SOVIET PHYSICS JETP

A translation of the Zhurnal Éksperimental'noĭ i Teoreticheskoĭ Fiziki.

Vol. 11, No. 3, pp. 481-731 (Russ. orig. Vol. 38, No. 3, pp. 669-1016, March, 1960) Sept., 1960

ACADEMICIAN IGOR' VASIL'EVICH KURCHATOV

ACADEMICIAN Igor' Vasil'evich Kurchatov, a leading Soviet physicist, died suddenly in Moscow on February 7, 1960.

I. V. Kurchatov was born on January 12, 1903 in the Sima mill settlement of the Ufa Province; his father was a land surveyor. In 1923 he graduated from the physico-mathematical faculty of the Crimean University. In the course of these years he developed an exceptional interest in scientific work. In 1925 he began working at the Leningrad Physico-Technical Institute.

Even as a young scientist Kurchatov made a series of important discoveries in the physics of dielectrics, a branch which was still little studied at that time. Already then he inaugurated the detailed study of a new class of materials — the ferroelectrics; his work led to a theoretical understanding of these phenomena, which subsequently took on a more practical significance.

During the following years Kurchatov occupied himself with studies of the atomic nucleus. In 1935 he discovered the phenomenon of nuclear isomerism.

In 1940 Kurchatov initiated and guided research which led to the discovery of the spontaneous fission of uranium nuclei.

During the second world war he devoted all his strength and knowledge to the consolidation of the defensive power of our country.

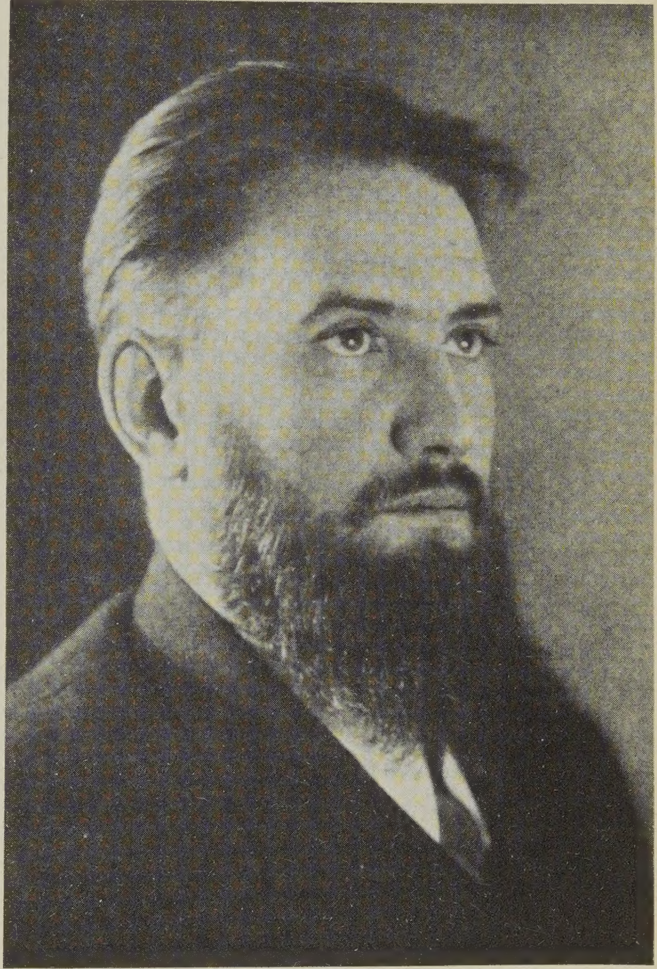

Thereafter all his activities were connected with the problems of utilizing atomic energy, and until the end of his life he continuously guided this work in the Soviet Union. He established the largest institute in the domain of nuclear physics — the Atomic Energy Institute of the U.S.S.R. Academy of Sciences (which will now bear his name). Under his scientific guidance and with his direct participation, an atomic technology was created in our country, and the study of the atomic nucleus was raised to a new and high level; work was developed on controllable thermonuclear reactions and ways of utilizing atomic energy in various branches of the national economy were found. Kurchatov trained numerous scientists and engineers in this new field.

In 1943 the U.S.S.R. Academy of Sciences elected him a full member of the Academy for his distinguished scientific merits.

Kurchatov was not only a great scientist but also a prominent figure in state affairs. He was several times elected a deputy to the Supreme Soviet.

Kurchatov was an ardent patriot. In a speech before the session of the Supreme Soviet on January 15, 1960, he said: "I am happy to have been born in Russia and to have dedicated my life to the atomic science of the great Soviet country. I deeply believe and strongly know that our people, our government, will devote the achievements of this science only to the welfare of humanity."

The brilliant ability of the scientist, his enormous energy, his remarkable gift for organizing, and his exceptional capacity for work, were happily combined with rare spiritual qualities. He enjoyed the respect and love of all those who were fortunate to work together with him and under his guidance.

For his distinguished merits on behalf of his native country, Kurchatov was honored three times with the title of Hero of Socialist Labor, and with the Lenin and Stalin prizes.

Together with all Soviet physicists, the editorial office of the JETP mourns the loss of a distinguished man and great scientist of our country.

Translated by Z. Barnea
137

SOVIET PHYSICS JETP VOLUME 11, NUMBER 3 SEPTEMBER, 1960

MEASUREMENTS OF THE SPECTRA AND AVERAGE NUMBER OF NEUTRONS EMITTED IN THE FISSION OF U^{235} AND U^{238} INDUCED BY 14.3-Mev NEUTRONS

Yu. A. VASIL' EV, Yu. S. ZAMYATNIN, Yu. I. IL' IN, E. I. SIROTININ, P. V. TOROPOV, and É. F. FOMUSHKIN

Submitted to JETP editor August 5, 1959

J. Exptl. Theoret. Phys. (U.S.S.R.) **38**, 671-684 (March, 1960)

The fission neutron spectra and average number of neutrons $\bar{\nu}$ emitted in the fission of U^{235} and U^{238} induced by 14.3-Mev neutrons were measured. The measurements were made at energies between 0.4 and 5 Mev by the time-of-flight technique, in which a pulsed source was used. The spectra obtained are interpreted as consisting of neutrons emitted by the fragments and of neutrons evaporated before fission of the nucleus. The following distribution parameters were found: $T_f = (1.06 \pm 0.03)$ Mev, $T = (0.37 \pm 0.04)$ Mev and α, the fraction of the evaporated neutrons, $= (16 \pm 2)\%$ for U^{235}; whereas $T_f = (1.16 \pm 0.03)$ Mev, $T = (0.4 \pm 0.04)$ Mev, $\alpha = (21 \pm 2)\%$ for U^{238}. The measured values of $\bar{\nu}$ are 4.17 ± 0.30 for U^{235} and 4.28 ± 0.30 for U^{238}, their ratio being $\bar{\nu}(U^{238})/\bar{\nu}(U^{235}) = 1.03 \pm 0.03$.

1. INTRODUCTION

MOST investigations into the various aspects of nuclear fission have been devoted to the study of nuclear fission by thermal neutrons and spontaneous fission. The study of nuclear fission by fast neutrons, especially the spectra and number of neutrons emitted, has been much more meager. This situation is largely due to the experimental difficulties inherent in recording fission neutrons in a background of many primary neutrons having approximately the same energy, as well as to the considerably smaller fission cross section for fast neutrons.

However, good reasons exist for the study of nuclear fission by fast neutrons: e.g., the occurrence of new fission channels at high excitation energies and the increase in the number of available fissionable isotopes.

At the present time data are available on the spectra of fission neutrons from the fission of U^{233}, U^{235}, Pu^{239}, and Pu^{241} induced by thermal neutrons[1-6] and from the spontaneous fission of Cf^{252}.[6] These measurements indicate that the spectra for all these isotopes are similar and can be approximated accurately enough by the expression

$$F(E) \sim \exp\left(-\frac{E}{T_f}\right) \sinh \frac{2\sqrt{wE}}{T_f} \qquad (1)$$

or

$$F(E) \sim \sqrt{E} e^{-E/B}. \qquad (2)$$

A slight hardening of the spectrum is noted in the transition from U^{235} to Pu^{239} and on to Cf^{252}. At present, because of insufficient experimental data, it is difficult to say whether the parameter Z^2/A plays a decisive role in this hardening.

Only the work of Zamyatnin et al.[7] contains data on the neutron spectrum for nuclear fission induced by neutrons with an energy of more than 1 Mev. In this work the photographic technique was used to study the fission neutron spectrum formed by the capture of 14-Mev neutrons by Th^{232}, U^{233}, U^{235}, U^{238}, and Pu^{239} nuclei.

The results of this study combined with computations by Bat' and Kudrin[8] give evidence of a slight hardening of the spectra with an increase in the primary neutron energy, though the data remain as yet insufficient for quantitative conclusions. Besides, the experimental setup described by Zamyatnin et al.[7] is such that it is impossible to distinguish the fission neutrons from neutrons emitted in the process of inelastic scattering and the (n, 2n) reaction.

Recently several papers[9-13] have been published on $\bar{\nu}$ measurements for the fission of various isotopes by 14-Mev neutrons. However, the results obtained lack satisfactory agreement among themselves and fail to provide a basis for conclusions as to variation of $\bar{\nu}$ from isotope to isotope.

This article describes an investigation undertaken to obtain additional data on the spectra and number of emitted neutrons from the fission of U^{235} and U^{238} induced by 14.3-Mev neutrons.

II. EXPERIMENTAL TECHNIQUE AND MEASUREMENT

Experimental arrangement. Figure 1 shows the layout of the experimental apparatus.

The time-of-flight technique was used in the measurements. An essential feature of this technique was the use of a pulsed primary neutron source.

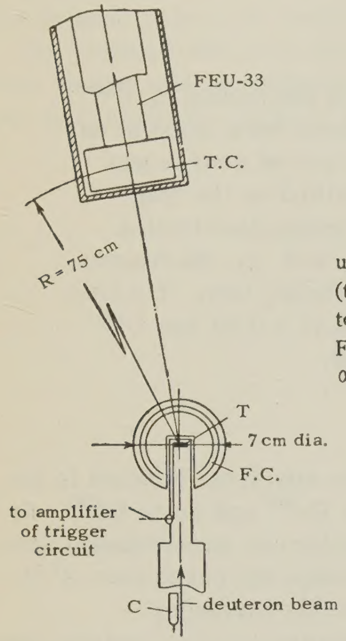

FIG. 1. Experimental setup; shaded area – Pb shield, (thickness = 2.5 mm), T.C. – tolane crystal, T – target, F.C. – fission chamber, C – α particle counter.

The primary neutron pulses were provided by a $T(d, n)He^4$ reaction in the target of the accelerator tube when the target was bombarded by short, periodic pulses of 150-kev deuterons. A fission chamber situated near the target served as the source of the fission neutrons. Since the fission incidents in the chamber occurred practically simultaneously with the primary neutron pulses, the target and the chamber constituted a pulsed source of primary and fission neutrons. Because the probability of fission inside the chamber was 10^{-4} per neutron pulse, most of the source pulses belonged to "background" and consisted of 14.3-Mev neutrons and neutrons formed by the inelastic interaction of these primary neutrons with the target materials and the fission chamber. If fission occurred in the chamber, fission neutrons likewise appeared in the source pulse. The presence of these "working" pulses was revealed by the appearance of ionization pulses in the fission chamber.

Pulses resulting from the deuteron beam bombarding the target were used as trigger pulses and determined the moment of emission of the neutrons from the source.

The neutron detector was a scintillation counter located 75 cm from the source. The time of flight of the neutrons was determined by measuring the time interval between the detector pulse and trigger pulse with an electronic circuit. The time distribution of the detector pulses was measured separately for "working" and "background" source pulses. If the total number of primary neutrons during a period of measurement was the same in the "working" and "background" source pulses, the difference in the measurements represented the time-of-flight distribution of fission neutrons. This distribution, when measured by a detector with a known energy sensitivity curve, permits one to determine the energy spectra of the fission neutrons, as well as average number of fission neutrons $\bar{\nu}$.

Pulsed source of 14.3-Mev neutrons. The pulsed deuteron flux was obtained by modulating a beam of accelerated deuterons with a sinusoidal electric field by the use of deflecting plates ($f = 2$ Mcs). The deuteron pulses and, correspondingly, the pulses of 14.3-Mev neutrons lasted 3 nanoseconds, and had a repetition rate of 4 Mcs. The average number of neutrons in a pulse, $\bar{n}$, was 4 (in fact $\bar{n} \approx \bar{\nu}$); any increase in the neutron yield was undesirable on account of the increase in the background. The average neutron emission was determined from the counting rate of the α monitor.

In intervals between pulses when deuterons struck the deflecting plates and the diaphragm, which was situated 80 cm from the target, 2.5-Mev neutrons were generated by the $D(d, n)He^3$ reaction. This resulted in a slight increase in background.

Fission chamber. Two fission chambers with layers of U^{235} (90%) and U^{238} (natural isotopic composition) were used. Each chamber consisted of three spheres 6, 7, and 8 cm in diameter and had a radial cylindrical channel 22 mm in diameter. The chamber electrodes and walls of the accelerator target block were constructed thin enough (0.5 mm) to reduce neutron scattering.

Layers of a fissionable substance were applied to both surfaces of the 7 mm diameter sphere. The layers in the U^{235} chamber were 2 mg/cm^2 thick and in the U^{238} chamber 3 mg/cm^2, with a thickness variation nowhere exceeding ±10%. The total weight of the fissionable substance was 0.6 g in the U^{235} chamber and 0.9 g in the U^{238} chamber. The detection efficiency of both chambers was about 60%.

The chambers were filled with a mixture of argon and carbon dioxide (10%) to a pressure of 760 mm Hg. The rise time of the chamber was $0.1 \pm 0.05\,\mu$sec.

The accelerator target was installed at the center of the chamber when spectra were being obtained. The spherically symmetrical arrangement of the fissionable substance in relation to the target eliminated the influence of anisotropy of fragment distribution on the measurements.

Neutron detector. The neutron detector was a tolane crystal, 80 mm in diameter and 25 mm thick, with a FEU-33 photomultiplier. This detector was set at a 15° angle to the axis of the accelerator tube. This placement of the detector made it possible to reduce the background due to the 2.5- Mev neutrons. The scintillation counter was sheathed in a lead shield 2.5 mm thick to protect it from x-rays from the accelerator tube.

The measurements were made in a room large enough to allow the detector to be installed no nearer than 4 m from the walls and floor and with the nearest scattering material (steel flooring 5 mm thick) 1.5 m away. Nevertheless, neutrons and γ rays that had been scattered in the room composed about half of the background in the 0.4 — 5 Mev range.

The efficiency of the detector for neutrons in the energy interval < 5 Mev was determined by Hardy's[14] method. Figure 2 shows computations for three threshold values, E_{th} (0.2, 0.25, and 0.3 Mev). To establish the energy threshold of the scintillation counter its absolute efficiency in the 0.2 — 1.5 Mev energy region was measured with an electrostatic accelerator. The $T(p, n)He^3$ reaction served as a source. A "long" counter and a U^{235} fission chamber were used as neutron flux monitors. Since the energy dependence of the counter efficiency for the 0.25 Mev threshold was in best agreement with the data obtained with the accelerator, this dependence was used in processing the measurements of the neutron spectra.

Electronic instrumentation. Electronic apparatus was used to measure the time distribution of the detector pulses which originated after the occurrence of working pulses from the pulsed source (i.e., after "effect + background" pulses). For our experimental conditions the time of flight for fission neutrons with energies in the 5 — 0.4 Mev region was 24 to 86 nanosec. This determined the minimum time-interval to be measured. In order to obtain data on prompt-fission γ rays and on the detector background, the time intervals measured were increased to 220 nanosec (150 nanosec after the working pulses and 70 nanosec before the pulses).

Figure 3 is a block diagram of the electronic apparatus. The system consisted of two channels — one slow, the other fast. In the slow channel, from the sequence of detector pulses those that happened to be in the interval being measured were selected; the time distribution of these pulses was measured in the fast channel. Coincidences in the slow channel were used to select the detector pulses. First, the trigger pulses that corresponded to working pulses were selected from the sequence of trigger pulses. For this purpose the trigger pulses, as well as shaped fission chamber pulses, which lasted $0.1\,\mu$sec, were fed into the slow gating circuit. With delay 1 properly selected, only working trigger pulses passed through the gating circuit; these then entered the coincidence unit with the detector pulses. If coincidence occurred, the fast gating circuit opened, and a time analyzer measured the time distribution of the corresponding detector pulses in the fast channel.

Thus, the fast channel measures the time distribution of only those detector pulses that had been produced within the exact time interval before or after the working pulses from the source. Moreover, the duration of the interval was determined by the resolution time of the coincidence circuit (220 nanosec), while the position of the interval in relation to the working trigger pulses was determined by the selection of delay 2. The interval position was maintained to within ±20 nanosec in the course of the measurements. The operation of the system is illustrated in the time diagram Fig. 4. The passage of the trigger pulses through the slow gating circuit is shown in the

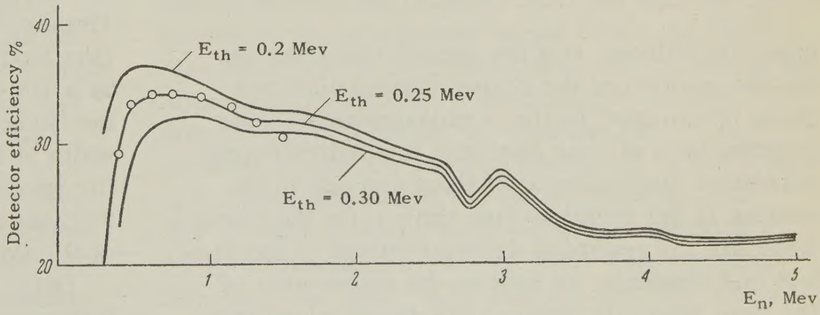

FIG. 2. Energy dependence of the detector efficiency; measurements with the electrostatic accelerator are designated by o.

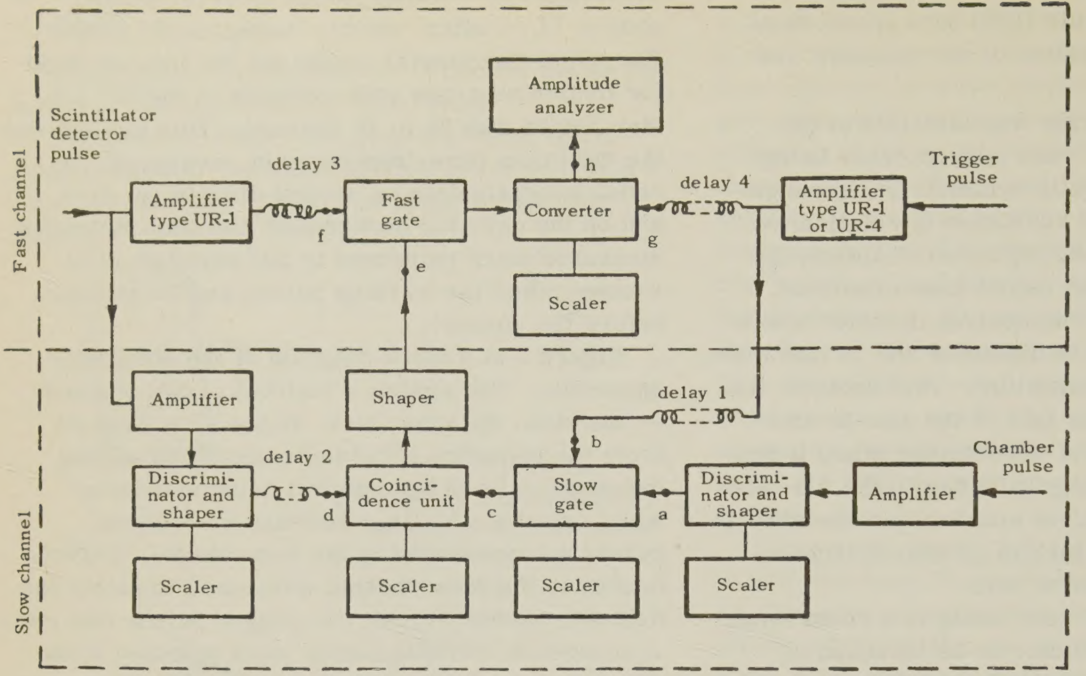

FIG. 3. Block diagram of the electronic apparatus.

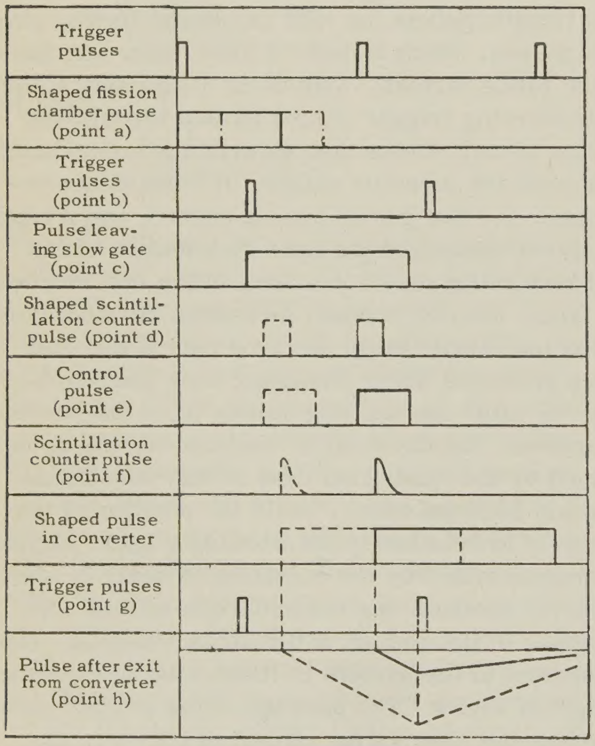
Trigger pulses
Shaped fission chamber pulse (point a)
Trigger pulses (point b)
Pulse leaving slow gate (point c)
Shaped scintillation counter pulse (point d)
Control pulse (point e)
Scintillation counter pulse (point f)
Shaped pulse in converter
Trigger pulses (point g)
Pulse after exit from converter (point h)

FIG. 4. Time diagram of pulses.

upper four lines. (On the second line from the top the position of the shaped fission chamber pulse is indicated during a measurement in the working interval; the dash-dot line indicates the maximum displacement of the pulse due to the scatter in the chamber rise time.) On the lower lines are the recorded detector pulses in the slow and fast channels, as well as the conversion of the time intervals between the detector and trigger pulses into an amplitude distribution. The solid and dotted lines show the pulses produced during the recording of neutrons with different times of flight.

The time distribution of the detector pulses was measured both after working source pulses (in working intervals) and after background pulses (in background intervals, which also lasted 220 nanosec). When the distribution in the background intervals was being measured, accelerator pulses instead of fission chamber pulses were admitted to the slow gating circuit. In this case, mostly background, randomly selected trigger pulses entered the coincidence circuit; the probability of transmitting working trigger pulses did not exceed 10^{-4}. The number of intervals recorded in these series of measurements was determined by the counting rate of the trigger pulses that entered the coincidence circuit (when the measurements were being made in the working intervals, the rates at which the trigger and fission chamber pulses were counted coincided).

The time analyzer used in the system operated on the principle of converting "time into amplitude." The amplitude distribution from the convertor (the input circuit of the analyzer) was measured by a 100-channel amplitude analyzer built along the lines of the ADA-50 analyzer. The average width of the time analyzer channel in the interval for recording fission neutrons and γ rays was 2.2 nanosec, and the non-linearity of the time scale did not exceed ±2%.

Data. Figure 5 (curve a) shows the time-interval distribution of the detector pulses ob-

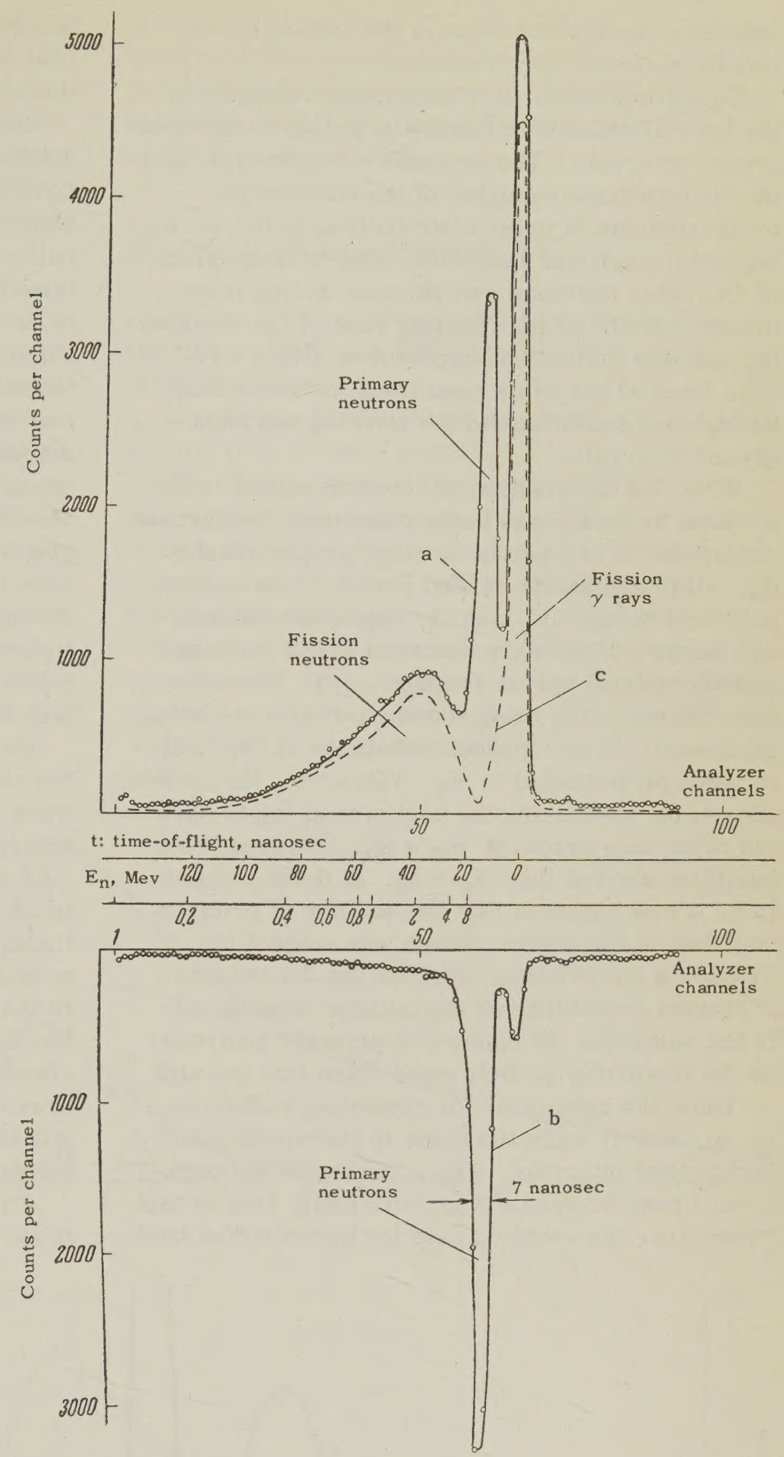

FIG. 5. Time-interval distribution of detector pulses obtained for the spectrum of neutrons from U^{238} fission; a – distribution of pulses in the working intervals, b – distribution of pulses in the background intervals, c – difference of curves a and b: time distribution of fission neutrons and γ rays.

tained in one of the series of measurements of the spectrum of neutrons emitted in U^{238} fission. On this graph one can see distinctly separate lines for the fission γ rays and 14-Mev neutrons; the broad maximum to the left corresponds to the fission neutrons.

In addition to the fission neutrons and γ rays in the working intervals, the following radiations were recorded: a) primary 14-Mev neutrons, as well as neutrons and γ rays formed in the interaction between the primary neutrons and the materials of the accelerator target block and the fission chamber; b) radiation due to the activation of materials, mostly of the scintillation counter, by fast primary neutrons; c) neutrons and γ rays formed by primary neutron scattering in the room; d) 2.5-Mev neutrons from the accelerator tube. The 14-Mev primary neutrons were separated from the fission neutrons by their time of flight. However, the other radiations enumerated above created a background even in the region where fission neutrons were recorded.

Background data were obtained by measuring the time distribution of detector pulses in the background intervals. The procedure for measuring the spectra thus consisted of the consecutive measurements of pulse distributions in the working and background intervals. The average yield of 14.3-Mev neutrons was checked during these measurements by the counting rate of the α monitor and was maintained constant to within ±3%. This insured the same conditions for recording background radiations in the working and background intervals.

When the distribution of detector pulses in the working intervals was being measured, background radiations a) and partly c) were proportional to $\bar{n}_W$, while radiations b) and partly c) were proportional to $\bar{n}_b$ ($\bar{n}_W$ and $\bar{n}_b$ represent the average number of primary neutrons in the working and background pulses respectively). When the distribution in the background intervals was being measured, all background radiations a), b), and c) were proportional to $\bar{n}_b$. Therefore, the method chosen for measuring the background might have led to serious error, if $\bar{n}_W \neq \bar{n}_b$. However, computations showed that $\bar{n}_W = \bar{n}_b$. In these computations it was assumed that the number of primary neutrons in the source pulses was subject to Poisson's distribution, and both the dependence of fission probability on the number of neutrons in the pulse and the capture of primary neutrons by the fissioning nucleus were taken into account.

Thus, the conditions for recording radiations a), b), and c) were the same in the working and background intervals. The accuracy of the background measurements was sufficiently high in this case, since the counting rate for uncontrolled background sources (2.5-Mev neutrons and characteristic detector noise) constituted less than 5% of the total background counting rate.

The measurements of the distributions in the working and background intervals gave rise to an equal number of recorded intervals. Figure 5 shows the frequency-time distribution of detector pulses in the background intervals that was obtained in one and the same set of measurements of the fission neutron spectrum for U^{238} (curve b). Figure 5 also shows the time distribution of neutrons and γ rays from U^{238} fission (curve c). As can be seen from the graph, the background amounted to 15 — 20% of the effect over a wide energy interval and at the limits of the 0.4 — 5 Mev energy interval amounted to 35%. This same graph shows the time and energy scales, with the zero time of the time-of-flight scale determined by the position of the fission γ-ray line. The time resolution of the apparatus as found from the half width of the fission γ-ray and primary-neutron line was 7 nanosec.

Corrections for fission neutrons scattered by the chamber and also for delayed fission γ rays[15] were applied to the data. The scattering of fission neutrons by detector materials, particularly by the lead shield, was shown by control measurements to have no effect on the spectrum measurements. Under the conditions of the experiment, measurements indicated that the effect of neutron scattering in the room could also be ignored. To illustrate the effect of the corrections Fig. 6 shows curve c (from Fig. 5) on an enlarged scale. (The shaded area corresponds to the corrections, which were subtracted during the processing of the measurements.)

To obtain the energy spectra of the fission neutrons use was made of the measurements of the

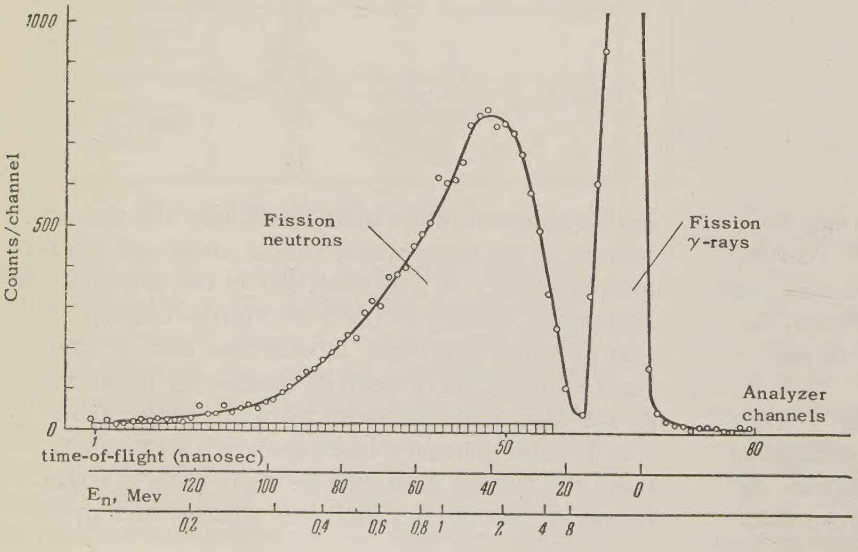

FIG. 6. Time distribution of neutrons and γ rays from U^{238} fission.

time distributions for time-of-flight intervals from 24 to 86 nanosec. The corresponding energy interval was 5 to 0.4 Mev. Data obtained outside this interval were not processed because of the strong background. Measurements for energies less than 0.4 Mev were also unreliable because of possible instability in the efficiency of the detector near the threshold.

The total number of recorded fission neutrons with energies in the 0.4 to 5 Mev interval was 2.2×10^4 for U^{235} and 2.6×10^4 for U^{238}, with the counting rate at 500 — 600 neutrons/hour. The statistical error was 3 — 4% in the 0.8- to 5-Mev interval and rose to 6% in the 0.4- to 0.8-Mev interval. The total error in the measurements may have been increased by inaccuracies in the numerical determination of the energy dependence of the detector efficiency.

To clarify the influence of energy resolution on the form of the fission neutron spectra, control measurements were made of the spectrum of secondary neutrons formed in the passage of 14.3-Mev neutrons through a layer of lead 6-cm thick, with three flight distances: 75, 100, and 125 cm. These measurements showed that as the energy resolution was improved, the form of the spectrum was the same within the limits of accuracy required in the experiments (2%).

III. RESULTS AND DISCUSSION

Figure 7 shows the spectra of neutrons from the fission U^{235} and U^{238} as obtained from the measurements.

To analyze the resultant spectra, $\ln\{F(E)/E\}$ curves (Fig. 8) were plotted.

The hard portion of the spectra ($E > 3$ Mev), due to neutrons emitted by fragments, was used to find the value of parameter T_f (w was assumed to be 0.5 Mev). The difference between the experimental data and Eq. (1) in the region where $E < 3$ Mev determined the spectrum of the neutrons that evaporated before fission. The spectra of fission neutrons from U^{235} and U^{238} were found to be represented by

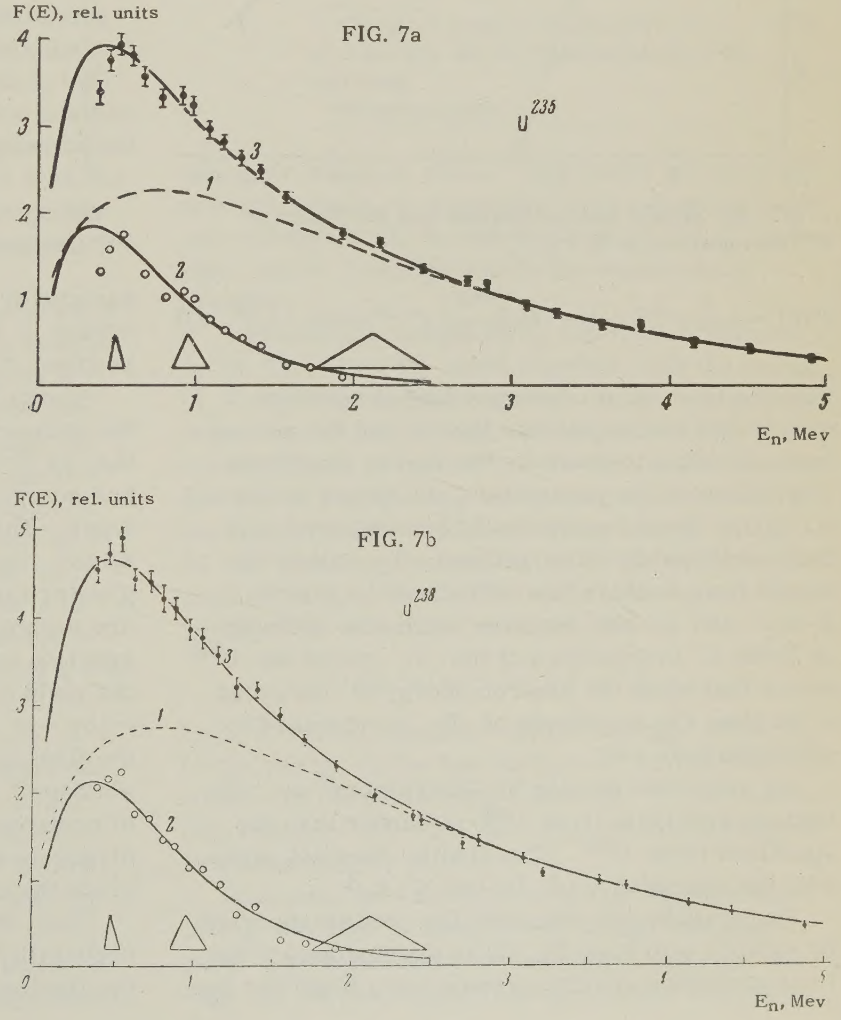

FIG. 7. Neutron spectra obtained from the fission of U^{235} (a) and U^{238} (b): ● — experimental results, ○ — the result of subtracting curve 1 from the experimental data; curve 1 — distribution given by Eq. (1), 2 — distribution $Ee^{-E/T}$, 3 — sum of curves 1 and 2 (distribution given by Eq. (3)).

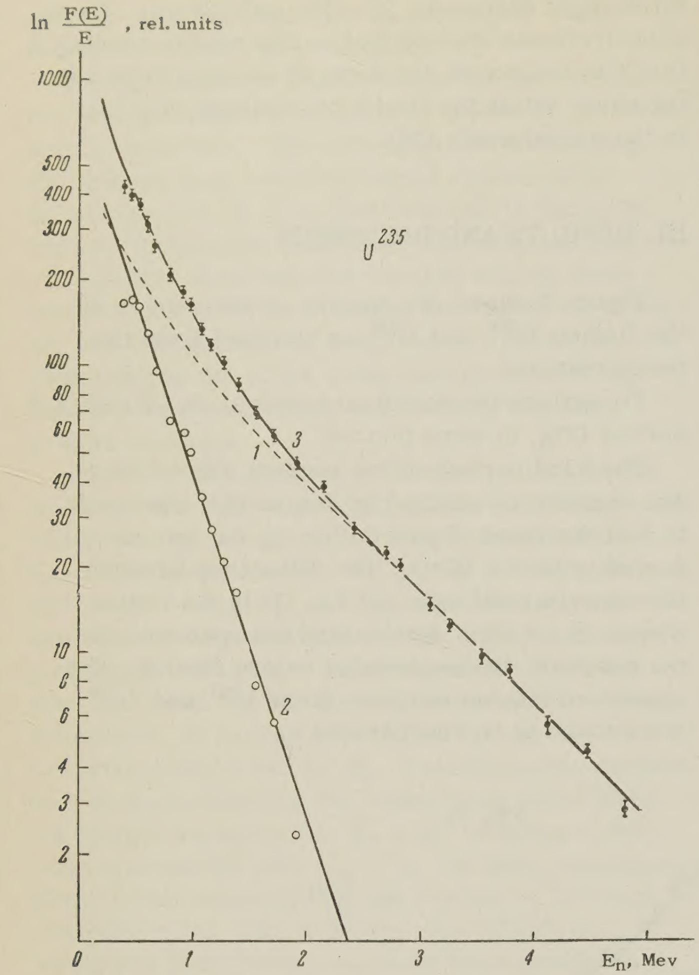

FIG. 8a. Neutron spectra obtained from the fission of U^{235} (designations as in Fig. 7).

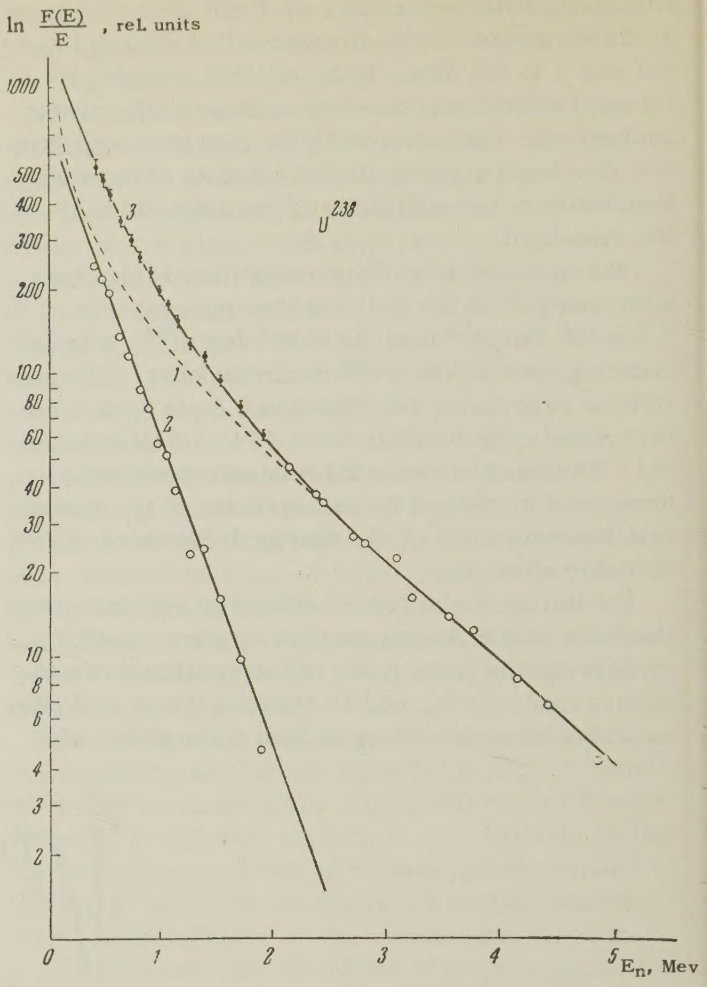

FIG. 8b. Neutron spectra obtained from the fission of U^{238} (designations as in Fig. 7).

$$F(E) = \alpha \frac{E}{T^2} e^{-E/T} + (1-\alpha) \frac{e^{-w/T_f}}{\sqrt{\pi w T_f}} e^{-E/T_f} \sinh \frac{2\sqrt{wE}}{T_f}, \quad (3)$$

with the first term corresponding to neutrons evaporated before nuclear fission and the second corresponding to neutrons emitted by fragments. The values of the parameters are shown in Table I.

So that these results could be compared with data published by other authors, T_f values obtained from nuclear fission induced by thermal, 4-Mev, and 14-Mev neutrons were also included in Table I. Comparison of the T_f values for U^{235} shows that when the neutron energy is increased to 14 Mev, the magnitude of T_f is increased by approximately 10%.

As was noted earlier by Zamyatnin et al.,[7] the neutron spectrum from U^{238} is harder than the spectrum from U^{235}. This finding does not agree with the dependence of T_f on Z^2/A.[18]

To compare our data with the results reported by authors who used Eq. (2) to approximate their fission neutron spectra, values were found for the parameter B. The values for B have been included in Table I and confirm the conclusions reached through comparison of the values of T_f.

As can be seen from Fig. 8, the spectrum of the evaporated neutrons is in good agreement with the $Ee^{-E/T}$ distribution, and the parameter T has nearly the same value for both uranium isotopes. The fraction of evaporated neutrons obtained (about 20%) proved to be considerably greater than expected. If the evaporated neutrons are assumed to occur solely through a (n, nf) reaction with a cross section $\sigma_f' = \sigma_{f_1} - \sigma_{f_0}$, then the yield of evaporated neutrons should be $\alpha = (\sigma_{f_1} - \sigma_{f_0})/\bar{\nu}\sigma_{f_1} \approx 10\%$, where σ_{f_0} and σ_{f_1} are the fission cross sections on the first and second plateaus[19] (see Fig. 9). Allowance for evaporation of neutrons by the (n, 2nf) reaction reduces the divergence somewhat but does not eliminate it, since the cross section for this process is small.[20]

Thus, the measurements indicate a greater probability for (n, nf) and (n, 2nf) processes in the fission of U^{235} and U^{238} by 14-Mev neutrons

TABLE I

Isotope	E_n, Mev	T_f, Mev	B, Mev	T, Mev	α
U^{235}	Thermal	0.965 [2]	1.290 [2,17]	—	—
	4.0	1.01±0.03 **	—	—	—
	14.0	1.05±0.06 [7]	—	0.4±0.05 [7]	—
	14.3	1.06±0.03*	1.36±0.04*	0.37±0.04*	0.16±0.02*
U^{238}	14.0	1.22±0.10 [7]	—	0.48±0.05 [7]	—
	14.3	1.16±0.03*	1.46±0.04*	0.40±0.04*	0.21±0.02*

*Results of the present experiment.

**Obtained on the basis of the relative value given by Bondarenko et al.[16] and the T_f value for thermal neutrons.

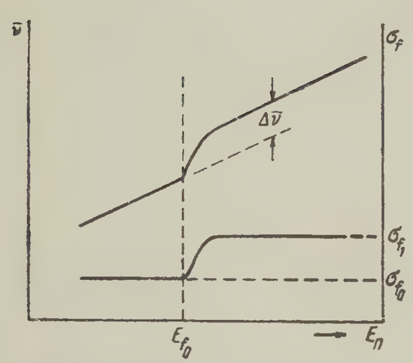

FIG. 9. Proposed $\bar{\nu}(E)$ dependence.

TABLE II

E_n, Mev	$\bar{\nu}(U^{235})$	$\bar{\nu}(U^{238})$
14.0	4.10±0.15 [17]	—
14.1	4.52±0.32 [17] 4.13±0.24 [11]	4.13±0.25 [17] 4.50±0.32 [11] 4.45±0.35 [12]
14.2	—	4.55±0.15 [13]
14.8	4.70±0.50 [10]	—
15.0	4.51±0.19 [9]	—
14.3	4.29±0.12* 4.17±0.30**	4.48±0.13* 4.28±0.30**

*Weighted mean; for reduction to E_n = 14.3 Mev the $d\bar{\nu}/dE_n$ obtained in our work was used.

**Results of this work.

than should result from the values for the fission cross sections on the first and second plateaus and, correspondingly, also indicate a reduction in the probability of nuclear fission without prior neutron evaporation. It is noteworthy that the experimental value of α for U^{238} is somewhat greater than for U^{235} and fits the assumption of a larger contribution by the (n, nf) process to the total fission cross section of U^{238}.

To obtain $\bar{\nu}$, the fission neutron spectra were integrated with allowance for the absolute scintillation-counter efficiency ϵ and the fraction β (≈ 0.15) of the spectrum which was beyond the measured range [β was computed from Eq. (3)]. The result obtained pertained to the fissions that were recorded during the measurement time. A correction was introduced in the calculation of $\bar{\nu}$ to take account of the moderation of the primary neutrons through scattering on the materials in the chamber and target block. The values for $\bar{\nu}$ obtained were 4.17 ± 0.30 for U^{235} and 4.28 ± 0.30 for U^{238}, and their ratio was $\bar{\nu}(U^{238})/\bar{\nu}(U^{235}) = 1.03 \pm 0.03$.

The error in $\bar{\nu}$ consists mostly of errors in determining the values of ϵ and β and on the average amounted to 7 — 8%. The error in the relative measurement was much smaller (~ 3%), since the absolute value of the efficiency was unimportant in this case.

For the sake of comparison, Table II includes values for $\bar{\nu}$ obtained from other investigations and their weighted mean. The values given in the present article are somewhat lower than the average values for $\bar{\nu}$, though both values for $\bar{\nu}$ and their ratios coincide within the experimental errors.

The absolute values of $\bar{\nu}_{14}$ for fission induced by 14-Mev neutrons taken together with the values of $\bar{\nu}_0$ for thermal neutrons or for low energy neutrons permit one to infer the dependence of $\bar{\nu}$ on the excitation energy E* of the fissionable nucleus (or on the energy, E_n, of the neutrons producing the fission). Moreover, the large change in E_n (to 14 Mev) and correspondingly in $\bar{\nu}$ permits one to find $d\bar{\nu}/dE_n$ with a sufficiently high degree of accuracy.[16] It is usually assumed that

$$d\bar{\nu}/dE_n = (\bar{\nu}_{14} - \bar{\nu}_0)/(14 - E_0),$$

i.e., $\bar{\nu}$ varies linearly with the energy. Here E_0 is the energy of the low energy or thermal neutrons. The experimental values for $\bar{\nu}$ for excitation energies E* < 10 Mev (E_n < 4 Mev) confirm this assumption.

However, the use of the value of $\bar{\nu}_{14}$ in computing $d\bar{\nu}/dE_n$ is complicated by the fact that when E_n is the same as the fission barrier energy E_f of the original nucleus, a new reaction channel is opened – (n, nf), and $\overline{\nu}(E)$ may undergo a discontinuity (Fig. 9). The magnitude of the $\Delta\overline{\nu}$ jump at E_f is

$$\Delta\bar{\nu} = \frac{\sigma'_f}{\sigma_{f_1}}\,[1 - \bar{\nu}(E_f) + \bar{\nu}(E_f - E_{\mathrm{b}} - 2T)],$$

and depends on the contribution σ'_f of the (n, nf) reaction to the total cross section σ'_f and on the difference $1 - [\overline{\nu}(E_f) - \overline{\nu}(E_f - E_b - 2T)]$ which may have either a positive or negative value. For those cases when the change in $\overline{\nu}$ is equal to unity, i.e., for E_f equal to the sum of the neutron binding energy, E_b, and the average neutron kinetic energy 2T, the discontinuity in $\overline{\nu}(E)$ is absent.*

To evaluate $\Delta\overline{\nu}$, we take for the value of E_b in U^{236} and U^{239}, 6.5 and 4.8 Mev respectively[21] and for the values for $d\overline{\nu}/dE_n$, those given by Bondarenko et al.[16] Thus we find that

$$\bar{\nu}(E_f) - \bar{\nu}(E_f - E_{\mathrm{b}} - 2T) = (E_{\mathrm{b}} + 2T)\,d\bar{\nu}\,/\,dE_n$$

is less than unity for both uranium isotopes. A calculation of the value of $\Delta\overline{\nu}$ with allowance for the reduction in $d\overline{\nu}/dE_n$ due to the discontinuity and also with allowance for a second discontinuity in the region of the threshold for the (n, 2nf) reaction indicates that in determining $d\overline{\nu}/dE_n$ it is necessary to reduce the difference $\overline{\nu}_{14} - \overline{\nu}_0$ by 0.10 for U^{235} and 0.16 for U^{238}. The value of $d\overline{\nu}/dE_n$ obtained on the basis of our results in the energy region $E_n < 2$ Mev proved to be 0.112 ± 0.011 for U^{235} and 0.115 ± 0.011 for U^{238}.

From our data we were also able to evaluate the relative yield of prompt fission γ rays. If the spectra of γ rays from the fission of U^{235} and U^{238} are assumed to be alike, then the ratio of the average numbers of γ rays emitted per fission event is $n_\gamma(U^{238})/n_\gamma(U^{235}) = 0.94$.

In conclusion the authors wish to express their gratitude to Yu. Ya. Glazunov, A. N. Maslov, N. I. Nemudrov, V. A. Parshina, A. I. Peshetov, V. S. Khorkhordin, and V. N. Shikin, who participated in the measurements, to the crew of radio technicians for setting up the electronic apparatus, to V. A. Komarova for her work on the computer, and also to the associates in V. A. Ivanov's group for seeing to the operation of the accelerator.

---

[1] B. E. Watt, Phys. Rev. **87**, 1037 (1952); Bonner, Ferrell, and Rinehart, Phys. Rev. **87**, 1032 (1952); D. L. Hill, Phys. Rev. **87**, 1034 (1952); Mukhin, Barkov, and Gerasimova, see B. G. Erozolimskiĭ, Атомная энергия (Atomic Energy) Supplement No. 1, p. 74 (1957); [Transl: The Physics of Fission, Consultants Bureau, Inc., New York, 1957, p. 51].

[2] Cranberg, Frye, Nereson, and Rosen, Phys. Rev. **103**, 662 (1956).

[3] J. A. Grundl and J. R. Neuer, Bull. Amer. Phys. Soc. Series II **1**, 95 (1956).

[4] Kovalev, Andreev, Nikolaev, and Guseĭnov, JETP **33**, 1069 (1957), Soviet Phys. JETP **6**, 825 (1958).

[5] V. P. Kovalev, JETP **34**, 501 (1958), Soviet Phys. JETP **7**, 345 (1958).

[6] Smith, Fields, Friedman, Cox, and Sjoblom, Paper No. 690, Second International Conference on the Peaceful Uses of Atomic Energy (Geneva, 1958), Vol. 15, p. 392.

[7] Zamyatnin, Safina, Gutnikova, and Ivanova, Атомная энергия (Atomic Energy) **4**, 337 (1958); Soviet Journal of Atomic Energy (Eng. Transl.) **4**, 443 (1958).

[8] G. A. Bat' and L. P. Kudrin, ibid. **3**, 15 (1957); Soviet Journal of Atomic Energy (English Translation) **3**, 735 (1957).

[9] Smirenkin, Bondarenko, Kutsaeva, Mishchenko Prokhoronova, and Shemetenko, ibid. **4**, 188 (1958); Soviet Journal of Atomic Energy (Eng. Transl.) **4**, 253 (1959).

[10] A. N. Protopopov and M. V. Blinov, ibid. **4**, 374 (1958); Soviet Journal of Atomic Energy (Eng. Transl.) **4**, 491 (1958).

[11] N. N. Flerov and V. M. Talyzin, ibid. **5**, 653 (1958); Soviet Journal of Atomic Energy (Eng. Transl.) **5**, 1593 (1958).

[12] N. N. Flerov and E. A. Tamanov, ibid. **5**, 654 (1958); Soviet Journal of Atomic Energy (Eng. Transl.) **5**, 1596 (1958).

[13] M. Gandin and J. L. Leroy, Paper No. 1186, Second International Conference on the Peaceful Uses of Atomic Energy (Geneva, 1958).

[14] J. E. Hardy, Rev. Sci. Instr. **29**, 705 (1958).

[15] Maienschein, Peele, Zobel, and Love, loc. cit. ref. 6, Paper No. 670, Vol. 15, p. 366

[16] Bondarenko, Kuz'minov, Kutsaeva, Prokhorova, and Smirenkin, ibid. Paper No. 2187, Vol. 15, p. 353.

[17] R. B. Leachman, ibid. Paper No. 2467, Vol. 15, p. 229.

[18] V. P. Kovalev and V. S. Stavinskiĭ, Атомная энергия (Atomic Energy) **5**, 649 (1958); Soviet Journal of Atomic Energy (Engl. Transl.) **5**, 1588 (1958).

[19] Yu. S. Zamyatnin, ibid., Supplement No. 1 p. 27 (1957); [Transl: The Physics of Fission, Consultants Bureau, Inc., New York, 1957].

[20] D. J. Hughes and R. B. Schwartz, Neutron Cross Sections, BNL-325, New York 1958.

[21] R. Vandenbosch and G. T. Seaborg, Phys. Rev. **110**, 507 (1958).

Translated by A. Skumanich
138

---

*In this case $\overline{\nu}$ is considered to be the same for neighboring isotopes.

SOVIET PHYSICS JETP VOLUME 11, NUMBER 3 SEPTEMBER, 1960

INTERACTION OF AN ELECTRON BEAM WITH A PLASMA

I. F. KHARCHENKO, Ya. B. FAĬNBERG, R. M. NIKOLAEV, E. A. KORNILOV, E. A. LUTSENKO, and N. S. PEDENKO

Physico-Technical Institute, Academy of Sciences, Ukrainian S.S.R.

Submitted to JETP editor August 12, 1959

J. Exptl. Theoret. Phys. (U.S.S.R.) **38**, 685-692 (March, 1960)

The results of an experimental investigation of the interaction of modulated and unmodulated high-energy electron beams with the plasma in a high-frequency discharge are presented. It is shown that the passage of an unmodulated beam through a plasma results in the production of plasma oscillations in the beam at a frequency close to the plasma frequency. The dependence of oscillation amplitude on frequency and the plasma parameters is determined. The coherent energy losses of electrons in modulated and unmodulated beams moving through a plasma have also been studied.

1. The first experiments in which plasma oscillations were produced by the interaction of an electron beam and a plasma were those reported by Langmuir, Tonks, and Penning.[1-3] Merill and Webb[4] and other authors[5] have investigated the oscillation regions and their relation to the anomalous dissipation of electron energy in a gas discharge. Interpretations of these results have been given by Vlasov[6] and by Bohm and Gross,[11] who showed that the oscillations are excited by a mechanism similar to that which operates in the klystron.

Looney and Brown[8] and Gabor and his coworkers,[9] using an external electron source, found that plasma oscillations are excited only when there are sheaths at the electrodes or at the surfaces which confine the discharge. As has been shown by Akhiezer and Faĭnberg[10] and Bohm and Gross,[7] an initially unmodulated beam characterized by a uniform density and constant velocity is unstable in passage through a uniform plasma (a plasma with no density gradients or sheaths). Under these conditions longitudinal electromagnetic waves of increasing amplitude are excited in the beam and in the plasma. The plasma is excited by the beam when the beam velocity is greater than the thermal velocity of the plasma, $v_0 \gg s$ and also when $v_0 \ll s$. However, when $v_0 \gg s$ the beam-plasma interaction is much more effective. The ratio of the excitation coefficients for these two cases is $v_0/s\,(\Omega/\omega_0)^{-1/3} \gg 1$, where ω_0 is the plasma Langmuir frequency and Ω is the plasma frequency of the beam.

Instabilities can be avoided if there is a velocity spread in the beam. The interaction mechanism described here also applies to the passage of an ion beam through a plasma.

In interacting with the plasma the beam becomes density modulated so that the initially uniform beam is broken up into separate bunches. Under these conditions coherent interactions can become important. The possibility of using the coherence effect for intensifying the interaction between charged particles and a plasma was first indicated by Veksler.[12] If the coherence conditions are satisfied the energy loss of an individual particle in a bunch is given by

$$\left|\frac{dE}{dx_z}\right| = \frac{e^2 N}{2v_0^2}\,\omega_0^2 \ln\left(1 + \frac{v_0^2}{\omega_0^2 b_\perp^2}\right), \qquad (1)$$

where N is the number of particles in the bunch and $b_\perp$ is the transverse dimension of the bunch. The fields produced by a coherent bunch can be intensified if the coherence conditions are satisfied for a number of such bunches simultaneously.[13]

A comparison of this interaction mechanism with that proposed by Tuck[14] indicates that the present excitation coefficient is much larger. The ratio of the excitation coefficients is $(c/v_0)^2 \times (\omega_0 r_0/v_0)(\omega_0/\Omega)^{2/3} \ll 1$, where r_0 is the classical electron radius. This difference is due to the fact that the Tuck analysis does not take account of the possibility of a coherent interaction.

The nature of the instability is of great importance in an analysis of the interaction of a particle beam with a plasma. A method of distinguishing between absolute and convective instability in hy-

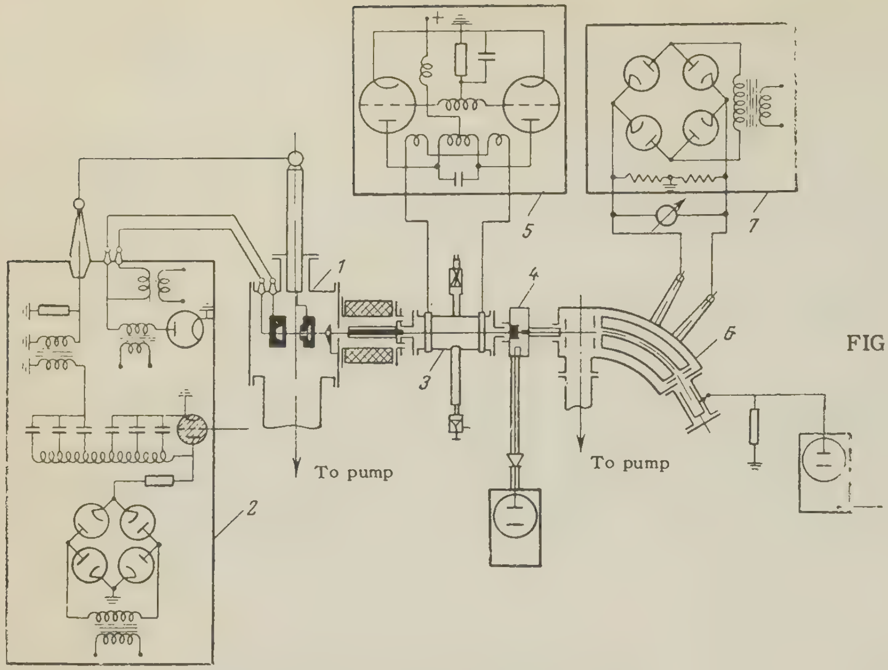

FIG. 1. Diagram of the experimental arrangement.

drodynamics has been pointed out by Landau and Lifshitz.[15] Essentially, this method is based on an investigation of the limiting behavior of the integral $\int \exp\{-i\omega(k)t\}\,dk$. Absolute instability obtains if the integral becomes infinite as $t \to \infty$. The difference between convective and absolute instabilities in beam interactions has been studied by Sturrock.[16] This criterion has been applied by Drummond[17] in an analysis of the excitation of a cold plasma by a beam and indicates that the instability is convective in this case. Investigations carried out by us,[18] using the Landau-Lifshitz technique, lead to the same result.

Experimental attempts to observe the interaction mechanism predicted by the theory[10,11] have been unsuccessful up to the present time.[8] It is probable that the reason for these failures is the fact that the interaction lengths were too small in these experiments and that the initial perturbations, due exclusively to fluctuations in the beam and plasma, were relatively small. This second suggestion has been verified by the work of Boyd, Field and Gould.[19]

2. We now consider the basic relations needed for an analysis of the experimental data.[10]

The gain factor, which characterizes the growth of the longitudinal waves in space (imaginary part of the wave vector **k** for a fixed value of the frequency ω) is given by the following expression when $v_0 \gg s$:

$$\gamma = \frac{3^{1/2}}{2^{4/3}} \frac{\omega_0}{s} \left(\frac{s}{v_0}\right)^{1/3} \left(1 - \frac{s^2}{v^2}\right) \left(\frac{\Omega}{\omega_0}\right)^{2/3}. \tag{2}$$

The excitation coefficient, which characterizes the growth of the oscillations in time (imaginary part of ω for a given **k**) is given by the expression:

$$\varepsilon = \Omega \left\{ \left(\frac{\omega_0}{\omega}\right)^2 \frac{1}{1 - s^2/v_0^2} - 1 + i\eta \right\}^{-1/2}, \tag{3}$$

where η characterizes the damping due to pair interactions or collective interactions. In the latter case, η is given by the Landau formula

$$\eta = \sqrt{\frac{3\pi}{2}} \frac{\omega}{ks} (ak)^{-2} \exp\left\{-\frac{3}{2}(\omega/ks)\right\}^2, \tag{4}$$

where a is the Debye radius.

For a cold plasma ($v_0 \gg s$, $s \to 0$) we have

$$\gamma = \Omega / v_0 \sqrt{(\omega_0/\omega)^2 - 1}, \tag{5}$$

$$\varepsilon = \Omega / \sqrt{(\omega_0/\omega)^2 - 1}. \tag{6}$$

As $\omega \to \omega_0$ the gain factor increases without limit while the excitation coefficient remains finite, being given by

$$\varepsilon = 2^{-4/3} \sqrt{3}\, \omega_0^{1/3} \Omega^{2/3}. \tag{7}$$

The frequency corresponding to maximum excitation is shifted with respect to ω_0 by an amount $\Delta\omega$:

$$\Delta\omega / \omega_0 = -2^{-4/3} (\Omega/\omega_0)^{2/3}. \tag{8}$$

The half width of the curve which describes the excitation coefficient as a function of frequency is given by the following relation (if damping is neglected):

$$\frac{\varepsilon_\omega}{\varepsilon_{\omega\, max}} = \frac{2^{4/3}}{3^{1/2}} \left(\frac{\omega_0^2}{\omega^2} - 1\right)^{-1/2} \left(\frac{\Omega}{\omega_0}\right)^{1/3}. \tag{9}$$

In the amplification case, as $\omega \to \omega_0$, if collisions are neglected, $\gamma \to \infty$. Under these conditions the half-width is determined by the damping due to collisions of plasma particles between themselves or with the walls.

3. We now describe the experimental investigation of the interaction of an electron beam with a plasma.

A schematic diagram and a general picture of the experimental arrangement are shown in Fig. 1. An electron beam with an energy of 80 kev at a current of one ampere (pulsed, pulse length of 2 μsec) is formed by the three-electrode gun 1. The electron acceleration pulse is produced by the double artificial line 2. At the output of the source the beam is focused by a longitudinal magnetic field of about 200 gauss. The plasma is formed in a quartz tube 3, 65 mm in diameter, by a radio-frequency oscillator 5 in which two GU27B tubes are used in push-pull. The oscillator provides up to one kilowatt of CW power into a real load at 16 Mcs. In these experiments the length of the tube is 10 cm and 20 cm.

In normal operation the pressure differential between the electron gun and the tube is produced by means of a copper tube (120 mm long with an aperture of 5 mm) through which the electron beam passes (the beam diameter at the output of the source is less than 5 mm). In this way a pressure variation from 10^{-2} mm Hg in the discharge tube to 10^{-5} mm Hg in the source chamber is obtained. The pressure in the discharge tube is controlled by a mechanical leak.

Beyond the tube there is a tunable coaxial cavity 4. If oscillations at the resonant frequency of the cavity are excited in the beam as it passes through the plasma the cavity is excited. Part of the energy of the cavity oscillations is coupled out by means of a crystal detector. After passing through the discharge tube and the cavity the beam strikes the Faraday cylinder in an electrostatic analyzer 6. The rectifier 7 supplies voltage for the plates of the analyzer. The current from the cylinder is fed to a dc amplifier with an integrating input and then to a loop oscilloscope. A saw-tooth voltage is applied to the plates of the analyzer so that the oscilloscope tape records the $I_{av}(U)$ curve, i.e., the electron energy spectrum averaged over several pulses. The analyzer and the source are isolated from the discharge tube which provides the necessary pressure differential between the tube and the analyzer.

The current pulse and the sweep of the measurement oscilloscope must be synchronized; for this reason all units of the system are triggered by a special synchronizing pulse generator.

Using the system described here we have been able to produce radio-frequency oscillations in an unmodulated beam passing through a plasma. The oscillations are observed in a plasma interaction tube 20 cm in length. If smaller interaction lengths are used (10 cm) it is possible to amplify the radio-frequency component of the beam current in a pre-modulated beam, but oscillations cannot be produced. Figure 2 shows oscillograms of the current pulse (upper oscillogram) and the radio-frequency oscillation pulse at the output of the cavity resonator (lower oscillogram). Oscillations are observed over the entire duration of the current pulse. There is some delay of the radio-frequency pulse with respect to the current pulse because of the time required for oscillations to build up in the cavity (several tenths of a microsecond).

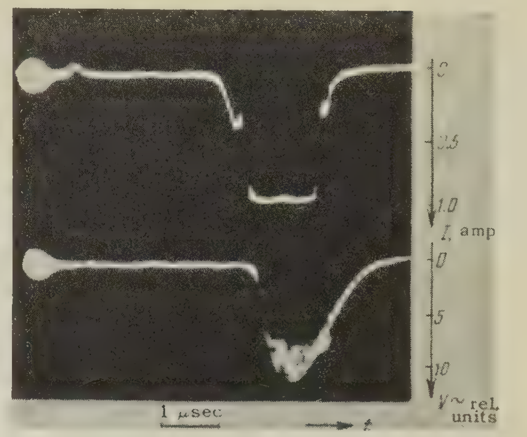

FIG. 2. Oscillogram showing the current pulse and the radio-frequency oscillations in the beam.

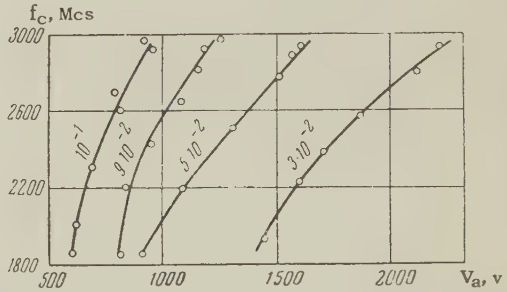

FIG. 3. Curves of the maximum oscillation amplitude at different pressures as a function of oscillator voltage (the figures on the curves are given in mm Hg).

In Fig. 3 the frequency f_c of the measuring cavity corresponding to the maximum oscillation amplitude is given as a function of the oscillator plate voltage V_a at different pressures in the discharge tube. The plate voltage determines the power supplied to the plasma by the oscillator, that is to say, the plasma density. The measurements have been carried out in the frequency range from 1800 to 3000 Mcs, the frequency limits of the oscillator.

At a given frequency the maximum oscillation amplitude is observed for some definite plate voltage or plasma density. In principle this density should correspond to the natural plasma frequency which, in the present case, is the resonant frequency of the measurement cavity. The displacement of the curves with pressure is due to the reduction in plasma density when the pressure in the discharge tube is reduced.

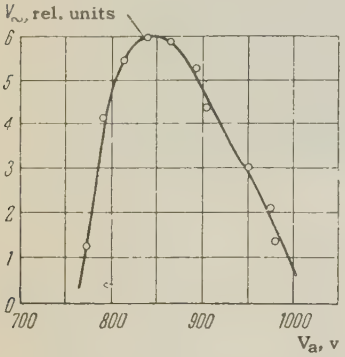

FIG. 4. Curve for oscillation amplitude at 2150 Mcs as a function of oscillator voltage ($p = 9 \times 10^{-2}$ mm Hg).

In Fig. 4, the oscillation amplitude at the output of the cavity $V_{\sim}$ is plotted in relative units as a function of the oscillator plate voltage with the cavity tuned to $f_c = 2150$ Mcs at a discharge tube pressure $p = 9 \times 10^{-2}$ mm Hg. It is apparent from the curve that at a given frequency and pressure a maximum oscillation amplitude is observed at one voltage, or plasma density. Similar curves are obtained at other frequencies and pressures. All these curves are characterized by a sharp rise in oscillation amplitude as the oscillator voltage increases to the resonance value and a slow reduction as the voltage is increased beyond this point. The nature of the oscillation spectrum can not be determined from the shapes of these curves because the plasma density is not a linear function of oscillator voltage.

A direct examination of the radio-frequency spectrum of the beam oscillations is made by measuring $V_{\sim}$ at the cavity output as the cavity is tuned to different frequencies with the plasma density held constant. Such a line trace is shown in Fig. 5; this figure refers to a generator voltage $V_a = 1000$ v and a pressure $p = 9 \times 10^{-2}$ mm Hg.

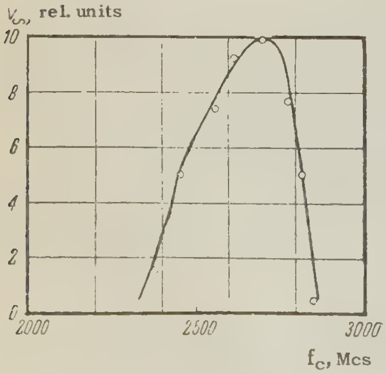

FIG. 5. The oscillation spectrum at a fixed plasma density ($p = 9 \times 10^{-2}$ mm Hg, $V_a = 1000$ v).

These parameters correspond to a plasma density $n = 7 \times 10^{10}$. There is no change in the nature of this spectrum at other plasma densities. Thus, direct measurement of the oscillation spectrum shows broadening at frequencies below the resonance frequency ω_0. The half width of the spectrum is approximately 250 Mcs on the low-frequency side and approximately 100 Mcs on the high-frequency side. This pattern is in qualitative agreement with the frequency dependence of the gain factor γ and the excitation factor ϵ. In the present experiments $v_0 \gg s$; hence, in accordance with Eqs. (5) and (6), γ and ϵ are real for $\omega > \omega_0$ and there is no amplification or excitation. When $\omega < \omega_0$, however, oscillations can be excited.

Inasmuch as γ and ϵ exhibit the same dependence on frequency, when $\omega \neq \omega_0$ this dependence cannot serve as a criterion to determine whether we are dealing with amplification or with self-excited oscillations due to an additional feedback mechanism.

The width of the experimental resonance curve is 350 Mcs. The half-width of the resonance curve for excitation of a cold plasma is given by Eq. (9). With a beam density of 10^8 or 10^9 electrons/cm^3 the half width can vary from 1000 to 1400 Mcs. Since $\gamma \rightarrow \infty$ if damping is neglected for amplification in a cold plasma at $\omega = \omega_0$, the notion of a half-width is not meaningful. The half-width for the gain factor as determined from Eq. (2) applies for a plasma at a finite temperature; in the present case $v_0/s \approx 10^3 - 10^4$ is extremely small. The half width observed in the present experiment cannot be explained by damping due to collective interactions (because in the present case $\eta_{\text{coll}} \approx \exp\{-(v_0/s)^2\} \ll 1$). Hence, if one assumes that the system is amplifying, then to explain the observed dependence of signal amplitude on frequency (Fig. 5) it must be assumed that the damping is due to pair collisions or collisions with the walls.

If we assume that oscillations are actually being excited by a feedback mechanism, the discrepancy between the experimental data and theory may be explained by the change in the density of the beam as it moves through the plasma. In order to compare the frequencies of the oscillations excited by the beam with the "natural" plasma frequencies, we have measured the plasma density by means of a radio-frequency double-probe method.[20] The results of these measurements are shown in Fig. 6. Curve 1 shows the density measured by the radio-frequency double-probe method while curve 2 shows the density determined from the frequency of the oscillations excited by passage of the beam through the plasma.

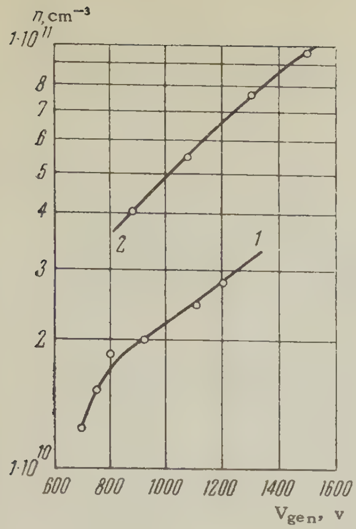

FIG. 6. Curves showing the dependence of plasma density on oscillator voltage ($p = 5 \times 10^{-2}$ mm Hg).

The discrepancy between those results may be due to the fact that the density is a maximum at the axis of the discharge tube while the radio-frequency double-probe method gives a value which represents an average over a diameter. The increase in plasma density due to the beam is insignificant since the beam density is 10^9 electrons/cm^3.

According to theory, when $v_0 \gg s$, excitation should be strongest near ω_0. In the present case the displacement with respect to the Langmuir frequency should be

$$\Delta\omega = 2^{-4/3}(\omega_0\Omega^2)^{1/3} \approx 10^9 \text{ cps}$$

This relation also applies for a cold plasma.

The frequency of maximum amplification in the cold plasma corresponds to $\omega = \omega_0$ (if collisions are neglected).

In Fig. 5, $\Delta\omega = 3 \times 10^9$ and the frequency corresponding to maximum excitation is higher than the Langmuir frequency indicated by the radio-frequency double-probe method rather than lower, as is indicated by the theory.

By comparing the oscillation amplitude in the cavity when it is excited by the beam and the amplitude when it is excited by a radio-frequency pulse generator of known power we have been able to estimate the power level of the oscillations in the cavity. This power level is several watts. It may be noted, however, that the amplitude of the oscillations excited in the beam when it passes through the plasma are comparable with the amplitude of oscillations which are excited when the beam is modulated by voltages up to 10 kv, indicating that the power in the beam is considerably higher; because of the poor beam-cavity coupling, however, only a small part of the true power is coupled out. The existence of coherent losses indicates a rather high field intensity in the plasma.

In a short tube (no oscillation) the energy loss of an unmodulated beam in a plasma is very small. We have not been able to observe this loss experimentally. If the tube length is increased, however, oscillations are excited and these are accompanied by losses. The measurements carried out in the tube 200 mm in length indicate that each electron loses 40 ev/cm at a plasma density of 2×10^{10} electrons/cm^3. A loss of this magnitude can be due only to a coherent interaction. The beam excites oscillations and the resulting field modulates the beam; eventually electron bunches of dimensions smaller than half a plasma wavelength are formed with a separation which represents a multiple of the plasma wavelength. This mechanism, as has been indicated above, leads to a strong interaction between the beam and plasma. According to theory[21] [Eq. (1)] coherent losses of this kind for a bunch consisting of 10^9 particles at plasma densities from 10^{10} to 10^{11} may amount to 10 or 100 ev/cm respectively. In measurements of the coherent energy losses in a modulated beam with different interaction lengths (10 and 20 cm) it has been found that the specific energy loss remains approximately equal to 80 ev/cm. The higher energy loss for bunches which are preformed (before entrance into the plasma) is due to a higher degree of coherence.

Experiments have also been carried out in which plasma oscillations are excited by bunching a beam with an external radio-frequency field at a frequency close to the natural plasma frequency (cf. reference 22). Bunching is accomplished by means of a cavity which is located at the point at which the beam leaves the electron gun (not shown in the diagram). The construction of this cavity is similar to that of the measurement cavity; the bunching cavity is driven by a pulsed magnetron.

The curves showing the amplification of the radio-frequency component in the beam as a function of plasma density are similar to the curve in Fig. 4 and the corresponding curve in reference 19. As has already been indicated, it is impossible to produce oscillations in an unmodulated beam with an interaction length of 10 cm. It would appear that this interaction length is too small and that the initial fluctuations in the beam and plasma are also small and cannot be observed experimentally, even when amplified. A prebunched beam provides a significant increase in the initial signal so that the amplification effect can be observed.

The data which have been obtained still do not furnish an answer to the question of whether we are dealing here with absolute or convective instability. In order to answer this question it will be necessary to measure the amplitude of the signal at different points along the plasma. It should be noted that in the present case we may be dealing with self-excitation due to a feedback mechanism. The plasma is bounded in the beam direction and its length is of the order of a perturbation wavelength.[23] Under these conditions, because of "feedback" due to reflection, an amplification process would lead to oscillations of this kind.

The excitation of plasma oscillations by an unmodulated beam is of great interest; interactions of precisely this type are undoubtedly instrumental in the excitation of plasma oscillations in various kinds of gas discharges in which "runaway" electrons appear.[24,25] This interaction is apparently responsible for the effective exchange of energy between the ordered motion of the charged particles and the rest of the plasma.

The experimental production of oscillations in an unmodulated beam passing through a plasma can be used directly for studying plasma parameters (electron density and ion temperature), for producing radio waves in the millimeter region, and for acceleration of particles in a plasma.[26]

In conclusion, we wish to thank K. D. Sinel'nikov and A. I. Akhiezer for discussion of the results of this work.

---

[1] F. Penning, Physica **6**, 241 (1926).

[2] I. Langmuir and L. Tonks, Phys. Rev. **33**, 195 (1929).

[3] I. Langmuir, Phys. Rev. **26**, 585 (1925).

[4] H. Merrill and H. Webb, Phys. Rev. **55**, 1191 (1939).

[5] G. Wehner, J. Appl. Phys. **21**, 62 (1950).

[6] A. A. Vlasov, J. Phys. (U.S.S.R.) **9**, 25 (1945).

[7] D. Bohm and E. Gross, Phys. Rev. **75**, 1851, 1864 (1949).

[8] D. Looney and S. Brown, Phys. Rev. **93**, 965 (1954).

[9] Gabor, Ashe, and Dracott, Nature **176**, 916 (1955).

[10] A. I. Akhiezer and Ya. B. Faĭnberg, JETP **21**, 1262 (1951); Dokl. Akad. Nauk SSSR **64**, 555 (1949).

[11] D. Bohm and E. Gross, Phys. Rev. **79**, 992 (1950).

[12] V. I. Veksler, Proc. CERN Symposium, 1956, Vol. 1, p. 80.

[13] B. M. Bolotovskiĭ, Dissertation, P. N. Lebedev Physics Institute, Acad. Sci. U.S.S.R. (1954).

[14] J. L. Tuck, Proceedings of 2nd International Conference on the Peaceful Uses of Atomic Energy, Geneva 1958, Report No. 1860.

[15] L. D. Landau and E. M. Lifshitz, Механика сплошных сред (Mechanics of Continuous Media) Fizmatgiz, 1953.

[16] P. Sturrock, Phys. Rev. **112**, 1488 (1958).

[17] E. Drummond and D. B. Chang, Bull. Am. Phys. Soc. **6**, 411 (1958).

[18] Kurilko, Shapiro, and Faĭnberg, Report, Phys.-Tech. Inst., Acad. Sci. Uk. S.S.R. 1959.

[19] Boyd, Field, and Gould, Phys. Rev. **109**, 1393 (1958).

[20] T. H. I. Leang and I. Sayers, Proc. Phys. Soc. **70**, 669 (1957).

[21] A. I. Akhiezer and Ya. B. Faĭnberg, Report, Phys.-Tech. Inst., Acad. Sci. Uk. S.S.R.

[22] K. D. Sinel'nikov, Proceedings of 2nd International Conference on Peaceful Uses of Atomic Energy, Geneva 1958, Report No. 2211.

[23] M. Sumi, Phys. Rev. Letters **2**, 2, 37 (1959).

[24] Bernstein, Chen, Heald, and Kranz, Proceedings of the 2nd International Conference on the Peaceful Uses of Atomic Energy, Geneva 1958, Report No. 358.

[25] H. Dreicer, ibid., Report No. 2292.

[26] Ya. Faĭnberg, CERN Symposium 1956, Vol. 1, p. 84.

Translated by H. Lashinsky
139

SOVIET PHYSICS JETP VOLUME 11, NUMBER 3 SEPTEMBER, 1960

THE INELASTIC SCATTERING OF PROTONS AND DEUTERONS FROM Mg^{24}

O. F. NEMETS and G. A. PROKOPETS

Physics Institute, Academy of Sciences, Ukrainian S.S.R.

Submitted to JETP editor August 22, 1959

J. Exptl. Theoret. Phys. (U.S.S.R.) **38**, 693-696 (March, 1960)

We have studied the angular distributions of protons and deuterons scattered inelastically from the excited 2^+ state of Mg^{24} lying at 1.37 Mev. The energy of the protons was 6.8 Mev while that of the deuterons was 13.6 Mev; the range of angles covered was 2.5 – 140°. We observed some previously unknown details in the angular distribution at small angles. A comparison with theories of inelastic scattering leads to inferences about the relative importance of direct interactions.

INTRODUCTION

THE angular distributions observed in nuclear reactions and in inelastic scattering are an important source of information about the properties of nuclei and the mechanisms involved. Direct interactions become significant even at moderate energies. This is especially true of the deuteron, which has a small binding energy so that often only one nucleon takes part in the reaction.[1,2] Direct interactions can also occur in which the deuteron behaves like one unit.[3-6]

Inelastic scattering need not occur through direct interactions but can also be associated with the formation of a compound nucleus. This is important mostly for protons.[7]

Measurements have shown that in the interaction between protons and Mg^{24} in the energy range 7.3 – 18 Mev, inelastic scattering can occur both through a direct interaction and also through the formation of a compound nucleus (these results are generalized in references 8 and 9; see also reference 10).

On the other hand, from measurements on the inelastic scattering of deuterons at 7.5 Mev,[11] 8.9 Mev,[12] and 15 Mev,[13] it appears that the most important mechanism is a direct interaction. Haffner[13] has noted that at small angles the electric interaction between the deuteron and the nucleus is also significant.[6]

Although the angular distribution at small angles is very interesting, since it can give important information about the mechanism involved in inelastic scattering, most of the authors referred to above have not examined the small angle region in detail. It is for this reason that we have attempted to examine the angular distribution in detail, particularly at small angles.

EXPERIMENTAL METHOD

The measurements were made on the external beam of the cyclotron at the Physics Institute of the Academy of Sciences of the Ukrainian SSR. Our spectrometer was an ionization chamber with split electrodes which allowed us to detect particles selectively.[14]

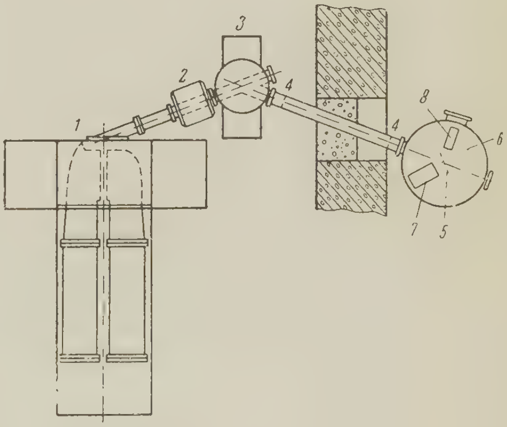

FIG. 1. Schematic diagram of the experimental setup.

The geometry of the experiment is shown in Fig. 1. The beam from the cyclotron, 1, is focused by quadrupole lenses, 2, bent by a deflecting magnet 3, collimated by diaphragms at 4, and is then incident on the target 5, which is at the center of the scattering chamber 6. The spectrometer 7 was placed at angles from 2.5° to 140° relative to the incident deuteron beam. Measurements were made at intervals of 2.5° at small angles and at intervals of 5° at larger angles. A scintillation counter at 8 served to monitor the beam and was place at 90° to it.

The statistical errors in the relative cross sections were about 15% at large angles and 25% at small ones. At angles less than 12.5° for deuterons and 15° for protons, the results are only qualitative because of the background arising from protons and deuterons which have first been inelastically scattered from the gas in the chamber and the 17 mg/cm^2 copper window, then elastically scattered in the target.

The target was a self-supporting magnesium foil which was 1.4 mg/cm^2 thick and was obtained by evaporation in a vacuum.

DISCUSSION OF THE RESULTS

Curve 1 in Fig. 2 shows the angular distribution we obtained for inelastically scattered deuterons, while curve 4 shows the result obtained in reference 13. In order to make the diagram clearer, the experimental results have not been normalized in the same way. Curve 2 shows the angular distribution calculated by Huby and Newns,[2] assuming a direct interaction, while curve 3 shows the calculations of Mullin and Guth.[6] According to the theory of Mamasakhlisov and Kopaleĭshvili,[3] the peak at 20° is related to collective behavior of Mg^{24}.

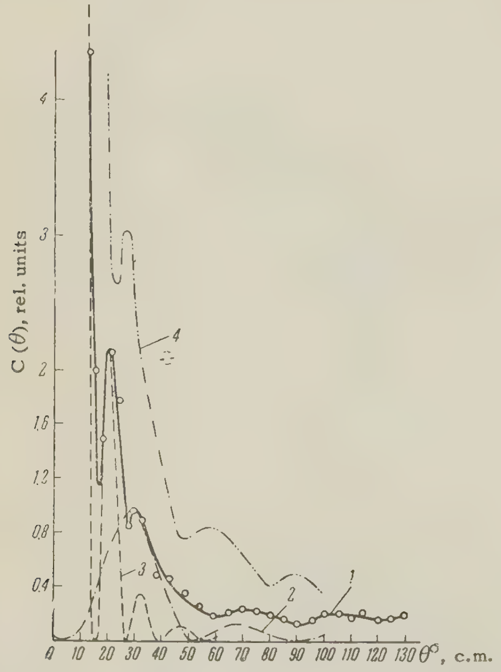

FIG. 2. Angular distribution of inelastically scattered deuterons Mg(dd′)Mg* (Q = −1.37 Mev); 1 – our data; 2 – theoretical curve for a nuclear interaction with $l = 2$ and $a = 6.3 \times 10^{-13}$ cm; 3 – theoretical curve for electrical interaction with $l = 2$, $a = 15.8 \times 10^{-13}$ cm; 4 – data from reference 13.

Best agreement between theory and experiment is obtained by taking an interaction radius $a = 6.3 \times 10^{-13}$ cm in the first case and $a = 15.8 \times 10^{-13}$ cm in the second case; at a radius of $a = 7 \times 10^{-13}$ cm, the peak in the theory of reference 2 occurs at 20°, as does the experimentally observed one. The angular momentum in both cases is 2; the experimental points for angles in the range 2.5 – 10° are not shown. At these angles the cross section rises with decreasing angle. Upon comparing the experimental results with the predictions of theory, one can conclude that direct interaction is the predominant mechanism in the inelastic scattering of deuterons at 13.6 Mev from the 1.37 Mev excited state of Mg^{24}. The electrical interaction is predominant at small angles.

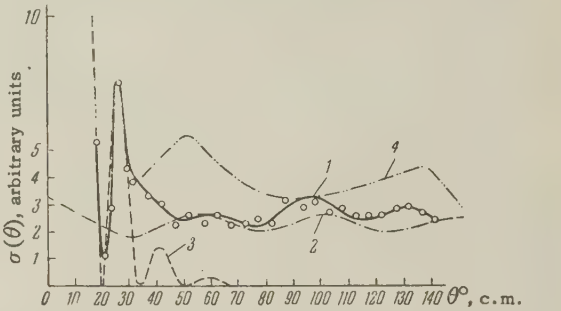

FIG. 3. Angular distribution of protons from the reaction Mg(pp′)Mg* (Q = −1.37 Mev). Curve 1 – our data; curve 2 – theoretical curve for direct interaction on the surface, $2.2 P_0 + P_7$; 3 – theoretical curve for surface electrical interaction ($l = 2$, $a = 24.7 \times 10^{-13}$ cm); 4 – data from reference 8.

Figure 3 shows the angular distribution obtained for protons (curve 1). Curve 2 shows the results of calculations made by Yoshida[4] on the basis of a direct surface interaction.

The theoretical curve 2 is $2.2 P_0 + P_7$, where the $P_n(\cos\theta)$ are Legendre polynomials; the term in P_7 must be included to get agreement with experiment. From this we may conclude that at middle and large angles most of the scattering occurs through the formation of a compound nucleus. At small angles some other mechanism must be important.

For small angles, the experimental results are difficult to reconcile with the theory of direct nuclear interaction proposed by Austern, Butler, and McManus:[15] the interaction radius R must be chosen anomalously large to give the right position for the minimum, and even then the function $j_2(KR)$ does not rise fast enough after passing through its minimum [$j_2(x)$ is the spherical Bessel function of order 2, $K = |\mathbf{K}_1 - \mathbf{K}_2|$ where $\mathbf{K}_1$ is the wave vector of the incident proton while $\mathbf{K}_2$ is the wave vector of the scattered one]. The agreement with the theory of electrical interaction[6] is somewhat better, as is indicated by curve 3 in Fig. 3, but here also an anomalously large interaction radius ($R = 24.7 \times 10^{-13}$ cm) is required if the function $[j_1(KR)/KR]^2$ is to fit the data at all well [$j_1(x)$ is the spherical Bessel function of order 1]. Such a large value of R can hardly be right.

Curve 4 in Fig. 3 represents the results of reference 8 for an energy 7.86 Mev.

In conclusion the authors would like to express their gratitude to Prof. M. V. Pasechnik for his constant interest, to Yu. A. Bin'kovskiĭ for preparing the targets, and to the personnel of the cyclotron laboratory.

---

[1] S. T. Butler, Proc. Roy. Soc. (London) **A208**, 559 (1951).

[2] R. Huby and H. C. Newns, Phil. Mag. **42**, 1442 (1951).

[3] V. I. Mamasakhlisov and T. I. Kopaleĭshvili, JETP **34**, 1169 (1958), Soviet Phys. JETP **7**, 809 (1958).

[4] S. Yoshida, Proc. Phys. Soc. (London) **A69**. 668 (1956).

[5] M. El' Nadi, JETP **34**, 1207 (1958), Soviet Phys. JETP 7, 834 (1958).

[6] C. J. Mullin and E. Guth, Phys. Rev. **82**, 141 (1951).

[7] M. M. Shapiro, Phys. Rev. **90**, 171 (1953).

[8] Greenlees, Haywood, Kuo, and Petravic, Proc. Phys. Soc. (London) **A70**, 331 (1957).

[9] P. C. Gugelot and P. R. Phillips, Phys. Rev. **101**, 1614 (1956).

[10] H. E. Conzett, Phys. Rev. **105**, 1324 (1957).

[11] J. R. Holt and C. T. Young, Nature **164**, 1000 (1949).

[12] Hinds, Middleton, and Parry, Proc. Phys. Soc. (London) **A70**, 900 (1957).

[13] J. W. Haffner, Phys. Rev. **103**, 1398 (1956).

[14] O. F. Nemets, Труды сессии АН УССР по мирному использованию атомной энергии (Proceedings of the Session of the Ukr. S.S.R. Academy of Sciences on the Peaceful Uses of Atomic Energy) Kiev, 1958, p. 145.

[15] Austern, Butler, and McManus, Phys. Rev. **92**, 350 (1953).

Translated by R. Krotkov
140

SOVIET PHYSICS JETP VOLUME 11, NUMBER 3 SEPTEMBER, 1960

ANOMALOUS DECAYS OF HYPERFRAGMENTS

S. A. AZIMOV, U. G. GULYAMOV, R. KARIMOVA, and B. G. RAKHIMBAEV

Physico-technical Institute, Academy of Sciences, Uzbek S.S.R.

Submitted to JETP editor August 24, 1959

J. Exptl. Theoret. Phys. (U.S.S.R.) **38**, 697-702 (March, 1960)

Two events of K-meson decay of hyperfragments are described. They are compared with previously described hyperfragment-decay events and some common features are noted. It is shown that the events cannot be explained by statistical deviations of the characteristics of the particle tracks in the emulsion.

SEVERAL events of hyperfragment decay have been recently described, in which a particle is emitted from the point of decay, with a mass equal to the K-meson mass[1-5] within the limits of measurement error. There are also known events of decay of hyperfragments with anomalously large values of liberated energy, which cannot be attributed to the decay of the bound Λ^0 particle.[6,7]

As a result of a systematic scanning of two emulsion chambers, one exposed to cosmic rays in the stratosphere and the other to pions of energy on the order of 4.5×10^9 ev, the authors have observed three events in which a particle with mass close to the K-meson mass was emitted from the stopping point of the heavy fragment. One of these cases was described earlier,[4] and the two others are described here.

The cases described were observed in an emulsion chamber, made up of layers of G-5 emulsion, exposed to pions of energy 4.5×10^9 ev, among 60,000 stars with $N_h \geq 8$. In both cases these particles stopped in the emulsion without any visible phenomena at the end of the track. We give here detailed descriptions of these cases.

Case 1. (Microphotograph shown in Fig. 1). Primary star of type $18 + 2\pi$. Particle F, emitted from this star, decays after a range of $101\,\mu$ in emulsion with emission of two charged particles 1 and 2. The dip of F in the unprocessed emulsion amounts to $5°20' \pm 30'$. Measurements of the width along the track of F have disclosed a tapering zone 65 to $76\,\mu$ long. According to references 8 and 9, the charge of the particle has been found to be $(8 \pm 2)e$, where e is the electron charge. The average width of the track in the portion where there is no tapering, equal to $(1.065 \pm 0.054)\,\mu$, does not contradict this result.

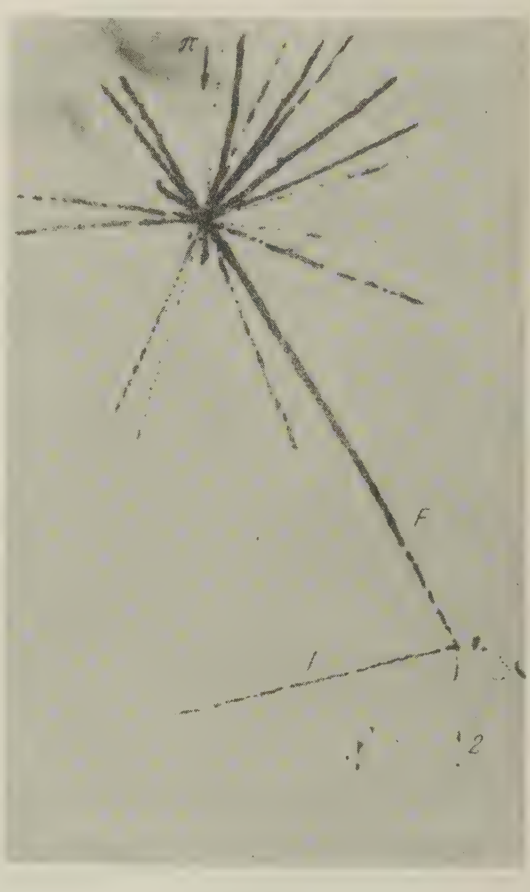

FIG. 1

The tracks of particles 1 and 2 terminate in the emulsion with ranges of (61 ± 0.4) and $(9362 \pm 122)\,\mu$, respectively. The angle between the tracks of particles 1 and 2 is $83°50' \pm 1°20'$.

A comparison of the width of track 1 with the widths of the tracks of an α particle, a lithium nucleus, and a proton, taken in the same plate and having approximately the same inclination, shows that the charge of particle 1 is equal to 2. If we consider track 1 to belong to an α particle, its energy and momentum are respectively (11.1 ± 0.1) Mev and (250 ± 1) Mev/c.

The mass of particle 2 was determined by two methods: by the range-scattering method and by the range-ionization method. The angle of multiple scattering was measured both by the method of constant cells, and by the method of constant inclinations.[10] The measurements were carried out by three observers and gave compatible results. The measurements with doubled intervals indicate the absence of a noticeable influence of noise on the result of the measurements. The width of the distribution curve of the second differences agrees well with the quantity predicted by the multiple-scattering theory.

The ionization was determined by comparing the density of the gaps in track 2 with the density of gaps in the tracks of the proton and pion, taken in the same plate.[11] The values of the mass of particle 2, obtained by these methods, coincide with each other and are equal to $M(J, R) = (856 \pm 167)\, m_e$ and $M(\langle\alpha\rangle, R) = (990 \pm 120)\, m_e$, respectively.

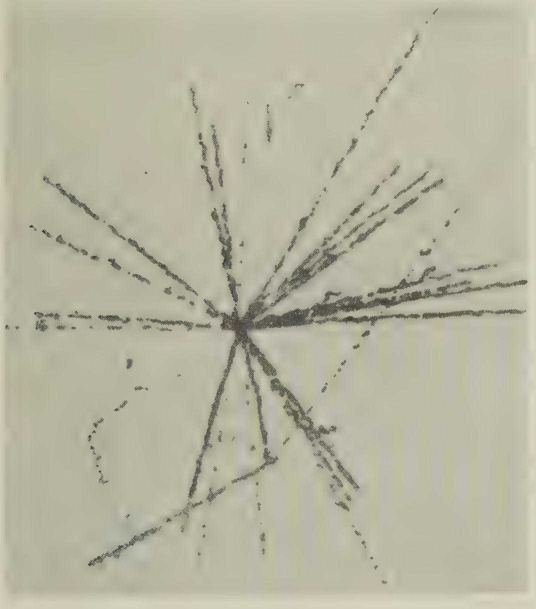

FIG. 2

Considering particle 2 to be a K meson, its energy and momentum were found to be respectively (38.3 ± 0.3) Mev and (197.6 ± 1.4) Mev/c. The minimum total momentum of particles 1 and 2 was found to be (307 ± 1.4) Mev/c. Assuming this momentum to be carried away by the residual nucleus, a track of this nucleus should be seen in the direction opposite to the direction of the total momentum of particles 1 and 2; this, however, was not observed. Starting with this fact, the most probable of all the decay schemes considered for particle F are found to be the following

$$^{*}C_6^{14} \rightarrow He_2^3 + K^- + n + B_5^{10}; \quad ^{*}O_8^{18} \rightarrow He_2^3 + K^- + n + N_7^{14}.$$

In all other schemes considered, either emission of neutrons is impossible, or the residual nucleus is found to be radioactive.

Case 2. Primary star of type 19 + 3π. Emitted from the primary star is the particle F, which decays after a range of 28 μ with emission of two charged particles 1 and 2 (Fig. 2).

The track of the particle F is inclined to the plane of the emulsion by 4° 40′ ± 1°. The track has two gaps 0.3 and 0.7 μ long. At the end of the range the track is strongly scattered. The width of the track of F is equal to the width of the tracks of singly-charged particles and is substantially less than the width of the tracks of particles with charge more than 1 (α particle and lithium nucleus). The tracks of particles 1 and 2 terminate in emulsion after ranges of (465 ± 8) and (13,640 ± 170) μ, respectively. The spatial angle between particles 1 and 2 is 141° ± 1° 30′.

The track of particle 1 was identified, by the density of gaps and by its width, as belonging to a particle of charge 2. The mass of particle 2 was determined from measurements of the average angle of multiple scattering, ionization, and range. Particular attention was paid to the reliability of measurements. The measurements were carried out by several observers, whose results coincided within the limits of errors.

The scattering was measured both by the method of constant cells, and by the method of constant inclinations. The effect of noise on the measurement results was first ascertained and was found to be negligibly small. The width of the distribution curve of the moduli of the second differences was within the limits of the predictions of the theory of multiple scattering. The ionization was determined by counting the grains and measuring the gap densities. In the second case a comparison was made of the corresponding quantity for track 2 and for control pions.

As a result of the measurement, the following values of the mass of particle 2 were obtained:

$M(J, \langle\bar{\alpha}\rangle) = (801 \pm 143)\, m_e$ —grain count;
$M(J, R) = (1170 \pm 120)\, m_e$ — gap density;
$M(\langle\bar{\alpha}\rangle, R) = (986 \pm 132)\, m_e$ —method of constant inclinations (c.i.)
$M(\langle\bar{\alpha}\rangle, R) = (764 \pm 170)\, m_e$ —method of constant cell.

From a comparison of the charges of particle F and of particle 1 it follows that $A_F = 3$ or 4, while $A_1 = 3$ or 4, where A_F and A_1 are the mass numbers of particles F and 1. The presence of the considerable residual momentum in particles 1 and 2, however, shows that this momentum should be compensated for by some neutral particle, emitted from the secondary star. It follows, therefore, that the only possible value of the mass numbers of particles F and 1 are $A_F = 4$ and $A_1 = 3$. Then the total momentum of particles 1 and 2 will be (294 ± 4.5) Mev/c, and the decay scheme of the particle will be

$$^{*}\mathrm{H}_1^4 \rightarrow \mathrm{He}_2^3 + K^- + n + Q.$$

The total energy liberated, considering the neutral particle to be a neutron, will be (110.4 ± 1.6) Mev (without allowance for the mass of the K meson proper).

Together with the decays described above, there are literature data on seven cases of K-meson decays of hyperfragments. In six of these cases the particle identified as the K meson stops in the emulsion, and in none of these cases is the stopping of this particlee accompanied by phenomena characteristic of the stopping of K mesons. It follows therefore that these particles are not K mesons and, like the muon, become absorbed in the nucleus without giving a visible disintegration. In case 4, however,[2] the particle identified as a K meson is absorbed in flight, indicating that this particle interacts strongly with the nucleus, although in this case no visible disintegration is observed. The identification of these particles is based only on the analysis of the characteristics of the particle tracks in the emulsion, and in all cases the masses determined on the basis of different characteristics of the track (the ionization-range, scattering-range, and scattering-ionization methods) agree with each other.

The most trivial explanation of these cases could be one in which all these particles are protons, but as a result of statistical deviations of the characteristics of their tracks in the emulsion, the mass measured is found to be close to that of the K meson, although under this assumption one cannot explain cases with anomalously large liberated energy (~ 500 Mev). This can occur when a correlation exists between the deviations of the different characteristics of the proton track, causing the proton masses, measured on the basis of any track characteristic, to be shifted to one side. If the foregoing assumption is correct, the probabilities of appearance of the discussed number of such events among the approximately 300 known* "normal" cases of mesonless decay of hyperfragments correspond to the number of observed cases.

To verify the foregoing assumption concerning the connection of the deviations of the track characteristics of the particle in the emulsion, we measured the masses of 140 known protons. The protons were taken from σ stars, produced by negative pions, which were identified visually. We choose only σ-star tracks with a residual range not less than 2500 μ and a dip angle to the plane of emulsion not more than 10 — 15°. In each individual case the mass of the particle was measured simultaneously by two methods: by the range-scattering method and by the range-ionization method. The average angle of multiple scattering was determined by the c.i. method with a cell for the proton;[10] the ionization was estimated from measurements of the density of the gaps of the measured track and by comparison of the density of the gaps of control pions, which were identified by the π-μ-e decay.[11]

Among the 140 investigated particles, there was not a single case where the statistical deviations caused the measured mass to be close to the mass of the K meson in either method of mass measurement.

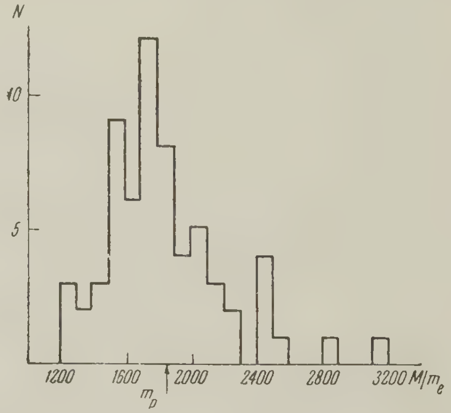

FIG. 3. Distribution of the masses of particles measured by the [$<\bar{\alpha}>$, R] method, for particles, the mass of which as given by the [g, R] method is greater than the proton mass.

To clarify the existence of a correlation between the deviations of the values of the measured mass from the proton mass in these two methods of measurements, we have compared the distribution of the masses measured by the scattering-range method, for particles whose mass, measured by the range-ionization method was greater (Fig. 3) or else smaller (Fig. 4) than the proton mass. The satisfactory agreement of these distributions indicates that there is no correlation between the deviations of the multiple scattering and the ionization.

The probability of random coincidence between the values of the proton mass and the mass of the K meson with accuracy of 400 m_e in the two meas-

---

*The number of known "normal" mesonless decays with emission of a fast proton does not amount to even half this number.

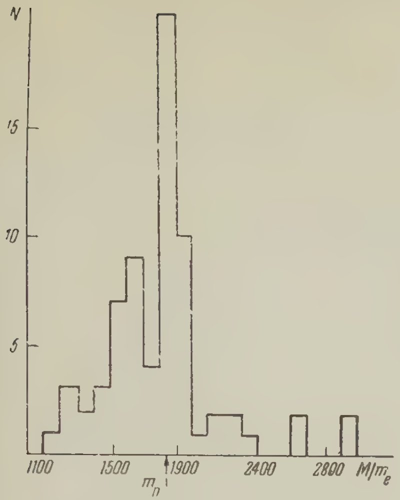

FIG. 4. Distribution of the masses of particles, measured by the [<$\bar{\alpha}$>, R] method, for particles whose mass is less than the proton mass when measured by the [g, R] method.

urement methods amounts according to our data to less than 0.5%, i.e., such a coincidence cannot explain more than one of the discussed cases. These data show that it is very unlikely that statistical deviations of the track characteristics can explain these cases.

A summary of the data on K-meson decays of hyperfragments is listed in the table. An analysis of the secondary stars shows certain singularities, which are common to all cases. With the exception of case 4 (reference 2), in all the other cases of K-meson decay of hyperfragments, the kinetic energies of the particles, identified as K mesons, are quite close to each other.

In all the cases discussed, the summary momentum of the charged particles is not equal to zero under any assumptions concerning the nature of the secondary particles, which is evidence that in these cases some neutral particles are emitted. In all cases where the unbalanced momentum can be estimated, the values of these momenta are close to each other. It follows, therefore, that in these cases we deal, perhaps, with a two-particle decay of some charged particle.

It follows, therefore, from the foregoing analysis of the anomalous cases of hyperfragment decay, that the particle emitted from the point of decay of the fragments has a mass on the order of 1000 m_e and its properties differ from those of K mesons.

Number of events	Literature reference	Mass of particle in m_e and method of determination of mass	Particle energy, Mev	Unbalanced momentum, Mev/c
1	Present work	[856±167]; [J, R] [990±120]; [⟨$\bar{\alpha}$⟩, R]	38.3±0.3	307±1.4 or 335±2
2	Present work	[801±143]; [J, ⟨$\bar{\alpha}$⟩] [1170±120]; [J, R] [986±132]; [⟨$\bar{\alpha}$⟩, R] [764±170]; c.i. method	48.1±0.2	294.5±4.5
3	[1]	[1103±190]; [R, J] [759±239]; [⟨$\bar{\alpha}$⟩, R] [1092±170]; [J, ⟨$\bar{\alpha}$⟩] [1170±200]; c.i. method	43.8	not less than 200
4	[2]	[1160±180]; [J, ΔR]π $\left[80^{+400}_{-180}\right]$; [g, ΔR]π $\left[950^{+330}_{-120}\right]$;]$J$, ΔR]p	65±5	
5	[3]	[850±300]; [J, R] [1200±320]; [⟨$\bar{\alpha}$⟩, R]	50.0	
6	[4]	$\left[725^{+170}_{-140}\right]$; [$J$, ⟨$\bar{\alpha}$⟩] [700± 85]; [1380±150];	46±4	337±21 or 463±25
7	[5]	[1005±200]; [⟨$\bar{\alpha}$⟩, R] [1024±150]; [$\bar{J}$, R]	42.0	207.0

In conclusion, the authors consider it their pleasant duty to thank M. I. Podgoretskiĭ for continuous interest and for useful advice in the performance of this work.

---

[1] Fry, Schneps, and Swami, Phys. Rev. 97, 1189 (1955).

[2] Varfolomeev, Gerasimova, and Karpova, Dokl. Akad. Nauk SSSR **110**, 959 (1956), Soviet Phys. "Doklady" **1**, 594 (1957).

[3] Toporkova, Fisenko, and Grigor'ev, Некоторые вопросы инженерной физики (Some Problems of Engineering Physics) No. 3, (1958).

[4] B. P. Bannik et al., JETP **34**, 286 (1958), Soviet Phys. JETP **7**, 198 (1958).

[5] Fry, Schneps, and Swami, Nuovo cimento **2**, 346 (1955).

[6] Costagnoli, Cortini, and Franzinetti, Nuovo cimento **2**, 550 (1955).

[7] W. F. Fry and M. S. Swami, Phys. Rev. **96**, 809 (1954).

[8] D. V. Viktorov and M. Z. Maksimov, JETP **32**, 135 (1957), Soviet Phys. JETP **5**, 42 (1957).

[9] Frier, Lofgren, Oppenheimer, and Ney, Phys. Rev. **74**, 1818 (1948).

[10] B. Judek, Nuovo cimento **5**, 886 (1957).

[11] D. M. Ritson, Phys. Rev. **91**, 1572 (1953).

Translated by J. G. Adashko
141

SOVIET PHYSICS JETP VOLUME 11, NUMBER 3 SEPTEMBER, 1960

EXPERIMENTAL INVESTIGATION OF THE ENERGY SPECTRUM OF THE PENETRATING COMPONENT OF EXTENSIVE AIR SHOWERS

É. L. ANDRONIKASHVILI and R. E. KAZAROV

Physics Institute, Academy of Sciences, Georgian S.S.R.

Submitted to JETP editor, September 4, 1959

J. Exptl. Theoret. Phys. (U.S.S.R.) **38**, 703-707 (March, 1960)

The energy spectrum of the μ-meson component of extensive air showers was measured in the range from 0.4 to 37 Bev. The investigations were carried out for three groups of showers with mean number of particles equal to 1.4×10^4, 7×10^4, and 2.9×10^5. The energy spectrum has been plotted for the three shower groups at a mean distance of ~ 28 m from the axis. The energy spectrum of the shower as a whole has also been determined. For all three shower groups, the power exponent of this spectrum is approximately equal to one.

AN investigation of the energy spectrum of the penetrating component of extensive air showers (EAS) was carried out by measuring the absorption of μ mesons in EAS at various depths underground. The measurements were carried out in several mines situated at an altitude of 400 m above sea level in various parts of the city of Tbilisi. Because of the need of transporting the array from place to place, the geometry of the setup that was used was not optimal from the point of view of statistics and of the accuracy of shower size determination and axis location. However, the setup corresponded to the best that could be attained under the conditions prevailing at each place.

The block diagram of the array is shown in Fig. 1. Triple coincidences between closely placed groups of Geiger-Müller counters, shown in Fig. 1 by the small circles, were used for the selection of EAS. The area of each group amounted to ~ 0.0257 m^2. The counters were placed in the vertices of a right-angle triangle, for which the radius of the circumscribing circle was equal to 1 m. These counter groups triggered four trays of hodoscope counters I — IV. The distance between the groups I, II and I, III was equal to ~ 10 m, while that between the groups I and IV was ~ 20 m. In each group of the hodoscope counters, counters of three different dimensions were used with a total sensitive area of 0.3 m^2. This ensured measurement of the density of the soft component in the range from 2 to 400 particles/m^2 with an average accuracy of ±40%.

The underground part of the array consisted of two Geiger-Müller counter trays. All the Geiger counters in each tray were connected in parallel. The total area of the tray amounted to ~ 1 m^2. The trays were placed one above the other and connected to a double-coincidence circuit. A lead absorber 8 cm thick was placed between the trays, and prevented the detection by the array of accidental background coincidences. The signals from the underground detector, as can be seen from Fig. 1, were fed to the circuit which selected their coincidences with the master pulse.

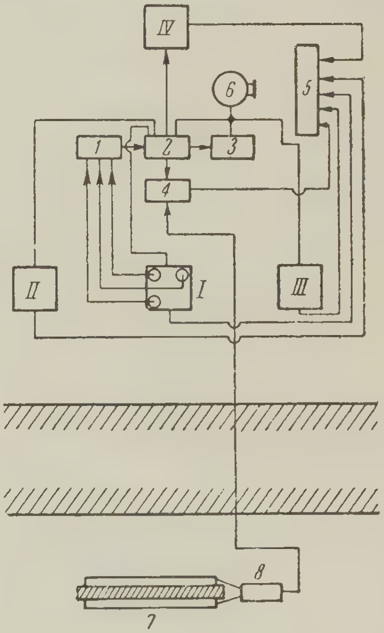

FIG. 1. Block diagram of the array: I, II, III, and IV — hodoscope trays, o — counters of the selection system, 1 — triple coincidence circuit, 2 — master-pulse shaping circuit, 3 — camera control circuit, 4 — master-pulse underground detector coincidence circuit, 5 — neon lamp panel, 6 — cine camera, 7 — underground counter trays, 8 — double coincidence circuit.

The master pulse, formed as the result of triple coincidences of the selection-system count-

Depth, m w.e.	$\overline{N}\cdot 10^{-4}$	n	n_μ	ρ_μ	$\sqrt{\overline{r^2}}$, m
3.2	1.4	562	59	0.44±0.06	10
	7	311	62	0.86±0.13	10
	29	222	71	1.48±0.25	10
61	1.4	257	32	0.13±0.03	13
	7	156	26	0.18±0.04	15
	29	217	82	0.48±0.08	16
127	1.4	348	19	0.058±0.014	27
	7	278	32	0.12±0.024	27
	29	302	63	0.23±0.04	27
162	1.4	1095	50	0.049±0.007	29
	7	737	60	0.086±0.012	29
	29	658	91	0.148±0.018	29

ers, was fed also to the hodoscope and to the circuit controlling the operation of a cine-camera which recorded the panel with the neon lamps. The resolving times of the systems were as follows: selection system — 2.5×10^{-6} sec, underground double coincidences — 2.5×10^{-6} sec, and hodoscope — 4×10^{-5} sec. These resolving times were sufficient to justify neglecting chance coincidences.

In a different series of experiments, the underground group of hodoscope counters was placed at depths of 162, 127, and 61 m water equivalent (w.e.). In one series of measurements, the penetrating-particle detector was placed on the surface of the earth under a layer of lead with a thickness of 3.2 m w.e. In the latter case, the detector consisted of three trays of hodoscope counters of the type GC-60 separated by lead layers. Each tray consisted of eight counters with a total area of 0.26 m^2. This detector made it possible to distinguish between the passage of μ mesons and the tracks of the nuclear-active component, according to the following criteria: an event was considered to be a μ meson if:

a) a single counter was discharged in each of the trays, so that one could reconstruct the particle track; and

b) if two or three adjoining counters in one of the trays were discharged together with single counter discharges in the remaining trays. In such a way, the δ-ray-producing μ mesons were also taken into account.

For the chosen selection system, 90% of all EAS detected by the array fell inside a circle 50 m in radius, the center of which coincided with the center of the selection system. Under these conditions, it was possible to determine the coordinates of the point of intersection of the shower axis with the plane of observation with an average error of ±50% from the information on the density of charged shower particles at the position of the hodoscope trays, and using the Nishimura-Kamata formula for the lateral distribution.[1] From these data, the shower size was determined with an error of +100%, −30%. It should be noted that we used the analytical expression for the Nishimura-Kamata distribution given by Greisen,[2] assuming that the age parameter $s = 1.25$.

All EAS detected by the array were divided into groups of various sizes. The groups contained showers with number of particles N from 7×10^3 to 4.5×10^5. Such a choice was made because of the fact that the size of showers smaller than 7×10^3 cannot be determined using the chosen array geometry (less than three hodoscopic trays are struck), and showers with $N > 4.5 \times 10^5$ were not considered because of poor statistics. According to the accuracy of shower size determination, the division into the three groups was as follows: $7 \times 10^3 - 2.8 \times 10^4$, $2.8 \times 10^4 - 1.1 \times 10^5$, and $1.1 \times 10^5 - 4.5 \times 10^5$, which correspond to mean weighted values of shower size 1.4×10^4, 7×10^4, and 2.9×10^5 respectively.

The results obtained in different series of measurements are collected in the table which presents, among other data, the average density of penetrating particles, and the mean square distance from the axis to which this density corresponds, for each shower group. The mean density ρ_μ of the μ-meson flux was determined from the expression

$$\rho_\mu = \frac{1}{\sigma} \ln \frac{n}{n - n_\mu}, \qquad (1)$$

where σ is the area of one tray of the detector, n is the number of detected showers of a given group, and n_μ is the number of showers of the given group with μ-meson accompaniment.

In spite of the fact that, in all series of measurements, the penetrating-particle detector was placed near the vertical passing through the center of the selection system (at a distance of 0 – 10 m), it can be seen from the table that the actual distance between the axis and the detector increases with depth. If the detector is placed at a depth h, and if the point of intersection of the vertical passing through it with the surface of the earth is taken as the origin of the coordinate system, then the distance r between the detector and the shower axis at the depth h is given by the formula

$$r^2 = R^2 \sin^2 \varphi + (R \cos \varphi \cos \vartheta - h \sin \vartheta)^2, \qquad (2)$$

where R is the distance from the shower axis trace on the earth's surface to the origin of coordinates, and φ and ϑ are the azimuth and zenith angles of the axis.

In order to obtain the required root-mean-square distance $(\overline{r^2})^{1/2}$, one should assume specific statistical distributions of the quantities entering into the right-hand side of Eq. (2). For φ we shall, obviously, take a uniform distribution. The angle ϑ, according to Greisen,[2] has a distribution of the form $J_\vartheta = J_0 \cos^{8.3} \vartheta$, while the distribution of A has been calculated by us from direct hodoscope measurements. The values of $(\overline{r^2})^{1/2}$ found in such a way are given in the table.

In order to construct the energy spectrum at a given distance from the shower axis, the numbers given in the table were recalculated for one average distance of 28 m from the axis. An analysis of the data given in the table shows that, in choosing the distance of 28 m, it is necessary to recalculate the μ-meson flux density only for the depths of 61 and 3.2 m w.e., for which the lateral distribution of the μ-meson flux in EAS is sufficiently well known.[3,4]

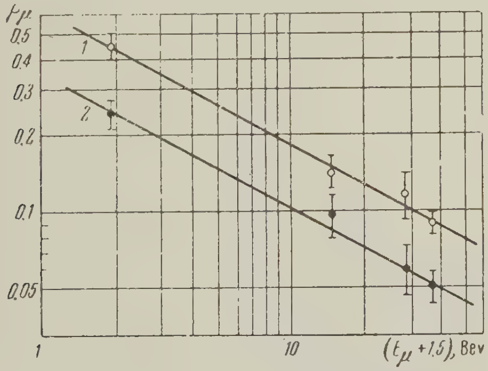

FIG. 2. Energy spectrum of the μ-meson component at a mean distance of 28 m from the axis of EAS: 1 – for $\overline{N} = 7 \times 10^4$, 2 – for $\overline{N} = 1.4 \times 10^4$. The x axis represents the energy of μ mesons increased by 1.5 Bev taking into account the average energy losses in the passage of the μ mesons through the atmosphere (corresponding to an average production height of μ mesons equal to 10 km). The y axis represents the μ-meson flux density at the distance of 28 m from the EAS axis, in terms of number of particles per m².

The shape of the energy spectrum, characteristic for the smaller of the investigated showers, is shown in Fig. 2. It can be seen that, for showers of 1.4×10^4 and 7×10^4 particles, the spectrum can be well represented by a straight line on log-log coordinates, with a slope equal to 0.54 ± 0.07. As far as larger showers, with an effective number of particles 2.9×10^5, are concerned, the spectrum is considerably steeper at greater depths, and the spectrum exponent approaches unity (see Fig. 3).

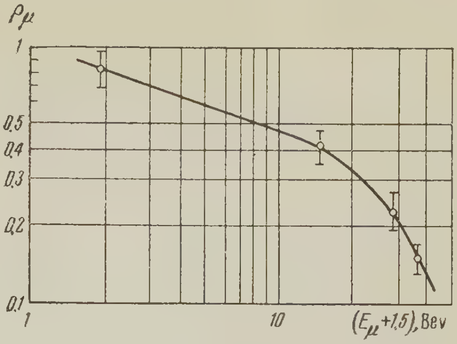

FIG. 3. Energy spectrum of the μ-meson component at an average distance of 28 m from the EAS axis for a shower with $\overline{N} = 2.9 \times 10^5$. The respective axes represent the same quantities as in Fig. 2.

Using the data on the lateral distribution of penetrating particles in EAS taken from references 3 and 5 for the depths of 61 and 127 m w.e., and also the measurements carried out in our laboratory at a depth of 160 m w.e., we have constructed the energy spectra of the showers as a whole. These spectra are shown in Fig. 4. It can be seen that each spectrum can be represented by a straight line with a slope close to unity. The maximum value of the exponent of the energy spectrum was obtained for showers with a mean number of particles equal to 2.9×10^5. This exponent is equal to 1.25 ± 0.20.

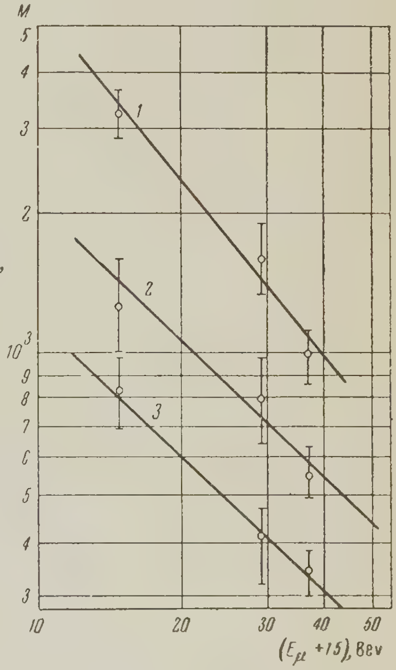

FIG. 4. Energy spectrum of the μ-meson component of EAS: 1 – for $\overline{N} = 2.9 \times 10^5$, 2 – for $\overline{N} = 7 \times 10^4$, 3 – for $\overline{N} = 1.4 \times 10^4$. The y axis represents the total number of μ mesons in EAS and the x axis the energy of μ mesons, taking into account the losses in their passage through the atmosphere.

According to the spectrum obtained, the mean energy of μ mesons of the penetrating component of EAS with $\bar{N} = 2.9 \times 10^5$ is, even at sea level, greater than 7 Bev, which fully confirms the results obtained by our group in previous years.

---

[1] I. Nishimura and R. Kamata, Prog. Theoret. Phys. **6**, 262, 628 (1951).

[2] K. Greisen, Progress in Cosmic Ray Physics (North-Holland Publishing Co., Amsterdam, 1956) vol.III, pp. 1-141

[3] É. L. Andronikashvili and M. F. Bibilashvili, JETP **32**, 403 (1957), Soviet Phys. JETP **5**, 341 (1957).

[4] Vavilov, Evstigneev, and Nikol'skiĭ, JETP **32**, 1319 (1957), Soviet Phys. JETP **5**, 1078 (1957).

[5] R. E. Kazarov and R. B. Lyudvigov, JETP **35**, 1310 (1958), Soviet Phys. JETP **8**, 903 (1959).

Translated by H. Kasha
142

SOVIET PHYSICS JETP VOLUME 38, NUMBER 3 SEPTEMBER, 1960

INTERACTIONS BETWEEN 630 Mev PROTONS AND He^4 NUCLEI

M. S. KOZODAEV, M. M. KULYUKIN, R. M. SULYAEV, A. I. FILIPPOV, and Yu. A. SHCHERBAKOV

Joint Institute for Nuclear Research

Submitted to JETP editor September 10, 1959

J. Exptl. Theoret. Phys. (U.S.S.R.) **38**, 708-715 (March, 1960)

A high-pressure diffusion cloud chamber was employed to study the scattering of 630 Mev protons on helium nuclei. The total, elastic, and inelastic cross sections were measured and found to be equal to $(150 \pm 13) \times 10^{-27}$ cm^2, $(24 \pm 5) \times 10^{-27}$ cm^2, and $(126 \pm 14) \times 10^{-27}$ cm^2, respectively. The angular distribution for the elastic scattering can satisfactorily be described in terms of the optical model using a complex potential with $V_R = 30$ Mev, $V_I = -(34 \pm 4)$, and $R = 1.45 \times 10^{-13}$ cm. Quasi-elastic proton-proton scattering and quasi-free proton-neutron interaction events were singled out. The cross sections for these reactions are $(15 \pm 2) \times 10^{-27}$ cm^2 and $(24 \pm 2) \times 10^{-27}$ cm^2 per nucleon, respectively. It is demonstrated that, in 20% of the events, either a cascade develops or the primary particle experiences a collision with a group of nucleons. Events involving π^- meson production in pn collisions were treated separately, and it was established that the cross section for this process is $(1.3 \pm 0.5) \times 10^{-27}$ cm^2 per neutron.

INTRODUCTION

A series of investigations devoted to the interaction of nucleons with the helium nucleus is being carried out at present. These experiments progress along two main directions. The first of these is related to the study of the structure of the He^4 nucleus. Among the structural properties, main attention is paid to the study of the nuclear size and the intranuclear nucleon motion,[1] as well as to a search of excited states.[2-4] Among research along this same direction belong also the experiments of Blankenbecler and Hofstadter on the charge distribution in the nucleus.[5] For research along the second direction, one should refer to the experiments devoted to the study of the mechanism of interaction of fast particles with the He^4 nucleus.[6,7] This nucleus has a sufficiently complex structure to exhibit the main features of interactions of fast particles with a complex nucleus in scattering processes and, at the same time, possesses a not too large number of nucleons, which makes it possible to discern easily the details of the observed events. Information obtained in such experiments can serve for creating a basis for the momentum-approximation method and for the optical model, which describe the interaction of fast particles with nucleons.

Although a large number of experiments have been devoted to the study of the interactions between nucleons and He^4 nuclei, only fragmentary data are available in the high-energy range (above 300 Mev). In this energy range, only two experiments have been carried out, those of Chamberlain et al.[6] and of Moulthrop.[7] In the first of these, the polarization and the elastic scattering of 315-Mev protons were investigated, while the second dealt only with the processes of π^--meson production in collisions of 300-Mev neutrons with He^4 nuclei.

It should be noted that investigations involving He^4 are more difficult as compared to those involving other light nuclei, since it is not always a simple problem to produce a target of liquid helium. Up to now, only two experiments[1,6] have used a liquid helium target.

In the present experiment, measurements on 630-Mev protons were carried out using a diffusion chamber. The method chosen made it possible to study both the processes of elastic scattering and the inelastic interactions in the same experiment. In connection with the latter, the possibility of studying the quasi-free scattering, and also of obtaining data on the multiple-interaction processes in a light nucleus, is of greatest interest.

EXPERIMENTAL METHOD

Proton scattering was studied by means of a diffusion chamber which, together with the auxiliary apparatus, has been described in detail in reference 8. The diameter of the working volume amounted to 30 cm. The height of the sensitive layer was 5 — 7 cm. The chamber was filled with helium to a pressure of 15 — 20 atmospheres.

A schematic diagram of the position of the apparatus during the experiment is shown in Fig. 1.

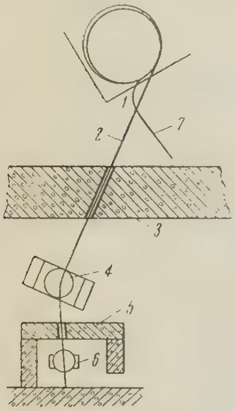

FIG. 1. Schematic diagram of the apparatus: 1 — accelerator chamber, 2 — proton beam, 3 — 4 m shielding wall, 4 — magnetic filter, 5 — additional chamber shield, 6 — diffusion chamber, 7 — π^--meson beam.

The protons were obtained by means of the synchrocyclotron of the Joint Institute for Nuclear Research. The particles were taken out of the accelerator chamber by means of an internal target. In this way, it was possible at the same time to work with another array placed in the π^--meson beam emerging from the same target. However, the proton energy was somewhat lower than the maximum obtainable in the accelerator and amounted to (630 ± 15) Mev, taking ionization losses into account.

The proton beam intensity was attenuated in an appropriate way so that a few tens of particles impinged upon the diffusion chamber during one cycle. The protons emerging from the accelerator were deflected at an angle of 19° by a deflecting magnet, and then directed through a 3 × 10 cm collimator to the diffusion chamber. The chamber was placed in a concrete hut with walls of 0.5 m thickness and which was, in addition, shielded by lead bricks to decrease the background of spurious radiation. A photograph was taken every 15 — 20 sec. The stereoscopic camera used had a basis of 120 mm, and the pictures were taken from a distance of 800 mm on Panchrom-X film with sensitivity $S_{0.85}$ = 1000 GOST units.

IDENTIFICATION OF INTERACTION EVENTS

About 20,000 stereograms were taken during the whole period of chamber exposure. Interaction events were selected by triple scanning through a stereoscopic magnifier. As the result of the scanning, 444 events of scattering of protons on helium nuclei were found. This number does not contain six events which were considered as interactions with C or O nuclei contained in methyl alcohol. The number of interactions with the nuclei of the admixture is roughly in agreement with the estimated expected number of such events.

The distribution of the interaction events of protons with helium nuclei, according to the number of prongs, is as follows:

Number of prongs	1	2	3	4	5
Number of events	0	204	228	8	4

Better sections of the film were used to obtain the total interaction cross section. The number of tracks in these was counted. Taking the necessary corrections into account, the value $\sigma_t = (150 \pm 13) \times 10^{-27}$ cm^2 was obtained for the total cross section.

The measurement of the spatial angles and also of the length of the tracks was carried out by means of a projector described earlier.[9] In several cases, the specific ionization of the particles was estimated by photometering the tracks by means of the MPH-4 microphotometer.[10]

A large number of reactions can occur on helium nuclei in the scattering of 630-Mev protons. For convenience of identification, they can be subdivided into separate groups according to the criterions for selection and analysis (see Table I).

Reactions of the first group, with the exception of reaction 4, represent coplanar two-prong stars, and are recognizable from kinematic conditions of the decay.

The second group of reactions also includes two-prong stars. The majority of events in this group consist of the quasi-elastic scattering of protons or neutrons (reaction 1). Other events, with the exception of reactions of types 2 and 4, refer to quasi-free interactions of protons. In the present experiment, it has not been possible to distinguish between reaction 1 and other reactions of this group.

The third group of reactions consists of three-prong stars, and includes not only the cases of quasi-free interactions of protons with protons, but also other processes in which a great number of nucleons take part in the interaction.

The quasi-elastic proton-proton scattering (reaction 1) was singled out from the reactions of this group. The selection of quasi-elastic scattering events was effected using the corresponding correlation of the emission angles of the particles, and also their momenta in the final state. The selection procedure of such events is analogous to that which has been used in the identification of quasi-elastic scattering of π mesons on protons, and which was described in detail in reference 16.

TABLE I

Reaction group	Serial Number	Reaction	Number of events
I	1	$p + \mathrm{He}^4 \to p + \mathrm{He}^4$	66
	2	$d + \mathrm{He}^3$	(1)*
	3	$\pi^+ + \mathrm{He}^5$	0
	4	$\pi^0 + \mathrm{Li}^5$	0
II	1	$p + \mathrm{He}^4 \to p + n + \mathrm{He}^3$	136
	2	$\pi^+ + n + \mathrm{He}^4$	
	3	$\pi^+ + 2n + \mathrm{He}^3$	
	4	$\pi^0 + p + \mathrm{He}^4$	
	5	$\pi^0 + (p, n) + \mathrm{He}^3$	
III	1	$p + \mathrm{He}^4 \to p + p + \mathrm{H}^3$	88 (19)*
	2	$\pi^+ + (3n, 2p)$	124
	3	$\pi^0 + (2n, 3p)$	
	4	$p + (2n, 2n)$	
VI	1	$p + \mathrm{He}^4 \to \pi^- + p + p + \mathrm{He}^3$	7 (3)**
	2	$\pi^- + p + p + p + d$	4

Note: Brackets with one star give the number of not completely certain events out of the total number of identified events. Brackets with two stars give the number of events which can be interpreted as production of a π^0 meson with consecutive decay into an electronic pair and a γ ray.

The fourth group of reactions consists of events referring to the production of π^0 mesons in p-n collisions. These events, in contrast to the reactions discussed above, represent four- and five-prong stars. The results for singled-out reactions of this group are given below.

In the interaction of 630-Mev protons with helium nuclei, the paired π-meson production can also occur, which can contribute to the number of four- and five-prong stars. However, it follows from the experiments of Block and others[12] that the cross section for processes of that type is very small even at the energy of 800 Mev, and is not greater than 0.8 mb per nucleon. One can assume that the contribution of paired production at 630 Mev is negligibly small, and it can be neglected in the above classification of reaction groups. Only one event which could be interpreted as a probable case of paired meson production was found in analyzing the five-prong stars. A picture of this event is shown in Fig. 2

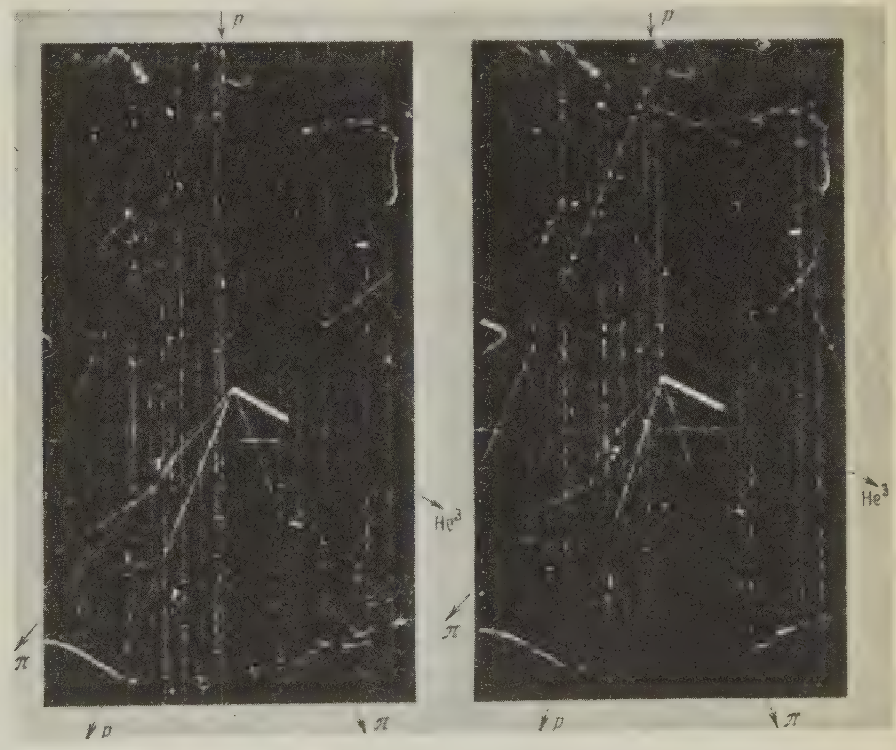

FIG. 2. Photograph of probable event of paired π-meson production.

ELASTIC SCATTERING

The angular distribution of elastic scattering is shown in Fig. 3. The minimum detection angle amounted to 5° in the c.m.s. Without a correction for the range of small angles, the following value was obtained for the total cross section for elastic scattering:

$$\sigma_{\text{el}} = (22.0 \pm 4.5) \cdot 10^{-27} \text{ cm}^2$$

From the optical theorem,[13] one can estimate the minimum correction to the cross section for the range of small angles. With the correction, the cross section amounts to $\sigma_{\text{el}} = (24.0 \pm 5.0) \times 10^{-27}$ cm², or 0.16 of the total cross section for the pHe interaction. This result shows that the cross section of elastic scattering remains practically constant from 315 to 630 Mev. (The integration of the angular distribution obtained by Chamberlain et al.[6] for 315 Mev gives $\sigma_{\text{el}} = 19 \times 10^{-27}$ cm².)

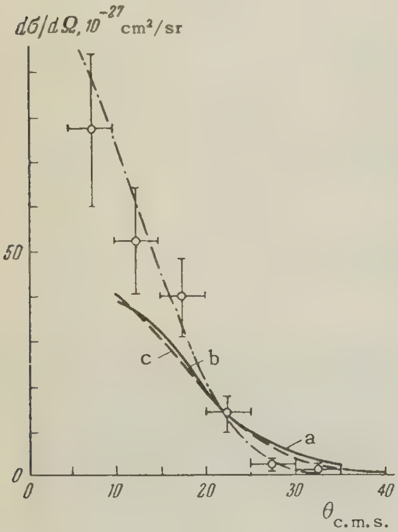

FIG. 3. Angular distribution of elastic scattering of proton on helium. The points represent the experimental distribution at 630 Mev; curve a – experimental distribution at 315 Mev;[6] b – angular distribution at 630 Mev, calculated according to the optical model with the parameters V = 45 Mev, R = 1.45 × 10^{-13} cm; c – angular distribution at 315 Mev calculated according to the optical model with parameters V = 17 Mev, R = 1.90 × 10^{-13} cm.

Estimates of the Coulomb scattering have shown that it is mainly concentrated in the range of angles 0 – 5° and, therefore, its contribution to the angular distribution given above is negligibly small.

Calculations of the angular distribution of the elastic scattering have been carried out within the framework of the optical model, using the Born approximation, and neglecting the spin-orbit and Coulomb interactions.

The scattering potential was taken as a rectangular well with radius R and depth $V = \sqrt{|V_R|^2 + |V_I|^2}$. The form of the angular distribution, consistent with the experimental data, is very sensitive to the value of the radius and to the potential. Acceptable distributions are obtained for radii in the range $(1.3 - 1.55) \times 10^{-13}$ cm. The possible values of the depth of the potential well amount to 40 – 50 Mev. A best fit with experimental points is obtained for the curve for which V = 45 Mev and $R = 1.45 \times 10^{-13}$ cm (Fig. 3).

If we use the value of the cross section for inelastic processes, then, for $R = 1.45 \times 10^{-13}$ cm, we obtain the value $V_I = -(34 \pm 4)$ Mev for the imaginary part of the potential. The real part of the potential is then equal to $V_R = 30$ Mev.

Analogous calculations were carried out for a proton energy of 315 Mev. The same figure (Fig. 3) shows the results of measurements of the elastic scattering of polarized protons on He^4 nuclei, obtained by Chamberlain et al.,[6] as well as the distribution calculated for $R = 1.9 \times 10^{-13}$ cm, and V = 17 Mev, which represents the best fit with the experimental points. If we assume $R = 1.9 \times 10^{-13}$ cm and set the Goldberger factor $\gamma = 0.8$, then, from the total pp and pn scattering cross section at 315 Mev, we obtain for the imaginary part of the potential $V_I = -18$ Mev; i.e., V_I is almost equal to the absolute value of the total potential.

A certain ambiguity is present in the choice of γ, since there is no information on the cross section for inelastic scattering at 315 Mev. This ambiguity, however, cannot affect the conclusion about the small value of the real part of the potential at this energy. This result is in agreement with calculations of the real part of the central potential carried out by Riesenfeld and Watson[14] from a phase-shift analysis of nucleon-nucleon scattering. The consistency of the results at 615 Mev may, within the framework of the accepted scheme, indicate that at 630 Mev the picture is sufficiently correct. Hence, we can conclude that the real part of the potential increases with increasing energy.

It should be mentioned that, within the framework of the above analysis, it is impossible to describe the angular distribution at the energies of 315 and 630 Mev with the same radius for the potential well.

INELASTIC SCATTERING

Multiple collisions inside the helium nucleus. The representation of cascade processes developed by Goldberger[15] can be applied to the He^4 nucleus. Cascade development at the energy under consideration can be due to recurring collisions both of nucleons and mesons produced in the first collision. The incident nucleons can also collide with a group of nucleons of the nucleus. The ejected nucleons are then found to be in both bound and free final states. In the latter case, the event can appear in such a way that it will be impossible to determine whether a cascade has developed, or whether a collision with a complex of nucleons has taken place. The term plural interaction will, in the following, be applied to processes of single or recurring interactions of the incident particle with several nucleons. From the data given above, one can estimate the contribution of such processes.

If we denote the total number of collisions between the incident proton and the neutrons of the nucleus by N_{pn}^{nuc}, we can write

$$N_{pn}^{nuc} = N_{pn} + N_{pn}^{pl} = N_2' + N_4 + N_5 + N_{pn}^{pl},$$

where N_{pn} is the number of cases of quasi-free interactions, N_2' is the number of two-prong stars including the elastic scattering events, N_4 and N_5 is the number of four- and five-prong stars, and N_{pn}^{pl} is the number of cases in which a multiple interaction has occured. This method of writing N_{pn}^{nuc} is possible only because of the fact that, among the two-prong stars, events related to multiple interaction processes are practially absent. Any repeated collisions will lead to an increase in the number of prongs, as a result of which a three-prong star will be detected. Exceptions to these are the reactions

$$p + \mathrm{He}^4 \to \pi^0 + p + \mathrm{He}^4, \qquad p + \mathrm{He}^4 \to \pi^+ + n + \mathrm{He}^4,$$

in which the development of the cascade may not lead to an increase in the number of prongs. However, it we use the results of Moulthrop,[7] it can be seen that the contribution of such reactions is small.*

The number of three-prong stars N_3 contains not only the events of quasi-free interactions between protons and protons N_{pp}, but also the events of plural interactions N_{pp}^{pl} and N_{pn}^{pl}. Therefore, the number of collisions between protons and protons N_{pp}^{nuc} can be written in the form

$$N_{pp}^{nuc} = N_{pp} + N_{pp}^{pl} = N_3 - N_{pn}^{pl}.$$

It is reasonable to assume that the cross sections for quasi-free scattering of nucleons have a ratio similar to that of the corresponding cross sections for free nucleons. Taking this into account, it is possible to estimate the contribution of the processes of plural interaction in the scattering of protons on He^4 as follows:

$$\varepsilon = \frac{(N_{pn}^{pl} + N_{pp}^{pl})}{(N_{pp}^{nuc} + N_{pn}^{nuc})} = \frac{N_3 - N_2' - N_4 - N_5}{N_3 + N_2' + N_4 + N_5} = 0.22 \pm 0.07.$$

The result obtained shows the considerable role of the plural interaction processes, even for such a light nucleus as He^4. The considerable role of such processes has also been established in the study of the scattering of fast π mesons on He^4.[16]

Quasi-free scattering of protons. The cross sections for various reactions singled out in the identification of interaction events are given in Table II. A comparison of the total cross section for inelastic processes with the sum of nucleon-nucleon cross sections results in a value of 0.82 for the quantity γ. These results indicate that, even for the energy of incident particle equal to ~ 600 Mev and for light nuclei, it is necessary to know the value of γ in order to estimate the value of the mean free path using the sum of the nucleon-nucleon cross sections. For 970 Mev protons, the value of γ still does not attain one, even for the deuteron, and amounts to 0.91.[11]

In row 7 of Table II, the data on the quasi-free scattering of neutrons on the neutrons of the helium nucleus are given. The total cross section for the quasi-free scattering amounts only to 0.65 of the corresponding cross section for free nucleons, without taking into account the processes of plural interaction. An analogous result has also been obtained for the quasi-elastic scattering of protons on protons (row 8). Introducing the corresponding correction for plural interaction, we obtain for γ roughly the same value as that obtained from the total cross section of inelastic scattering.

As can be seen from rows 5 and 6 of the same table, the cross section for meson production in collisions of protons with bound neutrons amounts to $(1.3 \pm 0.5) \times 10^{-27}$ cm^2, which is approximately equal to the cross section obtained in reference 17 for free neutrons.*

The angular distribution of protons emitted in quasi-elastic scattering is shown in Fig. 4. For a comparison, the angular distribution of elastic scattering of protons on protons at 660 Mev is also given in the same figure. The comparison of the distributions shows that, in quasi-elastic scattering, a certain number of nucleons are ejected both at small and large (close to 90°) angles. The observed difference is probably due mainly to the Pauli principle.

The form of the angular distribution of protons

---

*At 300 Mev, the output of π mesons from the $n + \mathrm{He}^4 \to \pi^- + P + \mathrm{He}^4$ reaction amounts to less than 6% of the total cross section for meson production.

*The results obtained are in agreement with the data of Dzhelepov, Kiselev, Oganesyan, and Flyagin, reported at the 1959 Kiev Conference in the paper of B. M. Pontecorvo.

TABLE II

	Reaction	Cross section per nucleus 10^{-27} cm²	Cross section per nucleon 10^{-27} cm²	$\frac{\sigma}{\sigma_{NN}}$	Cross section per nucleon with correction for plural processes, σ'	$\gamma=\frac{\sigma'}{\sigma_{NN}}$
1	**Inelastic scattering**	126±14	—	—	—	—
2	$p+n+\mathrm{He}^3$	46±4	23±2	—	—	—
3	$\pi^+ + n + n + \mathrm{He}^3$					
4	$p+\mathrm{He}^4 \rightarrow \pi^0 + (p,\ n) + \mathrm{He}^3$					
5	$\pi^- + p + p + \mathrm{He}^3$	1.3±0.7	1.3±0.5	—	—	—
6	$\pi^- + p + p + p + d$	1.3±0.7				
7	**Total quasi-free pn interaction**	48±4	24±2	0.65	29±3	0,78
8	$p+\mathrm{He}^4 \rightarrow p+p+\mathrm{H}^3$	29±3	15±2	0.6	18±2	0.73

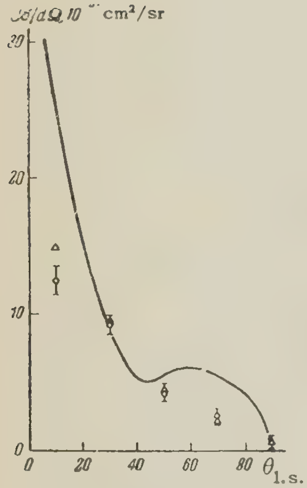

FIG. 4. Angular distribution of quasi-elastic scattering of protons on protons: o – experimental distribution, Δ – distribution calculated by the Monte-Carlo method, solid line – angular distribution of scattering of protons on free protons.

was calculated by the Monte Carlo method, taking the bond into account. In the calculation, the intranuclear momentum distribution of nucleons was taken as a Fermi distribution with a limiting momentum of 220 Mev/c. Plural interaction processes were not taken into account. Results of the calculation are also shown in Fig. 4. It can be seen that the angular distribution obtained experimentally is in satisfactory agreement with the calculated distribution. Such a fit indicates that the plural interaction processes which occur in helium do not, in the majority of cases, strongly distort the form of the distribution, but lead to a practically proportional ejection of protons at all angles.

In conclusion, the authors express their thanks to A. G. Potekhin and V. F. Poenko for help in setting up the experiment, and also to E. A. Shvanev for help in reducing the experimental data.

---

[1] W. Selove and J. Teem, Phys. Rev. **112**, 1658 (1958).

[2] Bogdanov, Vlasov, Kalinin, Rybakov, Samoĭlov, and Sidorov, Ядерные реакции при малых и средних энергиях (Nuclear Reactions at Low and Medium Energies), Acad. of Sciences U.S.S.R., Moscow, 1958.

[3] Tyren, Tibell, and Maris, Nucl. Phys. **4**, 277 (1957).

[4] R. M. Eisberg, Phys. Rev. **102**, 1104 (1956).

[5] R. Blankenbecler and R. Hofstadter, Bull. Am. Phys. Soc. **1**, 10 (1956).

[6] Chamberlain, Segrè, Tripp, Wiegand, and Ypsilantis, Phys. Rev. **102**, 1659 (1956).

[7] P. H. Moulthrop, Phys. Rev. **99**, 1509 (1955).

[8] Kozodaev, Kulyukin, Sulyaev, Filippov, and Shcherbakov, Приборы и техника эксперимента (Instruments and Measurement Engg.) No. 6, 47 (1958).

[9] Vasilenko, Kozodaev, Sulyaev, Filippov, and Shcherbakov, ibid., No. 6, 34 (1957).

[10] Voloshchuk, Kuznetsov, Sulyaev, Filippov, and Shcherbakov, ibid., No. 3, 1960.

[11] Batson, Culwick, Klepp, and Riddiford, Proc. Roy. Soc. **251**, 233 (1959).

[12] Block, Harth, Fowler, Shutt, Cocconi, Hart, Fowler, and Garrison, CERN Symposium 374 (1956).

[13] L. I. Lapidus, JETP **31**, 1099 (1956), Soviet Phys. JETP **4**, 937 (1957).

[14] W. Riesenfeld and K. Watson, Phys. Rev. **102**, 1157 (1956).

[15] M. Goldberger, Phys. Rev. **74**, 1269 (1948).

[16] Kozodaev, Kulyukin, Sulyaev, Filippov, and Shcherbakov, JETP **38**, 409 (1960), Soviet Phys. JETP **11**, 300 (1960).

[17] Yu. M. Kazarinov and Yu. N. Simonov, JETP **35**, 78 (1958), Soviet Phys. JETP **8**, 56 (1959).

Translated by H. Kasha
143

SOVIET PHYSICS JETP VOLUME 11, NUMBER 3 SEPTEMBER, 1960

FISSION OF URANIUM NUCLEI INDUCED BY 9-Bev PROTONS

N. A. PERFILOV, V. F. DAROVSKIKH, G. F. DENISENKO, and A. I. OBUKHOV

Radium Institute, Academy of Sciences, U.S.S.R.

Submitted to JETP editor September 10, 1959

J. Exptl. Theoret. Phys. (U.S.S.R.) **38**, 716-718 (March, 1960)

Some characteristics of uranium fission induced by 9-Bev protons are obtained. These include the magnitude of the cross section, the dependence of the yield on the ratio of the fragment ranges, data on the number of light particles involved in fission, and the angular distributions of the fragments.

EXPERIMENTAL CONDITIONS

We used the photographic method. Nuclear emulsions of type P-9ch with natural uranium introduced into the emulsion[1] were exposed to 9-Bev protons in the internal beam of the proton synchrotron of the Joint Institute for Nuclear Research. In scanning the emulsions, we classified as uranium-fission events also those cases of disintegration in which, along with tracks of light charged particles, essentially protons and α particles, two tracks which are similar in the darkening intensity to tracks of fragments of fission by thermal neutrons are observed. The overwhelming majority of the registered events has a light-to-heavy fragment ratio $L_l/L_h < 2$. We have, therefore, confined ourselves to that region of range ratios, particularly since for $L_l/L_h > 2$ the fragmentation admixture becomes substantial. A total of 1042 disintegrations classified as uranium fission were analyzed.

RESULTS

1. The fission cross section σ_f was calculated from the formula $\sigma_f = N_f/N_{nuc}N_p$, where N_f is the number of disintegrations per cubic centimeter, N_{nuc} is the number of uranium nuclei per cubic centimeter, and N_p is the neutron flux. The amount of uranium introduced was determined by calculating the number of tracks of α particles due to uranium decay over a known time interval. The proton flux was calculated by comparison of the number of disintegrations with fragments in the P-9ch emulsion, where the primary flux was not registered, but on which the basic experiment was performed, with that in the PR emulsion, in which the proton flux was determined by calculating the number of tracks in a known area.

The value obtained for the fission cross section was $\sigma_f = (1.3 \pm 0.4)$ b. However, in the interaction of 9-Bev protons with nuclei of the elements contained in the emulsion, a considerable number of secondary particles of different energy, less than 9 Bev, are produced and these also contribute to the fission of the uranium introduced in the photographic emulsion. A rough estimate of this background leads to a value of ~ 30%, and consequently, we have for the fission cross section of uranium by 9-Bev protons $\sigma_f \approx 0.9$ b.

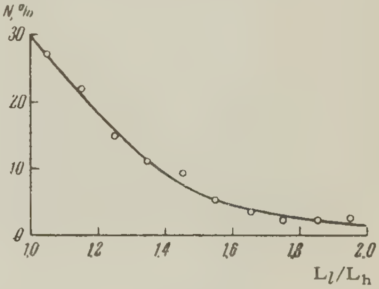

FIG. 1

2. The relations between the ranges of the light and heavy fragments in each individual fission event represent approximately the ratio of their masses.[2] Figure 1 shows the distribution of the fission events, accompanied by the emission of charged particles, as a function of the ratio of the ranges of the heavy and light fragments (the point of emission of the charged particles determines the point of fission). The character of the distribution is found to be similar to that observed in the fission by protons of energies on the order of hundreds of megavolts.[3] Thus, in the fission of uranium nuclei by 9-Bev protons, the most probable is fission by fragments that are of nearly equal mass.

Figure 2 shows the dependence of the average total range of fission fragments of uranium on the ratio of the ranges of the light and heavy fragments. The average total range of the fragments charac-

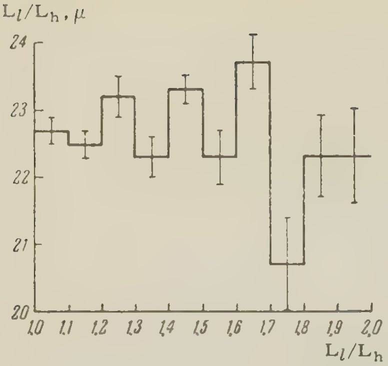

FIG. 2

terizes the liberated kinetic energy corresponding to a given type of fission as a function of the mass ratio. Figure 2 shows three maxima which are outside the limits of statistical errors. However, we shall not attempt so far to interpret them until more is known about their nature.

3. We list the results of the investigation of the angular distribution of the fission fragments — number of fissions N as a function of the angle θ between the direction of motion of the proton and the projection of the line of divergence of the fragments* on the plane of the microscope table.

	$\theta° = 0—15$	15—30	30—45	45—60	60—75	75—90
$n_{\alpha p} \geqslant 1$;	$N = 125$	107	120	124	111	110
$n_{\alpha p} \geqslant 0$;	$N = 179$	171	179	185	173	155

The first line refers here to the number of charged particles $n_{\alpha p}$, accompanying fission, starting with unity, and the second starting with zero.

For the ratio of the number of events in the interval 0 — 30° to the number of events in the interval 60 — 90° we obtain

$$N\,(0—30°)\,/\,N\,(60—90°) = 1.07 \pm 0.11,$$

i.e., an isotropic distribution within the limits of statistical errors.

4. Figure 3 shows the distribution of fissions by the number of accompanying "black" rays (by "black" rays we mean tracks which are registered by the P-9ch emulsion). The same figure shows for comparison the data obtained earlier in our laboratory for an energy of 660 Mev. The average value $\bar{n}_{\alpha p} = 3.82$ and E = 9 Bev, where at E = 660 Mev we have $\bar{n}_{\alpha p} = 1.16$. We can, therefore, conclude that the fissioning nuclei, obtained when 9-Bev protons act on the uranium nucleus have a much higher average excitation energy.

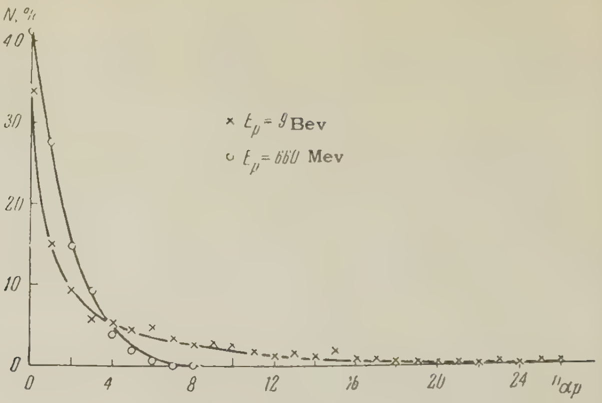

FIG. 3

5. Among the disintegrations that are produced when 9-Bev protons act on the uranium nucleus, one encounters disintegrations into two fragments of commensurate mass and a third lighter one. The relative frequency of appearance of such "triple" disintegrations with respect to "double" disintegrations is approximately 0.02, whereas at a proton energy of 660 Mev the frequency of triplet appearance is ~ 0.005 (reference 5). The average number of prongs accompanying triple fission is 11.0 and 1.6 respectively at 9 Bev and 660 Mev. We see that both the number of triple disintegration relative to the double ones, and the average number of charged particles accompanying the triple disintegration, increase considerably with increasing proton energy from 660 Mev to 9 Bev.

In conclusion, the authors express their gratitude to the staff of the high-energy laboratory of the Joint Institute for Nuclear Research for help in the irradiation.

Translated by J. G. Adashko
144

---

*As a rule, in the laboratory system of coordinates the angle between the fragments is less than 180°. As the line of divergence of the fragments in the system of the fissioning nucleus we used the line joining the ends of the tracks of two fragments.[4]

[1] Perfilov, Novikova, and Prokof'eva, Атомная энергия (Atomic Energy) **4**, 45 (1958).

[2] V. F. Darovskikh and N. A. Perfilov, JETP **36**, 652 (1959), Soviet Phys. JETP **9**, 1192 (1959).

[3] V. P. Shamov and O. V. Lozhkin, JETP **29**, 286 (1955), Soviet Phys. JETP **2**, 111 (1956).

[4] V. I. Ostroumov and N. A. Perfilov, JETP **31**, 716 (1956), Soviet Phys. JETP **4**, 603 (1957).

[5] N. A. Perfilov and G. F. Denisenko JETP **35**, 631 (1958), Soviet Phys. **8**, 1185 (1959).

SOVIET PHYSICS JETP VOLUME 11, NUMBER 3 SEPTEMBER, 1960

IONIZATION OF INERT GASES BY MULTIPLY CHARGED IONS

N. V. FEDORENKO, I. P. FLAKS, and L. G. FILIPPENKO

Leningrad Physico-Technical Institute, Academy of Sciences, U.S.S.R.

Submitted to JETP editor September 12, 1959

J. Exptl. Theoret. Phys. (U.S.S.R.) **38**, 719-725 (March, 1960)

The total ionization cross sections (σ_-) for single collisions between Ne^+, Ne^{2+}, Ne^{3+}, Kr^+, Kr^{2+}, Kr^{3+}, Xe^+, Xe^{2+}, Xe^{3+}, Xe^{4+} ions and inert gas atoms have been measured. In the investigated voltage range from 3 to 30 kv, it was found that the ionization cross section is practically independent of the charge of the primary ion for equal ion energy. For all ion-atom pairs, a continuous growth of the cross section with increase in kinetic energy of the primary ions was observed. In most cases the absolute values of the measured cross sections were close to those computed by Firsov's formula.[1]

INTRODUCTION

INFORMATION on the ionization of atoms by multiply charged ions is limited to the single work of Sherwin,[2] in which the ionization cross sections of molecules of hydrogen and atoms of helium by singly, doubly and triply charged ions of certain metals were measured for two values of the accelerating voltage (6 and 24 kv). Sherwin came to the conclusion that the ionization cross section increased in proportion to the square of the charge of the primary ion. As is well known, such a charge dependence is given by the theory of shock ionization for regions of high energy, when the condition $v \gg v_e$ is satisfied, where v is the velocity of relative motion and v_e is the velocity of the outer electrons in the atom.

Studies carried out in recent years[3] on the ionization of the atoms of a gas by singly charged ions in the velocity region $v \lesssim v_e$ have shown that the collisions accompanied by ionization do not reduce to the interaction of the ion with the individual electrons of the atom. It was established that the processes of ionization are realized in "penetrating" atomic collisions and the interaction of the electronic shells of the colliding atomic particles possesses great significance.

Recently a theoretical paper by Firsov[1] appeared, in which the ionization cross section for atomic collisions was calculated, on the basis of a quasi-classical representation, as a function of the number of electrons in the shells of the two particles.

Thus it is not difficult to explain the data of Sherwin on the ionization by multiply charged ions on the basis of recently developed ideas on the mechanism of ionization of atoms by singly charged ions in the region of velocities $v \leq v_e$. The present research was undertaken with a view toward carrying out a further investigation of ionization by ions of different charge with the application of a more reliable indication of monokinetic beams of multiply charged ions and with a method of measurement of the ion cross section developed in our laboratory.

In the present work, the study was limited to the ions Ne^+, Ne^{2+}, Ne^{3+}, Kr^+, Kr^{2+}, Kr^{3+}, Xe^+, Xe^{2+}, Xe^{3+}, Xe^{4+} and the atoms Ne, Kr, and Xe.

INVESTIGATION PROCEDURE

The study of ionization by ions of different charge was carried out on an experimental apparatus whose general description was given in our previous researches.[4-6] The primary ions were produced in an ion source which is a modification of the source of Ardenne.[7] A narrow ion beam of definite charge, composition and energy was separated by a magnetic mass spectrometer and passed through a rectangular slit S_1 (1 × 4 mm) in the collision chamber which was filled with the gas under investigation (Fig. 1). A sectionalized measuring capacitor, described in detail in reference 8, was placed in the collision chamber. The free electrons arising in the gas and the secondary ions were deflected by the electric field onto the plates 1 — 12 of the capacitor and the plates 13, 14 of the Faraday cage F_1. The plates of the measuring capacitor were screened by metallic grids with a transparency of about 90 per cent. A potential of ±45 v relative to the ground,

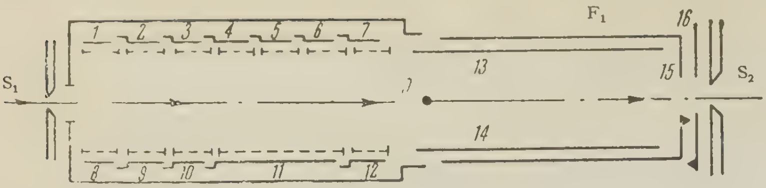

FIG. 1. Measuring capacitor.

was applied to the grids and to plates 13 and 14, while an additional +25 v relative to the grid was applied to plates 1 — 12. In this way, the secondary electrons emerging from the plates were held back by the electric field. Plates 5 and 6 in the middle part of the capacitor were chosen as the measuring plates. It was established by control experiments that the current of electrons and secondary ions were known to reach saturation, and only the charged particles appearing in the gas in a section equal to the length of the measuring plate were drawn off onto plates 5 and 6. A typical volt-ampere characteristic of the currents of the secondary ions and the free electrons on plates 5 and 6 is shown in Fig. 2.

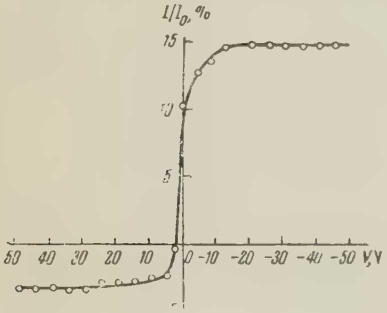

FIG. 2. Volt-ampere characteristic. The pair Kr^{2+} – Kr, energy 30 kev, gas pressure $p = 1.6 \times 10^{-4}$ atm, I — current in the measuring plates, I_0 — current of the primary beam.

The current of the primary beam was measured on the entire system of electrodes forming the measuring capacitor and the Faraday cage, and also on the suppressor plate 16, which covered the bottom of the cage at the time of measurement of the primary beam.

For correction of the beam inside the measuring condenser in the measurement of currents on plates 5 and 6, the collision chamber could be rotated about the axis O (which passes through the center of the chamber) by a small angle relative to the initial direction of the beam.[9] In this case the ion beam passed through the opening 15 into F_1 (8 × 12 mm) and the slit S_2 (6 × 10 mm), and was picked up on the monitor of the primary beam (not shown in Fig. 1).

To verify the recordings of the primary multiply-charged ions, measurements were made of the relative intensity of the lines of the different isotopes of the ions under study, which were then compared with the known tabular values. In addition, the presence of a magnetic analyzer after the collision chamber permitted us to observe the multiply-charged ions by means of the additional lines which appear in the ion beam after transmission through the gas [as the result of partial charge exchange (see references 4 — 6)].

The currents on plates 5 and 6 and the primary current were measured with an EMU-2 amplifier.

The experiments were carried out under conditions of single stage character of the collisions at gas pressures $\sim 1 \times 10^{-4}$ atm. The gas pressure drop amounted to $\sim 1:50$ at the slit S_1, and to $\sim 1:15$ at slit S_2. The residual pressure in the apparatus after shutting off admission of the gas into the collision chamber did not exceed 1×10^{-6} atm. The pressure was measured by an ionization manometer controlled by a McLeod gauge.

DETERMINATION OF THE CROSS SECTIONS

In the present research we measured the negative I_- and the positive I_+ saturation currents to the plates of the measuring condenser. Measurement of these currents permitted us to determine the total cross section for the formation of free electrons σ_- and the total cross section of formation of secondary ions σ_+ referred to a single charge:

$$\sigma_- = zI_- / NlI_0, \qquad \sigma_+ = zI_+ / NlI_0, \tag{1}$$

where I_0 is the current of the primary beam, z is the multiplicity of the charge of the primary ions, N is the number of atoms per cubic centimeter of gas, l is the length of the measuring electrodes.

The cross section σ_-, as also in reference 8, was of interest to us as the "total cross section" of ionization. Data on the cross section σ_+ were frequently used by us for the comparison with data on cross sections of capture of electrons by ions of the primary beam, obtained in references 4 — 6.

In the passage of a beam of singly charged ions through the gas, the cross sections σ_- and σ_+ are composed of the cross sections of the separate processes of three groups:

$$I^{i+} + A \to I^{i+} + A^{k+} + ke, \tag{I}$$

$$I^{i+} + A \to I^{f+} + A^{k+} + (f + k - i)e, \tag{II}$$

$$I^{i+} + A \to I^{l+} + A + (l - i)e. \tag{III}$$

The processes of group I have been named "pure" ionization of the gas atoms, those of the group II are known as ionization with capture, while those of group III as stripping of the primary ion. The processes of groups I and II can evidently exist simultaneously and lead to the release of electrons from the shells of both colliding atomic particles. Processes of group II are connected with the liberation of electrons from the shell of an atom and with partial neutralization of the primary ion. As the results of the existence of processes of groups I and II in the gas, secondary ions can be formed with different multiplicity of charge, and in the stripping (processes of group III), ions of much higher charge than that of the primary ions appear in the primary beam.

Complete account of all possible processes leads to the result that

$$\sigma_+ - \sigma_- = \sigma_0 - \sigma_l, \tag{2}$$

where σ_0 is the "total cross section" of ionization with capture, while σ_l is the "total cross section" of stripping, referred to a single charge. In the energy region under investigation, $\sigma_l \ll \sigma_0$ and

$$\sigma_+ - \sigma_- \approx \sigma_0. \tag{3}$$

In the general case of primary ions with i-fold charge,

$$\sigma_0 = \sum_{f=i-1}^{f=0} (i-f)\sigma_{if}, \tag{4}$$

where σ_{if} is the cross section for formation of ions with charge from $i-1$ to 0. The separate components of the sum (4) can be determined by analysis of the charge composition of the ion beam after passage through the gas.[4-6]

The currents I_- and I_+ entering into Eq. (1) were measured as the difference of the saturation currents in the gas under study and after pumping out of the collision chamber to the limiting vacuum.

The relative crudeness of the measurement of the cross sections σ_- and σ_+ is estimated by us to be of the order of 20 per cent, starting from the reproducibility of the results. It is connected with random errors in the measurement of the currents and of the gas pressure, and with a certain instability of the operation of the ion source.

RESULTS

The dependence of the total cross section of ionization of the gases under study by the various ions is shown in Fig. 3 as a function of the kinetic energy of the primary ions T.

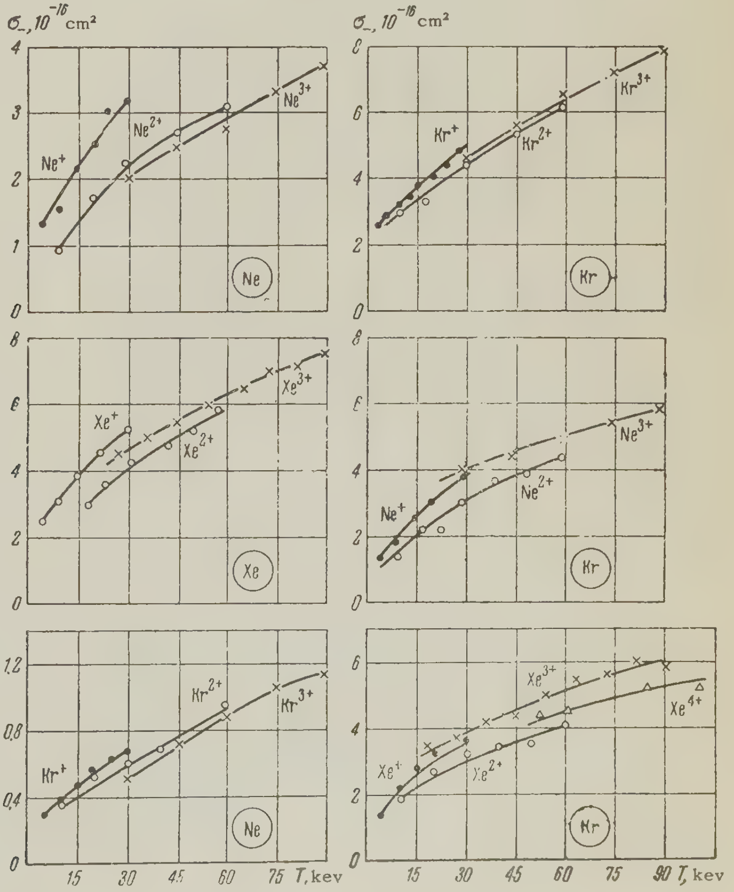

FIG. 3. Total ionization cross section of gases (shown in the circles) by ions (shown on the curves) as a function of the energy.

In the ionization of neon by neon ions, σ_- is somewhat larger for the Ne^+ ions at the same kinetic energy (or the same velocity of the ions). For the ions Ne^{2+} and Ne^{3+}, the cross sections are identical within the limits of error of the experiment.

In two other cases of ionization of a particular gas by ions of different charge, and in particular ionization of krypton by krypton ions and ionization of xenon by xenon ions, the cross sections σ_- are approximately the same for a given energy.

A similar conclusion can be reached from a consideration of the data for the ionization of gases by strange ions: krypton by neon ions, neon by krypton ions and krypton by xenon ions (see Fig. 3).

An uninterrupted increase in the ionization cross section was observed for all pairs of ions-atoms studied in the energy interval under consideration. In the middle part of the energy interval ($T \approx 50$ kev) the largest values were achieved for the ionization cross section of xenon by xenon ions and krypton by krypton ions ($\sigma_- \approx 6 \times 10^{-16}$ cm^2), and the smallest ionization cross section was that of neon by krypton ions ($\sigma_- \approx 8 \times 10^{-17}$ cm^2).

Two of the pairs studied by us, namely, Ne^+-Ne and Kr^+-Kr, were also measured by Gilbody and Hasted[10] in the energy ranges from 0.1 to 3 kev and from 5 to 40 kev. The cross section σ_- in reference 10 for the pair Ne^+-Ne is larger than ours by about 70 per cent, while that for Kr^+-Kr is 4 — 5 times larger. It should be noticed that these authors observed almost the same divergence for these pairs among the series of their own measurements completed in the region of small and high energies.

We carried out comparison of the difference in the cross sections $\sigma_+ - \sigma_-$ determined in our present work with the charge-exchange cross sections σ_{10} measured by us in reference 4 by the method of recording fast neutral atoms. This comparison was made for the pairs Ne^+-Ne and Kr^+-Kr. The results of the comparison are shown in Fig. 4. A similar comparison is shown in Fig. 5 for the pair Kr^{2+}-Ne, for which the cross section for capture of two electrons σ_{20} is very small in comparison with the cross section of capture of a single electron σ_{21} (see reference 5) and, consequently, by (4), $\sigma_+ - \sigma_- \approx \sigma_{21}$. As is seen from Fig. 5, in the case of doubly charged ions, a close correspondence is also observed between the results of independent measurements.

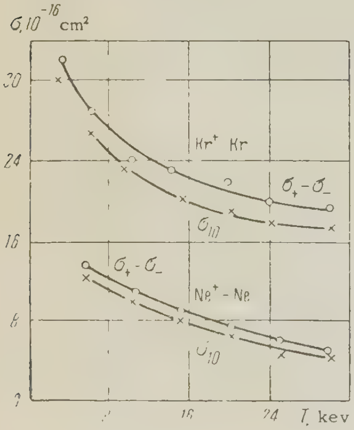

FIG. 4. Comparison of the capture cross section measured by the potential method $\sigma_+ - \sigma_-$ and by the method of registering fast atoms (σ_{10}). Pairs are Ne^+-Ne and Kr^+-Kr.

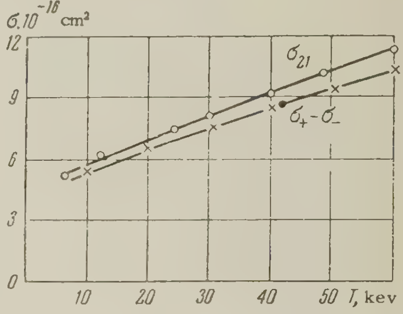

FIG. 5. Comparison of the capture cross section measured by the potential method $\sigma_+ - \sigma_-$ and by the mass spectrometer method (σ_{21}). The pair is Kr^{2+}-Ne.

DISCUSSION

The results of our investigation of the ionization of inert gases by multiply charged ions do not substantiate the quadratic dependence of the cross section on the charge of the primary ion found by Sherwin. It should be noted in passing that the cross sections in the work of Sherwin were compared, not for identical kinetic energy of ions of different charge, but for the same accelerating voltage. Thus a weaker dependence of cross section on charge actually follows from the data of Sherwin. In several cases (Cu^+, Cu^{2+}-He; C^+, C^{2+}-He), the cross sections are practically identical for singly and doubly charged ions. Some shortcomings in the method of the research of Sherwin were noted in reference 11. The absence of a reliable indication of multiply charged ions and the measurement of cross sections for comparatively high gas pressure ($\sim 5 \times 10^{-5}$ atm) also reduced the reliability of the data of Sherwin.

In the theoretical work of Firsov[1] which appeared recently, an estimate is given of the ionization cross section in atomic collisions, starting out from a quasiclassical consideration of the problem of the motion of electrons in the region of overlap of the shells of the colliding atomic particles. The ionization cross section is represented in the form of the approximate formula

$$\sigma = \frac{32.7 \cdot 10^{-16}}{(Z_1 + Z_2)^{2/3}} \left\{ \left[\frac{(Z_1 + Z_2)^{5/3} v}{23.3 \cdot 10^6 \varepsilon_i} \right]^{1/5} - 1 \right\}^2, \qquad (5)$$

where ϵ_i is the ionization energy, while Z_1 and Z_2 are the number of electrons in the ion and in the atom, respectively.

Introducing the characteristic velocity v_0 and the cross section σ_0 for each pair of colliding particles

$$v_0 = \frac{23.3\varepsilon_i}{(Z_1 + Z_2)^{5/3}} \cdot 10^6 \text{ cm/sec},$$

$$\sigma_0 = \frac{32.7}{(Z_1 + Z_2)^{2/3}} \cdot 10^{-16} \text{ cm}^2, \tag{6}$$

Firsov obtained a universal formula for the ionization cross section for an arbitrary pair of colliding particles:

$$\sigma / \sigma_0 = [(v / v_0)^{1/5} - 1]^2. \tag{7}$$

The dependence of σ/σ_0 on v/v_0, given by Eq. (7), is represented in Fig. 6 by the dashed curve. The experimental data for all ion-atom pairs that we investigated are also plotted in the same drawing. As is seen, for heavy ions and atoms (curves 10 — 19), and also for ions and atoms of neon (curves 1, 2, 3), the experimental data are grouped about the theoretical curve. Departures from the theoretical curve, as also for singly-charged ions [1,3] lie within a factor of 2.

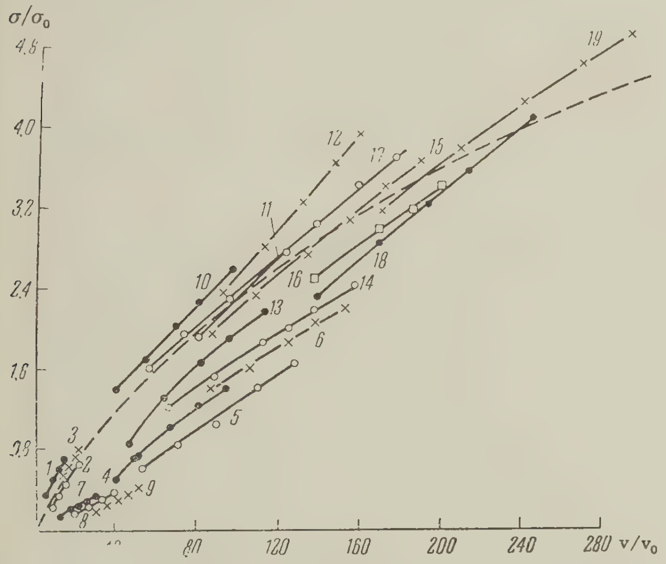

FIG. 6. Universal curve of Firsov (dashed) and experimental data on the ionization of atoms by ions of different charge

1 — Ne^+ — Ne; *2* — Ne^{2+} — Ne; *3* — Ne^{3+} — Ne; *4* — Ne^+ — Kr; *5* — Ne^{2+} — Kr; *6* — Ne^{3+} — Kr; *7* — Kr^+ — Ne; *8* — Kr^{2+} — Ne; *9* — Kr^{3+} — Ne; *10* — Kr^+ — Kr; *11* — Kr^{2+} — Kr; *12* — Kr^{3+} — Kr; *13* — Xe^+ — Kr; *14* — Xe^{2+} — Kr; *15* — Xe^{3+} — Kr; *16* — Xe^{4+} — Kr; *17* — Xe^+ — Xe; *18* — Xe^{2+} — Xe, *19* — Xe^{3+} — Xe

The essential experimental fact obtained in the present work, namely the absence of a significant effect of the charge of the primary ion on the magnitude of the ionization cross section, is in qualitative agreement with the Firsov theory. Actually, inasmuch as Z_1 and Z_2 are large numbers in Eq. (5), a decrease in Z_1 by several units in the case of multiply charged ions should not have a noticeable effect on the magnitude of the ionization cross section. Here it is interesting to observe that the ionization cross section for singly charged ions is as a rule always somewhat larger than for ions with a charge larger than unity (see Fig. 3).

For the cases of ionization of neon by krypton ions, and of krypton by neon ions, the Firsov formula gives cross sections that are too high by a factor of 2 — 4. It is possible that this is connected with the fact that individual peculiarities of the electron structure of the colliding atomic particles are not taken into account in the theory.

With the aim of further investigation of the phenomenon of ionization of gases by ions of different charge, we propose to extend the investigation to ions of elements of other groups of the periodic table, in particular to metallic ions.

In conclusion, the authors express their gratitude to Professor V. M. Dukel'skiĭ for discussion of the results of the research and to A. M. Shchenkov for practical assistance in carrying it out.

---

[1] O. B. Firsov, JETP **36**, 1517 (1959), Soviet Phys. JETP **9**, 1076 (1959).

[2] W. Sherwin, Phys. Rev. **57**, 814 (1940).

[3] N. V. Fedorenko, Usp. Fiz. Nauk **68**, 481 (1959), Soviet Phys. Uspekhi **2**, 526 (1959).

[4] I. P. Flaks and E. S. Solov'ev, J. Tech. Phys. (U.S.S.R.) **28**, 599 (1958), Soviet Phys.-Tech. Phys. **3**, 564 (1958).

[5] I. P. Flaks and E. S. Solov'ev, J. Tech. Phys. (U.S.S.R.) **28**, 612 (1958), Soviet Phys.-Tech. Phys. **3**, 577 (1958).

[6] I. P. Flaks and L. G. Filippenko, J. Tech. Phys. (U.S.S.R.) **29**, 1100 (1959), Soviet Phys.-Tech. Phys. **4**, 1005 (1960).

[7] M. Ardenne, Die Technik **11**, 65 (1956).

[8] Fedorenko, Afrosimov, and Kaminker, J. Tech. Phys. (U.S.S.R.) **26**, 1929 (1956), Soviet Phys.-Tech. Phys. **1**, 1861 (1957).

[9] Fedorenko, Filippenko, and Flaks, J. Tech. Phys. (U.S.S.R.) **30**, 49 (1960), Soviet Phys.-Tech. Phys., in press.

[10] H. B. Gilbody and J. B. Hasted, Proc. Roy. Soc. (London) **A240**, 382 (1957).

[11] M. M. Bredov and N. V. Fedorenko, J. Tech. Phys. (U.S.S.R.) **20**, 1464 (1950).

Translated by R. T. Beyer
145

SOVIET PHYSICS JETP VOLUME 11, NUMBER 3 SEPTEMBER, 1960

RELATIVE γ TRANSITION PROBABILITIES IN STRONGLY DEFORMED NUCLEI

A. V. GNEDICH, L. N. KRYUKOVA, and V. V. MURAV' EVA

Institute of Nuclear Physics, Moscow State University

Submitted to JETP editor September 14, 1959

J. Exptl. Theoret. Phys. (U.S.S.R.) **38**, 726-728 (March, 1960)

The relative intensities of the γ transitions in Lu^{175} and Hf^{177} have been determined from the photoelectron spectra. The discrepancy between the experimental values for the relative γ transition probabilities and the theoretical values derived by the Alaga rules is confirmed. A similar disagreement between the experimental and theoretical values is also found to hold for the Ib^{173} and W^{183} nuclei.

According to the collective model the internal wave functions of different states of the rotational band of strongly deformed nuclei can be assumed to be identical. In this case the ratio of the reduced probabilities of γ transitions going from some given state to various rotational states is found to depend only on geometrical factors, namely the Clebsch-Gordan coefficients (Alaga rules).[1]

We have considered two nuclei with large deformation parameters: Lu^{175} ($\delta = 0.28$) and Hf^{177} ($\delta = 0.26$) (see reference 2). The experimentally established level schemes[3] of Lu^{175} and Hf^{177} are in good agreement with the collective model of the nucleus of Bohr and Mottelson and with the Nilsson scheme.[4] The spins of the ground states and of the excited single particle levels correspond to the spins given by the Nilsson scheme with the corresponding δ. One observes rotational excitation of the ground states as well as single particle states. The deviation of the experimental values of the energy of the rotational levels from the values computed by the rotational formula is very small for both nuclei: $\Delta(E_2/E_1) = 0.5\%$.

However, the relative intensities of the γ lines obtained experimentally with scintillation[5,6] and crystal[7,8] spectrometers are very different from the values given by the Alaga rules. The data of references 5, 6 and 7, 8 are in slight disagreement. But it follows from either set of data that the γ transitions to excited states of the fundamental rotational band are much more intensive than is required by the intensity rules. In Lu^{175} the transitions from the 396 kev level to the first and second rotational states of the fundamental rotational band are faster by a factor of 7 and 55, respectively, than is predicted by the theory. In Hf^{177} the transitions from the 321 kev level to the first and second excited rotational states are faster by a factor of 1060 and 2200, respectively.

For a confirmation of this fact we have determined the relative intensities of the above-mentioned transitions by a different method. We took the photoelectron spectra of Yb^{175} and Lu^{177} with a magnetic lens spectrometer with a resolution of 0.5%. We used lead targets with the thickness 1.9 and 4.5 mg/cm^2 for Yb^{175} and 2.2 mg/cm^2 for Lu^{177}. The relative intensities were determined by the areas under the photoelectron lines with account of the experimentally established spectral sensitivity of the apparatus. The values of the relative intensities of the transitions under consideration are given in Table I.

It is seen from this table that our data are not in disagreement with the data obtained by other methods and, therefore, confirm the discrepancy between experiment and theory. In an effort to find analogous cases of disagreement between the experimental and theoretical values of the relative intensities we have investigated all nuclei with odd mass numbers in the region $150 < A < 192$. Owing to the insufficient amount of experimental data, we were able to choose only six nuclei for which it was possible to verify the above-mentioned intensity rules (we considered the ratio of the intensities of the competing transitions to the ground state and to the first two rotational levels from a level which does not belong to the basic rotational band E_0).

Some of the data relative to the nuclei under consideration are listed in Table II. It appears that only for two (Ta^{181}, Re^{187}) of the six nuclei do the relative intensities of the γ transitions conform to the Alaga rules. In the case of four nuclei (Yb^{173}, Lu^{175}, Hf^{177}, W^{183}) we observe considerable disagreement with the theory. It is interesting to note that the deviation from the theoretical values has uniform character: the transitions to the rotational states are faster than is predicted

TABLE I

Nucleus	E_γ, kev	Relative intensities of the lines		
		on the crystal spectrometer	on the scintillation spectrometer	on the magnetic spectrometer
		7, 8	5, 6	our data
Lu^{175}	396	100	100	100
	283	62	43	61
	145	5.9	2	13
Hf^{177}	321	100	100	100
	208	7300	1500	6000
	71	67	10	*

*Because of the x-radiation of Pb and Hf in the neighborhood of the photoelectron lines, it was impossible to separate the photoelectron L line for $E_\gamma = 71$ kev.

TABLE II

Nucleus	Deformation parameter, δ (reference 2)	Ratio of the intensities of the γ transitions $I_{\gamma_1} : I_{\gamma_2} : I_{\gamma_3}$ *		E_0 kev	Enhancement coefficient of the transitions	
		theoretical by Alaga's rules	experimental**		f_2	f_3
${}_{70}Yb^{173}_{103}$	0.29	100 : 14 : 0.43 (for $E1$)	100 : 1600 : 290 [11]	351	114	675
${}_{71}Lu^{175}_{104}$	0.28	100 : 8,3 : 0.108 (for $E1$)	100 : 71 : 7.5 [7]	396	8.5	70
${}_{72}Hf^{177}_{105}$	0.26	100 : 6.1 : 0.025 (for $E1$)	100 : 9700 : 83 [8]	321	1600	3300
${}_{73}Ta^{181}_{108}$	0.23	100 : 15 (for $E2$)	100 : 17 [12]	482	1.1	
${}_{74}W^{183}_{109}$	0.21	100 : 36.2 : 2.4 (for $M1$)	100 : 910 : 273 [12]	209	25	114
${}_{75}Re^{187}_{112}$	0.19	100 : 21 (for $E1$)	100 : 21 [12]	686	1	

*$\gamma_1, \gamma_2, \gamma_3$ are the transitions to the ground, first excited rotational, and second excited rotational states, respectively.

**With account of conversion and the composition of the multipole mixture.

by the intensity rules, where the enhancement coefficent* of the transition to the second rotational level is greater than that for the transition to the first level. It may be noted that all transitions which violate the intensity rules are accompanied by a change of K by −1. We have been unable to detect regularities with respect to any other quantum numbers.

The fact that the transition rates to the rotational state in the nuclei Lu^{175} and Hf^{177} are enhanced was noted by Marmier and Boehm[8] and also by Chase and Wilets.[9] Attempts were made to explain this enhancement by the argument that the E1 transitions are forbidden by the asymptotic quantum numbers but that the rotational motion leads to a certain violation of this forbiddenness rule. However, we do not find this a convincing explanation. Apparently there is some other reason for the systematic violation of the intensity rules. It may be that the adiabatic approximation which has been used in the derivation of the intensity rules is not applicable for the nuclei under consideration. In particular, the violation of the adiabatic hypothesis may lead to the mixing of states with different K.[1] Similar instances of inaccurate theoretical values of the relative intensities of the γ transitions are also observed in a number of even-even nuclei. Davydov and Filippov[10] showed that the asymmetry of the equilibrium shape of the nucleus may lead to the violation of the Alaga intensity rules in even-even nuclei. Analogous calculations for nuclei with odd A are not available.

---

*By enhancement coefficient we mean the ratio of the experimental value of the relative intensity of a given γ transition to the theoretical value.

[1] Alaga, Alder, Bohr, and Mottelson, Kgl. Danske Videnskab. Selskab, Mat.-Fys. Medd. **29**, No. 9 (1955).

[2] B. Mottelson and S. G. Nilsson, Phys. Rev. **99**, 1615 (1955).

[3] Strominger, Hollander, and Seaborg, Tables of Isotopes, Revs. Modern Phys. **30**, 585 (1958).

[4] S. G. Nilsson, Kl. Danske Videnskab. Selskab, Mat.-Fys. Medd. **29**, No. 16 (1955).

[5] Mize, Bunker, and Starner, Phys. Rev. **100**, 1390 (1955).

[6] P. S. Ofer, Nucl. Phys. **3**, 479 (1957).

[7] Hatch, Boehm, Marmier, and Du Mond, Phys. Rev. **104**, 745 (1956).

[8] P. Marmier and F. Boehm, Phys. Rev. **97**, 103 (1955).

[9] D. M. Chase and L. Wilets, Phys. Rev. **101**, 1038 (1956).

[10] A. S. Davydov and G. F. Filippov, JETP **35**, 440 (1958), Soviet Phys. JETP **8**, 303 (1959).

[11] Dzhelepov, Preobrazhenskiĭ, and Sergienko, Izv. Akad. Nauk SSSR, Ser. Fiz. **22**, 795 (1958), Columbia Tech. Transl. p. 789.

[12] B. S. Dzhelepov and L. K. Peker, Схемы распада радиоактивных ядер (Decay Schemes of Radioactive Nuclei), Acad. Sci. Press, M.-L., 1958.

Translated by R. Lipperheide
146

SOVIET PHYSICS JETP VOLUME 11, NUMBER 3 SEPTEMBER, 1960

SPIN-LATTICE RELAXATION IN CHROMIUM CORUNDUM

A. A. MANENKOV and A. M. PROKHOROV

P. N. Lebedev Physics Institute, Academy of Sciences, U.S.S.R.

Submitted to JETP editor September 15, 1959

J. Exptl. Theoret. Phys. (U.S.S.R.) **38**, 729-733 (March, 1960)

Spin-lattice relaxation of Cr^{3+} ions in corundum single crystals was studied at temperatures of 290, 77 and 4.2°K and at various magnetic dilutions. Continuous saturation of paramagnetic resonance absorption at a frequency of 9375 Mcs was employed. The spin-lattice relaxation times T_1, determined from the saturation of the lines of various electronic transitions, were found to depend on the degree of magnetic dilution. T_1 varies between $10^{-5} - 10^{-6}$ sec for $T = 77°K$ and between $10^{-2} - 10^{-5}$ sec for $T = 4.2°K$ when the Cr^{3+} ion concentration increases with respect to that of the Al^{3+} ions from $\sim 5 \times 10^{-4}$ to 6×10^{-3}. For a sample with a large magnetic dilution, the magnitude of T_1 at $T = 4.2°K$ depends on the saturating power, increasing with increase of the latter. The anomalous character of spin-lattice relaxation in chromium corundum is probably connected with energy transfer processes from the spin system to the thermostat (liquid helium) such as spin-phonon interaction, including phonon diffusion processes and transfer of energy from the lattice to the thermostat.

1. INTRODUCTION

INTEREST in the study of relaxation processes in paramagnets has recently developed in connection with the development of masers. Relaxation phenomena are also of great physical interest in themselves.

The theory of spin-lattice relaxation developed earlier by Kronig and van Vleck was in the main confirmed by the experiments on non-resonance paramagnetic absorption by Gorter and his collaborators, and also by some experiments on the saturation of paramagnetic resonance absorption (see, for example, references 1 and 2 and the bibliography contained in them). Recently "anomalous" spin-lattice relaxation effects have been observed in some paramagnetic crystals at very low temperatures (< 4°K).[1,2] It appeared that the spin-lattice relaxation time could not be explained on the basis of the Kronig-van Vleck theory. In particular, the theory does not explain the temperature and concentration dependence of the relaxation time.

To explain the observed anomalies, Gorter, Townes, Strandberg, Anderson* and others[1-3] put forward various hypotheses based on the assumption that the mechanism of transfer of the phonon energy to the thermostat (liquid helium) plays an important (sometimes dominant) part at low temperatures. Although some experimental data can be explained qualitatively by this mechanism, we should point out that the whole range of data on relaxation at low temperatures could not be explained on the basis of these hypotheses. At present, no rigorous quantitative theory of spin-lattice relaxation has been developed which describes the anomalous low temperature effects mentioned. For such a theory to be developed it is now very necessary to collect experimental data on spin-lattice relaxation over a wide temperature range, especially at low temperatures.

In the present work we present results of an investigation of spin-lattice relaxation of Cr^{3+} ions in single crystals of corundum (Al_2O_3) by the method of continuous saturation. The measurements were made at a frequency of 9375 Mcs at room temperature, liquid nitrogen and liquid helium temperatures. The effect of saturation of different electronic transitions of the "parallel" Cr^{3+} spectrum (see figure) was studied, i.e., for the external steady magnetic field parallel to the trigonal axis of the crystalline electric field.

2. EXPERIMENTAL METHOD

The single crystal specimens of chromium corundum ($Al_2O_3 \cdot Cr_2O_3$) had chromium concentrations (expressed as the ratio of the number of Cr^{3+} ions to the number of Al^{3+} ions, which formed the diamagnetic diluent) 2.2×10^{-5}, 1.5×10^{-4}, 5.3×10^{-4}, 0.9×10^{-3}, 4×10^{-3}, and 6.5×10^{-3}, and were grown from the melt by the Verneuil

---

*Paper delivered by P. Anderson at the Physics Institute, Academy of Sciences, U.S.S.R., 1959.

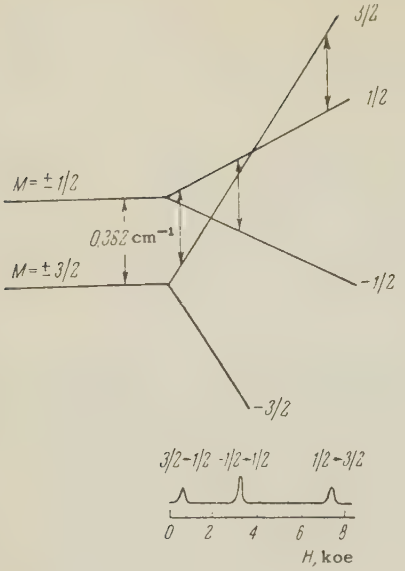

Energy levels and paramagnetic resonance spectrum for Cr^{3+} in corundum, observed at a frequency of 9375 Mcs for parallel orientation of the trigonal axis. The arrows show the electronic transitions corresponding to the spectrum observed.

process. Observation of the effect of saturation in the paramagnetic resonance spectrum of Cr^{3+} was made with a superheterodyne radio-spectrometer, similar to that described by us previously.[4] An automatic tuner and a special resonator with variable coupling are used to observe the resonance lines at low temperatures.[5]

The method of measuring the effect of saturation was the usual one, and consisted of measuring the line intensity of the absorption for various microwave power levels fed to the resonator. As is well known, when saturation occurs, the absorption line intensity is given by the relation

$$J = J_0/(1+\beta). \tag{1}$$

where J_0 is the intensity in the absence of saturation and β is the saturation factor equal to $2\gamma^2 H_1^2 T_1 T_2 w$, γ being the gyromagnetic ratio, H_1 the intensity of the microwave magnetic field in the resonator, T_1 the spin-lattice relaxation time, T_2 the spin-spin relaxation time, and w the square of the matrix element of the spin operator for the corresponding electronic transition. Two methods were used for determining the saturation factor. In the first β was determined from the ratio of the intensities of the Cr^{3+} resonance line for different levels of power fed to the resonator for constant power applied to the mixer of the superheterodyne receiver. In the second method β was determined from the ratio of intensities of the absorption line to an absorption line of a standard, the free radical diphenylpicrilhydrazine (DPPH), a specimen of which was included in the resonator with the substance under investigation. Our measurements showed that the DPPH line is not saturated at microwave power levels for which strong saturation of the Cr^{3+} line in corundum is observed. At T = 4.2°K the DPPH line is noticeably saturated for a power of about 30 mw and a loaded-resonator Q of 12×10^3. The saturation factor for the DPPH line was then 0.5.

The specimens were placed in the resonator in pairs to increase the accuracy of the determination of the relaxation times for different Cr^{3+} concentrations. The symmetry axes of the specimens were inclined at a small angle to one another (about 10°) to prevent coincidence of the absorption lines. The saturation factors were measured on the two specimens for the same power level, and parallel orientations for each was achieved by rotating the magnet, thus avoiding detuning of the resonator, which usually happens when the specimen is rotated inside. We checked the linearity of the radiospectrometer for all measurements (i.e., the dependence of the amplitude of the output signal to the oscillator on the power absorbed at resonance). Linearity was preserved in all cases, i.e., the absorption signal observed on the oscilloscope was proportional to the magnitude of the absorption coefficient (i.e., the imaginary part of the susceptibility — χ'').

The relaxation time is determined by the relation which follows from (1):

$$T_1 T_2 = 10^{-7}\nu V\beta/8\gamma^2 w Q P, \tag{2}$$

where ν is the frequency (cps) of the microwave source, V the volume (cc) of the resonator, Q the figure of merit of the loaded resonator, and P the power (w) fed to the resonator.

3. RESULTS AND DISCUSSION

As can be seen from Eq. (2), the spin-lattice relaxation time T_1 can be calculated if T_2 is known. T_2 can be derived from the line width if this is determined by homogeneous spin-spin interactions. However, for small Cr^{3+} concentrations the main contribution to the line width comes from the interaction of Cr^{3+} with Al^{27} nuclei, which leads to an inhomogeneous line broadening. As Portis[6] has shown, a formula different from (1) must be used for T_1, and T_2 must be determined only from the spin-spin width and not from the full line width. However, our investigation showed that the saturation effect in the Cr^{3+} line in corundum followed (1),[*] i.e., we must assume that the value of T_2 in (1) and (2) is determined

---

[*] This test was made on specimens 3 and 4 (see Table II) at a temperature of 77° K. See below for deviations from equation (1) at T = 4.2° K.

TABLE I. Relaxation time of Cr^{3+} in corundum for a specimen with relative concentration $Cr:Al = 5.3 \times 10^{-4}$

Transition	$T_1 \times 2.5$, sec			T_2, sec
	T,° K = 293	77	4,2	
$-{}^1/_2 \rightarrow +{}^1/_2$	$6.1 \cdot 10^{-6}$	$3.2 \cdot 10^{-4}$	$1.1 \cdot 10^{-1}$ *	$7.1 \cdot 10^{-9}$
${}^3/_2 \rightarrow {}^1/_2$	$8.4 \cdot 10^{-6}$	$4.5 \cdot 10^{-4}$	$2.7 \cdot 10^{-1}$ **	$5.5 \cdot 10^{-9}$
${}^1/_2 \rightarrow {}^3/_2$	$6.6 \cdot 10^{-6}$	$3.5 \cdot 10^{-4}$	—	$5.5 \cdot 10^{-9}$

*T_1 determined for a saturation factor $\beta = 1$.
**T_1 determined for a saturation factor $\beta = 1.5$.

TABLE II. Relaxation time of Cr^{3+} in corundum for specimens of various chromium concentrations. Electronic transition $-\frac{1}{2} \longrightarrow +\frac{1}{2}$

Specimen No.	Relative concentration	$T_1 \times 2.5$, sec			$T_2 \times 10^9$, sec
		T,° K = 293	77	4.2	
1	$2.2 \cdot 10^{-5}$	$5.3 \cdot 10^{-6}$	—	—	9.5
2	$1.5 \cdot 10^{-4}$	$5.0 \cdot 10^{-6}$	$3.8 \cdot 10^{-4}$	—	8.4
3	$5.3 \cdot 10^{-4}$	$6.1 \cdot 10^{-6}$	$3.2 \cdot 10^{-4}$	$1.1 \cdot 10^{-1}$*	7.1
4	$0.9 \cdot 10^{-3}$	$4.1 \cdot 10^{-6}$	$2.1 \cdot 10^{-4}$	$1.6 \cdot 10^{-2}$	6.0
5	$4 \cdot 10^{-3}$	—	$6.6 \cdot 10^{-5}$	$1.5 \cdot 10^{-3}$	2.9
6	$6.5 \cdot 10^{-3}$	—	$1.0 \cdot 10^{-5}$	$1.7 \cdot 10^{-4}$	1.3

*T_1 determined for a saturation factor $\beta = 1$.

by the full line width. Townes and his co-workers found an analogous situation in the effect of saturation for Cr^{3+} in cyanide.[2] We shall not discuss this effect here, although it is of interest in itself from the point of view of explaining the mechanism of saturation of the paramagnetic resonance line. Using the known line width to determine T_2,* we have in this way applied the experimental data on the saturation factors to determine the relaxation time of Cr^{3+} in corundum. These data are given in Tables I and II.

It can be seen from Table I that the values of T_1 corresponding to all three observed transitions of the "parallel" spectrum are not very different from one another. We should point out that because of the high relative accuracy of the measurements, the small differences in T_1, for different transitions at the same temperature, are outside the limits of error.

The small differences of T_1 for different transitions can be explained by considering the mechanism of saturation and spin-lattice relaxation in a system with many energy levels, as occurs for Cr^{3+} ions (four spin levels, corresponding to the electron spin $S = {}^3/_2$). In experiments on saturation, the equilibrium distribution of the paramagnetic ions among the levels (the Boltzmann distribution) during the saturation of one transition is achieved in the spin-lattice relaxation time T_1, which depends on the probability of relaxation transitions between all the spin energy levels of the given paramagnetic ions. The relaxation can be considered to take place via all levels. For multi-level systems, the relaxation time T_1 derived from experiments on saturation will therefore be an average over the relaxation transitions between all levels. It is then clear that although the probabilities of relaxation transitions between different levels may be very different, the difference between the values of T_1, determined by saturation of the lines of the corresponding transitions, may be small, as occurs for Cr^{3+} in corundum.

It can be seen from Table I that the temperature dependence of T_1 is slight, indicating that even at fairly high temperatures first order processes play an appreciable part in spin-lattice relaxation. The strong dependence of T_1 on Cr^{3+} concentration is unexpected (see Table II) and this dependence is different at different temperatures. The dependence of T_1 on concentration at $T = 4.2$°K is considerably greater than at $T = 77$°K. In addition, there is a departure from (1) for the effect of saturation at 4.2°K in specimens with large magnetic dilution. In specimen 3 (Table II) the value of β/P does not remain constant as β changes from 0.5 to 5, but increases by more than a factor of two. For the more concentrated specimen 4, the value of β/P does not change as β varies from 0.8 to 4.5.

---

*We have used the Lorentz formula for the line to calculate T_2, $T_2 = 1/\pi\Delta\nu$, where $\Delta\nu$ is the half-width in the absence of saturation, although in chromium corundum the lines lie between the Lorentz and Gauss shapes.[7] However, since the values of T_2 for Lorentz and Gauss lines are little different, and the line shape is very little dependent on Cr^{3+} concentration,[7] we have used Eq. (1) for T_2.

The experimental results obtained cannot be explained by the usual theory of spin-lattice relaxation. One must suppose that energy transfer processes from the spin system to the thermostat (liquid helium) are important, such as spin-phonon interaction, including phonon diffusion processes and energy transfer from the lattice to the thermostat. These anomalous relaxation processes in corundum are surprising as it has a high thermal conductivity, in contrast to crystals studied earlier in which such anomalous relaxation processes are found.[1,2]

The authors thank A. S. Bebchuk, R. P. Bashuk and L. M. Kharitonova for providing the chromium corundum single crystal specimens.

[1] Gorter, van der Marel, and Bölger, Physica **21**, 103 (1955); van der Marel, van der Broek, and Gorter, Physica **23**, 361 (1957); **24**, 101 (1958).

[2] Giordmaine, Alsop, Nash, and Townes, Phys. Rev. **109**, 320 (1958).

[3] M. W. Strandberg, Phys. Rev. **110**, 65 (1958).

[4] A. A. Manenkov and A. M. Prokhorov, Радиотехника и электроника (Radio Engg. and Electronics) **1**, 469 (1956).

[5] A. A. Manenkov, Paper presented at Conference on Paramagnetic Resonance, Kazan', June 1959.

[6] A. M. Portis, Phys. Rev. **91**, 1071 (1953)

[7] A. A. Manenkov and V. B. Fedorov, Paper presented at the Conference on Paramagnetic Resonance, Kazan', June 1959.

Translated by R. Berman
147

SOVIET PHYSICS JETP VOLUME 11, NUMBER 3 SEPTEMBER, 1960

*ELASTIC SCATTERING OF 128- AND 162-Mev NEGATIVE PIONS BY PROTONS**

Yu. A. BUDAGOV, S. WIKTOR, V. P. DZHELEPOV, P. F. ERMOLOV, and V. I. MOSKALEV

Joint Institute for Nuclear Research

Submitted to JETP editor September 18, 1959

J. Exptl. Theoret. Phys. (U.S.S.R.) 38, 734-746 (March, 1960)

A hydrogen-filled diffusion cloud chamber in a magnetic field was used to measure the angular distribution of 128 and 162-Mev negative pions elastically scattered on protons. The total elastic scattering cross sections for these energies are $(12.8 \pm 1.0) \times 10^{-27}$ and $(21.4 \pm 1.2) \times 10^{-27}$ cm^2, respectively. The angular distribution has the form $a + b \cos\theta + c \cos^2\theta$ with the coefficients given in Sec. 5d. At the above energies the real parts of the forward scattering amplitudes (in the c.m.s.) in $\hbar/m_\pi c$ units are 0.216 ± 0.031 and 0.216 ± 0.033, respectively. These values agree with those computed from the dispersion relations with a coupling constant $f^2 = 0.08$.

1. INTRODUCTION

MUCH attention has been paid recently to an experimental verification of dispersion relations. For the scattering of charged pions by protons, the dispersion relations were obtained first by Goldberger, Miyazawa and Oehme.[1] These relations connect the real parts of the forward scattering amplitudes with the lengths of the S scattering and the integral over the total cross sections of π^+-p and π^--p interactions over the entire range of energies. In the integration interval $0 \leqslant \omega < \mu$ a contribution exists from the "bound state," i.e., a contribution from the neutron, as a possible intermediate state of the system in scattering. This contribution can be expressed in terms of a renormalization coupling constant f^2, characterizing the pseudo-vector interaction. The derivation of the dispersion relations is also based on general physical principles, such as the principle of microscopic causality (the requirement that there be no signals propagating with a velocity greater than that of light) and the hypothesis of charge independence of nuclear forces. The correctness of these fundamental assumptions can be verified by comparison with the experimental results. It is also possible to determine independently the coupling constant and the S-scattering lengths.

A comparison of the dispersion relation with experiment, initially performed by Anderson, Davidon, and Kruse,[2] has shown good agreement. However, in 1957 Puppi and Stanghellini[3] called attention to the fact that for negative pions one observes a discrepancy between the experimental and theoretical data. While for positive pions the real parts of the forward scattering amplitudes, determined experimentally in the energy interval up to 400 Mev, were in agreement with those calculated from the dispersion relations with a coupling constant $f^2 = 0.09 \pm 0.01$, for negative pions in the energy interval up to 200 Mev, better agreement is obtained if the coupling constant is taken to be $f^2 = 0.04$. It was shown at the same time by Agodi, Cini, and Vitale[4] that effects dependent on the charge, electromagnetic corrections, and the contribution due to hyperons and K mesons cannot explain the observed discrepancy. On the other hand, as is seen from the original work by Puppi and Stanghellini,[3] this discrepancy is based essentially on the results of one experiment — the measurements of elastic π^--p scattering by the Carnegie Institute group[5] at a π^--meson energy of 150 and 170 Mev, since the remaining experimental data have in this energy region a relatively low accuracy. In this connection, the obtaining of new experimental data on elastic π^--p scattering in the energy range from 100 to 200 Mev, and a comparison of these data with the prediction of the dispersion relations, are of undoubted interest.

In the present article we report on the measurement of elastic scattering of negative pions by protons with energies 128 and 162 Mev, obtained with the aid of a hydrogen diffusion chamber. The use of such a procedure has made it possible to avoid many specific experimental difficulties, connected with the use of electronic measurement methods, and made it also possible to operate with smaller scattering angles, an important factor in the determination of the value of the differential scattering cross section at 0° angle.

---

*This work was reported upon at the 6th session of the Scientific Council of the Joint Institute for Nuclear Research (May, 1959) and at the Conference on the Physics of High-Energy Particles in Kiev (June, 1959).

2. EXPERIMENTAL CONDITIONS AND APPARATUS

Experimental setup. A diagram of the experimental setup is shown in Fig. 1. A beryllium target 3, 40 mm thick, was placed in the internal beam 2 (670 Mev) of the synchrocyclotron of the Laboratory of Nuclear Problems of the Joint Institute for Nuclear Research. The negative pions generated in the target (4) were extracted from the vacuum chamber 1 by the magnetic field, passed through additional concrete shield 5, and were collimated by collimator 6, 3.6 meters long with inside diameter 50 mm, built in shielding wall 7. The negative-pion beam was then deflected by clearing magnet 8 by 40° and entered the diffusion chamber 11, placed inside electromagnet 10. An additional lead collimator 9, with a rectangular opening 350 × 50 mm, was placed in front of the chamber. The negative-pion beam was guided in the usual manner by a flexible current-carrying filament. A total of 90,000 stereophotographs was obtained with the hydrogen chamber. This material, along with the elastic π^--p scattering considered in this article, has made it possible to observe the β decay of negative pions[6] ($\pi^- \rightarrow e^- + \bar{\nu}$) and to obtain certain data on the decays of neutral pions via the schemes $\pi^0 \rightarrow e^- + e^+ + \gamma$ (reference 7) and $\pi^0 \rightarrow 2e^- + 2e^+$ (reference 8).

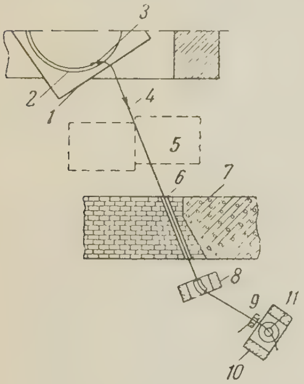

FIG. 1. Diagram of experimental setup.

Diffusion chamber. The diffusion chamber was constructed to operate with light gases at pressures up to 25 atm (reference 9). A schematic diagram of this chamber, placed in a magnet, is shown in Fig. 2. The chamber is built of stainless steel and comprises a three-part vessel. In the lower (principal) part of the chamber the required temperature gradient is produced with the aid of a system of heaters and a coil carrying cooled acetone. In the lower flange of the middle portion of the chamber there is a small trough for methyl alcohol, which is the working liquid of the chamber. At a bottom temperature of −70° and a trough temperature of +10° C, the temperature distribution produced in the sensitive volume of the chamber is approximately linear with a gradient of 7 deg/cm. The height of the sensitive layer becomes in this case 6 or 7 cm. The temperature is controlled and measured in various portions of the chamber with the aid of copper-constantan thermocouples.

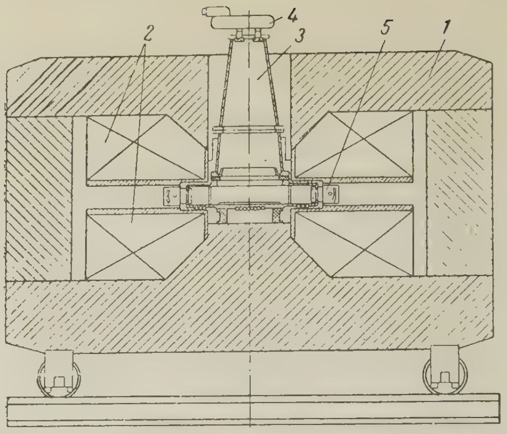

FIG. 2. Schematic diagram of the diffusion chamber, located in a solenoid magnet MS-4A. 1 – armature of electromagnet, 2 – coils, 3 – diffusion chamber, 4 – stereo camera, 5 – illuminators.

The chamber was illuminated at an angle of 90° to the photography axis through side windows, covered with plexiglas plates 30 mm thick. These windows were mounted on the ends of rectangular projections 150 mm long, welded to the lower cylindrical portion of the chamber, so that the working diameter of the chamber (380 mm) could be increased to a maximum for the specified opening diameter of 460 mm in the upper pole of the magnet.

The chamber was illuminated by two pulsed xenon lamps IFP-500, through which 200 microfarad capacitors, charged to 2000 volts, were discharged at the instant of flash. The light from each lamp was shaped into a parallel beam by two parabolic reflectors.

The photography was by means of a stereo camera with two "Gelios-37" GOI (State Optical Institute) lenses, of 62 mm focal length; Pankhrom-X 35 mm film, with a speed of 1000 GOST units, was used. The lens resolution was 50 lines per mm in the center of the field of view. The base of the stereo camera was 120 mm, and the photographs were taken from a distance of approximately 1 mm. The necessary depth of the photographed volumes was reached at a diaphragm setting of 5.6.

The operating cycle of the camera usually lasted eight seconds. The control of the time cycle was by means of an electronic system which performed the following principal operations: a) turning on the high-frequency voltage on the dee of the synchrocyclotron for a fixed number of cycles (usually 2 — 4); b) firing the pulse lamps at a delay of 0.2 — 0.3 seconds relative to the particle pulse; c) advancing the film; d) turning the electric clearing field on and off. The necessary time delays between operations were produced by monovibrator circuits. The beam intensity was maintained by adjusting the number of cycles of acceleration in such a way that in each photograph approximately 30 negative pion tracks were registered.

Electromagnet. A constant electromagnetic field of 9000 gauss was produced in the working volume of the chamber by a solenoid magnet of type MS-4A,* designed to operate both with dc and with pulsed excitation. The magnetic field was homogeneous within 3.5% along the height of the sensitive volume of the chamber and within 2.5% along the radius. The magnetization curve and the drop in magnetic field along the height and radius of the sensitive volume were plotted with a magnetometer, operating on the Hall-effect principle.† The instrument was calibrated by the proton-resonance method.

Negative-pion beams. The average meson energy in the beam and the energy spread were determined directly by measuring the radii of curvatures of the tracks in the photographs. To reduce the track distortion due to convection currents in the chamber, the measurements were made on films exposed with the ignition of the pulsed lamp delayed by approximately half the usual time. The energies determined in this manner were (128 ± 8) and (162 ± 10) Mev, where the indicated indeterminacies represent the half width of the energy distribution of the negative pions in the chamber.

To determine the admixture of μ^- mesons and electrons in the beam, and also to monitor the energy, absorption curves in copper were plotted by means of scintillation counters. The average energies of the beam, determined by these two methods, agreed with good accuracy. The total impurity of μ^- mesons and electrons in the beams amounted to (16 ± 2)%.

3. SCANNING OF PHOTOGRAPHS AND DATA REDUCTION

The photographs obtained were scanned with stereoscopes. All the films were scanned twice by several workers independently. Some of the films were scanned a third time with particular care, to estimate the effectiveness of the double scanning, which was found to be 97%. An investigation of the angular distributions of the omitted cases has shown that this effectiveness does not depend on the specific type of scattering event (scattering angle or azimuth angle).

As a result of a double scanning, 379 scattering events were observed at 128 Mev and 1113 cases at 162 Mev. The processing of these events was carried out by the reprojection method. Both frames of the stereoscopic pair were reprojected through the same optical system, with which the photographs were taken on a screen provided with an angle-measuring device. The structure of the reprojector is analogous to that described in reference 10. For each case of scattering, the following were measured: a) coordinates of the point of interaction (x, y, z) and the coordinates z_0 of the reference marker on the bottom of the chamber; b) scattering angles of the meson, θ_π, and of the recoil proton θ_p, accurate to approximately 1°); c) azimuth angle φ of the scattering plane, accurate to approximately 2° ($\varphi = 0$ corresponds to the case when the scattering plane is horizontal); d) range of recoil proton (in those cases where this was possible).

The coordinates x, y, and z were corrected for shrinkage of the film, usually amounting to 5 — 7%. For each case this correction was determined as a ratio of the true distance from the bottom of the chamber to the principal point of the objective and that measured. The effect of film shrinkage on the measurement of angles θ and φ was very small and was neglected.

Simultaneously with processing the scattering event, we measured on the same frame the z coordinate of the track of the random negative pion. A comparison of the distributions over the altitude of the sensitive volume, h, of the scattering cases with the corresponding distributions of the same number of random tracks has shown that there was no noticeable omission in the scanning of scattering cases, located near the bottom of the chamber and near the upper boundary of the sensitive layer (Fig. 3).

For further analysis we selected the events that satisfy the following criteria:

1. The particle tracks must be coplanar accurate to 2°, i.e., the angle between any one track

---

*The solenoid magnet MS-4A is a modification of the MS-4 magnet. These magnets were developed at the ÉFA Scientific Research Institute by N. S. Strel'tsov, A. V. Ugamm, N. N. Indyukov, Yu. P. Semenov, V. I. Sergeeva, and A. G. Studennikova.

†The authors are grateful to D. P. Vasilevskaya and Yu. N. Denisov for allowing them to use this instrument.

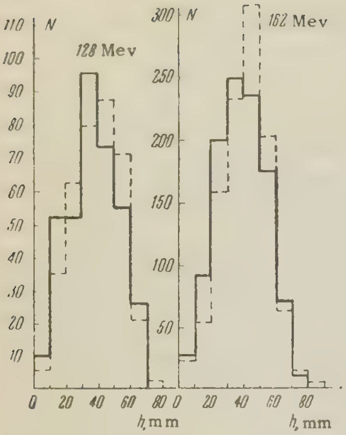

FIG. 3. Distribution of cases of elastic scattering (solid line) and of an equal number of random tracks of negative pions (dotted line) over the height h of the sensitive layer.

and the plane formed by two others must not exceed 2°.

2. The scattering angles of the negative pion and of the recoil proton should satisfy the kinematic requirements accurate to 2°; the curvatures of the tracks, the ionization density, and the recoil-proton range (in those cases when it can be measured) should also correspond to the kinematics.

3. The scattering angle of the negative pions should be more than 8° (laboratory system) (10° c.m.s.) i.e., greater than the maximum angle in π^--μ^- decay.

4. The length of each of the three tracks should be not less than 5 mm.

5. The point of interaction should not be located in an insensitive region measuring more than 5 mm or obscured by an accumulation of drops measuring more than 5 mm.

6. The point of interaction should be more than 1 cm away from the chamber walls.

7. The incoming negative pions should not be deflected from the principal direction of the beam by more than 5°.

8. Cases on frames having any defects and on frames with very large intensity were disregarded.

The foregoing selection rules were satisfied by 344 scattering events at 128 Mev and 941 events at 162 Mev. All further results on the angular distributions are based on this statistical material.

4. TOTAL ELASTIC SCATTERING CROSS SECTIONS

The total elastic π^--p scattering cross sections were determined by calculating the total length of the negative pion tracks. The calculation was made in the rectangular region S, separated in the central portion of the chamber (Fig. 4). In this region we counted all the scattering events satisfying the foregoing selection criteria. The coefficients β, which take into account failures to register cases whose scattering plane was close to vertical, were determined from the distributions over the azimuth angle φ, plotted for these cases (Fig. 5).

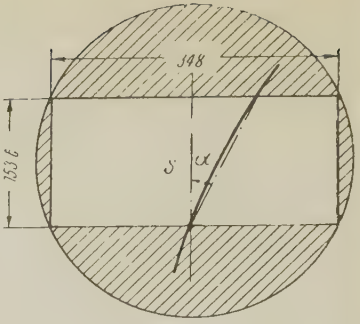

FIG. 4. Region S, separated in the chamber to calculate the total cross section of the elastic scattering.

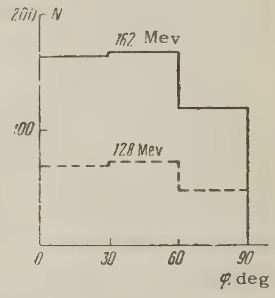

FIG. 5. Distribution of the scattering events located in region S over the axlmuth angle φ.

The total number of tracks in the region S was determined by counting the tracks in all frames whose number was a multiple of 25; the resultant figure was multiplied by 25 and corrected for the number of tracks located on the frames at the end of each film. The total track length L (cm) is given by the formula

$$L = 15.36\,T\delta / \cos\alpha_{\mathrm{av}}, \qquad (1)$$

where T is the total number of tracks, 15.36 is the width of the region S (in centimeters), α_{av} — the average angle of inclination of tracks relative to the edges of the region S (Fig. 4), and δ is a coefficient, that takes into account the substitution of a chord for the length of the arc (in our case we assumed $\delta = 1$). A correction was introduced in the total track length for broken tracks, the lengths of which were measured directly when counting the number of tracks. This correction does not exceed 4%. The total cross sections were determined from the formula

$$\sigma_{\mathrm{exp}} = N\beta / L n_{\mathrm{eff}} (1 - q)\, r, \qquad (2)$$

where N and L are the number of scattering events and the total track length; n_{eff} — effective number of hydrogen nuclei in one cubic centimeter; β is the coefficient that accounts for failure to register cases with φ near to 90°; q is the impurity of μ^- mesons and electrons in the beam; r is the film scanning efficiency. Table I lists the quantities used to calculate the total cross

TABLE I. Determination of total elastic-scattering cross sections

	128 Mev		162 Mev	
	Quantity	Δ, %	Quantity	Δ, %
Number N of scattering events in the region S	190	±7.2	449	±4.7
Correction for φ inefficiency, β	1.13	±2.5	1,10	±1.5
Total number of tracks, T	$0.991 \cdot 10^6$		$1.446 \cdot 10^6$	
Total length of tracks, L	$15.3 \cdot 10^6$ cm	±1	$22.3 \cdot 10^6$ cm	±1
Effective pressure in the chamber, p_{eff}	22.5 atm		23.0 atm	
Number of nuclei per cubic centimeter, n_{eff}, at a pressure p_{eff}	$1.22 \cdot 10^{21}$ cm^{-3}	±2	$1.24 \cdot 10^{21}$ cm^{-3}	±2
Admixture of μ^- mesons and electrons in beam, q	0,16	±2	0,16	±2
Scanning efficiency, r	0,97	±1	0,97	±1
Total cross section, σ_{exp}	$14.2 \cdot 10^{-27}$ cm^2	±8.2	$22.2 \cdot 10^{-27}$ cm^2	±5.8
Total cross section of Coulomb scattering by angles $\theta > 8°$ (l.s.)	$1.6 \cdot 10^{-27}$ cm^2		$1.1 \cdot 10^{-27}$ cm^2	
Correction for scattering in the angle interval $\theta < 8°$ (l.s.)	$0.24 \cdot 10^{-27}$ cm^2		$0.35 \cdot 10^{-27}$ cm^2	
Total elastic scattering cross section, σ_{el}	$12.8 \cdot 10^{-27}$ cm^2	±8.2	$21.4 \cdot 10^{-27}$ cm^2	±5.8

sections, along with the absolute mean-square error Δ (in percent). After subtracting the Coulomb corrections from the cross sections calculated by formula (2) (the method of calculating these corrections is given in Sec. 5b) and introducing corrections for scattering in the angle interval from 0 to 8° (laboratory system) (Table I), we obtain the total cross sections of elastic π^--p scattering for 128 and 162 Mev. As can be seen from Table II, the cross sections determined in the present paper (p.p.) are in good agreement with the other experimental data.

TABLE II. Total cross sections of elastic π^--p scattering in the energy interval 100 – 200 Mev

E, Mev	σ_{el}, 10^{-27} cm^2	E, Mev	σ_{el}, 10^{-27} cm^2
98	6.15±0.22 [11]	162	21.4±1.2 (p. p.)
118	9.6±2.0 [12]	165	22.5±1.5 [15]
120	11.3±1.6 [13]	169	21.2±2.0 [16]
128	12.8±1.0 (p. p.)	170	23.5±1.0 [5]
130	12.0[14]	187	22.5±1.3 [17]
144	17.0±2.4 [13]	189	23.0±1.4 [18]
150	20.0±1.0 [5]	194	26.4±2.7 [16]
152	18.8[14]	210	28.7±3.1 [16]

5. ANGULAR DISTRIBUTION OF ELASTIC SCATTERING

The negative-pion scattering angles were recalculated in the center-of-mass system, and then all the cases were grouped in eight angle intervals of 20° each from $\theta = 10°$ to $\theta = 170°$ (c.m.s.). The scattering cases obtained in the interval $\Delta\theta = 0 - 10°$ (one case for 128 Mev and nine cases for 162 Mev) were disregarded (see selection rules, Section 3), owing to the extremely low efficiency of observation, since the recoil protons have a very small range when the mesons are scattered by $\theta < 10°$, and the scattering cases could not be distinguished from π^--μ^- decays. In addition, the Coulomb scattering cross section is very large in this angle interval. The interval $\Delta\theta = 170 - 180°$ was also disregarded owing to the low efficiency (only one case, $\theta = 173°$, was observed although the expected number was 3 to 5).

Columns 1 and 2 of Tables III and IV list the angles θ corresponding to the centers of the angle intervals, and the number of scattering cases ΔN

TABLE III. Differential cross sections of elastic π^--p scattering at 128 Mev

θ (c.m.s.)	ΔN	α	$\left(\frac{d\sigma}{d\Omega}\right)_{exp}$, 10^{-27} cm^2/sr	$\left(\frac{d\sigma}{d\Omega}\right)_{nuc}$, 10^{-27} cm^2/sr
20°	61	1.22±0.06	3.63±0.50	2.01±0.54
40°	78	1.14±0.05	2.31±0.28	2.07±0.28
60°	44	1.08±0.02	0.91±0.14	0.85±0.14
80°	37	1.08±0.02	(1.00±0.08)×0.68±0.11	(1.00±0.08)×0.66±0.11
100°	33	1.08±0.02	0.60±0.10	0.60±0.10
120°	33	1.08±0.02	0.69±0.12	0.70±0.12
140°	34	1.08±0.06	0.95±0.17	0.98±0.17
160°	23	1.25±0.10	1.40±0.31	1.43±0.31

TABLE IV. Differential cross sections of elastic π^--p scattering at 162 Mev

θ (c.m.s.)	ΔN	α	$\left(\frac{d\sigma}{d\Omega}\right)_{\text{exp}}$, 10^{-27} cm²/sr	$\left(\frac{d\sigma}{d\Omega}\right)_{\text{nuc}}$, 10^{-27} cm²/sr
20°	139	1.20±0.04	4.76±0.43	3.60±0.46
40°	175	1.02±0.01	2.71±0.21	2.55±0.21
60°	159	1.09±0.01	1.96±0.16	1.91±0.16
80°	96	1.09±0.01	(1.00±0.06)×1.04±0.11	(1.00±0.06)×1.02±0.11
100°	86	1.09±0.01	0.93±0.10	0.92±0.10
120°	102	1.09±0.01	1.26±0.12	1.26±0.12
140°	124	1.12±0.03	2.11±0.20	2.13±0.20
160°	60	1.20±0.06	2.06±0.28	2.09±0.28

in each interval. To obtain the differential cross sections from these data, it is necessary to take into account the failure to register cases with φ close to 90°, Coulomb corrections, and corrections for averaging over the angle interval $\Delta\theta$.

a. Corrections for φ Ineffectiveness

The scattering cases, whose planes were close to vertical ($\varphi \sim 90°$) are more likely to be omitted in the scanning than cases located in planes close to horizontal. Here obviously the effectiveness should be lower for small and for very large scattering angles θ. Figures 6 and 7 show the distributions of the scattering cases by azimuth angle φ for different angular intervals $\Delta\theta$. The registration effectiveness obtained from these distributions for events in the interval $\Delta\theta = 45 - 135°$ amounts to 92 – 93%, and drops to 80 – 83% for the angular intervals $\Delta\theta = 10 - 30°$ and $\Delta\theta = 150 - 170°$. The coefficients α, which take into account the φ ineffectiveness, are listed in column 3 of Tables III and IV.

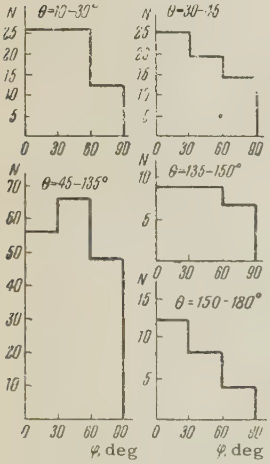

FIG. 6. Azimuthal distribution of scattering events at 128 Mev for different angular intervals $\Delta\theta$.

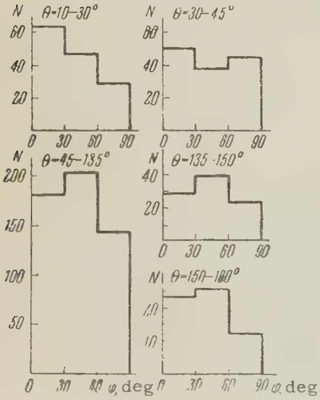

FIG. 7. Azimuthal distribution of scattering events at 162 Mev for different angular intervals $\Delta\theta$.

b. Coulomb Corrections

The Coulomb corrections were calculated using relativistic Coulomb-scattering amplitudes, obtained by Solmitz.[19] The differential scattering cross section due to Coulomb interaction can be written in the form

$$\left(\frac{d\sigma}{d\Omega}\right)_{\text{Coul+int}} = \Phi_1 \sin^{-4}\frac{\theta}{2} + \Phi_2 \sin^{-2}\frac{\theta}{2} + \Phi_3 + \Phi_4 \sin^2\frac{\theta}{2}, \tag{3}$$

where θ is the scattering angle in the c.m.s. The first term in (3) is the cross section of the pure Coulomb scattering, and the remaining terms are due to interference between the Coulomb and nuclear scatterings. The coefficients Φ are calculated from the following formulas

$$\begin{aligned}
\Phi_1 &= A^2(B+C)^2,\\
\Phi_2 &= 4A^2D^2 - 4A^2C(B+C) + A(B+C)(E+F),\\
\Phi_3 &= 4A^2(C^2-D^2) - 2AC(E+F)\\
&\quad - 2AF(B+C) - 4ADG,\\
\Phi_4 &= 4A(CF+DG),
\end{aligned} \tag{4}$$

where

$$\begin{aligned}
&A = e^2/2pc(\beta_\pi+\beta_p), \qquad B = 1 + \tfrac{1}{2}\beta_\pi\beta_p - \tfrac{1}{4}\beta_p^2(2\mu_p - 1),\\
&C = \tfrac{1}{2}\beta_\pi\beta_p + \tfrac{1}{4}\beta_p^2(2\mu_p - 1),\\
&D = \tfrac{1}{2}\mu_p\beta_\pi\beta_p + \tfrac{1}{4}\beta_p^2(2\mu_p - 1), E = \tfrac{1}{3}k^{-1}(2\sin 2\alpha_1 + \sin 2\alpha_3),\\
&F = \tfrac{1}{3}k^{-1}(2\sin 2\alpha_{11} + \sin 2\alpha_{31} + 4\sin 2\alpha_{13} + 2\sin 2\alpha_{33}),\\
&G = \tfrac{1}{3}k^{-1}(2\sin 2\alpha_{13} + \sin 2\alpha_{33} - 2\sin 2\alpha_{11} - \sin 2\alpha_{31}).
\end{aligned} \tag{5}$$

In these formulas $p = \hbar k$ is the momentum in the c.m.s., β_π and β_p are the velocities of the negative pion and the proton in the c.m.s., μ_p is the magnetic moment of the proton in nuclear magnetons. We give below the values of the coefficients Φ (in 10^{-27} cm^2/sr) for negative pion energies of 128 and 162 Mev, calculated from the foregoing formulas, and use for the calculation of E, F, and G the meson-nucleon interaction phases obtained by Chiu and Lomon:[20]

	$10^4\,\Phi_1$	$10^2\,\Phi_2$	$10^2\,\Phi_3$	$10^2\,\Phi_4$
$E = 128$ Mev:	2.18	3.61	—9.33	3.21
$E = 162$ Mev:	1.54	2.57	—7.26	2.96

The integration of (3) from 10° to 180° yields the corrections to the total elastic-scattering cross sections (see Table I)

$$\sigma_{\text{Coul+int}} = 2\pi \int\limits_{10^\circ}^{180^\circ} \left(\frac{d\sigma}{d\Omega}\right)_{\text{Coul+int}} \sin\theta\, d\theta = \begin{cases} 1.6\cdot 10^{-27}\ \text{cm}^2 & \text{for } 128 \text{ Mev}, \\ 1.1\cdot 10^{-27}\ \text{cm}^2 & \text{for } 162 \text{ Mev}. \end{cases}$$

To obtain the differential cross sections of pure nuclear scattering from the experimentally-obtained values $(d\sigma)_{\text{exp}}$, we calculated the cross sections

$$(d\sigma)_{\text{Coul+int}} = 2\pi \int\limits_{\Delta\theta} \left(\frac{d\sigma}{d\Omega}\right)_{\text{Coul+int}} \sin\theta\, d\theta,$$

in which the errors were determined by varying the phase shifts that enter into (5) over reasonable limits.

c. Correction for the Averaging Over the Angular Interval $\Delta\theta$

Since the midpoint of the interval θ is assigned a cross section value which is averaged over the finite angular interval $\Delta\theta$, the true value of the cross section for the angle θ will differ from the average one by an amount

$$d(\theta) = -\tfrac{1}{24}(\Delta\theta)^2\,[d\sigma(\theta)/d\Omega]'', \tag{6}$$

where $[d\sigma(\theta)/d\Omega]''$ is the second derivative of the differential cross section. As a first approximation we calculated $d(\theta)$ from the expressions $d\sigma(\theta)/d\Omega = a' + b'\cos\theta + c'\cos^2\theta$, obtained by the least-squares method from the experimental differential cross sections, corrected for Coulomb scattering. Then

$$d(\theta) = \tfrac{1}{24}(\Delta\theta)^2\,(b'\cos\theta + 2c'\cos 2\theta). \tag{7}$$

The maximum error as calculated by formula (7) did not exceed 2.5%.

d. Differential Cross Section of Elastic Scattering

The differential cross sections $(d\sigma/d\Omega)_{\text{exp}}$ (columns 4, Tables III and IV) were obtained from the angular distributions $dN/d\Omega$ by normalization to the total cross section σ_{exp} (Table I), with allowance for the coefficients α. Columns 5 of Tables III and IV list the differential cross sections of elastic π^--p scattering, due to purely-nuclear interaction. They were obtained by subtracting from $(d\sigma/d\Omega)_{\text{exp}}$ the Coulomb-scattering cross sections and by introducing corrections for averaging over the angle intervals. These errors are mean-square errors, due principally to statistical errors and to small indeterminacies due to introduction of corrections. The general factor in front of the cross sections is the error in the normalized total cross section.

Through the experimentally obtained cross sections $(d\sigma/d\Omega)_{\text{nuc}}$, the curves of the form $d\sigma/d\Omega = a + b\cos\theta + c\cos^2\theta$ were drawn by the method of least squares. We give below the values of the coefficients a, b, and c (in 10^{-27} cm^2/sr), and also the quantity $M = \sum\limits_i (\epsilon_i/\Delta\sigma_i)^2$ which is the sum of the squares of the deviations ϵ_i of the calculated cross sections from the experimental points, expressed in units of experimental errors $\Delta\sigma_i$, and the number of degrees of freedom $M_0 = n - m$ (n — number of experimental points, m — number of parameters of the curve). The fact that M is close to M_0 indicates good agreement between the drawn curves and the experimental cross sections

$$E = 128 \text{ Mev} \qquad \left.\begin{array}{r} a = 0.55 \pm 0.07 \\ b = 0.34 \pm 0.12 \\ c = 1.30 \pm 0.24 \end{array}\right\} \times (1.00 \pm 0.08); \quad M = 5.8; \quad M_0 = 5;$$

$$E = 162 \text{ Mev} \qquad \left.\begin{array}{r} a = 0.93 \pm 0.07 \\ b = 0.51 \pm 0.12 \\ c = 2.28 \pm 0.22 \end{array}\right\} \times (1.00 \pm 0.06); \quad M = 5.2; \quad M_0 = 5.$$

The error matrices $10^4\,G_{ij}^{-1}$, calculated by the method given in the paper by Klepikov and Sokolov,[21] have the following form

128 Mev			162 Mev		
53.53	—3.73	—118.15	49.78	0.76	—101.65
—4.1%	153.65	86.48	0.9%	140.28	39.35
—66.3%	28.6%	593.87	—64.8%	14.9%	494.60

The errors in the coefficients a, b, and c are the square roots of the diagonal elements of the matrices. The non-diagonal elements are the products of the corresponding standard deviations, multiplied by the correlation coefficient. In one half of the matrices, the non-diagonal elements are replaced by the correlation coefficients between a, b, and c (in percent).

The curves obtained, together with the experimental points, are shown in Fig. 8. They agree with the angular distributions of elastic π^--p scattering, measured by Ashkin et al.[5] at 150 and 170 Mev, and also with the results of Kruse and Arnold[14] at negative-pion energies of 130 and 152 Mev.

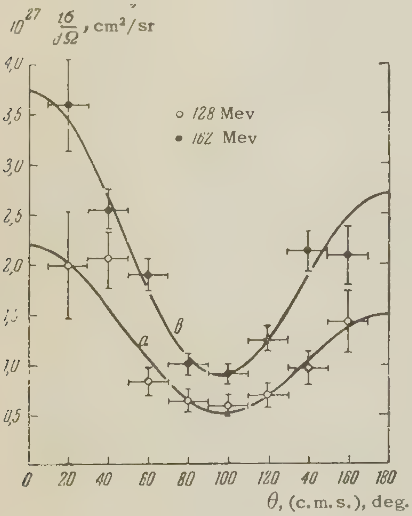

FIG. 8. Angular distributions of elastic π^--p scattering at 128 and 162 Mev. Curves a and b are found by the least-squares method with allowance for S and P waves only.

e. Determination of the Real Part of the Forward Scattering Amplitude

The differential forward-scattering cross sections $d\sigma(0)/d\Omega = a + b + c$ for 128 and 162 Mev are respectively equal to $(220 \pm 0.32) \times 10^{-27}$ and $(3.73 \pm 0.32) \times 10^{-27}$ cm²/sr. These errors take into account, in addition to the mean squared deviations of the coefficients a, b, and c, the correlation between the coefficients (non-diagonal elements of the error matrices). The magnitude of the real part of the forward-scattering amplitude Re $f(0, \omega)$ can be readily obtained from the optical theorem

$$\operatorname{Im} f(0, \omega) = k\sigma_t / 4\pi, \tag{8}$$

where σ_t is the total cross section of π^--p interaction. Then

$$D_-^b = \operatorname{Re} f(0, \omega) = \sqrt{\frac{d\sigma}{d\Omega}(0) - \frac{k^2}{16\pi^2}\sigma_t^2}. \tag{9}$$

The values of σ_t were taken from the curve of the energy dependence of the total cross sections, obtained by Klepikov, Meshcheryakov, and Sokolov[22] by analyzing all the experimental data on the total cross sections of π^+-p and π^--p interactions over a wide range of energies.

$$\sigma_t\,(128\,\text{Mev}) = (39.7 \pm 1.0)\cdot 10^{-27}\ \text{cm}^2,$$

$$\sigma_t\,(162\,\text{Mev}) = (63.3 \pm 1.0)\cdot 10^{-27}\ \text{cm}^2.$$

Then the real parts of the forward-scattering amplitude in the center-of-mass system (in units of $\hbar/m_\pi c$) are

$$D_-^b\,(128\,\text{Mev}) = 0.261 \pm 0.031,$$

$$D_-^b\,(162\,\text{Mev}) = 0.216 \pm 0.038.$$

The great relative error in D_-^b (162 Mev) is due to the fact that the formula for the error D contains D in the denominator, and therefore when resonance is approached, as D → 0, the relative error increases without limit.

6. DISCUSSION

During the performance of this experiment, several theoretical papers appeared[23-31] in which possible causes of the discrepancy observed by Puppi and Stanghellini are discussed. Zaidi and Lomon[23] have shown that the value of D_-^b depends greatly on the course of the curve of total cross sections of π^--p interaction near resonance. A detailed analysis of the errors that arise when the dispersions relations are applied to π-p scattering was carried out by Hamilton[25] and by Schnitzer and Salzman.[28] The latter have shown that by using the energy dependence obtained by Anderson[32] for the total cross sections, it is possible to reduce the discrepancy between the experimental and theoretical values of D_-^b by a factor of approximately 2. In addition, allowance for the normalization factor in the differential cross sections and for the correlation between the coefficients a, b, and c leads to an increase in the errors in the experimental values of D_-^b at 150 and 170 Mev, by a factor of approximately 2, compared with the errors indicated by Puppi and Stanghellini. In spite of this, a slight discrepancy still remains, and to explain it it is necessary to obtain more precise experimental data on the total cross section near resonance and to obtain new values of D_-^b.[28-30]

Most recently, Klepikov, Meshcheryakov, and Sokolov[22] have calculated the curve $D_-^b(\omega)$ for $f^2 = 0.08$, using new data on the total cross sections over a wide range of energies, including measured values of $\sigma_t(\pi^-\text{-p})$, accurate to 2 – 3%, obtained by Zinov, Konin, Korenchenko, and Pontecorvo[33] in the pion energy range 160 – 330 Mev. Figure 9 shows the curve by Klepikov et al. drawn with a solid line, while the dotted line represents the curve of Schnitzer and Salzman[28] for $f^2 = 0.08$. The solid bullets denote the values of D_-^b obtained in the present investigation. In addition, the figure shows recent results by Barnes et al. (41.5 Mev),[34] Edwards et al. (98 Mev),[11] and Kruse and Arnold (130 and 152 Mev),[14] and also the values of D_-^b at 150 and 170 Mev,[3] the errors of which were recal-

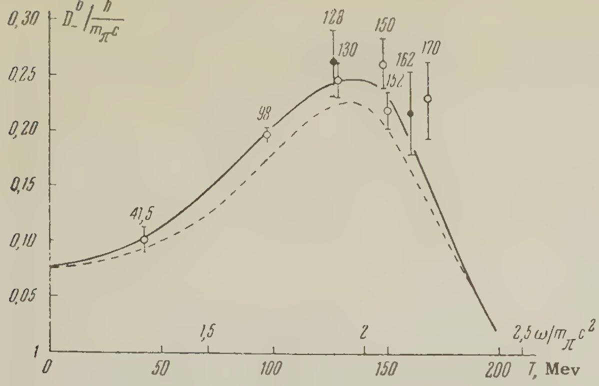

FIG. 9. Dependence of the real part of the forward scattering amplitude, D_-^b on the energy (ω – total negative-pion energy, T – kinetic energy). Solid curve – by Klepikov et al.[22] ($f^2 = 0.08$), dotted curve – by Schnitzer and Salzman[28] ($f = 0.08$).

culated by Schnitzer and Salzman.[28] As can be seen from Fig. 9, the results of our experiments and the data of all the later experimental investigations of elastic π^--p scattering in the energy range up to resonance agree quite satisfactorily with the new theoretical curve, calculated with a coupling constant $f^2 = 0.08$.

Thus, one can assume at present that the experimental data on elastic scattering of negative pions by protons also agrees with the dispersion relations at $f^2 = 0.08$, as was already established earlier for the scattering of positive pions.

The authors express their gratitude to L. I. Lapidus, S. N. Sokolov, V. A. Meshcheryakov for useful discussions, to L. I. Krasnoslobodtseva, T. S. Sazhneva, and Yu. L. Saĭkina for help in scanning the photographs, and to A. A. Andrianova and G. D. Malysheva for calculating the error matrices.

---

[1] Goldberger, Miyazawa, and Oehme, Phys. Rev. **99**, 986 (1955).

[2] Anderson, Davidon, and Kruse, Phys. Rev. **100**, 339 (1955).

[3] G. Puppi and A. Stanghellini, Nuovo cimento **5**, 1305 (1957).

[4] A. Agodi and M. Cini, Nuovo cimento **5**, 1256 (1957); **6**, 686 (1957); Agodi, Cini, and Vitale, Phys. Rev. **107**, 630 (1957).

[5] Ashkin, Blaser, Feiner, and Stern, Phys. Rev. **101**, 1149 (1956).

[6] Budagov, Viktor, Dzhelepov, Ermolov, and Moskalev, JETP **37**, 878 (1959), Soviet Phys. JETP **10**, 625 (1960).

[7] Budagov, Viktor, Dzhelepov, Ermolov, and Moskalev, JETP **35**, 1575 (1958), Soviet Phys. JETP **8**, 1101 (1959); JETP **38**, No. 4 (1960), Soviet Phys. JETP, in press.

[8] Budagov, Viktor, Dzelepov, Ermolov, and Moskalev, JETP **36**, 1080 (1959), Soviet Phys. JETP **9**, 767 (1959).

[9] Budagov, Viktor, Dzhelepov, Ermolov, and Moskalev, Материалы совещания по камерам Вильсона, диффузионным и пузырьковым камерам (Proceedings of the Conference on Cloud, Diffusion, and Bubble Chambers) Joint Institute for Nuclear Research, Dubna, 1958.

[10] Vasilenko, Kozodaev, Sulyaev, Filippov, and Shcherbakov, Приьоры и техника эксперимента (Instrum. and Meas. Engg.) No. 6 (1957).

[11] Edwards, Frank, and Holt, Proc. Phys. Soc. **73**, 856 (1959).

[12] J. Orear, Phys. Rev. **92**, 156 (1953).

[13] Anderson, Fermi, Martin, and Nagle, Phys. Rev. **91**, 155 (1953).

[14] U. Kruse and R. Arnold, Материалы конференции по физике высоких энергий, г. Киев, Proceedings of the Conference on High-energy Physics in Kiev) July, 1959, lecture by B. M. Pontecorvo.

[15] H. L. Anderson and M. Glicksman, Phys. Rev. **100**, 268 (1955).

[16] Fermi, Glicksman, Martin, and Nagle, Phys. Rev. **92**, 161 (1953).

[17] M. Glicksman, Phys. Rev. **95**, 1045 (1954).

[18] Kruse, Anderson, Davidon, and Glicksman, Phys. Rev. **100**, 279 (1955).

[19] F. T. Solmitz, Phys. Rev. **94**, 1799 (1954).

[20] H. Y. Chiu and E. L. Lomon, Ann. Phys. **6**, 50 (1959).

[21] N. P. Klepikov and S. N. Sokolov, Analysis of Experimental Data by the Method of Maximum Likelihood, preprint, Joint Institute for Nuclear Research, 1959.

[22] Klepikov, Meshcheryakov, and Sokolov, loc. cit. ref. 14.

[23] M. H. Zaidi and E. L. Lomon, Phys. Rev. **108**, 1352 (1959).

[24] V. A. Meshcheryakov, JETP **35**, 290 (1958), Soviet Phys. JETP **8**, 200 (1959).

[25] J. Hamilton, Phys. Rev. **110**, 1134 (1958).

[26] H. Y. Chiu, Phys. Rev. **110**, 1140 (1958).

[27] L. Bertocchi and L. Lendinara, Nuovo cimento **10**, 734 (1958).

[28] H. J. Schnitzer and G. Salzman, Phys. Rev. **112**, 1802 (1959).

[29] H. Y. Chiu and J. Hamilton, Phys. Rev. Lett. **1**, 146 (1958).

[30] H. P. Noyes and D. N. Edwards, Bull. Am. Phys. Soc. **4**, 50 (1959).

[31] H. J. Schnitzer and G. Salzman, Phys. Rev. **113**, 1153 (1959).

[32] H. L. Anderson, Proc. of the Sixth Ann. Roch. Conf., 1959 p. 20.

[33] Zinov, Konin, Korenchenko, and Pontecorvo, loc. cit. ref. 14.

[34] Barnes, Rose, Giacomelli, Ring, and Miyake, Phys. Rev., in press.

Translated by J. G. Adashko
148

SOVIET PHYSICS JETP VOLUME 11, NUMBER 3 SEPTEMBER, 1960

THE pn → pnπ^0 *REACTION IN THE ENERGY RANGE FROM THRESHOLD TO 665 Mev*

A. F. DUNAĬTSEV and Yu. D. PROKOSHKIN

Joint Institute for Nuclear Research

Submitted to JETP editor September 18, 1959

J. Exptl. Theoret. Phys. (U.S.S.R.) **38**, 747-757 (March, 1960)

By simultaneous investigation of π^0-meson production in pd and pp collisions, information is obtained on the magnitudes of the total cross sections and angular distributions for the pn → pnπ^0 reaction in the energy region from threshold up to 665 Mev. Comparison of these cross sections with those of other reactions shows that the condition imposed on the relation between the total cross sections of various meson productions by the isotopic invariance hypothesis is fulfilled (to within 10 per cent) in the investigated energy region. Production of π mesons in a state with isotopic spin T = 1 is almost twice as intense as that in states with T = 0. The angular distribution of π^0 mesons produced in nucleon-nucleon collisions at an energy of about 650 Mev was found to be approximately isotropic, in contrast to the distribution of charged π^+ mesons which is essentially anisotropic.[18] This difference contradicts the hypothesis of isotopic invariance.

1. INTRODUCTION

THE investigation of the reaction of production of neutral π mesons in pn collisions is of considerable interest at the present time in connection with the possibility of explaining by this means the role of transitions with isotopic spin T = 0 in processes of inelastic nucleon collisions. In addition, comparison of the magnitudes of the reaction cross sections mentioned with the cross sections of production of π mesons in other previously studied reactions permits one to establish the degree of validity of the hypothesis of charge invariance of nuclear forces.

Although the second of the two reactions for the production of π^0 mesons in nucleon collisions

$$p + p \rightarrow \pi^0 + p + p, \qquad (1)$$

$$p + n \rightarrow \pi^0 + \begin{cases} p + n \\ d \end{cases} \qquad (2)$$

is the more intense, its investigation has encountered significantly greater difficulties than in the case of reaction (1). The reaction (2) remains at the present time one of the least studied among processes of the type "nucleon + nucleon → π meson." This reaction can be studied by two means: by bombardment of a hydrogen nucleus by neutrons,[1-3] and by experimental comparison of the reaction cross sections of

$$p + d \rightarrow \pi^0 + \text{nucleons} \qquad (3)$$

with the cross sections of reaction (1).[4-7] In the first case, difficulties both of a methodological character (low intensity of neutron beams, etc) and in principle (large width of the neutron-energy spectrum[8]) arise. In the second case, the measurements are methodologically simpler but the interpretation of the experimental data is made much more difficult by reason of the motion of the nucleons in the nucleus of deuterium (which is equivalent to the problem of a broad neutron spectrum in the first case) and by reason of other effects brought about by the coupling of nucleons even in the presence of an extra nucleon in the final state of the reaction (3) in comparison with the reactions (2).

For a study of the reaction (2), we chose the second of the two possibilities pointed out above. Joint investigation of reactions (3) and (1) was carried out under identical experimental conditions over a wide range of energies. Measurements of the cross section were carried out both above and below the threshold of production of π mesons in the collision of free nucleons (280 Mev) with the aim of establishing the momentum distribution of the nucleons in the deuteron without which interpretation of the results of measurement in the region adjoining the threshold would be impossible. Chief interest in the work was devoted to the study of the angular distribution of π^0 mesons. This characteristic of reaction (2) was studied less: previously, at energies 400 and 590 Mev, the angular distribution was measured[9,10] for the second reaction channel (where the deuteron is produced in a final

TABLE I

E, Mev	$\theta°$	$\langle\langle\sigma'_{pn}\rangle\rangle=\sigma'_{pd}-\sigma'_{pp}$, %	σ'_{pd}, %	$d\sigma^{\gamma}_{pd}/d\Omega$, 10^{-27} cm²/sr
665	16	20.7±1.0	35.4±1.2	3.72±0.30
	20	20.5±1.5	35.9±1.8	3.41±0.30
	33	19.4±0.7	34.5±0.9	2.62±0.16
	45	20.4±1.5	34.9±1.7	2.20±0.25
	60	16.4±0.7	29.1±0.9	1.34±0.08
	75	19.1±1.0	30.7±1.3	1.17±0.07
	96	18.9±1.0	29.7±1.2	0.89±0.06
	120	16.3±1.3	26.2±1.4	0.66±0.05
	135	15.5±1.4	24.7±1.7	0.56±0.04
	145	14.1±1.4	23.5±1.7	0.52±0.04
	160	16.2±3.5	26.2±3.7	0.51±0.07
560	16	24.5±1.2	34.4±1.6	2.37±0.20
	34	22.1±1.4	31.5±1.6	1.56±0.13
	60	16.7±0.9	24.2±1.2	0.70±0.06
	90	17.6±0.7	24.4±0.9	0.47±0.03
	130	17.1±0.9	23.5±1.3	0.31±0.02
	150	19.9±1.0	25.9±1.3	0.33±0.03
485	16	21.5±1.0	26.6±1.4	0.96±0.09
	35	21.1±1.0	26.4±1.1	0.79±0.06
	60	16.0±1.0	21.3±1.3	0.41±0.04
	90	13.6±0.8	18.1±1.1	0.23±0.02
	130	16.5±1.4	20.5±1.6	0.19±0.02
	150	19.2±1.7	23.7±1.9	0.19±0.02

state) and the total angular distribution for both channels of the reaction was determined with low accuracy at an energy of 660 Mev.[6]

2. METHOD OF MEASUREMENT

The general setup and the method of measurement employed in the current research is similar to that described in our previous article.[11] Information on the angular distributions of π^0 mesons and on the magnitudes of the total cross sections for the reaction (2) were obtained by measurement of the yield of gamma quanta from the decay of π^0 mesons produced in targets upon transmission through them of a beam of protons. The experiments were completed on the external unpolarized proton beam of the sixty meter proton synchrotron of the Joint Institute for Nuclear Research. A γ telescope with a low energy threshold was used for recording the γ quanta; this telescope contained scintillation counters and a Cerenkov counter. As targets, we used heavy and light water, poured in thin-walled containers, and also plates of light graphite and polyethylene $(CH_2)_n$. Determination of the γ-quantum yield from these targets permitted us to find the values of the relation of the differential cross sections for the deuteron and hydrogen:

$$\sigma'_{pd} = (d\sigma^{\gamma}_{pd}/d\Omega)/(d\sigma^{\gamma}_{pC}/d\Omega)$$

and the differential cross sections for the deuteron (cross sections for hydrogen were measured earlier[11]). For the determination of the values of σ'_{pd} in the region of low proton energies, the data[11] obtained with a liquid hydrogen target were also used.

3. DIFFERENTIAL AND TOTAL CROSS SECTIONS FOR THE REACTION p + d → π^0 + nucleons

The angular dependences of the relative cross section σ'_{pd} and the differential cross section of the reaction (3) were measured in detail at proton energies E = 665, 560 and 485 Mev* (see Table I).

Here θ is the angle of emission of the γ photons in the laboratory system of coordinates (l.s.). For other proton energies, the ratios σ'_{pd} and the differential cross sections for hydrogen were measured either at the "isotropic" angles (see, for example, Table II), or at angles around 60 and 120° in the l.s., which permitted us to determine the magnitudes of the total cross sections without making assumptions on the character of the angular distribution of the π^0 mesons.[11,13] The values of the total cross sections $\sigma^{\pi^0}_{pd}$ for the reaction (3) thus found are given in Table III. In the determination of the cross section at the point E = 175 Mev, the extrapolated value is $\sigma'_{pd} = (10 \pm 4)$ per cent.

In the energy region 580 — 660 Mev, the relative cross sections σ'_{pd} found in the present work differ somewhat from those found earlier.[6] The reason for this discrepancy is evidently a local heating of the poor heat conducting target of LiD in irradiating it in the external beam of the accelerator, which produces a systematic error in the calorimetric method of determination of proton flux employed in reference 6. Heating of the tar-

---

*E – effective energy of the beam, determined with account of the energy loss in the target and of the dispersion of the beam.[12]

TABLE II. $\vartheta = 55^{0}$*

E, Mev	$\langle\langle\sigma'_{pn}\rangle\rangle$, %	σ'_{pd}, %	E, Mev	$\langle\langle\sigma'_{pn}\rangle\rangle$, %	σ'_{pd}, %
665	19.4±0.7	34.5±0.9	370	16.5±1.2	17.5±1.3
645	21.0±1.4	35.2±1.5	330	15.9±1.2	16.1±1.2
610	19.4±1.2	30.8±1.3	290	10.0±1.8	10.0±1.8
560	22.1±1.4	31.5±1.6	250	9.4±2.0	9.4±2.0
485	21.1±1.0	26.4±1.1	215	13±4	13±4
440	18.9±1.0	21.9±1.2	175 (extrap.)	10±4	10±4

*ϑ = angle of flight of γ photons in the center of mass system of the colliding nucleons.

TABLE III

E, Mev	$\sigma^{\pi^0}_{pd}$, 10^{-27} cm^2	$\sigma^{\pi^0}_{pd}$, rel. units	E, Mev	$\sigma^{\pi^0}_{pd}$, 10^{-27} cm^2	$\sigma^{\pi^0}_{pd}$, rel. units
665	7.9±0.4	1.00	485	2.35±0.18	0.30±0.02
652	7.6±0.5	0.96±0.06	440	1.54±0.12	0.19±0.01
645	8.0±0.5	1.01±0.04	437*	1.15±0.22	—
630	7.6±0.4	0.96±0.03	400	1.0±0.1	0.13±0.01
620	7.0±0.6	0.89±0.06	370	0.68±0.08	0.086±0.008
610	6.8±0.4	0.86±0.04	340**	0.59±0.15	—
597	6.1±0.5	0.77±0.05	330	0.38±0.06	0.048±0.007
590	5.8±0.4	0.73±0.03	290	0.19±0.04	0.024±0.005
560	4.45±0.30	0.56±0.02	250	0.08±0.02	0.010±0.002
520	3.1±0.2	0.39±0.02	215	0.06±0.02	0.008±0.002
508	2.9±0.2	0.37±0.02	175 (extrap.)	0.025±0.010	0.003±0.001

*According to the data of Stallwood et al.[7]

**According to the data of Hales and Moyer[4] and reference 11.

get decreases rapidly with decrease in the working radius of the target and the error should then disappear. Actually, at energies below 580 Mev, the values of σ'_{pd} obtained in the present work and in reference 6 agree within the limits of error of measurement (equal to 20 per cent in reference 6).

4. TOTAL CROSS SECTIONS OF THE REACTION (2)

A comparison of the cross sections obtained for the reaction $p + d \to \pi^0$ with the cross sections of the reaction $p + p \to \pi^0$ obtained earlier[11] permits us in principle to determine the cross section of the reaction (2) of interest to us, after calculation of the effects of the binding of the nucleons in the deuteron. The binding of the nucleons changes the values of the cross sections, as a result of which the cross section for the deuteron is not equal to the sum of the cross sections for the proton and the neutron. In the energy region under consideration, which is located not far from the threshold of the reaction of meson production, the change in the values of the cross sections because of the motion of the nucleon in the deuteron is fundamental because of the effect brought about by the coupling of the nucleons.[14] In researches previously completed,[5,6,15] the effect of the coupling was not taken into consideration. The cross section for the neutron was found by simple subtraction "D – H," which is valid only at a rough first approximation. Use of a similar approximation in these researches was quite correct, since the experiments were carried out in the high-energy region where the corrections which take into account the effect of binding were commensurate with the errors of determination of the cross section, which amounted to about 15 — 30 per cent in the researches mentioned. In order to make progress in the region of low energies, and also to decrease the crudeness of the determination of the cross section for high energies, it is necessary, if only approximately, to take into account the coupling of the nucleons. For the solution of this problem, it is necessary to know the momentum distribution of the nucleons in the deuteron.

In the energy region around and below threshold, the energy dependence of the cross sections of the reaction which takes place on the nucleons of the deuteron, and in particular the reaction (3), is entirely determined by the character of the momentum distribution of the nucleons, especially by the shape of its high momentum "tail." With decrease in the energy of the emitted proton, a more significant role is played in the reaction by the nucleons of a deuteron possessing high momenta at the moment of collision, while the contribution from the low energy part of the momentum distribution quickly disappears. For this reason, the investigation of the energy dependence of the cross section of reaction (3) in the region around threshold is a sufficiently sensitive method of studying the shape of the momentum distribution (and especially of its "tail"). The momentum distribution for the deuteron was found by this method in reference 14 from the data of Table III of the present work. It was shown to be close to the function calculated by Salpeter and Goldstein.[16] Knowing the momentum distribution, we can establish the magnitudes of the cross sections of reaction (2) by starting out from the data on the cross sections of reactions (3) and (1):[14]

$$\sigma_{pn}^{\pi^0} = \sigma_{pd}^{\pi^0} / k g_{pn} - \sigma_{pp}^{\pi^0} g_{pp} / g_{pn}. \qquad (4)$$

The functions g_p and g_{pp}, which characterize the change in the values of the cross sections because of intranuclear motion, and the coefficient k, which takes into account all other effects, are connected with the presence of a "spare" nucleon, computed in reference 14. By making use of these and the data of Table III, we obtain the total cross sections of the reaction (2) (Table IV).

TABLE IV

E, **Mev**	$\sigma_{pn}^{\pi^0}$, 10^{-27} **cm²**	$\sigma_{pn}^{\pi^0}$, **rel. units**	η_m*
665	6.3±0.4	1.00	1.90
652	6.1±0.5	0.97±0.06	1.86
645	6.5±0.5	1.03±0.04	1.84
630	6.1±0.4	0.97±0.03	1.79
620	5.6±0.5	0.89±0.06	1.76
610	5.5±0.4	0.87±0.04	1.73
597	4.9±0.4	0.79±0.06	1.69
590	4.6±0.3	0.75±0.03	1.66
560	3.41±0.25	0.54±0.02	1.56
520	2.2±0.2	0.35±0.02	1.43
508	2.02±0.17	0.32±0.02	1.38
485	1.57±0.13	0.250±0.015	1.30
440	0.95±0.10	0.151±0.010	1.12
400	0.56±0.06	0.089±0.007	0.95
370	0.34±0.04	0.065±0.007	0.81
330	0.15±0.03	0.033±0.006	0.59
290	0.011±0.003	0.0020±0.0005	0.25

*Here η_m is the maximum momentum of the π^0 mesons in the center of mass system, in units of the meson mass $m_\pi c$.

5. ANGULAR DISTRIBUTIONS OF γ QUANTA

The angular distributions of γ quanta from decay of π^0 mesons produced in reaction (3) were measured by us in the energy region 400 – 665 Mev. For these energies, the effect of coupling of nucleons in the deuteron on the angular distribution was still small and could be simply taken into account by means of the introduction of an effective center-of-mass system whose velocity in the laboratory coordinates, $\overline{\beta}_c$, differs slightly from the velocity of the center-of-mass system for the case of a collision with a nucleon at rest. The quantity $\overline{\beta}_c$ was determined by integration over $\mathbf{p}_2$ of the velocity of the center of mass of the emerging proton and nucleon, moving in the deuteron with momentum $\mathbf{p}_2$, with account of the Salpeter-Goldstein momentum distribution and the energy dependence of the cross section (these calculations are similar to those carried out in reference 14). The angular distribution of π^0 mesons in the effective center-of-mass system introduced in such fashion practically coincides with the angular distribution (in the center-of-mass system) of π mesons produced by collision of free nucleons.

The measured angular distribution of γ quanta produced in pd collisions at energy 665 Mev is shown in Fig. 1. As is seen from the drawing, the distribution $f_{pd}^{\gamma}(\vartheta)$ is slightly asymmetric relative to 90°, while the angular distributions for reactions (2) and (1) should be symmetric if the hypothesis of isotopic invariance is valid. The asymmetry arises by virtue of the absorption of the π meson at the emission of a proton. In such a simple and "porous" nucleus as the deuteron, the absorption must be small and the asymmetry of the angular distribution is not large. Actually, the contribution of the term proportional to $\cos\vartheta$ in the distribution $f_{pd}^{\gamma}(\vartheta)$ (Fig. 1) amounts to 5 per cent at most. This small correction can be sufficiently accurately taken into account (in view of its smallness) on the basis of a simpler model of a homogeneous nucleus with account of experimental data on the absorption of π mesons and nucleons in nuclear material. In the case of a complicated nucleus (carbon), where the absorption is large and the contribution of the asymmetric term to the angular distribution amounts to 30 per cent, the dependence of the coefficient k on the angle computed in such a fashion is in poor agreement with experimental data.[11,17]

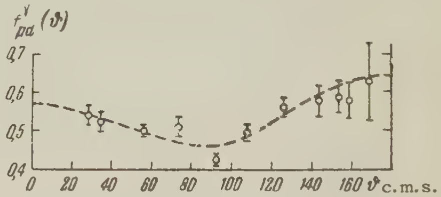

FIG. 1. Angular distribution in the effective center-of-mass system of γ quanta from the decay of π^0 mesons produced in pd collisions at an energy of 665 Mev. The dashed curve was obtained by the method of least squares with account of a small correction for screening.[17]

The angular distribution $f_{pn+pp}^{\gamma}(\vartheta)$ obtained from the distribution $f_{pd}^{\gamma}(\vartheta)$ after introduction in it of a computed correction to the absorption is well described by the polynomial

$$f^{\gamma}_{pn+pp}(\vartheta) \sim {}^1/_3 + (0.07 \pm 0.02)\cos^2\vartheta.$$

By computing from it the distribution found for the reaction (1) in reference 11, one can obtain the angular distribution of γ quanta in the reaction (2), $f^{\gamma}_{pn}(\vartheta)$, for E = 665 Mev. This distribution is approximated by the polynomial

$$f^{\gamma}_{pn}(\vartheta) \sim {}^1/_3 + (0.08 \pm 0.02)\cos^2\vartheta.$$

The distribution $f^{\gamma}_{pn}(\vartheta)$ was shown to be symmetric relative to 90°. If it is approximated by a polynomial, which in addition to the zero and second order terms also contains an asymmetric term proportional to $\cos\vartheta$, then the latter is shown to be insignificant: $(0.01 \pm 0.01)\cos\vartheta$. The correction to the total cross section is also small and of a much higher power of the cosine than the second. From this it follows (see reference 11) that, in the energy region up to 660 Mev, the distribution of γ quanta in the reaction (2) has the form

$$f^{\gamma}_{pn}(\vartheta) \sim {}^1/_3 + b_{\gamma}\cos^2\vartheta.$$

The quantities b_{γ} obtained for different proton energies are shown in Table V.

TABLE V

E, Mev	b_{γ}	E, Mev	b_{γ}
665	0.08±0.02	508	0.16±0.06
630	0.11±0.05	485	0.18±0.05
590	0.10±0.04	440	0.13±0.05
560	0.18±0.05	400	0.12±0.06
520	0.14±0.05		

6. DISCUSSION OF RESULTS

Total cross sections and the hypothesis of isotopic invariance. A well known consequence of the hypothesis of isotopic invariance is the relation connecting the total cross sections of formation of neutral and charged π mesons in nucleon-nucleon collisions:

$$(\sigma^{\pi^+}_{pp} + \sigma^{\pi^+}_{pn} + \sigma^{\pi^-}_{pn}) / 2(\sigma^{\pi^0}_{pp} + \sigma^{\pi^0}_{pn}) = 1. \qquad (5)$$

Making use of the values of the total cross sections of the reaction (2) found in the present work and of the cross sections of other reactions studied earlier,[11,18-22] one can verify the feasibility of Eq. (5) in the wide energy range from threshold to 665 Mev. As is seen from Fig. 2, this ratio is actually close to unity in the energy region under discussion.

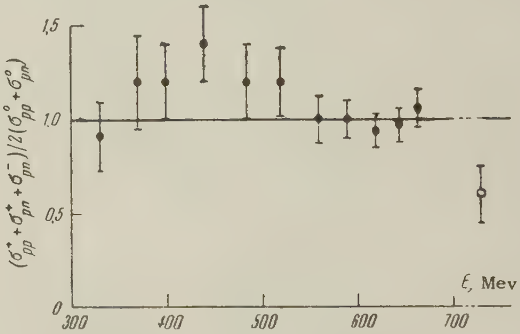

FIG. 2. Ratio of the total cross sections for production of charged and neutral π mesons at different proton energies: ● – according to the data of the present work and references 11, 18–22; □ – according to the data of Batson et al.,[23] E = 970 Mev.

For energies ≈ 600 Mev, where the total cross sec-

TABLE VI

E, Mev	σ_{01}, 10^{-27} cm²	σ_{10}, 10^{-27} cm²	σ_{11}, 10^{-27} cm²	σ_0, 10^{-27} cm²	σ_1, 10^{-27} cm²
660	1.7±1.1	10.9±0.5	3.22±0.17	5.1±3.3	17.1±0.6
645	2.6±1.1	10.2±0.5	2.93±0.17	7.8±3.3	16.0±0.6
630	3.1±0.9	9.1±0.5	2.74±0.16	9.3±2.7	14.5±0.6
620	2.7±1.1	8.5±0.5	2.55±0.17	8.1±3.3	13.5±0.6
610	2.9±0.9	8.1±0.5	2.25±0.14	8.7±2.7	12.5±0.6
597	2.3±0.9	7.5±0.5	1.96±0.14	6.9±2.7	11.5±0.6
590	1.9±0.8 1.9±0.9*	7.3±0.5	1.84±0.12	5.6±2.4	11.0±0.6
560	0.9±0.6	6.0±0.4	1.24±0.08	2.7±1.8	8.4±0.5
520	$0.1^{+0.6}_{-0.1}$	4.5±0.4	0.75±0.06	$0.3^{+1.8}_{-0.3}$	6.1±0.4
485	$0.1^{+0.5}_{-0.1}$	3.4±0.3	0.45±0.03	$0.3^{+1.5}_{-0.3}$	4.2±0.3
440	$0.1^{+0.4}_{-0.1}$	2.3±0.2	0.20±0.02	$0.3^{+1.2}_{-0.3}$	2.7±0.2
400	$0.1^{+0.3}_{-0.1}$ 0.22±0.08*	1.2±0.2	0.09±0.02	$0.3^{+0.9}_{-0.3}$ 0.65±0.25*	1.4±0.2
370	$0.1^{+0.2}_{-0.1}$	0.8±0.2	0.04±0.01	$0.3^{+0.6}_{-0.3}$	0.8±0.2
330	—	0.33±0.04	0.014±0.006	—	0.35±0.04

tions were measured with the least error, Eq. (5) is satisfied with an accuracy to within 8 — 10 per cent. Of the quantities entering into this equation, the least studied is the cross section $\sigma_{pn}^{\pi\pm}$, experimental information on which has been obtained only at two energies (400 (reference 20) and 590 Mev[21]). For other values of the energy, the values of $\sigma_{pn}^{\pi\pm}$ used in Fig. 2 were found by means of an approximation[22] of the energy dependence of the cross section $\sigma_{pn}^{\pi\pm}$ by the power function $\eta_m^{4-4.5}$. The errors connected with the use of a similar approximation cannot be large, since the contribution of the cross section $\sigma_{pn}^{\pi\pm}$ to Eq. (5) is comparatively small in the energy region under consideration. In the region of higher energies, the ratio (5) was recently measured at E = 970 Mev.[23] The cross section $\sigma_{pn}^{\pi^0}$ at this energy was shown to be unexpectedly large, which led to a value of the ratio (5) differing somewhat from unity (Fig. 2).

Making use of the cross section obtained for the reaction (2), it is possible to determine the value of the partial cross section[22] σ_{01} (which corresponds to the transition $T_N = 0 \rightarrow T_N = 1$; T_N is the isotopic spin of the nucleons)

$$\sigma_{01} = 2\sigma_{pn}^{\pi^0} + \sigma_{pp}^{\pi^0} - \sigma_{pp}^{\pi^+} \qquad (6)$$

at different energies (Table VI). The cross section σ_{01} can also be obtained from the relation

$$\sigma_{01} = 2\sigma_{pn}^{\pi\pm} - \sigma_{pp}^{\pi^0}. \qquad (7)$$

The values of σ_{01} marked in the table by an asterisk were found by the latter method. Along with the partial cross sections, values of the cross sections of production of π mesons in nucleon-nucleon collisions are given in Table VI for total isotopic spin T = 1 and 0: $\sigma_1 = \sigma_{pp}^{\pi^+} + \sigma_{pp}^{\pi^0}$ and $\sigma_0 = 3\sigma_{01}$.

Comparison of the magnitudes of the cross sections given in Table VI shows that in the energy region from threshold up to 665 Mev, σ_1 is approximately double σ_0 (Fig. 3). Better agreement with experimental data is obtained if, following Rosenfeld,[22] we assume that σ_{01} changes with the energy as η_m^4:

$$\sigma_{01} = 0.3\eta_m^4 \cdot 10^{-27}\ \text{cm}^2. \qquad (8)$$

The total cross sections of the reaction (2) found in the present work are close to the cross sections computed on the basis of the resonance phenomenological theory of Mandelstam[24] (Fig. 4). At energies E > 660 Mev, the increase of this cross section slowed down, in agreement with the theory of Mandelstam.

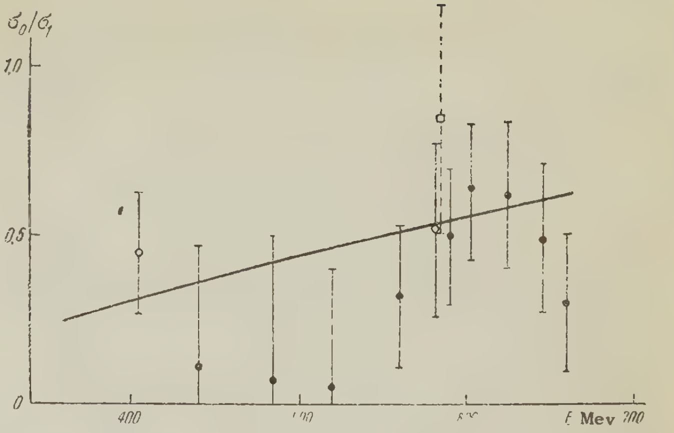

FIG. 3. Ratio of the cross section of production of π mesons by nucleons in states with isotopic spin T = 0 and T = 1: ● – obtained from the relation (6) from the data of the present work and references 11, 18, 19, and 22; ○ – obtained from the relation (7) from the data of references 11, 20, and 21; □ – obtained by starting out from the total cross sections.[21] The curve corresponds to the dependence (8).

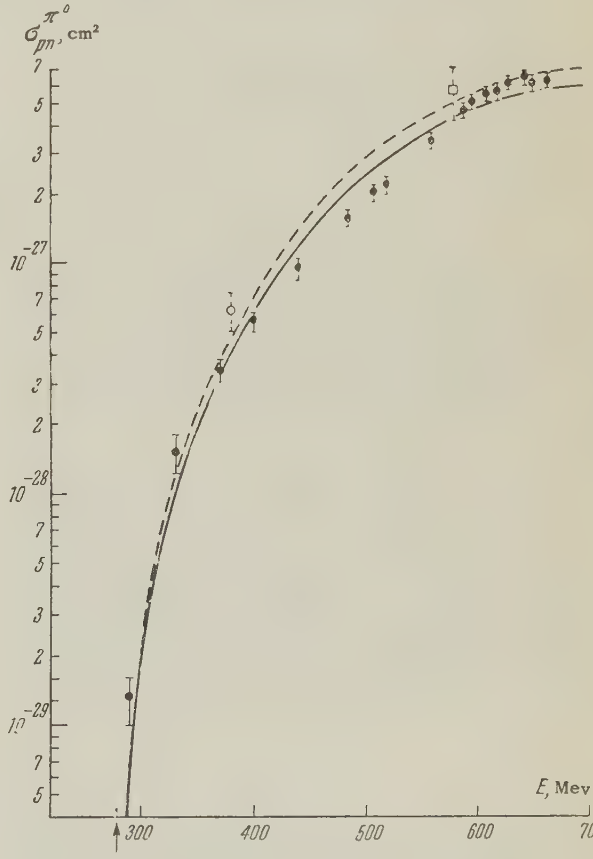

FIG. 4. Total cross sections of the reaction pn → pnπ⁰: ● – data of the present work; ○ – data of reference 2; □ – data of reference 3. The solid curve was computed on the basis of the resonant theory of Mandelstam, the dashed curve takes into account the non-resonant transition (8) in the state with T = 0. The arrow indicates the reaction threshold.

The angular distributions of π mesons and the hypothesis of isotopic invariance. The angular distributions of π⁰ mesons in the reaction (2), $f_{pn}^{\pi^0}(\vartheta)$, can be established according to the measured angular distributions of the γ quanta.[11] In the energy region from threshold up to 665 Mev, the function $f_{pn}^{\pi^0}(\vartheta)$ as also the function $f_{pn}^{\gamma}(\vartheta)$ has the form

$$f_{pn}^{\pi^0}(\vartheta) \sim {}^1/_3 + b_{\pi^0}\cos^2\vartheta.$$

The values obtained for b_π are given in Table VII.

As is seen from this table, the isotropy of the angular distribution of the π^0 mesons in reaction (2) increases along with increase in the energy of the emitted proton. This result agrees qualitatively (Fig. 5) with the predictions of the Mandelstam theory (private communication). The agreement with the theory is complete if, in addition to resonant transitions, we also take into account the non-resonant transition (8) from the state with T = 0, for which the isotropic angular distribution is characteristic.[11,21]

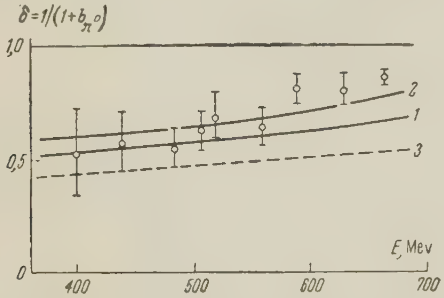

FIG. 5. Angular distributions of π° mesons produced from pn collisions. The quantity δ is the fraction of π° mesons distributed isotropically. The curve 1 was computed by Mandelstam on the basis of his resonance theory; curves 2 and 3 were computed with account of the non-resonant transition (8) under the assumption of an isotropic and $\sim\cos^2\vartheta$ distribution, respectively.

If the hypothesis of isotopic invariance is valid, then the total angular distributions of neutral and charged π mesons produced in nucleonic collisions must be the same [i.e., $f_{pp+pn}^{\pi^0}(\vartheta) = f_{pp+pn}^{\pi\pm}(\vartheta)$]. Since these angular distributions are accurately described for energies ≈ 650 Mev by a polynomial of the type $\frac{1}{3} + b_\pi\cos^2\vartheta$, then the latter confirmation is equivalent to the equation

$$b_{\pi^0} = b_{\pi\pm}. \tag{9}$$

Here b_{π^0} and $b_{\pi\pm}$ are the sums of the coefficient b_π normalized over the cross sections in angular distributions of neutral and charged π mesons.

The angular distribution of the π^0 mesons for energies ≈ 650 Mev are close to isotropic: $b_{\pi^0} = 0.16 \pm 0.04$ for E = 665 Mev according to the data of the present research and reference 11. At these energies, the distribution of charged π mesons produced in pn collisions is quite isotropic.[21] In contrast, the charged π-meson distribution produced in pp collisions is quite anisotropic: $b_{\pi^+} = 0.61 \pm 0.09$ according to the data of Neganov and Savchenko.[18] The difference between the value of the ratio $b_{\pi^0}/b_{\pi\pm}$ and the units characterizing the degree of violation of isotopic invariance is shown to be significant here:

$$b_{\pi^0}/b_{\pi\pm} = 0.38 \pm 0.11.$$

The difference shown between the angular distribution of neutral and charged π mesons is today perhaps the only violation of the hypothesis of isotopic invariance.[25] However, it should be noted that this difference is still not conclusively established experimentally. One must regard the value of the ratio $b_{\pi^0}/b_{\pi\pm}$ given above as a tentative one. On the other hand, the angular distribution of π^+ mesons can be shown to be more isotropic, as was observed in the recent experiments of Meshkovskiĭ, Shalamov, and Shebanov.[26] However, the angular distribution of neutral π mesons in the reaction (2) can differ somewhat from that given in the present research, inasmuch as interference is possible between the nucleonic state in the deuteron which leads to a change in the distribution of π^0 mesons in comparison to that which is the case for collisions of a proton with free nucleons. In this connection, accurate experimental data on the angular distributions of charged π mesons and the completion of researches on the angular distribution of π^0 mesons formed in free pn collisions are both necessary.

The reaction $pn \to \pi^\pm$ + nucleons. Making use of the values of the cross sections of reaction (2) obtained in the present research and the cross sections of production of π mesons in pp collisions,[11,18,19,22] one can determine the cross sections of the reaction $pn \to \pi^\pm$ over a wide energy range on the basis of Eq. (5). This is of considerable interest, inasmuch as direct studies of the reaction $pn \to \pi^\pm$ entail great experimental difficulties. The values found for the total cross sec-

TABLE VII

E, Mev	b_{π^0}	E, Mev	b_{π^0}	E, Mev	b_{π^0}	E, Mev	b_{π^0}
665	0.17±0.04	560	0.60±0.20	508	0.61±0.23	400	$0.9^{+1.3}_{-0.5}$
630	0.26±0.12	520	0.48±0.22	485	0.85±0.30		
590	0.25±0.10			440	$0.74^{+0.48}_{-0.34}$		

tions $\sigma_{pn}^{\pi^+}$ (or, what amounts to the same thing, $\sigma_{pn}^{\pi^-}$) are given in Fig. 6. As is seen from the drawing, the energy dependence of the cross section $\sigma_{pn}^{\pi^+}$ is well described by the function

$$\sigma_{pn}^{\pi^+} = (1.7 \pm 0.4)\, \eta_m^{4.6 \pm 0.4}. \qquad (10)$$

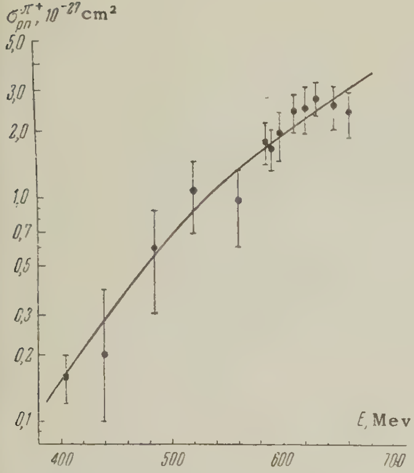

FIG. 6. Total cross sections of the reaction pn → nnπ^+ found under the assumption of the validity of the hypothesis of isotopic invariance: ● — according to the data of the present work and references 11, 18, 19, 22; ■ — are the results of direct measurement.[20,21] The curve corresponds to the dependence (10).

In conclusion, we take this opportunity to thank S. Mandelstam, who kindly sent us the results of his unpublished researches, B. Pontecorvo and B. S. Neganov for discussion of results of the present research, and I. V. Tsymbulov for help given in carrying out the measurements.

---

[1] B. Pontecorvo and G. I. Selivanov, Dokl. Akad. Nauk SSSR **102**, 495 (1955).

[2] Dzhelepov, Oganesyan, and Flyagin, JETP **29**, 886 (1955), Soviet Phys. JETP **2**, 757 (1956).

[3] Rosenfeld, Solmitz, and Hildebrand, Bull. Am. Phys. Soc. **1**, 72 (1956).

[4] R. Hales and B. J. Moyer, Phys. Rev. **89**, 1047 (1953).

[5] Tyapkin, Kozodaev, and Prokoshkin, Dokl. Akad. Nauk SSSR **100**, 689 (1955).

[6] Yu. D. Prokoshkin and A. A. Tyapkin, JETP **32**, 750 (1957), Soviet Phys. JETP **5**, 618 (1957).

[7] Stallwood, Sutton, Fields, Fox, and Kane, Phys. Rev. **101**, 1716 (1958).

[8] V. S. Kiselev and V. B. Flyagin, JETP **32**, 962 (1957), Soviet Phys. JETP **5**, 786 (1957).

[9] R. Hildebrand, Phys. Rev. **89**, 1090 (1953).

[10] Flyagin, Dzhelepov, Kiselev, and Oganesyan, JETP **35**, 854 (1958), Soviet Phys. JETP **8**, 592 (1959).

[11] A. F. Dunaĭtsev and Yu. D. Prokoshkin, JETP **36**, 1656 (1959), Soviet Phys. JETP **9**, 1179 (1959).

[12] I. M. Vasilevskiĭ and Yu. D. Prokoshkin, Атомная энергия (Atomic Energy) **9**, 237 (1959).

[13] A. A. Tyapkin, JETP **30**, 1150 (1956), Soviet Phys. JETP **3**, 979 (1957); Yu. D. Prokoshkin, JETP **31**, 732 (1957), Soviet Phys. JETP **4**, 618 (1957).

[14] Yu. D. Prokoshkin, JETP **38**, 455 (1960), Soviet Phys. **11**, 334 (1960).

[15] Dzhelepov, Oganesyan, and Flyagin, JETP **32**, 678 (1957), Soviet Phys. JETP **5**, 546 (1957).

[16] E. Salpeter and J. Goldstein, Phys. Rev. **90**, 983 (1953).

[17] Yu. D. Prokoshkin, Proc. CERN Symposium **2**, 385 (1956).

[18] B. S. Neganov and O. V. Savchenko, JETP **32**, 1265 (1957), Soviet Phys. JETP **5**, 1033 (1957).

[19] B. S. Neganov and L. B. Parfenov, JETP **34**, 767 (1958), Soviet Phys. JETP **7**, 528 (1958); M. G. Meshcheryakov and B. S. Neganov, Dokl. Akad. Nauk SSSR **104**, 360 (1955), and paper at the Conference on the Physics of High Energy Particles, Moscow, 1956; Fields, Fox, Kane, Stallwood, and Sutton, Phys. Rev. **109**, 1713 (1958).

[20] G. B. Yodh, Phys. Rev. **98**, 1330 (1955).

[21] Yu. M. Kazarinov and Yu. N. Simonov, JETP **35**, 78 (1958), Soviet Phys. JETP **8**, 56 (1959).

[22] A. H. Rosenfeld, Phys. Rev. **96**, 139 (1954).

[23] Batson, Cullwick, Klepp, and Riddiford, Proc. Roy. Soc. (London) **A251**, 233 (1959).

[24] S. Mandelstam, Proc. Roy. Soc. (London) **A254**, 491 (1958).

[25] Pontecorvo, Mukhin, Prokoshkin, and Soroko, Materials on the Conference on the Physics of High-Energy Particles, Kiev, 1959 (in press).

[26] Meshkovskiĭ, Shalamov, and Shebanov, JETP **35**, 64 (1958), Soviet Phys. JETP **8**, 46 (1959).

Translated by R. T. Beyer
149

SOVIET PHYSICS JETP VOLUME 11, NUMBER 3 SEPTEMBER, 1960

EXCITED STATES OF Cs^{134}

A. S. MELIORANSKIĬ, I. V. ÉSTULIN, L. F. KALINKIN, and B. S. KUDINOV

Institute of Nuclear Physics, Moscow State University

Submitted to JETP editor September 19, 1959

J. Exptl. Theoret. Phys. (U.S.S.R.) **38**, 758-764 (March, 1960)

Cascade γ transitions induced in cesium nuclei by thermal neutron capture were studied. The scheme of low energy Cs^{134} levels of excitation energies up to 320 kev is discussed.

INTRODUCTION

A large number of odd-odd nuclei are known; however, the excited states of most of them have been little studied. Also, theoretical ideas on the structure of the energy levels of such nuclei have not been developed, which is evidently connected both with the difficulty of the problem and with the lack of experimental material. At the same time, the character of the energy states of odd-odd nuclei can give additional information on the interaction of the odd proton with an odd neutron,[1] and also of these nucleons with the even-even core of the nucleus. In the present work, the low-lying excited states of the odd-odd nucleus Cs^{134} (55 protons, 79 neutrons) are studied.

Almost all odd-odd nuclei are radioactive. The energy states of similar nuclei can be studied in nuclear reactions and also by investigating the γ radiation emitted by nuclei in neutron capture.[2] The soft γ radiation emitted by nuclei in the radiative capture of thermal neutrons has been studied by us previously.[3,4] Here the position of the energy levels and their quantum characteristics were determined non-uniquely. More complete data can be obtained by measurement of cascade γ quanta, as has been shown by a number of authors.[2,5,6] In the present work, cascade γ radiation of radiative neutron capture has also been investigated.

For measurement of cascade γ quanta, use is made of a luminescence coincidence spectrometer. The method of the work and the subsequent results are described below; these results make it possible to establish the system of the low excited levels of Cs^{134}.

APPARATUS AND METHOD OF MEASUREMENTS

The block diagram of the luminescence coincidence spectrometer developed by one of the authors[7] is shown in Fig. 1. The spectrometer consists of the control and main channels. In the control channel, the pulses entering from the luminescence counter [FEU-11 with NaI(Tl) crystal], are fed after amplitude selection to the coincidence circuit which controls the bandpass filter. Pulses in the main channel [FEU-13 with NaI(Tl) crystal] are directed by the bandpass filter to the multi-channel amplitude analyzer. The spectrometer makes it possible to measure the spectrum of pulses that are coincident in time with the chosen energy interval (the resolving time of the coincidence selector was 8×10^{-8} sec). For measurement of the spectrum of random coincidences, a delay was introduced for the pulses in the main channel.

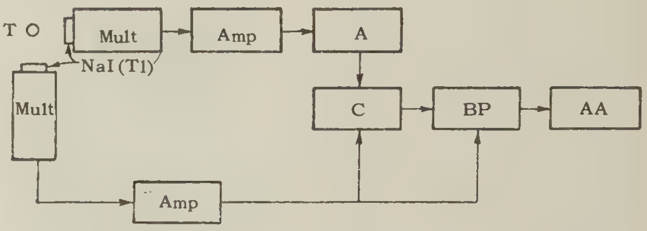

FIG. 1. Block diagram of the luminescence coincidence spectrometer: M – target, Amp – amplifier, A – amplitude analyzer, C – coincidence circuit, BP – bandpass filter, AA – 20-channel amplitude analyzer.

The target of CsF (a disk of diameter 20 mm and mass 0.25 g) was placed in the beam of neutrons emerging from the shield of the heavy-water reactor of the U.S.S.R. Academy of Sciences. The luminescence counters in the shield of lead and B_4C were located in a plane perpendicular to the beam of neutrons. In the absence of the target, the number of coincidences was negligibly small in comparison with the number of coincidences in the presence of the target. With the CsF target, the total number of coincidences amounted to 20 – 60 pulses/sec for an intensity of light in the channels of $2 - 5 \times 10^4$ pulses/sec. Approximately half the total number of coincidences were random. The spectrum of the random coincidences was

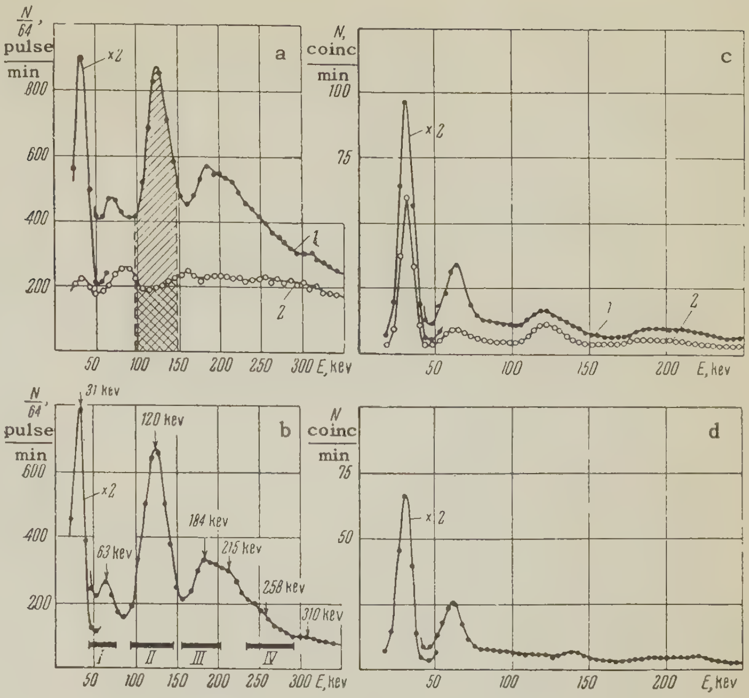

FIG. 2. Pulse spectra in the control channel for the following radiations: a – unfiltered and passed through 2 mm lead (curves 1 and 2, respectively), b – absorbed in 2 mm lead; the spectra of the coincidence pulses with the region 120 kev for control of the pulses; c – unfiltered and passed through 2 mm lead, curves 1 and 2 respectively, and d – absorbed in 2 mm lead. I, II, III, IV correspond to separate series of measurements. The exposure for measurement of the spectrum in c amounted to 40 minutes.

similar to the spectrum of the pulses in the channels. Each measurement of the spectrum of the total number of coincidences was accompanied by measurement of the spectrum of the random coincidences. The desired spectrum of true coincidences was obtained by finding the difference of these two successively measured spectra. In what follows only the spectra of the pure coincidences will be discussed.

Gamma radiation which takes place in the beam along with the neutrons can in the scattering produce noise readings in the counter. In experiments with a single crystal luminescence spectrometer[3] for consideration of this effect, the beam of neutrons at the exit of the neutron collimator was intercepted by a thin layer of B_4C. In the measurement of coincidences, this layer lowers the number of coincidences up to several per cent of the number of coincidences with an uninterrupted beam. In the experiments described, this correction was neglected.

The method of measurement is illustrated by the curves of Fig. 2. Curve 1 in Fig. 2a demonstrates the characteristic spectrum of pulses in a control channel produced by γ radiation of a CsF target. The peaks of the soft γ lines appear on a sizable "base" of Compton distribution of the harder γ lines. As was shown earlier[3] [by means of measurement with lead filters in the collimator of the γ rays (curve 2 in Fig. 2a)], one can separate the spectrum of the soft γ radiation. The curve of Fig. 2b shows the γ-ray spectrum absorbed in a lead filter of thickness 2 mm. The corresponding spectra of coincidences, obtained in one of the experiments, are shown by the curves of Fig. 2c and 2d. In these measurements, coincidences with light peaks of γ rays of energies 120 kev were neglected (the gap in the control channel is shown by the shaded region in Fig. 2a). Curve 1 of Fig. 2c was obtained in measurements without the filter. Curve 2 of the same drawing, which takes into account coincidences with the "base," was measured with a lead filter in the γ-ray collimator of the control channel. The difference of curves 1 and 2 in Fig. 2c, obtained in successive measurements, gives the coincidence spectrum (Fig. 2d) with soft γ radiation absorbed in a lead filter of 2 mm (see Fig. 2b).

The resulting coincidence spectra of the type shown in Fig. 2d will be discussed in the paper. In certain cases, control experiments were carried out with a lead filter in the γ-ray collimator, placed in front of a luminescence counter of the base channel; this served to make more accurate measurements of the low-intensity γ lines. These controls of measurement made it possible to reduce the noise in the coincidence spectra of the given type.

ISOMERIC TRANSITION OF Cs^{134m}

A peak appears in coincidence spectra, along with the peaks from the γ lines whose energy (31 ± 2) kev is equal to the energy of the x radiation of the Cs atom. This radiation is explained principally by internal conversion of γ quanta in the K shell of the atom, and in part by the photoeffect of γ quanta in self-absorption in the target.

For a thin target of CsF employed in the work, the effect of self-absorption was taken into account; it was not large. By comparison of the area of the peak from the x radiation with the area of the light peak, the coefficient of internal conversion of γ rays α_K in the K shell of the atom was determined. In this case, corrections[3,4] were introduced for the effectiveness of the luminescence counter for γ rays (ϵ), absorption of radiation on the path to the crystal of NaI(Tl), (k), and inside the target (κ). The experimentally measured values of α_K were compared with the theoretical[8] for determination of the multipolarity of the corresponding radiative transition.

With a view toward testing the accuracy of the determination of α_K in the introduction of the listed corrections, a control experiment was carried out with Cs^{134m} ($T_{1/2} = 3.1$ hours), the radiation of which was studied in researches of other authors.[9] In the experiments under consideration, the isomer was obtained in a sufficiently long exposure of the working target of CsF by a neutron beam. The spectrum from the induced activity was measured after turning off the beam with the same target and with the same geometry as for the measurement of the γ-ray (n, γ) reaction. The coincidence spectrometer was used in these experiments as a single crystal luminescence spectrometer. A γ-ray peak with energy 127 kev and a peak with energy 31 kev (x radiation of Cs) were observed in the spectrum. Comparison of the areas of these two peaks made it possible to determine the value of the coefficient of internal conversion of the γ rays of an isomeric transition in the K shell of the atom, $\alpha_K = 2.8 \pm 0.3$, which is in excellent agreement with the value obtained in the research of Sunyar, Mihelich and Goldhaber,[9] and with the theoretical value $\alpha_{\text{theor}} = 2.82$ for the E3 transition.[8]

γ RADIATION OF RADIATIVE NEUTRON CAPTURE IN Cs

In the investigation of cascade γ transitions that arise in the radiative capture of neutrons in Cs, four series of experiments were carried out (I, II, III, and IV in Fig. 2b) which differ in energy intervals isolated in the control channel. These experiments were supplemented by measurements with a single crystal spectrometer. As a result, the previous data[4] on energies and intensities of the γ quanta of the reaction $Cs^{133}(n, \gamma)Cs^{134}$ were made more precise, a number of new γ lines were revealed, and the coincidences between them were tested. A summary of the data is given in Table I.

TABLE I

Number of γ lines	Energy, kev	Number of γ quanta per neutron trapped, per cent	Appeared in coincidences
X	31±2	50±8	*I, II, III, V*
γ_1	63±2	9±2	*II, V*
γ_2	75±5	~1.5	**III, does not contradict I and II**
γ_3	120±3	18±3	*I, V*
γ_4	138±4	2±1	**III, V, does not contradict II**
γ_5	184±4	9±2	*V*
γ_6	195—260	3±2	*I*
γ_7	215±4	7±2	*V*
γ_8	258±4	5±1	*V*
γ_9	310±5	4±1	*V*

In the supplementary experiment, a crystal of NaI(Tl) 4 cm thick was inserted in the luminescence counter of the control channel. Pulses corresponding to γ quanta with energies close to the binding energy of the last neutron in the Cs^{134} nucleus, equal to $E_n = 6.8$ Mev (width of the gap 2 Mev) were selected. The γ lines observed in these experiments are listed in the last column of Table I by the symbol V. All the radiative transitions appearing in the measurement of coincidences have a lifetime of less than 4×10^{-8} sec, which is demonstrated by an estimate of the lifetime according to the method of lagging coincidences. Thus, the γ transitions under consideration are of the E1, M1, and E2 type. The M2 transitions or those of higher multipolarity would have a much longer lifetime.

In the series of experiments IV, the coincidence spectrum with light peaks from 258-kev γ quanta was measured. No coincidences of these γ lines with any other soft γ quanta were observed.

In series III, coincidences in the region of the peak from γ quanta with energy 184 kev were selected (see Feg. 2b). After introducing corrections in the spectrum of coincidences, peaks from two low intensity lines with energies of 75 and 138 kev and x radiation, whose intensity n_X was approximately three times the intensity of the γ quanta with energy 138 kev, were observed. As has already been noted, introduction of transitions of higher multipolarity contradicts the estimates of the lifetimes. For an explanation of the observed intensity n_X, it is necessary to take into account the conversion of the two previously mentioned γ lines in the K shell of the atom. In this case, the intensity of γ quanta with energies 75 kev is shown to be ~ 1.5 per cent for a single trapped neutron, which does not contradict the estimates of the intensity obtained in other researches. The transition with energy 75 kev can be E2 or a mixture M1 + E2. In the chosen scheme of transitions, preference is given to the latter.

In the series of experiments II, the spectrum was measured of coincidences with γ quanta of energies 120 kev. The results of one of these experiments are shown in Fig. 2d. Sharp peaks were discovered of x radiation, and a peak of γ quanta with energy 63 kev. Peaks from low intensity γ lines with energies 75 and 138 kev were also observed. Moreover, in the energy region 195 — 260 kev, unresolved γ lines appeared with a total intensity (3 ± 2) per cent per single trapped neutron. The intensity of the x radiation n_X relative to the number of 63-kev γ quanta, n_{63}, was found to be equal to $n_X/n_{63} = 4.9 \pm 0.6$. The coefficient of internal conversion of the 63-kev γ quanta was obtained with allowance for the possible conversion of the low-intensity γ lines appearing in the measurements. The corrected value of α_K is shown in Table II, as is also the experimental value. Comparison with theoretical values of α_K leads to the conclusion that the 63-kev, transition is electric quadrupole.

In series I, the spectrum of coincidences with the 63-kev γ line was measured. The result of one of these measurements is shown in Fig. 3.

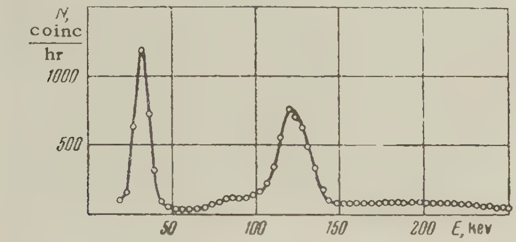

FIG. 3. Spectrum of coincidence pulses with 63-kev γ line.

Peaks from 120-kev γ quanta and a peak of x radiation are seen. The relative intensity of x radiation is $n_X/n_{120} = 0.81 \pm 0.20$. The coefficient of internal conversion of the 120-kev γ quanta in the K shell of the atom can be obtained here by introducing corrections for the possible conversion of the 75- and 138-kev γ quanta. This correction reduces the accuracy of the determination of α_K (120 kev). As is seen from Table II, an unambiguous choice between the transitions of type M1 and E2 cannot be made. In the most probable scheme of transitions, the 120-kev γ quanta are regarded as dipole.

DISCUSSION OF THE LEVEL SCHEME

A proposed scheme of excited levels of the Cs^{134} nucleus and the transition between them is shown in Fig. 4. In the construction of the scheme, consideration has been given to the coincidences which appeared in the research and to the anticoincidences of the separate γ transitions (see Table I). The values of the energy and the intensity of the transitions, lifetimes, spin, and parity of the levels (both those known previously and those assumed on the basis of the experimental data of the present research) are also taken into account. In addition to the levels whose existence has been established in this research, the levels 10.5 and 137 kev, known from the decay of the isomeric state Cs^{134m}, were also included in the scheme. The numbers of the γ transitions in Fig. 4 correspond to the numbers of the γ lines of Table I. The total probabilities of radiative transitions, including the intensity of the γ transition and the internal conversion in the K and L shells of the atom, are shown at the breaks of the arrows in the scheme. The accuracy of these data is defined by the accuracy of measurement of the intensities of the γ lines (Table I).

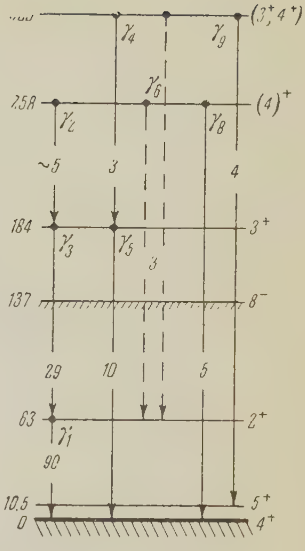

FIG. 4. Scheme of nuclear levels of Cs^{134}.

The most intense cascade, 63 — 120 kev, is fundamental in the construction of the scheme. It follows from intensity considerations that the 120-kev transition dominates the 63-kev transition. The large value of the absolute intensity of the latter suggests that it is located close to the ground state. The hypothesis that it terminates on the 10.5-kev level leads to worse agreement between the energies of cascade and direct transitions. In this case difficulties also arise in the choice of possible spin of the level from which the 63-kev transitions takes place.

The 63 — 120 kev cascade is not divided into intermediate levels, since there is a direct 184-kev transition, found in anticoincidences with the cascade in question. On the basis of coincidence measurements, levels are introduced in the scheme the energies of which, 258 or 320 kev, are equal, respectively, to the sums of the energies of 184- and 75-kev, or 184- and 138-kev γ lines.

In regard to direct transitions with energies of 258 and 310 kev, there is not sufficient convincing evidence that they terminate on the ground and first excited states, respectively. Furthermore, the doublet of these γ lines (transitions from corresponding levels can also lead to the ground and to the first excited levels) does not contradict the experimental result.

TABLE II

Energy of the transition, kev		63	120
Theory	$M1$	2.82	0.46
	$E2$	4.47	0.685
Experiment		4.3±0.6	0.6±0.25

In the proposed scheme, the characteristics of the 63-kev level are determined by the multipolarity of the transition found experimentally (Table II) with account of the characteristics of the isomeric and ground states. The characteristics of the 184-kev 3^+ level make it possible to explain the comparable intensities of transitions from it, if it is assumed that these transitions are magnetic dipole in nature.

The moment of the level with excitation energy 258 kev is selected from the same considerations, although less uniquely. The positive parity of this level follows from the fact that the 75-kev transition does not change the parity. The presence of concurrent transitions from the 320-kev level and consideration of their intensities makes it possible to assume the most appropriate characteristics of this level (3^+ or 4^+).

Measurements of the hard γ quanta of the reaction $Cs^{133}(n, \gamma)Cs^{134}$, carried out in a recently-published work,[10] confirm the existence in Cs^{134} of levels with energies 184 and 320 kev. In addition, transitions from the initial state to the level with energy 63 kev were not found. Therefore, the state which is realized in the capture of a thermal neutron probably has the characteristics of 4^+, not 3^+.

As is seen from the scheme of transitions, $_{55}Cs^{134}_{79}$ has many excited levels around the ground state; this is characteristic for odd-odd nuclei. We shall attempt to explain these levels by comparison with the levels of neighboring even-odd and odd-even nuclei. The configuration $(g_{7/2}, d_{3/2})$ corresponds to the ground state of Cs^{134}, where the shells of the last proton and neutron are indicated. The angular momentum and parity of the ground state 4^+ do not contradict the weak rule of Nordheim[1] for the addition of total momenta of the odd neutron and proton. The configuration $(g_{7/2}, d_{3/2})$ assumes states with characteristics 5^+, 4^+, 3^+, and 2^+. The level with excitation energy 10.5 kev was previously assigned to this configuration.[9] The level with excitation energy 63 kev also probably refers to it. Here we meet up with the multiplet structure of nuclear levels.[11] However, the probability of transition of type E2 from the 63-kev level is more than 200 times greater than the probability of a single particle transition.

Like the isomeric levels of the neighboring odd-even nuclei, the isomeric level of Cs^{134m} (137 kev) is interpreted as the first excited level of the neutron. The isomeric level is ascribed to the configuration $(d_{7/2}, h_{11/2})$. However, the energy of this level differs markedly from the energy of the isomeric transitions in the neighboring even-odd nuclei with the number of neutrons $N = 79$ the same as in the Cs^{134} nucleus (232 kev — $_{54}Xe^{133}$, 268 kev — $_{56}B^{135}$). Probably the interaction is that of odd nuclei.

The energy of the first excited level of the odd proton in the state $d_{5/2}$ in odd-even isotopes of Cs is equal to 82 kev (Cs^{133}) and 250 kev (Cs^{135}). In this region of excitation energies, one can expect the appearance of a multiplet structure corresponding to the configuration $(d_{5/2}, d_{3/2})$ with characteristics 4^+, 3^+, 2^+, and 1^+. It is possible that the levels of Cs^{134} with excitation energies 184 and 258 kev refer to this configuration. Unfortunately, there are no theoretical values with which one could compare the splitting of the levels of the nuclear multiplet.

In conclusion the authors thank their co-workers operating the physical reactor for their assistance in the research.

---

[1] C. J. Gallagher and S. A. Moszkowski, Phys. Rev. **111**, 1282 (1958).

[2] Bartholomew, Campion, Knowles, and Manning, Nucl. Phys. **10**, 590 (1959).

[3] Éstulin, Kalinkin, and Melioranskiĭ, JETP **32**, 979 (1957), Soviet Phys. JETP **5**, 801 (1957).

[4] Kalinkin, Melioranskiĭ, and Éstulin, JETP **35**, 592 (1958), Soviet Phys. JETP **8**, 410 (1959).

[5] V. G. Burmistrov, Izv. Akad. Nauk SSSR, Ser. Fiz. **23**, 898 (1959), Columbia Tech. Transl., in press.

[6] R. E. Segel, Phys. Rev. **113**, 844 (1959).

[7] A. S. Melioranskiĭ, Приьоры и техника эксперимента (Instrum. and Meas. Engg.), in press.

[8] L. A. Sliv and I. M. Band, Таблицы коэффициентов внутренней конверсии гамма-излучения (Tables of Internal Conversion Coefficients of

Gamma Radiation), Acad. Sci. Press, Moscow-Leningrad, 1958.

[9] Sunyar, Mihelich, and Goldhaber, Phys. Rev. **95**, 570 (1954).

[10] Balzer, Knoepfel, Lang, Stoll, and Wölfli, Helv. Phys. Acta **32**, 264 (1959).

[11] L. V. Groshev and A. M. Demidov, Атомная энергия (Atomic Energy) **3**, 91 (1957).

Translated by R. T. Beyer
150

SOVIET PHYSICS JETP VOLUME 11, NUMBER 3 SEPTEMBER, 1960

INVESTIGATION OF THE GAMMA SPECTRUM OF Ce^{140}

S. F. ANTONOVA, S. S. VASILENKO, M. G. KAGANSKIĬ, and D. L. KAMINSKIĬ

Leningrad Physico-technical Institute, Academy of Sciences, U.S.S.R.

Submitted to JETP editor September 29, 1959

J. Exptl. Theoret. Phys. (U.S.S.R.) **38**, 765-767 (March, 1960)

Gamma radiation with energy above $2mc^2$ from Ce^{140} was investigated by measuring the internal pair-conversion positron spectrum of decaying La^{140}. The multipolarities and intensities of γ quanta with energies $E_\gamma = 1596$, 2330, and 2525 kev have been determined by comparison with the corresponding K-shell electron-conversion lines. It is shown that for transitions involving energies above $2mc^2$ such a method of determining γ-quantum characteristics has certain advantages.

AN investigation of γ quanta of energy greater than 1 Mev, which accompany the transition of nuclei from the excited state to the ground state, entails many difficulties. The principal method of investigating low-energy γ rays, by means of the internal-conversion electrons, has little effectiveness at energies > 1 Mev, since the internal conversion becomes very small and in addition depends weakly on the multipolarity of the transition. Gamma rays with energy $E_\gamma > 2mc^2$ can also be investigated by internal conversion with production of electron-positron pairs, but the probability of this process is relatively low. Consequently, γ radiation from nuclei was investigated by means of the internal pair-conversion process only in a few cases.[1]

In the present work we investigated the hard γ radiation from Ce^{140} by simultaneously measuring the spectrum of the pair-conversion positrons and the corresponding K-shell conversion lines. This method has several advantages. Thus, for example, in determining the multipolarity of the γ radiation by the absolute value of the conversion coefficient one must have not only the conversion spectrum but also data on the γ-ray intensity. On the other hand, when determining the multipolarity by the ratio of the internal pair coefficient (Γ_p) and the electron conversion on the K shell (α_K), no data on the γ-ray intensity are necessary, and both the spectra of the positron pair conversion and of the electron conversion can be obtained with the same instrument. Furthermore, as seen from Table I, the ratio of the coefficients of pair conversion to electron conversion depends more strongly on the multipolarity than on the absolute values of these coefficients. Thus, for example, for Ce^{140} at $E_\gamma = 5mc^2$ the conversion coefficients from the K shell, for M1 and E2 radiations, differ by 10%, whereas the ratio Γ_p/α_K differs in this case by 50%.

The spectrometer used for the measurements has been described earlier.[2,3] The La^{140} sources were obtained by bombarding lanthanum oxide, deposited on an aluminum foil 5 μ thick, with thermal neutrons. The source density was 1 — 2 mg/cm², the source dimensions 25 × 10 mm. The spectrometer resolution $\Delta(H\rho)/H\rho$ was 1.5%.

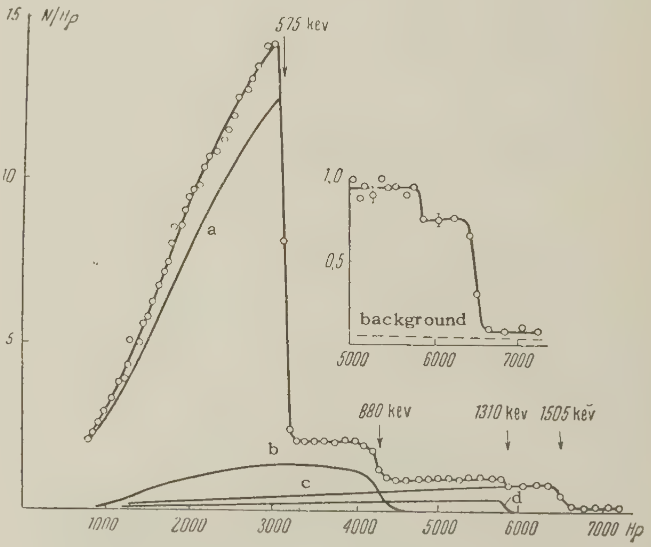

Positron spectrum of internal conversion of Ce^{140}; a,b,c,d,— partial positron spectra, due to internal pair conversion of transitions with respective energies 1597, 1902, 2527, and 2332 kev.

The spectrum of the internal-conversion positrons is shown in the diagram. As can be seen, the positron spectrum is complex. Many steep drops, observed in the spectrum, are due to the presence of corresponding energy transitions for the Ce^{140} nucleus. The transition energies, ac-

TABLE I

γ-quantum energy, kev	Quantity	Calculated data[5,6]					Measurement data
		E1	E2	E3	M1	M2	
1597	$10^3\ \alpha_K$	0:32	0.68	1.24	0.87	1.91	
	$10^4\ \Gamma_p;\ Z=0$	3,48	1.23	0.48	0,64	0.28	
	$10^4\ \Gamma_p;\ Z=84$	2.14	0.92				
	$10^2\ \Gamma_p/\alpha_K;\ Z=0$	109	18.1	3,86	7.35	1.45	$I_{e+}/I_{e-} = 15.5 \pm 0.5$
	$10^2\ \Gamma_p/\alpha_K;\ Z=84$	67	13.5				
2332	$10^3\ \alpha_K$	0.16	0.33	0.56	0.38	0.76	
	$10^4\ \Gamma_p;\ Z=0$	8.84	4,80	2.56	3.20	1.95	
	$10^4\ \Gamma_p;\ Z=84$	7,32	3,70				
	$10^2\ \Gamma_p/\alpha_K;\ Z=0$	550	145	45.5	84	25.8	$I_{e+}/I_{e-} = 116$
	$10^2\ \Gamma_p/\alpha_K;\ Z=84$	460	112				
2527	$10^3\ \alpha_K$	0.15	0.30	0.48	0.33	0.64	
	$10^4\ \Gamma_p;\ Z=0$	10.1	5.84	3.44	4.20	2.60	
	$10^4\ \Gamma_p;\ Z=84$	8.68	4.44				
	$10^2\ \Gamma_p/\alpha_K;\ Z=0$	680	194	71,5	130	40.5	$I_{e+}/I_{e-} = 105$
	$10^2\ \Gamma_p/\alpha_K;\ Z=84$	580	148				

cording to our data, are 1597, 1902, 2332, and 2527 kev. These values are in good agreement with those obtained by others.[4] The partial spectra (see diagram) were separated by the value of the steep drop in the summary positron spectrum. It was assumed here that the energy distribution of the internal pair-conversion positrons for Ce^{140} ($Z = 58$) differs little from the distribution for $Z = 84$.

As already noted, the multipolarity of the γ rays was determined from the ratio Γ_p/α_K. The calculated and the experimental values of Γ_p/α_K are listed in Table I. The values of α_K were calculated from the Sliv and Band tables.[5] The Γ_p/α_K ratios listed in Table I are given for two values of Γ_p (for $Z = 0$ and $Z = 84$), since calculations are available at present only for these values of Z.[6] The experimental ratio of the coefficients of pair conversion and electron conversion was determined from the ratio of the areas of the corresponding partial positron spectra and the conversion K lines. Since the internal-conversion electron spectrum was measured only partially, data on the weakest conversion lines were taken from the work of Dzhelepov, Prikhodtseva, and Khol'nov.[4]

As can be seen from Table I, γ quanta with energy 1597 and 2332 kev have multipolarity of type E2, while the γ quantum of energy 2527 kev is of type M1. Knowing the multipolarity of γ quanta from the ratio Γ_p/α_K, one can determine the values of Γ_p.

Since the intensities of the partial positron spectra are known, then, by knowing Γ_p, one can determine the intensity of the γ quanta. These data are listed in Table II. The same table gives the results of references 4 and 7. As seen from the table, our data on the energy, multipolarity, and intensities of the γ rays are in good agreement with those of Dzhelepov et al.

It was established recently[4] that the 1902-kev transition is a 0 — 0 transition. Our results confirm this. The experimentally obtained value of the ratio of the conversion probabilities on the K shell and with pair production was $W_K/W_p = 6.3$. At the same time, calculation by the Thomas formula[8] gives for this case a value close to the experimental, $W_K/W_p = 7.6$.

TABLE II. Data on γ radiation from Ce^{140}

Our data				Data of Dzhelepov et al.[4,7]		
E_γ, kev	Multipolarity	$10^4\ \Gamma_p$	Relative Intensity	E_γ, kev	Multipolarity	Relative Intensity
1597	E2	1.15	100	1597	E2	100
2332	E2	3.9	0.9	2343	M1, E2	0.78
2527	M1	3.2	5.0	2525	M1	3.7
2900			0.3	2910	E2, M1	0.08

---

[1] K. Siegbahn, Beta- and Gamma-Ray Spectroscopy, North Holland, Amsterdam, 1955.

[2] D. L. Kaminskiĭ and M. G. Kaganskiĭ, Приьоры

и техника эксперимента (Instrum. and Meas. Engg.) No. 1, 32 (1959).

[3] Antonova, Vasilenko, Kaganskiĭ, and Kaminskiĭ, JETP **37**, 667 (1959), Soviet Phys. JETP **10**, 477 (1960).

[4] Dzhelepov, Prikhodtseva, and Khol'nov, Dokl. Akad. Nauk SSSR **121**, 995 (1958), Soviet Phys.-Doklady **3**, 803 (1959).

[5] L. A. Sliv and I. M. Band, Таблицы коэффициентов внутренней конверсии (Tables of Coefficients of Internal Conversion) Academy of Sciences Press (U.S.S.R.), 1956.

[6] M. E. Rose, Phys. Rev. **78**, 184 (1950).

[7] V. P. Prikhodtseva and Yu. V. Khol'nov, Izv. Akad. Nauk SSSR, Ser. Fiz. **22**, 176 (1958), Columbia Tech. Transl. p. 173.

[8] R. Thomas, Phys. Rev. **58**, 714 (1940).

Translated by J. G. Adashko
151

SOVIET PHYSICS JETP VOLUME 11, NUMBER 3 SEPTEMBER, 1960

NUCLEON EMISSION BY A ROTATING NUCLEUS

G. A. PIK-PICHAK

Submitted to JETP editor September 29, 1959

J. Exptl. Theoret. Phys. (U.S.S.R.) **38**, 768-772 (March, 1960)

The effect of a large angular momentum on the emission of nucleons by an excited nucleus is determined in the independent particle model. The mean characteristics of neutron emission as a function of temperature and angular momentum are calculated. An estimate is made of the mean excitation energy which remains after the emission of the nucleons and which is carried off by the γ quanta.

In recent times experiments have begun to be performed in which heavy ions are used as bombarding particles.[1-3] The compound nucleus formed in these reactions usually has a relatively high excitation energy and a large angular momentum. The existence of a large moment of inertia has a great effect on the physics of the decay processes of the compound nucleus and, in particular, on the emission of nucleons.

We shall assume that the compound nucleus formed in the reaction is in thermodynamic equilibrium, which is in fact the condition for the existence of a compound nucleus. Then the excitation energy of the nucleus, E, can be written as

$$E = E(T) + E_{\text{rot}} \qquad E_{\text{rot}} = j^2 \hbar^2 / 2I,$$

where $E(T)$ is the thermal energy, E_{rot} is the energy of rotation, j is the angular momentum, I is the moment of inertia of the nucleus, and $T = \sqrt{10\,E(T)/A}$ is the temperature of the nucleus of mass A.

Generally speaking, the nuclear moment of inertia is not equal to the moment of inertia of a rigid body and depends on the formation of pairs on the Fermi surface.[4,5] However, even for relatively small thermal excitation these pairs are destroyed, and consequently the nuclear moment of inertia becomes equal to the moment of inertia of a rigid body. The effect of the rotation of the nucleus on the formation of pairs is similar to the effect of a magnetic field, i.e., the increase of the moment of inertia counteracts the formation of pairs, and starting from some angular momentum j_c, all pairs are destroyed. The quantity j_c can be estimated by comparing the energy of rotation with the change of energy connected with the formation of pairs:

$$\hbar^2 j_c^2 / 2I \sim \Delta^2 \rho / 4,$$

where Δ is the magnitude of the gap and ρ is the level density on the Fermi surface; $j_c \sim 7$ for nuclei with $A \sim 50$ and $j_c \sim 15$ for nuclei with $A \sim 250$. Even for vanishing thermal excitation energy the moment of inertia of the nucleus therefore becomes equal to the moment of inertia of a rigid body I_0 already for relatively small angular momenta (the compound nucleus usually has the maximal angular momentum $j \gtrsim 30$ for $A \sim 50$ and $j \gtrsim 70$ for $A \sim 250$). We shall assume in the following that the nucleus has spherical shape, i.e., $I_0 = \frac{2}{5}\mu AR^2$, where μ is the mass of the nucleon, and $R = r_0 A^{1/3}$ is the radius of the nucleus.

The probability for the evaporation of a nucleon from a nucleus with small angular momentum per unit time is usually determined (by using the principle of detailed balance or the reciprocity theorem) from the cross section of the reverse process, in this case from the cross section for compound nucleus formation, which is known experimentally. Since no experiments have been performed to determine the cross section for nucleon capture by a nucleus with high angular momentum, the decay probability for such a nucleus must be found directly.

The characteristics of the emission of nucleons by a nucleus with large angular momentum can be found in the independent particle model. We shall regard the nucleus as a set of spinless particles moving in a spherical square well of depth V and radius R. In the ground state of the nucleus all nucleons are distributed pairwise over the levels such that their angular momenta compensate each other and give the total angular momentum zero. If the nucleus has nonvanishing angular momentum, some of the nucleons must be placed on higher levels such that the total angular momentum of the nucleons is equal to the given one. For given angular momentum the state with the lowest energy corresponds to the state in which the energy of thermal motion is zero.

As the angular momentum increases, more and more nucleons go to higher levels, and for sufficiently high angular momentum it becomes possible that some of the nucleons find themselves above the well and can leave the nucleus. This process of emission of a nucleon from the nucleus has nothing in common with the usually considered process of evaporation and is only due to the rotation of the nucleus. Since the orbital angular momentum of the nucleons above the well is different from zero, the emission of neutrons will be hindered by the centrifugal barrier and that of the protons by the centrifugal and Coulomb barriers. The lifetime of these states will therefore be greater than the characteristic nuclear periods. To obtain a rough qualitative estimate for nucleons above the well, we can thus use the expression for the single particle level density in a spherical well of infinite depth.

In the quasi-classical approximation the number of particles within the interval $d\epsilon$ with orbital angular momentum l and projection m in a system with the total angular momentum j and temperature T is equal to[6]

$$dn_{lm} = \frac{1}{2\pi\varepsilon}\left[\exp\left\{\frac{\varepsilon-\theta-\gamma m}{T}\right\}+1\right]^{-1}\sqrt{\frac{2\mu R^2}{\hbar^2}-(l+{}^1/_2)^2}\,d\varepsilon, \tag{1}$$

where $\gamma = j\hbar^2/I_0$, and θ is the chemical potential of the rotating system, which up to terms of order E_{rot}/A is equal to θ_0, the chemical potential of a system with angular momentum zero. In what follows this correction will be neglected.

The width for the emission of a nucleon is of the order of magnitude of the quantity

$$\Gamma = \sum_{l,\,m}\int dn_{lm}T_l(E)\,\varepsilon,$$

where $T_l(E)$ is the penetrability of the barrier and E is the kinetic energy of the nucleons at infinity. For neutrons with $E/\epsilon \ll 1$ we may use the approximate expression for $T_l(E)$:[7]

$$T_l(E) = (4x/X)\,v_l(x);$$

$$x = \sqrt{2\mu R^2E}/\hbar;\ \ X = \sqrt{2\mu R^2\varepsilon}/\hbar;$$

$$v_l(x) = 2/\pi x\,(J^2_{l+1/2}(x)+N^2_{l+1/2}(x)),$$

$J_{l+1/2}(x)$ and $N_{l+1/2}(x)$ are the Bessel and Neumann functions. Tables of $v_l(x)$ are given in reference 8.

In the case of protons we used the formula for the penetrability of the Coulomb barrier with account of the angular momentum of the proton obtained in the quasi-classical approximation:[6]

$$T_l(E) = \exp(-2C_l);$$

$$\frac{C_l}{g} = \frac{1}{2}t^{-1/2}\left(\frac{\pi}{2}+\arcsin\frac{1-2t}{\sqrt{1+4yt}}\right)-$$

$$-\sqrt{1+y-t}+y^{1/2}\ln\frac{1+2t^{1/2}(t^{1/2}+\sqrt{1+y-t})}{\sqrt{1+4yt}};$$

$$g^2 = 2\mu Ze^2R/\hbar^2, \qquad y = l(l+1)/g^2, \qquad t = E/B_C,$$

and $B_C = Ze^2/R$ is the Coulomb barrier for a nucleus with atomic number Z.

The penetrability of the centrifugal barrier becomes close to unity for $E \geq \hbar^2l^2/2\mu R^2$. On the other hand, the probability of finding a particle in the given interval $d\epsilon$ [formula (1)] is close to unity for $\epsilon \leq \theta + \gamma m$. Therefore, in order that the lifetime of the compound nucleus be greater than the characteristic nuclear period, the inequalities

$$V + \hbar^2l^2/2\mu R^2 > \mu + \gamma l \geqslant \mu + \gamma m$$

must be fulfilled for all l. This leads to the condition

$$E_{rot} < \tfrac{2}{5}BA,$$

where $B = V - \theta_0$ is the binding energy of the neutron.

If the thermal energy is equal or close to zero, a nucleon can be emitted only if the change of the energy of the nucleons at the Fermi surface due to the rotation of the nucleus exceeds the binding energy:

$$B < \gamma m_f \leqslant \gamma l_f \approx \gamma\sqrt{2\mu R^2\theta_0}/\hbar.$$

For $E_{rot} > E^k_{rot} = B^2A/10\theta_0$ the rotating nucleus will emit neutrons. For $E_{rot} < E^k_{rot}$ there will be no emission of nucleons, and the nucleus will be in an excited state until the excitation energy is carried off by the emission of γ quanta. If this state of the nucleus is the result of the emission of several particles, the excitation energy of the nucleus will with equal probability take on any value inside some interval of excitation energies which is larger than B. The average excitation energy of a nucleus with small angular momentum is therefore equal to the known value B/2, while it is equal to $E^k_{rot} - B/2$ for a nucleus with large angular momentum $(T = 0)$.

In heavy-ion reactions the compound nucleus may have arbitrary angular momenta — from zero up to some maximal value. For small values of the angular momentum, when the exponential in the denominator of (1) can be expanded in terms of γ after which the exact expression for the penetrability of the centrifugal barrier is replaced

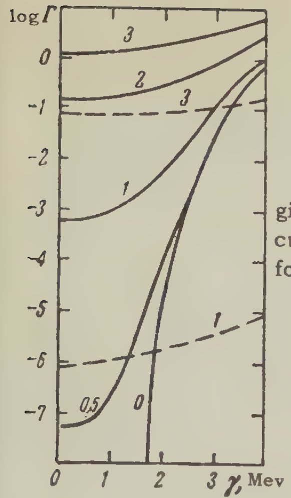

FIG. 1. The numbers at the curves give the temperature in Mev. Dotted curves – for protons, solid curves – for neutrons.

by its classical approximation, the probability for evaporation depends on the kinetic energy of the neutron in the same way as usual.[9] The only difference is that we use the temperature of the initial nucleus instead of that of the final nucleus. This inaccuracy can be easily taken account of, however, by taking the correct temperature (this was done in the calculation of the cascade emission of neutrons). Since the replacement of the penetrability of the centrifugal barrier by its classical approximation is legitimate if the denominator of (1) changes slowly as compared to $T_l(E)$, the condition of applicability of the formulas obtained in references 10 and 11 is not determined by the smallness of the parameter E_{rot}/TA (the parameter of the thermodynamic perturbation theory) alone.

We calculated Γ numerically for the nucleus with $2\mu R^2/\hbar^2 = 1$ Mev^{-1}, V = 40 Mev, B = 8 Mev, $B_C = 8$ Mev, $g^2 = 8$ ($A \approx 50$, $Z \approx 25$, $r_0 = 1.23 \times 10^{-13}$ cm). Figure 1 shows the dependence of the logarithm of the neutron and proton emission widths on the temperature and angular momentum of the nucleus. It is seen from the figure that the proton emission probability is almost independent of the angular momentum, whereas the neutron emission probability depends very strongly on it, especially at small temperatures. This behavior of Γ_n and Γ_p as functions of the angular momentum has as a consequence that the number of protons emitted by a rotating nucleus is smaller than in the case where the nucleus has a small angular momentum.

Figure 2 gives the energy distribution of the neutrons. The scale of the curves is arbitrary. The existence of separate energetical groups of neutrons for T = 0 is due to the discrete values of m.

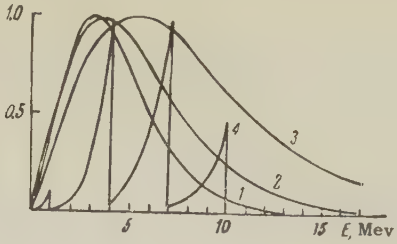

FIG. 2

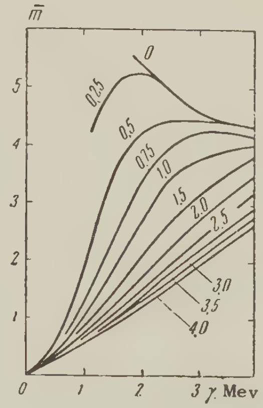

FIG. 4

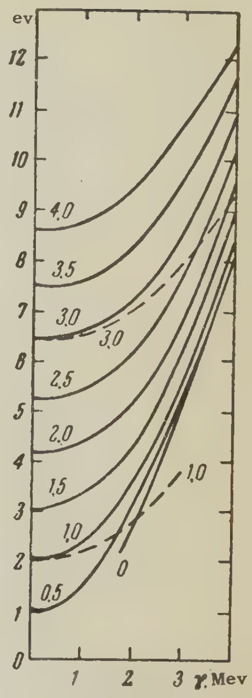

FIG. 3

FIG. 2. Curve 1: T = 1 Mev, γ = 2 Mev; 2: T = 2 Mev, γ = 1 Mev; 3: T = 3 Mev, γ = 0; 4: T = 0, γ = 3 Mev.

FIG. 3 The numbers at the curves give the temperature in Mev; the dotted curves are calculated with $T_l(E)$ taken from references 10 and 11.

FIG. 4. The numbers at the curves give the temperature in Mev.

Figure 3 shows the behavior of

$$\overline{E} = \sum_{lm} \int dn_{lm} T_l(E)\, \varepsilon E / \Gamma$$

the average kinetic energy of the neutron as a function of temperature and angular momentum. We note that even for $(E_{rot}/TA) \ll 1$ the quantity $\overline{E}$ is quite different from that obtained in reference 10.

Figure 4 shows the behavior of

$$\overline{m} = \sum_{lm} \int dn_{lm} T_l(E)\, \varepsilon m / \Gamma$$

the average projection of the angular momentum as a function of γ and T. For small T, an increase of γ leads to a decrease of the admissible projection m of the emitted neutrons and hence also to a decrease of $\overline{m}$.

The average excitation energy carried off by the neutron is equal to $B + \overline{E}$. Since the neutron changes the angular momentum of the nucleus by $\overline{m}$, the rotational energy carried off is equal to

$$(\hbar^2/2I_0)\,[j^2 - (j-m)^2] \approx (\hbar^2/2I_0)\, 2j\overline{m} = \gamma\overline{m}.$$

Hence the change in thermal energy of the nucleus is equal to $B + \bar{E} - \gamma\overline{m}$. If the thermal excitation energy of the nucleus is zero, the neutron carries off only mechanical energy and for $T = 0$ we have $B + \bar{E} = \gamma\overline{m}$. This equation may serve as a check on the accuracy of the numerical calculations. It turns out that it is satisfied with an accuracy up to 6%.

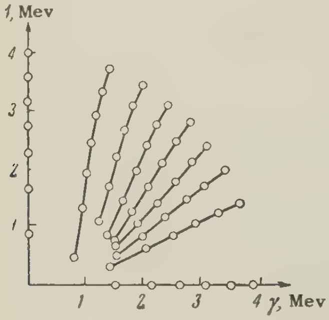

FIG. 5

Knowing the mean characteristics of the neutron emission process, we can find the approximate behavior of the nucleus during the time of the cascade process. In Fig. 5 we show an example of a cascade process with an initial total excitation energy of 80 Mev. The initial points correspond to identical values of the intervals ΔE_{rot}. It is seen from the figure that the ratio γ/T increases during the course of the cascade process. This leads to a large average excitation remaining after the emission of the neutrons and hence to a displacement of the maximum yield of a given isotope toward higher excitation energies of the nucleus. In the given case this displacement turns out to be equal to ~ 8 Mev for the maxima of the yield of the isotopes corresponding to the emission of 5 to 6 neutrons. The average excitation energy remaining in the nucleus is also equal to ~ 8 Mev.

In conclusion I express my gratitude to B. T. Geĭlikman, V. M. Galitskiĭ, and V. M. Strutinskiĭ for a useful discussion of this work and for valuable comments.

---

[1] Baraboshkin, Karamyan, and Flerov, JETP **32**, 1294 (1957), Soviet Phys. JETP **5**, 1055 (1957).

[2] Gerlit, Karamyan, and Myasoedov, Тр. Всес. конф. по ядерным реакциям при малых и средних энергиях, ноябрь 1957 (Transactions of the All-Union Conference on Nuclear Reactions at Low and Intermediate Energies, November 1957) Acad. Sci. Press, 1958.

[3] Knox, Quinton, and Anderson, Phys. Rev. Lett. **2**, 402 (1959).

[4] S. T. Belyaev, Kgl. Danske Videnskab. Selskab, Mat.-Fys. Medd. **31**, 11 (1959).

[5] A. B. Migdal, JETP **37**, 249 (1959), Soviet Phys. JETP **10**, 176 (1960).

[6] H. A. Bethe, Nuclear Physics, pt. II, M.-L. (1948) (Russ. Transl.).

[7] J. Blatt and V. Weisskopf, Theoretical Nuclear Physics, J. Wiley and Sons, N. Y. (1952).

[8] M. Lax and H. Feshbach, J. Acoust. Soc. Amer. **20**, 108 (1948).

[9] W. Heisenberg, Theory of the Atomic Nucleus, M., 1953 (Russ. Transl.).

[10] V. M. Strutinskiĭ, loc. cit. ref. 2.

[11] T. Ericson and V. Strutinski, Nucl. Phys. **8**, 284 (1958).

Translated by R. Lipperheide
152

THE CHANGE OF ATOMIC MAGNETIC MOMENTS IN FERROMAGNETIC METALS UNDER HYDROSTATIC COMPRESSION

E. I. KONDORSKIĬ and V. L. SEDOV

Moscow State University

Submitted to JETP editor October 3, 1959

J. Exptl. Theoret. Phys. (U.S.S.R.) **38**, 773-779 (March, 1960)

A study was made of the change of magnetic moment σ and electrical resistance R under hydrostatic compression for iron, nickel, iron-nickel alloys with nickel contents of 34% or more, and nickel-copper alloys containing up to 48% copper; the study was made at helium temperatures using magnetic fields up to 8600 oe. It was established that, in iron-nickel alloys with nickel contents between 34 and 45% (Invar alloys), the change of σ and R under pressure was approximately an order greater than in the other alloys and metals studied. In all the metals and alloys studied the magnetic moment decreased under hydrostatic compression. The electrical resistance decreased under hydrostatic compression for iron and nickel, and increased for Invar alloys. Possible reasons are considered for the changes of σ and R which were found, and it is shown that the comparatively large changes of these quantities under pressure and the other peculiarities of Invar alloys can be explained by the existence of "latent" anti-ferromagnetism, existing due to the negative sign of the exchange integral between atoms of iron in the face-centered lattice.

THE authors have previously shown[1] that the quantity $(1/\sigma_0)\Delta\sigma/\Delta p = K_\sigma$ (where σ_0 is the saturation magnetic moment of unit mass) does not tend to zero at T = 0°K for Invar alloys. It was also established that the change of magnetization under hydrostatic compression cannot be completely attributed to a displacement of the Curie point.

For pure ferromagnetic metals K_σ is much smaller than for Invar alloys. The values of K_σ, quoted in the literature by various authors for nickel and iron at room temperature, differ greatly from one another. This is associated with experimental difficulties arising because of the smallness of the effect sought for ($\Delta\sigma/\sigma_0 \approx 10^{-4}$ at 1,000 atm[2-4]). With regard to data on the behavior of this quantity at low temperatures, there has been only one attempt[5] to determine $(1/\Psi_0)\Delta\Psi/\Delta p$ for iron at liquid nitrogen temperature (Ψ is the magnetic flux through the specimen).

In the present work we have studied the effect of hydrostatic compression on the saturation magnetization of nickel, iron, a single crystal of meteoric iron, and iron-nickel and copper-nickel alloys, at temperatures of 20.4° and 4.2°K. It was also of interest to find what connection K_σ had with the effect of hydrostatic compression on the electrical resistance of these metals, i.e., the quantity $(1/R_0)\Delta R/\Delta p = K_R$.

MEASUREMENT PROCEDURE AND RESULTS

The arrangement for measuring the quantity $(1/\Psi)\Delta\Psi/\Delta p$ is shown schematically in Fig. 1. A bomb of beryllium bronze containing the specimen, 1, is situated in the field of a water-cooled solenoid, 3. A pressure of approximately 150 atm was provided by gaseous helium which was supplied to the bomb from a gas cylinder through a capillary, 4. The measuring coil, 2, disposed outside the bomb, had two sections, an internal and an external. The sections were connected in series in opposite sense. The number of turns in each section was chosen so that, on reversing the magnetic field in the solenoid with no specimen present, the signals arising in each section cancelled one another out. The change of magnetic moment of the specimen was recorded because of the different number of turns in the inner and outer sections; the difference in the number of turns in our case was 7643. The measuring coil was connected to a photoelectric fluxmeter with sensitivity 5 maxwells/division. In the experiment, the movement of the fluxmeter pointer, due to the change of magnetic flux through the specimen on applying and removing the pressure, was measured directly. The error of the measurements, referred to unit cross-sectional area of the specimen $\delta[(1/4\pi s)\Delta\Psi/\Delta p]$, was

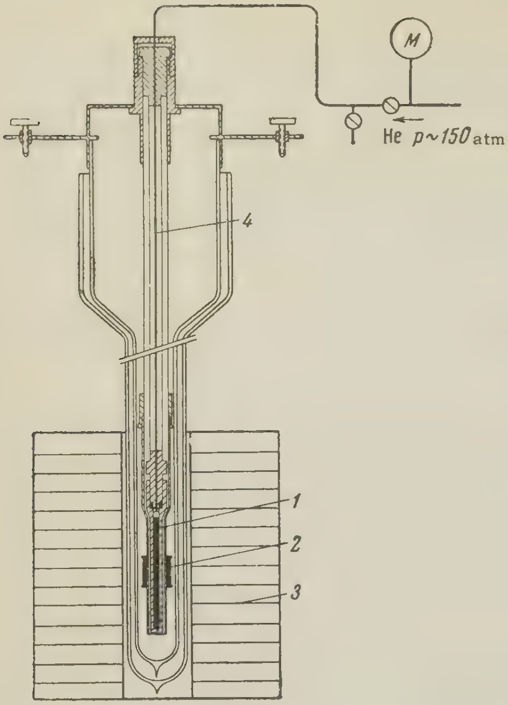

FIG. 1. Diagram of the basic part of the apparatus.

0.2×10^{-4} gauss/atm. The specimens used were in the form of cylinders 112 mm long and 5.9 mm in diameter. The specimens were fabricated from technically pure materials. After fabrication they were subjected to a vacuum anneal for 8 hours at a temperature of 1,000°C and were subsequently cooled in the furnace.

For the measurements on K_R, the pressure was created by freezing an aqueous solution of alcohol (~ 3%) at constant volume. We used the same method as in references 6 and 7.

The main results are shown in Fig. 2. Curves 1 and 2 display, respectively, the dependence of $(1/\Psi_0)\,\Delta\Psi_0/\Delta p$ and K_R on specimen composition. The specimens were at a temperature of 4.2°K, and a field of 8600 oe was applied, magnetic saturation being obtained. The quantity $(1/\Psi_0)\,\Delta\Psi/\Delta p$ had the same value at 20.4° and 4.2°K within the limits of accuracy of our measurements. The value of K_R generally depended on the temperature, and for all the ferromagnets studied the dependence was such that $\partial/\partial T\,(\Delta R/\Delta p) < 0$. In the region of Invar alloys where $(1/\Psi_0)\,\Delta\Psi/\Delta p$ and K_R are large, the behavior of curves 1 and 2 is approximately similar, and while the magnetization of the specimen decreased under hydrostatic compression, its electrical resistance increased. The increase of $(1/\Psi_0)\,\Delta\Psi/\Delta p$ for nickel-copper alloys with increasing copper content is associated with the decrease of Ψ_0, as can be seen from the table. K_σ is related to $(1/\Psi_0)\,\Delta\Psi/\Delta p$ by the relationship

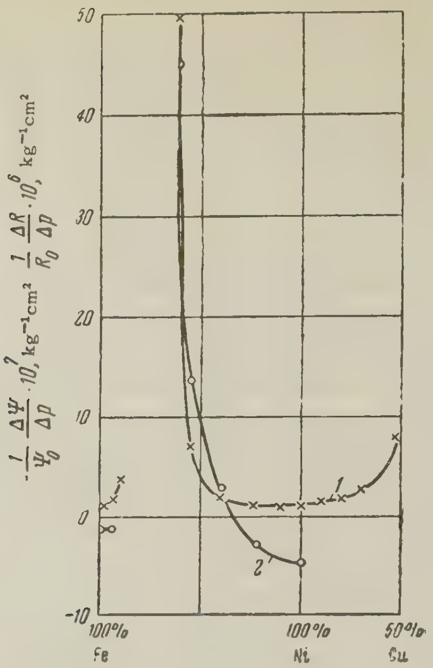

FIG. 2. Values of the quantities $(1/\Psi_0)\Lambda\Psi_0/\Delta p$ (curve 1) and $(1/R_0)\Delta R_0/\Delta p = K_R$ (curve 2) for iron, nickel, iron-nickel and copper-nickel alloys in the magnetic saturation region. Ψ_0 is the magnetic flux of the specimen obtained by extrapolation to absolute field, R_0 is the residual resistance.

$$K_\sigma = (1/\Psi_0)\,\Delta\Psi/\Delta p + {}^1/_3\,\Delta V/V\Delta p.$$

Since both the terms on the right-hand side have negative signs, $|K_\sigma| > |(1/\Psi_0)\,\Delta\Psi/\Delta p|$. The calculated values of K_σ* are given in the table.

The values of K_R for pure electrolytic nickel ($R_{300°}/R_{4.2°} = 250$) and for technically pure nickel ($R_{300°}/R_{4.2°} = 6$) are equal.

The variation of $(1/\Psi_0)\,\Delta\Psi_0/\Delta p$ with magnetic field H at 20.4°K is given in Fig. 3. Curve 1 refers to a specimen of polycrystalline nickel, curve 2 to a specimen of single-crystal meteoric iron (5.5% Ni) cut in the direction of the [100] axis, i.e., along the direction of easy magnetization. In Fig. 4 are given the curves showing the variation of the electrical resistance of nickel with magnetic field at a temperature of 4.2°K for two pressures, atmospheric (curve 1) and 1380 atm (curve 2). The curves cross at low magnetic fields. This is associated with the increase of $(1/\Psi_0)\,\Delta\Psi/\Delta p$ on reducing the magnetic field H.

DISCUSSION OF RESULTS

The authors have previously[1] enumerated the possible reasons for the changes of specific spontaneous magnetization σ_0 and residual electrical resistance R_0 close to absolute zero under hydro-

---

*We took the values of $\frac{1}{3}\Delta V/V\Lambda p$ for T = 300°K from reference 2.

Ni content in NiFe alloy specimens %	Saturation magnetization I_0, gauss	Specific electrical resistance ρ_0 at T = 4.2°K μohm cm	$\frac{1}{4\pi s}\cdot\frac{\Delta\Psi}{\Delta p}\cdot 10^4$, gauss kg^{-1} cm^2	$\frac{1}{\Psi_0}\cdot\frac{\Delta\Psi}{\Delta p}\cdot 10^7$, kg^{-1} cm^2	$K_\sigma\cdot 10^7$, kg^{-1} cm^2	$K_R\cdot 10^6$, kg^{-1} cm^2
0	1751*	2.58	—1.9	—1.1±0.2	—3.1	—1.4±0.3
10.0	1750	—	—6.7	—3.8±0.4	—5.9	—
34.7	1250	50	—131	—105±15	—109	+38±3
38.0	1360	31.2	—68	—50±8	—54	+45±3
44.9	1380	18.8	—9.66	—7±1.5	—11	+13.5±2
59.9	1100	10.4	—2.03	—1.9±0.2	—4.4	+2.6±0.5
76.0	948	6.15	—1.01	—1.1±0.25	—3.6	—2.9±0.5
90.2	680	—	—0.57	—0.85±0.3	—3	—
100	512	0.034** 1.18***	—0.56	—1.1±0.4	—2.9	—4.7±1.5
Cu content in NiCu alloy specimens %						
10.2	415	—	—0.63	—1.5±0.5	—	—
19.6	350	—	—0.60	—1.7±0.6	—4.3	—
29.0	235	—	—0.64	—2.7±0.8	—5.6	—
48.4	82.5	—	—0.65	—7.9±2.5	—	—

*Value for I_0 for iron from reference 8.

**For electrolytically pure nickel.

***For technically pure nickel.

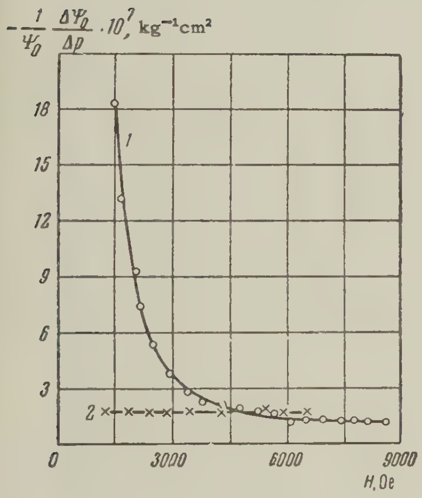

FIG. 3. Variation of the relative change of magnetic flux under pressure on magnetic field at T = 20.4°K: 1 – nickel, 2 – single-crystal meteoric iron (magnetic field directed along the [100] axis).

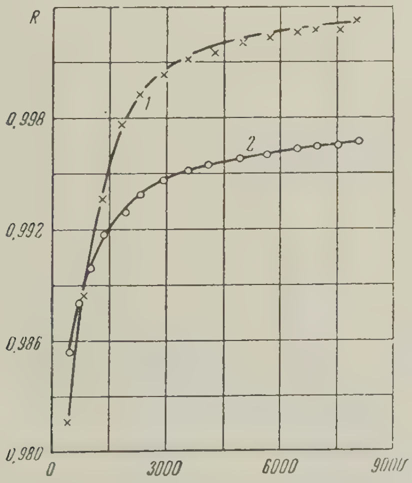

FIG. 4. Variation of the electrical resistance of nickel (R in relative units) with magnetic field at T = 4.2°K: 1 – at atmospheric pressure, 2 – at pressure of 1380 atm.

static compression.*

1. A change in the value of the d-d exchange integrals J_{dd} on changing the interatomic distances under pressure. If some of these integrals are negative ("latent" antiferromagnetism), the change of J_{dd} involves a change in the number of anti-parallel spins in the lattice; consequently, there is a decrease (or increase) of the spontaneous magnetization. Therefore the electrical conductivity decreases (or increases); this can occur due to the change in degree of magnetic order and the change in the value of the spontaneous magnetization.

2. A change in the values of the s-d exchange integrals J_{sd} on changing the interatomic distances. Changing J_{sd} alters the molecular field acting on the conduction electrons, which affects their contribution to the spontaneous magnetization.[9] In this case the electrical conductivity can either decrease or increase, because the degree of scattering of the conduction electrons at inhomogeneities of the magnetic moment depends on the quantities J_{sd},[10] and because there are changes in the effective mass and mean free path of the conduction electrons associated with their polarization in the molecular field.[9]

3. The transfer of electrons from the s into the d band or vice versa under lattice compression. Here the number of unfilled sites in the d band changes, as well as the number of s electrons, which alters the magnetic moment and the electrical conductivity. In this case the electrical

---

*The order in which these are enumerated is different from that in reference 1.

conductivity changes because the number of carriers alters and because there is an increase or decrease of the number of "holes" and the degree of scattering of electrons at "holes."

Electrical conductivity changes can also be due to a "smoothing" of irregularities in the potential — which is possible under hydrostatic compression.

According to the way in which σ_0 and R_0 change under hydrostatic compression, the metals and alloys studied can be divided into two groups: a) iron-nickel alloys with nickel contents of 34, 38, and 45% (Invar alloys), in which the absolute values of K_σ and K_R are approximately an order of magnitude greater than in the other materials studied, and in which these quantities have opposite signs ($K_\sigma < 0$, $K_R > 0$); b) iron, nickel, iron-nickel alloys with nickel contents 10, 60, 76, and 90%, and copper-nickel alloys, in which the absolute values of K_σ and K_R are comparatively small and both are negative — K_R being approximately the same for specimens with different values of residual resistance. The difference referred to between the quantities K_σ and K_R shows that the changes of σ_0 and R_0 observed under hydrostatic compression in materials of the first and second groups, are due essentially to different factors.

A. The changes of σ_0 and R_0 under hydrostatic compression for materials of the first group (Invar alloys). It has been remarked above that the absolute values of K_σ and K_R in Invar alloys are an order of magnitude greater than in other iron-nickel alloys, iron, and nickel. It is well known that Invar alloys also show a number of other anomalies (anomalous coefficient of thermal expansion, high electrical resistance, etc). It is natural to look for a general explanation of all these anomalies. In reference 11 we have shown that such an explanation can be given starting from the hypothesis of a negative exchange interaction between the d electrons of iron in the face-centered lattice. This hypothesis is based on experimental data obtained in reference 12, where it was established that an alloy of iron, nickel and chromium with face-centered lattice, containing 72% iron, becomes antiferromagnetic at a temperature of about 40°K.

As shown in reference 11, small changes in the exchange integral for d electrons on neighboring iron ions displaces the transitional concentration region (i.e., the alloy concentrations lying intermediate between antiferromagnetic and ferromagnetic) towards nickel, and therefore strongly affects σ_0. With decreasing interatomic distance the absolute value of the negative exchange integrals increases more rapidly than it decreases; therefore, under hydrostatic compression a displacement of the transitional region towards the nickel side and, consequently, a decrease of magnetic moment would be expected. Due to the increase in the number of anti-parallel spins, the electrical resistance of the alloys would thus be expected to increase. Therefore, if the hypothesis on the role of antiferromagnetism in iron as an explanation of the anomalies in Invar alloys is true, and if the first of the reasons enumerated above for the change of σ_0 and R_0 is the most potent, then the quantities K_σ and K_R in iron-nickel alloys should attain their greatest absolute values in the same concentration region as that in which the fall of magnetic moment with increasing iron content is observed, and they should have different signs in this region. From the curves given in Figs. 2 and 5, it is seen that the greatest values of K_σ and K_R do, in fact, correspond to the concentration region referred to, and these quantities have different signs in this region, and $\Delta\sigma_0/\Delta p < 0$.

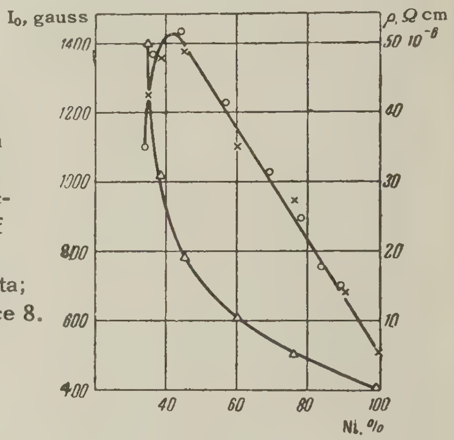

FIG. 5. Saturation magnetization I_0 and residual specific electrical resistance ρ_0 of iron-nickel alloys; ×, Δ – the authors' data; ○ – data from reference 8.

Another fact supporting the explanation given of the effect of pressure on σ_0 and R_0 in Invar alloys is obtained by comparing the change of these quantities under hydrostatic compression with their changes during a small decrease of the strong magnetic field which magnetizes the alloys to saturation. If the cause of the changes discussed is the increase of the number of anti-parallel spins, then the ratios $(\Delta R_0/R_0)$, $(\Delta\sigma_0/\sigma_0)$ in both cases should be approximately equal in magnitude and sign. As the comparison made by us in reference 1 shows, these ratios in fact lie close to one another for Invar alloys.

The considerations given support the idea that the most probable basic reason for the changes of σ_0 and R_0 in Invar alloys under hydrostatic compression is the first of the reasons enumerated above. If it were assumed that the basic cause of these changes lay in the second or third reasons, then it is difficult to explain, without artificial assumptions, why in Invar alloys the variations of σ_0 and R_0 under pressure are an order greater than in other iron-nickel alloys and in metals.

B. The changes of σ_0 and R_0 under hydrostatic compression in iron, nickel, and alloys belonging to the second group. It was remarked above that in metals and alloys belonging to the second group, both K_σ and K_R are negative. At the same time it is well known that $(1/\sigma_0)\Delta\sigma/\Delta H$ and $(1/R_0)\Delta R/\Delta H$ for these materials in strong fields have different signs. A comparison of the ratio K_R/K_σ, calculated for specimens of the metals according to our data, with the ratio $[(1/R_0)(\Delta R/\Delta H]/[(1/\sigma_0)\Delta\sigma/\Delta H]$ at room temperature, derived from data in the literature,[13-15] shows that these ratios in a number of cases differ significantly from one another. The first is insensitive to the quantity R_0, but the second varies with change of this quantity. Thus, in the materials considered, changes of J_{dd} cannot be the basic cause of changes in σ_0 and R_0 under hydrostatic compression.

It follows from the usual ideas about the relation between the magnetic moments of ferromagnetic metals and the degree of filling of the d band, that on transferring electrons from the d band to the s band, together with a fall of electrical resistance, a rise of magnetic moment should be observed (at least in cobalt and nickel, where the conductivity is mainly due to s electrons). Thus, $(\Delta\sigma_0/\sigma_0)_{d\rightarrow s} \approx -\alpha\Delta R_0/R_0$, where α is the ratio of the number of electrons to the number of unfilled sites in the d band (for nickel $\alpha = 1$). It is seen from the table that for electrolytic nickel K_R is approximately 15 times greater in absolute terms than K_σ. Consequently, without additional assumptions on the various mechanisms of compensating $(\Delta\sigma/\sigma_0)_{d\rightarrow s}$, this assumption contradicts the experimental data on the effect of pressure on K_σ in nickel. The reverse assumption — that, under the influence of pressure, electrons are transferred from the s into the d band, and that this is the basic cause of the fall of σ_0 under hydrostatic compression observed in iron and nickel — leads to a quantitative contradiction of the experimental data on the effect of pressure on the electrical resistance of iron.

Thus, the third of the possible reasons enumerated above, as well as the first, cannot be the basic reason for the changes of σ_0 and R_0 in the metals under hydrostatic compression. There remains the assumption that the basic cause for these changes in the metals is the second one (i.e., the effect of pressure on the values of the J_{sd} s-d exchange integrals), and that in Invar alloys this effect exceeds the effect of the first one. Unfortunately, it is at present difficult to estimate how the electrical resistance would change during variations of σ_0 associated with changes of J_{sd}.

We note that, if the basic reason for the observed fall of electrical resistance in the metals under pressure is "smoothing" of irregularities of potential, then the quantity K_R should be insensitive to the value of the residual resistance; this is confirmed by the measurements for pure electrolytic nickel and technically pure nickel.

---

[1] E. I. Kondorskiĭ and V. L. Sedov, JETP **35** 845 (1958), Soviet Phys. JETP **8**, 586 (1959).

[2] M. Ebert and A. Kussman, Z. Physik **38**, 437 (1937).

[3] K. H. v. Klitzing and J. Gielessen, Z. Physik **146**, 59 (1956).

[4] D. Gugan, Proc. Phys. Soc. **72**, 1013 (1958).

[5] Gal'perin, Larin, and Shishkov, Dokl. Akad. Nauk SSSR **89**, 419 (1953).

[6] B. G. Lazarev and L. S. Kan, JETP **14**, 439 (1944).

[7] N. B. Brandt and A. K. Tomashchuk, Приборы и техника эксперимента (Instrum. and Meas. Engg.) **2**, 113 (1958).

[8] E. I. Kondorskiĭ and L. N. Fedotov, Izv. Akad Nauk SSSR, Ser. Fiz. **16**, 432 (1952).

[9] S. V. Vonsovskiĭ, Современное учение о магнетизме (The Modern Theory of Magnetism), M.-L. (1955).

[10] E. A. Turov, Izv. Akad. Nauk SSSR, Ser. Fiz. **19**, 474 (1955), Columbia Tech. Transl. p. 426.

[11] E. I. Kondorskiĭ, JETP **37**, 1819 (1959), Soviet Phys. JETP **10**, 1284 (1960).

[12] E. I. Kondorskiĭ and V. L. Sedov, JETP **35**, 1579 (1958), Soviet Phys. JETP **8**, 1104 (1959).

[13] E. Englert, Ann. Physik **14**, 589 (1932).

[14] P. Weiss and R. Forrer, Ann. Physik **12**, 279 (1929).

[15] A. R. Kaufmann, Phys. Rev. **55**, 1142 (1939).

Translated by K. F. Hulme
153

SOVIET PHYSICS JETP VOLUME 11, NUMBER 3 SEPTEMBER, 1960

PHOTOPROTONS FROM Cu^{65}

N. V. LIN'KOVA, R. M. OSOKINA, B. S. RATNER, R. Sh. AMIROV* and V. V. AKINDINOV*

P. N. Lebedev Physical Institute, Academy of Sciences, U.S.S.R.

Submitted to JETP editor October 5, 1959

J. Exptl. Theoret. Phys. (U.S.S.R.) **38**, 780-789 (March, 1960)

The energy and angular distributions of photoprotons produced in a Cu^{65}-enriched sample by bremsstrahlung with maximum energies $E_{\gamma\,max} = 17.9$, ~ 20, 24.5, and 28.5 Mev were studied by means of photographic emulsions. The dependence of the Cu^{65} photoproton yield on $E_{\gamma\,max}$ was measured and the excitation curve for reactions involving proton emission was determined. An analysis of the experimental data shows that at least 80% of the proton yield is due to a mechanism other than evaporation. If this mechanism is assumed to be a direct photoeffect in which all the gamma-ray energy minus the binding energy is imparted to the ejected proton it is found from the energy distributions that only a small fraction of the protons results from the photoeffect at the highest nuclear level, the principal contribution being due to transitions from lower-lying shells. Two proton emission peaks are observed, $E_p = \sim 4.7$ and ~ 6.0 Mev. The angular distributions are represented by $a + b \sin^2\theta$ for $E_{\gamma\,max} = 17.9$ and 20.0 Mev, and by $a + b \sin^2\theta + c \sin^2\theta \cdot \cos^2\theta$ for $E_{\gamma\,max} = 24.5$ and 28.5 Mev. This indicates dipole absorption of gamma rays for $E_\gamma < 20$ Mev, with quadrupole absorption becoming appreciable at higher energies.

INTRODUCTION

IN investigating the mechanism of interactions between gamma rays and nuclei valuable information is obtained by studying angular and energy distributions and the yields of photonuclear products. The observed departures from statistical theory for the (γp) reaction[1-3] have suggested the existence of a direct nuclear photoeffect,[4] although details of this mechanism and the part it plays in giant resonance have thus far not been determined. It is of special interest to investigate the (γp) reaction in isotopes where proton evaporation is not favored. The direct photoeffect is an important participant in the (γp) reaction for $Z \approx 28$.[5,6] For example, in a natural mixture of copper isotopes it accounts for 20 — 40% rather than 5 — 10% as previously estimated.[3,7] We used a Cu^{65}-enriched sample for the purpose of verifying these results.

According to statistical theory, if all other conditions are identical proton evaporation is limited by competition with neutron evaporation and is strongly dependent on the difference between the neutron binding energy B_n and the proton binding energy B_p. The ratio of proton to neutron emission probability w_p/w_n contains the factor $\exp\{B_n - B_p\}$.[8] On the basis of the binding energy ratio in Cu^{63} and Cu^{65} the proton evaporation yield from Cu^{65} should be only about one-tenth as large as from Cu^{63}.

We may therefore expect that the contribution of the direct photoeffect to the (γp) yield from copper should increase with the Cu^{65} content. Preliminary data[9] have shown that the ratio of (γp) yields in Cu^{65}-enriched and natural copper samples for $E_{\gamma\,max} = 29.0$ Mev is considerably greater than that predicted by the statistical theory. An estimate of $\sim 85\%$ for the direct photoeffect in Cu^{65} and $\sim 40\%$ in Cu^{63} was confirmed by an analysis of angular and energy distributions of photoprotons from natural copper.[5] A subsequent more careful measurement of the photoproton energy distribution from Cu^{65} for $E_{\gamma\,max} =$ 19.5, 24.5, and 28.5 Mev revealed separate peaks in the spectrum,[10] although the statistical accuracy was unsatisfactory and additional measurements were performed to provide the necessary confirmation. All data for Cu^{65} are summarized in the present paper.

EXPERIMENTAL PROCEDURE

Nuclear emulsions were used in this work. Figure 1 shows the experimental arrangement including the interior geometry of the chamber containing the target and plates. The target was a 29 mg/cm^2 foil containing 93.5% Cu^{65} and 6.5% Cu^{63}. The plates were positioned on both sides of the target at angles θ equal to 30, 50, 70, 90, 110, 130, and 150° with respect to the gamma-ray direction (Fig. 1a), except in the case of $E_{\gamma\,max}$

---

*At Saratov State University.

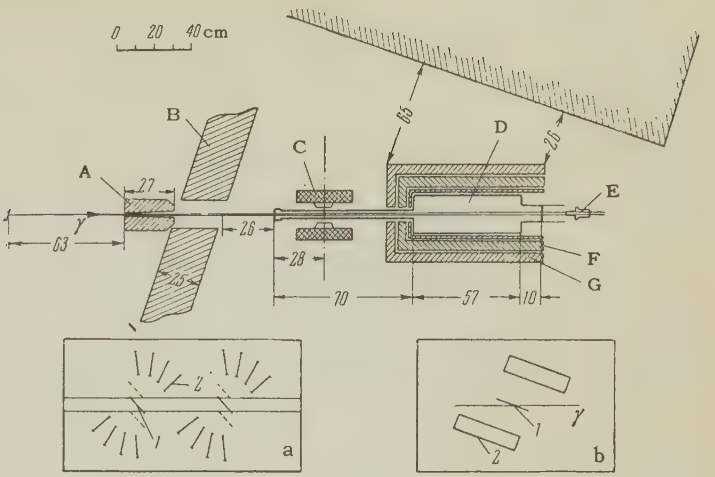

FIG. 1. Experimental arrangement: A – lead collimator, B – lead shield, C – sweeping magnet, D – vacuum chamber containing target and plates, E – monitor, F – paraffin, G – lead. a – interior geometry of chamber; dashed lines represent plate positions for yield measurements; b – the same for irradiation at $E_{\gamma\,max} = 20.0$ Mev; 1 – target, 2 – plates.

= 20.0 Mev, the geometry for which is shown in Fig. 1b. Plates located close to the target were also irradiated in order to determine the yield curve at low energies ($E_{\gamma\,max} < 18$ Mev) and to determine the photoproton yield ratio from Cu^{65}-enriched and natural copper samples.

Protons were registered in NIKFI Ya-2 and T-3 emulsions of 300 μ and 400 μ thicknesses. Dosages were monitored by an integrating ionization chamber which was calibrated by a thick-walled ionization chamber of known sensitivity.

The results given below were corrected only for the scattered gamma-ray background, which was measured in the absence of the target. This background was small (1 – 5%) and was concentrated mainly in the low proton-energy region $\epsilon_p < 5 - 7$ Mev.

An additional background associated with the target cannot easily be evaluated quantitatively. We shall now proceed to estimate the contributions of the principal processes.

1. (γd) and ($\gamma\alpha$) reactions. The emulsions used in the present work do not permit very good discrimination of charged-particle tracks. Therefore we assigned to the effect in question all tracks starting at the emulsion surface, moving in the required direction and having lengths corresponding to proton energies $\epsilon_p \geq 3$ Mev. We thus actually measured the results of the combined reactions (γp) + (γnp) + (γd) + ($\gamma\alpha$).

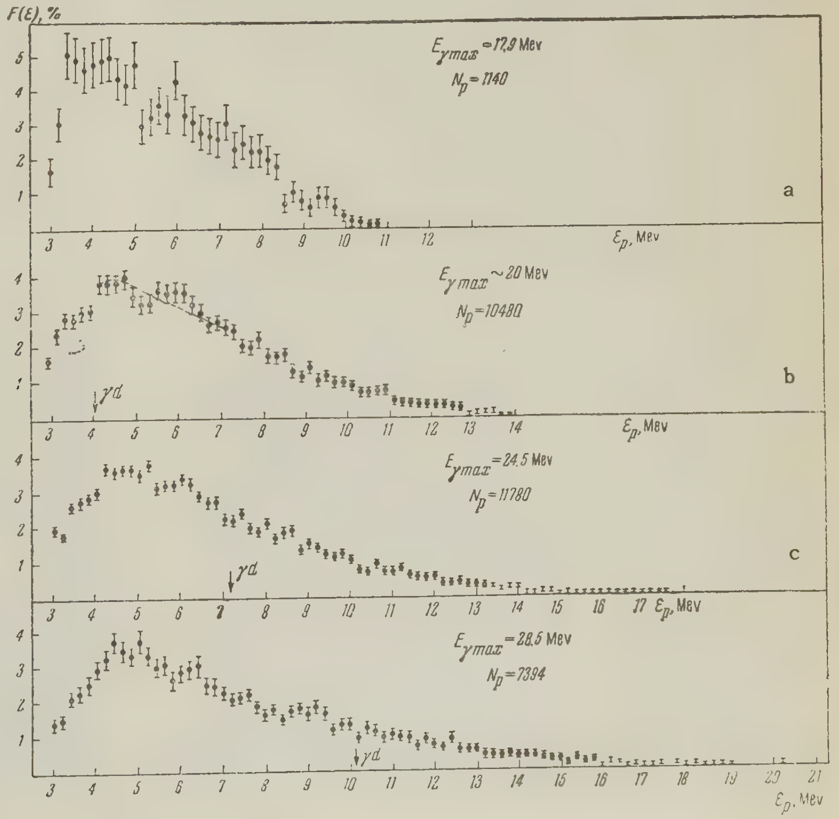

FIG. 2. Energy distributions of photoprotons from Cu^{65} for different values of $E_{\gamma\,max}$. Statistical errors are indicated.

Rough estimates of the contributions of the (γd) and $(\gamma \alpha)$ reactions, based on measurements obtained from natural copper,[3,11,12] indicate that the photodeuteron contribution is not greater than 10% (for $E_{\gamma \max} > 25$ Mev) while the contribution of alpha particles may be disregarded altogether. For lower values of $E_{\gamma \max}$ this contribution will obviously be still smaller.

2. Contribution from Cu^{63}. The sample contained about 6.5% Cu^{63}. An estimate based on the measured photoproton yield ratio of natural and Cu^{65}-enriched samples indicates that Cu^{63} contributed 10 — 15% for all four values of $E_{\gamma \max}$.

EXPERIMENTAL RESULTS

The proton energy spectra in Fig. 2, for $E_{\gamma \max} = 17.9$, ~ 20, 24.5, and 28.5 Mev, represent combined measurements obtained with plates that were placed at different angles θ with respect to the gamma-ray beam. The total numbers N_p of tracks used in plotting the spectra were 1140, 10,480, 11,780, and 7394, respectively, for the different values of $E_{\gamma \max}$. Relative units are used. $F(\epsilon)$ is the ratio of the number of tracks in the $\epsilon_p \pm 0.1$ Mev interval to the number with $\epsilon_p \geq 3.0$ Mev. Arrows indicate the proton energy limit below which the spectra may be distorted by photodeuterons.

The spectra were plotted with special care in order to determine whether a structure is present. We first plotted for each plate a histogram of the track number $N(L)$ in the length interval $\Delta L = 5\,\mu$ as a function of measured track length L. A correction for proton energy loss in the target was then introduced by shifting the range scale toward larger values by an amount l equivalent in a given plate to half of the target thickness. (The average energy loss was 0.5 Mev for $\epsilon_p = 5$ Mev and ~ 0.3 Mev for $\epsilon_p = 11$ Mev.) Using the ranges $L' = L + l$ and the corresponding energies with 0.2-Mev intervals in accordance with the range-energy curve we computed the number of tracks in each energy interval and subtracted the background. The range-energy curve for Ilford C-2 emulsions[13] was used for the NIKFI Ya-2 emulsion. The NIKFI T-3 emulsion, which contains a little less AgBr than the Ilford C-2, was calibrated according to the recoil-proton range produced by 14-Mev neutrons and the aforementioned range-energy curve was corrected. Range intervals $\Delta L'$ corresponding to energy intervals $\epsilon_p \pm 0.$ Mev were determined very carefully, with special attention to the monotonic increase of these intervals with ϵ_p. The proton spectra were thus free of possible peaks resulting from systematic errors associated with inaccurate determination of the intervals $\Delta L'$.

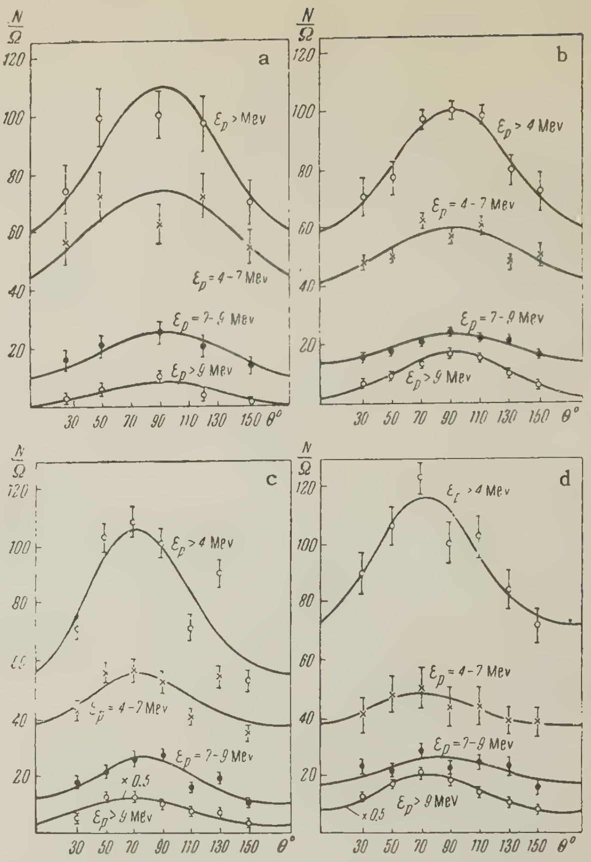

FIG. 3. Angular distributions of photoprotons from Cu^{65} (in relative units): (a) $E_{\gamma \max} = 17.9$ Mev, (b) 20.3 Mev, (c) 24.5 Mev, (d) 28.5 Mev. The number of protons with energies $\epsilon_p \geqslant 4$ Mev is taken as 100. Statistical errors are indicated.

Figure 3 shows the angular distributions of photoprotons for the different energy groups. The continuous curves represent the following distributions:

$$I(\theta) = a + b \sin^2 \theta \quad \text{(Fig. 3a and b)} \qquad (1)$$

$$I(\theta) = a + b \sin^2 \theta + c \sin^2 \theta \cos \theta \quad \text{(Fig. 3c and d)} \qquad (2)$$

The following table contains the least-squares values of b/a and c/b.

In Fig. 4 the photoproton yield of a Cu^{65}-enriched sample is shown as a function of $E_{\gamma \max}$; data obtained at different times are connected by the curves. The yield is given for unit solid angle and identical ionization in a thick-walled ionization chamber. The curve may be attributed primarily to (γp) and (γnp) reactions in Cu^{65}, the cross section for which (denoted by $\sigma_{\gamma p}$ for brevity) is shown in Fig. 5. The cross sections were calculated from the yield curve by the method of photon differences.[14] The absolute normalization of this curve will be discussed below.

Parameters in the Angular Distribution of Protons.

ε_p, **Mev**	$E_{\gamma\,max} = 17.9$ **Mev**	20.0 **Mev**	24.5 **Mev**		28.5 **Mev**	
	b/a	b/a	b/a	c/b	b/a	c/b
⩾4	0.81	0.68	0.76	0.79	0.52	0.86
4—7	0.50	0.87	0.40	0.83	0.22	0.19
7—9	1.60	0.75	1.20	0.69	0.47	0.42
>9	83	10.0	1.90	0.87	1.23	0.91

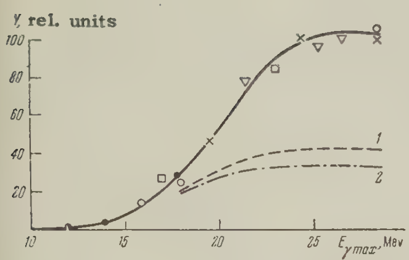

FIG. 4. Cu^{65} photoproton yield as a function of $E_{\gamma max}$. Different symbols represent different sets of data. The broken lines were calculated from the statistical model: curve 1 for a = 16 Mev^{-1};[15] curve 2 for a = 8 Mev^{-1}.[16]

FIG. 5. Cross section for Cu^{65} photoproton emission. The dashed curve provides comparison with the cross section for $Cu^{65}(\gamma n)Cu^{64}$.[17]

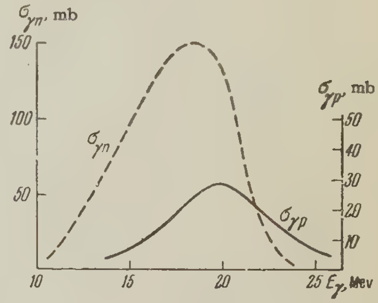

DISCUSSION OF RESULTS

1. Photoproton yield from Cu^{65}. Using the measured photoproton yield ratio for natural copper and a Cu^{65}-enriched sample (1.5 ± 0.2 for $E_{\gamma max} = 25.2$ Mev) and the fractional isotopic abundance of Cu^{63} and Cu^{65} in the samples, the photoproton yield ratio from these isotopes at the given $E_{\gamma max}$ was found to be 1.9. By comparison, the statistical theory of nuclear reactions gives the value 9 for the ratio. The calculation resembled that of Byerly and Stephens,[3] assuming $\omega(E_R) \sim \exp(aE_R)^{1/2}$ for the level density in both final nuclei Ni^{62} and Ni^{64}. The following constants were used: $a_1 = 3.35(A-40)^{1/2} \approx 16$ Mev^{-1},[15] $a_2 = 8$ Mev^{-1};[16] $r_0 = 1.5 \times 10^{-13}$ cm; $\sigma_{\gamma n}$ was taken from reference 17. The proton binding energy B_p and the neutron binding energy B_n were taken to be 6.5 and 11.0 Mev, respectively, in Cu^{63} and 7.5 and 10.0 Mev in Cu^{65}.

It should be noted that the assumption of equal level densities in Ni^{62} and Ni^{64} is not strictly justified. There are indications of considerable fluctuations of nuclear-level density near magic numbers.[18,19] If it should be found that the level density in Ni^{64} is 4 or 5 times greater than in Ni^{62} the observed proton yield ratio for Cu^{65} and Cu^{63} would not disagree with statistical theory. However, Ni^{64} and Ni^{62} differ only[20] by the circumstance that in the unfilled $4f_{5/2}$ neutron level the former contains two neutrons while the latter contains two vacancies; we can therefore hardly expect the level densities to differ so strongly. The statistical theory also cannot account for the sharp rise of the photoproton yield in the region $E_{\gamma max} = 20-25$ Mev (Fig. 4). To account for these facts it must be assumed that most of the Cu^{65} proton yield results from a mechanism other than evaporation. A calculation based on the assumption that the proton yields from Cu^{65} and Cu^{63} as a result of evaporation differ by a factor of 9 indicates that this additional mechanism contributes at least 80% to the Cu^{65} photoproton yield.

2. Energy distributions. The photoproton spectra in Fig. 2 are marked by the following characteristics:

a) Although a large fraction of the proton yield is apparently produced by a mechanism different from evaporation (at least for $E_{\gamma max} = 24.5$ and 28.5 Mev) a considerable fraction of the protons is found at relatively low energies ($\epsilon_p = 4-6$ Mev).

b) The fraction of protons close to the maximum possible energy, $\epsilon_{p\,max} = E_{\gamma max} - B_p$, is small and falls off sharply as $E_{\gamma max}$ increases. It therefore is a relatively infrequent occurrence that the entire energy of a gamma ray, minus the binding energy, is transferred to a proton from an upper level. This conclusion follows even more convincingly from an examination of proton spectra produced by gamma rays in narrower energy intervals. In work on bremsstrahlung such spectra can be obtained by taking the differences between proton spectra measured at two values of $E_{\gamma max}$ and normalized to unit solid angle and identical ionization in a thick-walled ionization chamber. Figure 6 shows such differences between proton spectra,

$$\Delta Y(\varepsilon) = [YF(\varepsilon)]_{E^{(1)}_{\gamma max}} - [YF(\varepsilon)]_{E^{(2)}_{\gamma max}};$$

Y and $F(\epsilon)$ are taken from Figs. 2 and 4, respectively. The corresponding bremsstrahlung spectra are also shown:

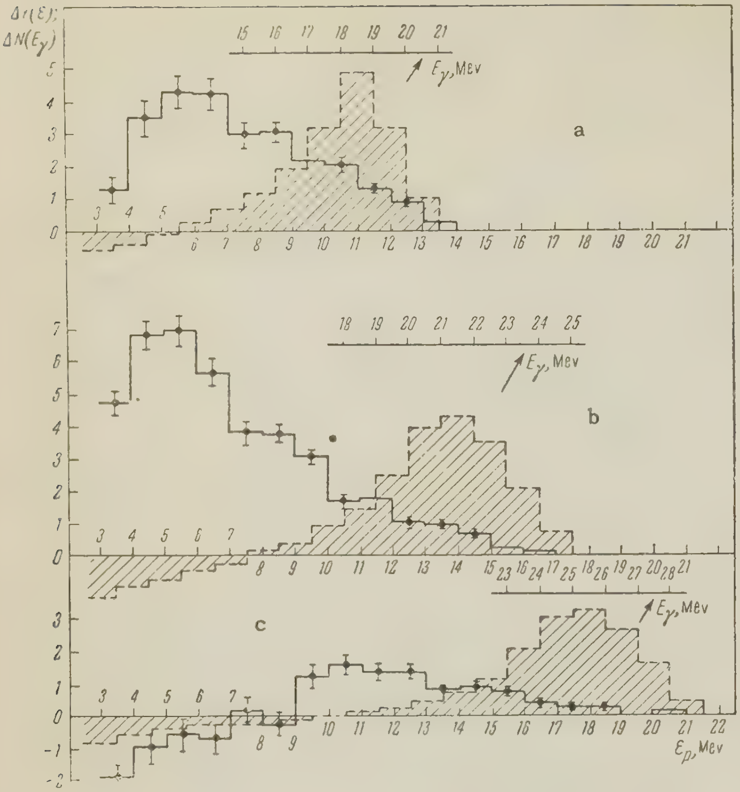

FIG. 6. Differences between proton spectra: a – for $E^{(1)}_{\gamma\max} = 20.0$ Mev and $E^{(2)}_{\gamma\max} = 17.9$ Mev; b – for $E^{(1)}_{\gamma\max} = 24.5$ Mev and $E^{(2)}_{\gamma\max} = 20.0$ Mev; c – for $E^{(1)}_{\gamma\max} = 28.5$ Mev and $E^{(2)}_{\gamma\max} = 24.5$ Mev. The dashed lines represent the differences between the corresponding bremsstrahlung spectra.

$$\Delta N(E_\gamma) = N(E_\gamma, E^{(1)}_{\gamma max}) - N(E_\gamma, E^{(2)}_{\gamma max}),$$

also reduced to identical ionization. The differences of the proton and gamma-ray spectra are given in arbitrary units, with the gamma-ray energy scale shifted by an amount equal to the proton binding energy $B_p = 7.5$ Mev. It is consequently evident that protons emitted from the upper level should overlap the gamma-ray spectrum. Figure 6a shows a considerable fraction of these protons overlapping the gamma-rays from 17 to 20 Mev. For $E_\gamma > 20$ Mev this fraction is small (Fig. 6b and c).

The proton spectrum in Fig. 6b, corresponding to gamma rays from 19 to 24 Mev, contains a large number of slow protons with ϵ_p from 3 to 8 Mev. Therefore the sharp rise of the yield in this gamma-ray region (Fig. 4) results mainly from the emission of low-energy particles which cannot be attributed to evaporation, since (as already indicated) the statistical theory does not account for the observed rise of the yield; no important change results when the (γnp) process is taken into account. In the case of direct interactions the presence of a large number of slow particles may result either from the large part played by processes in which gamma-ray energies are transferred to two or more particles simultaneously or because there is a large probability for nucleon extraction from deep shells.

The available experimental data do not definitely favor either of these explanations. If we assume that a single-particle mechanism exists, then from the difference ΔE between the proton and gamma-ray peaks in Fig. 6b we can roughly estimate the proton binding energy B_p at the level making the principal contribution to the Cu^{65} photoproton yield. In the case of copper this is most likely the filled $4f_{7/2}$ level. It is easily seen that $B_p(4f_{7/2}) \approx \Delta E \sim 15 - 16$ Mev.

It is of interest that in the spectrum of protons from gamma rays with energies 24 – 28 Mev in Fig. 6b there are no particles with $\epsilon_p < 9$ Mev and that ΔE derived from this figure is also ~ 15 Mev. Gamma rays in the given energy region thus evidently extract protons from the $4f_{7/2}$ level.

c) In the proton spectrum for all four energies two peaks are observed at $\epsilon_p \sim 4.7$ and 6.0 Mev, which are most pronounced for $E_{\gamma\max} = 20.0$ Mev. We attempted to approximate the proton spectrum in the region $\epsilon_p = 4 - 7$ Mev for the given value of $E_{\gamma\max}$ by means of the smooth curve represented by the broken line in Fig. 2b. The χ^2 goodness of fit of this curve is defined by

$$\chi^2 = \sum_i (F_i(\varepsilon) - \bar{y}_i)^2 / \sigma_i^2,$$

where $F_i(\epsilon)$ is the experimental value, $\bar{y}_i$ is the curve ordinate and σ_i is the root-mean-square error of $F_i(\epsilon)$. The probable validity of the curve was estimated to be about 10%.

Statistical fluctuations can therefore evidently not account for the observed peaks in the proton spectrum. All other errors associated with finite target thickness and experimenters' errors would result in the smoothing of the spectral shape rather than in peaks.

The presence of two peaks in the energy distribution might be attributed to the observation of two spectra with noncoinciding maxima. Possible sources could be, for example, 1) (γp) and (γnp) reactions; 2) photoprotons from Cu^{65} with Cu^{63} admixture; 3) photoprotons resulting from evaporation as well as from a direct photoeffect.

The first of these possibilities cannot account for the presence of two peaks, which are most pronounced for $E_{\gamma\,max} = 20$ Mev, where the (γnp) reaction in copper is possible energetically only with $\epsilon_p < 4$ Mev. When a correction is made for protons from Cu^{63} (from measurements on natural copper[5]) or for the evaporation contribution the observed peaks do not disappear, since in both instances it is necessary to subtract the spectrum with a broad peak in the ϵ_p region from 4 to 6 Mev. The observed peaks therefore do not appear to result from the superposition of two noncoinciding spectra.

Separate peaks in the proton spectrum might also result from transitions between distinct states of the initial and final nuclei, accompanied by proton emission. In our case nuclei are irradiated with continuous bremsstrahlung; therefore distinct initial states can be excited only if the gamma-ray absorption cross section exhibits resonances.

It would be strange if distinct final states were singled out, because of the high nuclear-level density for $A > 50$. It should be noted, however, that proton spectra from the (np) reaction with 14-Mev neutrons and $A > 50$ also sometimes exhibit peaks.[21,22]

3. Angular distributions. Figure 3a shows that the angular distributions of photoprotons for $E_{\gamma\,max} = 17.9$ and 20.3 Mev is quite well approximated by (1). For $E_{\gamma\,max} = 24.5$ and 28.5 Mev (Fig. 3b) the peaks are shifted forward and these distributions are represented by (2).

The table shows that the anisotropy b/a is always appreciably different from zero and that for given $E_{\gamma\,max}$ it increases with ϵ_p. This rise is most pronounced for $E_{\gamma\,max} = 17.9$ and 20.0 Mev, where the angular distribution of the most energetic pronouns, resulting from the photoeffect involving the upper level ($\epsilon_p > 9$ Mev), becomes, as in the case of ordinary copper,[3,5] practically completely anisotropic: $I(\theta) \sim \sin^2\theta$. According to the models of Courant[4] and Wilkinson[23] such a distribution corresponds to transitions from the S shell and cannot be the result of a photoeffect in the upper $3p_{3/2}$ proton level in copper. However, it was shown in reference 24 that a completely anisotropic distribution may accompany a photoeffect in a P shell if interference of the $l \rightarrow l+1$ and $l \rightarrow l-1$ transitions is taken into account. It is significant that the angular distribution of fast photoprotons from silver, which also has an upper p level, is likewise represented by $I(\theta) \sim \sin^2\theta$.[25] The diminished fast-proton anisotropy as we go to $E_{\gamma\,max} = 24.5$ and 28.5 Mev is, as in the case of natural copper,[5] apparently associated with the fact that a photoeffect in the lower-lying $4f_{7/2}$ level begins to play a part.

It follows from the 90° peak of the angular distributions for $E_{\gamma\,max} = 17.9$ and 20.0 Mev that for $E_\gamma < 20.0$ Mev gamma-ray absorption is of dipole character. The forward shift of the peak $(c \neq 0)$ at higher values of $E_{\gamma\,max}$ indicates that quadrupole absorption is beginning to appear. It can easily be shown that the lower limit of the ratio between the integrated quadrupole and dipole gamma absorption cross sections is given by $\sigma_q^{int}/\sigma_{dip}^{int}\quad (c/b)^2/10(3a/b+2)$, which is estimated to be $\sim 1\%$ for $E_{\gamma\,max} = 24.5$ and 28.5 Mev (for $\epsilon_p > 4$ Mev).

4. Proton emission cross section. The cross section $\sigma_{\gamma p}$ is represented in Fig. 5, with the $Cu^{65}(\gamma n)Cu^{64}$ cross section shown for comparison.[17] $\sigma_{\gamma p}$ has a half-width of about 7 Mev and peak $E_{\gamma p}^{max} = 20.0$ Mev, shifted upward by about 1.5 Mev compared with $\sigma_{\gamma n}$.

By using the known[3,17] ratios of the photoproton and photoneutron yields from Cu^{63} and Cu^{65} together with our own data we determined the absolute maximum of $\sigma_{\gamma p}$ through a comparison with the cross section for $Cu^{63}(\gamma n)Cu^{62}$.[17] From $\sigma_{\gamma p}^{max}(Cu^{65}) = 27$ mb obtained in this manner we have $\sigma_{\gamma p}^{int}(Cu^{65}) = 190$ Mev-mb.

It was shown above that at least 80% of the Cu^{65} proton yield results from a mechanism other than evaporation. If gamma rays are absorbed through a single-particle mechanism we can assume that about half of the integrated gamma absorption cross section $\sigma_\gamma^{int} \approx \sigma_{\gamma p}^{int} + \sigma_{\gamma n}^{int}$ represents absorption by proton shells. The fraction of these absorptions resulting in direct proton emission is thus $\delta_{exp} \approx 0.8\,\sigma_{\gamma p}^{int}/(\sigma_\gamma^{int}/2) \approx 20\%$ when $\sigma_{\gamma n}^{int}(Cu^{65}) = 1110$ Mev-mb.[17]

The Wilkinson model[23] was used to estimate the same quantity, following the procedure of Lokan.[25]

It was assumed that transitions from the $4f_{7/2}$ shell are most important and that they determine the position of the maximum $E_{\gamma p}^{max}$. From the spectrum of protons emitted as a result of gamma irradiation with energy close to $E_{\gamma p}^{max}$ (Fig. 6b) it follows that particles emitted from the $4f_{7/2}$ shell have an average energy of 6 — 7 Mev. We have found $\delta \approx 10\%$, using $r_0 = 1.5 \times 10^{-13}$ cm and W, the imaginary part of the complex potential, given by 2W = 4 Mev.[25] The agreement with experiment is satisfactory, considering the roughness of the estimate.

The authors are deeply indebted to N. A. Ponomareva and R. D. Rozhdestvenskaya for scanning of the plates and assistance with the treatment of the data.

---

[1] O. Hirzel and H. Wäffler, Helv. Phys. Acta **20**, 373 (1947).

[2] B. C. Diven and G. M. Almy, Phys. Rev. **80**, 407 (1950).

[3] P. R. Byerly and W. E. Stephens, Phys. Rev. **83**, 54 (1951).

[4] E. D. Courant, Phys. Rev. **82**, 703 (1951).

[5] Lejkin, Osokina, and Ratner, Nuovo cimento Suppl. **3**, 105 (1956).

[6] R. M. Osokina and B. S. Ratner, JETP **32**, 30 (1957), Soviet Phys. JETP **5**, 1 (1957).

[7] M. E. Toms and W. E. Stephens, Phys. Rev. **95**, 1209 (1954).

[8] W. V. Weisskopf, Phys. Rev. **52**, 295 (1937).

[9] R. M. Osokina and B. S. Ratner, Physica **22**, 1147A (1956).

[10] Akindinov, Amirov, Osokina, and Ratner, Report at All-Union Conference on Nuclear Reactions, 1957.

[11] B. Forkman, Arkiv Fysik **11**, 265 (1956).

[12] Medicus, Grant, and Demers, Bull. Am. Phys. Soc. **3**, 382 (1958).

[13] J. Rotblat, Nature **167**, 550 (1950).

[14] L. Katz and A. G. W. Cameron, Can. J. Phys. **29**, 518 (1951).

[15] V. F. Weisskopf, Statistical Theory of Nuclear Interactions, Russ. Transl., IIL, 1952.

[16] J. M. Blatt and V. F. Weisskopf, Theoretical Nuclear Physics, Wiley, N. Y., 1952.

[17] L. Katz and A. G. W. Cameron, Can. J. Phys. **29**, 1209 (1951).

[18] J. W. Butler and C. R. Gossett, Phys. Rev. **108**, 1473 (1957).

[19] T. Ericson, Nuclear Phys. **11**, 481 (1959).

[20] P. F. Klinkenberg, Revs. Modern Phys. **24**, 63 (1952).

[21] D. L. Allan, Nuclear Phys. **6**, 464 (1958).

[22] D. L. Allan, Proc. Phys. Soc. (London) **A70**, 195 (1957).

[23] D. H. Wilkinson, Physica **22**, 1039 (1956).

[24] J. Eichler and H. A. Weidenmuller, Z. Physik **152**, 261 (1958).

[25] K. H. Lokan, Proc. Phys. Soc. (London) **A73**, 697 (1959).

Translated by I. Emin
154

SOVIET PHYSICS JETP VOLUME 11, NUMBER 3 SEPTEMBER, 1960

EQUATION OF STATE FOR ALUMINUM, COPPER, AND LEAD IN THE HIGH PRESSURE REGION

L. V. AL' TSHULER, S. B. KORMER, A. A. BAKANOVA, and R. F. TRUNIN

Submitted to JETP editor October 7, 1959

J. Exptl. Theoret. Phys. (U.S.S.R.) **38**, 790-798 (March, 1960)

An equation of state for metals is considered, which differs from the Mie-Grüneisen equation of state for a solid body in taking into account the electronic components of the energy and pressure. New data from the dynamic compression of metals are presented, on the basis of which equations of state are derived for aluminum, copper, and lead in the high pressure region.

INTRODUCTION

THE behavior of metals under pressures of several million atmospheres and temperatures of some tens of thousands of degrees may be described by an equation of state, if their compressibility curves at the absolute zero of temperature, the specific heats of the lattice and the electron gas, and their Grüneisen coefficients (defined as the ratio of the thermal pressure to the thermal energy density) are known. Such equations of state cannot be obtained theoretically, since quantum-statistical calculations of the compressibility by the Thomas-Fermi and Thomas-Fermi-Dirac methods lead to an increased pressure which does not reduce to zero at normal density. Solid state theory also does not allow the calculation of Grüneisen coefficients for the lattice, establishing merely the connection between these coefficients and the extrapolated "cold" compression curve.[1-3] For the non-transition metals, our knowledge of the thermal components of energy and pressure caused by the excitation of the electron gas is quite complete and reliable. The validity of the theoretical results in this field are confirmed by measurements of the electronic specific heat at temperatures close to absolute zero. At the present time, of course, we can deal only with semi-empirical equations of state, based on direct experimental measurements of the compressibility.

As a source of information about the pressure region of interest to us, the authors have made use of data from individual single dynamic compressions. The transition from a dynamic adiabatic to the general equation of state connecting the pressure with the density and temperature is possible if additional data is available, for example on the shock compressibility of porous bodies,[4] or with the aid of the theoretical relationships, mentioned above, between the Grüneisen coefficients and the curve of cold compression. This second method has been put into practice in a work by Walsh and his collaborators,[5] devoted to the state equations for metals up to pressures of 5×10^5 atm.

The main difference between our work and the above consists in the considerably wider range of pressures and temperatures covered, and in taking into account the electronic components of energy and pressure, which cannot in any case be neglected for temperatures of 1 – 2 ev. In this paper we also present data on the dynamic compression of aluminum up to pressures of 2×10^6 atm and the results of new measurements of the compressibility of copper, lead, and iron at pressures of 10^6, 2×10^6, and 4×10^6 atm.

1. DYNAMIC ADIABATS OF ALUMINUM, COPPER, LEAD, AND IRON

The dynamic adiabats of copper and lead up to 5×10^5 atm have been described by Walsh[5] and in reference 6. In the present paper we also present the results of dynamic compression measurements on these metals up to pressures of 3.5×10^6 atm. For aluminum the observed range of pressures has amounted to 5×10^5 atm.[5,7,8] In this section we present the results of the compression of aluminum by strong shock waves up to 2×10^6 atm, obtained in the authors' laboratory, and new results on copper, lead, and iron in the pressure range from 10^6 to 4×10^6 atm. To improve the precision, it was necessary to make new measurements for the following reason. The dynamic adiabat for iron, used in reference 6 as a reference standard for determining the compressibilities of other elements at 1.3

TABLE I

Serial No.	Striker material	Striker speed, km/sec	D, km/sec	U, km/sec	P, 10^{10} d/cm^2	ρ/ρ_0	D, km/sec	U, km/sec	P, 10^{10} d/cm^2	ρ/ρ_σ
			Aluminum				Copper			
I	Aluminum	5.60	9.13	2.80	69.3	1.442	6.64	1.82	107.9	1.377
II	Iron	5.60	10.39	3.70	104.2	1.553	8.06	2.71	195.0	1.506
III	Iron	9.10	—	—	—	—	10.58	4.43	418.7	1.720
IV	Iron	8.64	12.94	5.62	197,1	1.767	10.12	4.14	374.0	1.692
			Lead				Iron			
I	Aluminum	5.60	4.92	1.88	104.9	1.618	7.01	1.90	104.5	1.372
II	Iron	5.60	6.07	2.76	190.0	1.834	8.44	2.80	185.5	1.496
III	Iron	9.10	8.26	4.45	417.0	2,168	11.26	4.55	402.2	1.678
IV	Iron	8.64	7.74	4.18	366.9	2,174	10.67	4.26	356.8	1.664

$\times 10^6$ atm, was obtained in reference 4 by the "splitting-off" method, i.e., by a comparison of the shock wave velocity in an iron plate with the speed W of expansion of the rear surface of the plate after the passage of the shock wave through it. The material velocity in this case was taken to be approximately $\frac{1}{2}$W, since the calculated corrections for the failure of the rule of doubled material velocity were small. The actual error due to violation of the doubling rule could have been larger. Accordingly, new measurements of the dynamic compressibility of iron, lead, and copper in this region have been carried out by the deceleration method,[4] by recording the speed of a shock wave in the receiver and the speed of a plate, smoothly accelerated by explosion products, which strikes the receiver.

Another reason for possible inaccuracies in the previous measurements arises from the decay of the shock wave in the material of the screen which protects the sample, and in the sample itself. In order to exclude this error, the new experiments were carried out with thin screens, using a short base-line of 3 to 4 mm for the measurements. Both these effects lead to errors of the same sign, increasing the degree of compression. The suggestion that the adiabat may have a "stiffer" slope in the region of 2×10^6 atm pressure has also been expressed by Walsh (private communication).

In the first group of experiments, the pressure was created by the impact of an aluminum plate 2 mm thick and 70 mm in diameter.* After being put in place on the explosive charge, the plate was surrounded by a steel ring 120 mm in diameter and of the same thickness. The higher pressure of the explosion products caused by reflection of the detonation wave from the surface of the steel ring prevented the edges of the plate from lagging behind. In the second group of experiments the striker was a steel disk 1.5 mm thick and 70 mm in diameter, driven by the products of an explosion inside a massive lead cylinder, 90 mm thick, to a speed of 5.6 km/sec. By this means, pressures close to 2×10^6 atm were attained in iron, copper, and lead (185.5×10^{10}, 195.0×10^{10}, and 190.0×10^{10} d/cm^2). Pressures of 4×10^6 atm were obtained with steel striker speeds of 9.1 km/sec. The heating of the aluminum and steel strikers during the driving process was approximately equal in all runs, and it is estimated that it did not exceed a few hundred degrees. In the first two groups of experiments the screens were made of the same material as the test samples; in the third group it was made of the same material as the striker.

The striker speed, the results of the wave-velocity measurements in the test piece, and the parameters obtained for the points by graphical constructions on the pressure-velocity diagrams are shown in Table I. The following notation has been used in the table: D is the wave velocity, U the material velocity behind the shock wave front, P the pressure, ρ the density behind the wave front, ρ_0 the density of the initial state ahead of the front, and $\sigma = \rho/\rho_0$ is the relative compression. Each value in the table was obtained as the mean of the values from 4 to 6 experiments. In each run the time recording was carried out on three double-beam oscilloscopes. The inaccuracy in the determination of the quantities D and W did not exceed 1%.

In Group IV of the table are shown the parameters of the shock waves in copper, lead, and iron obtained for a striker velocity of 8.64 km/sec, taken from reference 6. The slight changes in the

---

*The possibility of obtaining high pressures by impact of a plate driven by explosion products was indicated in 1948 by E. I. Zababakhin. Using this method, Yu. F. Alekseev measured in 1949 the compressibility of aluminum up to pressures of 500,000 atm.

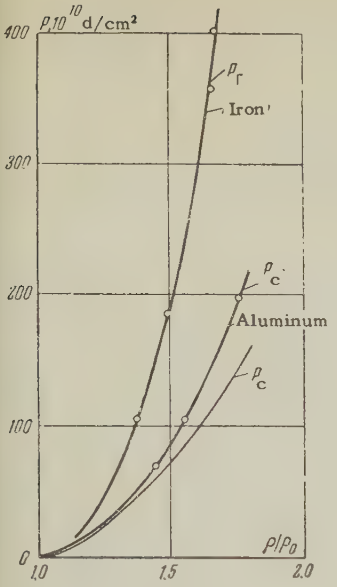

FIG. 1. Shock adiabats for iron and aluminum, and the curve of cold compression for aluminum.

parameters as compared with reference 6 are due to the introduction of the corrections to allow for the decay of the shock wave in the screen and the sample. New data have also been included on the compressibility of aluminum at pressures close to 2×10^6 atm (197.1×10^{10} d/cm^2).

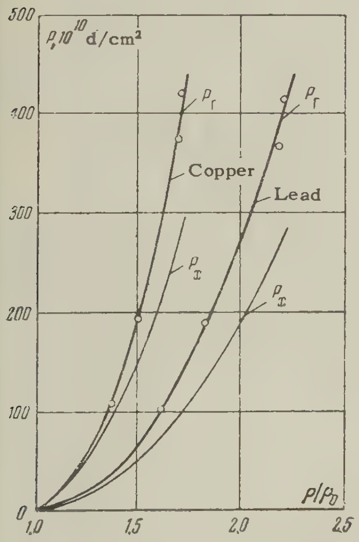

FIG. 2. Shock adiabats and curves of cold compression for copper and lead.

The points on the shock adiabat thus obtained are shown in Figs. 1 and 2. The thick lines in the figures represent the positions of the adiabats constructed from the data in the present paper. By comparison with references 4 and 6, the greatest change is in the position of the lead adiabat, which has been shifted to the left, in the direction of lower σ, by 3 to 5%. For copper and iron the changes are small.

Analytical expressions for the dynamic adiabats in the form

$$P_\Gamma = \Sigma a_k (\sigma - 1)^k \tag{1}$$

contain the coefficients a_k, the first three of which are determined by the parameters of the material under normal conditions in the case of copper, aluminum, and lead, as will be shown below. The dynamic adiabat for iron in the pressure range from 5×10^5 to 5×10^6 atm is described by five coefficients. There is no connection between these coefficients and the parameters for iron under normal conditions, since, according to Bancroft,[9] a phase transition occurs in iron at a pressure of 1.3×10^5 atm. The coefficients a_k are shown in Table II. The relationships between the wave and material velocities is given in Table III. For the values of P_Γ as a function of σ, see Tables V to VII below.

TABLE II

k	Values of a_k, 10^{10} d/cm^2			
	Aluminum	Copper	Lead	Iron
1	73.1	137.0	41.4	30.3
2	152.7	271.7	101.7	724.5
3	143.5	224.0	120.0	—271.2
4	—887	1078	—43	—14
5	2862	—2967	547	852
6	—3192	3674	—801	—
7	1183	—1346	312	—

2. THE FORM OF THE EQUATIONS OF STATE

We shall write the equation of state and the expression for the internal energy in the additive form

$$P = P_c + P_{\text{t.l.}} + P_{\text{t.e.}}, \quad E = E_c + E_{\text{t.l.}} + E_{\text{t.e.}} \tag{2}$$

In equation (2), P_c and E_c are terms characterizing the interactions of the atoms at $T = 0°$K; $P_{t.l}$ and $E_{t.l}$ are thermal terms due to the vibration of the atomic lattice; $P_{t.e}$ and $E_{t.e}$ are the terms due to the thermal excitation of the electrons. The necessity for taking the electronic terms into account is due to the fact that, in the regions of temperature and pressure which we are considering, their contribution is already important, as will become evident from what follows later.

Let us consider the individual terms in (2). It has been shown that the function $P_c(v)$, and consequently also $E_c = \int_v^{v_{0k}} P_c \, dv$, must be found from experimental measurements (v_{0k} is the specific volume at $P = 0$ and $T = 0°$K). We shall write the thermal terms for the lattice, in conformity with the conclusions of solid state theory, in the form

$$E_{\text{t.l.}} = C_{vl}\left(T - T_0 + \frac{E_0}{C_{vl}}\right) \tag{3a}$$

$$P_{\text{t.l.}} = \gamma_l(v)\frac{C_{vl}}{v}\left(T - T_0 + \frac{E_0}{C_{vl}}\right). \tag{3b}$$

TABLE III

U, km/sec	D, km/sec				U, km/sec	D, km/sec			
	Aluminum	Copper	Lead	Iron		Aluminum	Copper	Lead	Iron
0	5.20	3.92	1.91	—	3.5	10.41	9.19	7.00	9.54
0.5	5.94	4.68	2.75	—	4.0	10.81	9.93	7.59	10.33
1.0	6.64	5.44	3.56	5.38	4.5	11.48	10.67	8.18	11.10
1.5	7.32	6.22	4.33	6.30	5.0	12.16	—	—	—
2.0	8.02	6.96	5.07	7.15	5.5	12.82	—	—	—
2.5	8.71	7.70	5.75	7.96	6.0	13.45	—	—	
3.0	9.41	8.45	6.38	8.76					

TABLE IV

	Aluminum	Copper	Lead		Aluminum	Copper	Lead
ρ_0, g/cm³	2.71	8.93	11.34	$(d\ln\gamma_l/d\ln v)_{v_0}$	1.175	1.265	1.400
C_{vl}, 10^6 erg/g-deg	8.960	3.825	1.293	m	3.5	4.3	5.0
E_0, 10^7 erg/g	161.0	77.1	32.3	n	6.0	6.0	7.0
$\varkappa_0$, 10^{-12} cm²/d	1.367	0.730	2.415	β_0, erg/g-deg²	500	110	144
α, 10^{-6} deg⁻¹	23.1	16.5	29.0	v_{0k}/v_0	0.988	0.990	0.979
γ_0	2.088	1.983	2.457	$-v_0(dP_c/dv)_{v_{0k}}$, $10^{10}\frac{\text{d}}{\text{cm}^2}$	77.10	142.82	45.89

Here C_{vl} is the specific heat of the lattice; E_0 is the internal energy under normal conditions; $\gamma_l(v)$ is the Grüneisen coefficient for the lattice, which is a function of the specific volume; and v is the specific volume.

In Eq. (3) it is assumed that the specific heat is independent of the temperature and density, as a consequence of which the Grüneisen coefficient also becomes independent of the temperature. The assumption of constant C_{vl} is, of course, an approximation which does not take into account the anharmonicity of the vibrations in the solid.

Solid state theory provides a connection between the Grüneisen coefficients and the derivatives of the curve $P_c(v)$. According to Slater[1] and Landau[2]

$$\gamma_l(v) = -\frac{v}{2}\left[\frac{d^2P_c/dv^2}{dP_c/dv}\right] - \frac{2}{3}. \tag{4a}$$

According to Dugdale and MacDonald[3]

$$\gamma_l(v) = -\frac{v}{2}\left[\frac{d^2(Pv^{2/3})/dv^2}{d(Pv^{2/3})/dv}\right] - \frac{1}{3}. \tag{4b}$$

Let us consider the limits of variation of $\gamma_l(v)$.

Under normal conditions, by definition

$$\gamma_0 = \gamma_l(v_0) = -\frac{v_0^2}{C_{vp}}\left(\frac{\partial P}{\partial v}\right)_{T=T_0}\frac{1}{v_0}\left(\frac{\partial v}{\partial T}\right)_{P=0} = \frac{3\alpha}{\rho_0 C_{v\,l}\varkappa_0}, \tag{5}$$

where α is the coefficient of linear thermal expansion; κ_0 is the coefficient of volume compressibility for $P = 0$ and $T = T_0$; and $v_0 = 1/\rho_0$ is the specific volume under normal conditions. The values of the parameters E_0, ρ_0, C_{vl}, α, κ_0, and γ_0 for aluminum, copper, and lead are given on the left hand side of Table IV. For these metals the initial values γ_0 are close to 2, and are all included within a rather narrow range of values.

Some idea of the behavior of the function $\gamma_l(v)$, for v close to v_0, can be obtained by substituting the expression for $P_c(v)$ resulting from the Mie-Lennard-Jones potential[10] into the relation (4a) or (4b). Using formula (4b),

$$\gamma_l(v_0) = \tfrac{1}{6}(n + m + 3), \tag{6}$$

$$(d\ln\gamma_l/d\ln v)_{v_0} = (n+2)(m+2)/18. \tag{7}$$

The quantities $(d\ln\gamma_l/d\ln v)_{v_0}$ from (7) are given in Table IV. The exponents m and n used

TABLE V. Aluminum

ρ/ρ_0	P_c, 10^{10}d/cm²	E_c, 10^8 erg/g	P_Γ, 10^{10} d/cm²	T, °K	γ_l	ρ/ρ_0	P_c, 10^{10}d/cm²	E_c, 10^8 erg/g	P_Γ, 10^{10} d/cm²	T, °K	γ_l
1.05	3.1	2.0	4.2	315	2.00	1.45	61.9	249.0	71.3	1980	1.41
1.10	7.8	10.5	9.0	348	1.81	1.50	72.7	306.0	86.1	2640	1.44
1.15	13.4	26.0	14.5	401	1.56	1.55	84.5	368.0	103.0	3440	1.44
1.20	19.7	47.0	21.1	488	1.37	1.60	97.0	435.0	121.7	4410	1.43
1.25	26.6	76.0	28.8	625	1.28	1.65	110.0	508.0	142.7	5530	1.41
1.30	34.5	111.0	37.4	818	1.28	1.70	125.0	585.0	165.2	6790	1.39
1.35	42.9	151.0	47.2	1097	1.31	1.75	140.0	667.0	189.7	8180	1.34
1.40	51.9	198.0	58.2	1476	1.37	1.80	157.0	754.0	216.0	9670	1.30

TABLE VI. Copper

ρ/ρ_0	P_c, 10^{10}d/cm^2	E_c, 10^8 erg/g	P_Γ, 10^{10} d/cm^2	T, °K	γ_l	ρ/ρ_0	P_c, 10^{10}d/cm^2	E_c, 10^8 erg/g	P_Γ, 10^{10} d/cm^2	T, °K	γ_l
1.05	6,1	1.3	7,5	317	1.89	1.40	105.2	117.0	122.5	2300	1.63
1.10	15,1	6.3	46.7	360	1,85	1.45	127.2	148.7	152.2	3180	1,59
1.15	25,4	15,1	28.0	438	1.87	1.50	151,8	184.8	185.8	4350	1.55
1.20	37,5	27.9	41,3	577	1.88	1.55	178.3	224.0	225.2	5760	1.53
1.25	51.6	44.6	56.6	802	1,84	1.60	207.5	267.2	271.4	7530	1.53
1.30	67.4	64,7	75.5	1150	1,77	1.65	238,7	314.5	324.7	9710	1.53
1.35	85.3	89.1	97.1	1630	1.70	1.70	273.0	366.0	388.0	12425	1.54

in equation (7) are shown in the same place.* The sign and absolute magnitude of $(d \ln \gamma_l / d \ln v)_{v_0}$ show that the Grüneisen coefficient increases rapidly with a decrease in the specific volume. From Gilvarry's data,[11] as the pressure increases without limit, γ_l tends to a limiting value of $2/3$.

The electronic heat terms in the energy and pressure are proportional to the square of the temperature for a degenerate electron gas. This conclusion follows not only from free electron theory, but also from the solution of the Thomas-Fermi equations obtained by Gilvarry.[12] By making use of the concept of an electronic specific-heat coefficient β, they can be rewritten in the form

$$E_{\text{t.e.}} = \tfrac{1}{2}\beta T^2, \quad P_{\text{t.e.}} = \gamma_e E_{\text{t.e.}}/v = \tfrac{1}{2}\gamma_e \beta T^2/v. \qquad (8)$$

Here γ_e is a coefficient defined as the ratio of the electrons' thermal pressure to their thermal energy.

A comparison of Latter's data,[13] giving an accurate solution of the Thomas-Fermi equation for the case $T \neq 0$, with Gilvarry's data for the case $T \approx 0$ shows that the electronic specific heat coefficient remains almost constant up to temperatures of the order of 30 to 50×10^3 °K. Furthermore, as the density increases, this constancy is maintained up to higher temperatures. In order to explain the dependence of the electronic specific heat coefficient on the degree of compression, we make use of the thermodynamic identity

$$(\partial E/\partial v)_T = T(\partial P/\partial T)_v - P.$$

Substituting $E_{t.e}$ and $P_{t.e}$ from (8) into this expression we obtain, after integration,

$$\beta = \beta_0 \exp\left\{\int_{v_0}^{v} \gamma_e \frac{dv}{v}\right\}.$$

An analysis of the data of Gilvarry and Latter shows that the magnitude of the Grüneisen coefficient for electrons, γ_e, varies within the rather narrow limits 0.5 to 0.6, tending at extremely high pressures to the value $2/3$, characteristic of a free electron gas. If we take $\gamma_e = 1/2$ over the region of interest to us, we obtain $\beta = \beta_0 (v/v_0)^{1/2}$ and accordingly

$$E_{\text{t.e.}} = \tfrac{1}{2}\beta_0 (v/v_0)^{1/2} T^2; \quad P_{\text{t.e.}} = \tfrac{1}{4}\beta_0\rho_0 (v_0/v)^{1/2} T^2. \qquad (9)$$

The value of β_0 may be taken from experimental measurements at low temperatures. It is well known that the electronic specific heat, which under normal conditions is an extremely small fraction of the lattice specific heat (~3%), becomes noticeable at temperatures close to the absolute zero, because in this region the specific heat due to lattice vibrations drops off as T^3, while the specific heat of the electron gas is proportional to T. The values of the experimentally determined electronic specific heat coefficients β_0, used in the calculations below, are given in Table IV.

Adding the terms P_c and E_c to the electronic and lattice thermal terms, we obtain the following expressions for the pressure and energy:

$$P = P_c + \frac{\gamma_l C_{vl}}{v}\left[T - T_0 + E_0/C_{vl}\right] + \tfrac{1}{4}\rho_0\beta_0 (v_0/v)^{1/2} T^2; \qquad (10a)$$

$$E = \int_{v}^{v_{0k}} P_c\, dv + E_0 + C_{vl}(T - T_0) + \tfrac{1}{2}\beta_0 (v/v_0)^{1/2} T^2. \qquad (10b)$$

Let us now, following Walsh,[5] establish a connection between the parameters of the metal in its initial state and the coefficients a_k of the dynamic adiabats. In order to obtain the necessary relations, we recall that the isentropic curve which passes through the origin of coordinates has a second-order tangency with the Hugoniot adiabat. Its coefficients, when expressed in a series analogous to (1),

$$P_s = \sum_k a_k(s)(\sigma - 1)^k,$$

are connected with the coefficients of the Hugoniot adiabat by the expressions:

$$a_1(s) = a_1; \quad a_2(s) = a_2;$$
$$a_3(s) = a_3 - \tfrac{1}{6}\gamma_0 (a_1 + a_2). \qquad (11)$$

The first coefficient $a_1(s)$ is the isentropic modulus of bulk compression, i.e., the reciprocal of the compressibility coefficient κ. For all practical purposes it does not differ from the isothermal modulus measured by Bridgman.[14]

---

*m and n have been chosen from the experimental values of the sublimation energies and the coefficients $\gamma_l(v_0)$.

Substituting P_S into (4a) and then differentiating leads to the equation

$$a_2(s) = a_1(s)\,\gamma_0;$$

$$\gamma_0\left(\frac{d\ln\gamma}{d\ln v}\right)_{v=v_0} = 2\left(\frac{a_2(s)}{a_1(s)}\right)^2 - \frac{10}{6}\left(\frac{a_2(s)}{a_1(s)}\right) - 3\,\frac{a_3(s)}{a_1(s)} - \frac{1}{y}\,.$$

In view of (11), we obtain finally

$$a_1 = \frac{1}{\varkappa_0};\quad a_2 = \frac{\gamma_0}{\varkappa_0};$$

$$a_3 = \frac{a_1}{3}\left[\frac{5}{2}\left(\frac{a_2}{a_1}\right)^2 - \frac{7}{6}\left(\frac{a_2}{a_1}\right) - \gamma_0\left(\frac{d\ln\gamma}{d\ln v}\right)_{v_0} - \frac{1}{9}\right]. \quad (12)$$

In calculating the coefficients a_1, a_2, and a_3, the values of κ_0, γ_0, and $(d\ln\gamma_l/d\ln v)_{v_0}$ were taken from Table IV.

3. RESULTS OF THE CALCULATIONS

The results of dynamic experiments, expressed in the form (1), determine the pressure P_Γ, and also the energy $E_\Gamma = E_0 + \frac{1}{2}P_\Gamma(v_0 - v)$. Substituting these quantities into the left hand side of (10a) and (10b) gives us two equations, containing three unknown functions P_c, γ_l, and T. The missing third equation is (4b). The initial conditions of the system will be

$$P_c(v_{0k}) = 0 \text{ and } (dP_c/dv)_{v_{0k}}.$$

The method of calculating v_{0k} and $(dP_c/dv)_{v_{0k}}$ is given in Walsh's paper,[5] and the values of these quantities which have been used in the calculations are given in Table IV.

The results of the numerical solution of the system for aluminum, copper, and lead are given in Tables V to VII, respectively. In these tables are given the pressures and compressional energies at the absolute zero of temperature, the pressures and temperatures of the Hugoniot adiabat, and the values of the Grüneisen coefficient.

The relative positions of the Hugoniot adiabats and the curves of "cold" compression are demonstrated in Figs. 1 and 2. As the figures show, thermal pressure plays an important role in the compression of metals by strong shock waves. Thus, for pressures of 216×10^{10} d/cm^2 in aluminum, 388×10^{10} d/cm^2 in copper, and 401×10^{10} d/cm^2 in lead, the thermal components of the pressure are equal to 59×10^{10}, 115×10^{10}, and 124×10^{10} d/cm^2, respectively.

The role of the heat in the internal energy balance is even larger. In this case, for the same compressive shock pressures as above, the thermal energy has become the major fraction, amounting to 57% for aluminum, 60% for copper, and 69% for lead.

The temperatures attained were 9700, 12,400, and 26,200 degrees, which are approximately twice as high as the melting points of the metals, as estimated for the high pressure region by Gilvarry.[11] High temperatures lead to a considerable increase in the specific heat of the metal, due to its electronic component βT. There is a corresponding increase in the contribution of the electrons to the internal energy balance. For example, in the shock compression of lead to $\rho = 2.2\,\rho_0$ the electronic fraction of the thermal energy amounts to about 34% of the total internal energy change, and to 50% of its thermal part. The corresponding proportions of the thermal pressure due to the electrons are 10% and 34%.

As expected, in all three metals a general tendency was observed for $\gamma_l(v)$ to decrease with density. It should be noted that the value of the function $\gamma_l(v)$ depends markedly on small variations in the positions of the dynamic adiabatics. On the other hand, the shape of the cold compression curves is much less sensitive to possible variations in the dynamic adiabatics, especially in the region of large thermal pressures. The positions of the P_c curves also change very little when the expression (4b) for γ_l is substituted for the Landau-Slater formula (4a), or when the quantity β_0 is varied.

TABLE VII. Lead

ρ/ρ_0	P_c, 10^{10}d/cm^2	E_c, 10^8 erg/g	P_Γ, 10^{10} d/cm^2	T, °K	γ_l	ρ/ρ_0	P_c, 10^{10}d/cm^2	E_c, 10^8 erg/g	P_Γ, 10^{10} d/cm^2	T, °K	γ_l
1.10	4.2	1.2	5.3	364	2.20	1.80	123.7	127.3	176.5	11590	1.48
1.20	11.6	6.2	13.4	563	2.00	1.85	139.5	144.6	200.7	13260	1.42
1.30	21.6	15.3	25.0	1045	1.90	1.90	156.0	163.2	225.5	15000	1.35
1.40	34.6	28.8	42.3	2000	1.84	1.95	173.8	182.8	251.2	16720	1.28
1.50	51.0	46.7	65.5	3550	1,77	2.00	192.6	203.5	277.6	18470	1.21
1.55	60.7	57.2	79.7	4570	1.73	2.05	212.3	225.2	305.5	20300	1.14
1.60	71.3	69.0	95.5	5730	1.69	2.10	233.0	248.2	335.5	22150	1.07
1.65	82.7	81.7	113.5	7070	1.65	2.15	254.5	272.0	367.7	24125	1.02
1.70	95.3	95.8	133.0	8485	1.60	2.20	277.0	297.0	401.0	26230	0.98
1.75	109.2	111.1	154.0	10000	1.54						

The shape of the curves $P_c(v)$ is also apparent from the results of the present work.

The authors express their thanks to A. I. Funtikov for valuable discussions and participation in the series of experiments, and also to R. V. Malyshev and I. P. Dudoladov for the large volume of computational work which they accomplished. With especial gratitude the authors acknowledge the valuable consultations with Prof. K. A. Semendyaev.

---

[1] J. C. Slater, Introduction to Chemical Physics, McGraw, New York (1939).

[2] L. D. Landau and K. P. Stanyukovich, Dokl. Akad. Nauk SSSR **46**, 399 (1945).

[3] J. S. Dugdale and D. K. MacDonald, Phys. Rev. **89**, 832 (1953).

[4] Al'tshuler, Krupnikov, Lebedev, Zhuchikhin, and Brazhnik, JETP **34**, 874 (1958), Soviet Phys. JETP **7**, 606 (1958).

[5] Walsh, Rice, McQueen, and Yarger, Phys. Rev. **108**, 196 (1957).

[6] Al'tshuler, Krupnikov, and Brazhnik, JETP **34**, 886 (1958), Soviet Phys. JETP **7**, 614 (1958).

[7] J. M. Walsh and M. H. Rice, J. Chem. Phys. **26**, 815 (1957).

[8] H. D. Mallory, J. Appl. Phys. **26**, 555 (1955).

[9] Bancroft, Peterson, and Minshall, J. Appl. Phys. **27**, 291 (1956).

[10] E. Grüneisen, Handbuch der Physik, Springer, Berlin, (1926), vol. 10, p. 1.

[11] J. J. Gilvarry, Phys. Rev. **102**, 317 (1956).

[12] J. J. Gilvarry, Phys. Rev. **96**, 934, 944 (1954); J. J. Gilvarry and G. H. Peebles, Phys. Rev. **99**, 550 (1955).

[13] R. Latter, Phys. Rev. **99**, 1854 (1955).

[14] P. V. Bridgman, The Physics of High Pressure, Bell (1949); Recent Work in the Field of High Pressures, Revs. Modern Phys. **18**, 1 (1946).

Translated by D. C. West
155

SOVIET PHYSICS JETP VOLUME 11, NUMBER 3 SEPTEMBER, 1960

SECOND SOUND IN HELIUM II

V. P. PESHKOV

Institute for Physics Problems, Academy of Sciences, U.S.S.R.

Submitted to JETP editor October 8, 1959

J. Exptl. Theoret. Phys. (U.S.S.R.) **38**, 799-805 (March, 1960)

An investigation of second sound in helium has been conducted by the resonance method down to a temperature of 0.38°K. At temperatures below 0.5°K the attenuation of second sound is so great that resonances are not observed, and the second sound is transformed into rapidly-attenuated thermal waves. Experimental values of u_2 are presented from the λ-point to 0.55°K (1958 temperature scale). It is shown that the computed data for u_2 obtained by Bendt et al.[16] from experiments on the scattering of cold neutrons in helium agree well with the data from direct measurements of the second sound velocity.

THE velocity of second sound in superfluid helium has been measured at temperatures above 0.8°K and up to the λ-point by both resonance and pulse methods.[1-5] Its values as determined by various authors and by various methods agree among themselves to within the limits of experimental error. At temperatures below 0.8°K second sound has been studied by a number of authors[6-9] using the pulse method. In these papers, unfortunately, no account was taken of experimental peculiarities, and data are presented on the second sound velocity down to temperatures of 0.1 – 0.2°K. In pure He^4, however, the mean free path of the thermal quanta, for $T < 0.6$°K, becomes comparable with the dimensions of the containers used and with the second-sound wavelength, as noted in one of the papers cited.[8] The phenomenon of second sound itself therefore disappears, being transformed into ordinary, rapidly-attenuated thermal waves. The thermal effect observed in conjunction with the pulses is associated with the reception of acoustic waves of first sound, excited by thermal expansion of the liquid helium. In the work of Osborne,[10] measurements are performed on the phase of the temperature oscillations of a thermometer, placed at one end of a resonator, as related to the phase of the oscillations of a continuously operating radiator located at the other end of the resonator. The measurements are carried out over the temperature range 0.25 – 0.58°K. In this case, as in those preceding, it is hardly possible to speak of second sound.

The goal of the present work was the measurement of the velocity of second sound down to the very lowest temperatures at which second sound still exists. Such measurements may most reliably be made by the resonance method. Considerable difficulties naturally arise in this case, associated with the attainment and maintenance of temperatures of 0.5 – 0.8°K within a large volume of He^4, in the presence of appreciable heat inputs, and also with the necessity for receiving extremely weak second sound signals.

In order to produce and maintain temperatures in the range 0.4 – 1.2°K the He^3 cryostat described previously[11] was employed. Two resonators were used. The first was made from a glass tube 33 mm in internal diameter and 50 mm in length, to the ground ends of which plane glass disks were cemented with BF cement. To one of the disks was fixed a radiator of constantan wire 40 microns in diameter, with a resistance of 160 Ω; to the other, a thermometer of 30-micron phosphor bronze wire with an initial resistance ~ 100 Ω. Leads from heater and thermometer were passed separately through two one-millimeter apertures drilled in the tube at its center, between the disks. The resonator was placed within a receptacle filled with He^4 and cooled by He^3 vapor pumping. The second resonator was made of copper and was also a cylinder, but of greater size. Its internal diameter was 60 mm and its length 70 mm. Within, on a disk which was soldered to the He^3 bath container, was fixed a radiator of 30-micron constantan wire. The radiator was made in the form of a closely-wound single-layer bifilar spiral of 1000 Ω total resistance. At the opposite end of the resonator were placed two thermometers, of 30- and 40-micron bronze, each with ~ 100 Ω resistance, as well as samples of 50-micron aluminum wire and 67-micron cadmium wire.

The bronze thermometers were calibrated

against the He^3 vapor pressure in accordance with the data presented by Roberts and Sydoriak.[12] In addition, during the course of each experiment the operation of the thermometers was controlled according to the aluminum and cadmium superconducting transition points. Owing to insufficient purity of the aluminum, its transition was broadened over 0.02°. The temperature $T = 1.13°K$, at which the sample had lost half of its residual resistance, was taken as the aluminum transition point. The cadmium was adequately pure (99.999%); its transition was sharp and corresponded to $T = 0.52°K$. (The terrestrial magnetic field was not compensated for.) The thermometers and the super-conducting reference standards were connected in series and supplied with a stabilized measuring current of 1 ma. An apparatus developed by Vetchinkin[13] served as the stabilizer. The stabilizer guaranteed constancy of the current to 0.001% for a variation in the circuit resistance of 500 Ω. The current in the potentiometer circuit was likewise stabilized with an accuracy of 0.001%, with the aid of a simple system using a galvanometer and photo-resistors.[13] The use of stabilizing devices greatly simplified the work, since the necessity of controlling for constancy of the current was completely eliminated. During the measurements we determined the temperature from the direct deflection of a galvanometer, connected to the thermomenter as shown in the circuit of Fig. 1.

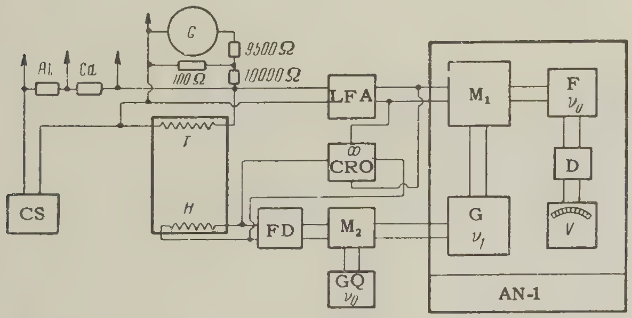

FIG. 1. Diagram of apparatus for observation of second sound (for symbols, cf. text).

For generation and measurement of the second sound oscillations an apparatus having high sensitivity and low noise level was prepared in the Institute's electronics shop. An AN-1 voltage analyzer was selected as a foundation, having its own internal generator G (cf. Fig. 1), working at frequencies from 56 to 76 Kc, a mixer M_1, and a narrow-band quartz filter F, tuned for a frequency of 56 Kc. Following the filter are a detector D and a voltmeter. The operating range of the AN-1 is from 100 to 20 kcs in frequency, and in voltage from 100 μv to 100 v; the passband width is 25 cps. An attachment was made for the AN-1 consisting of a generator, GQ, quartz-stabilized at the frequency of the filter F (56 kcs), a mixer M_2 with a filter passing frequencies from 100 cps to 10 kcs, and a divider FD to halve the frequency. In addition, the low-noise amplifier LFA described previously by Zinov'eva[14] was connected at the input of the AN-1.

The principle of operation of the circuit was as follows: a frequency $\nu = \nu_1 - \nu_0$ was produced (and high-frequency components filtered out) in the mixer M_2. In the divider FD this frequency was divided by two and applied to the heater H in the resonator. The heater radiated second sound of frequency ν, which was received by the thermometer T. From the thermometer the signal, amplified by the LFA, entered the mixer M_1 of the AN-1 analyzer. There it was mixed again with the frequency ν_1, and a signal of frequency $\nu_0 = \nu_1 - \nu$ passed through the quartz filter F, was detected by the detector D, and registered on the voltmeter V. The exact value of the frequency was determined from the number of periods recorded with the aid of a counting circuit during a known time interval.

The system described made it automatically possible to have in the receiving circuit, for any frequency of the generator, a narrow-band quartz filter set precisely at the frequency of the received signal. Together with the low-noise amplifier at the input, it assured positive registration of signals exceeding by a few times the noise level, which was $\sim 0.03\,\mu$v. In addition, the voltage supplied to the heater was simultaneously applied to the horizontal sweep of the cathode-ray oscilloscope CRO, to the vertical plates of which was fed the amplified signal from the thermometer. With the aid of the oscilloscope it was possible to determine the phase of the second sound oscillations relative to the phase of the radiator. Inasmuch as it was very difficult to avoid pickup from the circuit at frequencies which were multiples of 50, especially at the uneven harmonics, the measurements in the low temperature region were carried out in the following manner: a frequency was selected at which the pickup was at a minimum. Near 1°K, where the resonance peaks are extremely narrow, the temperature was adjusted to correspond exactly to resonance, and a Lissajous figure in the form of a symmetrical figure-eight was produced on the oscilloscope CRO by adjusting the LFA amplifier. Then with slow cooling or warming-up of the resonator, which had previously been cooled to 0.4°K, the temperatures corresponding to resonances were recorded, according to the readings of the circuit of the cathode-ray oscilloscope.

In addition, a more detailed investigation of the dependence of the amplitude of the second sound oscillations within the resonator upon temperature was carried out in the copper resonator. Curves of this sort, obtained in the copper resonator for frequencies of 633.6, 730 and 816.8 cps, are presented in Fig. 2. As can be seen from Fig. 2, the second sound resonances are strongly washed out as the temperature is lowered. For the frequency of 816.8 cps at T = 0.535°K it is evident from the phase of the oscillations on the oscilloscope that the conditions for resonance are present; due to the great damping, however, the amplitude maximum is no longer observed.

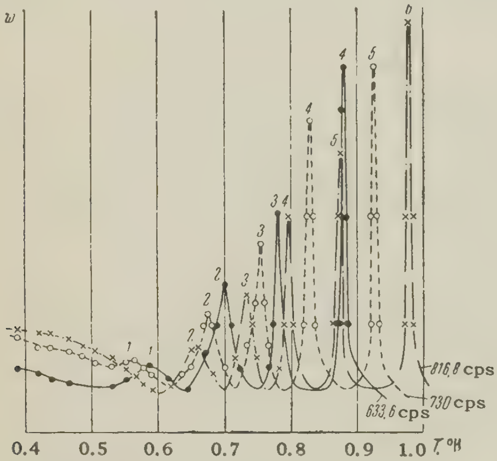

FIG. 2. Dependence of amplitude of second sound oscillations in resonator upon temperature. Number of resonances indicated by numbers on curves. Frequency and current supplied to heater held constant.

In determining the velocity u_2 from observation of the amplitude maxima, it is necessary to introduce for the washed-out peaks a correction to the value of u_2. If the length of the resonator is designated by l, and the law for propagation of second sound in the resonator is taken in the form

$$w = w_1 e^{-\gamma l} \sin(\omega t - \omega x / u_2),$$

then near resonance $\omega l/u_2 = n\pi + \delta$, and the amplitude of the oscillations will be[15]

$$w_1 = w_0 / 2\sqrt{\delta^2 + (\gamma l)^2}.$$

The condition for a maximum in w_1 will be a minimum value for the expression under the radical; i.e.,

$$\delta\, \partial\delta / \partial T + \gamma l^2\, \partial\gamma / \partial T = 0.$$

But

$$\partial\delta / \partial T = -(\omega l / u_2^2)\, \partial u_2 / \partial T$$

and the maximum will be observed at

$$\frac{\omega l}{u_2} = n\pi + \frac{u_2^2 \gamma l\, \partial\gamma / \partial T}{\omega\, \partial u_2 / \partial T} \quad \text{or} \quad u_2 = \frac{\omega l}{n\pi}\left(1 - \frac{u_2^3 \gamma\, \partial\gamma / \partial T}{\omega^2\, \partial u_2 / \partial T}\right).$$

This correction amounts, at low temperatures, to approximately 3%. If the observation is carried out using the cathode-ray oscilloscope — i.e., according to the phase of the oscillations — then it is not necessary to introduce the correction. The correction corresponding to the change in l from room temperature down to that of the helium is, in all, 0.3% for copper, and even less for glass.

Results of the measurement of u_2 at temperatures below 1°K are presented in Fig. 3. The curve of du_2/dT is also given in the figure, at the bottom. With the copper resonator the measurements were carried out at frequencies of 634, 730, 817, 930 and 1440 cps (all indicated by the same symbol), and with the glass resonator, at frequencies of 990 and 1352 cps. In Fig. 3 are shown the data of Bendt, Cowan and Yarnell[16] obtained for u_2, by calculation, from the spectrum of the thermal excitations in liquid helium, using the spectrum established experimentally[17] from measurements of the scattering of cold neutrons in helium II. The data of Kramers and co-authors,[9] from measurements of u_2 by the pulse method, are also presented. Inasmuch as at T = 0.7°K and below there is observed a considerable dispersion of second sound, due to the great attenuation, the pulses are strongly distorted, and the method does not yield satisfactory results. Kramers and his co-authors succeeded in obtaining more or less reasonable results, thanks to a special method for reducing the experiments, but these only at temperatures above 0.7°K. Data for u_2 by other authors[6-8] at temperatures below 0.8°K have not had dispersion taken into account in the proper

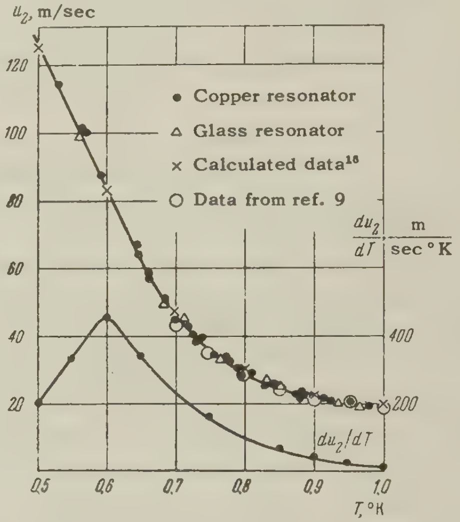

FIG. 3. Dependence of second sound velocity upon temperature.

T, °K	u_2, m/sec experiment	u_2, m/sec calculation[16]	T, °K	u_2, m/sec experiment	u_2, m/sec calculation[16]	T, °K	u_2, m/sec experiment	u_2, m/sec calculation[16]	T, °K	u_2, m/sec experiment
0.50		125	1.12	18.30		1.65	20.32		2.025	15.7
0.55	105		1.15	18.33		1.70	20.3	20.0	2.05	14.7
0.60	83	83.2	1.20	18.4	18.9	1.75	20.15		2.075	13.5
0.65	62		1.25	18.7		1.80	19.85	19.2	2.10	12.2
0.70	46.5	47.2	1.30	19.1	19.2	1.825	19.55		2.11	11.5
0.75	36.0		1.35	19.4		1.850	19.3		2.12	10.8
0.80	29.0	29.9	1.40	19.7	19.7	1.875	19.0		2.13	10.0
0.85	24.4		1.45	19.9		1.90	18.7	17.8	2.14	9.1
0.90	21.6	22.6	1.50	20.1	20.0	1.925	18.3		2.15	8.1
0.95	19.8		1.55	20.25		1.950	17.8		2.16	6.7
1.00	18.9	19.8	1.60	20.3	20.1	1.975	17.1		2.17	4.7
1.05	18.5		1.63	20.33		2.00	16.4	15.2	2.175	2.5
1.10	18.33	18.9								

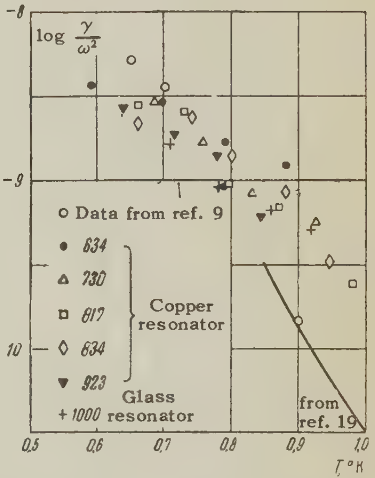

FIG. 4. Dependence of log (γ/ω^2) upon temperature (numbers following symbols in list are frequencies in cps).

way, and differ even more from those obtained in the present experiment.

In the copper resonator, the measurement of u_2 was carried out in the region of higher temperatures as well, up to T = 2.175° K (T_λ = 2.176° K). The combined results from the measurement of the second sound velocity u_2 under saturated vapor pressure over the whole temperature range are presented in the table. These data are obtained by averaging the most trustworthy measurements performed at the Institute for Physics Problems, and are referred to the 1958 temperature scale.[18] For comparison, the calculated data of Cowan et al.[16] are also given in the table. As is evident, the two sets of data are very close to one another, and practically agree to within the limits of error for the calculated and experimental data.

Measurement of the width of the resonance peaks makes it possible to determine the second sound attenuation. The attenuation at low temperatures is large; therefore it is no longer possible to take the quantity γl as equal to the half-width δ of the resonance curve. It is necessary to use the following approximation. With an accuracy up to terms in δ^7

$$\gamma l \quad \delta(1-\delta^2/3).$$

At low temperatures, the correction reached 20%. For weak signals, moreover, it was necessary to introduce a correction for background. If a is the background amplitude, w_0 the amplitude of the signal at maximum, w_1 the whole amplitude at maximum, and w_2 the amplitude at which the half-width is equal to δ, then

$$w_1 = \sqrt{w_0^2 + a^2}, \quad w_2 = \sqrt{w_0^2/2 + a^2} = \sqrt{(w_1^2 + a^2)/2}\,.$$

Inasmuch as in our case the resonators were broad and short, the surface losses were incomparably smaller than the volume losses, and it was possible to neglect them. Data on the second sound attenuation are represented in Fig. 4. The y axis represents log (γ/ω^2); this quantity is frequency-independent, since the volume losses are proportional to the square of the frequency. The data obtained by Kramers and co-authors,[9] and a curve constructed from the measurements of Zinov'eva,[19] are also shown in the figure. It should be noted that according to the data of Zinov'eva and Kramers the attenuation at temperatures above 0.8° K is much smaller than in the present work. This is explained by the fact that in such broad, short resonators, beginning as early as the third resonance, several types of oscillations arise at once. In our case, at the higher temperatures, resonances beyond the second were the ones observed, and it was impossible to determine from them the attenuation of plane waves of second sound. The attenuation as determined from the first and second resonances, however, lies on a prolongation of Zinov'eva's curve, and close to the data of Kramers. In several papers,[9,10] a mean free path for the phonons is determined from the second sound attenuation. At low temperatures, however, there are few rotons, and a fundamental role is played by the scattering of phonons on phonons. In this case the mean free path depends very strongly upon the angle of incidence of the phonons, and is a maximum when the directions coincide. At the same time, collisions of phonons having the same direction cannot lead to the generation of second sound. The problem of the mean free path at low temperatures must therefore be investigated separately; in any case a model in the form of elastic spheres is not suitable for them.

Second sound might be observed at temperatures below 0.55° by using lower frequencies; in this case, however, the dimensions of the apparatus will grow considerably. Thus for observation of a resonance of identical form — i.e., maintaining the same $\gamma l = \gamma_0 l_0$ — taking $u_2 = l\omega/\pi$ and the increase in attenuation $d \log(\gamma/\gamma_0)/dT = -4$, for $T = 0.5°K$ as compared with $T = 0.55°K$, it is necessary to use a resonator with $l = 2l_0$, and by comparison with $T = 0.6°K$, a resonator with $l = 6l_0$, or, in the present case, a length ~ 0.4 m. Under the usual experimental conditions it is thus impossible to observe second sound at temperatures below 0.5°K.

Osborne[10] has carried out an investigation of the propagation of periodically-radiated heat, at temperatures between 0.25 and 0.58°K and frequencies from 60 to 2000 cps. The radiating heater was located at one end of a closed tube 2 cm in diameter. At the other closed end was placed a receiving thermometer. The phases of the oscillation were compared for various lengths of the tube (0.38, 3.16, 9.26, and 12.35 cm). The conditions in Osborne's experiment were close to those described in the present work; in the overlapping region the values should therefore agree, but Osborne's $u_2 = 145$ m/sec for the point at 0.54°K, while at 0.58°K, the quantity $u_2 = 115$ m/sec. The considerable increase in Osborne's values for u_2 can be explained by the fact that, in reducing the experiment, the author tacitly assumes the phonon-phonon scattering process to be analogous to the scattering of elastic spheres. The cardinal difference between these processes, however, lies in the fact that for elastic spheres any other sort of collision has a much greater probability than a collision in closely similar directions. The greatest contribution to the generation and propagation of second sound oscillations, though, is provided by collisions at large angles. However, in collisions of phonons the opposite picture prevails. Proceeding from these considerations, he obtained the extremely strange result that the phonon mean free path increases by a factor of three, in all from 0.58 to 0.25°K. From Osborne's experiments it is thus possible to affirm only the considerable likelihood of the conclusion that the concept of the phonon mean free path as applied to the propagation of heat in helium at temperatures below 0.7°K must be investigated in greater detail. In any case, to speak of second sound at temperatures below 0.5°K under presently attainable experimental conditions seems scarcely expedient. Here, phenomena will appear completely different.

In conclusion, I take this opportunity to thank Academician P. L. Kapitza for his interest in the work, Prof. I. M. Khalatnikov for valued discussions, and also A. I. Filimonov for his aid in carrying out the experiments.

---

[1] V. P. Peshkov, JETP **16**, 1000 (1946); **18**, 951 (1948); **23**, 687 (1952).

[2] V. P. Peshkov, K. N. Zinov'eva, JETP **18**, 438 (1948).

[3] Lane, Fairbank, and Fairbank, Phys. Rev. **71**, 600 (1947).

[4] J. R. Pellam, Phys. Rev. **75**, 1183 (1949).

[5] R. D. Maurer and M. A. Herlin, Phys. Rev. **76**, 948 (1949).

[6] K. R. Atkins and D. V. Osborne, Phil. Mag. **41**, 1078 (1950).

[7] V. Mayper and M. A. Herlin, Phys. Rev. **89**, 523 (1953).

[8] de Klerk, Hudson, and Pellam, Phys. Rev. **93**, 28 (1954).

[9] Kramers, Van Peski-Tinbergen, Wiebes, Van den Burg, Gorter, Physica **20**, 743 (1954).

[10] D. V. Osborne, Phil. Mag. **1**, 301 (1956).

[11] Peshkov, Zinov'eva, and Filimonov, JETP **36**, 1034 (1959), Soviet Phys. JETP **9**, 735 (1959).

[12] T. R. Roberts and S. G. Sydoriak, Phys. Rev. **106**, 175 (1957).

[13] A. N. Vetchinkin, Приборы и техника эксперимента (Instrum. and Meas. Engg.), in press.

[14] K. N. Zinov'eva, JETP **25**, 235 (1953).

[15] V. P. Peshkov, JETP **18**, 857 (1948).

[16] Bendt, Cowan, and Yarnell, Phys. Rev. **113**, 1386 (1959).

[17] Yarnell, Arnold, Bendt, and Kerr, Phys. Rev. **113**, 1379 (1959).

[18] Van Dijk, Durieux, Clement, and Logan, Suppl. Physica **24**, 129 (1958).

[19] K. N. Zinov'eva, JETP **31**, 31 (1956), Soviet Phys. JETP **4**, 36 (1957).

Translated by S. D. Elliott
156

SOVIET PHYSICS JETP VOLUME 11, NUMBER 3 SEPTEMBER, 1960

A CRYOSTAT FOR NEUTRON DIFFRACTION STUDIES

R. A. ALIKHANOV

Institute for Physics Problems, Academy of Sciences, U.S.S.R.

Submitted to JETP editor October 10, 1959

J. Exptl. Theoret. Phys. (U.S.S.R.) **38**, 806-808 (March, 1960)

A low temperature (including helium temperatures) cryostat is described for studying scattering of thermal neutrons by polycrystalline specimens.

We have constructed an apparatus for studying the magnetic properties of antiferromagnetics at low temperatures,[1,2] in which neutron diffraction can be investigated over a wide range of Bragg angles. As the requirements of accuracy in interpreting the diffraction pattern are high, we took account of many reflections and high orders. It was therefore experimentally desirable to be able to measure the scattering up to angles $\Theta_B = 45°$, i.e., for rotation of the detector through 90°. The optimum rate for the automatic rotation of our detector around the specimen is 1° in 3.5 min. It follows, then, that the exposure time for recording the diffraction pattern can be 5 hours, and if the picture is taken point by point this time is doubled.

The main requirement for a cryostat for this purpose is, then, to maintain the specimen at a low temperature for a long time with, naturally, minimum background scattering produced by the cryostat itself.

The cryostat used for our measurements was constructed from the hydrogen Dewar proposed for the purpose by Kapitza in 1932.[3] Figure 1 shows a sketch of the Dewar after it had been turned into the cryostat. "Appendix" 2, of 0.2 mm wall thickness stainless steel, is attached below the inner vessel 1, which holds 5 *l* of liquid. The thin walled (0.2 mm) aluminum cup 3, containing the specimen, is attached to the base of the "appendix." The aluminum was tinned with an ultrasonic soldering iron before being soldered on. The leads to the thermometer 6 were passed to the outside through a 3 mm diameter stainless tube 4, extending through the whole cryostat, from the bottom of the appendix to a sealed glass tube 5, provided with platinum leads.

The 5-liter sphere 1 is surrounded by a copper shield 7 cooled by nitrogen fed from a 3-liter "sputnik," 9, through a copper rail 8. The aluminum foil cylinder 11 is attached to shield 7. There is a flange connection 12 below the outer layer of the cryostat by means of which the aluminum pressure vessel 13 is attached to the outer layer with 4 mm screws through a rubber seal. This vessel is thinned down to a thickness of 0.2 mm over the specimen height, namely 60 mm, with stiffening rings 1.5 mm thick left on the surface at 20 mm intervals. The suspension tubes 18 and 19 of the vessels 1 and 9 were changed to stainless steel to reduce the heat inflow. The rubber seal, aluminum soldering and thinned-down cylinder operated without trouble after a year and half.

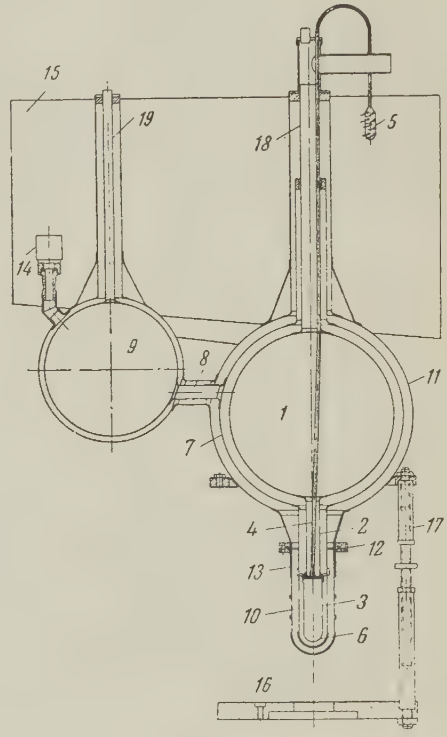

FIG. 1

The vacuum space between the spheres is pumped through the sylphon tube 14, fixed to the Plexiglas shield 15, by a special vacuum system connected by a flexible metal tube. The original vacuum achieved, 2×10^{-5} mm Hg, did not deteriorate during operation. A series of measurements on any one specimen could be carried on for several months without further pumping. This was aided by activated charcoal at the bottom of sphere 1 and the nitrogen sphere, which on cooling absorbed the gas given off the inner surfaces of the cryostat.

During the experiments the sputnik was constantly supplied with nitrogen by an oxygen-regulated automatic filler. When assembled, the cryostat with the specimen is located at the center of the mounting of the neutron spectrometer by means of the aluminum disc 16 and the three supports 17.

When experiments are made at helium temperatures, the helium evaporated from the cryostat is collected by a pumping system attached for the purpose. Helium from a portable Dewar (see reference 4) is siphoned into the 5-liter volume kept at a constant pressure of 20 mm Hg, produced by the forevacuum pump. The pump exhaust is connected to a (2.5 m^3) rubber and a (0.5 m^3) metal gas holder. The helium is compressed at 5 m^3 per hour into a high pressure container by a compressor. The use of a rubber gas holder avoids an expensive and bulky metal holder and also allows the expermenter to carry out the whole process of filling and pumping helium without assistance.

As has been found from many experiments, the cryostat fulfilled all the requirements demanded of it. The background from the aluminum casing is 20% of the counter background and does not distort the neutron diffraction pattern of the specimen. The coolants kept for a sufficiently long time, and at the end of the diffraction measurements had to be boiled off from inside the 5-liter sphere by a special heater.

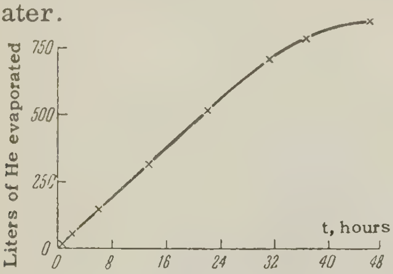

FIG. 2

The apparatus could keep a specimen at helium temperature for two days and nights. The total amount of helium used for an experiment, including the cooling, was then 7.5 l. A typical evaporation curve is shown in Fig. 2, which shows the evaporation of 1.3 l He. The rate of evaporation is at first constant (1 l of liquid is boiled off in 29 hours), and then gradually decreases up to 69 hours. This corresponds to the moment when helium only remains in the "appendix" 2. Most of the helium is, therefore, boiled off while the apparatus is cooling down, the evaporation itself being small. We have calculated that ~ 4 l of liquid He are necessary to cool the vessel.

We used an experimental thermometer obtained from Yu. V. Sharvin, prepared from coal[5]. Such thermometers, especially the resistance thermometers made by the Allen-Bradley company, show a strong temperature dependence of resistance at low temperatures. This makes them very convenient as low-temperature thermometers. They are advantageous for neutron diffraction work because of their extremely small size. A small thermometer can be placed on one end of the cylinder with the specimen and so does not affect the diffraction pattern.

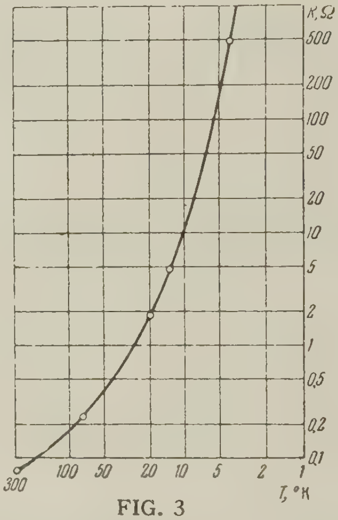

FIG. 3

Our thermometer was 1 × 2 × 3.5 mm in size and was secured with BF-2 adhesive to the bottom of the aluminum cylinder containing the specimen. Potential and current leads from it were connected to a compensated potentiometer circuit. Figure 3 shows the thermometer calibration, measured at five temperatures.

In some cases, temperature control of the specimen for long experiments was achieved by a recording potentiometer EPP-09 with 100 scale divisions for 10 mv.

I am deeply grateful to Acad. P. L. Kapitza for his constant interest in the work. I thank Yu. V. Sharvin for supplying me with an experimental thermometer model.

---

[1] R. A. Alikhanov, JETP **36**, 1690 (1959), Soviet Phys. JETP **9**, 1204 (1959).

[2] R. A. Alikhanov, JETP **37**, 1145 (1959), Soviet Phys. JETP **10**, 814 (1960).

[3] P. Kapitza and J. D. Cockcroft, Nature **129**, 224 (1932).

[4] A. B. Fradkov, Приборы и техника эксперимента (Instruments and Meas. Engg.) No. 4, 108 (1958).

[5] Yu. V. Sharvin, ibid., No. 1, 147 (1959).

Translated by R. Berman
157

SOVIET PHYSICS JETP VOLUME 11, NUMBER 3 SEPTEMBER, 1960

HIGH-ENERGY PHOTONUCLEAR DEUTERONS AND TRITONS

V. P. CHIZHOV

Leningrad Physico-Technical Institute, Academy of Sciences, U.S.S.R.

Submitted to JETP editor October 21, 1959

J. Exptl. Theoret. Phys. (U.S.S.R.) **38**, 809-818 (March, 1960)

The ratios of (γ, d) to (γ, p) cross sections for 15.5 – 30 Mev protons and deuterons produced by bremsstrahlung of $E_{\gamma\,\mathrm{max}} \approx 90$ Mev are given as function of atomic number A for 14 elements from Li^6 to Au. For medium and heavy nuclei $\sigma(\gamma, d)/\sigma(\gamma, p) \sim A^{5/3}Z$, corresponding to the picture of production of photodeuterons in the capture process. The energy dependence of $\sigma(\gamma, d)/\sigma(\gamma, p)$ is given for Li^6 and Li^7, together with the energy distribution of photodeuterons from Li^6 and Li^7 and of phototritons from Li^7. A relatively large yield of high-energy phototritons from Li^6, Li^7 and B was observed. The angular distributions of photoprotons and photodeuterons from Li^6, Li^7, Be, and C are compared. The shape of the experimental photodeuteron angular distributions is found to agree with those computed on the assumption that the photodeuterons are produced in the capture process. Angular distributions of high-energy phototritons from Li^6, Li^7 and Be are also given.

1. INTRODUCTION

IN the study of deuterons and protons of energy > 15 Mev produced in photodisintegration of the nucleus by bremsstrahlung of $E_{\gamma\,\mathrm{max}} \approx 90$ Mev, ratios $\sigma(\gamma, d)/\sigma(\gamma, p)$ were obtained previously[1] for Be and C as functions of particle energy E_d and E_p, as well as the energy dependence of $\sigma(\gamma, d)$ In this work, a rough, semi-empirical analysis was carried out, assuming that the photodeuterons are produced in the so-called capture process. This gave results in good agreement with the experimental data. It was noted that analogous experimental data on photodeuterons of energy > 40 Mev produced[2] in photodisintegration of the nucleus by bremsstrahlung of $E_{\gamma\,\mathrm{max}} \approx 300$ Mev could also be interpreted as following from this capture mechanism. Further light would be shed on the mechanism of the (γ, d) reaction by establishing such important characteristics as the dependence of photodeuteron yield on atomic number A and by obtaining angular distributions, and comparing these with the same characteristics for photoprotons.

In work carried out with the Pennsylvania betatron[3-5] with $E_{\gamma\,\mathrm{max}} = 24$ Mev, using the method of counting grains in photoemulsion tracks, the following data on the yields $Y(\gamma, d)/Y(\gamma, p)$ of photodeuterons relative to photoprotons for energies up to 10 Mev were found: Cu[3], 0.31; In[4], < 0.01, Ce, 0.04; Bi, 0.01; Co[5], < 0.02. The large fluctuations in the ratio $Y(\gamma, d)/Y(\gamma, p)$ from element to element would seem to establish the basic influence of the specific structure of the nucleus on the yield of photodeuterons, whereas a similar effect on the yield of photoprotons, at least for Cu and Co, was not observed. However, Forkman[6] showed later, using bremsstrahlung of $E_{\gamma\,\mathrm{max}} = 30$ Mev and the same method of detecting protons and deuterons, that it was impossible to identify protons and deuterons for each individual track by the method of grain counting in the energy region studied, and that some possibility of separating deuterons from protons could be realized only by a statistical processing of the data for a large number of tracks. Forkman found the following ratios $Y(\gamma, d)/Y(\gamma, p)$ for Co and Cu: Co, 0.22; Cu, 0.16, which are not very different. Using the same method, Makhnovskiĭ obtained $Y(\gamma, d)/Y(\gamma, p) = 0.14$ for Au.

It is clear that these works suffer from the shortcoming of poor statistical accuracy. Values for the ratio $Y(\gamma, d)/Y(\gamma, p)$ of 0.76 and 0.15 were obtained for Cu[8] and S[9], respectively, with γ rays from a synchrotron with $E_{\gamma\,\mathrm{max}} = 65$ Mev using a Wilson chamber in a magnetic field. Here, again, a surprisingly large number of photodeuterons were found in the case of Cu. In preliminary data of the Cornell group,[10] who used a synchrotron with $E_{\gamma\,\mathrm{max}} \approx 300$ Mev and studied the high-energy protons and deuterons with a scintillation telescope of two crystals, the ratios $Y(\gamma, d)/Y(\gamma, p)$ increased gradually for a series of elements from 0.12 for C to 0.24 for Pb. The ratio $Y(\gamma, d)/Y(\gamma, p)$ of 0.21 for Be stood out. Comparison of relative yields of photodeuterons of a given energy produced by bremsstrahlung of $E_{\gamma \max} \approx 90$ Mev[1] and $E_{\gamma \max} \approx 300$ Mev[2] shows a substantial difference in the magnitudes of the yields. This fact shows that in comparing yields of photodeuterons from different nuclei, it is necessary to compare yields obtained for the same value of $E_{\gamma \max}$.

In the data obtained on the Cornell synchrotron with $E_{\gamma \max} = 300$ Mev, the photodeuterons from C, Cu, Ag and Pb of energies near 40 Mev have approximately the same angular distribution as photoprotons of the same energy.[10] It was found on the synchrotron of the Physico-Technical Institude with $E_{\gamma \max} \approx 90$ Mev that photodeuterons from Be of energy greater than 18 Mev have an angular distribution analogous to that of photoprotons[1] in the interval 40 — 90°. These works exhaust the published information that we know of on the angular dependence of (γ, d) reactions. It can be seen that the questions noted above require further investigation.

In the present work the relative yields of (γ, d) and (γ, p) reactions were studied for a wide interval of mass numbers from Li to Au for protons and deuterons of energy 15 to 30 Mev, produced by bremsstrahlung with $E_{\gamma \max} \approx 90$ Mev. In order to elucidate possible fluctuations in the yields of photodeuterons, nuclei of neighboring mass, but different occupation of upper nucleon shells, were chosen. The angular distributions of photodeuterons from the photodisintegration of the light nuclei Li^6, Li^7, Be, and C were also studied and compared with angular distributions of photoprotons of the same energy. In addition, some information about high-energy phototritons was obtained.

2. EXPERIMENTAL ARRANGEMENT AND DISCRIMINATION BETWEEN PARTICLES

Fast charged particles — products of the photodisintegration of the nucleus — were counted and identified by a telescope of scintillation counter-spectrometers. This was done by measuring $\Delta E \sim dE/dx$ of the particle, from the pulse of the first counter which had a thin crystal, and the energy E of the particle lost in the thick crystal of the rear counter. This method has been described in detail previously.[1] Measurements were carried out with four independent telescopes, each of which could be set at arbitrary angle to the direction of the γ-ray beam, at a definite distance from the target held strictly the same for all telescopes. The particle yields were studied mainly at 90°. Angular distributions were determined from measurements at 35, 57.5, 80, 102.5, 125, and 145° relative to the direction of the γ-ray beam in both left and right parts of the hemisphere, centered upon the target. Different telescopes gave the same results, within the limits of statistical errors, when placed at the same angles. Readings of the telescopes at each angle were lumped together. Targets for the angular distributions consisted of hollow cylinders with thick walls, corresponding to the range of protons of energy about 4 Mev, and for measurements of yields, of rectangular plates. The targets were placed in a vacuum chamber in order to exclude background due to nuclear reactions in air. The absolute intensity of γ rays was measured using a thick-walled ionization chamber, calibrated by the calorimetric method of Kruglov.[11]

Distributions of particles with ΔE and E for boron and cobalt are given in Figs. 1 and 2. In Fig. 1, which relates to boron, three distinct groups of particles registered by the telescope are seen. From measurements of ΔE and E, they are identified as protons, deuterons and tritons. In the case of cobalt, there are only two distinct groups of particles, lying in the regions of protons and deuterons, and only a few points fall in the triton region although the number in the deuteron region is about the same as for boron. The results for these and for all other nuclei were ob-

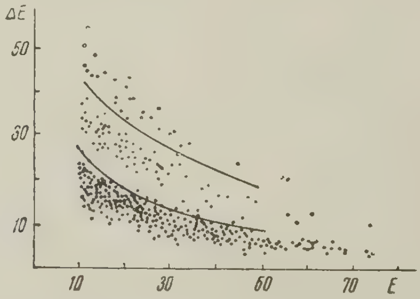

FIG. 1. Distribution of particles for B with energy ΔE lost in the first thin crystal of the scintillation telescope, and energy E absorbed in the rear thick crystal. ΔE and E are given in arbitrary units. The solid lines give the calculated upper limits of proton and deuteron regions.

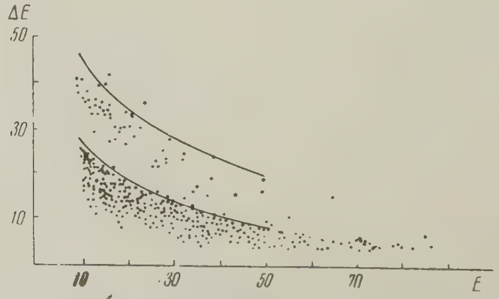

FIG. 2. Same as Fig. 1, but for Co.

FIG. 3. Ratio of (γ, d) to (γ, p) cross sections for protons and deuterons of energies 15.5–30 Mev as function of atomic weight A. The solid curve shows the dependence given by Eq. (2), arbitrarily normalized.

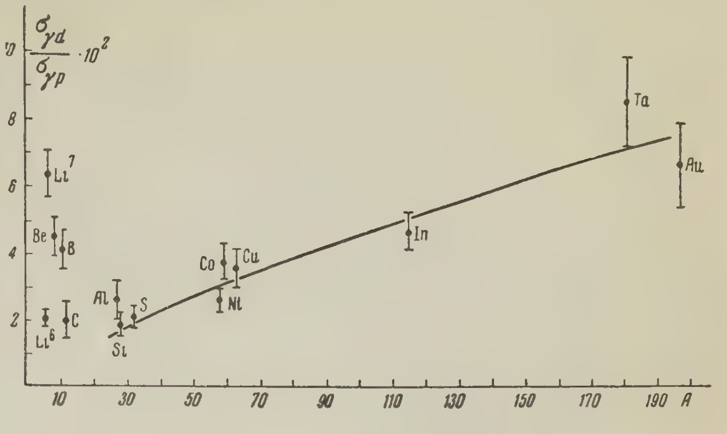

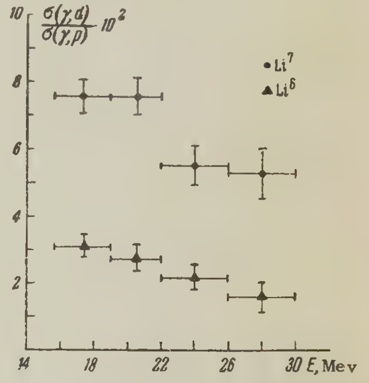

FIG. 4. Dependence of the ratio of (γ, d) to (γ, p) cross sections on the particle energy E for Li^6 and Li^7.

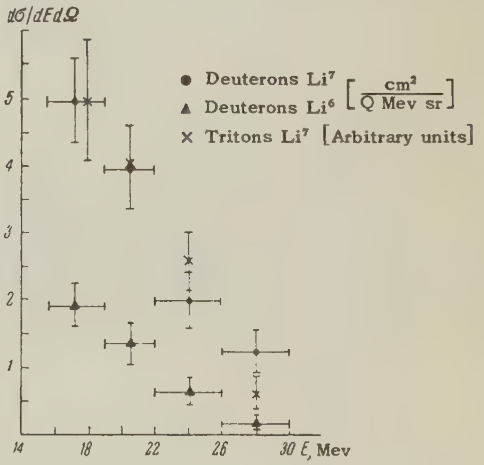

FIG. 5. Energy distributions of photodeuterons from Li^6 and Li^7 and phototritons from Li^7. The scale of the ordinate for phototritons is arbitrary.

tained by a frequent interchange of targets, so as to avoid errors from any uncontrollable fluctuations in the apparatus. The reproducibility of the results was very satisfactory.

The yields of phototritons were estimated in the following way. A calculated curve connecting E with ΔE for protons was normalized to the upper limit of the proton region which was very sharply defined so that above this curve lay only a negligible number of proton points. After such a normalization, the calculated upper limit to the deuteron region was determined. Points above the upper deuteron limit can relate only to tritons. In Figs. 1 and 2 these calculated curves are represented by solid lines. With this method, points relating to tritons, but falling in the region below the calculated upper limit for deuterons, are naturally not taken into account. However, from Fig. 1, where the whole triton region is displayed more or less distinctly, it can be seen that the loss of points from the lower tail of the triton distribution is insignificant. The measurements include protons and deuterons of energy 15.5 — 30 Mev and tritons of energies 17 — 30 Mev.

3. EXPERIMENTAL RESULTS

The ratios of $\sigma(\gamma, d)/\sigma(\gamma, p)$ of cross sections for (γ, d) and (γ, p) reactions for protons and deuterons of energy 15.5 — 30 Mev are given in Fig. 3 as function of mass number A for 14 elements. The data are for angle $\theta = 90°$ relative to the direction of the γ rays. For the Li^6 and Li^7 targets, $\theta = 80°$. Only statistical root-mean-square errors are indicated. Figure 4 shows the energy dependence of $\sigma(\gamma, d)/\sigma(\gamma, p)$ for Li^7 and Li^6. This was obtained by summing data for angles 35 to 145°. The energy distributions of photodeuterons at $\theta = 80°$ for Li^7 and Li^6 are given in Fig. 5 in units of cm^2/Q Mev-sr. For comparison, the energy distribution of phototritons from Li^7, obtained by summing tritons at angles 35, 57.5, 80, 102.5, 125, and 145° is given in the same figure. The ordinate gives numbers of tritons in arbitrary units. In all cases, only statistical errors are indicated. The error in measurement of the absolute cross section was estimated to be ± 35%.

Relative yields of phototritons in numbers of phototritons per 100 deuterons are given in Table I. Here the data for Li^6, Li^7, and Be was obtained by summing results for angles 35, 57.5, 80, 102.5, 125, and 145° relative to the γ rays.

TABLE I

Element	$100N_t/N_d$	Element	$100N_t/N_d$	Element	$100N_t/N_d$	Element	$100N_t/N_d$
Li^6	30±3	B	39±8	Ni	10±4	In	5±2.5
Li^7	22.5±2.5	Si	10±4	Co	2.5±2	Ta	10±4
Be	13±2.6	S	8±4	Cu	2.2±2	Au	3±3

The data for the other elements relate to 90° and, because of large statistical errors, can serve as only preliminary estimates of the yields of fast phototritons.

It should be noted that the yield of photoprotons of the energy considered rises smoothly with Z for the elements plotted in Fig. 3, and that starting already with Al, no direct proportionality to Z is observed on account of the effect of the Coulomb barrier. For illustration, we give the yields of photoprotons Y(γ, p) per proton in the nucleus for several elements in relative units (the error in these measurements was estimated to be ±10%):

	Li^6	Li^7	Be	C	Al	Cu
$Y(\gamma,p) =$	1.49	1.57	1.5	1.31	1.00	0.56

Angular distributions of photoprotons of energies 15.5 — 30 Mev are given in Fig. 6 for Li^6, Li^7, Be, and C. The cross section for (γ, p) reactions is plotted, in relative units, along the ordinate, and the angle between the axis of the telescope and the direction of the γ-ray beam, along the abscissa. Only statistical errors are indicated. The dashed lines show smoothed curves, characterizing the form of the experimental angular distribution of photoprotons.

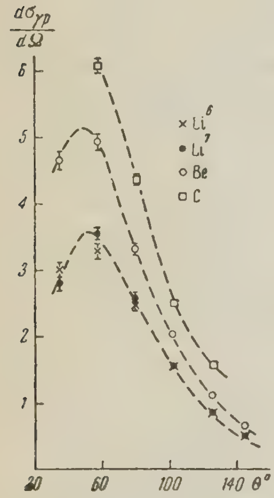

FIG. 6. Angular distributions of photoprotons of energies 15.5–30 Mev for Li^6, Li^7, Be, and C. The errors are statistical.

Figure 7 shows the angular distributions of photodeuterons of energies 15.5 - 30 Mev from the same nuclei. The cross section for (γ, d) reactions is plotted along the ordinate in relative units, against the abscissa, the same angle as in Fig. 6.

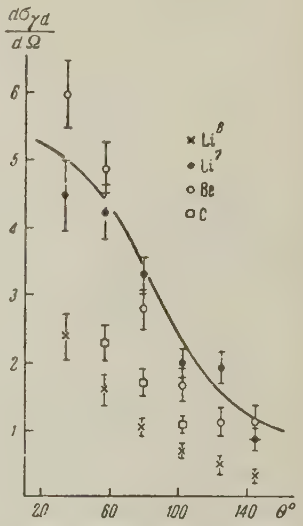

FIG. 7. Angular distributions of photodeuterons of energies 15.5–30 Mev for Li^6, Li^7, Be, and C. The errors are statistical. The solid curve gives the calculated results for photodeuterons from Be.

Figure 8 displays the differences in the shapes of the angular distributions of photoprotons and photodeuterons from Li^7, Li^6, and Be, the ordinate giving the ratios of (γ, d) to (γ, p) cross sections in percentages. The dashed line is a smoothed curve characterizing the shape of the ratio $\sigma(\gamma, d)/\sigma(\gamma, p)$ as a function of angle relative to the γ-ray beam. In Figs. 7 and 8, only statistical errors are shown.

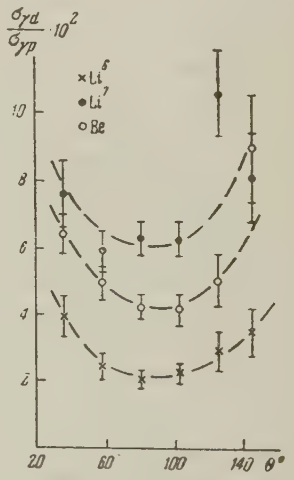

FIG. 8. Angular dependence of the ratio of (γ, d) to (γ, p) cross sections for Li^6, Li^7, and Be. The errors are statistical.

Figure 9 shows the angular distributions of phototritons of energy 17 — 30 Mev from Li^7, Li^6, and Be. In this case the indicated errors can be seen to be rather large; therefore, the results given in Fig. 9 should be considered preliminary. The cross section for (γ, t) reactions is given in

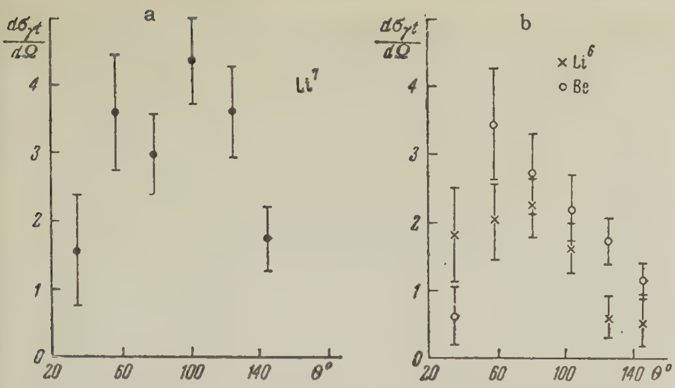

FIG. 9. Angular distributions of phototritons of energies 17–30 Mev for Li^7, Li^6, and Be. a – Li^7; b – Li^6 and Be. The scale is the same in a and b. The errors are statistical.

relative units. Some quantitative comparisons of these cross sections with the cross sections for (γ, d) and (γ, p) reactions are given in Table II for 80° and the above intervals of particle energy.

TABLE II

	$\sigma_{\gamma p}\cdot 10^{30}$, $\frac{cm^2}{Q\text{-sr}}$	$\frac{\sigma_{\gamma d}}{\sigma_{\gamma p}}\cdot 10^2$	$\frac{\sigma_{\gamma t}}{\sigma_{\gamma p}}\cdot 10^2$
Li^7	66.0±1.3	6,3±0.55	1.0±0.25
Li^6	62.5±1.3	2.10±0.25	0.79±0.20

4. DISCUSSION OF EXPERIMENTAL RESULTS

a) Yields. The experimental results shown in Fig. 3 make it possible to show the main features of the dependence of the ratio $\sigma(\gamma, d)/\sigma(\gamma, p)$ on atomic number A. It can be seen that this ratio decreases in the region of light nuclei but, in the region of medium (beginning with $A \approx 30$) and heavy nuclei, gradually rises with increasing A. For neighboring nuclei, in particular, for Co and Cu, the ratios $\sigma(\gamma, d)/\sigma(\gamma, p)$ are very close to each other. An exception is Li^6 where the reaction $Li^6(\gamma, d)He^4$, which is energetically favorable for the absorption of electric dipole γ rays, is forbidden by isotopic-spin selection rules.[12] Such a reaction can proceed by magnetic-dipole and electric-quadrupole absorption of γ rays. In addition, the reactions $Li^6(\gamma, d)He^3 + n$ and $Li^6(\gamma, d)H^3 + p$ are not forbidden also in the case of electric-dipole absorption, but have a high energy threshold. The excitation function for photodeuterons of energy 15.6 – 22 Mev is given for Li^6 in Fig. 10. The maximum bremsstrahlung energy is plotted along the abscissa, and the cross section for (γ, d) reactions per effective quantum, in relative units, along the ordinate. The arrows in the region $E_{\gamma\,max} = 20$ Mev delimit the region of the energy threshold for the reaction $Li^6(\gamma, d)He^4$ for the given case. The arrows in the region of 40 Mev delimit the region of threshold for the reactions $Li^6(\gamma, d)He^3 + n$ and $Li^6(\gamma, d)H^3 + p$. It is seen that the (γ, d) reaction becomes large in Li^6 only for γ-ray energy above the second threshold region. Because of this, it is clear why the ratio $\sigma(\gamma, d)/\sigma(\gamma, p)$ is so much smaller for Li^6 than for Li^7.

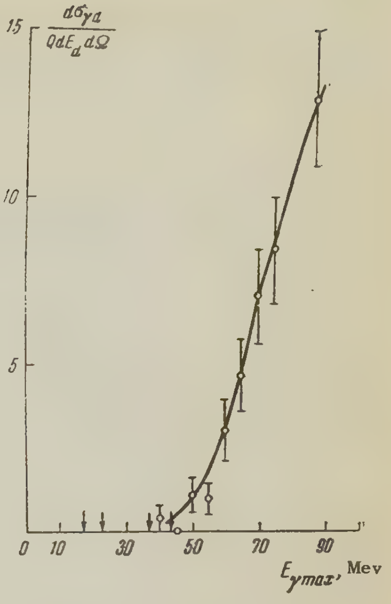

FIG. 10. Excitation function for photodeuterons of energies 15.6–22 Mev from Li^6.

When the capture mechanism is operative, the (γ, d) reaction can be considered to take place in two stages. In the first stage, the γ ray is absorbed by the proton or neutron in the nucleus, and in the second stage, the excited nucleon picks up a second nucleon, forming the emitted deuteron. If we assume such a process, then the ratio $\sigma(\gamma, d)/\sigma(\gamma, p)$ can be written in the following form:

$$\frac{\sigma(\gamma, d)}{\sigma(\gamma, p)} \sim \frac{[\sigma'(\gamma, p) + \sigma'(\gamma, n)]\, P_3 F_d}{\sigma'(\gamma, p)\, F_p}. \tag{1}$$

Here, $\sigma'(\gamma, p)$ and $\sigma'(\gamma, n)$ are the cross sections for (γ, p) and (γ, n) reactions neglecting the potential barrier, P_3 is some average probability of the proton or neutron capturing a second nucleon with emission of a deuteron, F_d and F_p are barrier penetrabilities for deuterons and protons, respectively. On the basis of work carried out to date,[13,14] one can take $[\sigma'(\gamma, p) + \sigma'(\gamma, n)] \sim A$ and $\sigma'(\gamma, p) \sim Z$. Further, it is natural to consider that such a weakly bound system as the deuteron can be formed and emitted from medium and heavy nuclei mainly from the surface region only; consequently, one can assume that $P_3 \sim A^{2/3}$. Finally, the ratio F_d/F_p for medium and heavy nuclei depends only weakly on A. Thus, one can expect that if the capture mechanism is operative, the dependence of $\sigma(\gamma, d)/\sigma(\gamma, p)$ on A will go roughly as

$$\sigma(\gamma, d)/\sigma(\gamma, p) \sim A \bullet A^{2/3}/Z. \tag{2}$$

The solid curve in Fig. 3, normalized arbitrarily to experimental results, reproduces the dependence (2). It can be seen that the calculated curve reproduces the trend of experimental ratios $\sigma(\gamma, d)/\sigma(\gamma, p)$ rather well. Equation (2) is, of course, not applicable in the region of light nuclei, where the concept of nuclear surface loses meaning because of the small number of nucleons. The ratios $\sigma(\gamma, d)/\sigma(\gamma, p)$ for high-energy deuterons ($\approx$ 40 Mev) produced[10] by bremsstrahlung with $E_{\gamma\,\max} = 310$ Mev, are 0.21 for Be, 0.12 for C, and 0.24 for Pb. Noting that $\sigma(\gamma, d)/\sigma(\gamma, p)$ here increases gradually with increasing A between C and Pb,[10] we come to the conclusion that the dependence of $\sigma(\gamma, d)/\sigma(\gamma, p)$ on A has the same character at high energies as that shown in Fig. 3 of this article. There is a difference, in that the ratios $\sigma(\gamma, d)/\sigma(\gamma, p)$ obtained in reference 10 are substantially larger. This fact was explained by the semi-empirical calculations based on the capture mechanism.[1] The energy dependence of the ratios $\sigma(\gamma, d)/\sigma(\gamma, p)$ for Li^6 and Li^7 and the energy distributions of photodeuterons given in Figs. 4 and 5 are, in the main, similar to those for Be and C given in reference 1.

In Table I, where the relative yield N_t of fast phototritons is given, it can be seen that for all nuclei given, with the exception of Li^6, Li^7, and B, the magnitude of the ratio $\sigma(\gamma, t)/\sigma(\gamma, d)$ is about the same, within the limits of statistical error, as the magnitudes of the ratio $\sigma(\gamma, d)/\sigma(\gamma, p)$ for the same nucleus. It is possible that these phototritons are produced by a mechanism of double capture. The noticeable larger yield of phototritons from Li^6, Li^7 and B is striking. From Fig. 5 it is seen that the shape of the energy distribution of phototritons from Li^7 is similar to the energy distribution of photodeuterons.

b) Angular distributions. It can be seen from Figs. 6 and 7 that the angular distributions of photoprotons and photodeuterons in the same energy interval are rather similar in shape. However, it is striking that the shapes of the angular distributions of photodeuterons are completely different in one definite characteristic. This is especially clear in Fig. 8 for Li^6, Li^7, and Be. The characteristic difference consists in the fact that the cross section for (γ, d) reactions drops much less quickly with increasing angle in the large angle region, and in the small angle region does not have such a sharp drop as that observed in the (γ, p) cross section. The fact that the form of the angular distribution of the (γ, d) cross section resembles that of the analogous (γ, p) distribution, does not qualitatively contradict the earlier assumption,[1] justification for which was given in reference 1, that the deuterons are formed in the process of capture. We can try, on the basis of this assumption, to estimate the shape of the angular dependence of the (γ, d) reactions. Under this assumption, the γ ray is absorbed by a single nucleon in the nucleus and the excited nucleon either goes right out of the nucleus at angles θ', φ' to the γ-ray beam, or, with a definite probability, picks up another nucleon to form a deuteron emitted at angles θ, φ. Then, in a rough approximation, the angular distribution for (γ, d) reactions looks like

$$\frac{d\sigma_{\gamma d}(\theta, \varphi)}{d\Omega} \sim \int_0^{\pi}\int_0^{2\pi}\left[\frac{d\sigma_{\gamma p}(\theta', \varphi')}{d\Omega'} + \frac{d\sigma_{\gamma n}(\theta', \varphi')}{d\Omega'}\right] P_3(\omega)\, d\Omega'. \tag{3}$$

When applied to results given in Fig. 7, $d\sigma_{\gamma d}(\theta, \varphi)/d\Omega$ denotes the cross section for the (γ, d) reaction at angles θ, φ, integrated over photodeuteron energy from 15.5 to 30 Mev, while $d\sigma_{\gamma p}(\theta', \varphi')/d\Omega$ and $d\sigma_{\gamma n}(\theta', \varphi')\, d\Omega'$ are the cross sections for (γ, p) and (γ, n) reactions at angles θ', φ', integrated over energies from the minimum value for which the proton and neutron can form a deuteron of energy $E_d = 15.5$ Mev to the maximum observed in the experiment. The connection between the energy of the photodeuteron and the energy of the photoproton (photoneutron) which would be emitted without formation of a photodeuteron, is found from energy conservation for (γ, p) and (γ, d) reactions in which the residual nucleus is formed in its ground state. $P_3(\omega)$ is some capture probability, averaged over deuteron energy and depending on angle ω between the directions of emission of the proton (or neutron) and deuteron. In carrying out the calculations for Be, one can consider the angular dependence of the (γ, n) reaction[15] to be very near in form to that of the (γ, p) reaction. Consequently, we need only the dependence of $d\sigma_{\gamma p}(\theta', \varphi')\, d\Omega'$, given directly by experiment. This dependence is not shown separately, since it does not differ essentially from that given in Fig. 1. In analogy with the usual capture process,[16,17] the angular distribution of the probability of capture can be written, in a well-known approximation, as

$$P_3(\omega) \sim N(\mathbf{n}) \sim e^{-E'/E_0}, \tag{4}$$

where $N(n)$ is the distribution function of nucleon momentum in the nucleus, E' is the energy of the captured nucleon in the nucleus, $E_0 \approx 20$ Mev for Be^{18}. For the dependence of the averaged capture probability on angle ω in Eq. (3), we substituted $P_3(\omega)$ calculated for some mean deuteron energy in the interval 15.5 — 30 Mev studied.

Results of the calculations for photodeuterons from Be, using Eqs. (3) and (4), are given in Fig. 7 by the solid line, arbitrarily normalized to the experimental data. It is seen that agreement between the calculation and experiment is rather good. Everything said above applies also to photodeuterons from Li^7, and since the dependence of $d\sigma_{\gamma p}(\theta', \varphi')/d\Omega'$ and $P_3(\omega)$ for Li^7 and Be are very similar, the calculated results agree well with experiment also in the case of Li^7. Consequently, by application of the capture mechanism, one can explain not only the rough similarities of the characteristics of angular distributions of photoprotons and photodeuterons, but also the difference between them, as shown in Fig. 8.

The angular distributions of high-energy phototritons from Li^7, Li^6, and Be given in Fig. 9, differ markedly in form from the angular distributions of photodeuterons and, it would appear, could not be explained by a mechanism analogous to double capture in (p, t) and (n, t) reactions. The dependence of the (γ, t) cross section on angle is approximately as $A + B \sin^2 \theta$. It is possible that here direct electric-dipole absorption of γ rays by quasitritons formed inside the nucleus takes place. The probability that these exist part of the time cannot be excluded.

The author would like to express his gratitude to Prof. A. P. Komar, and to colleagues L. A. Kul'chitskiĭ, E. B. Bazhanov, Yu. M. Volkov, A. B. Kulikov, and G. M. Shklyarevskiĭ for useful discussions and help. He would also like to express his gratitude to the synchrotron group of the Physico-Technical Institute.

[1] V. P. Chizhov and L. A. Kul'chitskiĭ, JETP **36**, 345 (1959), Soviet Phys. JETP **9**, 239 (1959).

[2] DeWire, Silverman, and Wolfe, Phys. Rev. **92**, 519 (1953).

[3] P. R. Byerly, Jr. and W. E. Stephens, Phys. Rev. **83**, 54 (1951).

[4] M. E. Toms and W. E. Stephens, Phys. Rev. **92**, 362 (1953).

[5] M. E. Toms and W. E. Stephens, Phys. Rev. **95**, 1209 (1954).

[6] B. Forkman, Ark. f. Fysik **11**, 265 (1956).

[7] E. D. Makhnovskiĭ, JETP **36**, 739 (1959), Soviet Phys. JETP **9**, 519 (1959).

[8] W. H. Smith and L. J. Laslett, Phys. Rev. **86**, 523 (1952).

[9] L. S. Ring, Jr., Phys. Rev. **99**, 137 (1955).

[10] Edwards, Wolfe, Silverman, and DeWire, Phys. Rev. **95**, 629 (1954).

[11] S. P. Kruglov, J. Tech. Phys. (U.S.S.R.) **28**, 2310 (1958), Soviet Phys.-Tech. Phys. **3**, 2120 (1959).

[12] A. Gamba and L. V. Wataghin, Nuovo cimento **10**, 174 (1953).

[13] S. A. E. Johansson, Phys. Rev. **98**, 705 (1955).

[14] J. W. Rosengren and J. M. Dudley, Phys. Rev. **89**, 603 (1953).

[15] L. A. Kul'chitskiĭ and V. Presperin, JETP **37**, 1524 (1959), Soviet Phys. JETP **10**, 1082 (1960).

[16] G. F. Chew and M. L. Goldberger, Phys. Rev. **77**, 470 (1950).

[17] W. Selove, Phys. Rev. **101**, 231 (1956).

[18] Azhgireĭ, Vzorov, Zrelov, Meshchyeryakov, Neganov, Ryndin, and Shabudin, JETP **36**, 1631 (1959), Soviet Phys. JETP **9**, 1163 (1959).

Translated by G. E. Brown
158

SOVIET PHYSICS JETP VOLUME 11, NUMBER 3 SEPTEMBER, 1960

SCATTERING BY A SINGULAR POTENTIAL IN PERTURBATION THEORY AND IN THE MOMENTUM REPRESENTATION

Ya. B. ZEL' DOVICH

Institute for Theoretical and Experimental Physics, Academy of Sciences, U.S.S.R.

Submitted to JETP editor September 24, 1959

J. Exptl. Theoret. Phys. (U.S.S.R.) **38**, 819-824 (March, 1960)

A method is developed for treatment of scattering by a singular potential in the momentum representation and in perturbation theory. Application of such renormalization techniques permits one to derive well-known results for cross sections, despite the fact that the integrals diverge and the matrix elements entering into the wave equation in the momentum representation vanish.

THE problem is considered below of scattering in the presence of a nearby resonant level — real, as a deuteron in the triplet state, or virtual, as in the singlet np scattering. In the limit, this problem can be regarded as scattering by a potential U, acting for $r < r_0$, where $U \to -\infty$, $r_0 \to 0$, such that

$$Ur_0^2 \to -\pi\hbar^2/8m + wr_0$$

(the coefficients refer to a rectangular well).

The usual solution of this problem is found in space coordinates by replacing the action of the potential by a boundary condition applied to the wave function $\varphi = r\psi$ at the origin:

$$d \ln \varphi / dr = mw/\hbar^2 = -1/a;$$

This boundary condition follows from a solution of the Schrödinger equation for $r \leq r_0$. As is well known, the value of a completely determines the value of the scattering cross section:

$$\sigma = 4\pi a^2 [1 + (ap/\hbar)^2]^{-1}$$

for $pr_0 \ll 1$. If $a > 0$, there is also a single bound state with energy $E = -\hbar^2/2ma^2$.

The problem becomes singular if treated by perturbation theory. By considering the transition from a state with one momentum p into a state with another momentum p′ under the action of a potential U, it is easy to establish the fact that the corresponding matrix element

$$U(p, p') = (2\pi)^{-3} \int U(\mathbf{r}) e^{i(\mathbf{p}-\mathbf{p}')\mathbf{r}} d^3\mathbf{r} \tag{1}$$

does not exceed $U \cdot \frac{4}{3}\pi r_0^3$ and, consequently, in the limit as $r_0 \to 0$, the matrix element also tends to zero as r_0, inasmuch as $U \sim r_0^{-2}$.

It is evident that in the limit not only the first approximation of perturbation theory disappears, but also the sum of any finite number of terms of the series; however, the sum of the entire infinite series of perturbation theory preserves completely a definite value of the transition probability, i.e., the scattering cross section. As we shall see below, in the transition to the limit $r_0 \to 0$, along with the transition to zero of each term of the series of perturbation theory, the number of terms of the series which must be taken into consideration tends to infinity. Since one ordinarily uses not the coordinate representation, as in field theory, but precisely perturbation theory in momentum representation, a complete explanation of such a peculiar situation in a simple example can be of interest.

Perturbation theory uses plane waves as a base, i.e., it is essentially close to a consideration of the problem in the momentum representation.* In this representation the matrix element U(p, p′) enters into the equation and the surmounting of the difficulties associated with $U(p, p') \to 0$ also opens up a path to the solution of the problem in perturbation theory. The method of obtaining the correct result in the momentum representation in the transition to the limit of the quantities entering into it is very instructive and has general similarities with the methods of renormalization, especially in that form in which they were applied by Heisenberg[3] to the Lee model.

1. THE EQUATION IN THE MOMENTUM REPRESENTATION

Substituting in the Schrödinger equation ($\hbar = m = 1$)

---

*Scattering and the bound state in the momentum representation were considered by Salpeter;[1] see also reference 3.

$$\psi = (2\pi)^{-3/2} \int \chi(p)\, e^{i\mathbf{p}\mathbf{x}} d^3\mathbf{p}, \tag{2}$$

we get an equation for $\chi(\mathbf{p})$

$$(p^2 - 2E)\,\chi(p) = -2 \int d^3p'\chi(p')\, U(p',\ p) \tag{3}$$

[$U(\mathbf{p}, \mathbf{p}')$ is determined by Eq. (1)]. In the problem of the determination of the bound level, we set $E = -\kappa^2/2$; Eq. (3) is rewritten in the form

$$(\mathbf{p}^2 + \varkappa^2)\,\chi(p) = -2 \int d^3p'\chi(p')\, U(p', p). \tag{4}$$

In the scattering problem, we set $E = k^2/2 > 0$; the momentum $\mathbf{k}$ and energy $E = k^2/2$ of the incident wave are given. Equation (3) is rewritten in the form

$$(\mathbf{p}^2 - k^2)\,\chi(p) = -2 \int d^3p'\chi(p')\, U(p',\ p). \tag{5}$$

Its solution must contain the incident wave and the scattered wave of the same energy, i.e.,

$$\chi(p) = \delta(\mathbf{p} - \mathbf{k}) + f(\mathbf{p}),$$

such that the problem reduces to the determination of $f(\mathbf{p})$ for $\mathbf{p}^2 = k^2$.

Returning to the specifics of the singular potential, we observe that for $r_0 \to 0$, the function $U(\mathbf{p}, \mathbf{p}') \to 0$, but the dependence of U on $|\mathbf{p}|$, $|\mathbf{p}'|$ simultaneously vanishes up to $|\mathbf{p}| \sim 1/r_0$, $|\mathbf{p}'| \sim 1/r_0$. We set

$$U(p,\ p') = -C \quad \text{for } |p| < b,\quad |p'| < b;$$
$$U(p,\ p') = 0 \quad \text{for } |p| > b,\quad |p'| > b, \tag{6}$$

in order to make the subsequent transition to the limit $C \to 0$, $b \to \infty$.

For the bound state we get from the equation

$$(p^2 + \varkappa^2)\,\chi(p) = 2C \int\limits_0^b \chi(p')\, d^3p' \tag{7}$$

$$\chi(p) = q/(p^2 + \varkappa^2), \qquad q = 8\pi C \int\limits_0^b dp' q p'^2/(p'^2 + \varkappa^2). \tag{8}$$

For scattering, it follows from the equation

$$(p^2 - k^2)\,\chi(p) = 2C \int\limits_0^b \chi(p')\, d^3p' \tag{9}$$

that

$$\chi(p) = \delta(\mathbf{p} - \mathbf{k}) + \frac{q}{p^2 - k^2},$$

$$q = 2C\Big[\int\limits_0^b dp' 4\pi q p'^2/(p'^2 - k^2) + 1\Big]. \tag{10}$$

2. TRANSITION TO THE SINGULAR POTENTIAL

It is now seen why the equation can have a finite solution: in spite of the transition to zero $C = -U(\mathbf{p}, \mathbf{p}')$, the limiting value of the momentum b, for which decrease of U begins, increases along with decrease in r_0. The quantity C enters into Eqs. (8) and (10) multiplied by an integral which diverges as b for $b \to \infty$.

We set

$$2C \int\limits_0^b \frac{4\pi p^2}{p^2}\, dp = 8\pi C b = 1 + 4\pi^2 Z C. \tag{11}$$

This is the connection between the transition $C \to 0$ and $b \to \infty$, which is necessary in order that we obtain a finite answer, i.e., in order that resonance take place. It is easy to prove that the condition $Cb = \text{const}$ is equivalent to $Ur_0^2 = \text{const}$, $r_0 \to 0$. Here Cb must have a completely determined value for the existence of a solution. The coefficient Z, which shows just how Cb tends toward its limiting value, is also important for the result. The factor $4\pi^2$ is introduced in the term $4\pi^2 ZC$ only for convenience.

We further divide the diverging (as $b \to \infty$) integral (8), (10) into a constant diverging integral and a converging integral which depends on the quantities entering into the conditions of the problem. Making use of the identities

$$(p^2 + \varkappa^2)^{-1} = p^{-2} - \varkappa^2/p^2(p^2 + \varkappa^2), \tag{12a}$$

$$(p^2 - k^2)^{-1} = p^{-2} + k^2/p^2(p^2 - k^2), \tag{12b}$$

we find

$$\int\limits_a^b \frac{p^2}{p^2 + \varkappa^2}\, dp = \int\limits_0^b dp - \int\limits_0^b \frac{\varkappa^2}{p^2 + \varkappa^2}\, dp$$
$$= b - \varkappa \tan^{-1}\frac{b}{\varkappa} \to b - \frac{\pi}{2}\varkappa \quad (b \to \infty) \tag{13}$$

and, by substituting in (8), we obtain

$$q = 8\pi C q\,(b - \pi\varkappa/2), \qquad 4\pi^2(ZC - C\varkappa) = 0. \tag{14}$$

We now let $C \to 0$. The real level exists only for $Z > 0$, and its energy is given by the value $\kappa = Z$.

The scattering problem is solved in similar fashion. Substituting (12b) and (11) in (10), we obtain

$$q = q\,(1 + 4\pi^2 ZC) + 8\pi q C k^2 \int\limits_0^b \frac{dp}{p^2 - k^2} + 2C. \tag{15}$$

After division by q and C we allow the limiting transition $C \to 0$, $b \to \infty$ in Eq. (15). In taking the integral

$$\int_0^\infty dp/(p^2-k^2)$$

it is necessary to take into account that $\kappa(p)$ must be written as a diverging wave. As is well known,[2] it is necessary to integrate in this case over the real axis of the variable p, assuming that p has a small imaginary part: $p \rightarrow p + i\epsilon$, $\epsilon > 0$, $\lim \epsilon = 0$. Carrying out the integration in this fashion, we get

$$\int_0^\infty \frac{dp}{p^2-k^2+i\varepsilon} = \frac{1}{2}\int_{-\infty}^{+\infty} \frac{dp}{p^2-k^2+i\varepsilon} = \frac{\pi i}{2k}.$$

Substitution of the resulting integral in (15) gives

$$q = (2\pi^2)^{-1}(Z+ik)^{-1} \tag{16}$$

and consequently the wave function of the scattering problem in the momentum representation has the form

$$\chi(p) = \delta(\mathbf{p}-\mathbf{k}) + \frac{1}{2\pi^2(Z+ik)}\frac{1}{p^2-k^2+i\varepsilon} = \delta(\mathbf{p}-\mathbf{k}) + \chi_s(p). \tag{17}$$

We find the asymptotic form of the function, corresponding to the second term χ_s of (17) in the coordinate representation:

$$\psi(\mathbf{r}) = \int e^{i\mathbf{pr}}\chi_s(p)\,d^3p = \frac{2\pi}{ir}\int_0^\infty (e^{ipr}-e^{-ipr})\,p\chi_s(p)\,dp = \frac{2\pi}{ir}\int_{-\infty}^{+\infty} e^{ipr}\chi_s(p)\,p\,dp = 4\pi^2\frac{e^{ikr}}{r}\mathrm{Res}\{\chi_s(p)\} = \frac{1}{Z+ik}\frac{e^{ikr}}{r_0}. \tag{18}$$

By comparing the scattered current with the current in the incident wave, we find the scattering cross section in the form

$$\sigma = 4\pi\left|\frac{1}{Z+ik}\right|^2 = \frac{4\pi}{Z^2+k^2}, \tag{19}$$

as was to have been expected. In the presence of a bound level $(Z = \kappa)$ a quantity appears in the numerator of (19), which is proportional to the sum of the collision energy and the binding energy of the level; in the absence of a bound level $(Z < 0)$, Z^2 is a quantity proportional to the energy of the virtual level.

3. PERTURBATION THEORY

The solution of the problem by the method of perturbation theory consists of iteration of the integral equation (5). In the zeroth approximation, we have only the incident wave

$$\chi_0 = \delta(\mathbf{p}-\mathbf{k}). \tag{20}$$

Substituting (5) on the right hand side, we get

$$\chi_1 = \chi_0 - \frac{2}{p^2-k^2}\int_0^\infty d^3p'\chi(p')\,U(p,\ p') = \delta(\mathbf{p}-\mathbf{k}) + \frac{2C}{p^2-k^2}. \tag{21}$$

The subsequent approximation gives

$$\chi_2 = \delta(\mathbf{p}-\mathbf{k}) + \frac{2C}{p^2-k^2} + \frac{2}{p^2-k^2}\int_0^\infty d^3p'U(p',\ p)\frac{2C}{p'^2-k^2}. \tag{22}$$

The integral on the right hand side is transformed by the method applied in Sec. 2:

$$\int U(p,\ p')\frac{2C}{p'^2-k^2}\,d^3p' = 8\pi C\left[Cb + C\,\frac{k^2\pi i}{2k}\right], \tag{23}$$

from which it follows that

$$\chi_2 = \delta(\mathbf{p}-\mathbf{k}) + \frac{2C}{p^2-k^2} + \frac{2C}{p^2-k^2}\,[8\pi Cb + i4\pi^2k]. \tag{22a}$$

It is easy to prove that the perturbation-theory series is a geometric progression, the denominator of which is the expression in the square brackets in (22a), while the first term is $2C/(p^2-k^2)$. We then immediately obtain the sum of the infinite number of terms

$$\chi_\infty = \delta(\mathbf{p}-\mathbf{k}) + \frac{1}{p^2-k^2}\,\frac{2C}{1-8\pi Cb-iC4\pi^2k}. \tag{24}$$

It is now evident that for the result to be finite it is necessary that the difference $(1-8\pi Cb)$ be of order C. Taking for Cb the limiting expression in Eq. (11), we get the expression $\chi(p)$ of Eq. (17) from (24). Thus, in the limit the denominator α of the geometric progression actually tends to unity (the difference $1-\alpha \sim C$), while the effective number of terms of the series tends to infinity as $1/C$, which also compensates the trend to zero of each separate term of the series, which is proportional to C.

We note that Eq. (24) remains in force even when $Z > 0$, $|\alpha| > 1$ (the case of the existence of a bound level), in spite of the divergence of the series of perturbation theory for $|\alpha| > 1$.

4. MORE RIGOROUS METHOD

The transformations connected with the elimination of the zeros $(C \rightarrow 0)$ and the infinities $(b \rightarrow \infty)$ were carried out above schematically under the assumption that $U(p, p')$ is broken off sharply for $p > b$. Evidently, all the discussions can be carried out more rigorously if we write

$$U = Cf(|p-p'|/b), \qquad \chi = \frac{q}{p^2+\varkappa^2}\,g(|p|/b),$$

where the characteristic functions f and g satisfy the condition $f(0) = g(0) = 1$ and coincide at large values of the arguments. The condition connecting C and b is written as follows:

$$2C\int_0^\infty f(|p-p'|/b)\,g(|p-p'|/b)\,\frac{1}{p^2}\,d^3p = 1 + 4\pi^2ZC.$$

After subtraction similar to (12a) and (12b), we obtain integrals of the form

$$\varkappa^2 \int_0^\infty \frac{f(|p-p'|/b)\, g(|p-p'|/b)}{(p'^2+\varkappa^2)}\, d^3p',$$

$$k^2 \int_0^\infty \frac{fg}{p^2-k^2+i\varepsilon}\, d^3p'.$$

It is important that these integrals converge independently of the decrease of f and g, because of the high power of the denominator. Therefore, their values and dependence on κ can be immediately computed for $b \rightarrow \infty$, i.e., in the approximation $f = g = 1$.

Thus the connection between the scattering cross section and the location of the level (the real or virtual) is shown to be independent of the concrete form of U(r). Computations carried out in all their triviality and absence of new results are instructive. A mechanism is given for obtaining a finite scattering cross section of a bound level under the action of a potential which gives a vanishing matrix element in perturbation theory of arbitrary (n-th) order. One can easily show that only an infinitely short duration of such a perturbation is capable (at a given relation between the zero and the infinity) of giving a finite effect.

---

[1] E. E. Salpeter, Phys. Rev. **84**, 1226 (1951).

[2] M. Lippman and J. Schwinger, Phys. Rev. **79**, 469 (1950).

[3] W. Heisenberg, Nucl. Phys. **4**, 532 (1957).

Translated by R. T. Beyer
159

SOVIET PHYSICS JETP VOLUME 11, NUMBER 3 SEPTEMBER, 1960

ON THE THEORY OF NON-EQUILIBRIUM STATISTICAL PROCESSES

R. L. STRATONOVICH

Moscow State University

Submitted to JETP editor June 17, 1959; resubmitted October 10, 1959

J. Exptl. Theoret. Phys. (U.S.S.R.) **38**, 825-833 (March, 1960)

A stochastic equation is derived by means of the phenomenological equations of motion under well-defined assumptions. The thermal noise of a nonlinear resistance is considered as an example.

IN view of the fact that a mathematical analysis of the exact dynamical picture of non-equilibrium statistical processes is very difficult, it is advisable to study such processes using equations of the phenomenological type. This leaves only a small number of coordinates to be considered (the coordinates of a Brownian particle, the charge or current in an electrical circuit, and so on). The participation of a huge number of other particles in the process expresses itself implicitly in two ways. Firstly, there is dissipation, which is described by the phenomenological equation for the average velocity-dependent force (elementary dynamical interactions are non-dissipative). Secondly, there are the fluctuating impacts from the surrounding medium. The average phenomenological force defines the first-derivative term in the stochastic equation, while the fluctuating impacts cause the occurrence of terms (or a term) with higher derivatives. An evaluation of the statistics of the fluctuating actions so as to determine the form of these terms is a more difficult problem than the determination of the average phenomenological force. The latter can be determined experimentally and can be considered as given in the theory. From general considerations it follows that there is a connection between the statistics of the fluctuating actions and the dissipation in the system. The determination of these statistics from the dissipation mechanism is a general and important problem in statistical physics and has many diverse applications.

For the case where the dissipative force depends linearly on the velocity the above problem was solved in the classical papers on Brownian motion (Langevin and others). The problem is, however, appreciably more complicated in the case of a nonlinear mechanism of dissipation, and has not yet been solved in general form at the present. Some authors (see, for instance, reference 1) even deny the existence of a necessarily unique connection between the average force and the intensity of the impacts in the general case. The papers of Magalinskiĭ and Terletskiĭ[2-4] were devoted to a consideration of the above mentioned problem, but gave rise to important objections.

In the present paper we give an exact solution of a well-defined problem; that is to say, we derive a stochastic equation under the assumption that the relaxation time for the velocity is much smaller than the relaxation time for the coordinate. To do this we apply a method based on a corrected and extended version of the method proposed in references 2 — 4.

Let q be one or several coordinates of an arbitrary mechanical system described by a Hamiltonian H (p, p′, q, q′) (the q′ are the remaining coordinates). The process of motion is determined by the dynamical equations

$$\dot{q} = \partial H / \partial p, \qquad \dot{p} = -\partial H / \partial q. \tag{1}$$

The totality of the influence of the variables q′, which correspond to the medium through which the particle moves, can be described phenomenologically by introducing a frictional force (in the general case nonlinear) and fluctuating forces. The exact Eqs. (1) are then replaced by a phenomenological equation of the Langevin type

$$\ddot{q} = \Phi(\dot{q}, q, t) = F(\dot{q}, q) + \xi(t, \dot{q}; q). \tag{2}$$

We assume that the kinetic energy pertaining to the coordinate q is equal to $m\dot{q}^2/2$. The function Φ in (2) has the meaning of a force divided by the mass m. The division by m was performed to simplify the formulae and we shall continue to call Φ a “force.”

The force Φ is given in (2) as the sum of an average force, $F = \bar{\Phi}$, and a fluctuating term which by definition has an average value of zero:

$$\overline{\xi(t,\ q,\ q)} = 0. \tag{3}$$

For the sake of simplicity, we have chosen to write our equations in one-dimensional form (q is one coordinate).

The dependence of the force on the coordinate and on the velocity can be determined experimentally. One must average the action of the fluctuating force in that case over some time interval τ_y, which must be longer than the correlation time τ_1 of the fluctuating force: $\tau_y \gg \tau_1$. The length of the time interval over which it is averaged has no upper bound. However, to obtain as detailed a phenomenological description of the system as possible, it is desirable to choose the smallest value compatible with the above-mentioned inequality.

What we can measure is essentially not the exact force Φ as a function of q and $\dot{q}$, but an average force $\tilde{\Phi}$ as a function of the average values q and $\tilde{\dot{q}}$. The tilde on top indicates here an average over the time τ_y, for instance,

$$\tilde{\dot{q}} = \frac{1}{\tau_y} \int_t^{t+\tau_y} \dot{q}\,dt = \frac{q(t+\tau_y) - q(t)}{\tau_y}. \tag{4}$$

Because of the condition $\tau_y \gg \tau_1$ $\tilde{\Phi}$ is the same as F. If we wish to find out how $\tilde{q}$ and $\tilde{\dot{q}}$ are connected with the instantaneous values q and $\dot{q}$, we must take into account the relaxation times of the latter. We introduced along with τ_1 the velocity relaxation time

$$\tau_2 \sim \tilde{\dot{q}}/\tilde{\ddot{q}} \sim \tilde{\dot{q}}/F \tag{5}$$

and the coordinate relaxation time

$$\tau_3 \sim \tilde{q}\,/\,\tilde{\dot{q}}. \tag{6}$$

Different relations are possible between the time constants τ_1, τ_2, and τ_3. We consider the case where

$$\tau_2 \ll \tau_3 \tag{7}$$

and where we can consider phenomenological equations that correspond to a time of averaging which satisfies the inequalities

$$\tau_y \ll \tau_3, \tag{8}$$

$$\tau_y \gg \tau_2. \tag{9}$$

Assume, in particular, that (7) is satisfied and the force relaxation time τ_1 is comparable with τ_2

$$\tau_1 \sim \tau_2. \tag{10}$$

If we then choose our averaging time so that $\tau_1 \ll \tau_y \ll \tau_3$, we satisfy conditions (8) and (9).

Because of inequality (8), $\tilde{q}$ is the same as q but $\tilde{\dot{q}}$ differs from the instantaneous value of $\dot{q}$. The trajectory in phase space is no longer a Markov process. Because of (7) the $q(t)$ process can, however, be considered to be a Markov process. Our problem is to express its statistical characteristics through the experimental function $F(\tilde{\dot{q}}, q)$, which is supposed to be known.

Inequality (9) enables us to state that the time average is the same as the statistical average

$$\tilde{\dot{q}} = \bar{\dot{q}} \tag{11}$$

[we are considering an ensemble for which $q(t_0) = q_0$]. This average value is independent of the initial velocity $\dot{q}(t_0)$, the influence of which vanishes within a period of time of the order of τ_2. It is thus some phenomenological function of the coordinate,

$$\bar{\dot{q}} = f(q). \tag{12}$$

Taking (11) into account we can write the phenomenological equation (2) in the form

$$\dot{v} = F(\bar{v},\ q) + \xi(t,\ \bar{v},\ q) \quad (v = \dot{q}). \tag{13}$$

The function (12) can be determined from Eq. (13). Indeed, averaging (13) and taking (3) into account, we find

$$\bar{\dot{v}} = F(\bar{v},\ p).$$

Substituting (12) and performing the transformation

$$\bar{\dot{v}} = \overline{\dot{f}(q)} = (\partial f/\partial q)\,\bar{v},$$

we obtain the equation

$$\partial f/\partial q = F(f,\ q)/f, \tag{14}$$

from which we can determine $f(q)$. One can simplify this with the aid of (7). To do this we take into account Eqs. (5) and (6) which define τ_2 and τ_3. The latter can be written

$$\bar{\tau}_3^{-1} \sim f/q \sim \partial f/\partial q. \tag{15}$$

According to (5) $F/\bar{v}$ is of the order of $1/\tau_2$ for most values of $\bar{v}$; in our case, however, it is of order $1/\tau_3$, [i.e., appreciably smaller, because of (7)] as can be seen from (14) and (15). This exceptional value must be determined from the equation

$$F(\bar{v},\ q) = 0. \tag{16}$$

The latter states that an average velocity is set up in such a way that it corresponds to a zero force acting upon the particle.

Turning to the dynamical equations (1), we shall consider instead of the variables q and p the coordinate and velocity q and $v = \dot{q}$. In that case Eq. (1) is transformed into

$$\dot q = v, \quad \dot v = G(q, v, p', q') = -m^{-1}\partial H/\partial q. \tag{17}$$

Here $G(q, v, p', q')$ is the dynamical expression for the force, corresponding to the phenomenological expression Φ. The probability distribution density $w = w(q, v, p', q')$ changes according to the equation

$$\dot w = -\frac{\partial}{\partial q}(vw) - \frac{\partial}{\partial v}(Gw) + \frac{\partial H}{\partial q'}\frac{\partial w}{\partial p'} - \frac{\partial H}{\partial p'}\frac{\partial w}{\partial p'} \equiv Aw. \tag{18}$$

We are especially interested in the well-defined initial condition $q = q_0$ at $t = t_0$, which corresponds to

$$[w]_{t=t_0} = \delta(q - q_0)\, w_0(v, p', q') \tag{19}$$

(the initial distribution $w_0(v, p', q')$ does not play a large part since it relaxes rapidly).

We introduce the functions

$$W = e^{uq}w, \tag{20}$$

$$Z(u) = \int W d\Omega = \int e^{uq} w d\Omega, \tag{21}$$

$$\tilde w = W/Z(u) \tag{22}$$

($d\Omega = dq\, dv\, dp'\, dq'$) and ascertain their time variation. Writing (18) in the form

$$e^{-uq}\dot W = A(e^{-uq}W)$$

and differentiating we get

$$\dot W = AW + uvW. \tag{23}$$

If we integrate this equation over v and q we get

$$\dot Z(u) = u\bar v W, \tag{24}$$

where

$$\bar v = Z^{-1}\int vW d\Omega = \int v\tilde w d\Omega. \tag{25}$$

Differentiating $\tilde w$ with respect to time and substituting (23) and (24), we find

$$\dot{\tilde w} = A\tilde w + u(v - \bar v)\tilde w. \tag{26}$$

We write the last term in (26) as a differential expression

$$(v - \bar v)\tilde w = \sum_{m,\, n=0}^{\infty} \frac{1}{m!\, n!}\left(-\frac{\partial}{\partial q}\right)^m \left(-\frac{\partial}{\partial v}\right)^n (\beta_{mn}\tilde w). \tag{27}$$

Here $\beta_{mn} = \beta_{mn}(q_0)$ are suitably chosen coefficients. It is shown in the Appendix that they can easily be expressed in terms of the correlation functions of the velocity fluctuations; in particular,

$$\beta_{01} = \overline{(v - \bar v)^2} = k_2(0),$$

$$\beta_{10} = \overline{(q - \bar q)(v - \bar v)} = \int_0^\infty k_2(\tau)\, d\tau. \tag{28}$$

Because of (27), Eq. (26) is equivalent to

$$\dot q = v + a(t), \quad \dot v = G(q, v, p', q') + b(t), \tag{29}$$

where $a(t)$ and $b(t)$ are random functions with average values

$$\bar a = u\beta_{10}, \quad \bar b = u\beta_{01}, \tag{30}$$

and with correlation functions (for r quantities a and s quantities b)

$$k_{(r)a,\,(s)b}(t_1, \ldots, t_{r+s}, q_0)$$

$$= u\beta_{rs}\delta(t_2 - t_1) \ldots \delta(t_{r+s} - t_1) \tag{31}$$

(cf. reference 5).

Equations (29) enable us to interpret $\tilde w$ as the distribution density for some new mechanical system subjected to additional forces a and b, each with a steady and a fluctuating term.

The additional forces can be included not only in the dynamic, but also in the phenomenological equations. In accordance with (29), Eqs. (13) are replaced by

$$\dot q = v + a(t), \quad \dot v = F(\bar v, q) + \xi(t) + b(t), \tag{32}$$

We use (32) to find a new phenomenological function

$$\dot{\bar q} = f(q, u), \tag{33}$$

which determines the average velocity. Averaging (32), we have

$$\dot{\bar q} = \bar v + \bar a, \quad \dot{\bar v} = F(\bar v, q) + \bar b. \tag{34}$$

As in the derivation of Eq. (16), we find from the second equation of (34)

$$F(\bar v, q) + \bar b = 0. \tag{35}$$

Solving with respect to $\bar v$ and denoting the corresponding function by f_1, we get

$$\bar v = f_1(q, u). \tag{36}$$

Substituting (36) into the first equation of (34), we get the required function (33):

$$\dot{\bar q} = f(q, u) = f_1(q, u) + \bar a. \tag{37}$$

The function (12) is, of course, none other than a particular value, $f(q, 0)$.

We now turn to the problem of the diffusion of an initial distribution of the type (19). In the first period, while $t - t_0 \lesssim \tau_2$, the fluctuations of $q(t)$ are not like a Markov process. Thereafter, when $\tau_2 \ll t - t_0 \ll \tau_3$ the average velocity $\dot{\bar q}$ approaches the function (12), which is independent of the initial velocity. For those intervals of time, the fluctuating process $q(t)$ can at the same time be considered to be a Markov process. The distribution $w(q, q_0)$, obtained from the initial distribution $\delta(q - q_0)$, then generates a Markov transition probability and characterizes completely the fluctuating process. For time intervals satisfying the condition

$$\tau_2 \ll t - t_0 \ll \tau_3,$$

the coordinate q does not have time to change strongly, and we have from Eq. (33), for the chosen initial condition,

$$\overline{q} = q_0 + (t - t_0) f(q_0, u). \qquad (38)$$

According to what has been said above, the averaging $\overline{q}$ is then done over an ensemble corresponding to the included additional forces a, b, i.e., with the weight of w. According to (20) -- (22), this average can be written as

$$\overline{q} = \int q\tilde{w}d\Omega = \frac{1}{Z}\int qe^{uq}wd\Omega = \frac{1}{Z}\frac{\partial Z}{\partial u}. \qquad (39)$$

Because of this (38) goes over into the equation

$$\partial \ln Z(u)/\partial u = q_0 + (t - t_0) f(q_0, u), \qquad (40)$$

from which we can determine Z (u). When integrating this we take into account the initial condition Z (0) = 1, which follows from (21), and we get

$$Z(u) = \exp\{q_0 u + (t - t_0)\int_0^u f(q_0, u)\,du\}. \qquad (41)$$

For imaginary values of the argument u = iv the function Z (u) is none other than the characteristic function $\overline{\exp(iv)}$. The required transition probability can thus be obtained from it by a Fourier transformation

$$w(q, q_0) = \frac{1}{2\pi}\int e^{-ivq} Z(iv)\,dv. \qquad (42)$$

Knowing the transition probability one can evaluate how any other initial distribution $w(q_0, t_0)$ will change. The Markov condition leads to

$$w(q, t) = \int w(q, q_0)\, w(q_0, t_0)\, dq_0. \qquad (43)$$

The choice of the initial moment is arbitrary; giving t_0 increasing values we can follow the complete evolution of the distribution density.

It is convenient to consider a differential stochastic equation. To get it we expand (40) in powers of $t - t_0$. Retaining only the first two terms we have

$$Z(u) = e^{q_0 u} + (t - t_0)\, e^{q_0 u}\sum_{s=1}^{\infty}\frac{u^s}{s!}K_s(q_0). \qquad (44)$$

The function $\int_0^u f(q_0, u)\,du$ is here expanded in a Maclaurin series and

$$K_s(q_0) = [\partial^{s-1} f(q_0, u)/\partial u^{s-1}]_{u=0}. \qquad (45)$$

After substituting (44) into (42) we find

$$w(q, q_0) = \delta(q - q_0) + (t - t_0)\sum_{s=1}^{\infty}\frac{1}{s!}\left(-\frac{\partial}{\partial q}\right)^s K_s(q_0)\,\delta(q - q_0). \qquad (46)$$

To obtain the stochastic equation we must still substitute (46) into (43). The term $w(q, t_0)$ obtained after integrating with $\delta(q - q_0)$ is shifted to the left-hand side and $[w(q, t) - w(q, t_0)]/(t - t_0)$ is denoted $\dot{w}$. The result is

$$\dot{w}(q) = \sum_{s=1}^{\infty}\frac{1}{s!}(-1)^s\frac{\partial^s}{\partial q^s}[K_s(q)\, w(q)]. \qquad (47)$$

From a mathematical point of view, the main result here is that the correlation functions [or, what is the same, the moments $\overline{\eta(t_1, q)\ldots\eta(t_s, q)}$] of the random functions $\eta(t, q)$ in the equation

$$\dot{q} = f(q) + \eta(t, q), \qquad (48)$$

which is equivalent to (47), cannot be given arbitrarily, but are uniquely determined by the force function F (q, v).

First example. A particle experiencing nonlinear friction. Let a conservative force g (q) and a nonlinear frictional force $\varphi(v)$ act upon the particle. The phenomenological Eq. (13) is of the form

$$m\dot{v} = g(q) - \varphi(v) + m\xi, \qquad \dot{q} = v. \qquad (49)$$

In this case

$$\tau_2 \sim m/\varphi', \qquad \tau_3 \sim q\varphi'/g.$$

The condition for the applicability of the theory given here is thus of the form

$$m/\varphi' \ll \tau_y \ll q\varphi'/g. \qquad (50)$$

The system with the additional forces included is described by the phenomenological equations

$$\dot{q} = v + a, \qquad m\dot{v} = g(q) - \varphi(\overline{v}) + m\xi + mb.$$

Averaging these and solving the equation

$$\varphi(\overline{v}) = g(q) + m\overline{b},$$

which corresponds to Eq. (35), we find

$$\overline{\dot{q}} = \overline{a} + \psi(m\overline{b} + g).$$

Here ψ is the inverse of $\varphi(v)$. According to (28) and (30) we then have

$$\overline{a} = u\beta_{10} = u\overline{(q - \overline{q})(v - \overline{v})}, \qquad \overline{b} = u\beta_{01} = u\overline{(v - \overline{v})^2}.$$

In view of the fact that the velocity distribution at time $t - t_0 \gg \tau_2$ is practically the same as at equilibrium, i.e., a Maxwell distribution, we have $m\overline{b} = u\Theta$ (Θ is the temperature).

The coefficients in (47) are evaluated from the equations

$$f(q,u) = u\beta_{10} + \psi(u\Theta + g); \qquad K_1 = \psi(g),$$

$$K_2 = \beta_{10} + \Theta\psi'(g), \quad K_n = \Theta^{n-1}\psi^{(n-1)}(g) \quad (n = 3, 4, \ldots). \tag{51}$$

To evaluate β_{10} it is expedient to take into account that

$$\overline{(q-\bar{q})(v-\bar{v})} = \tfrac{1}{2}\, d\,\overline{(q-\bar{q})^2}/dt = \tfrac{1}{2}\, d(K_2 t)/dt$$

and, thus, $\beta_{10} = \frac{1}{2} K_2$.

Taking (37) and (45) into account we get

$$K_2 = 2\Theta\psi'(g) = 2\Theta/\varphi'(K_1). \tag{52}$$

In the particular case where the frictional function is linear $[\varphi(v) = \beta v]$ the relation given here gives the usual expressions

$$K_1 = g/\beta, \qquad K_2 = 2\Theta/\beta, \qquad K_3 = \cdots = 0.$$

Second example. The mechanical example considered is analogous to an electrical circuit containing a nonlinear resistance and a nonlinear capacitance (Figure). q is then the charge on the capacitance and $\dot{q} = I$ the current in the circuit, while the induction L plays the role of the mass. The relaxation times are in this case equal to

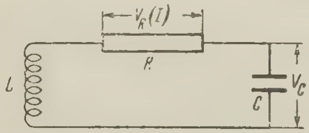

$$\tau_2 \sim L/R, \qquad \tau_3 \sim RC$$

$[R = dV_R/dI,\ C = V_C/q = g(q)/q]$. We can use for this circuit Eq. (46) with the values of the coefficients from (51), if

$$L/R \ll RC \tag{53}$$

and if $\varphi(I)$ is taken to mean the function that describes the dependence of the average potential across the resistance on the average current after a time $\tau_y \gg L/R$

$$V_R = \varphi(\bar{I}).$$

When the dependence of the voltage on the instantaneous current

$$V_R = V(I)$$

(which corresponds to $\tau_1 \ll \tau_y \ll \tau_2$) is known from experiments, we can find the function φ corresponding to longer averaging times from the formula

$$\varphi(\bar{I}) = \sqrt{L/2\pi\Theta}\int V(I)\exp\left\{-\frac{L}{2\Theta}(I-\bar{I})^2\right\}dI. \tag{54}$$

In the region of stationary fluctuations the quantity $\bar{I}^2 L/\Theta$ (which is of the same order of magnitude as $(\bar{I}/V)^2 L/C$) is small because of the inequality (53). This enables us to expand (54) in a power series in $\bar{I}$. Restricting ourselves to the first term we have

$$\varphi(\bar{I}) = \beta\bar{I} = R_{\mathbf{eq}}\bar{I},$$

where

$$R_{\mathbf{eq}} = \frac{1}{\sqrt{2\pi}}\left(\frac{L}{\Theta}\right)^{3/2}\int_{-\infty}^{\infty} V(I)\, I \exp\left\{-\frac{L}{2\Theta}I^2\right\}dI \tag{55}$$

is the equivalent linear resistance by which we can replace the given nonlinear resistance.

The consideration given here was restricted by the condition of fast relaxation of the velocity: $\tau_2 \ll \tau_3$. It would be of great interest to get rid of this restriction.

The author expresses his gratitude to Academician M. A. Leontovich and Professor Ya. P. Terletskiĭ for their interest in the present paper and for a number of helpful discussions.

APPENDIX

We shall find the coefficients β_{mn} of the expansion (27). We multiply both sides of this equation by $E = \exp[(q-\bar{q})x + (v-\bar{v})y]$ and integrate over q and v. The integral $\int(v-\bar{v})E\tilde{w}\,dq\,dv$ can be written in the form $\partial\Theta(x,y)/\partial y$, where

$$\Theta(x,y) = \int E\tilde{w}\,dq\,dv$$

is the two-dimensional characteristic function of the quantities $q-\bar{q}$ and $v-\bar{v}$. Further integrations by parts give

$$\int\left(-\frac{\partial}{\partial q}\right)^m\left(-\frac{\partial}{\partial v}\right)^n(\beta_{mn}\tilde{w})\,E\,dq\,dv = x^m y^n \beta_{mn}\Theta(x,y).$$

(27) is thus equivalent to the equation

$$\frac{\partial\Theta}{\partial y} = \Theta\Sigma\frac{x^m y^n}{m!\,n!}\beta_{mn} \quad \text{or} \quad \frac{\partial \ln\Theta}{\partial y} = \Sigma\frac{x^m y^n}{m!\,n!}\beta_{mn}.$$

At the same time, the two-dimensional characteristic function can, as is well known, be expressed in terms of the cumulants k_{mn} corresponding to the random functions $q-\bar{q}$, $v-\bar{v}$ by the equation

$$\ln\Theta(x,y) = \sum_{m,\,n=1}^{\infty}\frac{x^m y^n}{m!\,n!}k_{mn}.$$

Equating the last two equations we find

$$\beta_{mn} = k_{mn+1}.$$

If we know the $(m+p)$th velocity correlation function

$$k_{(m+p)v}(t_1, \ldots, t_{m+p}),$$

we can, by integrating, obtain the cumulant

$$k_{mp} = \int_{-\infty}^{t} \cdots \int k_{(m+p)v}(t_1, \ldots, t_m, t, \ldots t)\, dt_1 \ldots dt_m.$$

In particular, we find for the coefficients β_{10} and β_{01} (which are respectively equal to k_{11}, k_{02}) that they are expressed in terms of $k_2(\tau) = k_{(2)V}(t, t+\tau)$ by Eqs. (28).

---

[1] D. K. C. MacDonald, Phys. Rev. **108**, 541 (1957).

[2] V. B. Magalinskiĭ and Ya. P. Terletskiĭ, JETP **34**, 729 (1958), Soviet Phys. JETP **7**, 501 (1958).

[3] V. B. Magalinskiĭ, JETP **36**, 1423 (1959), Soviet Phys. JETP **9**, 1011 (1959).

[4] V. B. Magalinskiĭ and Ya. P. Terletskiĭ, JETP **36**, 1731 (1959), Soviet Phys. JETP **9**, 1234 (1959).

[5] Kuznetsov, Stratonovich, and Tikhonov, JETP **26**, 189 (1954).

Translated by D. ter Haar
160

SOVIET PHYSICS JETP VOLUME 11, NUMBER 3 SEPTEMBER, 1960

DEPENDENCE OF THE PARAMETERS OF THE NUCLEAR POTENTIAL ON THE NUMBER OF PARTICLES

M. Ya. AMUS' YA

Leningrad Physico-technical Institute, Academy of Sciences, U.S.S.R.

Submitted to JETP editor July 2, 1959

J. Exptl. Theoret. Phys. (U.S.S.R.) **38**, 834-842 (March, 1960)

The dependence of the oscillator potential parameters on the number of nucleons is determined starting from the assumption that the mean energy per nucleon in the nucleus is constant. The possible effect of three-particle interactions is considered.

THE present work is concerned with the problem of how well the shell model describes the integral properties of heavy nuclei, especially the separation energies Q of the last nucleon and the mean energy per nucleon E_m.

It is well known (see, for example, reference 1) that E_m is approximately constant for all nuclei. (E_m decreases slowly through the entire periodic system, from $E_m = 8.8$ Mev for $A = 55$, to $E_m \cong 7.6$ Mev for $A = 238$.) Therefore, to a rather high degree of accuracy, one can consider that*

$$\partial E_m / \partial A = 0. \tag{1}$$

For a system consisting of two-particle interactions, Eq. (1) is equivalent to

$$E_m = E_F, \tag{2}$$

where E_F is the Fermi energy of the system.

In order to demonstrate Eq. (2) in general, it is necessary to define E_F. Let the Hamiltonian of the system have the form

$$H_A = -\sum_{i=1}^{A} (\hbar^2/2m)\nabla_i^2 + \frac{1}{2}\sum_{i,k=1}^{A} U_{ik}, \tag{3}$$

$$H_A\psi = AE_m\psi. \tag{4}$$

We define E_F as

$$E_F = \left(\psi\left| -(\hbar^2/2m)\nabla_A^2 + \sum_{k=1}^{A-1} U_{Ak}\right|\psi\right),$$

where it is assumed that all

$$E_i = (\psi| -(\hbar^2/2m)\nabla_i^2 + \sum U_{ik}|\psi) \leqslant E_F.$$

Then, differentiating Eq. (4) with respect to A, multiplying by ψ^* and integrating over all A coordinates, we find that

$$E_m = E_F + \tfrac{1}{2}\left(\psi\left|\sum_{i,k}\partial U_{ik}/\partial A\right|\psi\right), \tag{5}$$

from which Eq. (2) follows if $\partial U_{ik}/\partial A = 0$.

We will illustrate Eq. (2) using the Hartree self-consistent field as an example:

$$E_m = \frac{1}{A}\Big(\sum_{i=1}^{A} T_i + \frac{1}{2}\sum_{i,k=1}^{A}\bar{U}_{ik}\Big),$$

$$T_i = -\int\psi_i^*(\hbar^2/2m)\nabla^2\psi_i\,d\tau_i,$$

$$\bar{U}_{ik} = \int\psi_i^*\psi_k^* U(\mathbf{r}_i - \mathbf{r}_k)\psi_i\psi_k\,d\tau_i\,d\tau_k.$$

From Eq. (1) it follows that

$$\frac{E_m}{A} = \frac{1}{A}\Big(T_A + \sum_{i=1}^{A-1}\bar{U}_{iA}\Big) + \frac{1}{A}\Big(\sum_i\frac{\partial T_i}{\partial A} + \frac{1}{2}\sum_{ik}\frac{\partial\bar{U}_{ik}}{\partial A}\Big),$$

but in so far as

$$\Big[-\frac{\hbar^2\nabla^2}{2m} + \sum_i\int\psi_i^*U\psi_i\,d\tau_i\Big]\psi_k = E_k\psi_k, \qquad \int\psi_k^*\psi_k\,d\tau_k = 1,$$

we have

$$\frac{1}{A}\Big(\sum_i\frac{\partial T_i}{\partial A} + \frac{1}{2}\sum_{i,k}\frac{\partial\bar{U}_{ik}}{\partial A}\Big) = 0,$$

which means that*

$$E_m = E_A = E_F.$$

Such a conclusion would be unjustified if tertiary collisions were present, since then U would depend upon A.

1. We assume that the potential well in the nucleus results from two-particle collisions only. Since we are interested in qualitative aspects of the problem, we consider, for simplicity, that the self-consistent potential is an oscillator well. Then the total number of particles in the system is equal to

$$A = \frac{1}{2}\sum_{n=0}^{N}(n+1)(n+2) + P_{N+1}, \tag{6}$$

---

*It can easily be seen that the conclusions below are not changed if $\partial E_m/\partial A \leq 0.01$.

*See reference 2, where it is shown that if $\partial E_m/\partial\rho = 0$, where ρ is the density of nuclear matter, then $E_m = E_F$ for arbitrary weak interaction.

where N is the principal quantum number of the last filled shell, P_{N+1} is the number of nucleons outside filled shells.

If

$$H = -(\hbar^2/2m)\nabla^2 - V_A + \tfrac{1}{2} m\omega_A^2 r^2,$$

then

$$E_{\mathrm{m}}^{(A)} = \frac{3}{4A}\sum \hbar\omega_A \left(n+\frac{3}{2}\right) - \frac{1}{2}V_A \tag{7}$$

and Eq. (1) can be written in the form*

$$\begin{aligned}\frac{3}{4}A\hbar\frac{\partial\omega_A}{\partial A}\left[\sum\left(n+\frac{3}{2}\right)+P_{N+1}\left(N+\frac{5}{2}\right)\right] &= \frac{A^2}{2}\frac{\partial V_A}{\partial A}+\frac{3}{4}\hbar\omega_A\left[\sum\left(n+\frac{3}{2}\right)\right.\\ &\left.+P_{N+1}\left(N+\frac{5}{2}\right)-A\left(N+\frac{5}{2}\right)\right].\end{aligned} \tag{8}$$

We then set

$$V_A = \hbar\omega_A\left[\left(N+\tfrac{3}{2}\right)+(1-\delta(P))\right]+\theta,$$

$$\delta(P) = \left.\begin{matrix}1\\0\end{matrix}\right\} \begin{matrix}\text{for } P=0;\\ \text{for } P\neq 0;\end{matrix} \tag{9}$$

where θ is the total energy of the last nucleon which, as will be shown, is not equal to its separation energy. Comparing V_A and V_{A+1}, we find

$$\partial V_A/\partial A = \hbar\left(N+\tfrac{5}{2}\right)\partial\omega_A/\partial A + \hbar\omega_A\delta(P) + \partial\theta/\partial A. \tag{10}$$

We introduce the notation:

$$B_N = \tfrac{1}{6}(N+1)(N^2+5N+6),$$

$$C_N = \tfrac{1}{8}(N+1)(N^3+7N^2+16N+12),$$

with $A = P + B_N$. Then, from Eqs. (8) – (10) we find

$$\begin{aligned}\hbar\left[\tfrac{3}{4}C_N+\tfrac{3}{4}P\left(N+\tfrac{5}{2}\right)-\tfrac{1}{2}A\left(N+\tfrac{5}{2}\right)\right]\partial\omega_A/\partial A &\approx \tfrac{1}{2}A\partial\theta/\partial A\\ +\hbar\left[\tfrac{3}{4}C_N/A+\tfrac{3}{4}P\left(N+\tfrac{5}{2}\right)/A-\tfrac{3}{4}\left(N+\tfrac{5}{2}\right)\right.&\\ \left.+\tfrac{1}{2}A\delta(P)\right]\omega_A.&\end{aligned} \tag{11}$$

Let $\partial\theta/\partial A = 0$. Assume that for a nucleus composed of closed shells +1 nucleon, $\omega_A \cong 5$ Mev. Starting from this assumption and Eq. (11) we will try to construct $\omega = \omega(A)$. For closed shells $\delta(P) = 1$ and $\partial\omega_A/\partial A > 0$, whereas for $P \neq 0$, $\partial\omega_A/\partial A > 0$. From Eq. (11) we obtain an equation determining the change in ω inside the shells in the process of filling:

$$\omega = \omega^{(1)}\frac{(B_N+P)\left[3C_N-2B_N\left(N+\frac{5}{2}\right)\right]}{B_N\left[3C_N+(P-2B_N)\left(N+\frac{5}{2}\right)\right]}, \tag{12}$$

where $\omega^{(1)}$ denotes the ω of the nucleus consisting of closed shells only. It is easy to see that the shape of the curve (12) is nearly independent of the principal quantum number. In the region of closed shells, the curve for ω undergoes a jump.*

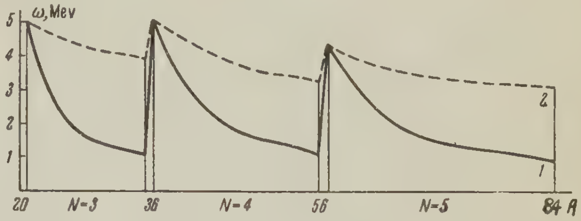

Change in the oscillator frequency with A. Curve 1 is for $\alpha = 0$, 2 for $\alpha = 0.5$ (qualitative curve).

For P = 0, we obtain $\partial\omega/\partial A$ from Eq. (11). The curve constructed from Eqs. (11) and (12) with $\omega_{A=21} = 5$ Mev is given in the figure. It is of interest that in the case of two-particle interactions, $\omega \cong$ const for $\partial\theta/\partial A = 0$ for nuclei consisting of closed shells +1 nucleon. We note that the requirement of constant volume per nucleon in the nucleus leads to a change in ω qualitatively analogous to that displayed in the figure. This is quite understandable, in so far as the conditions of constancy of volume and Eq. (1) are essentially equivalent. It is of interest to see how much $\omega(A)$ is affected by taking into account several factors which were neglected earlier. It was noted above that taking the dependence of E_m on A into account does not change the curve shown in the figure.

We did not take into account the fact that there can be two nucleons in each state. As can be seen from Eqs. (11) and (12), this does not change $\partial\omega/\partial A$ for closed shells, and diminishes $\partial\omega/\partial A$ inside the shell by a factor of about two. The shape of the curve is unchanged.

Taking into account the difference of $\partial\theta/\partial A$ from zero can qualitatively change the dependence of $\omega = \omega(A)$ if, as seen from Eq. (11), $\partial\theta/\partial A < 0$ and $|\partial\theta/\partial A| > \omega_A$. A substantial change in θ from an additional particle is, however, improbable. We shall therefore assume that $|\partial\theta/\partial A| \ll \omega_A$. For $P \neq 0$, even a small value of $\partial\theta/\partial A$ can substantially change the trend of the curve. If one assumes[1] that for a value of the order of $\partial\theta/\partial A \cong \partial Q/\partial A$ and P near (but not equal to) zero, one can neglect all of the terms in Eq. (11) except $\partial\theta/\partial A$, then, as numerical evaluation shows, one obtains

$$\hbar\partial\omega/\partial A = A\left[\tfrac{3}{2}C_N+\tfrac{3}{2}P\left(N+\tfrac{5}{2}\right)-A\left(N+\tfrac{5}{2}\right)\right]^{-1}\partial\theta/\partial A. \tag{13}$$

---

*If $\partial\omega/\partial A = \partial V_A/\partial A$ then Eq. (8) cannot be fulfilled.

*Use of a potential more realistic than the oscillator one would clearly lead to smoothing of the curve $\omega = \omega(A)$ in the region of shell closing.

If a substantial number of nucleons are outside closed shells, a term proportional to ω must be included in (11). In so far as ω is a discontinuous function, as we have seen earlier, one might wonder about the validity of expressions obtained by differentiating ω. However, it is clear that one can avoid differentiation by writing Eq. (1) as $E_m^{(A)} = E_m^{(A+1)}$. The result so obtained coincides with the above.

In all of the above results we neglected the presence of residual interaction. In order to include it, the total energy of the nucleus is written in the form

$$E = E_{\text{s.c.}} + \tfrac{1}{2} \sum_{ik} u_{ik}, \tag{14}$$

where U_{ik} is the energy of a residual interaction between pairs, $E_{\text{s.c.}}$ is the total energy of the system described by the self-consistent field. Setting $u_{ik} \cong u$, we find a formula differing from Eq. (11) by the presence of terms on the right-hand side:

$$\tfrac{1}{2} A (A-1)\, \partial u / \partial A + \tfrac{1}{2} (A-1)\, u. \tag{15}$$

Even a small change in the residual interaction can change the dependence of ω on A substantially. However, the applicability of the shell model in describing single-particle excitations indicates that $u \ll \hbar\omega$, at least. In this case, inclusion of the residual interaction does not change the jumps in ω in the region of closed shells; however, it might greatly change the dependence of ω on A inside the shells.

It is easy to relate $\partial V_i / \partial A$ and $\partial u_{ik} / \partial A$. To do this, one should consider that with a self-consistent field, the Hamiltonian (3) should be replaced by

$$H_A = -\sum_i \frac{\hbar^2 \nabla_i^2}{2m} + \sum_i V_i + \frac{1}{2} \sum_{ik} u_{ik}. \tag{16}$$

If the Hamiltonian (3) leads to (2), then an analogous relation follows also for (16). In so far as $\partial E_m / \partial A = 0$, then from (16) it follows that

$$E_m = E_F + \left(\psi \left| \sum_i \partial V_i / \partial A \right| \psi\right) + \tfrac{1}{2} \sum_{ik} (\psi \,|\, \partial u_{ik} / \partial A \,|\, \psi),$$

from which, taking Eq. (2) into account, we find

$$\left(\psi \left| \sum_i \partial V_i / \partial A \right| \psi\right) + \left(\psi \left| \tfrac{1}{2} \sum_{ik} \partial u_{ik} / \partial A \right| \psi\right) - \left(\psi \left| \tfrac{1}{2} \sum_{i,k} \partial U_{ik} / \partial A \right| \psi\right). \tag{17}$$

The potential V_i usually used in nuclear theory, which depends only on r and includes spin-orbit interaction, does not lead to $\partial E_m / \partial A = 0$. Therefore, $\partial V_i / \partial A \neq 0$ (this is confirmed by calculations of excited levels of several nuclei[3]). Since, as we shall show, in the nucleus $\theta \neq E_m$, i.e., $\partial U_{ik} / \partial A \neq 0$, it follows from Eq. (17) that $\partial V_i / \partial A$ and $\partial u_{ik} / \partial A \neq 0$ in general. We note that only indirect experimental data on u_{ik} exists, and this in insufficient quantity.

In so far as the calculation of residual interaction, the energy of which is $W = 2E_{A+1} - E_A - E_{A+2}$, is concerned, Eq. (1) leads to $W \equiv 0$. The experimentally observed values, $W = 1.5 - 3$ Mev, show that Eq. (1) is not exactly fulfilled in nuclei. Taking W into account, just as taking into account $\partial E_m / \partial A \ll 0.01$, does not change the curve 1 substantially.

We shall try now to take into account the effect of deformations of nuclei with a considerable number of nucleons outside closed shells on the dependence of ω on particle number. Employing the model of Inglis,[4] we write the total energy of the nucleus as (the nucleus is assumed to be stretched along the z axis)

$$E = E_1 + \beta E_2 + \beta^2 E_3, \tag{18}$$

where β is the nuclear deformation, parameter

$$E_1 = \tfrac{3}{4} \sum' \hbar\omega \left(n + \tfrac{3}{2}\right) - \tfrac{1}{2} V_A A,$$

$$E_2 = \tfrac{1}{2} \sum \hbar\omega \,(n - 3n_z),$$

$$E_3 = \tfrac{1}{2} \sum \hbar\omega \,(n + 3 + 3n_z), \tag{19}$$

and the sum is carried out over all occupied states. For close shells, $\beta = 0$; therefore, the positions of the jumps in $\omega = \omega(A)$ do not change by including the effect of deformations. For $\beta \neq 0$, we can write the expression for V_A, remembering that V_A does not increase gradually, but in jumps, with the filling of subshells (a subshell consists of a group of nucleons with the same n and n_z):

$$V_A = \hbar\omega \Big[\left(N + \tfrac{3}{2}\right) + \tfrac{2}{3} \beta (N - 3N_z - 3) + \tfrac{2}{3} \beta^2 (N + 3N_z + 6) + (1 - \delta(P)) + 2\beta (1 - \delta(s)) - 2\beta^2 (1 - \delta(s))\Big] + \theta, \tag{20}$$

where s is the number of nucleons in the last unfilled subshell, N_z is the quantum number along the symmetry axis corresponding to the last filled subshell. Then, instead of Eq. (11), we have:

$$\hbar(\partial\omega/\partial A)\left\{\tfrac{3}{4}C_N+\tfrac{3}{4}P\left(N+\tfrac{5}{2}\right)-\tfrac{1}{2}A\left(N+\tfrac{5}{2}\right)+\beta\left[\tfrac{1}{2}\sum(n-3n_z)-\tfrac{1}{3}A(N-3N_z)\right]+\beta^2\left[\tfrac{1}{2}\sum(n+3n_z+3)\right.\right.$$
$$\left.\left.-\tfrac{1}{3}A(N+3N_z+3)\right]\right\}=\tfrac{3}{4}\hbar\omega\left[C_N/A+P\left(N+\tfrac{5}{2}\right)/A-\left(N+\tfrac{5}{2}\right)+\tfrac{2}{3}A\delta(P)\right]+\beta\hbar\omega\left[A\delta(s)\right.$$
$$\left.+\left(\tfrac{1}{2}A^{-1}-\tfrac{1}{2}\partial/\partial A\right)\sum(n-3n_z)\right]+\beta^2\hbar\omega\left[-A\delta(s)+\left(\tfrac{1}{2}A^{-1}-\tfrac{1}{2}\partial/\partial A\right)\sum(n+3+3n_z)\right]$$
$$+\hbar\omega(\partial\beta/\partial A)\left[\tfrac{1}{3}A(N-3N_z)-\tfrac{1}{2}\sum(n-3n_z)\right]+\beta(\partial\beta/\partial A)\hbar\omega\left[\tfrac{2}{3}A(N+3N_z+3)-\sum(n+3n_z+3)\right]+\tfrac{1}{2}A\partial\theta/\partial A;$$
$$P=\tfrac{1}{2}(N-N_z)(N-N_z+3)+s_N+1. \tag{21}$$

The formula obtained is analogous to Eq. (11). If, as earlier, it is assumed that the total energy of the last nucleon changes so that $\beta\hbar\omega > \frac{1}{2}\partial\theta/\partial A$, then jumps in ω (small in magnitude) appear also in the region of the filling of subshells. In order to compare Eqs. (21) and (11), we give the relations between $\partial\omega/\partial A$ and ω, obtained from Eqs. (21) and (11) with $\beta_{max} = 0.3$ and $\beta = 0$ at the limits of the shells (see Table I):

The increase in absolute value of the quantity $\partial\omega/\partial A$ is explained by the appearance of jumps in the filling of subshells ($P = 1, 10, 21$). For $P = 0$

$$\hbar\partial\omega/\partial A=2.63\hbar\omega+2.80\,\partial\theta/\partial A.$$

The separation energies of the last nucleon and the mean energy per nucleon are known from experiment; from these, one can obtain θ and $\partial\theta/\partial A$. It does not follow that $\theta = E_F$ can be identified with the separation energy of the last nucleon Q:

$$Q=E_{A+1}-E_A\approx\tfrac{3}{4}C_N\hbar\partial\omega/\partial A+\tfrac{3}{4}P\hbar\partial\omega/\partial A$$
$$+\tfrac{3}{4}\hbar\omega\left(N+\tfrac{5}{2}\right)-\tfrac{1}{2}A\partial V/\partial A-\tfrac{1}{2}V_A+E_2\partial\beta/\partial A$$
$$+\beta\partial E_2/\partial A+2\beta E_3\partial\beta/\partial A+\beta^2\partial E_3/\partial A. \tag{22}$$

From Eqs. (7), (9), (19), and (22), θ and $\partial\theta/\partial A$ can be expressed in terms of Q and $E_m \equiv Q$ [if Eq. (1) is valid]. In particular, in the neighborhood of closed shells

$$\theta=2\hbar\omega\left[\tfrac{3}{4}A^{-1}C_N+\tfrac{3}{4}A^{-1}P\left(N+\tfrac{5}{2}\right)-\tfrac{1}{2}\left(N+\tfrac{5}{2}\right)+\tfrac{1}{2}\delta(P)-E_m/\hbar\omega\right],$$
$$\frac{\partial\theta}{\partial A}=\frac{2}{A}\left\{\left(\hbar\frac{\partial\omega}{\partial A}-\frac{\hbar\omega}{A}\right)\left[\tfrac{3}{4}C_N+\tfrac{3}{4}P\left(N+\tfrac{5}{2}\right)-\tfrac{1}{2}A\left(N+\tfrac{5}{2}\right)\right]\right.$$
$$\left.+\hbar\omega\left[\frac{N}{4}+\frac{1}{8}-\frac{A}{2}\delta(P)\right]\right\}. \tag{23}$$

From Eq. (23) it follows that, as assumed above, $\partial\theta/\partial A \ll \omega$. This conclusion remains valid if terms depending on β are taken into account. For closed shells, for example, $\theta \cong -2E_m$ and $\frac{1}{2}A\partial\theta/\partial A \geq 0$. Inside shells $\theta \leq -2E_m$ and $\frac{1}{2}A\partial\theta/\partial A \leq 0$. Consequently, within the framework of our assumptions

$$E_m \neq E_F. \tag{24}$$

It was shown above that in systems with two-particle interactions, $E_m = E_F$ in Eq. (1) is valid. We calculated E_m for nuclei, assuming that the two-particle interaction led to a self-consistent oscillator potential, took account of (1) and came to Eq. (24), in contradiction to Eq. (2). In addition, it turned out that if $\partial\theta/\partial A \cong 0$, ω changes sharply in the region of closed shells. The difference between E_m and E_F can be explained either by the dependence of the two-particle interaction on A or by the inclusion of a three-particle force.

2. Within the Hartree approximation, a system with three-particle interactions is equivalent to one with two-particle interactions if

$$U_{ik}=\sum_l(\psi_l|v_{ikl}|\psi_l).$$

Here $\partial U_{ik}/\partial A \neq 0$. We assume that the inclusion of the three-particle interaction, together with the two-particle one, leads to an oscillator self consistent potential. Then, in the expression for E_m, the potential energy will be prefixed by the coefficient $\frac{1}{2}-\frac{1}{3}\alpha$, rather than $\frac{1}{2}$, where α characterizes the relative contribution of the three-particle interaction in the mean energy per nucleon.

We shall first show that inclusion of the three-

TABLE I. Values of $\hbar\partial\omega/\partial A = a\hbar\omega + b\partial\theta/\partial A$ for $N = 5$

	P	1	2	10	11	21	22
$\beta\neq0$	a	−0.094	−0.251	0.354	−0.095	0.212	−0.204
	b	+1.07	+1.07	+1.10	+1.10	+1.29	+1.29
$\beta=0$	a	−0.122	−0.122	−0.047	−0.047	−0.050	−0.050
	b	+2.18	+2.18	+1.12	+1.12	+0.765	+0.765

TABLE II. Values of $\hbar\partial\omega/\partial A = a\hbar\omega + b\partial\theta/\partial A$ for N = 5

	P	1	2	10	11	21	22
$\beta=0$	a	≈ -0.023	≈ -0.023	≈ -0.015	-0.015	-0.020	-0.020
	b	$+0.317$	$+0.317$	$+0.266$	$+0.266$	$+0.234$	$+0.234$
$\beta\neq 0$	a	-0.031	-0.072	-0.066	-0.036	0.047	-0.037
	b	$+0.274$	$+0.274$	$+0.251$	$+0.251$	$+0.26$	$+0.26$

particle interaction does not lead to a qualitative change in the dependence of ω on A:

a) for closed shells it follows from Eq. (11) that the sign of $\partial\omega/\partial A$ changes for $\alpha \neq 0$ if

$$\left\{\tfrac{3}{4} C_N - \tfrac{1}{2} A\left(N + \tfrac{5}{2}\right)\right\} \to \left\{\left(\tfrac{3}{4} - \tfrac{1}{6}\alpha\right) C_N - \left(\tfrac{1}{2} - \tfrac{1}{3}\alpha\right) A\left(N + \tfrac{5}{2}\right)\right\}$$

changes sign with the growth of α from 0 to 1. In so far as $C_N > \tfrac{2}{3}A(N+\tfrac{5}{2})$ then $C_N > A(N+\tfrac{5}{2}) \times (\tfrac{1}{2} - \tfrac{1}{3}\alpha)/(\tfrac{3}{4} - \tfrac{1}{6}\alpha)$ if $\alpha \geq 0$;

b) inside shells the coefficient of $\partial\omega/\partial A$ does not change sign as α increases from 0 to 1, since the sign of the coefficient of ω in Eq. (11) does not depend on α (within the limits $0 \leq \alpha \leq 1$). Consequently, the character of the curve, i.e., the signs of $\partial\omega/\partial A$ and the positions of jumps in ω, is unchanged.

The situation with the mean energy is different; its magnitude depends essentially on α. This is connected with the fact that the coefficient of $\partial\omega/\partial A$ in Eq. (11) changes within very large limits with changing α. For example, for $N=5$, $\alpha = 0$, the quantity $\{\tfrac{3}{4}C_N - \tfrac{1}{2}A(N+\tfrac{5}{2})\} = 10$ for $\alpha = 0.5$, whereas it is equal to 56 for $\alpha = 0.5$ and 100 for $\alpha = 1$. Already, for $\alpha = 0.1$, the coefficient of $\partial\omega/\partial A$ is doubled. Inclusion of the three-particle interaction, while not changing the character of the curve* 1, can diminish the jumps in ω several times and can make the dependence of ω on A smoother.

The parameters of the potential well obtained from calculations of low-lying excited states of nuclei are roughly equal[3] for nuclei consisting of closed shells ±1 nucleon. From this it is difficult to assert that the scheme of a two-particle type of self-consistent potential is inapplicable, and that it is necessary to introduce a three-particle interaction. However, if one succeeds in showing that $\partial\theta/\partial A \cong 0$, then the constancy of the potential would have to be explained by introducing a three-particle interaction.

The dependence of ω on A for $\alpha \neq 0$ is obtained analogously to Eq. (12)

$$\omega = \omega^{(1)} \frac{(B_N + P)\left[(9-2\alpha) C_N - (6-4\alpha) B_N (N + {}^5/_2)\right]}{B_N\left[(9-2\alpha)C_N - (6-4\alpha)B_N(N + {}^5/_2) + (3+2\alpha)P(N+{}^5/_2)\right]}. \tag{25}$$

For closed shells, $\partial\omega/\partial A$ is obtained from Eq. (11) by the substitutions $\tfrac{3}{4} \to \tfrac{3}{4} - \tfrac{1}{6}\alpha$; $\tfrac{1}{2} \to \tfrac{1}{2} - \tfrac{1}{3}\alpha$; The formulas (13) and (23) are modified, and the coefficient 2 in Eq. (14) is replaced by $6/(3-2\alpha)$. For example, $\theta \cong -3E$ for $\alpha = 0.5$.

We now take into account effects of nucleon deformation. Proceeding in the same way as in the derivation of Eq. (21), and taking into account the three-particle interaction, we obtain instead of Eq. (21)

$$\begin{aligned}
&\hbar(\partial\omega/\partial A)\left\{\tfrac{1}{12}(9-2\alpha)C_N + \tfrac{1}{12}(9-2\alpha)P\left(N+\tfrac{5}{2}\right)\right.\\
&\quad - \tfrac{1}{6}(3-2\alpha)A\left(N+\tfrac{5}{2}\right) + \beta\left[\sum \tfrac{1}{18}(9-2\alpha)(n-3n_z)\right.\\
&\quad \left.- \tfrac{1}{9}(3-2\alpha)A(N-3N_z)\right] + \beta^2\left[\sum\tfrac{1}{18}(9-2\alpha)(n+3+3n_z)\right.\\
&\quad \left.\left.- \tfrac{1}{9}(3-2\alpha)(N+3N_z+3)\right]\right\} = \tfrac{1}{12}(9-2\alpha)\hbar\omega\left[C_N/A\right.\\
&\quad \left.+ (P/A-1)\left(N+\tfrac{5}{2}\right) + (6-4\alpha)/(9-2\alpha)A\delta(P)\right]\\
&\quad + \beta\hbar\omega\left[\tfrac{1}{3}(3-2\alpha)A\delta(s) + \tfrac{1}{18}(9-2\alpha)(A^{-1}-\partial/\partial A)\right.\\
&\qquad \left.\sum(n-3n_z)\right] + \beta^2\hbar\omega\left[-\tfrac{1}{3}(3-2\alpha)A\delta(s)\right.\\
&\quad \left.+ \tfrac{1}{18}(9-2\alpha)(A^{-1}-\partial/\partial A)\sum(n+3n_z+3)\right]\\
&\quad + \hbar\omega(\partial\beta/\partial A)\left[\tfrac{1}{9}(3-2\alpha)A(N-3N_z)\right.\\
&\quad \left.- \tfrac{1}{18}(9-2\alpha)\sum(n-3n_z)\right] + \hbar\omega\beta\,\partial\beta/\partial A\left[\tfrac{2}{9}(3-2\alpha)\right.\\
&\qquad \left.A(N+3N_z+3) - \tfrac{1}{9}(9-2\alpha)\sum(n+3n_z+3)\right]\\
&\quad + \tfrac{1}{6}(3-2\alpha)A\,\partial\theta/\partial A.
\end{aligned} \tag{26}$$

The effect of α in the quantity $\partial\omega/\partial A$ can most easily be shown by a concrete example. Values of $\hbar\partial\omega/\partial A$ for $\alpha = 0.5$, $N = 5$, $\beta_{\max} = 0.3$ are given in Table II. It is easy to obtain expressions for $\theta = E_m$, analogous to Eqs. (22) and (23), including the three-particle interaction.

Recently a number of authors have discussed the use of a potential which depends on momentum (or, which is the same thing, the so-called effective mass approximation) in the shell model. A number of arguments can be adduced, according to which a system of strongly-interacting nucleons can be replaced by a model system of weakly-interacting quasiparticles (of number equal to the number of nucleons) so that the energies of the ground and low-excited states coincide in the two cases.[5]

---

*Equations (11) and (23) are not independent, but are connected by Eq. (1). Therefore, there is left to our disposal one parameter $\partial\theta/\partial A$ which can be and should be chosen so that for nuclei consisting of closed shells +1 nucleon, $\omega \cong$ const.

Construction of a self-consistent potential for quasiparticles in nuclear matter leads to its dependence on the momentum of the quasiparticle, or to an effective mass, which, in turn, depends (but only weakly) on the momentum.[5] In the case of finite nuclei it is also possible to go over to a model system of quasiparticles, moving with effective mass in the field of a self-consistent potential (and the self-consistent potential and effective mass depend on the quantum numbers defining the quasiparticle state, see reference 6). Therefore, it might be hoped that replacement of the true mass by the effective mass would diminish the magnitude of the residual interaction [see Eq. (14)]. It is of interest to see how much the introduction of an effective mass changes the conclusions reached above. It is easy to see that introduction of the same effective mass for all nucleons is equivalent to increasing the frequency ω_A by the factor $(m/m_{\text{eff}})^{1/2}$. Repeating the above development, we see that the qualitative character of curve 1 is not changed, but that the depth of the potential well is increased by a factor of about $(m/m_{\text{eff}})^{1/2}$.

We note that the discontinuous changes in the parameters of the shell-model potential came, as seen from the above conclusions, from changes in the depth of the potential well with the addition of a single nucleon outside a closed shell. In fact, for arbitrary potential, the following relation is valid [compare Eq. (9)]:

$$V = -\sum_{i<j} \Delta E_{ij} - \theta,$$

where ΔE_{ij} is the distance between energy shells (the summation is carried out over the totality of filled or partially filled energy shells). Addition of a particle outside a closed shell adds one term to the sum over $i < j$ [see the term $\hbar\omega\,[1 - \delta(P)]$ in Eq. (9)]. Consequently, the discontinuous change in parameters also appears in use of a potential more realistic than the oscillator one.

It is known that the data on scattering of nucleons by nuclei are rather well described by an optical potential of constant depth and radius $R \sim A^{1/3}$. This does not, however, contradict the conclusions reached earlier about the shell-model potential. The situation is that for higher energies of the incident nucleon, the real part of the optical potential depends essentially on the energy of the incident nucleon and differs from the shell-model potential. We give below several considerations, according to which the real part of the optical potential should, for arbitrary energy of the incident nucleon, differ in general from the shell-model potential.

3. Up to now the problem of the change in the potential well of the nucleus necessary to ensure fulfilment of Eq. (1) was considered. In the problem of the interaction of an incident nucleon with the nucleus, the Hamiltonian is written as

$$(-\hbar^2\nabla^2/2m + U^{(A+1)}).$$

If the incident nucleon leads to a complete recomposition of the target nucleus, then

$$U^{(A+1)} = U^{(A)} + \partial U^{(A)}/\partial A, \qquad (27)$$

or if there is no recomposition, $U^{(A+1)} = U^{(A)}$.

In the present work, using Eq. (1), the magnitude of $\partial U^{(A)}/\partial A$ was found, i.e., the correction to the real part of the optical potential for low energies. From this it is clear that calculations of excited states of nuclei by several authors using the optical potential do not have a strong basis in view of Eq. (27). For an oscillator potential we have

$$V^{(A+1)} = -(N + \tfrac{5}{2})(\hbar\omega + \hbar\partial\omega/\partial A)$$
$$+ \tfrac{1}{2} m(\omega + \partial\omega/\partial A)^2 r^2 - \theta - \partial\theta/\partial A,$$

where $\partial\omega/\partial A$ is determined either from Eq. (11) or from Eqs. (21) and (26).

In conclusion, it is my pleasant duty to express my deep gratitude to L. A. Sliv for numerous discussions and interest.

---

[1] V. A. Kravtsov, Usp. Fiz. Nauk **54**, 1 (1954).

[2] N. M. Hugenholtz and L. van Hove, Physica **24**, 363 (1958).

[3] L. A. Sliv and B. A. Volchok, JETP **36**, 539 (1959), Soviet Phys. JETP **9**, 374 (1959).

[4] D. Inglis, Phys. Rev. **96**, 1059 (1954).

[5] K. A. Brueckner and J. L. Gammel, Phys. Rev. **109**, 1023 (1958).

[6] K. A. Brueckner, Proc. of the Int. Conf. on the Nuclear-Optical Model, Tallahasee, 1959.

Translated by G. E. Brown
161

SOVIET PHYSICS JETP VOLUME 11, NUMBER 3 SEPTEMBER, 1960

DISPERSION IN HIGH-DENSITY, HIGH-TEMPERATURE MEDIA

G. S. SAAKYAN

Erevan State University

Submitted to JETP editor July 2, 1959

J. Exptl. Theoret. Phys. (U.S.S.R.) **38**, 843-849 (March, 1960)

The dispersion properties of high-density, high-temperature media are investigated; media of this kind may exist in the inner regions of irregular stars (white super dwarfs). Single photon annihilation and electron pair creation occur at electron densities $N_e \gtrsim 10^{32}$ cm^{-3}. At frequencies which satisfy the inequality in Eq. (31) electromagnetic waves are scattered on nucleons rather than electrons. The index of refraction at these frequencies and densities is given approximately by $n \approx 1 + 1.05 \times 10^{-41} N$ (N is the neutron density). Hard Cerenkov radiation can be excited in a medium of this kind. The energy of the Cerenkov photons satisfies the inequality in Eq. (35).

SCATTERING OF ELECTROMAGNETIC WAVES BY ELECTRONS

WE have shown earlier[1] that under certain physical conditions single photon annihilation and electron pair production $\gamma \rightleftarrows e^+ + e^-$ can occur in a scattering medium with a refractive index smaller than unity. In vacuum these processes can take place only in the presence of an additional particle. However, single photon annihilation and pair production do not occur in all media with refractive indices smaller than unity. In addition to this condition there are certain requirements on the density of particles and the temperature of the medium. The density requirement follows directly from a consideration of the meaning of the refractive index in a medium. Obviously, a refractive index is meaningful only if the following condition is satisfied:

$$\lambda\!\!\!^{-} \gg l, \qquad (1)$$

where l is the mean distance between electrons and $\lambda\!\!\!^{-}$ is the length of the electromagnetic wave divided by 2π.

From (1) and the fact that the production and annihilation of electron pairs require a photon energy greater than $2mc^2$, where m is the mass of the electron, it follows that the effect being discussed here can occur only when the particle density in the medium is sufficiently high:

$$N \gg 8\lambda\!\!\!^{-}_e{}^{-3} \approx 1.4 \cdot 10^{32} \text{ cm}^{-3}, \qquad (2)$$

where $\lambda\!\!\!^{-}_e$ is the electron Compton wavelength divided by 2π. It would appear that densities of this kind are in fact found in the inner regions of white super dwarfs.

It is apparent that atoms are completely ionized under these physical conditions so that the ensemble of electrons constitutes a relativistic ideal gas. At densities given by (2) the mean kinetic energy of electrons is of order mc^2 and higher while the ratio of potential energy Ze^2/r to kinetic energy cp is $Ze^2/crp \approx Ze^2/\hbar c \ll 1$.

For the densities of interest here the degeneration temperature of the electron gas is

$$T_0 \gg 4 \cdot 10^{10}. \qquad (3)$$

It is difficult to say whether the electron gas in a star is degenerate or nondegenerate. It is possible that there are white dwarfs of both types in nature. These two cases lead to completely different physical results. In the first case, at sufficiently high densities we are dealing with a medium whose dispersion properties at very high frequencies are determined by neutrons rather than by electrons. In a medium of this kind the refractive index is greater than unity; hence the process $\gamma \rightleftarrows e^+ + e^-$ is forbidden. On the other hand, another phenomenon can occur: charged particles moving with velocities exceeding the phase velocity of light can emit hard Cerenkov radiation, with photon energies up to 150 Mev. In the absence of degeneracy, however, the dispersion properties of a medium are always determined by the electrons. In a medium of this kind at densities given by (2) the process $\gamma \rightleftarrows e^+ + e^-$ is allowed while Cerenkov radiation is not. Both of these limiting cases will be discussed in detail below.

When the electron gas is not degenerate it is apparent that the dispersion is always determined by the electrons. As is well known, at frequencies greater than characteristic atomic frequencies the refractive index of a medium is given by the relation

$$n^2 = 1 - 4\pi N e^2 / m\omega^2. \tag{4}$$

However, this relation cannot be used in the present case because its derivation assumes that the electrons are nonrelativistic whereas the electrons are relativistic in the case at hand.

At densities given by (2) electrons are quasi-classical particles. Provisionally, we may also assume that the quasi-classical approach is valid at relatively low electron densities; in particular we require that the mean distance between particles be somewhat smaller than the Fermi radius of the atom $l \ll Z^{1/3}\hbar^2/me^2$.

In order to calculate the refractive index we must find the additional velocity $\mathbf{v}' = \mathbf{v} - \mathbf{v}_0$ acquired by a free electron under the influence of the electromagnetic field. Solving the Hamiltonian-Jacoby equation for an electron in a field of a plane electromagnetic wave $\mathbf{A}(\mathbf{r}, t) = \mathbf{A}_0 \exp\{i(\mathbf{k}\cdot\mathbf{r} - \omega t)$

$$[\nabla S - (e/c)\,\mathbf{A}]^2 - c^{-2}(\partial S/\partial t)^2 + m^2c^2 = 0 \tag{5}$$

and then computing the velocity $\mathbf{v}$ from the formula

$$(1 - \beta^2)^{-1/2} m\mathbf{v} = \nabla S - (e/c)\,\mathbf{A}, \tag{6}$$

we obtain the additional velocity $\mathbf{v}'$:

$$\mathbf{v}' = -\frac{ec}{E_0}\mathbf{A} + \frac{ec^2(\mathbf{p}_0\mathbf{A})\,\mathbf{k}}{E_0[c(\mathbf{p}_0\mathbf{k}) + kE_0]} - \frac{ec^4(\mathbf{p}_0\mathbf{k})(\mathbf{p}_0\mathbf{A})\,\mathbf{p}_0}{E_0^3[c(\mathbf{p}_0\mathbf{k}) + kE_0]} + \frac{ec^3}{E_0^3}(\mathbf{p}_0\mathbf{A})\,\mathbf{p}_0, \tag{7}$$

where p_0 and $E_0 = c(p_0^2 + m^2c^2)^{1/2}$ are the initial momentum and energy.

We now determine the current induced by the electromagnetic field:

$$\mathbf{j}' = e\int \mathbf{v}' f(p_0)\, dp_0 \sin\vartheta\, d\vartheta\, d\varphi, \tag{8}$$

where $f(p)$ is the electron distribution in momentum space.* Substituting Eq. (7) in Eq. (8) and carrying out the integration over angles (i.e., over the initial direction of motion of the electron), we obtain

$$\mathbf{j}' = i\frac{2\pi e^2c^2}{\omega}\mathbf{E}\int\left(1 + \frac{m^2c^3}{Ep}\ln\frac{E + cp}{mc^2}\right)\frac{f(p)}{E}\, dp, \tag{9}$$

where $\mathbf{E}$ is the electric field intensity. Now, comparing the microscopic and macroscopic field equations and taking account of Eq. (9) we find the following formula for the index of refraction:

$$n^2 = 1 - \frac{8\pi^2e^2c^2}{\omega^2}\int\left(1 + \frac{m^2c^2}{Ep}\ln\frac{E + cp}{mc^2}\right)\frac{f(p)}{E}\, dp. \tag{10}$$

First we consider the case in which the gas is degenerate. In this case

$$f(p) = p^2/4\pi^3\hbar^3 \text{ for } p < p_f,$$
$$f(p) = 0 \text{ for } p > p_f; \tag{11}$$

where p_f is the limiting Fermi momentum, which is given by

$$p_f = (3\pi^2)^{1/3}\hbar N^{1/3}. \tag{12}$$

When $p_f \ll mc$ we obtain the familiar formula (4); when $p_f \geq mc$ we have

$$n^2 = 1 - (\omega_0/\omega)^2, \tag{13}$$

$$\omega_0^2 \approx 3\pi ce^2 N / p_f \approx 3c^2 N^{2/3} / 137. \tag{14}$$

Thus, for a relativistic degenerate gas the constant ω_0^2 is proportional to $N^{2/3}$ rather than N.

We now consider the case in which the electron gas is not degenerate. Under these conditions we have[2]

$$f(p) = N\varphi(T)[p^2/4\pi(mc)^3]\exp(-E/\chi T), \tag{15}$$

$$\varphi(T) = [2u^{-2}K_1(u) + u^{-1}K_0(v)]^{-1}. \tag{16}$$

The quantities K_1 and K_0 are Bessel functions of the second kind of imaginary argument while $u = mc^2/\chi T$ (χ is the Boltzmann constant). When $u \gg 1$ we have

$$\varphi \approx 4\pi(mc)^3(2\pi m\chi T)^{-3/2}e^u,$$

and when $u \ll 1$ we have $\varphi \approx u^3/2$.

As in the preceding case, upon substitution of Eq. (15) in Eq. (10) we obtain an integral which cannot be integrated exactly. When $u \lesssim 1$, as an approximation we have

$$n^2(\omega) \approx 1 - \frac{4.8\,\pi e^2}{m\omega^2}\frac{N\varphi}{u}e^{-u}. \tag{17}$$

When $u \gg 1$, Eq. (17) no longer applies and does not give the proper transition to the familiar formula. As we see, in the absence of degeneracy the refractive index depends on temperature.

It is apparent that in the absence of degeneracy, in the region in which one can apply the notion of the dielectric constant of a medium, the dispersion is always determined by the electrons. Consequently, at electron densities $N_e \gtrsim 1.4 \times 10^{32}$ cm^{-3} photon annihilation and electron pair production can occur in a medium.

We now consider the second limiting case; here the electron gas is highly degenerate (temperatures $T \ll 4 \times 10^{10}$). (In this case there are still two possibilities: either the neutrons are not degenerate or the neutron gas is also degenerate.) Under these physical conditions it turns out to be more favorable thermodynamically to have reactions in which the nucleus captures an electron and simultaneously emits a neutrino.[2] Because of this reaction the number of protons in the nucleus is reduced sharply and eventually the nucleus becomes unstable and decays. As a result we must in fact consider an ideal gas of electrons, protons, and neutrons.

---

*We omit from now on the subscript "zero" from the symbols for the momentum and energy.

The number of particles of each kind is determined from the equilibrium condition, that is to say, from the condition that the thermodynamic potential be a minimum for a given pressure and temperature. For the reactions

$$p + e^- \rightarrow n + \nu \text{ and } n \rightarrow p + e^- + \bar{\nu}.$$

where e^-, p, n, ν and $\bar{\nu}$ denote the electron, the proton, the neutron, the neutrino and the antineutrino respectively, the equilibrium condition is

$$\mu_p + \mu_e = \mu_n, \tag{18}$$

where μ_e, μ_p and μ_n are the chemical potentials for the corresponding particles. The electron chemical potential is

$$\mu_e = E_f \approx \pi c\hbar N_e^{1/3}, \tag{19}$$

where E_f is the limiting Fermi energy.

If the nucleon gas is not degenerate, we have[2]

$$\mu_p = \chi T \ln\left[\frac{N_p}{2}\left(\frac{2\pi\hbar^2}{M\chi T}\right)^{3/2}\right]; \ \mu_n = \chi T \ln\left[\frac{N_n}{2}\left(\frac{2\pi\hbar^2}{M_n\chi T}\right)^{3/2}\right]. \tag{20}$$

Substituting the values of the chemical potentials in Eq. (18) and using the obvious relation $N_p = N_e$, we find*

$$N_n = N_e \exp(\pi c\hbar N_e^{1/3}/\chi T). \tag{21}$$

Since the electron gas is assumed to be highly degenerate $\chi T \ll \pi c\hbar N_e^{1/3}$ and, consequently, $N_n \gg N_e$.

Now we assume that at the densities being considered the temperatures are so low that the neutron and proton gases are also highly degenerate. In this case

$$\mu_p = Mc^2 + (\hbar^2/2M)(3\pi^2 N_e)^{2/3},$$
$$\mu_n = M_n c^2 + (\hbar^2/2M_n)(3\pi^2 N_n)^{2/3}, \tag{22}$$

where $M_n = M + \alpha m$ is the mass of the neutron and $\alpha \approx 2.54$ is the difference in the masses of the neutron and proton expressed in units of electron mass. Here we assume that the proton and neutron are nonrelativistic particles, as is the case for matter densities up to the order of nuclear densities. Substituting Eqs. (19) and (22) in the equilibrium relation (18) we find

$$N_e = \varkappa^{-3} N_0 \{[1 + \alpha\varkappa/\pi + \varkappa^2 (N_n/N_0)^{2/3}]^{1/2} - 1\}^3, \tag{23}$$

where we have introduced the notation $N_0 = 8\lambda\!\!\!^-{}_e^{-3} = 1.4 \times 10^{32}\ \text{cm}^{-3}$ and $\kappa = 2\pi m/M$.

If we limit ourselves to densities of the order of nuclear densities or smaller, $N_n \lesssim 10^{38}\ \text{cm}^{-3}$, Eq. (23) can be simplified:

$$N_e \approx (N_0/8)[\alpha/\pi + \varkappa (N_n/N_0)^{2/3}]^3. \tag{23'}$$

In order to ascertain whether the process $\gamma \rightleftarrows e^+ + e^-$ with the participation of the medium is possible or not, we must first understand the role played by the nucleons in the scattering of electromagnetic waves.

2. SCATTERING OF ELECTROMAGNETIC WAVES ON NUCLEONS

Under certain physical conditions, i.e., high matter densities, low temperatures (so that the electron gas may be considered highly degenerate), and high frequencies, electromagnetic waves are scattered on nucleons rather than on electrons, Under these conditions hard Cerenkov radiation is produced of necessity.

To understand the nature of this effect, we investigate the dispersion properties of a medium consisting of neutrons. We compute the refractive index of such a medium for electromagnetic waves and determine the frequencies and neutron densities for which the dispersion properties of the medium are determined by the neutrons rather than by electrons (we should speak generally of nucleons; however, under the physical conditions of interest the number of protons is small compared with the number of neutrons, so that we shall consider only the latter although the results also apply to protons).

Although it is electrically neutral, the neutron is capable of scattering γ quanta. This effect is related to the well-known phenomenon of meson photoproduction. Both virtual and real mesons can be created in the interaction of photons with neutrons. The creation of real mesons corresponds to absorption of a wave; hence the refractive index of a medium consisting of neutrons is a complex quantity:

$$\sqrt{\varepsilon} = n + in_1. \tag{24}$$

The following relation obtains between the real and imaginary parts of the index of refraction:[3]

$$n(\omega) = 1 + \frac{2}{\pi}\int_0^\infty \frac{\varkappa n_1(\varkappa)}{\varkappa^2 - \omega^2}\, d\varkappa, \tag{25}$$

where the bar means that the integral is to be understood in the sense of the principal value. Expressing $n_1(\kappa)$ in terms of the photoproduction cross section:

---

*It is appropriate to note that there are no positrons in the medium at the temperatures being considered here. These particles appear only when $\chi T > mc^2$ (cf. reference 2, page 334). Because the electron gas is degenerate pair production is forbidden by the Pauli principle.

$$n_1(\varkappa) = (c/2\varkappa)\, N_n \sigma(\varkappa), \tag{26}$$

we find

$$n(\omega) = 1 + \frac{cN_n}{\pi} \int_0^\infty \frac{\sigma(\varkappa)\, d\varkappa}{\varkappa^2 - \omega^2}. \tag{27}$$

To compute n we start with the experimental curves for the cross sections for photoproduction of neutral pions on protons.[4-6] This curve exhibits two maxima: the first is very narrow and well defined ($\hbar\omega = 320$ Mev) while the second is very weak and broad ($E \sim 700$ Mev).

The neutron density increases towards the center of the star and, in accordance with (1), the region for which we can use the notion of a refractive index shifts towards the higher-energy quanta. In the limiting case we deal with nuclear densities. Under these conditions the mean distance between particles is $\hbar/\mu c$ (μ is the mass of the pion) and, correspondingly, the limiting photon energy should be of the order of 150 Mev. Hence, we can speak of a refractive index for neutron matter only at photon energies $\hbar\omega \lesssim 150$ Mev. In this energy region $\sigma(\omega) = 0$ and the principal maximum is found at an energy which is twice 150 Mev. It is thus clear that, since we are interested in frequencies $\hbar\omega \lesssim 150$ Mev, the detailed dependence of $\sigma(\omega)$ on ω is unimportant for the determination of $n(\omega)$. As a good approximation to the true curve shown in the figure we can use a discontinuous curve (shown by dashes); the dashed curve is chosen to make the area between it and the abscissa axis approximately the same as the area formed by the experimental curve. Further, we assume that the cross sections for photoproduction of neutral and positive pions on protons are the same (as is approximately the case[5,6]) and that the cross sections for photoproduction on neutrons and protons are also equal. Thus, for $\sigma(\omega)$ we have:

$$\sigma(\omega) = \begin{cases} 0 & \text{for} \quad \omega < \omega_1, \\ \sigma_1 & \text{for} \quad \omega_1 < \omega < \omega_2, \\ \sigma_2 & \text{for} \quad \omega > \omega_2; \end{cases} \tag{28}$$

where $\sigma_1 = 5 \times 10^{-28}$ cm², $\sigma_2 = 0.62 \times 10^{-28}$ cm², $\omega_1 = 3.7 \times 10^{23}$ is the frequency corresponding to a photon energy of 240 Mev, and $\omega_2 = 6.1 \times 10^{23}$ is the same quantity for an energy of 400 Mev.

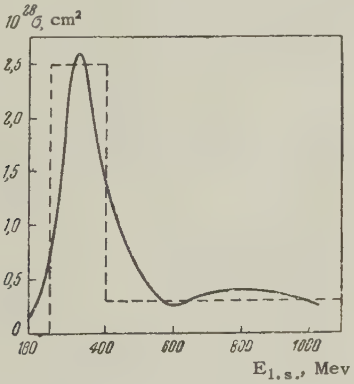

Since we are interested only in the frequency region $\hbar\omega \ll 150$ Mev $\sim \hbar\omega_1$ we can neglect ω in the integrand in Eq. (27). Then, using Eq. (28) we have

$$n^2 - 1 \approx \frac{2cN}{\pi} \left(\frac{\sigma_1}{\omega_2} - \frac{\sigma_1 - \sigma_2}{\omega_2} \right) = 2{,}1 \cdot 10^{-41}\, N_n. \tag{29}$$

Thus, the dielectric constant of neutron matter is essentially independent of frequency and always very close to unity.

In the final analysis, to determine whether the dispersion properties of the medium are determined by the electrons or by the neutrons, we must compare Eq. (29) with Eq. (13). The dispersion is determined by the neutrons when

$$(n^2 - 1)/(1 - n_e^2) = 2{,}1 \cdot 10^{-41} N_n\, (\omega/\omega_0)^2 > 1, \tag{30}$$

where the subscript e refers to the electron. From Eq. (14), substituting the value of ω_0 we find

$$\omega^2 N_n > 10^{60} N_e^{2/3}. \tag{31}$$

First we consider the case in which the nucleon gas is not degenerate. According to Eqs. (21) and (31) the condition that dispersion be determined by electrons is given by the relation

$$N_e^{1/3} \exp(aN_e^{1/3}/T) < 3{,}6 \cdot 10^{17}\, (\omega_0/\omega)^2, \tag{32}$$

where we have introduced the following notation: $\hbar\omega_0 = 2mc^2$, $a = \pi c\hbar/\chi \approx 0.72$. Taking account of the inequality in (1) $\omega \lesssim cN_e^{1/3}$, we find that when $aN_e^{1/3}/T \lesssim 15$ the process $e^+ + e^- \rightarrow \gamma$ is possible in the medium. At lower temperatures, however, this process is forbidden. The inverse process, $\gamma \rightarrow e^+ + e^-$, is forbidden by the Pauli principle; it becomes possible, however, if vacancies appear in the electron distribution because of various processes. The dispersion is determined by the neutrons when

$$3{,}6 \cdot 10^{17}\, (N_0/N_e)^{2/3} \exp(-2aN_e^{1/3}/3T) \leqslant 3.6 \cdot 10^{17} (\omega_0/\omega)^2$$
$$< N_e^{1/3} \exp(aN_e^{1/3}/T); \tag{33}$$

Here, the condition at the left means $\omega \lesssim cN_n^{1/3}$. Whence it is apparent that when $aN_e^{1/3}/T = 15$ and $\omega \gtrsim 7\,\omega_0$ the dispersion is determined by the neutrons; at frequencies below $7\,\omega_0$ the dispersion is determined by the electrons.

When the nucleon gas is also degenerate the electron density becomes a relatively weak function of neutron density. When $N_n < 10^{36}$ we have $N_e \sim N_0/8$ and $cN_e^{1/3} \approx 0.5\,\omega_0$ so that the processes $\gamma \rightleftarrows e^+ + e^-$ either do not occur at all in the medium or appear at the very threshold for the effect ($\hbar\omega \approx 2mc^2$). At densities of $N \gtrsim 8 \times 10^{35}$, however, the electron density becomes sufficient for creation and annihilation of pairs. As before, in order to determine whether this effect actually occurs we must find the frequencies at which dispersion is determined by the electrons and those at which it is determined by the neutrons. To find these frequencies we again use the condition in (31). According to Eqs. (23′) and (31) dispersion is determined by the neutrons when

$$N_n > 2.4 \cdot 10^{38} \nu^{-2} [\alpha/\pi + \varkappa (N_n/N_0)^{2/3}]^2, \qquad (34)$$

where $\nu = \omega/\omega_0$. As always, Eq. (34) must be supplemented by the criterion which must be satisfied if we are to use the idea of a medium, i.e., $\omega \lesssim cN_n^{1/3}$. When $N_n \lesssim 10^{36}$ the process $\gamma \rightleftarrows e^+ + e^-$ is possible and will occur only at threshold energy; the condition $N_n \gtrsim 10^{36}\ \mathrm{cm}^{-1/3}$ is necessary and sufficient (obviously we still must satisfy the requirement for this process $\omega \lesssim cN_e^{1/3}$).

On the basis of the material presented in this section we can conclude that for a given matter density there is a certain critical frequency above which dispersion is determined by neutrons; below this frequency the dispersion is due to electrons. According to Eq. (29), above the critical frequency the refractive index is greater than unity and remains essentially constant, being independent of frequency. It is clear that charged particles moving with velocities exceeding the phase velocity of light in such a medium will emit Cerenkov radiation. In accordance with the conditions in (1) and (31), only photons which satisfy the following inequality are radiated:

$$10^3 N_e^{1/3} N_n^{-1/2} < \hbar\omega \lesssim \hbar c N_n^{1/3}. \qquad (35)$$

In this energy range the number of photons radiated per energy interval is uniform. According to Eq. (29) the Cerenkov effect appears at particle energies $E \geq 2.2 \times 10^{20} N_n^{-1/2} Mc^2$ where Mc^2 is the self energy of the particle.

When the nucleon gas is not degenerate the relation between the densities N_e and N_n is given by Eq. (21). For purposes of illustration we take $aN_e^{1/3}/T = 10$; then, from Eq. (35) with $N_e = 10^{32}$ (i.e., $N_n = 2.2 \times 10^{36}$) we find $20 < \hbar\omega \lesssim 28$ Mev while with $N_e = 4.5 \times 10^{33}$ (i.e., $N_n = 10^{38}$) we have $10 < \hbar\omega \lesssim 100$ Mev.

When the nucleon gas is also degenerate the relation between N_e and N_n is given by Eq. (23′). In this case (35) assumes the following form:

$$2.6 \cdot 10^{13} N_n^{-1/2} [\alpha/\pi + \varkappa (N_n/N_0)^{2/3}] < \hbar\omega \lesssim hcN_n^{1/3}. \qquad (35')$$

Whence we find that the neutron density must be $N_n \gtrsim 8 \times 10^{35}$. With $N_n = 10^{36}\ \mathrm{cm}^{-3}$, from Eq. (35′) we find $13 < \hbar\omega \lesssim 20$ Mev while with $N_n = 10^{38}$ we find $1.6 < \hbar\omega \lesssim 100$ Mev.

In conclusion I wish to express my gratitude to Academician V. A. Ambartsumyan for valuable comments and also to N. M. Kocharyan, I. I. Gol'dman, G. M. Garibyan, and A. Ts. Amatuni for many discussions and for their interest in this work.

---

[1] G. S. Saakyan, Dokl. Akad. Nauk ArmSSR **29**, 23 (1959); JETP **38**, 1593 (1960), Soviet Phys. JETP **11**, in press.

[2] L. D. Landau and E. M. Lifshitz, Статистическая физика (Statistical Physics) Gostekhizdat, 1951.

[3] L. D. Landau and E. M. Lifshitz, Электродинамика сплошных сред (Electrodynamics of Continuous Media) Gostekhizdat, 1957.

[4] M. Gell-Mann and K. M. Watson, Ann. Rev. Nuclear Sci. Vol. 4, 1954, Stanford.

[5] Heinberg, McClelland, Turkot, Woodward, Wilson, and Zipoy, Phys. Rev. **110**, 1211 (1958).

[6] J. I. Vette, Phys. Rev. **111**, 622 (1958).

Translated by H. Lashinsky
162

SOVIET PHYSICS JETP VOLUME 11, NUMBER 3 SEPTEMBER, 1960

INSTABILITY OF LONGITUDINAL OSCILLATIONS OF AN ELECTRON-ION PLASMA

L. M. KOVRIZHNYKH and A. A. RUKHADZE

P. N. Lebedev Physical Institute, Academy of Sciences, U.S.S.R.

Submitted to JETP editor July 4, 1959

J. Exptl. Theoret. Phys. (U.S.S.R.) **38**, 850-853 (March, 1960)

The problem of the instability of longitudinal oscillations of low temperature electron-ion plasma is discussed. In an isotropic plasma the oscillations are always damped, while in an anisotropic one the ion motion may lead to the appearance of solutions that increase with time, i.e., to instability.

RECENTLY problems connected with the instability of a current flowing through a plasma, and particularly those connected with the instability of longitudinal plasma waves, have come in for ever increasing attention. Thus, Bohm and Gross[1] and Akhiezer and Faĭnberg[2] have investigated the oscillations of a plasma containing an electron beam and have demonstrated that the oscillations increase with time. In these studies ion motion was altogether neglected. In some cases, however, inclusion of ion motion may prove essential and produce new forms of plasma instability due to electron-ion interaction (see below).

Let $f_{0e}(\mathbf{v})$ and $f_{0i}(\mathbf{v})$ represent equilibrium electron and ion distribution functions (normalized to unity). For a given equilibrium distribution the asymptotic behavior of the solution is determined, as is known,[3] by the roots of the dispersion equation

$$1 = \frac{i\omega_{0e}^2}{k^2}\left\{\int d\mathbf{v}\,\frac{\mathbf{k}\partial f_{0e}/\partial\mathbf{v}}{s + i\mathbf{k}\mathbf{v}} + \delta\int d\mathbf{v}\,\frac{\mathbf{k}\partial f_{0i}/\partial\mathbf{v}}{s + i\mathbf{k}\mathbf{v}}\right\}, \tag{1}$$

where $\omega_{0e}^2 = 2\pi e^2 n_e/m_e$, $\delta = zm_e/m_i$ (z is the ion charge), $\mathbf{k}$ is the wave vector, and $s = i\omega + \gamma$. Since we shall be concerned only with solutions that increase with time ($\gamma > 0$), the integrals in (1) can be taken along the real axis. Before proceeding to the discussion of a concrete case, we shall make a few general remarks.

If we transform Eq. (1) by integration by parts and separate the result into a real and imaginary part we obtain a system of two equations for ω and γ. One of these equations has the following form:

$$\gamma\int d\mathbf{v}\,[f_{0e}(\mathbf{v}) + \delta f_{0i}(\mathbf{v})]\,\frac{\omega + \mathbf{k}\mathbf{v}}{[(\omega + \mathbf{k}\mathbf{v})^2 + \gamma^2]^2} = 0. \tag{2}$$

Two conclusions follow directly from this equation.

First, oscillations with frequency $\omega > k\bar{v}$ are always stable, while oscillations with frequency $\omega < k\bar{v}$ may be unstable. Thus, the following inequality is a condition for instability:

$$\bar{v} > \omega/k = v_{\mathrm{ph}}, \tag{3}$$

where $\bar{v}$ represents some average value of the velocity. Condition (3) means that only waves whose phase speed is less than the average speed of the particles can be unstable. (This condition was first noted by Bohm and Gross.[1]) We shall show that condition (3) is necessary but insufficient; this will become apparent from an example discussed below.

Secondly, in the case of an isotropic plasma the oscillations are always stable for arbitrary distributions of the form $f_{0e}(v^2)$ and $f_{0i}(v^2)$. Actually, by integrating Eq. (2) over all directions in the velocity space, we find

$$\gamma\omega\int_0^\infty v^2 dv\,\frac{f_{0e}(v^2) + \delta f_{0i}(v^2)}{[\gamma^2 - \omega^2 + k^2v^2]^2 + 4\omega^2\gamma^2} = 0, \tag{4}$$

whence it follows that $\gamma = 0$. The contrary assertion in the article by Bohm and Gross[1] is the result of an error in the computation of the integral appearing in the dispersion relation. Their result would have been incorrect none the less if only because of the fact that when the integration is along the real axis, as Landau has demonstrated,[3] it is in principle impossible to obtain damped solutions.

Let us examine a case where the electron gas is described by a drifting Maxwellian distribution, while the ion distribution is isotropic and likewise Maxwellian, i.e.,

$$\begin{aligned} f_{0e}(\mathbf{v}) &= (m_e/2\pi\varkappa T_e)^{3/2}\exp\{-m_e(\mathbf{v} - \mathbf{u})^2/2\varkappa T_e\}, \\ f_{0i}(\mathbf{v}) &= (m_i/2\pi\varkappa T_i)^{3/2}\exp[-(m_i\mathbf{v}^2/2\varkappa T_i)]. \end{aligned} \tag{5}$$

Such a case might occur in a plasma located in a strong electric field.[4]

Substituting (5) in Eq. (1), we obtain the following dispersion equation:

$$F([s+i\mathbf{ku}]^2, \alpha_e) + \delta F(s^2, \alpha_i) + \omega_{0e}^{-2} = 0. \tag{6}$$

The following designations apply here

$$\alpha_e = m_e/2\varkappa T_e, \qquad \alpha_i = m_i/2\varkappa T_i;$$

$$F(s^2, \alpha) = \frac{2\alpha}{k^2}\left\{1 - \sqrt{\pi\alpha}\,\frac{s}{k}\,w\left(i\alpha^{1/2}\frac{s}{k}\right)\right\},$$

$$w(z) = e^{-z^2}\left(1 + \frac{2i}{\sqrt{\pi}}\int_0^z e^{t^2}\,dt\right). \tag{7}$$

Equation (6) with $u = 0$ was studied by Silin[5] and Kovrizhnykh[6] who showed that when k is small, two modes of plasma oscillations occur, which are entirely different in their properties. The first mode, called optical, is characterized by comparatively large oscillations of the charge density while the ion motion is insignificant. For this mode of plasma oscillations, $\omega(k) \neq 0$ with $k = 0$. The optical mode is obtained by solving Eq. (6) with $u = 0$ and with the second term neglected. The second, or acoustic mode, on the other hand, is characterized by small oscillations of the charge density and a linear dependence of s on k.

An analogous division into optical and acoustic modes may also be adopted for the case where $u \neq 0$. The optical mode will correspond, as for the case $u = 0$, to the solution of Eq. (6) with the second term omitted. Naturally the solution of this equation will differ from the corresponding solution where $u = 0$ due to the appearance of the imaginary term $i\mathbf{k}\cdot\mathbf{u}$, which corresponds to a Doppler effect due to the electron motion. The character of the oscillations specified by the real part of s does not change, i.e., the optical oscillations are attenuated regardless of the magnitude of u. This circumstance indicates the insufficiency of condition (3). It is a different matter with the second, or acoustic, mode of plasma oscillations. When $u \neq 0$, the acoustical solution of Eq. (6) may be unstable. The frequency region where $s^2\alpha_i/k^2 \gg 1$ corresponds to the unstable solutions of Eq. (6). Therefore, if we make use of the asymptotic representation of $\omega(z)$ in the region where $\mathrm{Re}(s) > 0$, we obtain from Eq. (6) the following dispersion equation, correct to terms $\sim k^2/s^2\alpha_i$:

$$[(s+i\mathbf{ku})^2 + k^2v_e^2]^{-1} + \delta/(s^2 + k^2v_i^2) + \omega_{0e}^{-2} = 0, \tag{8}$$

where $v_e^2 = 3kT_e/m_e$, $v_i^2 = 3kT_i/m_i$, represent the thermal speed of the electrons and ions respectively. As was noted above, the linear dependence of s on k is characteristic of the acoustic mode. Therefore, it is always possible to isolate a region of k-space in which $s^2 \ll \omega_{0e}^2$. In this case the last term in Eq. (8) can be neglected. This also corresponds to neglecting oscillations of the charge density. Finally, we obtain the following solution for Eq. (8):

$$s = -i\mathbf{ku}\delta + [\delta(\mathbf{ku})^2 - k^2(\delta v_e^2 + v_i^2)]^{1/2}. \tag{9}$$

Because of the asymptotic representation used for w(z), Eq. (9) is correct when $|\mathbf{k}\cdot\mathbf{u}|^2/k^2 \gg v_e^2$, v_i^2/δ and $(\mathbf{k}\cdot\mathbf{u})^2 \ll \omega_{0e}^2$. In this region Eq. (9) predicts unstable plasma oscillations.*

In addition to solution (9), an acoustic solution of Eq. (8) can be obtained when the term ω_{0e}^2 is included but with $|s| \ll |\mathbf{k}\cdot\mathbf{u}|$. In this case, neglecting terms of the order of $\sqrt{\delta}$ in comparison with unity, we find

$$s = \gamma = \omega_{0e}\delta^{1/2}(\mathbf{ku})\,[\omega_{0e}^2 - (\mathbf{ku})^2]^{-1/2}, \tag{10}$$

which is applicable when $\omega_{0e}^2 - (\mathbf{k}\cdot\mathbf{u})^2 > \omega_{0e}^2\delta^{1/3}$.

Thus in a plasma whose electrons have an average speed greater than their thermal speed, the acoustic oscillations may become unstable. In this case, the energy of the electron motion is converted into energy of acoustic oscillations and is the source of the instability. We note that a similar instability can occur in a plasma in which part of the electrons have a fast drift, i.e., in a plasma containing so-called "runaway" electrons. In this case, besides the excitation of unstable acoustic oscillations, there will be excitation of unstable optical oscillations with s given by an expression of the form of Eq. (10) but with δ equal to the ratio of the number of runaway electrons to the total number of electrons.

In conclusion we note that an instability of this type appears to have been observed experimentally.[8]

The authors are grateful to M. S. Rabinovich and V. P. Silin for their helpful comments.

---

[1] D. Bohm and E. P. Gross, Phys. Rev. **75**, 1864 (1949).

[2] A. I. Akhiezer and Ya. B. Faĭnberg, JETP **21**, 1262 (1951).

[3] L. D. Landau, JETP **16**, 574 (1946), see J. Phys. (U.S.S.R.) **10**, 25 (1946).

[4] L. M. Kovrizhnykh, JETP **37**, 1394 (1959), Soviet Phys. JETP **10**, 989 (1960).

[5] V. P. Silin, JETP **23**, 649 (1952).

[6] L. M. Kovrizhnykh, JETP **37**, 1692 (1959), Soviet Phys. JETP **10**, 1198 (1960).

[7] G. V. Gordeev, JETP **27**, 19 (1954).

[8] Bernstein, Chen, Heald, and Kranz, Phys. Fluids **1**, 430 (1958).

Translated by A. Skumanich
163

---

*The case where $u^2 \ll v_e^2$ and $n_eT_e \gg n_iT_i$ has been investigated by Gordeev.[7]

SOVIET PHYSICS JETP VOLUME 11, NUMBER 3 SEPTEMBER, 1960

ON THE PROCESSES INVOLVING TRANSFER OF MOMENTUM TO THE MEDIUM

M. I. RYAZANOV

Moscow Engineering Physics Institute

Submitted to JETP editor July 18, 1959

J. Exptl. Theoret. Phys. (U.S.S.R.) **38**, 854-862 (March, 1960)

The change of the transition probability caused by the Coulomb scattering of particles by the atoms of the medium is found for a certain class of processes in which there are one charged particle and an arbitrary number of neutral particles in the initial and final states.

1. INTRODUCTION

EXPERIMENTAL studies of processes of interaction of high-energy particles are often made in rather dense substances. As a rule the data obtained in such experiments are compared with the theoretical results of calculations of the probability of the given process in vacuum. This means an implicit use of the hypothesis that possible participations of the atoms of the surrounding substance in the process lead only to vanishingly small corrections to the transition probability. In particular, this applies to the possible transfer of some part of the momentum to atoms of the medium through Coulomb scattering of the particles involved in the process.

The incorrectness of this assumption was first pointed out by Landau and Pomeranchuk,[1] who showed that multiple scattering of a particle by atoms of the medium causes a considerable change in the bremsstrahlung. In the case of bremsstrahlung a transfer of momentum to the medium would occur even if the Coulomb scattering were not taken into account. Therefore it is convenient to take account of the additional transfer of momentum to the medium in the treatment of the basic process. The position is different, however, when one treats a process that occurs spontaneously in vacuum. Transfer of momentum to atoms of the medium leads to the appearance of a new type of process, qualitatively different from the basic process. For example, spontaneous π-μ decay is possible in vacuum. In matter one has besides the spontaneous type of decay the possibility of an "induced" or "deceleration" type of decay, in which atoms of the medium take part in the process, receiving part of the momentum of the initial particle. Since in the usual experimental arrangement the momentum transferred to the medium is not measured, the experimentally observed transition probability must include both the spontaneous and the "induced" processes.

We present below a general method for calculating probabilities of processes with transfer of momentum to atoms of the medium taken into account, and we consider the change of the transition probability owing to this effect for the simplest cases. We note that this effect occurs already in the approximation linear in the density of medium atoms, in which the action of each atom is considered independently. Therefore in most cases it is not necessary to deal with multiple scattering, and we can confine ourselves to first-order perturbation theory in the potential of the atoms of the medium.

We consider only cases of very fast charged particles, with momenta large in comparison with the reciprocal of the Thomas-Fermi radius of the atom, $\lambda = me^2Z^{1/3}$ ($\hbar = c = 1$). This means that we can consider only Coulomb scattering by the nuclei of the atoms, including the action of the electron shells in terms of a screening factor only.

We also note the following fact: The occurrence of finite energy losses in the motion of a charged particle through matter has the consequence that, unlike the situation for vacuum, the imaginary term in the mass of the particle, which Feynman introduced to prescribe the correct way of going around the poles for the Green's function, is now a finite, though indeed small, quantity. The finite value of this quantity is also due to the presence of the electron shells of the atoms. We shall neglect here effects associated with the finiteness of the imaginary term in the mass.

In treating the interaction of a charged particle with an individual atom we shall neglect retardation and the recoil of the atom, restricting the treatment to not very large momentum transfers. Under the assumptions that have been made the total potential of all the atoms of the medium, $U(x) = \sum_a U_0(x - x_a)$ [$U_0(x - x_a)$ is the potential of an individual atom], can be regarded as an external field. The total potential $U(x)$ depends on the specific (but unknown) distribution of the atoms of an amorphous medium. Therefore in the final results there must be an averaging over the coordinates x_a of the atoms; this is denoted by the symbol $\langle \ldots \rangle$. Because the medium as a whole is neutral, $\langle U(x) \rangle$ is a constant independent of x. To simplify the writing it is convenient to introduce instead of U the potential $V(x) = U(x) - \langle U(x) \rangle$, including the constant $\langle U(x) \rangle$ in the definition of the fourth component of the momentum of the charged particle. Thus the problem reduces to the calculation of the transition probability in an external field $V(x)$.

2. THE MATRIX ELEMENT OF THE PROCESS IN AN EXTERNAL FIELD

Let us consider a process whose initial and final states involve one charged particle, the initial and final four-momenta being p_1 and p_2. Besides this particle, there can be an arbitrary number of neutral particles in both the initial and the final states. Let us denote the difference of the four-momenta of the neutral particles in the initial and final states by k. Assuming that the Coulomb scattering of virtual particles can be neglected, we shall deal with the effects of the scattering of the initial and final charged particles by the potential V.

The matrix element of the process in vacuum can always be put in the form

$$M_0 = \int dx \bar{\psi}_{02}(x)\, O(k)\, \psi_{01}(x) \exp(ikx), \qquad (2.1)$$

where $\psi_{01}(x)$ and $\psi_{02}(x)$ are the wave functions of the initial and final charged particles in vacuum. In what follows we shall assume them normalized so that there is one particle in a large volume Ω. For example, for spin ½ we have $\psi_{01}(x) = \Omega^{-1/2} u_1 \times \exp(-ip_1x)$. In this connection we shall always understand the three-dimensional integral over momenta to mean the sum,

$$\int d^3p \to (2\pi)^3 \Omega^{-1} \sum_{\mathbf{p}}, \qquad \delta(\mathbf{p} - \mathbf{p}') = \Omega (2\pi)^{-3} \delta_{\mathbf{p},\mathbf{p}'}.$$

The matrix element of the process in the external field can be obtained from Eq. (2.1) by replacing the vacuum wave functions ψ_{01} and ψ_{02} by the wave functions of the charged particles in the external field. Assuming that the effect of the external field is small, we can determine the desired wave functions by perturbation theory. Assuming the momentum l transferred to the external field small in comparison with the momentum of the particle, in the first nonvanishing approximation in l/p and in second-order perturbation theory in V we can get the expression

$$\psi_{1(2)}(x) = C_{1(2)} \{1 + f_{1(2)}(x)\} \psi_{01\,(2)}(x); \qquad (2.2)$$

where $f(x)$ denotes the quantity

$$f(x) = 2E \int \frac{dl V(l) \exp(ilx)}{l^2 + 2pl + i\delta} \left\{1 + 2E \int \frac{dl' V(l') \exp(il'x)}{(l + l')^2 + 2p(l + l') + i\delta}\right\}, \qquad (2.3)$$

and the normalization constant C is determined from the requirement that the wave function of the particle in the medium be normalized just like that of the particle in vacuum (one particle in the volume Ω). It follows that the normalization constant C is given by

$$C^{-1} = \Omega^{-1/2} \left[\int dx\, |1 + f(x)|^2\right]^{1/2}. \qquad (2.4)$$

It may seem that the normalization constant C should be set equal to unity, since the difference $1 - C^2$ contains the large volume Ω in its denominator. Actually this must not be done, since in the numerator of the difference $1 - C^2$ there is a quantity proportional to the total number N of the atoms of the medium. The ratio of these quantities is proportional to the number of atoms per unit volume, and remains constant as the normalization volume goes to infinity. Therefore we must not neglect the difference between the normalization constant C and unity.

From what has been said it follows that the matrix element of the process in the external field can be written in the form

$$M = \int dx \exp(ikx) (\bar{\psi}_{02}(x)\, O(k)\, \psi_{01}(x)) (1 + f_2^*(x)) (1 + f_1(x)). \qquad (2.5)$$

Assuming for definiteness that the charged particles have spin ½, and denoting the momentum $p_1 - p_2 - k$ transferred to the external field by s, we can transform Eq. (2.5) to the form

$$M = \int dx \exp(-isx) (\bar{u}_2 O(p_1 - p_2 - s) u_1) \times (1 + f_2^*(x)) (1 + f_1(x)). \qquad (2.6)$$

3. THE TRANSITION PROBABILITY IN THE EXTERNAL FIELD

From Eq. (2.6) it is easy to get the square of the absolute value of the matrix element and the transition probability for the process in the external field. As is well known, the differential transition probability is connected with the matrix element by the formula

$$dW = \frac{d}{dt} |M|^2 d^3p_1 d^3p_2 d^3k_1 \ldots d^3k_\nu (2\pi)^{-3(\nu+2)}, \quad (3.1)$$

where ν is the number of neutral particles in the final state, and $k_1, \ldots, k_\nu$ are the momenta of these particles. We can replace the integration over one of the momenta of the neutral particles in the final state by integration over k, and then go over from integration over k to integration over the momentum s transferred to the medium. Since for a process in vacuum the integration over the momentum of one particle is always taken between infinite limits by means of a δ function, we can perform the integration over s between infinite limits without destroying the correspondence with the vacuum case.

Using this idea, we easily get from Eq. (3.1)

$$dW = \frac{d}{dt} C_1^2 C_2^2 \iint dx\, dx' \int d^3s \exp[is(x - x')]$$
$$\times |(\bar{u}_2 O(p_1 - p_2 - s)\, u_1|^2 \; (1 + f_1(x))$$
$$\times \; (1 + f_1^*(x'))(1 + f_2(x'))$$
$$\times \; (1 + f_2^*(x))(2\pi)^{-3(\nu+2)} d^3p_1\, d^3p_2\, d^3k_1 \ldots d^3k_{\nu-1}. \quad (3.2)$$

Carrying out the integration over x and x′, one easily convinces oneself that only small values of s play any part in the integral over s. Therefore, provided the difference $p_1 - p_2$ is not small, the quantity $|\bar{u}_2 O(p_1 - p_2 - s) u_1|^2$ is a slowly varying function of s as compared with the exponential. Taking this slowly varying function from under the integral sign, we can relate the transition probability in the external field to the transition probability dW_0 in vacuum:

$$dW = \frac{dW_0 \Omega \int d^3x\, (1 + b_1(x))\, (1 + b_2(x))}{\int d^3x\, (1 + b_1(x)) \int d^3x'\, (1 + b_2(x'))}, \quad (3.3)$$

where we have used the notation

$$b(x) = |1 + f(x)|^2 - 1.$$

It is easy to see from Eq. (3.3) that inclusion of the normalization leads to cancellation from the final result of all terms associated with the effect of the external field on only the initial or only the final particle. In fact, using the smallness of b(x), we can get from Eq. (3.3) the formula

$$dW = dW_0 (1 + \Omega^{-1} \int d^3x b_1(x)\, b_2(x) - \Omega^{-2}$$
$$\times \int d^3x b_1(x) \int d^3x' b_2(x')). \quad (3.4)$$

When we substitute in Eq. (3.4) the explicit expression for $b_1(x)$ and $b_2(x)$ we must remember that we are using perturbation theory for the external field, so that in Eq. (3.4) we must include only the part of b(x) linear in the field, dropping terms quadratic in the field. Besides this we must note that in the cases we are concerned with, in which the external field is that of an individual atom, or else we are using the external potential $V(x) = U(x) - \langle U(x) \rangle$, the last term in Eq. (3.4) is zero. Therefore the final expression for the transition probability in the medium is connected with the transition probability in vacuum by the formula

$$dW = dW_0 \{1 + (2\pi)^3 \Omega^{-1} 4E_1E_2 \int d^3l\, |V(\mathbf{l})|^2 [(\mathbf{l}^2 + 2\mathbf{p}_1\mathbf{l} - i\delta)^{-1}$$
$$+ (\mathbf{l}^2 - 2\mathbf{p}_1\mathbf{l} + i\delta)^{-1}][(\mathbf{l}^2 + 2\mathbf{p}_2\mathbf{l} + i\delta)^{-1}$$
$$+ (\mathbf{l}^2 - 2\mathbf{p}_2\mathbf{l} - i\delta)^{-1}]\}. \quad (3.5)$$

Let us apply this formula to the case in which we are dealing with the external field of an individual atom. Then in virtue of the fact that in our approximation the effects of the atoms on the process are treated independently, to get the total effect of N atoms we must multiply the correction for one atom by the total number of atoms. Thus we get from Eq. (3.5) the result

$$dW = dW_0 \{1 + n(2\pi)^3 4E_1E_2\, 2\,\mathrm{Re} \int d^3l\, |U_0(\mathbf{l})|^2$$
$$\times (\mathbf{l}^2 + 2_2\mathbf{p}\mathbf{l} - i\delta)^{-1} [(\mathbf{l}^2 + 2\mathbf{p}_1\mathbf{l} - i\delta)^{-1}$$
$$+ (\mathbf{l}^2 - 2\mathbf{p}_1\mathbf{l} - i\delta)^{-1}]\}, \quad (3.6)$$

where n is the number of atoms per unit volume.

Exactly the same formula is obtained if we consider the process in the external potential $V(x) = U(x) - \langle U(x) \rangle$. If we use the fact that in the momentum representation the total potential U is connected with the potential U_0 of an individual atom by the relation $U(p) = U_0(\mathbf{p})\,\delta(p_4) \times \sum_a \exp(i\mathbf{p} \cdot \mathbf{r}_a)$, we easily show that $\langle |V(\boldsymbol{l})|^2 \rangle = N|U_0(\boldsymbol{l})|^2$. By using this result one gets Eq. (3.6) from Eq. (3.5).

4. APPLICATION OF THE DIAGRAM TECHNIQUE

The result obtained above can also be found by a different method, by using an analogy with the diagram technique of quantum field theory. In the derivation of Eq. (3.6) the averaging over the positions of the medium atoms was carried out only in the concluding stage of the calculations. We can arrive at the analogy with quantum field theory if we do the averaging over the positions of the atoms somewhat earlier. Let us consider the average value of the product of two potentials V(l) and V(l') in the momentum representation. Using the fact that

$$\left\langle \sum_a \exp(i\mathbf{p}\mathbf{r}_a) \right\rangle = N\delta_{\mathbf{p},0} = n(2\pi)^3\delta(\mathbf{p}),$$

we easily get

$$\langle V(l)V(l')\rangle = F(l)\delta^{(4)}(l+l'),$$

$$F(l) = n(2\pi)^3|U_0(\mathbf{l})|^2\delta(l_4). \qquad (4.1)$$

The presence of the four-dimensional δ function on the right enables us to regard Eq. (4.1) as an expression analogous to the propagation function of a quasi-particle. If both potentials V(l) and V(l') are in the same matrix element, the averaging of their product leads to a transfer of momentum from one particle to another (from one point of a diagram to another). Therefore the average value (4.1) can be graphically represented by connecting the points of action of the potentials on a Feynman diagram by a dotted line. In other words, such average values are taken into account in the same way as the exchange of a virtual photon, but with the propagation function (4.1).

There is also another possible case, in which one of the potentials to be averaged is in the matrix element M and the other in the Hermitian adjoint matrix element M^+. Using the fact that there is always an integration over the momenta l and l' transferred to the external field, we can put the result of integrating the expression (4.1) in the form

$$n(2\pi)^3\int d^3l\,|U_0(\mathbf{l})|^2. \qquad (4.2)$$

It is easily seen that the average values (4.2) are to be taken into account in just the same way as the emission of real photons, but with the factor $e(2\omega)^{-1/2}$ replaced by $n^{1/2}(2\pi)^{3/2}U_0(\mathbf{l})^2$ and with an integration over the momenta of the emitted "quasi-particles." Average values of this type correspond to a mean transfer of momentum to atoms of the medium.

These arguments make our problem of the calculation of the probability of a process with account taken of transfer of momentum to the medium entirely analogous to the problem of the calculation of radiative corrections to the process in question; we are here concerned not with corrections caused by the electromagnetic interaction, but with those caused by interactions with "quasi-particles." As is well known, in the calculation of radiative corrections to the experimentally observable cross section one must include not only radiative corrections owing to the exchange of virtual photons, but also those processes occurring in the same order of the perturbation theory and involving the emission of small quanta that are not registered by the experimental apparatus. The corresponding diagrams are shown in Fig. 1.

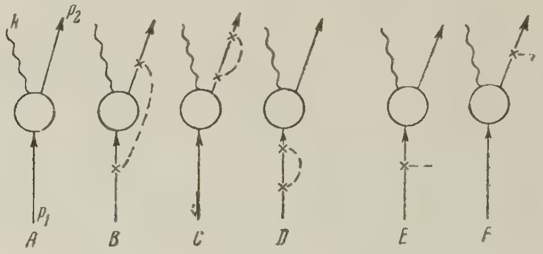

FIG. 1

Diagrams C and D contain proper-energy parts in external lines. A renormalization of the wave function must be carried out in the corresponding parts of the matrix element; it can, for example, be performed by the Feynman method.[2] This renormalization leads to the same results as the normalization of the wave function in the external field which was done in the preceding section.

The cancellation in the final result of all expressions involving the effect of the external field on only one initial or one final particle is analogous to the cancellation of the infrared divergence in the case of the electromagnetic radiative corrections.

It is convenient to represent all the terms contributing to the final result by so-called generalized Feynman diagrams, in which together with the graph corresponding to the matrix element there is also drawn its mirror image, corresponding to the Hermitian adjoint matrix element. Figure 2 shows

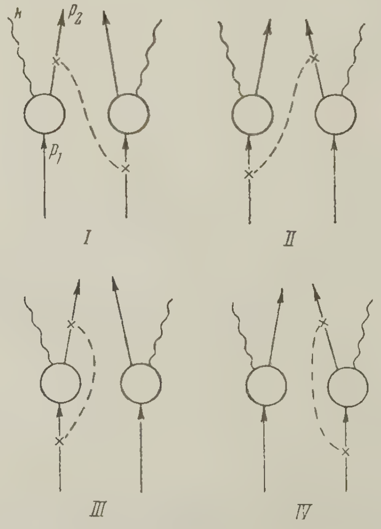

FIG. 2

all the diagrams of this kind; diagrams I and II correspond to transfer of momentum to the medium (emission of "quasi-particles"), and diagrams III and IV correspond to the process without mean momentum transfer to the medium (exchange of virtual "quasi-particles").

It is easily verified that by means of the diagram technique one again gets Eq. (3.6).

5. THE EXPERIMENTALLY OBSERVED TRANSITION PROBABILITY

To obtain the probability of a process in the medium we must substitute in Eq. (3.6) the explicit expression for the potential U_0 of an individual atom:

$$U_0(r) = (Ze^2/r)\exp(-\lambda r); \quad U_0(\mathrm{p}) = (Ze^2/2\pi^2)(\mathrm{p}^2+\lambda^2)^{-1}. \tag{5.1}$$

From Eqs. (3.6) and (5.1) we get the formula for the transition probability in the medium

$$dW = dW_0\Big\{1 + (2/\pi)\,4E_1E_2\,2\,\mathrm{Re}\int d^3l\,(\mathbf{l}^2+\lambda^2)^{-2} \times (\mathbf{l}^2 + 2\mathbf{p}_2\mathbf{l} - i\delta)^{-1}\,[(\mathbf{l}^2 + 2\mathbf{p}_1\mathbf{l} - i\delta)^{-1} + (\mathbf{l}^2 - 2\mathbf{p}_1\mathbf{l} - i\delta)^{-1}]\Big\}. \tag{5.2}$$

The calculation of the integral is carried out in the Appendix; for not too small angles ϑ between the momenta of the charged particles, $\mathbf{p}_1$ and $\mathbf{p}_2$ $(2\,|\mathbf{p}_1|\,|\mathbf{p}_2|\,\sin\vartheta > \lambda\,|\mathbf{p}_1 + \mathbf{p}_2|)$ we have the following formula:

$$dW = dW_0\{1 - 4\pi^2Z^2e^4n\lambda^{-3}E_1E_2/\sqrt{p_1^2p_2^2 - (\mathbf{p}_1\mathbf{p}_2)^2}\}. \tag{5.3}$$

In ordinary units this is

$$dW = dW_0\{1 - 4\pi^2Zn(\hbar/mc)^3(\hbar c/e^2) \times E_1E_2/|\mathbf{p}_1|\,|\mathbf{p}_2|\,|\sin\vartheta|\}. \tag{5.4}$$

In the derivation of this formula we have taken into account only the Coulomb scattering of the initial and final charged particles and have neglected the scattering of virtual particles. Let us estimate in what cases this neglect is justified. It is easy to see that in the averaging of the product of a pair of potentials $V(l)$ and $V(l')$ over the coordinates of the atoms there appear in the matrix element integrals of the type

$$\int \frac{d^4l\,\delta(l_4)\,|U_0(\mathbf{l})|^2}{\prod\limits_i [(p_i + l)^2 - m_i^2]}.$$

We have taken into account only those factors in the denominator for which $p^2 = m^2$, neglecting the terms containing l in the factors for which $p^2 \neq m^2$. This is justified in cases in which the effective values of the momenta of the virtual particles satisfy the inequality $p^2 - m^2 \gg \lambda^2$. If this condition is satisfied the formula (5.4) remains valid for a process of arbitrary order, if in the initial and final states there is one charged particle together with an arbitrary number of neutral particles.

We note that Eq. (5.4) is valid both for particles of spin $1/2$ and also for particles of spin 0. In fact, all formulas up to Eq. (2.6) are valid for arbitrary spin; the change of Eq. (2.6) for spin 0 is trivial, so that Eqs. (3.3) – (3.6) are also valid for arbitrary spin.

Equation (5.4) cannot be used for small values of the difference $\mathbf{p}_1 - \mathbf{p}_2$, that is, in cases in which $\mathbf{k}$ is small in magnitude. In this case the quantity $|\bar{u}_2O(\mathbf{p}_1 - \mathbf{p}_2 - \mathbf{s})u_1|^2$ in Eq. (3.2) cannot be regarded as a slowly varying function of $\mathbf{s}$. Besides this, Eq. (5.4) is invalid in the region of small angles ϑ between $\mathbf{p}_1$ and $\mathbf{p}_2$, such that $2\,|\mathbf{p}_1|\,|\mathbf{p}_2| \times \sin\vartheta < \lambda\,|\mathbf{p}_1 + \mathbf{p}_2|$. These cases require further consideration, since in this region it may be necessary to include the effect of higher orders of perturbation theory in the external potential of the atoms of the medium.

Let us estimate the size of the corrections to the transition probability for some media. Introducing the speeds β_1 and β_2 of the charged particles, we can write Eq. (5.4) in the form

$$dW = dW_0(1 - B/\beta_1\beta_2\,|\sin\vartheta|), \tag{5.5}$$

where for lead, water, and liquid hydrogen the coefficient B has the values 0.75×10^{-3}, 0.9×10^{-4}, and 0.6×10^{-5}, respectively. It follows that for small angles the change of the transition probability in dense substances near the end of the periodic table can become appreciable. On the other hand it is well known that for high energies of the initial particle the process occurs only in a small range of angles $(\vartheta \leq (1 - \beta_1^2)^{1/2})$. In such cases we can also expect that the corrections to total transition probabilities will be large. We shall illustrate these results with the example of π-μ decay.

6. APPLICATION TO π-μ DECAY

As is well known, the probability of π-μ decay in vacuum can be written in the form

$$dW_0 = \frac{g^2}{8\pi}\,\frac{\mu^2(M^2 - \mu^2)}{E_1p_1}\,dE_2. \tag{6.1}$$

It follows from Eq. (5.4) that the decay probability in a medium can be written in the form

$$dW = dW_0\{1 - 4\pi^2Z^2e^4n\lambda^{-3}/\beta_1\beta_2\,|\sin\vartheta|\}. \tag{6.2}$$

As has already been pointed out, at very small angles $\vartheta < \lambda\,|\mathbf{p}_1 + \mathbf{p}_2|/2\,|\mathbf{p}_1|\,|\mathbf{p}_2|$ Eq. (5.4), and consequently also Eq. (6.2), is incorrect. Such small angles, however, make only a negligibly small contribution to the total decay probability. Therefore we can get the total decay probability by integrating the approximate formula (6.2). Instead of integrating over the angle ϑ it is convenient to use the conservation laws to express ϑ in terms of the μ-meson energy E_2 and intergrate over E_2 from its minimum value $(E_1/2)[1+\mu^2M^{-2}-\beta(1-\mu^2M^{-2})]$ to its maximum value $(E_1/2)[1+\mu^2M^{-2}+\beta(1-\mu^2M^{-2})]$ (M and E_1 are the mass and energy of the π meson). After the intergration we can write the total decay probability for a meson passing through the medium with speed β_1 in the form

$$W = W_1\left\{\sqrt{1-\beta_1^2} - \frac{2\pi^3 Z^2 e^4 n}{\beta\lambda^3}\frac{M^2+\mu^2}{M^2-\mu^2}\right\}.$$

$$W_1 = (g^2/8\pi)\,\mu^2 M\,(1-\mu^2 M^{-2})^2. \qquad (6.3)$$

Thus the Coulomb scattering of the decaying particle and the decay products leads to a decrease of the total decay probability, i.e., to an increase of the lifetime of the unstable particle.

Let us emphasize once again that this result applies only to the decay of a π meson moving swiftly through the medium, and cannot be extended to a π meson at rest. Furthermore, for a π meson at rest in the medium the influence of the Coulomb scattering can act only on the μ meson produced in the decay, i.e., just on the final charged particle. As has been shown above, in this case there is on the average no change of the transition probability.

The change of the decay probability is especially marked at high π-meson energies, since the main term, the decay probability in vacuum, falls off linearly with increase of the energy, and the correction term approaches a constant value as the energy increases. For lead, water, and liquid hydrogen the coefficient $2\pi^3Z^2e^4n\lambda^{-3}(M^2+\mu^2)(M^2-\mu^2)^{-1}$ has the values 3×10^{-3}, 4×10^{-4}, and 2×10^{-5}, respectively. Therefore in lead, for example, at π-meson energies of the order of 10^{10} ev the correction term is 30 percent of the main effect, and in water at the same energy the correction is about 4 percent of the main effect. The use of perturbation theory to treat the total potential of the atoms of the medium makes the result only qualitatively correct for large values of the correction. Therefore it is interesting to treat processes with transfer of momentum to the medium without handling V by the perturbation method; such a treatment will be presented elsewhere. Finally, for the motion of particles of very high energy in a medium one should take into account losses in the medium. This fact makes the results obtained here inapplicable at very high energies.

We note that in its nature and properties the effect treated here is an analog of the Landau-Pomeranchuk effect for bremsstrahlung. In both cases a change of the transition probability is caused by the Coulomb scattering of the charged particles by the atoms of the medium and the effect reduces to the transfer of momentum to the atoms of the medium. The only difference is that in the case of bremsstrahlung it is convenient to take the transfer of momentum to the medium into account as part of the bremsstrahlung process itself, and in the case of decay we have to deal with a further process of decay in an external field which is qualitatively different from the main decay process.

The effect of transfer of momentum to the atoms of the medium must be taken into account for all processes involving at least two fast charged particles. The extension to the case of several charged particles is obvious. If the scattering of the virtual particles can be neglected, the averaged differential transition probability for the case of several charged particles will have a form analogous to Eq. (5.4). To get the total transition probability a separate treatment is required in each concrete case.

In conclusion, I take this occasion to thank E. L. Feĭnberg and V. M. Galitskiĭ for helpful discussions.

APPENDIX

The integral in Eq. (5.2)

$$J = \mathrm{Re}\int d^3l\,(\mathbf{l}^2+\lambda^2)^{-2}(\mathbf{l}^2+2\mathbf{p}_1\mathbf{l}-i\delta)^{-1}$$

$$\times\{(\mathbf{l}^2+2\mathbf{p}_2\mathbf{l}-i\delta)^{-1}+(\mathbf{l}^2-2\mathbf{p}_2\mathbf{l}-i\delta)^{-1}\}$$

can be put in the form

$$J = \mathrm{Re}\left(1+\frac{\lambda}{2}\frac{\partial}{\partial\lambda}\right)\int_{-1}^{+1}du\int_0^1 2x\,dx\int_0^1 3y^2dy\int d^3l$$

$$\times[\mathbf{l}^2-4\mathbf{l}\,(\mathbf{p}_2ux+\mathbf{p}_1(1-x))\,y+\lambda^2(1-y)-i\delta]^{-4}$$

$$= \mathrm{Re}\,\frac{i\pi^2}{8}\left(1+\frac{\lambda}{2}\frac{\partial}{\partial\lambda}\right)\int_{-1}^{+1}du\int_0^1 2x\,dx\int_0^1 3y^2dy$$

$$\times[y^2(\mathbf{p}_2ux+\mathbf{p}_1(1-x))^2-\lambda^2(1-y)+i\delta]^{-5/2}.$$

Integrating over y and taking the real part, we have

$$J = 4\pi^2\left(1+\frac{\lambda}{2}\frac{\partial}{\partial\lambda}\right)\frac{1}{\lambda}\int_{-1}^{+1}du\int_0^1 x\,dx\,[4(\mathbf{p}_2ux+\mathbf{p}_1(1-x))^2+\lambda^2]^{-2}$$

$$= -\frac{\pi^2}{\lambda}\frac{\partial^2}{\partial\lambda^2}\int_{-1}^{+1}du\int_0^1 x\,dx\,[4(\mathbf{p}_2ux+\mathbf{p}_1(1-x))^2+\lambda^2]^{-1}.$$

Changing to the variables $\zeta = ux + (1 - x)$ and $\eta = ux - (1 - x)$ and abbreviating $\mathbf{p}_1 + \mathbf{p}_2 = \mathbf{q}$ and $\mathbf{p}_1 - \mathbf{p}_2 = \mathbf{k}$, we get after integrating over ζ

$$J = -\frac{\pi^2}{2\lambda}\frac{\partial^2}{\partial\lambda^2}\int_{-1}^{+1} d\eta\,[\lambda^2 q^2 + \eta^2(q^2k^2 - (\mathbf{qk})^2)]^{-1/2}$$

$$\times\left\{\tan^{-1}\frac{\eta\,(q^2 + \mathbf{qk})}{\sqrt{\lambda^2q^2 + \eta^2\,(q^2k^2 - (\mathbf{qk})^2)}}\right.$$

$$\left.-\tan^{-1}\frac{\eta\,(\mathbf{qk} - \mathbf{q}^2)}{\sqrt{\lambda^2q^2 + \eta^2\,(q^2k^2 - (\mathbf{qk})^2)}}\right\}.$$

For $q^2k^2 - (\mathbf{qk})^2 \gg \lambda^2 q^2$ the behavior of the integrand is determined by the square root in the denominators, and the main contribution is from small values of η. Assuming that the inequality just stated holds, we can then get the approximate result

$$J = -(\pi^3 / 4\lambda^3)\,(p_1^2 p_2^2 - (\mathbf{p}_1\mathbf{p}_2)^2)^{-1/2}.$$

---

[1] L. D. Landau and I. Ya. Pomeranchuk, Dokl. Akad. Nauk SSSR **92**, 735 (1953).

[2] R. P. Feynman, Phys. Rev. **76**, 769 (1949).

Translated by W. H. Furry
164

SOVIET PHYSICS JETP VOLUME 11, NUMBER 3 SEPTEMBER, 1960

PERIPHERAL NUCLEON INTERACTION IN THE TWO-MESON APPROXIMATION

A. F. GRASHIN and I. Yu. KOBZAREV

Submitted to JETP editor June 22, 1959; resubmitted December 10, 1959

J. Exptl. Theoret. Phys. (U.S.S.R.) **38**, 863-869 (March, 1960)

Triplet nucleon-nucleon scattering phase shifts are computed at nonrelativistic energies in the two-meson approximation. A comparison of the two-meson and one-meson phase shifts shows that the one-meson approximation is excellent for all mixing parameters (starting with ^3S-^3D). This permits the use of theoretical values of mixing parameters in order to obtain a unique solution in a phase-shift analysis. The peripheral part of the two-meson potential, which corresponds in first Born approximation to the correct scattering amplitude, is also derived.

GALANIN et al.[1] have proposed a method of calculating nucleon-nucleon scattering phase shifts for large orbital angular momenta l in the two-meson approximation. The method makes it possible to obtain, for two-meson phase shifts, the lowest order term in a series expansion in the parameter

$$1/L = \sqrt{1 + p^2/\mu^2}/(l+1),$$

where μ is the pion mass and p is the nucleon momentum in the barycentric system. Specific calculations were carried out in reference 2 for the singlet state, in the nonrelativistic approximation including corrections of order $\sim p^2/m^2$, where an expansion in a second parameter $\zeta = \epsilon\sqrt{L}/2$ was simultaneously introduced ($\epsilon = \mu/m$, m = nucleon mass). Thus the singlet scattering phase shifts are obtained in the form of a double series expansion in the parameters 1/L (lowest order term) and ζ (first three terms) which insures good accuracy in the intermediate region $1 \ll L \ll 4/\epsilon^2$.

In the approximation indicated, calculations can be performed in an analogous fashion for the triplet state which makes it possible to find the nucleon-nucleon scattering operator due to the exchange of two mesons. For comparison with theoretical investigations and phenomenological models we also calculate the nucleon-nucleon potential corresponding to the two-meson scattering operator obtained in this work. An expansion in 1/L of the phase shifts corresponds to an expansion in 1/x of the potential, where x is the distance between the nucleons in units of $1/\mu$; i.e., the present method makes it possible to obtain the peripheral part of the two-meson potential for distances $x > 1$ with an accuracy of order $\sim 1/x$.

1. SCATTERING AMPLITUDES AND PHASE SHIFTS

The calculation of the scattering operator $M^{(2)}(q^2)$ in the vicinity of the nearest singular point* $q^2 = -4\mu^2$ differs from the corresponding singlet amplitude calculation[2] only in the replacement of the singlet matrix elements w, w_1, w_2, and w_3 [see Eqs. (1.7), (1.16), and (1.23) in reference 2] by the corresponding spin operators. Also, in the calculation of the contribution from one of the perturbation theory diagrams (B_4 in the notation of reference 2) it is necessary to include terms of order $\sim s^2$, where $s^2 = 1 + q^2/4\mu^2$. The nonexchange part of the scattering operator near the point $q^2 = -4\mu^2$, with corrections of order $\sim p^2/m^2$ included, may be written as follows:

$$M^{(2)}(q^2) = M_S(q^2) + \frac{i}{m^2}(\mathbf{S}[\mathbf{p}'\times\mathbf{p}])\, M_{LS}(q^2) + \frac{(\boldsymbol{\sigma}^{(1)}\mathbf{q})(\boldsymbol{\sigma}^{(2)}\mathbf{q})}{m^2} M_T(q^2), \tag{1.1}$$

where

$$M_S(q^2) = -\frac{3g^4}{8mE}\left\{c_{0S}s + c_{1S}\varepsilon\ln(\varepsilon + 2s) + \frac{3+2\lambda_\tau}{6}\frac{\varepsilon s}{\varepsilon + 2s} + \frac{3-2\lambda_\tau}{12E}\frac{\varepsilon}{v}\left[\ln\frac{2Es + \varepsilon v}{E(1+v)\mu/p} - \frac{i\pi}{2\sqrt{1-s^2}}\right]\right\},$$

$$c_{0S} = (\alpha - 1)^2, \qquad c_{1S} = \alpha - 1;$$

$$M_{LS}(q^2) = -\frac{3g^4}{8mE}\left\{c_{0(LS)}s + c_{1(LS)}\varepsilon\ln(\varepsilon + 2s) + \frac{3+2\lambda_\tau}{12}\frac{\varepsilon s}{\varepsilon + 2s} + \frac{3-2\lambda_\tau}{12E}\frac{\varepsilon m^2}{p^2}\left(\frac{1}{v} - v\frac{\mu^2}{\mu^2+p^2}\right)\left[\ln\frac{2Es+\varepsilon v}{E(1+v)\mu/p} - \frac{i\pi}{2\sqrt{1-s^2}}\right]\right\}.$$

$$c_{0(LS)} = -\frac{1}{2}(\alpha - 1)^2 + \frac{3-2\lambda_\tau}{12}\frac{\mu^2}{p^2+\mu^2} + \frac{2}{3}\lambda_\tau\beta_2,$$

---

*We use the notation introduced by Galanin et al.[1,2] except for a change in sign of the momentum transfer q^2. Our choice has the convenient feature that $q^2 = \mathbf{q}^2$.

$$c_{1(LS)} = -\frac{1}{2}\alpha - (1-2s^2)\frac{3-2\lambda_\tau}{12E}\frac{m^2}{p^2+\mu^2} - \frac{\lambda}{3}\left(\beta_2 + 2\beta\frac{s^2}{\varepsilon^2}\right);$$

$$M_T(q^2) = -\frac{3g^4}{8mE}\left\{c_{0T}s + c_{1T}\varepsilon\ln(\varepsilon+2s) - \frac{3-2\lambda_\tau}{48E}\frac{\varepsilon v m^2}{\mu^2+p^2}\left[\ln\frac{2Es+\varepsilon v}{E(1+v)\mu/p} - \frac{i\pi}{2\sqrt{1-s^2}}\right]\right\},$$

$$c_{1T} = \frac{3+2\lambda_\tau}{48} + (1-2s^2)\frac{3-2\lambda_\tau}{48}\frac{m^2+\mu^2/2}{\mu^2+p^2} - \frac{\lambda_\tau}{24}\beta_1\left(1-4\frac{s^2}{\varepsilon^2}\right);$$

$$c_{0T} = -\frac{1}{8}\left(1+\frac{1}{2}\frac{\mu^2}{\mu^2+p^2}\right) - \frac{\lambda}{12}\left(1-\beta_1-\frac{1}{2}\frac{\mu^2}{\mu^2+p^2}\right),$$

$$v = \sqrt{4s^2p^2+\mu^2}/\mu; \qquad E^2 = 1 + p^2/m^2; \qquad \alpha = 1{,}2;$$

$$\beta_1 = 0.025, \qquad \beta_2 = -0.029, \qquad \beta = -\beta_1 - \beta_2;$$

and $\lambda_T = 1, -3$ corresponds to isotopic spin $T = 1, 0$.

The coefficient $a_l(S, S'_z, S_z, T)$ in an expansion of the amplitude in associated Legendre polynomials may be obtained by calculating the matrix elements of the operator (1.1) in the angular momentum representation and integrating over $|s|$ entirely analogously to what was done in references 1 and 2. The triplet amplitudes corresponding to a change in the spin projection $|\Delta S_z| = 1$ and 2 are expanded in terms of the polynomials $P_l^{(1)}$ and $P_l^{(2)}$ and the expansion coefficients are expressed in terms of integrals over the cut of the associated Legendre functions of the second kind $Q_l^{(1)}$ and $Q_l^{(2)}$. Replacing the associated functions by Q_l we obtain, accurate to order $\sim 1/L$,

$$a_l(1, 1, 0, T) = -p\frac{4(\mu/p)^3}{i\pi l}\sqrt{1+\frac{\mu^2}{p^2}}\,Q_l(1+2\mu^2/p^2) \times\int_0^\infty e^{-L|s|^2}\Delta[M(1, 1, 0, T)/\sin\theta]\,|s|\,d|s|,$$

$$a_l(1, 1, -1, T) = -p\frac{2(\mu/p)^2}{i\pi l^2}Q_l(1+2\mu^2, p^2) \times\int_0^\infty e^{-L|s|^2}\Delta M(1, 1, -1, T)\,|s|\,d|s|.$$

where we denote by the symbol Δf the discontinuity in the function f across the cut $q^2 \leq -4\mu^2$ $(s^2 \leq 0)$. Finally, the various scattering phase shifts* are expressed in terms of the coefficients $a_l(S, S'_z, S_z, T)$ with the following result

$$\eta_l^J = \frac{3g^4\varepsilon\mu}{8E\sqrt{\pi}pL^{3/2}}Q_l(1+2\mu^2/p^2)\{d_0^J + 2\sqrt{\pi}\zeta d_1^J + \zeta^2 d_2^J\}. \tag{1.2}$$

Here it is understood that the superscript J is to be omitted for the singlet state. We find for the coefficients of the powers of ζ appearing in Eq. (1.2)

$$d_0 = (\alpha-1)^2, \qquad d_1 = \alpha - 1 + \frac{3-2\lambda_\tau}{6}\left(1-\frac{p^2}{2m^2}\right)\Psi(z),$$

$$d_2 = -4(\alpha-1) + p^2/m^2 + \tfrac{1}{3}\lambda_\tau(4-2p^2/m^2),$$

$$z^2 = L\mu^2/4p^2, \qquad \Psi(z) = ze^{-z^2}\int_0^z e^{x^2}dx; \qquad d_i^l = d_i,$$

$$d_i^{l\pm1} = d_i \pm \varepsilon\sqrt{\varepsilon^2+p^2/m^2}D_i \qquad (i = 0, 1, 2);$$

$$D_0 = (\alpha-1)^2 - \tfrac{4}{3}\lambda_\tau(\beta_2 - \tfrac{1}{2}\beta),$$

$$D_1 = \alpha - (3-2\lambda_\tau)\left(1-\frac{p^2}{2m^2}\right)\frac{m^2}{3p^2}\left(\Psi(z)-\frac{1}{2}\right) - \frac{\lambda_\tau}{3}\frac{\beta}{\zeta^2},$$

$$D_2 = -2(2\alpha+1). \tag{1.2'}$$

The triplet phase shift with $J = l$ and the singlet phase shift η_l coincide, and the triplet phase shifts $\eta_l^{l\pm1}$ (with $J = l\pm1$) differ from them by terms due to the spin-orbit interaction.

The mixing parameter is given by

$$\xi_J = \frac{3g^4\varepsilon^3\mu}{8E\sqrt{\pi}pL_J^{3/2}}Q_{J+1}\left(1+2\frac{\mu^2}{p^2}\right) \left(1+2\frac{\mu^2}{p^2}+2\frac{\mu}{p}\sqrt{1+\mu^2/p^2}\right)\{h_0 + 2\sqrt{\pi}\zeta_J h_1\},$$

$$h_0 = 1 - \tfrac{2}{3}\lambda_\tau\beta_1,$$

$$h_1 = -\frac{9+2\lambda_\tau}{24} - \frac{(3-2\lambda_\tau)(1-p^2/2m^2)m^2}{12(\mu^2+p^2)}\frac{\Psi(z_J)}{z_J^2} + \frac{\lambda_\tau}{6}\frac{\beta_1}{\zeta^2},$$

$$L_J = (J+2)/\sqrt{1+p^2/\mu^2}, \quad \zeta_J = \varepsilon\sqrt{L_J}/2, \quad z_J^2 = L_J\mu^2/4p^2. \tag{1.3}$$

Equations (1.2) and (1.3) represent the first terms of the expansion of two-meson phase shifts in $1/L$ and ζ. Therefore we omit corrections of order ϵ^2 in the calculations since such terms are of the same order of smallness as $\sim 1/L$ corrections to higher order terms in the expansion in ζ (note that $\epsilon^2 = 4\zeta^2/L$). An interesting feature of our results is the strong cancellation in the phase shifts η_l, η_l^J of the contributions from perturbation theory and from the "smooth" part of the meson-nucleon amplitude containing the coefficient α (the main terms contain $\alpha - 1 \ll \alpha, 1$). The contributions from the meson-nucleon amplitude containing β_1 and β_2 are small and may be neglected in rough estimates.

Expression (1.3) for the mixing parameter does not contain the coefficient α. This is explained by the fact that the corresponding part of the meson-nucleon amplitude is spin-independent and does not contribute to the tensor forces. Since the coefficient β_1 entering into (1.3) makes a small contribution, the mixing parameters are approximated well by perturbation theory. This makes it possible to obtain more accurate expressions for them than Eq.

---

*For that purpose we make use of Eq. (6) of Grashin[3] accurate to terms of order $1/l$. The notation for the phase shifts and expansion coefficients of the amplitude coincides with that introduced by Grashin;[3] only their real parts concern us here.

TABLE I

E_{lab}, Mev	10	40	100	200	300	400	670
$^1D_2$	0.04	0.1	0.25	0.5	—	—	—
$^1G_4$	0	0.01	0.04	0.1	0.2	0.3	—
$^3P_0$	0.06	0.03	0.02	—	—	—	—
$^3P_1$	—0.07	—0.1	—0.15	—	—	—	—
$^3P_2$	1	2	2	—	—	—	—
ξ_2	—0.001	—0.003	—0.01	—0.02	—0.04	—0.05	—
$^3F_2$	0.02	0.04	0.06	0.07	0.08	0.07	—
$^3F_3$	—0.01	—0.02	—0.04	—0.08	—0.1	—0.15	—
$^3F_4$	0.05	0.2	0.4	0.7	1	1	—
ξ_4	0	0	—0.002	—0.008	—0.015	—0.02	—0.04
$^3H_4$	0	0.01	0.03	0.06	0.07	0.08	0.1
$^3H_5$	0	0	—0.01	—0.03	—0.05	—0.07	—0.1
$^3H_6$	0.01	0.02	0.1	0.3	0.4	0.5	0.9

TABLE II

E_{lab}, Mev	10	40	100	200	300	400	670
$^1P_1$	—0.15	—0,2	—0.2	—	—	—	—
$^1F_3$	0	—0.02	—0.04	—0.07	—0.1	—0.1	—
$^1H_5$	0	0	—0.01	—0.02	—0.03	—0.04	—0.1
ξ_1	—0.005	—0.02	—0.02	—0.01	—	—	—
$^3D_1$	—0.07	—0.01	0.05	0.07	—	—	—
$^3D_2$	0.02	0.03	0.03	0.04	—	—	—
$^3D_3$	0.3	—0.6	—0.8	—0.8	—	—	—
ξ_3	0	—0.003	—0.006	—0.006	—0.005	—0.002	—
$^3G_3$	—0.01	—0.02	0.01	0.03	0.05	0.06	—
$^3G_4$	0	0.01	0.01	0.02	0.02	0.03	—
$^3G_5$	0.02	—0.08	—0.2	—0.3	—0.3	—0.4	—

(1.3) by taking into account higher order terms in the $1/L$ expansion.*

Tables I and II show the ratios of the two-meson phase shifts, Eqs. (1.2) and (1.3), to the corresponding one-meson phase shifts calculated by Grashin.[3] Ratios smaller than 1% for η_l, η_l^J, and smaller than 0.1% for the mixing parameters ξ_J, were replaced by zero. The ratios were not calculated for the cases when $1/L \gg 1$. However, the ratios given in the tables also correspond to rather large values of $1/L$ $(0.4-0.8)$ and therefore the results should be viewed as rough estimates only and may be used with sufficient reliability only to establish the limits of applicability of the one-meson approximation.

It can be seen from the tables that the ratios are very large for the phase shifts with $J = l + 1$. As was already pointed out[3] this is due to the fact that the one-meson contributions to these phase shifts are anomalously small since at low energies they have the "anomalous" energy dependence p^{2l+3}. An interesting feature of our results is the high accuracy of the one-meson mixing parameters (beginning with ξ_1), which is very important for a comparison of theoretical and experimental data, since polarization data make it possible to obtain the mixing parameters with sufficient accuracy experimentally. Thus a comparison of the theoretical and experimental ξ_2 for pp scattering at 310 Mev[4] makes it possible, from just this one parameter, to reject two of the eight solutions of Stapp et al., namely the second and the fourth. The subsequent more accurate analysis with higher phase shifts taken into account in the one-meson approximation[5] showed that the two solutions become one (No. 2 in the notation of Cziffra et al.[5]).

One is inclined to believe, as suggested by one of the authors[3] and by Cziffra et al.,[5] that fewer solutions will also be found at other energies if use is made of peripheral one-meson phase shifts (for example, those for which Tables I and II give ratios smaller than 10%) in the phase shift analysis.

We next discuss briefly the analytic properties of two-meson phase shifts as a function of p^2. All present calculations, as well as those of Galanin et al.,[1,2] were carried out for physical energies; however it is trivial to generalize the method used to arbitrary energies and therefore Eqs. (1.2) and (1.3) are also valid for complex p^2 accurate to order $1/|L|$, $|\xi|^2$. In the unphysical region the two-meson phase shifts have a branch point at

---

*To this end it is necessary to obtain higher order terms in the expansion of the perturbation theory amplitudes in powers of s^2. For one of the diagrams, which gives an anomalously large contribution to Eq. (1.3), the exact singular part (all powers of s^2) is calculated in reference 2.

$p^2 = -\mu^2$ and a cut from $-\mu^2$ to $-\infty$. The function $Q_l(1 + 2\mu^2/p^2)$ is single-valued in the entire cut p^2 plane, and for an analytic continuation of the function $\Psi(z)$ which appears in Eqs. (1.2′) and (1.3) it is convenient to use an expansion in the neighborhood of $p^2 = 0$ $(z = \infty)$: $\Psi(z) = \frac{1}{2} + \frac{1}{4}z^{-2} + \ldots$ However the integration over dq^2 by the saddle-point method used in the calculation of the two-meson shifts, as well as the expansion in s^2 for one of the perturbation theory diagrams, are only valid under the condition $|p^2 + \mu^2| \gg \mu^2/|L|$, and consequently Eqs. (1.2), (1.3) cannot be used in the vicinity of the singular point $p^2 = -\mu^2$.

2. NUCLEON-NUCLEON POTENTIAL

The calculated two-meson phase shifts are determined by the interaction in the peripheral region $x > 1$, which may be considered as weak. This makes it possible to use the Born approximation to construct a potential* corresponding to the scattering amplitude. By inverting the usual Born formula we find for the potential

$$U = -\frac{1}{2\pi^2 m}\int e^{i\mathbf{qr}} M(q^2)\, d\mathbf{q}. \qquad (2.1)$$

We introduce the scattering operator (1.1) into Eq. (2.1) and write the two-meson potential as follows:

$$U = U_S + (\mathbf{LS})\, U_{LS} + (\sigma^{(1)}\nabla_x)(\sigma^{(2)}\nabla_x)\, U_T, \qquad (2.2)$$

where $(\mathbf{LS})$ is the spin-orbit operator with eigenvalues $\frac{1}{2}[J(J+1) - l(l+1) - S(S+1)]$ and the functions U_S, U_{LS}, and U_T, after integration over the angles of the vector $\mathbf{q}$, are given by

$$U_S = \frac{i}{\pi m r}\int_{-\infty}^{+\infty} e^{iqr} M_S(q^2)\, q\, dq,$$

$$U_{LS} = \frac{i}{\pi m^3 r}\frac{\partial}{\partial r}\frac{1}{r}\int_{-\infty}^{+\infty} e^{iqr} M_{LS}(q^2)\, q\, dq,$$

$$U_T = -\frac{i\mu^2}{\pi m^3 r}\int_{-\infty}^{+\infty} e^{iqr} M_T(q^2)\, q\, dq. \qquad (2.3)$$

To integrate over dq we close the contour in the upper half-plane going around the cut on the imaginary axis $\mathrm{Im}\, q \geq 2\mu$ in the manner shown in the figure. The integral over the semicircle at infinity may only give a delta-function-like contribution in those cases when $M(q^2)$ does not fall off sufficiently rapidly as $q^2 \to \infty$. Therefore the peripheral part of the potential is determined by the integral over the cut only and for $x \gg 1$ only a small portion near the singular point $q = 2i\mu$ plays an important role. Going over to the variable s and using the saddle point method we obtain accurate to order $\sim 1/x$:

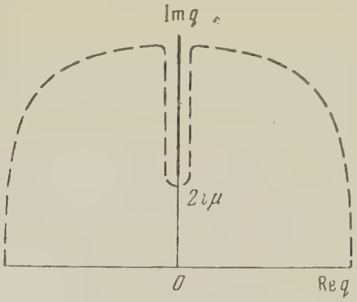

$$\int_{-\infty}^{+\infty} e^{iqr} M(q^2)\, q\, dq = 4\mu^2 e^{-2x}\int_0^{-\infty} e^{-x|s|^2}\Delta M(s^2)\, |s|\, d|s|. \qquad (2.4)$$

The remaining integration over $d|s|$ in Eq. (2.4) coincides with the integral of the discontinuity in the amplitude, $\Delta M(s^2)$, which was encountered in calculating phase shifts and differs from it by the formal replacement of L by x. Making use of the previous results and denoting by $d_1(x)$, $D_1(x)$, and $h_1(x)$ the functions obtained from d_1, D_1, and h_1 [see Eqs. (1.2′) and (1.3)] by the formal substitution $L \to x$, we obtain for $1 \ll x \ll 4/\epsilon^2$

$$U_S = -\frac{3g^4\varepsilon^2\mu}{4\sqrt{\pi}}\frac{e^{-2x}}{x^{5/2}}\left\{d_0 + \varepsilon\sqrt{\pi x}\, d_1(x) + \frac{\varepsilon^2 x}{4} d_2\right\}, \qquad (2.5)$$

$$U_{LS} = -\frac{3g^4\varepsilon^4\mu}{4\sqrt{\pi}}\frac{e^{-2x}}{x^{7/2}}\left\{D_0 + \varepsilon\sqrt{\pi x}\, D_1(x) + \frac{\varepsilon^2 x}{4} D_2\right\}, \qquad (2.6)$$

$$U_T = -\frac{3g^4\varepsilon^4\mu}{16\sqrt{\pi}}\frac{\varepsilon^{-2x}}{x^{5/2}}\{h_0 + \varepsilon\sqrt{\pi x}\, h_1(x)\}. \qquad (2.7)$$

In accordance with the expansion of the phase shifts in $1/L$ and ζ, the coefficients of the exponentials in the potentials are lowest order terms in an expansion in $1/x$ and $\epsilon\sqrt{x}/2$. Therefore only lowest order terms in $1/x$ should be kept when differentiating with respect to x the tensor or spin-orbit parts [see Eq. (2.3)] of the potential (2.2) [e.g., differentiation in Eq. (2.3) is equivalent to multiplication by -2].

The two-meson potential (2.2), (2.5), (2.6), and (2.7) represents the next correction to the well-known one-meson potential (see, e.g., reference 6), and consists of a central, spin-orbit, and tensor part. Interactions of the type $\sigma^{(1)}\sigma^{(2)}$ and $(\sigma^{(1)}\mathbf{L}) \times (\sigma^{(2)}\mathbf{L})$ give corrections to the phase shifts η_l, η_l^J of order ϵ^2, $1/L$, and are therefore not included in our approximation. The tensor interaction contributes to η_l, η_l^J corrections of the same order, but, in contrast, fully determines the mixing parameters. For this reason we kept the tensor terms in the scattering operator (1.1) and the potential (2.2), but ignored interaction terms of the form $\boldsymbol{\sigma}^{(1)}\boldsymbol{\sigma}^{(2)}$ and $(\boldsymbol{\sigma}^{(1)}\mathbf{L})(\boldsymbol{\sigma}^{(2)}\mathbf{L})$. A characteristic feature of the two-meson potential is its substantial energy dependence contained in the function $\Psi(\mu\sqrt{x}/2p)$, as well as its dependence on isotopic spin.

---

*We note that, strictly speaking, a potential in the conventional sense (local) describing the nucleon interaction does not exist. This is reflected in the fact that our equivalent potential depends on p^2 and is therefore nonlocal. Furthermore, in higher orders of smallness in our expansion the operation of constructing a potential is not even unique.

We emphasize in conclusion that this potential is equivalent to the scattering amplitude only in the first Born approximation. The question of a more correct construction of the potential will be discussed separately.

The authors are grateful to L. B. Okun' and I. Ya. Pomeranchuk for useful discussions.

[1] Galanin, Grashin, Ioffe, and Pomeranchuk, JETP **37**, 1663 (1959), Soviet Phys. JETP **10**, 1179 (1960); Nucl. Phys. (in press)

[2] Galanin, Grashin, Ioffe, and Pomerancuhk, JETP **38**, 475 (1960), Soviet Phys. JETP **11**, 347 (1960); Nucl. Phys. (in press).

[3] A. F. Grashin, JETP **36**, 1717 (1959), Soviet Phys. JETP **9**, 1223 (1959).

[4] Stapp, Ypsilantis, and Metropolis, Phys. Rev. **105**, 302 (1957).

[5] Cziffra, MacGregor, Moravcsik, and Stapp, Phys. Rev. **114**, 880 (1959).

[6] Bethe and de Hoffmann, Mesons and Fields, v. 2 (Russ. transl.) IIL, 1957, p. 363.

Translated by A. M. Bincer
165

SOVIET PHYSICS JETP VOLUME 11, NUMBER 3 SEPTEMBER, 1960

EFFECT OF DEFORMATION OF THE NUCLEUS ON THE ELECTRONIC WAVE FUNCTIONS. APPLICATION TO BETA DECAY

R. WEINER and Ch. IUSIM

Physics Institute, Academy of the Rumanian People's Republic, Bucharest; Parhon University, Bucharest

Submitted to JETP editor August 5, 1959

J. Exptl. Theoret. Phys. (U.S.S.R.) 38, 870-876 (March, 1960)

The effect of the quadrupole interaction on the wave functions of an electron-nucleus system is studied. In the case of a nonspherical nucleus the electron and nuclear variables cannot be separated. This has the result that there are "satellite" nuclear and electronic angular momenta I and j, which satisfy the inequalities $|I - I_0| \leq 2$ and $|j - j_0| \leq 2$, where I_0 and j_0 are the total nuclear and electronic angular momenta in the absence of quadrupole interaction. The wave function of an electron-nucleus system for a nucleus with axial symmetry is determined by a perturbation calculation. An explicit expression is given for the wave functions in the region $r \leq R$ (R is the radius of the nucleus). The "satellite" states cause the appearance of new matrix elements, which in some cases can greatly change the value of the probability of the corresponding transitions. In the case of beta decay, for $Z \sim 70$ and $Q_0 \sim 5 \cdot 10^{-24}$ cm^2, with $\Delta I \geq 3$, where ΔI is the difference of the nuclear spins of the initial and final states, the new matrix elements can exceed by one to two orders of magnitude the values calculated without taking the nuclear-deformation effect into account.

INTRODUCTION

ELECTRONIC wave functions (e.w.f.) play an important part not only in atomic transitions but also in all nuclear processes in which electrons take part, such as β decay, internal conversion, and so on. Since in these latter phenomena the electron density in the region of the nucleus is important, the probability of such transitions must depend to a considerable degree on the finite dimensions of the nucleus. The effects of the finite size of the nucleus on the e.w.f. have been studied in a number of papers, both in connection with β decay (cf., e.g., references 1, 2) and also with internal conversion.[3,4] These treatments, however, dealt only with the nonsingular charge distribution of the nucleus and did not take into account effects of the shape of the nucleus on the e.w.f. and on nuclear transitions. To speak more exactly, in these papers it was always assumed that the nucleus is spherical. There exists in nature, however, a rather extensive class of nonspherical nuclei, for which a number of specific properties are observed, and special models must be devised to explain these properties.

It can be expected that also the e.w.f., in particular in their behavior near the nucleus, are sensitive to the shape of the nucleus, and that there are resulting effects on nuclear transitions (the influence of the form of the nucleus on nuclear transitions by means of nuclear wave functions was studied in a number of papers devoted to deformed nuclei;[5-8] a paper by Smorodinskiĭ[9] predicts an increase of the probabilities of forbidden β-decay transitions owing to effects of the dependence of the interaction constant on the shape of the nucleus). Indeed, the form of the e.w.f. is determined by the interaction of the electron with the nucleus. For spherically symmetrical nuclei this interaction is characterized by the fact that the total angular momenta of the nucleus and the electron are exact quantum numbers, in terms of which selection rules hold for the nuclear transitions.

The situation is different in the case of deformed nuclei. For example, the existence of an electric quadrupole moment destroys the spherical symmetry of the electric field of the nucleus; in this case it is already impossible to separate the electronic and nuclear variables, and we can no longer speak of electronic and nuclear states separately, but only of the state of the nucleus-electron system. In other words, instead of exactly defined electronic and nuclear angular momenta we must consider their superposition. This effect can change the selection rules, and thus also the probabilities of nuclear transitions. Under some circumstances these changes can be large.

In the present paper we determine, in the framework of perturbation theory, the wave functions of a system consisting of one electron and a deformed axially symmetrical nucleus. We have confined ourselves to the first approximation in the deformation parameter. We give a formula for the new functions which is suitable for the calculation of matrix elements for electron capture and β decay.

THE WAVE FUNCTIONS OF THE NUCLEUS-ELECTRON SYSTEM

The Hamiltonian of a system consisting of one electron and a nucleus is

$$H = H_n + H_e + H_{en}, \tag{1}$$

where H_n is the Hamiltonian of the nucleus, which depends only on the nuclear variables; H_e is the electron Hamiltonian, containing only the electronic variables; and H_{en} is the interaction term, depending on both the nuclear and the electronic variables.

In the calculation of the wave functions the electrostatic part of the interaction is the most important. Let us consider deformed axially symmetrical nuclei. In first approximation we can confine ourselves to a treatment of the quadrupole term (we include the monopole term, the part of the interaction independent of the angles, in H_e)

$$H_{en} = -\tfrac{1}{2} Q_0 \alpha f(r) P_2(\cos\theta_{en}), \tag{2}$$

where Q_0 is the intrinsic quadrupole moment of the nucleus, α is the fine-structure constant, and $f(r)$ is a radial function determined by the distribution of the electric charge of the nucleus (r is the distance between the electron and the center of mass of the nucleus). In the case of a distribution uniform throughout the volume of the nucleus $f(r)$ has the following form:

$$f(r) = \begin{matrix} r^2/R^5 & \text{for } r \leqslant R, \\ r^{-3} & \text{for } r > R, \end{matrix} \tag{3}$$

where R is the radius of the corresponding spherical nucleus; θ_{en} is the angle between the radius vector of the electron and the axis of symmetry of the nucleus.

Since H_{en} is the Hamiltonian for the interaction of the electron with the nucleus as a whole, we shall be interested in only that part of H_n that determines the orientation of the nucleus.[10] The eigenfunctions of H_n will be the symmetrical-top functions:

$$\psi_{I\mu K} = [(2I+1)/8\pi^2]^{1/2} D^{I*}_{\mu K}(\theta_n), \tag{4}$$

where θ_n are the three Euler angles of the axes of the nucleus, I is the spin of the nucleus, and K and μ are its projections on the axis of symmetry and the z axis, respectively. The phases of the $D^I_{\mu K}$ are defined as in reference 11.

H_e is the ordinary Dirac Hamiltonian[12]

$$H_e = \alpha \mathbf{p} + \beta m - eA_0(r), \tag{5}$$

where $A_0(r)$ is the monopole electrostatic potential of the nucleus. The solutions of the equations

$$H_e \varphi^0 = \varepsilon_e \varphi^0, \tag{6}$$

in the representation of j^2, j_z, ϵ_e, and the parity $(-1)^l$ have the form

$$\varphi^0_{jlj_z} = \begin{pmatrix} i g_{jl}(r) Y^{j_z}_{jl\,1/2} \\ f_{jl}(r) \frac{\sigma \mathbf{r}}{r} Y^{j_z}_{jl\,1/2} \end{pmatrix} \equiv \begin{pmatrix} i r^{-1} \Phi^{0+}_{jl}(r) Y^{j_z}_{jl\,1/2} \\ r^{-1} \Phi^{0-}_{jl}(r) \frac{\sigma \mathbf{r}}{r} Y^{j_z}_{jl\,1/2} \end{pmatrix}, \tag{7}$$

(we shall always omit the index ϵ_e from wave functions), where the spinors $Y^{jz}_{jl\,1/2}$ are defined as in the book of Blatt and Weisskopf.[13]

Our problem is that of solving the equation

$$H\Psi = \varepsilon\Psi, \tag{8}$$

with H_{en} playing the part of a perturbation. The unperturbed wave functions are products of the $\psi_{I\mu K}$ and $\varphi^0_{jlj_z}$. Instead of these products it is convenient to choose the linear combinations

$$\Psi^0_{FM\ldots} = \sum_{\mu + j_z = M} C(I_0 j_0 F;\ \mu j_z)\, \psi_{I_0 \mu K} \varphi^0_{j_0 l_0 j_z}, \tag{9}$$

where F is the total angular momentum, M is its projection along the z axis, and $C(\ldots.)$ are Clebsch-Gordan coefficients.[11] Since H_{en} is invariant under rotations, F and M are also exact quantum numbers for Eq. (8). Therefore we shall look for the solution of Eq. (8) in the form

$$\Psi_{FM} = \Psi^0_{FM} + \Psi^c_{FM}. \tag{10}$$

In first approximation in Q_0 the correction function Ψ^c_{FM} satisfies the equation

$$(H_n + H_e - \varepsilon_{I_0} - \varepsilon_e)\Psi^c_{FM} = (\varepsilon_c - H_{en})\Psi^0_{FM}, \tag{11}$$

where ϵ_{I_0} is the rotational energy of the nucleus and ϵ_c is the correction to the total energy of the unperturbed system. These quantities are connected by the relation

$$\varepsilon = \varepsilon_{I_0} + \varepsilon_e + \varepsilon_c. \tag{12}$$

Let us expand the function Ψ^c_{FM} in the orthonormal system

$$\chi_{FMIKjl} = \sum_{\mu + j_z = M} C(IjF;\ \mu j_z)\, \psi_{I\mu K} Y^{j_z}_{jl\,1/2}. \tag{13}$$

Then

$$\Psi^{c}_{FM..} = \begin{pmatrix} \sum\limits_{Ijl} ir^{-1}\Phi^{+}_{Ijl}(r)\,\chi_{FMIKjl} \\ \sum\limits_{Ijl} r^{-1}\Phi^{-}_{Ijl}(r)\,(\sigma\mathbf{r}/r)\,\chi_{FMIKjl} \end{pmatrix}, \tag{14}$$

where the expansion coefficients $\Phi^{\pm}_{Ijl}(r)$ are radial "electronic" correction functions. To determine them, we substitute Eqs. (14) and (9) in Eq. (11). Using the properties of the functions χ_{FMIKjl}, after some simple calculations we get the following equation for $\Phi^{\pm}_{Ijl}$:

$$[d/dr \pm r^{-1}\varkappa_{jl}]\,\Phi^{\pm}_{Ijl} \mp [\bar{\varepsilon} \pm m + eA_0(r)]\,\Phi^{\mp}_{Ijl} = \pm[\varepsilon_c\delta_{II_0}\delta_{jj_0}\delta_{ll_0} + A_{Ijl;\,I_0j_0l_0}f(r)]\,\Phi^{0\mp}_{j_0l_0}; \tag{15}$$

here

$$A_{Ijl;\,I_0j_0l_0} = \tfrac{1}{2}Q_0\alpha(-1)^{I_0+j_0-F}[(2I_0+1)(2j_0+1)(2l_0+1) \times (2j+1)]^{1/2}\,C(2I_0I;\,0K)\,C(2l_0l;\,00) \times W(II_0jj_0;\,2F)\,W(2lj_0{}^1/_2;\,l_0j); \tag{16}$$

$$\varkappa_{jl} = \begin{matrix} -(l+1) & \text{for } j = l + {}^1/_2, \\ l & \text{for } j = l - {}^1/_2; \end{matrix} \tag{17}$$

$$\bar{\varepsilon} = \varepsilon_e + \varepsilon_{I_0} - \varepsilon_I; \tag{18}$$

The W's are the well known Racah coefficients (cf., e.g., reference 11). From the properties of the Clebsch-Gordan and Racah coefficients in Eq. (16) it follows that the "satellite" angular momenta I, j, l are connected with the basic angular momenta by the relations

$$|I - I_0| \leqslant 2, \qquad |j - j_0| \leqslant 2, \quad l = l_0, \qquad l_0 \pm 2. \tag{19}$$

From the equations (15) one can calculate both the energy correction ϵ_c caused by the quadrupole moment and the corrections $\Phi^{\pm}_{Ijl}(r)$ to the wave functions. The calculation of ϵ_c essentially means the determination of the hyperfine splitting of the atomic levels. We shall not concern ourselves with this problem, which has been sufficiently thoroughly studied. Moreover, we shall not go into the calculation of the wave-function corrections $\Phi^{\pm}_{I_0j_0l_0}(r)$ that correspond to the basic angular momenta I_0, j_0, l_0, since they do not give new matrix elements. Accordingly, the quantity ϵ_c will always be omitted hereafter.

The relations (15) are a system of inhomogeneous equations which are to be solved with the following boundary conditions:[14]

$$\lim_{r\to 0}\Phi^{\pm} = 0, \qquad \lim_{r\to\infty}\Phi^{\pm} \neq \infty. \tag{20}$$

For $|\bar{\epsilon}| > m$ we must also impose the radiation condition.[14,15] The solution that satisfies the boundary conditions is of the form

$$\Phi^{\pm} = \frac{1}{\Phi_1^{+}\Phi_2^{-} - \Phi_1^{-}\Phi_2^{+}}\Big[\Phi_1^{\pm}\int\limits_{\infty}^{r}(\mathcal{A}^{-}\Phi_2^{-} + \mathcal{A}^{+}\Phi_2^{+})\,dr - \Phi_2^{\pm}\int\limits_{0}^{r}(\mathcal{A}^{-}\Phi_1^{-} + \mathcal{A}^{+}\Phi_1^{+})\,dr\Big], \tag{21}$$

$$\mathcal{A}^{\pm} = A_{Ijl;I_0j_0l_0}f(r)\,\Phi^{0\pm}_{j_0l_0}; \tag{22}$$

$\Phi_1^{\pm}$ and $\Phi_2^{\pm}$ are the two linearly independent solutions of the homogeneous equation

$$(d/dr \pm r^{-1}\varkappa_{jl})\,\Phi^{\pm} \mp (\bar{\varepsilon} \pm m + eA_0(r))\,\Phi^{\mp} = 0, \tag{23}$$

which satisfy the following boundary conditions:

$$\lim_{r\to 0}\Phi_1^{\pm} = 0, \qquad \lim_{r\to\infty}\Phi_2^{\pm} \neq \infty \qquad (\text{for } (|\bar{\varepsilon}| < m); \tag{24}$$

$$\lim_{r\to\infty}\Phi_2^{\pm} \sim e^{i(pr+\delta)} \qquad (\text{for } |\bar{\varepsilon}| > m). \tag{25}$$

Here $p = (\bar{\epsilon}^2 - m^2)^{1/2}$ and δ is a radial function whose form depends on $A_0(r)$.

To get a concrete solution, we must know the spherically symmetrical potential $A_0(r)$, which determines the form of the functions $\Phi_1^{\pm}$ and $\Phi_2^{\pm}$, and the unperturbed functions $\Phi^{0\pm}$. In the choice of $A_0(r)$ the finite dimensions of the spherical nucleus should be taken into account. For simplicity we shall omit this refinement, however; this is quite permissible in determining the order of magnitude of the effect for β-decay transitions.

Thus we take A_0 to be the Coulomb potential of a point nucleus:

$$eA_0(r) = Z\alpha/r. \tag{26}$$

The corresponding functions $\Phi_1^{\pm}$ and $\Phi_2^{\pm}$ are

$$\Phi_1^{\pm} = \sqrt{1 \pm \bar{\varepsilon}/m}\,\rho^{-1/2}[(\varkappa + N_0)\,M_{N-1/2,\gamma} \mp (\gamma + iN)\,M_{N+1/2,\gamma}],$$

$$\Phi_2^{\pm} = \sqrt{1 \pm \bar{\varepsilon}/m}\,\rho^{-1/2}[(\varkappa + N_0)\,W_{N-1/2,\gamma} \pm W_{N+1/2,\gamma}], \tag{27}$$

$$\rho = 2\lambda r, \qquad \lambda = \sqrt{m^2 - \bar{\varepsilon}^2} \qquad (\text{for } |\bar{\varepsilon}| < m);$$

$$\Phi_1^{\pm} = a_{\pm}\rho^{-1/2}[(\varkappa - i\nu_0)\,M_{-i\nu-1/2,\gamma} \mp (\gamma - i\nu)\,M_{-i\nu+1/2,\gamma}],$$

$$\Phi_2^{\pm} = F(\gamma) + F(-\gamma), \quad \lambda = i\sqrt{\bar{\varepsilon}^2 - m^2} \quad (\text{for } |\bar{\varepsilon}| > m), \tag{28}$$

where

$$N = Z\alpha\bar{\varepsilon}/\sqrt{m^2 - \bar{\varepsilon}^2}, \qquad N_0 = Z\alpha m/\sqrt{m^2 - \bar{\varepsilon}^2},$$

$$\gamma = \sqrt{\varkappa^2 - Z^2\alpha^2}, \qquad a_{+} = \sqrt{\bar{\varepsilon}/m + 1},$$

$$a_{-} = i\sqrt{\bar{\varepsilon}/m - 1}, \tag{29}$$

$$\nu = Z\alpha\bar{\varepsilon}/\sqrt{\bar{\varepsilon}^2 - m^2}, \qquad \nu_0 = Z\alpha m/\sqrt{\bar{\varepsilon}^2 - m^2};$$

$$F(\gamma) = e^{i\pi\gamma}\Gamma(\gamma - i\nu)\,\Gamma(-2\gamma)\,\Phi_1^{\pm} \quad (|\bar{\varepsilon}| > m), \tag{30}$$

and $M(\rho)$ and $W(\rho)$ are the well known solutions of the Whittaker equation.[16]

As for the functions $\Phi^{0\pm}$, they are solutions of the unperturbed equation. Here we must distinguish bound states ($\epsilon_e < m$) from unbound states ($\epsilon_e > m$). In the former case the $\Phi^{0\pm}$ are the well known electronic functions of the hydrogenlike atom, and in the latter case they are continuous-spectrum Coulomb functions.[12] The $\Phi^{0\pm}$ are normalized, and here in the determination of the normalization constants we can also take screening into account, as is usually done in the derivation of formulas for β decay.

APPLICATION TO BETA DECAY

Let us now return to the solutions (21). In the general case $\Phi^{\pm}_{1,2}$ and $\Phi^{0\pm}$ have simple forms only at very small or very large values of the argument. For β decay, however, we are interested in the behavior of the electronic functions only for $r < R$. We note that ρ, the argument of the functions $\Phi^{\pm}_{1,2}$, defined in Eq. (27), has a parametric dependence on the relation between $\overline{\epsilon}$ and m, whereas the argument of $\Phi^{0\pm}$ depends on ϵ_0/m. For strongly deformed nuclei the difference $\epsilon_{I_0} - \epsilon_I$ with $|I - I_0| \leq 2$ ordinarily does not exceed 2m (1 Mev). As for the electron's energy ϵ_e, in β decay it is limited by the energy of the transition. If we consider β-decay transitions with energies not exceeding 1 Mev (which is always the case for transitions between rotational levels), then $\overline{\epsilon} \leq 5m$ (2.5 Mev). From the relation $\rho = 2\lambda r$ for $R \sim 6 \times 10^{-13}$ cm (rare earths) and $\overline{\epsilon} = 5m$ we have $\rho(r = R) \approx 1/6$. The smaller $\overline{\epsilon}$, the smaller the error in expanding $\Phi^{\pm}$ in powers of ρ. There is another simplifying circumstance for $\rho(r = R) \leq 1$; this is that the integral

$$\int_{\infty}^{r} (\mathcal{A}^{-}\Phi_2^{-} + \mathcal{A}^{+}\Phi_2^{+})\,dr$$

in Eq. (21) is determined by the behavior of the integrand for small ρ.

In what follows we confine ourselves to the first term of the expansion in powers of ρ. Then the quantities $\Phi^{0\pm}$ have the same form both for the discrete spectrum $\epsilon_e < m$ (capture) and for the continuous spectrum $\epsilon_e > m$ (β decay):

$$\Phi^{0\pm}_{r\to 0} \approx C^{\pm}(\varepsilon_e)\, r^{\gamma_0}, \tag{31}$$

where γ_0 is the value of γ for the unperturbed state j_0, l_0. Owing to this the functions $\Phi^{\pm}$ will also be the same in this approximation for the bound and free states. As the result of calculation we get for $r \leq R$:

$$\Phi^{+}_{Ijl}(r) = \frac{A_{Ijl;I_0j_0l_0}}{R^2}\Phi^{0+}_{j_0l_0}(r)\left\{\left(\frac{r}{R}\right)^{\gamma-\gamma_0}\frac{5Z\alpha\,[1+(\varkappa-\gamma)/(\varkappa_0-\gamma_0)]}{2\gamma(\gamma_0+3-\gamma)(\gamma+2-\gamma_0)} - \left(\frac{r}{R}\right)^3\frac{Z\alpha}{(\gamma_0+3)^2-\gamma^2}\left(1+\frac{\varkappa-\gamma_0-3}{\varkappa_0-\gamma_0}\right)\right\}; \tag{32}$$

$$\Phi^{-}_{Ijl}(r) = \frac{A_{Ijl;I_0j_0l_0}}{R^2}\Phi^{0+}_{j_0l_0}(r)\left\{\left(\frac{r}{R}\right)^{\gamma-\gamma_0}\frac{5\,[\varkappa+\gamma+Z^2\alpha^2/(\varkappa_0-\gamma_0)]}{2\gamma(\gamma_0+3-\gamma)(\gamma+2-\gamma_0)} - \left(\frac{r}{R}\right)^3\frac{1}{(\gamma_0+3)^2-\gamma^2}\left(\varkappa+\gamma_0+3+\frac{Z^2\alpha^2}{\varkappa_0-\gamma_0}\right)\right\}. \tag{33}$$

It can be seen from Eqs. (32) and (33) that the correction functions depend only on ϵ_e (but not on $\overline{\epsilon}$), through the unperturbed functions. This fact is essential in applications. The proportionality between $\Phi^{\pm}$ and $\Phi^{0\pm}$ also has another consequence; namely, since in the region of the nucleus the $\Phi^{0\pm}$ have appreciable values only for small angular momenta of the electron, in practice the only important corrections will be those to states with small j_0, l_0.

It is easy to see that for β decay inclusion of the new "satellite" states can change the order of magnitude of the probabilities of forbidden transitions. In fact, for a given type of β interaction the value of the matrix element is determined by the difference ΔI of the nuclear spins of the initial and final states, and in the case of electron capture also by the electronic states j_0, l_0. The correction functions (14) contain new nuclear and electronic states, which leads to an effective decrease of the order of forbiddenness. The quantitative calculation of this effect of course depends on the type of interaction. It will be presented in another paper, in which we shall also examine the influence of the "satellite" states on the shape of the β-ray spectrum, and in which the results of calculations will be compared with the experimental data. We here mention only that at energies up to 1 Mev and with $\Delta I \geq 3$, for $Z \sim 70$ and $Q_0 \sim 5 \times 10^{-24}$ cm^2 (both for β decay and for capture) the transition probabilities can be increased by several orders of magnitude. Moreover, the matrix elements of transitions with $\Delta I = 3, 4, 5$ are of the same order of magnitude, which is not so in the case of spherical nuclei. Similar results can also be expected in the case of internal conversion.

V. Rittenberg took part in the initial stages of this work, and we express our sincere gratitude to him. We regard it as our pleasant duty to give our thanks also to Academician S. Titejca and to A. Gelberg for helpful discussions.

Note added in proof (February 13, 1960). It has recently become known to us [private communication from J. M. Pearson; see also Bull. Am. Phys. Soc. **4**, No. 4, 229 (1959)] that Pearson is now studying the influence of the nuclear quadrupole moment on the relative intensities of first-forbidden β transitions for Np^{236}. For this purpose the appropriate Dirac equations are being solved numerically. Pearson's preliminary results are negative (corrections ~ 4 percent), which agrees with the conclusion of the present paper.

[1] L. A. Sliv, JETP **17**, 1049 (1947).

[2] Z. Matumoto and M. Yamada, Progr. Theoret. Phys. **19**, 285 (1958).

[3] L. A. Sliv, JETP **21**, 770 (1951).

[4] L. A. Sliv and M. A. Listengarten, JETP **22**, 29 (1952).

[5] A. Bohr and B. Mottelson, Kgl. Danske Videnskab. Selskab, Mat.-fys. Medd. **27**, No. 16 (1953).

[6] Alaga, Alder, Bohr, and Mottelson, Kgl. Danske Videnskab. Selskab, Mat.-fys. Medd. **29**, No. 9 (1955).

[7] M. G. Redlich and E. P. Wigner, Phys. Rev. **95**, 122 (1954).

[8] S. G. Nilsson, Kgl. Danske Videnskab. Selskab, Mat.-fys. Medd. **29**, No. 16 (1955).

[9] Ya. A. Smorodinskiĭ, Usp. Fiz. Nauk **68**, 653 (1959), Sov. Phys.-Uspekhi **2**, 557 (1960).

[10] L. Wilets, Kgl. Danske Videnskab. Selskab, Mat.-fys. Medd. **29**, No. 3 (1954).

[11] M. E. Rose, Elementary Theory of Angular Momentum, New York (Wiley and Sons), 1957.

[12] A. Akhiezer and V. Berestetskiĭ, Квантовая электродинамика (Quantum Electrodynamics), Gostekhizdat, Moscow, 1953, AEC Tr. No. 2876.

[13] J. M. Blatt and V. F. Weisskopf, Theoretical Nuclear Physics, Wiley, N.Y., 1952.

[14] N. F. Mott and H. S. W. Massey, The Theory of Atomic Collisions, Oxford, 1933, Chapter 6.

[15] L. D. Landau and E. M. Lifshitz, Квантовая механика (Quantum Mechanics), Gostekhizdat, Moscow, 1948, Section 113.

[16] I. Ryzhik and I. Gradsheĭn, Таблицы интегралов, сумм, рядов, произведений, (Tables of Integrals, Sums, Series, and Products), Gostekhizdat, Moscow-Leningrad, 1951.

Translated by W. H. Furry
166

SOVIET PHYSICS JETP VOLUME 11, NUMBER 3 SEPTEMBER, 1960

THE SINGULAR POINTS OF SOME FEYNMAN DIAGRAMS

V. A. KOLKUNOV, L. B. OKUN', and A. P. RUDIK

Submitted to JETP editor August 10, 1959

J. Exptl. Theoret. Phys. (U.S.S.R.) **38**, 877-881 (March, 1960)

The positions of the singular points are determined for the two Feynman diagrams shown in Figs. 1 and 7.

BECAUSE of the recent interest in the singularities of scattering amplitudes it seems worthwhile to examine in detail the method of finding the singular points of complicated Feynman diagrams. We here use a method developed earlier[1,2] to calculate the singular points of the two Feynman diagrams shown in Figs. 1 and 7. We shall look for those singular points of these diagrams for which the values of all the integration parameters α_i in the corresponding Feynman integrals are different from zero (cf. reference 2).

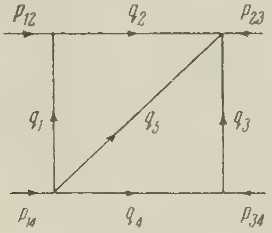

FIG. 1

1. Let us consider the Feynman diagram shown in Fig. 1. We shall assume that the masses of all the particles involved in this diagram are equal, and take them equal to unity. Then this diagram is a special case of the scattering of scalar mesons. By symmetry we have the following equalities, which greatly simplify the further calculations:

$$q_{54} = q_{25}, \quad q_{53} = q_{15}, \tag{1}$$

where $q_{ik} = q_i q_k$ is the scalar product of the four-vectors q_i and q_k.

The singular points of the Feynman diagram of Fig. 1 can be found by two methods: either by a trigonometric computation based on the properties of the scheme corresponding to the diagram of Fig. 1, or by an analysis of the determinants corresponding to the condition $\Sigma_i \alpha_i q_i = 0$ for each of the contours of the diagram of Fig. 1.

The Trigonometric Method. The scheme corresponding to the diagram of Fig. 1 is shown in Fig. 2, where we have introduced the usual notations $W^2 = (p_{12} + p_{14})^2$ and $Q^2 = (p_{12} + p_{23})^2$.

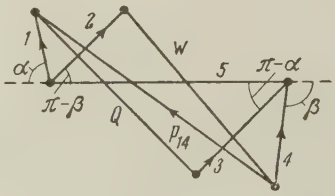

FIG. 2

As has been shown previously,[2] the lines 3, 4, and 5 must lie in one plane, and the lines 1, 2, and 5 in some other plane. We shall denote the angle between these two planes by φ. Then from the relation $p_{14}^2 = (q_1 + q_4 + q_5)^2 = 1$ we have

$$(1 + \cos\alpha)(1 + \cos\beta) = \sin\alpha \sin\beta \cos\varphi; \tag{2}$$

from the relation $W^2 = (q_2 + q_4 + q_5)^2$,

$$W^2 = 1 + 2(1 + \cos\alpha)^2 - 2\sin^2\alpha \cos\varphi; \tag{3}$$

and from the relation $Q^2 = (q_1 + q_3 + q_5)^2$,

$$Q^2 = 1 + 2(1 + \cos\beta)^2 - 2\sin^2\beta \cos\varphi. \tag{4}$$

Substituting the value of $\cos\varphi$ obtained from Eq. (2) in Eqs. (3) and (4), we get the following parametric representation of the function $F(W^2, Q^2) = 0$:

$$Q^2 = 1 + 2(1 + \cos\beta)^2 - 2(1 + \cos\alpha)(1 + \cos\beta)\sin\beta/\sin\alpha,$$
$$W^2 = 1 + 2(1 + \cos\alpha)^2 - 2(1 + \cos\alpha)(1 + \cos\beta)\sin\alpha/\sin\beta, \tag{5}$$

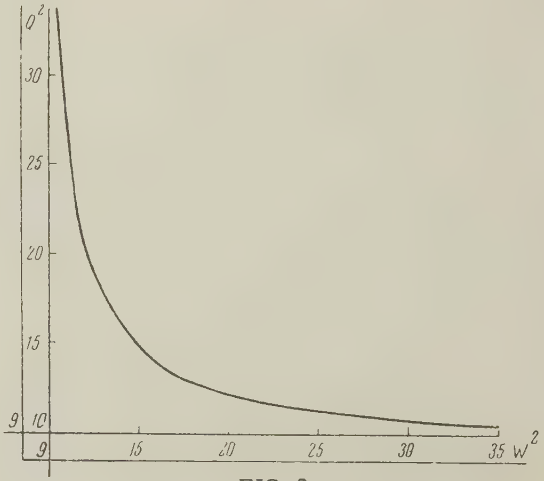

FIG. 3

where the angles α and β are connected by the relation

$$\alpha-\beta=-\pi/3. \tag{6}$$

The curve $F(W^2, Q^2)=0$ is shown in Fig. 3.

The value $\alpha=0$ corresponds to the asymptote $Q^2\to\infty$, $W^2\to 9$; $\beta=0$ corresponds to the asymptote $W^2\to\infty$, $Q^2\to 9$. These asymptotes arise from the two dipole patterns of Figs. 4 and 5, respectively, which are obtained by reductions of the diagram of Fig. 1. To the point $W^2=Q^2$ there correspond the values $\alpha=-\beta=-\pi/6$; at this point $W^2=Q^2=4(2+3^{1/2})$.

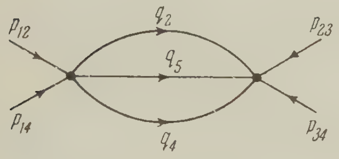

FIG. 4

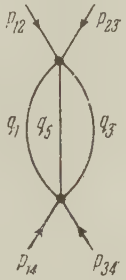

FIG. 5

The Determinant Method. From Eq. (1) and the conservation laws of the four-momenta one easily gets the following relations:

$$W^2=3+2q_{24}+4q_{25},\quad Q^2=3+2q_{13}+4q_{15}, \tag{7}$$

$$q_{14}=q_{23}=-(1+q_{15}+q_{25}). \tag{8}$$

We then use the equation $\alpha_1 q_1+\alpha_2 q_2-\alpha_5 q_5=0$. Multiplying it successively by the four-vectors (q_1, q_2, q_5), (q_1, q_2, q_3), and (q_1, q_2, q_4), we get the following three determinants:

$$\begin{vmatrix} 1 & q_{12} & q_{15} \\ q_{12} & 1 & q_{25} \\ q_{15} & q_{25} & 1 \end{vmatrix}=0, \tag{9$'$}$$

$$\begin{vmatrix} 1 & q_{12} & q_{15} \\ q_{12} & 1 & q_{25} \\ q_{13} & q_{23} & q_{53} \end{vmatrix}=0, \tag{9$''$}$$

$$\begin{vmatrix} 1 & q_{12} & q_{15} \\ q_{21} & 1 & q_{25} \\ q_{14} & q_{24} & q_{54} \end{vmatrix}=0. \tag{9$'''$}$$

Since q_{12} is known $(q_{12}=\frac{1}{2})$, the condition (9′) gives a connection between q_{15} and q_{25}. Figure 6 shows the curve $\varphi(q_{15}, q_{25})=0$, which is an ellipse with the semiaxes $(\frac{3}{2})^{1/2}$ and $(\frac{1}{2})^{1/2}$. In virtue of the condition that the Feynman parameters α_i are positive, only the part of the ellipse with $q_{25}>0$, $q_{15}>0$ is used.

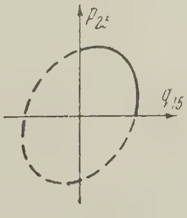

FIG. 6

Solving Eq. (9″) for q_{13} and Eq. (9‴) for q_{24} and using Eq. (8), after substitution in Eq. (7) we get

$$W^2=9+4(q_{25}-1)-2\left(\tfrac{3}{2}+q_{15}+q_{25}\right)\frac{q_{25}/2-q_{15}}{q_{25}-q_{15}/2},$$

$$Q^2=9+4(q_{15}-1)-2\left(\tfrac{3}{2}+q_{15}+q_{25}\right)\frac{q_{25}-q_{15}/2}{q_{25}/2-q_{15}}, \tag{10}$$

where q_{15} and q_{25} are connected by the condition (9′). The expressions (10) with the condition (9′) are equivalent to the expressions (5) with the condition (6).

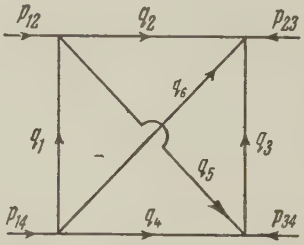

FIG. 7

2. As a second example we shall consider one of the Feynman diagrams for the scattering of pseudoscalar mesons (Fig. 7). The masses of all particles in the diagram of Fig. 7 are unity. This diagram is interesting because it is of the same order as the diagrams considered by Mandelstam for π-π scattering[3] (cf. Figs. 8 and 9).

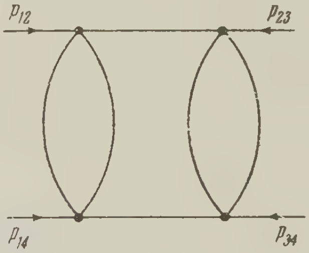

FIG. 8

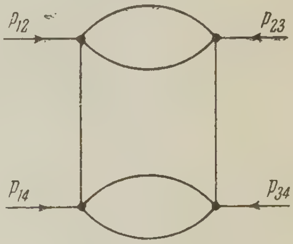

FIG. 9

To determine the singular point of the diagram of Fig. 7 it is more convenient to use the determinant method. From the conditions of symmetry it is easy to get the following equalities:

$$q_{15}=q_{35}=-q_{16}=-q_{36},\quad q_{25}=q_{45}=q_{26}=q_{46},$$

$$q_{12}=q_{34}=-q_{14}=-q_{23}. \tag{11}$$

Using these relations, we get the following expressions for $W^2=(p_{12}+p_{14})^2$ and $Q^2=(p_{12}+p_{23})^2$:

$$W^2=4+2q_{24}+8q_{25}+2q_{56},$$

$$Q^2=4+2q_{13}-8q_{15}-2q_{56}. \tag{12}$$

Let us now determine the connections between the scalar products that occur in the right members of the expressions (12). From the relation $p_{12}^2 = (q_2 + q_5 - q_1)^2 = 1$ we have

$$q_{12} = 1 - q_{15} + q_{25}. \qquad (13)$$

We then use the equation $\alpha_1 q_1 + \alpha_2 q_2 - \alpha_6 q_6 = 0$. By multiplying this equation successively by (q_1, q_2, q_6), (q_1, q_2, q_4), (q_1, q_2, q_3), and (q_1, q_2, q_5), we obtain determinants which we denote respectively by Δ_{126}, Δ_{124}, Δ_{123}, and Δ_{125}. Each of these determinants is equal to zero. Using Eqs. (13) and (11), we get from Δ_{126} a connection between q_{25} and q_{15}:

$$q_{25}^2 (1 + q_{15}) + q_{25} (1 - q_{15}^2) - q_{15} (1 - q_{15}) = 0. \qquad (14)$$

In solving the equation (14) one must remember the condition $\alpha_i > 0$.

From $\Delta_{124} = 0$ we get an expression for q_{24}:

$$q_{24} = 1 - 2q_{12} \, (q_{12}q_{25} + q_{15})/(q_{25} + q_{12}q_{15}), \qquad (15)$$

from $\Delta_{123} = 0$ an expression for q_{13}:

$$q_{13} = 1 - 2q_{12} (q_{25} + q_{12}q_{15})/(q_{12}q_{25} + q_{15}), \qquad (16)$$

and from $\Delta_{125} = 0$ an expression for q_{56}:

$$q_{56} = (q_{25}^2 - q_{15}^2)/(1 - q_{12}^2). \qquad (17)$$

In the expressions (15) — (17), q_{12} must be expressed in terms of q_{15} and q_{25} as shown in Eq. (13).

Thus by substituting Eqs. (15), (16), and (17) in Eq. (12), we get the following one-parameter form of the curve $F(W^2, Q^2) = 0$:

$$W^2 = 6 - 4q_{12} \frac{q_{12}q_{25} + q_{15}}{q_{25} + q_{12}q_{15}} + 8q_{25} + 2 \frac{q_{25}^2 - q_{15}^2}{1 - q_{12}^2},$$

$$Q^2 = 6 - 4q_{12} \frac{q_{25} + q_{12}q_{15}}{q_{12}q_{25} + q_{15}} - 8q_{15} - 2 \frac{q_{25}^2 - q_{15}^2}{1 - q_{12}^2}, \qquad (18)^*$$

where q_{12}, q_{15}, and q_{25} are connected by the relations (13) and (14).

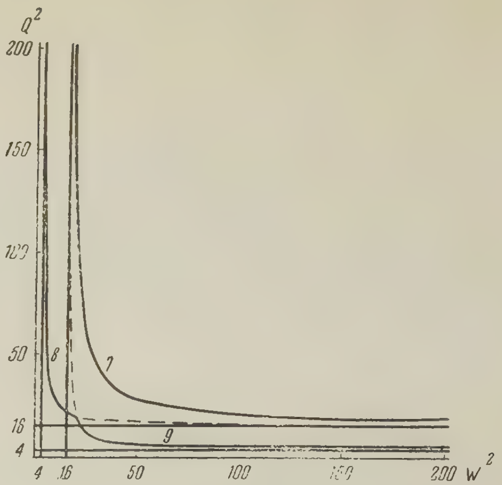

FIG. 10

Figure 10 shows the curve of $F(W^2, Q^2) = 0$. To the asymptote $Q^2 \to \infty$, $W^2 \to 16$ there correspond the values $q_{16} \to \infty$, $q_{24} = q_{25} = q_{56} = 1$, and to the asymptote $W^2 \to \infty$, $Q^2 \to 16$ the values $q_{25} \to \infty$ and $q_{13} = -q_{15} = -q_{56} = 1$. These asymptotes are obtained as the singular points of the dipole patterns reduced from the diagram of Fig. 7. To the point $W^2 = Q^2$ there correspond the values $q_{25} = -q_{15} = (1 + 5^{1/2})/2$, $q_2 = 2 + 5^{1/2}$. At this point $W^2 = Q^2 = 18 + 8 \times 5^{1/2}$.

In Fig. 10 curve 7 corresponds to the diagram of Fig. 7, and curves 8 and 9 correspond respectively to the diagrams of Figs. 8 and 9. As can be seen from Fig. 10, curve 7 lies much higher than curves 8 and 9.

The writers express their gratitude to Academician L. D. Landau for his interest in this work.

---

*The expressions for W^2 and Q^2 can be transferred to the form

$$W^2 = 6 + 8q_{25} - 4 \frac{1 + q_{25}}{1 + q_{15}} + 2 \frac{q_{15} + q_{25}}{q_{15} - q_{25} - 2};$$

$$Q^2 = 6 - 8q_{15} - 4 \frac{1 - q_{15}}{1 - q_{25}} - 2 \frac{q_{15} + q_{25}}{q_{15} - q_{25} - 2}.$$

[1] L. D. Landau, JETP **37**, 62 (1959), Soviet Phys. JETP 10, 45 (1960).

[2] L. B. Okun' and A. P. Rudik, Nuclear Phys. (in press).

[3] G. Chew and S. Mandelstam, Preprint.

Translated by W. H. Furry
167

ON THE QUANTUM ANALOG OF THE COLLISION INTEGRAL FOR ELECTRONS IN MAGNETIC AND ELECTRIC FIELDS

A. M. KOSEVICH and V. V. ANDREEV

Physico-technical Institute, Academy of Sciences, Ukrainian S. S. R.

Submitted to JETP editor August 10, 1959

J. Exptl. Theoret. Phys. (U.S.S.R.) **38**, 882-888 (March, 1960)

The influence of an electric field on the quantum analog of the collision integral for electrons in a magnetic field is investigated. For this purpose the quantum mechanical transport equation for electrons in a metal in crossed magnetic and electric fields is derived for low temperatures when the electron scattering occurs mainly on impurities. It is found that the purely quantum mechanical term in the "collision integral" which is proportional to the electric field and was not taken into account in the transport equation in reference 1 plays an important role in the discussion of quantum effects in strong magnetic fields. The oscillations of the elements of the "transverse" electrical conductivity tensor due to variations of the magnetic field are considered.

INTRODUCTION

I. M. LIFSHITZ[1] has constructed a quantum theory of the conduction of metals in a magnetic field at low temperatures. In this work essential use is made of the correspondence principle, according to which the kernel of the integral transformation that describes the collisions of the electrons with the impurities can be replaced by its classical value in the quasi-classical approximation. By making this replacement one neglects, of course, the effect of the electric field on the collision integral, as in the classical case.

In the present paper it is our aim to investigate the influence of the electric field on the quantum analog of the collision integral in a magnetic field and to point out possible consequences arising from taking this circumstance into account. Our interest in this problem was prompted to a large extent by remarks contained in the paper by Adams and Holstein.[2]

To obtain a qualitative idea of the possible role of those corrections in the quantum mechanical transport equation which are caused by the influence of the electric field **E** on the "collision integral" we consider the fundamental equation of the paper by I. M. Lifshitz,[1] which is in its simplest form

$$\{i(n-n')\omega^* + 1/\tau\}\rho^1_{nn'} = -e\mathbf{E}\mathbf{v}_{nn'}(f^0_n - f^0_{n'})/(\varepsilon_n - \varepsilon_{n'}). \tag{1}$$

Here ρ^1 is a correction to the equilibrium density matrix for the electrons, n is the quantum number of the orbital motion of the electron in the magnetic field **H**, $f^0_n \equiv f_0(\epsilon_n)$ is the Fermi function, $\omega^* = eH/m^*c$, m^* is the effective mass of the electron, τ is the relaxation time, and **v** is the velocity of the electron.

The most interesting region for the application of equation (1) is the region of strong magnetic fields, when $\omega^*\tau \gg 1$. In the following we will be interested only in this region of fields, so that we shall regard $1/\omega^*\tau$ as a small parameter the powers of which define the order of smallness of the corresponding expressions.

When the electric field is taken account of in the "collision integral" in (1), a small quantum term of the order of

$$(eEa/\hbar\omega^*)(f_0/\tau), \tag{2}$$

will appear, where a is some characteristic length related to the collision process. Observing that the estimate (2) depends on f_0 but not on ρ^1, we consider the largest possible alteration of Eq. (1). The estimate (2) depends critically on the determination of the order of magnitude of the parameter a. In the case of a longitudinal electric field ($\mathbf{E} \parallel \mathbf{H}$), the parameter a is of the same order of magnitude as the de Broglie wavelength of the electron. With such an a, the quantity (2) is so small that the longitudinal electric field may be neglected in the "collision integral." In the case of a transverse electric field ($\mathbf{E} \perp \mathbf{H}$) the parameter a should be of the order of magnitude of the classical radius of the Larmor orbit of the electron, r. This is easily understood by noting that the motion of the electron is quantized in a direction perpendicular to the magnetic field, so that even in the scattering from a point center the result depends on the radius of the orbit as on one of the parameters describing the state of the electron

Since the right hand side of (1) has for $n \neq n'$ the order of magnitude

$$eEv\,(f_0/\hbar\omega^*), \tag{3}$$

it may turn out that even in the case of a transverse field the correction (2) is smaller than the leading term of the right hand side of (1) by the factor $r/v\tau \sim 1/\omega^*\tau \ll 1$. However, for uniform fields the basic term on the right hand side of (1) does not give any contribution to the electric current in the zeroth approximation with respect to $1/\omega^*\tau$; to investigate the role of the additional term in the transport equation we must therefore estimate the ratio of the quantities (2) and (3) multiplied by $\omega^*\tau$. This last circumstance permits us to believe that in quantum phenomena the role of the term due to the influence of the electric field on the "collision integral" is comparable to that of the basic term included in Eq. (1).

In order to substantiate the qualitative remarks made above, we must analyze the equation for the density matrix of the electrons in the magnetic field and establish rigorously the corresponding quantum mechanical transport equation. Without pretense to completeness we consider, in Sec. 1, the quantum mechanical transport equation obtained from the general equation for the density matrix of perturbation theory, i.e., in the same approximation as in the work of Adams and Holstein.[2] The "collision integral" of this equation is derived by the method developed by Bogolyubov[3] and used by Gurzhi[4] for the calculation of the electron-phonon interaction in the field of an electromagnetic wave. This method is similar to that proposed by Kohn and Luttinger.[5]

In Sec. 2 we illustrate the role of the additional term in the transport equation on the example of the calculation of the oscillations of the tensor of the "transverse" electric conductivity (Shubnikov-de Haas effect). It will be shown in this section that the quantum oscillations of the tensor of electrical conductivity can, as has also been done earlier,[6] be expressed in terms of the classical "mobility" tensor and the oscillatory part of the magnetic moment of the electron gas. This connection between the classical and quantum characteristics was obtained for the first terms of the expansion of the tensor of electrical conductivity in powers of $1/\omega^*\tau$, but it is not essentially linked to perturbation theory by which τ was computed.

1. THE QUANTUM MECHANICAL TRANSPORT EQUATION IN MAGNETIC AND ELECTRIC FIELDS

Let us consider a gas of electrons which interact with particles of a different kind. As we are interested in the elastic scattering by the impurities, we consider only the interactions of the electrons with the heavy neutral particles (the interaction with the phonons can be treated in an analogous fashion). If the mass of the heavy particle is M, we can assume that $M \gg m$ (m is the mass of the electron), and consider the interaction of the electrons with fixed impurities. We assume that the heavy particles are distributed uniformly in space (the state of free motion of the particle is described by the momentum $\mathbf{s}$). The energy of the interaction between the electron and the heavy particle will be denoted by $V(\mathbf{r})$, where $\mathbf{r}$ is the distance between the two particles.

Following Bogolyubov,[3] we can write down a chain of equations for the partial statistical operators of the system of electrons and heavy particles and cut it off at the equation for the binary density matrix. We can then use perturbation theory to obtain a system of two equations for the one-particle density matrices of the electrons, ρ, and the heavy particles. The equation for ρ has the form

$$\partial\rho/\partial t + (i/\hbar)\,[\mathcal{H}, \rho] + D\{\rho\} = 0, \tag{4}$$

where $D\{\rho\}$ is the quantum analog of the collision integral. The expression for $D\{\rho\}$ is quadratic in the matrix elements of V and depends on the density matrix of the heavy particles.

In writing down the expression for $D\{\rho\}$ for the elastic scattering by the impurities, we regard the gas of heavy particles to be in equilibrium (the corresponding density matrix is diagonal in $\mathbf{s}$), and assume that the mass of the heavy particle is infinite as compared to the mass of the electron ($M \gg m$). These assumptions replace the usual averaging over the positions of the impurities and lead to the following expression for $D\{\rho\}$ in the representation in which the Hamiltonian of the electron in the given fields, $\mathcal{H}$, is diagonal ($\mathcal{H}_{\mu\nu} = \epsilon_\mu \delta_{\mu\nu}$):*

$$\begin{aligned}(D\rho)^{\mu\nu} = N\,(2\pi/\hbar) \sum \delta_+(\varepsilon_l - \varepsilon_\mu)\,[\rho^{\mu l'} V_{\mathbf{s}}^{l' l} V_{-\mathbf{s}}^{l\nu} - V_{\mathbf{s}}^{\mu l'} \rho^{l' l} V_{-\mathbf{s}}^{l\nu}] \\ - \delta_+(\varepsilon_\nu - \varepsilon_l)\,[V_{\mathbf{s}}^{\mu l} \rho^{l l'} V_{-\mathbf{s}}^{l'\nu} - V_{\mathbf{s}}^{\mu l} V_{-\mathbf{s}}^{l l'} \rho^{l'\nu}].\end{aligned} \tag{5}$$

The summation in (5) goes over all Latin indices, N is the number of scattering centers per unit volume, and

---

*All calculations leading to (5) are completely analogous to the calculations of references 3 and 4 and can therefore be omitted.

$$\delta_+(x) = \tfrac{1}{2}\delta(x) + i/2\pi x. \tag{6}$$

If we assume that $\rho^{\mu\nu}$ is diagonal, i.e., that there exists a distribution function, then formula (5) goes over into the classical collision integral for impurities.

Equation (4), with a Hamiltonian $\mathcal{H}$ which allows stationary states of the electron, determines the equilibrium density matrix of the electron gas. It is easy to verify that, up to terms which are quadratic in V [with accuracy corresponding to expression (5)], the equilibrium density matrix ρ_0 has the form

$$\rho_0^{\mu\nu} = f_0(\varepsilon_\mu)\,\delta_{\mu\nu} + F_0^{\mu\nu}, \tag{7}$$

$$F_0^{\mu\nu} = N\sum_{l,s} V_s^{\mu l} V_{-s}^{l\nu}\,(g^{\mu l} - g^{\nu l})/(\varepsilon_\mu - \varepsilon_\nu),$$

$$g^{\mu\nu} = (f_\mu^0 - f_\nu^0)/(\varepsilon_\mu - \varepsilon_\nu). \tag{8}$$

The physical meaning of the nondiagonal part of ρ_0 (i.e., of the matrix F_0) is very simple: expression (7) gives the first terms of the expansion of the operator $f_0(\mathcal{H} + W)$ in powers of $W = \Sigma V$ (sum over all impurities) averaged over the positions of the fixed impurities.

In order to establish the explicit form of Eq. (4) for the electron gas in constant magnetic (**H**) and electric (**E**) fields with $\omega^*\tau \gg 1$, we must take account of the existence of stationary states of the electron for mutually perpendicular **H** and **E**. This last circumstance leads, as we shall see below, to the dependence of $D\{\rho\}$ on the component of **E** perpendicular to **H**. A simple analysis shows at the same time that in our approximation $D\{\rho\}$ does not depend on the component of **E** along **H**. This means that the longitudinal electric field is fully included in the equations of type (1) in reference 1. In order to keep the appearance of the equations simple, we shall in the following not consider the component of **E** along the magnetic field at all, i.e., we shall investigate the simplest case of mutually perpendicular **H** and **E** ($H = H_z$, $E = E_y$).

Let $\hat{\epsilon}$ be the Hamiltonian for the motion of the electron in the magnetic field (its eigenvalues are $\epsilon_\mu \equiv \epsilon_n(p_z)$, $\mu = n, p_x, p_z$). We use the representation corresponding to this Hamiltonian in order to facilitate the comparison of our equation with the equations of reference 1 (the result given below can be obtained in a more direct way by using the representation in which the total Hamiltonian $\mathcal{H} = \hat{\epsilon} - eE\hat{y}$ is diagonal).

In the representation $\hat{\epsilon}$ the total Hamiltonian takes the form

$$\mathcal{H}_{\mu\nu} = (\varepsilon_\mu - eEy_0)\,\delta_{\mu\nu} - eE\xi_{\mu\nu}, \tag{9}$$

where $y_0 = -cp_x/eH$ plays the role of y, the coordinate of the center of the classical Larmor orbit of the electron,[7,8] and ξ is the displacement of the electron with respect to this center.

It is an essential characteristic of Eq. (9) that the electric field enters in the diagonal part of $\mathcal{H}$. It then follows by straight mathematical manipulation that the δ-functions of the "collision integral" $D\{\rho\}$, which describe the law of energy conservation, will also contain E explicitly. From a physical point of view this is extremely reasonable, since the term $-eEy_0$ in (9) has the meaning of the potential energy of the electron in the electric field. However, by virtue of the quantum nature of the motion of the electron in the Larmor orbit in the magnetic field (the electron is "smeared out" over the orbit), its "potential" energy depends on the location of the center of this orbit. Since the location of the center of the classical orbit changes in collisions, it is natural that E enters explicitly in the law of energy conservation.*

The nondiagonal part of $\mathcal{H}$ is very simply accounted for in writing down $D\{\rho\}$. If we express the density matrix ρ in the form $\rho = \rho_0 + \rho_1$ (ρ_0 is determined by (7), where ϵ_μ are the energy levels of the electron in the magnetic field) and linearize Eq. (4) with respect to E, we obtain as a result the following form of the quantum mechanical transport equation:

$$\partial\rho_1/\partial t + (i/\hbar)[\varepsilon, \rho_1] + eEgv_y + D\{\rho_1\}$$
$$= eED\{(cp_x/eH)\,df_0/d\varepsilon - \xi g\} + (i/\hbar)[eEy, F_0]. \tag{10}$$

The matrix product ga in (10) is to be understood as a direct product: $(ga)^{\mu\nu} = g^{\mu\nu}a^{\mu\nu}$. The matrix F_0 is given by formula (8).

The right hand side of (10), which vanishes in the classical case of scattering by point centers, takes account of the influence of E on $D\{\rho\}$ and distinguishes (10) from the quantum mechanical transport equation used by I. M. Lifshitz.[1]

In the stationary case ($\partial\rho_1/\partial t = 0$) a solution of (10) can be found in the form of an expansion of ρ_1 in powers of $1/\omega^*\tau$: $\rho_1 = \rho_1^{(0)} + \rho_1^{(1)}$. The first term, which is independent of the relaxation time, has the form

$$\rho_1^{(0)} = -eE\xi g. \tag{11}$$

---

*Noting that in the quasi-classical approximation the inclusion of E is essential only in the conservation law, the influence of the electric field on the "collision integral" can be described within the framework of the basic transport equation of reference 1 by using the representation in which the Hamiltonian $\mathcal{H}$ is diagonal and by replacing $\delta(\epsilon - \epsilon')$ by $\delta(\epsilon - eEy_0 - \epsilon' + eEy_0')$ in formula (27) of reference 1.

For $\rho_1^{(1)}$ we obtain the relation

$$(i/\hbar)[\varepsilon, \rho_1^{(1)}] = eED\{(cp_x/eH)\,df_0/d\varepsilon\} + (i/\hbar)[eEy, F_0], \tag{12}$$

which is in agreement with the result of Adams and Holstein.[2] The last term on the right hand side of (12) does not contribute to the current along the y axis and was therefore neglected.

In the classical approximation, expressions (11) and (12) go over into

$$\rho_1^{(0)} = -eE\xi df_0/d\varepsilon, \tag{13}$$

$$\partial\rho_1^{(1)}/\partial\varphi = eED_0\{(cp_x/eH)\,df_0/d\varepsilon\}, \tag{14}$$

respectively, where φ is an angular variable that describes the position of the electron on the classical orbit in momentum space, which we introduce following Lifshitz et al.[1,9] The determination of $D_0\{\rho\}$ is formally the same as before, with the only difference that the matrix elements of V which enter in the expression are replaced by the corresponding Fourier components,[1] and the functions $\delta_+(x)$ are changed to $\frac{1}{2}\delta(x)$.

It is easily seen that expressions (13) and (14) give the first terms of the expansion of the solution of the classical transport equation in a magnetic field in powers of $1/\omega^*\tau$.

2. THE TRANSVERSE ELECTRICAL CONDUCTIVITY OF A METAL IN A MAGNETIC FIELD

The electric current transverse to the magnetic field is given by the usual expression

$$j^\alpha = e\,\mathrm{Sp}\,\{\rho_1 v^\alpha\} \quad (\alpha = x, y). \tag{15}$$

It immediately follows from (15) and (11) that the terms proportional to 1/H in the expansion of the elements of the electrical conductivity tensor $\sigma^{\alpha y}$ are determined in the obvious way:[1]

$$\sigma_{yy}^{(0)} = 0, \quad \sigma_{xy}^{(0)} = (ec/H)(n_e - n_h), \tag{16}$$

where n_e is the number of electrons and n_h is the number of "holes" in the case of a closed Fermi surface. The expression (16) for $\sigma_{xy}^{(0)}$ includes the current along the x axis due to the last term in (12); it gives the following contribution to σ_{xy}:

$$\Delta\sigma_{xy}^{(0)} = (ec/H)\,\mathrm{Sp}\,\{F_0\}. \tag{17}$$

It is clear from the meaning of the diagonal elements of the matrix $F_0^{\mu\nu}$ that the additional term (17) can be included in the renormalized chemical potential of the electron gas, so that it is indeed taken account of in expression (16).

The part of $\sigma^{\alpha y}$ which is determined by the "collision integral" can be written in the form

$$\sigma_{\alpha y}^{(1)} = -2\sum_{\varepsilon_n}\int \frac{df_0}{d\varepsilon_n}\chi_{\mathrm{qu}}^{\alpha y} m^*\Delta\varepsilon_n dp_z. \tag{18}$$

The quantities $\chi_{\mathrm{qu}}^{\alpha y}$ entering in (18) are given in an obvious way by (15) and (12). They correspond to the linear terms of the expansion in powers of $1/\omega^*\tau$ of the analogous quantities χ introduced in reference 1.

The classical part of $\sigma_{\alpha y}^{(1)}$ is obtained from (18) by going directly from the summation over ϵ_n to the integration over ϵ and replacing $\chi_{\mathrm{qu}}^{\alpha y}$ by its classical value $\chi^{\alpha y}$:

$$\sigma_{\alpha y}^{(1)} = -2\iint \frac{df_0}{d\varepsilon}\chi^{\alpha y} m^* d\varepsilon dp_z. \tag{19}$$

Following reference 1, we replace the quantities $\chi_{\mathrm{qu}}^{\alpha y}$ in (18) by their classical values $\chi^{\alpha y}$. This operation was discussed in reference 1, and its validity was proven for the scattering by impurities. Its meaning is merely that we consider only the basic term in the expansion of the quantum corrections to $\sigma^{\alpha y}$ in powers of λ/r, where λ is the de Broglie wavelength, and r is the radius of the Larmor orbit of the electron. Since $\lambda/r \ll 1$ in metals, the magnitude of any quantum effect is determined by the basic term of the expansion.

Starting from (18) and (19) and using the method of calculation developed earlier,[6,7] we easily obtain the oscillatory parts of the elements of $\sigma^{\alpha y}$:

$$\Delta\sigma_{\mathrm{osc}}^{\alpha y} = h^3 (\chi m^*)_m^\zeta \frac{dS_m^{-1}(\zeta)}{d\zeta} H^2 \frac{\partial\Delta M_z}{\partial H}, \tag{20}$$

where $S_m(\xi)$ is the maximal area of the intersection of the Fermi surface with the plane perpendicular to **H**; the index m indicates that the corresponding quantity is evaluated at the maximal section of this surface. ΔM_z denotes the oscillatory part of the component of the magnetic moment of the electron gas along the magnetic field and is determined in reference 7.

We note that the classical formula for $\sigma_{\alpha y}^{(1)}$ with $kT \ll \xi_0$ (ξ_0 is the chemical potential of the electron gas at T = 0°K) can be written in terms of the same quantities which determine the amplitude of the oscillations in (20):

$$\sigma_{\alpha y}^{(1)} = n_0\bar{u}_{\alpha y}(\zeta), \tag{21}$$

where n_0 is the number of current carriers in a given group and $u_{\alpha y}$ has the meaning of an element of the "mobility tensor":

$$u^{\alpha y}(\varepsilon, p_z) = \chi^{\alpha y} m^*/S(\varepsilon, p_z) \tag{22}$$

the averaging is performed over the Fermi surface:

$$\bar{u}(\zeta) = \int u(\zeta, p_z)\,S(\varepsilon, p_z)\,dp_z \Big/ \int S(\varepsilon, p_z)\,dp_z. \tag{23}$$

The quantity $S(\xi, p_z)$ in (23) denotes the area of the intersection of the Fermi surface with the plane $p_z = \text{const}$, so that the integral $\int S(\zeta, p_z)\,dp_z$ gives the volume bounded by the Fermi surface.

Using (22), we rewrite (20) in the form

$$\Delta\sigma^{\alpha y}_{\text{osc}} = -H^2 u^{\alpha y}_m(\zeta)\left(\frac{d\ln S_m(\zeta)}{d\zeta}\right)\frac{\partial\Delta M_z}{\partial H}. \tag{24}$$

In this way we see that, as in the work of I. M. Lifshitz,[1] the oscillations of $\sigma^{\alpha y}$ are expressed in terms of the oscillations of ΔM_z, where the amplitude of the oscillations is determined by the classical "mobility tensor."

The oscillation amplitudes given by formula (24) are in agreement with the results of Adams and Holstein[2] and are larger than the amplitudes determined in reference 6 by the factor $\zeta_0/\hbar\omega^*$. This last circumstance allows us to neglect the oscillations of the chemical potential of the electron gas in the investigation of the oscillations.

We thank I. M. Lifshitz for his advice and valuable comments and also for giving us the opportunity to acquaint ourselves with the preprint of the paper by Adams and Holstein. We are also grateful to R. N. Gurzhi for a discussion.

---

[1] I. M. Lifshitz, JETP **32**, 1509 (1957), Soviet Phys. JETP **5**, 1227 (1957). J. Phys. Chem. Solids **4**, 11 (1958).

[2] E. N. Adams and T. D. Holstein, J. Phys. Chem. Solids **10**, 254 (1959).

[3] N. N. Bogolyubov, Проблемы динамической теории в статистической физике (*Problems of Dynamical Theory in Statistical Physics*), Gostekhizdat (1946). N. N. Bogolyubov and K. P. Gurov, JETP **17**, 614 (1947).

[4] R. N. Gurzhi, JETP **33**, 451 (1957), Soviet Phys. JETP **6**, 352 (1958).

[5] W. Kohn and J. M. Luttinger, Phys. Rev. **108**, 590 (1957).

[6] I. M. Lifshitz and A. M. Kosevich, JETP **33**, 88 (1957), Soviet Phys. JETP **6**, 67 (1958). J. Phys. Chem. Solids **4**, 1 (1958).

[7] I. M. Lifshitz and A. M. Kosevich, JETP **29**, 730 (1955), Soviet Phys. JETP **2**, 636 (1956).

[8] A. M. Kosevich, JETP **35**, 738 (1958). Soviet Phys. **8**, 512 (1959).

[9] Lifshitz, Azbel', and Kaganov, JETP **31**, 63 (1956), Soviet Phys. **4**, 41 (1957).

Translated by R. Lipperheide
168

SOVIET PHYSICS JETP VOLUME 11, NUMBER 3 SEPTEMBER, 1960

EQUATIONS OF STATE DETERMINING THE MAGNETOELASTIC PROPERTIES OF FERROMAGNETIC MONOCRYSTALS

K. B. VLASOV

Institute of Metal Physics, Academy of Sciences, U.S.S.R.

Submitted to JETP editor August 14, 1959

J. Exptl. Theoret. Phys. (U.S.S.R.) 38, 889-894 (March, 1960)

A thermodynamic derivation is given of the equations of state (for small magnetization changes and deformations) that determine the magnetomechanical properties of magnetically polarized ferromagnetic monocrystals possessing hexagonal symmetry. It is shown that in the case of nonuniform strains, the equilibrium values of the mechanical stresses and of the magnetic field intensity are connected by equations of state not only with the magnetization vector and strain tensor, but also with the rotation tensor, which determines the orientation of the volume element under consideration. On the basis of the equations obtained, conclusions are drawn regarding special features of the velocity of propagation and rotation of the plane of polarization of transverse elastic waves in ferromagnets.

1. In works of the author,[1,2] equations of "state" have been obtained that describe the magnetoelastic properties of magnetically polarized magnetoelastic media in the dynamic regime; and on the basis of these equations, it has been shown[3] that in the propagation of transverse elastic waves along the direction of the magnetization, a rotation of their plane of polarization is to be expected. To determine the physical nature of certain constants that enter in the equations mentioned above and in the equation for the angle of rotation of the plane of polarization, it is necessary to consider specific types of magnetoelastic media.

2. We consider ferromagnetic monocrystals. To make the calculation more definite, we choose for consideration ferromagnetic monocrystals possessing hexagonal symmetry, in which the sixfold axis is the axis of easy magnetization. With respect to their elastic, magnetic, and magnetoelastic properties for small magnetization changes, such monocrystals behave like magnetoelastic magnetically polarized media possessing uniaxial symmetry, whose properties were treated in references 1 — 3. We shall furthermore consider equilibrium processes and treat the crystal as infinite.

Let a change of the magnetization **I** occur in such a monocrystal, and let the monocrystal undergo an arbitrary elastic deformation, defined by the vector displacement **u** of an element of volume as a whole, the strain tensor $\epsilon_{ij} = \frac{1}{2}(\partial u_i/\partial x_j + \partial u_j/\partial x_i)$, and the rotation tensor $\omega_{ij} = \frac{1}{2}(\partial u_i/\partial x_j - \partial u_j/\partial x_i)$ of the volume element. The equations of state that connect the equilibrium values of the strains and magnetization with the magnetic field intensity **H** and with the symmetric components σ_{ij} and the antisymmetric components σ_{ij}^* of the mechanical "stress" tensor σ_{ij}^{**} can be found from the condition that the thermodynamic potential

$$\Phi = u_{\mathbf{ex}} + u_{\mathbf{c}} + u_{\mathbf{me}} + u_{\mathbf{el}} - H_m I_m - \sigma_{ij}\varepsilon_{ij} - \sigma_{ij}^*\omega_{ij}, \qquad (1)$$

be a minimum; here u_{ex}, u_c, u_{me}, and u_{el} are respectively the exchange, magnetocrystalline-anisotropy, magnetoelastic (magnetostrictive), and elastic energies. They are defined as follows:

$$u_{\mathbf{ex}} = {}^1/_2\, a_1 |\mathbf{I}|^2 + {}^1/_4\, a_2 |\mathbf{I}|^4, \qquad (2)$$

$$u_{\mathbf{me}} = {}^1/_2\, q_{mnij} I_m I_n \varepsilon_{ij}, \qquad (3)$$

$$u_{\mathbf{el}} = {}^1/_2\, c_{ijkl}\varepsilon_{ij}\varepsilon_{kl}. \qquad (4)$$

For the case of monocrystals of hexagonal symmetry, when the x_3 coordinate axis is chosen along the sixfold axis, the magnetocrystalline-anisotropy energy in the first approximation is equal to

$$u_{\mathbf{c}} = K_1 |[\mathbf{I}\times\mathbf{k}]|^2 / |I|^2, \qquad (5)$$

where **k** is the unit vector along the x_3 axis. In this case the tensor q_{mnij} has the following independent nonvanishing components:

$$q_{1111} = q_{2222}, \quad q_{3333}, \quad q_{1122} = q_{2211}, \quad q_{1133} = q_{2233},$$
$$q_{3311} = q_{3322}, \quad q_{2323} = q_{2332} = q_{3223} = q_{3232} = q_{1313} = q_{1331}$$
$$= q_{3113} = q_{3131}, \quad q_{1212} = q_{1221} = q_{2112} = q_{2121}$$
$$= (q_{1111} - q_{1122})/2. \qquad (6)$$

The choice of u_{me} in the form (3), with (6) taken into account, assumes that in magnetically uniaxial monocrystals, the magnetostriction is not determined solely by the orientation of the vector magnetization, as had been assumed earlier,[4,5] but depends also on the value of the magnitude of the magnetization.[6]

The tensor c_{ijkl}, in contrast to the tensor q_{mnij}, is invariant with respect to interchange of pairs of indices ij and kl. Therefore it has the same form as the tensor q_{mnij} except that $c_{3311} = c_{1133}$.

3. As an initial state, we may choose the state of the ferromagnetic crystal that one obtains by applying along the sixfold axis a uniform, constant polarizing magnetic field $H_0\mathbf{k}$, strong enough so that the crystal will be uniformly magnetized along the x_3 axis. From the minimization condition for the thermodynamic potential (1), we find the equilibrium values of the magnetization $I_0\mathbf{k}$ and of the stresses σ^0_{ij} in the initial state:

$$H_0 = (a_1 + a_2 I_0^2)\, I_0, \tag{7}$$

$$\sigma^0_{11} = \sigma^0_{22} = {}^1/_2\, q_{3311} I_0^2,$$
$$\sigma^0_{33} = {}^1/_2\, q_{3333} I_0^2, \qquad \sigma^0_{12} = \sigma^0_{23} = \sigma^0_{31} = 0. \tag{8}$$

In practice, it is convenient to choose another state as initial state, namely in which the initial stresses are zero. This is dependent on the fact that the crystal is usually not in an absolutely rigid environment, and under the influence of the stresses σ^0_{ij} it is uniformly strained, i.e., acquires uniform strains $\epsilon^0_{11} = \epsilon^0_{22}$ and ϵ^0_{33}.

4. We now consider the case in which there are present in the crystal a weak magnetic field $\mathbf{h}$ and mechanical stresses, alternating both in time and in space. In the crystal there will occur deformations determined by the strain tensor ϵ_{ij} and the rotation tensor ω_{ij} of the volume element, and the vector magnetization in each volume element will change its value slightly both in magnitude and in direction.

Expressions (2) — (5) for the various energies have already been written in a definite coordinate system, related to the crystallographic axes [that is, a system in which the tensor constants have a completely definite form characteristic of the given crystal symmetry, for example the form (6)]; they are correct, strictly speaking, only for uniform strains and rotations (which were not contemplated in the theory of elasticity). In the general case, nonuniform strains are connected with nonuniform rotations of the volume elements of the crystal, and consequently also with nonuniform rotations of the crystallographic axes of the volume elements.

We assume that the form of the expressions (2) — (5) for the energy densities, in which the tensor constants have a completely definite form characteristic of the given type of symmetry, remains valid also for nonuniform strains, but that these energies must be referred to coordinate axes x'_1, x'_2, x'_3 related to the crystallographic axes of the volume element under consideration.[7] We therefore introduce two coordinate systems: 1) a fixed coordinate system x_1, x_2, x_3 attached to the crystallographic axes of the crystal in its initial state, with the x_3 axis oriented along the sixfold axis; 2) a local movable coordinate system x'_1, x'_2, x'_3 attached to (and rotating with) the volume element under consideration, with the x'_3 axis oriented along the sixfold axis of the given volume element.

5. We now obtain the explicit form of the thermodynamic potential in the fixed system of coordinates. We first write the energies u_c and u_{me} in the movable coordinate system. For this purpose it is necessary in formula (5) to replace the unit vector $\mathbf{k}$ by the unit vector $\mathbf{k}'$, connected with $\mathbf{k}$ by the relation

$$\mathbf{k}' = \mathbf{k} + [\boldsymbol{\omega} \times \mathbf{k}], \tag{9}$$

and in the expression (3) to substitute the values of the components of the vector magnetization and of the strain tensor in the movable coordinate system, I'_m and ϵ'_{ij}, which are connected with the values of the components of these quantities in the fixed system of coordinates by the relations

$$\mathbf{I}' = \mathbf{I} + [\mathbf{I} \times \boldsymbol{\omega}], \qquad \varepsilon'_{11} = \varepsilon_{11} + 2\,(\omega_3\varepsilon_{12} - \omega_2\varepsilon_{13}), \ldots,$$
$$\varepsilon'_{12} = \varepsilon_{12} + \omega_1\varepsilon_{13} - \omega_2\varepsilon_{23} + \omega_3\,(\varepsilon_{22} - \varepsilon_{11}), \ldots, \tag{10}$$

where $\boldsymbol{\omega}$ is the vector rotation of the volume element, dual to the rotation tensor ω_{ij}, with components given by the known relations $\omega_1 = \omega_{32} = -\omega_{23}, \ldots$.

We next transform, according to formulas (9) and (10), to the fixed coordinate system. Here we choose as independent variables, determining the value of the change of the vector magnetization, the value of the change of absolute value ΔI and the vector angle of rotation $\boldsymbol{\theta}$, which determines the rotation of the vector magnetization with respect to the fixed coordinate axes. For changes of the vector magnetization that are small in comparison with its initial value $I_0\mathbf{k}$, its new value can be determined from the relation

$$\mathbf{I} = (I_0 + \Delta I)\,(\mathbf{k} + [\boldsymbol{\theta} \times \mathbf{k}]) - {}^1/_2\, I_0\,(\boldsymbol{\theta}^2\mathbf{k} - (\boldsymbol{\theta},\ \mathbf{k})\,\boldsymbol{\theta}), \tag{11}$$

and we obtain

$$u_c = K_1\,\{(\boldsymbol{\omega} - \boldsymbol{\theta})^2 - (\mathbf{k},\ \boldsymbol{\omega} - \boldsymbol{\theta})^2\}, \tag{12}$$

$$u_{me} = {}^1/_2\, q_{3311} I_0^2\,(\varepsilon_{11} + \varepsilon_{22}) + {}^1/_2\, q_{3333} I_0^2 \varepsilon_{33} + q_{3311}\, I_0 (\varepsilon_{11} + \varepsilon_{22})\Delta I$$
$$+ q_{3333}\, I_0 \varepsilon_{33} \Delta I - 2q_{2323} I_0^2\,(\varepsilon_{23}\theta_1 - \varepsilon_{13}\theta_2)$$
$$+ (2q_{2323} - q_{3333} + q_{3311})\, I_0^2\,(\varepsilon_{23}\omega_1 - \varepsilon_{13}\omega_2). \tag{13}$$

The exchange and elastic energies have the same form in both coordinate systems, since the first depends on the absolute value of the vector magnetization, and since the expression for the second differs by terms of the third order of small quantities when written in the fixed and in the movable systems.

On using the minimization conditions $\partial\Phi/\partial\theta = 0$, $\partial\Psi/\partial\Delta I = 0$, and $\partial\Phi/\partial\epsilon_{ij} = 0$ for the thermodynamic potential, and on taking account of (7) and (8), we obtain the following equations of state:

$$h_m = \gamma_{mn}I_n + h_{mf}\varepsilon_f + \overset{*}{h}_{mq}\omega_q,$$
$$\sigma_g = h'_{gn}I_n + c_{gf}\varepsilon_f + \overset{*}{c}_{gq}\omega_q, \tag{14}$$

where now by I_n are understood the small values of the change of magnetization from its initial state, and where the new symbols ϵ_f and ω_q have been introduced; they are connected with the previous quantities ϵ_{ij}, ω_m, and ω_{ij} by the following scheme: $\epsilon_1 = \epsilon_{11}, \ldots, \epsilon_6 = 2\epsilon_{12}, \ldots, \omega_6 = -2\omega_3 = 2\omega_{12}$. Here and hereafter we shall assume that the indices m, n, i, and j run through the values 1, 2, and 3; the indices f and g through the values 1, 2, . . . , 6; and the indices p and q through the values 4, 5, and 6.

Here the following components are different from zero:

$$\gamma_{11} = \gamma_{22} = (H_0/I_0 + 2K_1/I_0^2), \qquad \gamma_{33} = (H_0/I_0 + 2a_2I_0^2), \tag{15}$$

$$h_{31} = h_{32} = h'_{13} = h'_{23} = q_{3311}I_0, \qquad h_{33} = h'_{33} = q_{3333}I_0, \tag{16}$$
$$h_{15} = h_{24} = h'_{51} = h'_{42} = q_{2323}I_0,$$

$$\overset{*}{h}_{15} = -\overset{*}{h}_{24} = K_1/I_0, \tag{17}$$

$$c_{11} = c_{22} = c_{1111}, \quad c_{33} = c_{3333}, \quad c_{12} = c_{21} = c_{1122},$$
$$c_{13} = c_{23} = c_{31} = c_{32} = c_{1133},$$
$$c_{44} = c_{55} = c_{2323}, \qquad c_{66} = (c_{11} - c_{12})/2, \tag{18}$$

$$\overset{*}{c}_{44} = -\overset{*}{c}_{55} = -(2q_{2323} - q_{3333} + q_{3311})I_0^2/4$$
$$= -(2h_{15} - h_{33} + h_{31})I_0/4. \tag{19}$$

If as initial state we choose not the state with the initial stresses (8), but the state usually encountered in practice, in which these stresses are absent, then we still get equations of state of the type (14), except that the constant c_{44}^* will have the new value

$$\overset{*}{c}_{44} = -q_{2323}I_0^2/2 = -h_{15}I_0/2. \tag{19'}$$

6. On further setting $\partial\Phi/\partial\omega_m = 0$, we get an expression for the antisymmetric component of the mechanical "stress" tensor, σ_{ij}^*, to which is equivalent (dual) a certain axial vector T_m. Here

$$T_p = \overset{*'}{h}_{pn}I_n + \overset{*''}{c}_{pf}\varepsilon_f + \overset{**}{c}_{pq}\omega_q, \tag{20}$$

where

$$\overset{*'}{h}_{51} = -\overset{*'}{h}_{42} = \overset{*}{h}_{15}, \qquad \overset{*'}{c}_{44} = -\overset{*'}{c}_{55} = \overset{*}{c}_{44}, \qquad \overset{**}{c}_{44} = \overset{**}{c}_{55} = K_1/2, \tag{21}$$

and T_p is connected with T_m and σ_{ij}^* by relations of the type $T_4 = -T_1/2 = \sigma_{23}^*, \ldots$.

We shall explain the physical meaning of the antisymmetric part of the mechanical "stress" tensor σ_{ij}^*. The right member of (20) was obtained by differentiating, with respect to the components of the vector angle that describes the orientation of the volume element, the magnetocrystalline-anisotropy and magnetoelastic energies, which depend on interaction of the magnetization (spin system) with the crystal lattice. Therefore these derivatives should give expressions for the components of the force couples (with sign reversed), $-T_m^*$, exerted by the spin system on the crystal lattice of the volume element under consideration. Since in equilibrium no resultant couple should act on the volume element, this couple must be balanced by forces transmitted across the surface of the volume element from its environment. These forces can be described by the antisymmetric component σ_{ij}^* of the mechanical "stress" tensor σ_{ij}^{**}. From this it follows that the force couple T_m^* exerted by the spin system on the lattice is determined by the vector $-T_m$ ($T_m^* = -T_m$) dual to the antisymmetric component σ_{ij}^* of the mechanical "stress" tensor. However, the resultant force and couple (which figure in the equations of elasticity theory) on the volume element are determined by the symmetric part σ_{ij} of the mechanical "stress" tensor (or simply of the mechanical stress σ_{ij}). This is easy to show if one considers that the force on a volume element is determined by the divergence either of the tensor σ_{ij}^{**} or of the tensor T_{ij}^* dual to the vector force couple T_m^*, and if one takes account of the requirement that the resultant force moment must be expressed solely in the form of a surface integral.

7. In the absence of equilibrium, the derivatives of the thermodynamic potential Φ with respect to the components of the vector $\boldsymbol{\theta}$, which describe the orientation of the vector magnetization, determine the components of the resultant force moment that acts on the magnetization. On taking account of this and using (14), we get for this moment the relation

$$\mathbf{T} = [\mathbf{I}_0 \times \mathbf{h}^{\mathrm{ef}}], \tag{22}$$

where $h_m^{\mathrm{ef}} = h_m - \bar{h}_m$, and where $\bar{h}_m$ is that value of the magnetic field intensity which would correspond to the given values of magnetization and strain if the process were an equilibrium process; that is, we must substitute for $\bar{h}_m$ its value determined by formula (14). Knowing the couple that acts on the magnetization, we can construct the equation of motion of the magnetization.

8. We shall compare the relations obtained with the relations deduced earlier by a formal method. Equations (14) and (20) agree with Eqs. (7) of reference 1 and (17) of reference 2. (We remark, in this connection, that in Eqs. (7) and (17) of the articles cited, ϵ_4, $\epsilon_5, \ldots, \omega_6$ must be replaced not by ϵ_{23}, $\epsilon_{13}, \ldots, \omega_{12}$, but by their doubled values.) However, the constants h_{15}^*, c_{44}^*, and c_{44}^{**} introduced earlier by the formal method are now expressed through basic constants I_0, K_1, and q_{mnif} that describe the ferromagnetic.

9. Finally, we shall apply the relations obtained to the analysis of concrete physical processes.

In reference 3 it was shown that rotation of the plane of polarization of elastic waves may be determined, in particular, by the term containing the expression $h_{15}(h_{15} - h_{15}^*)$, which according to (17) can be written in the form $h_{15}^2(1 - K_1/I_0 h_{15})$. It follows that the rotation of the plane of polarization is determined not solely by the magnetostriction constant, but also by the magnetocrystalline anisotropy constant. In particular, for $h_{15} > 0$, the sign of the angle of rotation can depend on the ratio of the quantities K_1 and $I_0 h_{15}$, which can change with change of temperature. In order of magnitude, $h_{mf} \sim c_{ijkl}\lambda_s / I_0$, where λ_s is the saturation magnetostriction, and $c_{ijkl} \sim 10^{12}$ d/cm^2; thus we find that a calculation of the term $K_1/I_0 h_{15}$ (that is, of the constant h_{15}^*) is necessary for ferromagnetics that possess a relatively large anisotropy constant and small magnetostriction. For example, for $K_1 \geq 10^6$ erg/cm^3 and $\lambda_s \leq 10^{-6}$ this term is greater than unity.

As a second example, we calculate the speed c_t of propagation of transverse elastic waves propagated along the sixfold axis in a magnetodielectric. On solving the equation of motion of the theory of elasticity, $\rho\ddot{\mu}_i = \partial\sigma_{ij}/\partial x_j$, and taking account of (14), we get

$$c_t = c_t^0 \{1 - [h_{15}(h_{15} - \overset{*}{h}_{15}) - \gamma_{11}\overset{*}{c}_{44}]/\gamma_{11}c_{44}\}^{1/2}, \qquad c_t^0 = (c_{44}/\rho)^{1/2}. \tag{23}$$

This expression differs somewhat from the expression for c_t derived by Akhiezer, Bar'yakhtar, and Peletminskiĭ[8] (on going over to the case of propagation of the wave along the symmetry axis and to low frequencies); namely, in it there are additional terms, containing the constants h_{15}^* and c_{44}^*, which take account of rotations of the volume elements. In this connection we note that the expression for c_t from reference 8, mentioned above, can be easily obtained by calculating the speed of propagation of elastic waves by the formula $c_t = (c_{44}^H/\rho)^{1/2}$, where c_{44}^H is the value of the elastic modulus measured at constant magnetic field. For quasistatic processes, there is a definite relation[9] between the components of the elastic modulus tensor measured at constant field, c_{ijkl}^H, and at constant magnetization, $c_{ijkl}^I = c_{ijkl}$. For the present case this has the form $c_{44}^H = c_{44}(1 - h_{15}^2/\gamma_{11}c_{44})$. This difference between c_{44}^H and c_{44} bears the name "Δg-effect." Thus the difference between the relations for c_t given by Akhiezer and others[8] and by us [formula (23)] consists in this, that in the derivation of formula (23), along with calculation of the Δg-effect, which received attention in reference 8, account has been taken of the rotation of the volume elements that takes place in propagation of elastic waves transverse with respect to the polarizing magnetic field H_0.

We shall assume that in the initial state the ferrodielectric is in an unstressed state. Then in accordance with (15), (17), and (19′), we get

$$c_t = c_t^0 [1 - (h_{15}^2 + {}^1/_2 h_{15} H_0)/\gamma_{11}c_{44}]^{1/2}.$$

Thus in this case the speed of propagation of elastic waves is determined by the Δg-effect alone when $H_0 = 0$. On increase of H_0 ($H_0 \gg 2K_1/I_0$), c_t tends, if we take account of (15), not to c_t^0 but to the value $c_t^0(1 - h_{15}I_0/2c_{44})^{1/2}$, which may be either larger or smaller than c_t^0 according to the sign of the magnetostriction.

---

[1] K. B. Vlasov, Физика металлов и металловедение (Phys. of Metals and Met. Res.) **5**, 385 (1957).

[2] K. B. Vlasov, Izv. Akad. Nauk SSSR, Ser. Fiz. **22**, 1159 (1958), Columbia Tech. Transl. p. 1149.

[3] K. B. Vlasov and B. Kh. Ishmukhametov, JETP **37**, 745 (1959), Soviet Phys. JETP **10**, 545 (1960).

[4] F. Bitter, Introduction to Ferromagnetism, New York, 1937.

[5] S. V. Vonsovskiĭ and Ya. S. Shur, Ферромагнетизм (Ferromagnetism), Gostekhizdat, M.-L., 1948.

[6] L. D. Landau and E. M. Lifshitz, Электродинамика сплошных сред (Electrodynamics of Continuous Media), Gostekhizdat, 1957.

[7] W. F. Brown, Jr., Amer. J. Phys. **19**, 290 and 333 (1951).

[8] Akhiezer, Bar'yakhtar, and Peletminskiĭ, JETP **35**, 228 (1958), Soviet Phys. JETP **8**, 157 (1959).

[9] K. B. Vlasov, Тр. Института физики металлов, Уральский филиал АН СССР, Свердловск (Transactions of the Institute of Metal Physics, Ural Branch, Academy of Sciences, U.S.S.R.), Sverdlovsk, 1958, Number 20, page 71.

Translated by W. F. Brown, Jr.
169

SOVIET PHYSICS JETP VOLUME 11, NUMBER 3 SEPTEMBER, 1960

A STUDY OF THE LIMITS OF APPLICABILITY OF THE THEORY OF IONIZATION LOSSES

M. L. TER-MIKAELYAN

Physical Institute, Academy of Sciences, Armenian S.S.R.

Submitted to JETP editor August 25, 1959

J. Exptl. Theoret. Phys. (U.S.S.R.) 38, 895-905 (March, 1960)

The energy losses of an arbitrary moving particle are calculated by means of the macroscopic Maxwell equations. A separation into ionization losses and radiation losses is made, outside the framework of perturbation theory. Effects on the formulas for ionization losses owing to multiple Coulomb scattering are examined, and also effects of the finiteness of the path length. It is found that because of the existence of the density effect the influence of multiple Coulomb scattering on this part of the losses can be neglected.

1. INTRODUCTION

IN this paper we study the limits of applicability of the theory of energy losses by excitation, ionization, and Cerenkov radiation at ultrahigh energies (hereafter for brevity we shall call these losses ionization losses). As will be shown below, for ionization losses, just as for radiation losses,[1] large longitudinal distances which increase with the energy of the particle are effective in a collision with an individual atom. This can be intuitively understood from the fact that the "collision times" $\Delta t_1 \approx (\rho/v)(1 - v^2/c^2)^{1/2}$ (ρ is the impact parameter) correspond to large "passage times," during which the field of the particle is formed. From the relation

$$t = t_1 - R(t)/c = t_1 - \sqrt{v^2t^2 + \rho^2}/c$$

we at once get the required connection

$$t_{\text{eff}} \approx \rho/c\sqrt{1 - v^2/c^2} \quad \text{for} \quad t_1 = 0, \ \Delta t_{\text{eff}} \approx \Delta t_1/(1 - v/c).$$

Thus the field of the particle at the atom ($t_1 = 0$) during the time Δt_1 is determined by large passage-time intervals Δt_{eff} at large distances vt_{eff} from the atom.

If the effective distances become sufficiently large, various external causes can disturb the path of the charge, and this leads to a change in the theory of ionization losses. We shall consider the influences of three effects: multiple scattering, polarization of the medium, and finiteness of the trajectory. Inclusion of these effects in the radiation losses[2-4] has led to a sharp change of the formulas for bremsstrahlung and pair production. As regards the inclusion of the polarization of the medium in the calculation of ionization losses, its effect reduces to the well known density effect of Fermi and the Cerenkov radiation. Therefore the main part of this paper (Sec. 2 and 3) will be devoted to a study of the influence of multiple elastic scattering on the ionization losses.

For a qualitative estimate of this effect we consider the field produced by an arbitrarily moving charge. The Fourier components of the potentials are easily found from the Maxwell equations (cf. Sec. 2). For example, the vector potential is given by the expression

$$\mathbf{A}(\mathbf{k}, \omega) = -\frac{e}{4\pi^3 c}\left(\varepsilon\frac{\omega^2}{c^2} - k^2\right)^{-1}\int e^{-i\mathbf{kr}(t)+i\omega t}\,\mathbf{v}(t)\,dt,$$
$$\mathbf{A}(\mathbf{r}, t) = \int \mathbf{A}(\mathbf{k}, \omega)\,e^{i\mathbf{kr}-i\omega t}\,d\mathbf{k}\,d\omega.$$

If, starting from these expressions, we now calculate the flux of pseudoquanta, multiply it by the absorption coefficient of photons and integrate over $d\mathbf{k}$ and $d\omega$, we get an expression for the energy loss of an arbitrarily moving particle. The effect on the losses of deviations from rectilinear motion is determined by an integral of the form

$$\iint e^{-i\mathbf{k}(\mathbf{r}_1-\mathbf{r}_2)+i\omega(t_1-t_2)}\,dt_1\,dt_2,$$

in estimating which it is convenient to integrate over the direction of the vector $\mathbf{k}$.

If we forgo the scattering, then $|\mathbf{r}_1 - \mathbf{r}_2| = v(t_1 - t_2)$, $\omega = k_z v$, and the effective times will be of the order $t_{\text{eff}} \sim (\omega \pm kv)^{-1}$. Since $k = (\kappa^2 + \omega^2/v^2)^{1/2}$, for $\kappa \ll \omega/v$ we have

$$t_{\text{eff}} \sim \omega/\varkappa^2 v \tag{1}$$

(we are using $t \sim (\omega - kv)^{-1}$, omitting the terms with $\omega + kv$).

Let us now estimate the effect of the scattering. In this case[2,3]

$$|\mathbf{r}_1 - \mathbf{r}_2| = v(t_1 - t_2) + \Delta r, \quad \Delta r = v^2t^2E_s^2/E^2L$$

and in the exponent there is the additional quantity

$$k\Delta r \approx kv^2t^2E_s^2/E^2L \approx \omega vt^2E_s^2/2E^2L \tag{2}$$

(E is the energy of the electron, E_s is a constant of the order of 21 Mev, and L is the shower length). This quantity becomes comparable with the main term in the exponent, $(kv - \omega)t$, for a time t_1 that can be determined from the relation

$$(kv - \omega)\, t_1 \approx \omega v t_1^2 E_s^2/2E^2L. \tag{3}$$

Consequently, if $t_1 < t_{eff}$, then for momentum transfers in the direction perpendicular to the motion that satisfy

$$\varkappa_1^2 \lesssim (\omega E_s/Ev_1)\sqrt{\omega/Lv} \tag{4}$$

the scattering must be taken into account.

It is well known that there is a logarithmic contribution to the ionization loss from all values of the impact parameter (a quantity inversely proportional to κ) from minimum values to maximum values

$$\rho_{max} \approx \varkappa_{min}^{-1} \lesssim v/\omega_{at}\sqrt{1 - v^2/c^2} \tag{5}$$

(ω_{at} is a quantity of the order of atomic frequencies).

Comparing Eqs. (4) and (5), we see that the influence of scattering begins to be appreciable for the calculation of ionization loss if

$$\varkappa_1 \gtrsim \varkappa_{min},$$

that is, beginning at energies

$$E_1/mc^2 \gtrsim (L\omega_{at}/v)^{1/2}\, mc^2/E_s. \tag{6}$$

The situation is much changed, however, if we take into account the effect of the density of the medium. It will become clear from what follows that the density effect cuts off the effective range of κ at a value

$$\varkappa \approx \sqrt{4\pi Ne^2Z/mc^2} \tag{7}$$

(N is the density of particles in the medium). Comparing with Eq. (5), we find that the density effect becomes appreciable for

$$E_2/mc^2 \gtrsim (\omega_{at}/v)\sqrt{mc^2/4\pi NZe^2}, \tag{8}$$

that is, at smaller energies, and therefore the contribution to the ionization loss from the impact parameters at which the multiple scattering has a large effect is practically unimportant.

In the present paper we also consider the effect of the finiteness of the path on the ionization loss. Since lengths of the order of

$$ct_{eff} \sim c/(\omega - kv) \approx 2\omega_{at}/v\varkappa^2 \lesssim 2c/\omega_{at}(1 - v^2/c^2), \tag{9}$$

are effective for the ionization, the ionization curve must be changed if the length cT of the path is comparable with ct_{eff}. This condition sets in when

$$cT \lesssim (E/mc^2)^2\, c/\omega_{at}. \tag{10}$$

If the density effect is important at a given energy, we must substitute in Eq. (9) the value of κ from Eq. (7). Then we get

$$ct_{eff} \lesssim mc\omega_{at}/2\pi NZe^2 \tag{11}$$

In this case the finiteness of the path length will affect the ionization loss if

$$cT \lesssim mc\omega_{at}/2\pi NZe^2. \tag{12}$$

The effect of the finiteness of the path on the Cerenkov radiation was first considered by Tamm.[5]

2. THE TOTAL ENERGY LOSS

We shall calculate the energy loss by using the macroscopic Maxwell equations ($\mu = 1$):

$$\nabla^2 \mathbf{A} - \frac{\varepsilon}{c^2}\frac{\partial^2\mathbf{A}}{\partial t^2} = -\frac{4\pi}{c} e\mathbf{v}\delta(\mathbf{r} - \mathbf{r}(t)),$$

$$\nabla^2 \varphi - \frac{\varepsilon}{c^2}\frac{\partial^2\varphi}{\partial t^2} = -\frac{4\pi}{\varepsilon} e\delta(\mathbf{r} - \mathbf{r}(t)). \tag{13}$$

The solution for the potentials and the Lorentz condition are

$$\mathbf{A}(\mathbf{k},\omega) = \frac{e}{4\pi^3 c}\left[k^2 - \frac{\omega^2}{c^2}\varepsilon(\omega)\right]^{-1}\int_{-\infty}^{+\infty} \mathbf{v}(t)\, e^{i\omega t - i\mathbf{k}\mathbf{r}(t)}\, dt,$$

$$\varphi(\mathbf{k},\omega) = \frac{e}{4\pi^3\varepsilon(\omega)}\left[k^2 - \frac{\omega^2}{c^2}\varepsilon(\omega)\right]^{-1}\int_{-\infty}^{+\infty} e^{i\omega t - i\mathbf{k}\mathbf{r}(t)}\, dt,$$

$$\int_{-\infty}^{+\infty} (\mathbf{k}\mathbf{v}(t) - \omega)\, e^{i\omega t - i\mathbf{k}\mathbf{r}(t)}\, dt = 0. \tag{14}$$

The energy loss is given by the work done against the retarding force acting on the particle, according to the formula

$$F = -e\int_{-\infty}^{+\infty} \mathbf{E}(\mathbf{r},t)\, \mathbf{v}(t)\, dt, \tag{15}$$

where $\mathbf{E}(\mathbf{r}, t)$ is the electric field produced by the particle moving along the path $\mathbf{r}(t)$ with the velocity $\mathbf{v}(t)$. The Fourier component of the field is given by the relation

$$\mathbf{E}(\mathbf{k},\omega) = (i\omega/c)\,\mathbf{A}(\mathbf{k},\omega) - i\mathbf{k}\varphi(\mathbf{k},\omega). \tag{16}$$

Using these expressions, we easily get the formula that is the basis of our further calculations:

$$F = -\frac{ie^2}{4\pi^3}\int_{-\infty}^{+\infty} \frac{d\mathbf{k}\,\omega\, d\omega}{k^2 - \omega^2\varepsilon(\omega)/c^2}\left\{\left|\int \frac{\mathbf{v}}{c}\, e^{i\mathbf{k}\mathbf{r}(t) - i\omega t}\, dt\right|^2 - \frac{1}{\varepsilon}\left|\int e^{i\mathbf{k}\mathbf{r}(t) - i\omega t}\, dt\right|^2\right\}. \tag{17}$$

Regarding the limits of applicability of this formula we must make the following remarks. The energy $h\omega$ transferred to the medium must be much smaller than the energy of the electron, since $\mathbf{r}(t)$ is a prescribed trajectory, and recoil cannot be taken into account by such a method. In particular, since, as we shall see later on, Eq. (17) contains the loss to bremsstrahlung, the energy of the emitted quanta must be much smaller than that of the electron. For $\mathbf{r}(t)$ we must substitute the classical trajectory determined by the scattering by the Coulomb centers of force. Since, however, $Ze^2/hc < 1$, the concept of a classical trajectory is not valid, and the classical connection between the impact parameter and the angle of deviation does not exist. Actually this does not affect the result, because the procedure for obtaining the final result reduces to an averaging of the expression (17) over all possible trajectories, i.e., over all possible deviations from a straight path. Naturally, the averaging depends on the laws of multiple scattering, which are the same for the classical cases in virtue of the accidental circumstance that the Rutherford formula is always valid. Thus on this point the quantum nature of the phenomena is unimportant. Finally, we are using macroscopic electrodynamics. This means that the effective lengths must exceed interatomic distances, or in terms of momentum transfers this means that $\kappa \ll h/R_{at}$, where R_{at} is of the order of interatomic distances, and κ is the component of the vector $\mathbf{k}$ perpendicular to the direction of motion. This restriction must be made if we do not introduce explicitly the dependence of ϵ on the vector $\mathbf{k}$ (spatial dispersion), i.e., if we use the usual expression $\epsilon(\omega)$ which is legitimate in macroscopic electrodynamics.

For large values of κ we come to collisions with individual particles, so that a quantum calculation is necessary and we have to join it on to the formulas valid for small κ in a suitable way. On this point our calculations do not differ from the usual ones.

Finally, we shall make one more remark regarding the passage of Eq. (17) into an analogous formula when there is only one atom and we can neglect the effect of the medium. Here it is helpful to think of the loss as a quantity proportional to the imaginary part of $\epsilon(\omega)$, i.e., to the absorption coefficient. To get this result we replace the integration over ω between infinite limits by an integration from zero to infinity; using the property[6] of the dielectric constant, $\epsilon(-\omega) = \epsilon^*(\omega)$, we get

$$F_1 = -\frac{ie^2}{4\pi^3}\int\limits_{-\infty}^{+\infty} d\mathbf{k}\int\limits_0^{\infty}\frac{d\omega\,(\varepsilon-\varepsilon^*)\,\omega}{|k^2-\omega^2\varepsilon/c^2|^2}\left\{\left|\int\frac{\mathbf{v}}{c}\,e^{i\mathbf{kr}(t)-i\omega t}\,dt\right|^2\frac{\omega^2}{c^2}+\frac{k^2-\omega^2(\varepsilon+\varepsilon^*)/c^2}{|\varepsilon|^2}\left|\int e^{i\mathbf{kr}(t)-i\omega t}\,dt\right|^2\right\}. \tag{18}$$

The absorption coefficient is defined by the formula

$$N\sigma(\omega) = i\omega(\varepsilon-\varepsilon^*)/2c.$$

Here $\sigma(\omega)$ is the cross section for absorption of a quantum of frequency ω by an individual atom. Formula (18) can easily be obtained in a different way. We must calculate the flux of pseudoquanta from the moving particle, multiply it by the absorption coefficient, and integrate over all $\mathbf{k}$ and all ω. This makes clear how to make the passage to the case of collision with a single atom. To do this we must set $\epsilon = 1$ wherever it occurs in Eq. (18), except in the absorption coefficient. Then we are neglecting the influence of the density effect, and for a given motion $\mathbf{r}(t)$ we get as the formula for the loss:

$$F_2 = -\frac{ie^2}{4\pi^3}\int d\mathbf{k}\int\limits_0^{\infty}\frac{(\varepsilon-\varepsilon^*)\,\omega d\omega}{(k^2-\omega^2/c^2)^2}\left\{\left(k^2-\frac{2\omega^2}{c^2}\right)\left|\int e^{i\mathbf{kr}(t)-i\omega t}\,dt\right|^2 + \frac{\omega^2}{c^2}\left|\int\frac{\mathbf{v}(t)}{c}e^{i\mathbf{kr}(t)-i\omega t}\,dt\right|^2\right\}. \tag{19}$$

Let us now turn to the problem of separating out from the formula (17) the losses by ionization and bremsstralung. We first intergrate Eq. (17) over the direction of $\mathbf{k}$ relative to $\mathbf{r}(t_1) - \mathbf{r}(t_2)$. Then we get

$$F = -\frac{ie^2}{\pi^2}\int\frac{k^2dk\omega d\omega}{k^2-\omega^2\varepsilon(\omega)/c^2} \times\left[\iint\limits_{-\infty}^{+\infty}\left(\frac{\mathbf{v}_1\mathbf{v}_2}{c^2}-\frac{1}{\varepsilon}\right)e^{-i\omega(t_1-t_2)}\frac{\sin k|\mathbf{r}_1-\mathbf{r}_2|}{k|\mathbf{r}_1-\mathbf{r}_2|}dt_1\,dt_2\right]. \tag{20}$$

We shall assume the deviations from rectilinearity small and expand Eq. (20) in terms of these deviations. It must be noted that although the deviations are small the trigonometric functions can oscillate strongly, so that in general they cannot be expanded. If we denote the small deviations from rectilinearity by $\Delta\mathbf{r}$ and $\Delta\mathbf{v}$

$$\Delta\mathbf{r} = \mathbf{r}_2-\mathbf{r}_1-\mathbf{v}(t_2-v_1), \quad \Delta\mathbf{v} = \mathbf{v}_2-\mathbf{v}_1, \quad \mathbf{v} = \mathbf{v}_1 = \text{const}$$

and introduce $t_1 - t_2 = t$ and t_1 as variables of integration, then since all the quantities in the integrand depend only on the difference of the times and the integral over t_1 gives the total time of passage, we shall have for the energy loss in unit time

$$F' = -\frac{ie^2}{\pi^2}\iint\frac{k^2dk\omega d\omega}{k^2-\omega^2\varepsilon(\omega)/c^2}\left\{\int\limits_{-\infty}^{+\infty}\left(\frac{v^2}{c^2}-\frac{1}{\varepsilon} + \frac{\mathbf{v}_1\Delta\mathbf{v}}{c^2}\right)\frac{\sin(kvt+k\Delta r)}{kvt+k\Delta r}\,dt\right\}. \tag{21}$$

We further average the expression (21) over all possible paths. We use the formulas of multiple scattering

$$\overline{\mathbf{v}\Delta\mathbf{v}} = -\theta^2 v^2/2 = -E_s^2 v^3 |t|/2E^2 L,$$

$$\overline{(\mathbf{r}_1-\mathbf{r}_2)^2 - v^2(t_1-t_2)^2} = -v^2 t \overline{\int_0^t \theta_\tau^2 d\tau} + v^2 \overline{\left(\int_0^t \theta_\tau \, d\tau\right)^2}$$
$$= -v^2 E_s^2 t^2 |t| / 6E^2 L. \tag{22}$$

Substituting Eq. (22) in Eq. (21), we get ($F' = F_1 = F_2$)

$$F_1 = -\frac{2ie^2}{\pi^2 v} \iint \frac{k dk \omega d\omega}{k^2 - \omega^2 \varepsilon(\omega)/c^2} \left(\frac{v^2}{c^2} - \frac{1}{\varepsilon}\right)$$
$$\times \int_0^\infty \cos\omega t \cdot \sin\left(kvt - \frac{kv^2 t^2 E_s^2}{12E^2 L}\right) \frac{dt}{t},$$

$$F_2 = -\frac{2ie^2}{\pi^2 v} \iint \frac{k dk \omega d\omega}{k^2 - \omega^2 \varepsilon(\omega)/c^2} \left[\left(\frac{v^2}{c^2} - \frac{1}{\varepsilon}\right) \frac{vE_s^2}{12E^2 L} - \frac{v^3 E_s^2}{2c^2 E^2 L}\right]$$
$$\times \int_0^\infty \cos\omega t \, \sin\left(kvt - \frac{kv^2 t^2 E_s^2}{12E^2 L}\right) dt. \tag{23}$$

The lack of exactness of the expressions is due to the use of the simple averaging procedure used by Landau and Pomeranchuk,[2] which reduces to the replacement of averages of products of functions by products of functions of the averaged arguments. For the first term, F_1, the lack of exactness is due only to the fact that the average value of the sine is replaced by the sine of the average value. In what follows we shall be interested in only the first term of the expansion. If in the argument of the sine we neglect the term proportional to E_s^2 we arrive at the usual expression for the ionization loss in distant collisions of a particle with uniform rectilinear motion (cf. Sec. 3).

For relativistic particles and for $h\omega \gg h\omega_{at}$ the second term in the expansion as given by Eq. (23) differs from the formula for bremsstrahlung[2,3] with inclusion of effects of multiple scattering and ionization of the medium only in its coefficient. This can be shown in the following way. For large energy transfers $h\omega \gg h\omega_{at}$, the absorption coefficient falls off sharply. This means that the medium becomes transparent, and in the integration over ω we can assume that ϵ has an infintely small imaginary part (we emphasize that for this approximation it is necessary that the thickness of the target be smaller than the length in which a quantum is absorbed). We now carry out the integration over the variable k in the expression (23), using the relation[6]

$$\int_{-\infty}^{+\infty} d\omega \int_0^{k_{max}} \frac{\omega k^2 dk A(\omega, k)}{k^2 - (\omega^2/c^2)\varepsilon_1(\omega) - (i\omega^2/c^2)\varepsilon_2(\omega)}$$
$$= \int_0^\infty \frac{\pi i \omega^2}{c} \sqrt{\varepsilon} A\left(\omega, \frac{\omega}{c}\sqrt{\varepsilon}\right) d\omega. \tag{24}$$

In the derivation of this equation we have used the fact that ϵ_1 is an even function and $\epsilon_2 \rightarrow 0$ is an odd function of ω. The function $A(\omega, k)$ is an arbitrary even function of its arguments. Substituting the result (24) in the expression for F_2, we finally arrive at the formula for the bremsstrahlung

$$F_2 = -\frac{E_s^2}{E^2} \frac{e^2}{\pi L} \int_0^\infty d\omega \int_0^\infty \cos\omega t \sin\left(kvt - \frac{kv^2 t^2 E_s^2}{12E^2 L}\right) dt, \tag{25}$$

where $k = \omega\epsilon^{1/2}/c$.

The formula (25) differs by a factor 3 from the analogous formula obtained in references 2 and 3 by the same method of calculation. The starting expression used in those papers differs from Eq. (17) by the presence of a factor $\mathbf{k}\cdot\mathbf{v}/\omega$ in the integrand of the second term in the curly brackets in Eq. (17). Using the Lorentz condition (15), however, one can easily verify the equivalence of the two expressions (in this case it is a matter of the emission of quanta larger than atomic energies, so that one must use Eq. (24) and the procedure of integration described above). The reason for the lack of agreement of the coefficients is that in references 2 and 3 terms were dropped which after an integration by parts make contributions to the integral (17) that are of the same order as the main terms.

Finally, let us examine the limits of applicability of the expansion (23), and also the connection between the distant and close collisions. As we have already pointed out, the expansion is in terms of the deviations from rectilinear motion, which are always small (we note that in such an expansion the degree of the terms in the integrand with respect to t increases, but the integration over t always extends effectively to t_{eff}, so that the expansion remains valid). Nevertheless we know that the radiation energy loss of a relativistic electron is larger than the loss by ionization. This is so owing to the presence of the factor $v^2/c^2 - 1/\epsilon$ in F_1 [Eq. (23)], i.e., an accidental circumstance which sharply decreases the loss at frequencies higher than atomic frequencies. Thus when the energy loss occurs in large portions the main contribution to the loss in the expression (23) is given by the second term. This is easy to show. In fact, the second term gives the energy loss in the emission of quanta of energies smaller than $h\omega$ (the effect of the medium does not change the estimate):

$$F_2 \approx 4vr_0^2 Z^2 N L_{rad} h\omega / 137,$$

whereas the first term (we integrate it over all energy transfers, noting that the main contribution comes from atomic energies) gives

$$F_1 \approx 2\pi v Z e^4 N L_{ion} / mv^2.$$

A crude comparison of these two expressions shows that for large losses $h\omega$ the second term is in fact more important than the first, and it would seem that to get a knowledge of F_1 we would need to use an exact method of averaging, so as to confirm that the small terms dropped from F_2 do not change the expression for F_1. The situation is much better than this, however, because hereafter we shall use the expression F_1 only for small energy transfers, of the order of atomic energies. For large energy transfers in the ionization loss we must use the formulas for free collisions. According to the calculations of Bethe,[7] already at energy transfers of the order of $5me^4/h^2$ the main contribution to the ionization loss in hydrogen comes from free collisions. It is clear that for such values of $h\omega$ the effect of F_2 is quite unimportant.

Thus in the range of energy transfers in which we are interested our approximation consists of the replacement of the average value of the sine by the sine of the average value, which leads to logarithmic accuracy, as we shall see below.

3. INVESTIGATION OF F_1

Let us rewrite F_1 in the form

$$F_1 = -\frac{2ie^2}{\pi^2 v}\int\limits_0^\infty d\omega \int\limits_0^\infty dk \frac{\omega k(\varepsilon - \varepsilon^*)}{|k^2 - \omega^2\varepsilon/c^2|^2 |\varepsilon|^2}\left[\frac{\omega^2}{v^2}\left|\frac{v^2}{c^2}\varepsilon - 1\right|^2 - \frac{\omega^2}{v^2} + k^2\right] \int\limits_0^\infty \sin\left(kvt - \frac{kv^2t^2}{12L}\frac{E_s^2}{E^2}\right)\cos\omega t\,\frac{dt}{t} \tag{26}$$

and consider the integral over t:

$$I = I_1 + I_2 = \frac{1}{2}\int\limits_0^\infty \sin\left[(\omega + kv)t - \frac{kv^2t^2}{12L}\frac{E_s^2}{E^2}\right]\frac{dt}{t} + \frac{1}{2}\int\limits_0^\infty \sin\left[(kv - \omega)t - \frac{kv^2t^2E_s^2}{12LE^2}\right]\frac{dt}{t}. \tag{27}$$

In the first integral I_1 the effective range of integration is $t \sim 1/(\omega + kv)$. It is easy to show that the second term in the argument of the sine is always smaller than unity for all values of the variable of integration that are important for the integral I_1. That is, in I_1 we can always neglect the term with the scattering and integrate over t. We then find that $I_1 = \pi/4$ for all positive values of $\omega + kv$.

Let us now consider I_2. In the range

$$-(vE_s/E)\sqrt{k/12L} \gg kv - \omega \gg (vE_s/E)\sqrt{k/12L} \tag{28}$$

of the variables the term with the scattering can be neglected, and we have $I_2 = \pi/4$ if $\omega < kv$, and $I_2 = -\pi/4$ if $\omega > kv$. Since it can be seen from the condition (28) that the scattering is important only when $|kv - \omega|/kv \ll 1$, we can assume that $\omega \approx kv$. Outside the range (28), on the other hand, we can neglect the first term and get

$$I_2 = -\frac{1}{2}\int\limits_0^\infty \frac{\sin \xi^2}{\xi}\,d\xi = -\frac{1}{4}\int\limits_0^\infty \frac{\sin x}{x}\,dx = -\frac{\pi}{8}. \tag{29}$$

Let us rewrite F_1 in the following form:

$$F_1 = -\frac{2ie^2}{\pi^2 v}\int\limits_0^\infty d\omega \left\{\frac{\pi}{8}\int\limits_{\sim\varkappa_1}^{\sim\varkappa_2} \frac{\omega\varkappa(\varepsilon - \varepsilon^*)\,d\varkappa}{|k^2 - \omega^2\varepsilon^2/c^2|^2|\varepsilon|^2}\left[\frac{\omega^2}{v^2}\left|\frac{v^2}{c^2}\varepsilon - 1\right|^2 + \varkappa^2\right] + \frac{\pi}{2}\int\limits_{\sim\varkappa_2}^{\varkappa_{max}} \frac{d\varkappa\,\omega\varkappa(\varepsilon - \varepsilon^*)}{|k^2 - \omega^2\varepsilon/c^2|^2|\varepsilon|^2}\left[\frac{\omega^2}{v^2}\left|\frac{v^2}{c^2}\varepsilon - 1\right|^2 + \varkappa^2\right]\right\}. \tag{30}$$

Here we have introduced instead of k the variable $\kappa^2 = k^2 - \omega^2/v^2$, which in the case of rectilinear motion is a quantity inversely proportional to the square of the impact parameter. In calculating the integral (30) we neglect the density effect. As we already know, to do this we must introduce the absorption coefficient, according to Eq. (19), and set $\epsilon = 1$ in the other parts of Eq. (30). After integrating over κ we get

$$F_1 = -\frac{Ne^2c}{\pi v}\int\limits_0^\infty d\omega\,\sigma(\omega)\left\{\frac{1}{4}\ln\Big/\frac{\varkappa_2^2 + \omega^2(1 - v^2/c^2)/v^2}{\varkappa_1^2 + \omega^2(1 - v^2/c^2)/v^2} + \ln\frac{\varkappa_{max}^2}{\varkappa_2^2 + \omega^2(1 - v^2/c^2)/v^2} - \frac{v^2}{c^2} + \frac{\omega^2(1 - v^2/c^2)/c^2}{\varkappa_2^2 + \omega^2(1 - v^2/c^2)/v^2} - \frac{\omega^2(1 - v^2/c^2)/c^2}{\varkappa_1^2 + \omega^2(1 - v^2/c^2)/v^2}\right\}. \tag{31}$$

To reduce the integral to final form we use the well known properties of the absorption coefficient:[6]

$$\int\limits_0^\infty \omega\varepsilon''(\omega)\,d\omega = 2\pi^2 Ne^2 Z/m, \tag{32}$$

$$\ln\bar{\omega} = \frac{m}{2\pi^2 Ne^2 Z}\int\limits_0^\infty \omega\varepsilon''(\omega)\ln\omega\,d\omega. \tag{33}$$

At first we neglect the term associated with the scattering. This is legitimate if the inequality opposite to the inequality (6) is satisfied. The formula (31) takes the form

$$F_1 = \frac{2\pi Ne^4 Z}{mv}\left\{\ln\frac{v^2\varkappa_{max}^2}{\omega^2(1 - v^2/c^2)} - \frac{v^2}{c^2}\right\}. \tag{34}$$

If the inequality (6) holds, the formula for the loss takes a different form:

$$F_1 = \frac{2\pi Ne^4 Z}{mv}\left\{\ln\frac{\varkappa_{max}^2 E(12L)^{1/2}}{2\alpha(\bar{\omega}/v)^{3/2}E_s} - \frac{v^2}{c^2}\right\}, \quad \alpha \approx 1. \tag{35}$$

We shall now show that this case never occurs. The reason for this is the density effect, which we have temporarily neglected. If, on the other hand, we neglect the effect of the scattering, the total loss (in this case including also the loss by Cerenkov radiation) will be given by the formula of Fermi

$$F_1 = \frac{2\pi N Z e^4}{mv} \ln \frac{mc^2 \varkappa_{max}^2}{4\pi N Z c^2}. \qquad (36)$$

Comparing Eqs. (34) and (36), we note that the density effect begins to be appreciable when the condition (8) holds. A comparison of the conditions (6) and (8) shows that the density effect is always important at lower energies ($E_2 \ll E_1$). This means that when the energy is further increased (for $E > E_2$) the contribution to the ionization comes from the same impact parameters as for $E < E_2 \ll E_1$, at which the scattering still has no effect.

We can also examine the question of the influence of the scattering on the large-quantum energy loss. If $h \gg h\omega_{at}$, we can use the limiting value for the dielectric constant

$$\varepsilon = 1 - 4\pi N Z e^2 / m\omega^2. \qquad (37)$$

It is easy to see that the factor $4\pi NZe^2/mc^2$ appears in the argument of the logarithm in Eq. (31). As can be verified without difficulty, the frequency range in which the scattering is of importance is given by

$$\left(\frac{4\pi N Z e^2}{mc^2}\right)^{2/3} \left(\frac{E}{mc^2}\right)^{2/3} \frac{vL^{1/3}mc^2}{E_s} \ll \omega \ll \left(\frac{E_s}{mc^2}\right)^2 \frac{vE^2}{Lm^2c^4} \ll \frac{E}{h} \qquad (38)$$

and occurs at energies

$$E / mc^2 > (4\pi N Z e^2 / m)^{1/2} (mc^2 / E_s)^2 L / c. \qquad (39)$$

A comparison of Eqs. (38) and (39) with the analogous conditions in the formulas for the bremsstrahlung[3] shows that they are just the same. Furthermore, if the condition (38) is satisfied a pole appears in the integration of Eq. (30), and passage around this pole also leads to an additional contribution to the loss.

As we already noted above, however, these results do not change our conclusions about the total energy loss, because for large energy transfers the absorption coefficient is so small that the contribution to the loss calculated from Eq. (30) (without integration over ω) can be neglected in comparison with the contribution from free collisions (for energies that satisfy Eq. (39), Eq. (38) shows that the lower limit of the frequencies considerably exceeds atomic frequencies). Furthermore, the pole that appears in the first integral of Eq. (30) leads to a contribution to the emission of hard quanta satisfying the condition (38); but the intensity of the radiation is much smaller than that given by the term F_2. The latter term has been calculated inexactly because of the approximate method of averaging. Thus also for large energy transfers, although Eq. (30) is indeed changed, the contribution of F_1 to the large energy transfers can be neglected in comparison with the other losses.

4. INFLUENCE ON THE LOSSES OF THE EFFECT OF FINITENESS OF THE PATH

Let us consider the energy loss of a particle that has suddenly started its motion and has stopped after a time interval T. We shall neglect the effect of scattering. Integration of the basic formula (17) with the use of the Lorentz condition (15) gives

$$F = -\frac{2ie^2}{\pi^2} \int_0^{\varkappa_{max}} \iint_{-\infty}^{+\infty} \frac{\omega\, d\omega\, \varkappa\, d\varkappa\, dk_z}{\varkappa^2 + k_z^2 - \omega^2 \varepsilon(\omega)/c^2} \left\{ \frac{v^2}{c^2} - \frac{k_z^2 v^2}{\varepsilon \omega^2} \right\}$$
$$\times \frac{\sin^2((k_z\vartheta - \omega)T/2)}{(k_z v - \omega)^2}. \qquad (40)$$

To evaluate the integral we shall use a method described above. We at first neglect the density effect and look to see that change in the loss is caused by the presence of the limits on the trajectory. For this purpose we rewrite Eq. (40) in the form

$$F = -\frac{2ie^2}{\pi^2} \int_0^{\varkappa_{max}} d\varkappa \int_0^{\infty} d\omega \int_{-\infty}^{+\infty} dk_z \frac{\omega(\varepsilon - \varepsilon^*)\varkappa}{|\varepsilon|^2 |\varkappa^2 + k_z^2 - \omega^2\varepsilon/c^2|^2} \left\{ \left[\frac{\omega^2}{v^2} \left| \frac{v^2}{c^2}\varepsilon - 1 \right|^2 \right.\right.$$
$$\left.\left. - \frac{\omega^2}{v^2} + k^2 \right] \frac{k_z^2 v^2}{\omega^2} + \frac{|\varepsilon|^2 v^2 \omega^2}{c^4} \left(1 - \frac{k_z^2 v^2}{\omega^2} \right) \right\} \frac{\sin^2((k_z v - \omega)T/2)}{(k_z v - \omega)^2}. \qquad (41)$$

As we already know, the neglect of the density effect means that in Eq. (41) we are to set $\epsilon = 1$ everywhere in Eq. (41) except in the absorption coefficient (19). Then we can integrate over the parameter κ (we discuss the treatment of the pole later) and introduce the new variable of integration $x = (k_z v - \omega)T/2$.

We see from the expression (41) that the main contribution to the integral comes from the region $x \lesssim 1$ and $\omega \approx \omega_{at}$. We get (for $v \approx c$, $|k_z v - \omega|/\omega \ll 1$)

$$F = -\frac{ie^2 T}{2\pi^2 v} \int_0^{\infty} \omega\, d\omega\, (\varepsilon - \varepsilon^*)$$
$$\times \int_{-\infty}^{+\infty} dx \frac{\sin^2 x}{x^2} \left\{ \ln \frac{c^2 \varkappa_{max}^2}{2\omega^2 |2x/T\omega + 1 - v/c|} - 1 \right\}. \qquad (42)$$

From Eq. (42) we at once get the conditions for the effect of finiteness of the path to be appreciable.

If the condition (10) is satisfied, then the existence of the limits on the path has no effect, and integrating over x we arrive at the usual loss theory [Eq. (34)]. In the opposite case we can neglect the quantity $1 - v/c$ in comparison with $2x/T\omega$ in the argument of the logarithm and integrate over x:

$$F = -\frac{ie^2T}{2\pi v}\int_0^\infty \omega\, d\omega\, (\varepsilon - \varepsilon^*) \ln \frac{Tc^2\varkappa_{max}^2}{4\omega}. \tag{43}$$

Using Eqs. (32) and (33), we get

$$F = (2\pi Ne^4 Z/mv) \ln (Tc^2\varkappa_{max}^2/4\overline{\omega}). \tag{44}$$

This formula is valid if the logarithm is large.

Now let us estimate the influence of the density effect. As we have already seen, the density effect sets in when the condition (8) is satisfied. In this case the formula for the loss is Eq. (36). The combination of conditions (7) and (9) leads us to the criterion (12) given in the Introduction, under which the formula (43) holds. In this case the losses enter a plateau, the beginning and height of which are now determined not by the density effect, but by the finiteness of the path. It must be noted that the presence of limits to the path leads to the appearance of additional losses, which for a transparent medium appear in the form of radiation "at the stop."[5]

To separate this from the total loss [cf. Eq. (40) or (41)] we have to pass around the poles in the integration over κ. The passage around the poles [cf. Eq. (24)] leads to a formula for the loss by radiation

$$F_{\mathbf{rad}} = \frac{2e^2}{\pi}\int_0^\infty \omega\, d\omega \int_{-\infty}^{+\infty} dk_z \left\{\frac{v^2}{c^2} - \frac{k_z^2 v^2}{\varepsilon\omega^2}\right\} \frac{\sin^2((\omega - k_z v)T/2)}{(\omega - k_z v)^2}. \tag{45}$$

Let us rewrite the last formula, introducing the new variable

$$x = \omega - k_z v = 1 - (v\sqrt{\varepsilon}/c)\cos\vartheta \tag{46}$$

(ϑ is the angle the emitted quantum makes with the x axis):

$$F_{\mathbf{rad}} = \frac{2e^2}{\pi v}\int_0^\infty \omega\, d\omega \int_{\omega(1-v\sqrt{\varepsilon}/c)}^{\omega(1+v\sqrt{\varepsilon}/c)} dx \left[\left(\frac{v^2}{c^2} - \frac{1}{\varepsilon}\right)\frac{\sin^2(xT/2)}{x^2} + \frac{2\sin^2(xT/2)}{\varepsilon\omega x} - \frac{\sin^2(xT/2)}{\varepsilon\omega^2}\right]. \tag{45'}$$

Suppose that

$$v\sqrt{\varepsilon}/c > 1, \tag{47}$$

$$x_{min}T \gg 1. \tag{48}$$

Then we can use the equation

$$x^{-2}\sin^2(xT/2) = \tfrac{1}{2}\pi T\delta(x)$$

and get the loss by Cerenkov radiation

$$F_{\mathrm{C}} = T\frac{e^2 v}{c^2}\int_{v\sqrt{\varepsilon}/c>0} \omega\, d\omega\, (1 - c^2/v^2\varepsilon). \tag{49}$$

If the condition (47) is not satisfied, but Eq. (48) is, then we can average the rapidly oscillating factor (i.e., replace $\overline{\sin^2(xT/2)}$ by ½). Then Eq. (45′) can be rewritten in the form

$$F_{\mathbf{stop}} = -\frac{v^2e^2\sqrt{\varepsilon}}{\pi c^3}\int_0^\infty d\omega \int_0^\pi \frac{\sin^2\vartheta\, d(\cos\vartheta)}{(1 - (v\sqrt{\varepsilon}/c)\cos\vartheta)^2}. \tag{50}$$

For $\epsilon = 1$ this last expression becomes the well known formula (with a factor 2) for the stopping radiation. If the condition (48) is not satisfied there is a change of the formulas that have been given, because of the effect of finiteness of the path. Equation (49) is practically unchanged. Equation (50) (sic) will be decidely changed, since the main contribution to the integral comes from the region around $x_{\min}$. Here there is a complete analogy with the formulas for bremsstrahlung, and therefore the effect of multiple scattering which we omitted in Eq. (40) will also be very important at high energies.[2]

---

[1] M. L. Ter-Mikaelyan, JETP **25**, 289 (1953); **25**, 296 (1953).

[2] L. D. Landau and I. Ya. Pomeranchuk, Dokl. Akad. Nauk SSSR **92**, 535 (1953); **92**, 735 (1953).

[3] M. L. Ter-Mikaelyan, ibid. **94**, 1033 (1954).

[4] A. B. Migdal, JETP **32**, 633 (1957), Soviet Phys. JETP **5**, 527 (1957).

[5] I. E. Tamm, J. Phys. (U.S.S.R.) **1**, 439 (1939).

[6] L. D. Landau and E. M. Lifshitz, Электродинамика сплошных сред (Electrodynamics of Continuous Media), Gostekhizdat, Moscow, 1957.

[7] H. Bethe, Quantum Mechanics of the Simplest Systems (Russian Translation), Gostekhizdat, 1935 [Handb. Physik, 24/1, 1933].

Translated by W. H. Furry
170

SOVIET PHYSICS JETP VOLUME 11, NUMBER 3 SEPTEMBER, 1960

ELECTOMAGNETIC WAVES IN A MEDIUM WITH A CONTINUOUS ENERGY SPECTRUM. I.

V. S. MASHKEVICH

Kiev Polytechnic Institute

Submitted to JETP editor September 3, 1959

J. Exptl. Theoret. Phys. (U.S.S.R.) 38, 906-911 (March, 1960)

The dependence of the polarization vector on the electric field strength is found for a medium with a continuous energy spectrum. An integral expression which defines the polarizability is derived. Dispersion relationships are found between the Hermitian and anti-Hermitian parts of the kernel.

THE wave functions of states of a continuous spectrum extend widely in space. Therefore when such states are excited by electromagnetic waves, the polarization at any point of the medium will depend on the values of the field throughout the entire medium; i.e., there will be a spatial dispersion. Under these conditions the concept of polarizability, defined as the coefficient of proportionality between the polarization vector and the field strength, loses its meaning; one can speak only of a "polarizability kernel" which enters into the corresponding integral expression. The effect of spatial dispersion has been studied by Pekar[1] for exciton states. We consider here the case of arbitrary currentless states.

1. PERTURBATION THEORY FOR A CONTINUOUS SPECTRUM

We use a variant of the method of Weisskopf and Wigner, similar to the one used by Born and Kun Huang[2] to investigate the influence of anharmonicity on the dispersion. The Hamiltonian of the system is

$$\hat{H} = \hat{H}^0 + \hat{H}_d' + \hat{H}',$$

where $\hat{H}_0$ is the unperturbed Hamiltonian, $\hat{H}_d'$ is the dissipative perturbation, and $\hat{H}'$ is the electromagnetic perturbation. The corresponding wave function in the medium (the field is considered classical) is

$$\Psi = \Psi^0 + \Psi' + \Psi_d',$$

where

$$\Psi^0 = a_0 \exp(-i\omega_0 t)\,\psi_0$$

describes the ground state,

$$\Psi' = \sum_n a_n \exp(-i\omega_n t)\,\psi_n$$

describes the states into which direct transitions from Ψ^0 can be induced by $\hat{H}'$, and

$$\Psi_d' = \sum_s a_s \exp(-i\omega_s t)\,\psi_s$$

are the states of the quasi-continuous spectrum, into which transitions from Ψ' are possible as a result of $\hat{H}_d'$. For electronic states n, the operator $\hat{H}_d'$ can be found from the interaction of the electrons with the lattice vibrations; for the phonon states, it can be found from the anharmonicity. In the expressions given above, the ψ_m ($m = 0, n, s$) do not depend on time, and are normalized to unity; $\omega_m = E_m/\hbar$, E_m being the energy of the unperturbed state.

Assuming that at the initial moment of time the system is in the ground state, neglecting interference of the energy dissipations of different n-states and the width of the ground state, and postulating a harmonic electromagnetic perturbation of the form

$$\hat{H}' = \hat{h}^{(+)} \exp(-i\omega t) + \hat{h}^{(-)} \exp(i\omega t), \tag{1}$$

we obtain the stationary solution

$$\Psi' = -\frac{1}{\hbar}\left\{\exp[-i(\omega_0+\omega)t] \sum_n \frac{(n|\hat{h}^{(+)}|0)}{\omega_{n0}-\omega-i\gamma_n(\omega)}\psi_n + \exp[-i(\omega_0-\omega)t] \sum_n \frac{(n|\hat{h}^{(-)}|0)}{\omega_{n0}+\omega-i\gamma_n(-\omega)}\psi_n\right\}$$

$$(\omega_{n0} = \omega_n - \omega_0),$$

$$\gamma_n(\omega) = \frac{\pi}{\hbar^2} \lim_{\Delta\omega\to 0} \sum_{s_n}^{\omega,\,\omega+\Delta\omega} |(s_n|\hat{H}_d'|n)|^2,$$

in which the summation is carried out over the states s_n which produce dissipation in the states n, the frequencies of which lie in the interval from $\omega_0 + \omega$ to $\omega_0 + \omega + \Delta\omega$.

Ψ' is of the same order of smallness as $\hat{H}'$; Ψ_d', obviously, is of the order of $\hat{H}'\hat{H}_d'$. Hence the principal (of the order of $\hat{H}'$) time-dependent part of the operator $\hat{f}$ is

$$\bar{f}(t) = -\frac{1}{\hbar}\sum_n \left\{\frac{(0|\hat{f}|n)(n|\hat{h}^{(+)}|0)}{\omega_{n0}-\omega-i\gamma_n(\omega)} + \frac{(n|\hat{f}|0)(n|\hat{h}^{(-)}|0)^*}{\omega_{n0}+\omega+i\gamma_n(-\omega)}\right\}\exp(-i\omega t) + \text{c.c.} \tag{2}$$

2. DEPENDENCE OF THE POLARIZATION ON THE ELECTRIC FIELD

Let us consider the penetration of a transverse field into the medium. If a Coulomb calibration is used, the Coulomb interaction reduces to the portion $\hat{H}^0 + \hat{H}_d'$ of the Hamiltonian, and $\hat{H}'$ is determined by the solenoidal field only;

$$\hat{H}' = -\frac{1}{c}\sum_i (e_i/m_i)\,\mathbf{A}(\mathbf{r}_i, t)\,\hat{\mathbf{p}}_i, \qquad \operatorname{div}\mathbf{A}(\mathbf{r}, t) = 0, \quad (3)$$

where $\mathbf{r}_i$, e_i, m_i, and $\hat{\mathbf{p}}_i$ are the coordinates, charge, mass, and momentum operator of the i-th particle, respectively, $\mathbf{A}(\mathbf{r}, t)$ is the vector potential of the field, and c is the velocity of light in vacuum. In the case of harmonic time dependence,

$$\mathbf{A}(\mathbf{r}, t) = \mathbf{A}(\mathbf{r})\exp(-i\omega t) + \text{c.c} \quad (4)$$

Substituting (4) into (3) and comparing with (1), we find

$$\hat{h}^{(+)} = -\frac{1}{c}\sum_i (e_i/m_i)\,\mathbf{A}(\mathbf{r}_i)\hat{\mathbf{p}}_i, \qquad \hat{h}^{(-)} = \hat{h}^{(+)+}.$$

For the matrix elements appearing in (2) it is easy to obtain

$$(n|\hat{h}^{(+)}|0) = -\frac{1}{c}\int \mathbf{A}(\mathbf{r})\Pi_n(\mathbf{r})\,d\mathbf{r}, \quad (5)$$

where

$$\Pi_n(\mathbf{r}) = \sum_i (e_i/m_i)\int \psi_n^*(\mathbf{r}_1, \ldots, \mathbf{r}_{i-1}, \mathbf{r}, \mathbf{r}_{i+1}, \ldots, \mathbf{r}_N)$$
$$\times\, \hat{\mathbf{p}}\psi_0(\mathbf{r}_1, \ldots, \mathbf{r}_{i-1}, \mathbf{r}, \mathbf{r}_{i+1}, \ldots, \mathbf{r}_N)$$
$$\times\, d\mathbf{r}_1 \ldots d\mathbf{r}_{i-1}\,d\mathbf{r}_{i+1} \ldots d\mathbf{r}_N. \quad (6)$$

The intensity of the solenoidal field is

$$\mathbf{E}^{(\perp)}(\mathbf{r}, t) = -\frac{1}{c}\frac{\partial \mathbf{A}(\mathbf{r}, t)}{\partial t} = \frac{i\omega}{c}\mathbf{A}(\mathbf{r})\exp(-i\omega t) + \text{c.c.}$$
$$= \mathbf{E}^{(\perp)}(\mathbf{r})\exp(-i\omega t) + \text{c.c.}$$

Expressing $\mathbf{A}(\mathbf{r})$ in terms of $\mathbf{E}(\mathbf{r})$ in (5) and substituting the result and the analogous expressions for $(n|\hat{h}^{(-)}|0)$ into (2), we obtain

$$\bar{f}(t) = \exp(-i\omega t)\int \mathbf{K}_f(\mathbf{r}; \omega)\,\mathbf{E}^{(\perp)}(\mathbf{r})\,d\mathbf{r} + \text{c.c.}, \quad (7)$$

$$\mathbf{K}_f(\mathbf{r}, \omega) = -\frac{i}{\hbar\omega}\sum_n \left\{\frac{(0|\hat{f}|n)\,\Pi_n(\mathbf{r})}{\omega_{n0} - \omega - i\gamma_n(\omega)} + \frac{(n|\hat{f}|0)\,\Pi_n^*(\mathbf{r})}{\omega_{n0} + \omega + i\gamma_n(-\omega)}\right\}. \quad (8)$$

In order to obtain the material Maxwell equation connecting the polarization with the field, we must take for $\hat{f}$ the operator of the electric moment per unit volume

$$\mathbf{G}(\mathbf{r}) = \frac{1}{\Delta v}\sum_i \gamma_{\Delta v}(\mathbf{r}_i)\,e_i(\mathbf{r}_i - \mathbf{r}),$$

where Δv is a physically infinitesimal element of volume around the point $\mathbf{r}$ and

$$\gamma_{\Delta v}(\mathbf{r}) = \begin{matrix} 1, & \mathbf{r} \text{ inside } \Delta v \\ 0, & \mathbf{r} \text{ outside } \Delta v \end{matrix}.$$

In characterizing the electrical state of the material by a polarization vector, we are limiting ourselves to the dipole approximation. The same limitation therefore applies in (5) and (6). The corresponding calculations yield

$$\Pi_n(\mathbf{r}) = (n|\dot{\mathbf{G}}(\mathbf{r})||0) = i\omega_{n0}(n|\mathbf{G}(\mathbf{r})|0). \quad (9)$$

Substituting (9) and (8) into (7), we obtain

$$\mathbf{P}(\mathbf{r}, t) \equiv \{\bar{\mathbf{G}}(\mathbf{r})\}(t) = \mathbf{P}(\mathbf{r})\exp(-i\omega t) + \text{c.c.}, \quad (10)$$

$$P_{x'}(\mathbf{r}) = \sum_{y'}\int K_{x'y'}(\mathbf{r}, \mathbf{r}_0; \omega)\,E_{y'}^{(\perp)}(\mathbf{r}_0)\,d\mathbf{r}_0, \quad (11)$$

where the polarizability kernel is

$$K_{x'y'}(\mathbf{r}, \mathbf{r}_0; \omega) = \frac{1}{\hbar\omega}\sum_n \omega_{n0}\left\{\frac{(0|G_{x'}(\mathbf{r})|n)(n|G_{y'}(\mathbf{r}_0)|0)}{\omega_{n0} - \omega - i\gamma_n(\omega)}\right.$$
$$\left. - \frac{(n|G_{x'}(\mathbf{r})|0)(0|G_{y'}(\mathbf{r}_0)|n)}{\omega_{n0} + \omega + i\gamma_n(-\omega)}\right\}. \quad (12)$$

We shall write the polarizability kernel in the form

$$K_{x'y'}(\mathbf{r}, \mathbf{r}_0; \omega) = Q_{x'y'}(\mathbf{r}, \mathbf{r}_0; \omega) + R_{x'y'}(\mathbf{r}, \mathbf{r}_0; \omega), \quad (13)$$

where

$$Q_{x'y'}(\mathbf{r}, \mathbf{r}_0; \omega) = \frac{1}{\hbar\omega}\sum_n \omega_{n0}\left\{\frac{(\omega_{n0} - \omega)(0|G_{x'}(\mathbf{r})|n)(n|G_{y'}(\mathbf{r}_0)|0)}{(\omega_{n0} - \omega)^2 + \gamma_n^2(\omega)}\right.$$
$$\left. - \frac{(\omega_{n0} + \omega)(n|G_{x'}(\mathbf{r})|0)(0|G_{y'}(\mathbf{r}_0)|n)}{(\omega_{n0} + \omega)^2 + \gamma_n^2(-\omega)}\right\},$$

$$R_{x'y'}(\mathbf{r}, \mathbf{r}_0; \omega) = \frac{i}{\hbar\omega}\sum_n \omega_{n0}\left\{\frac{\gamma_n(\omega)(0|G_{x'}(\mathbf{r})|n)(n|G_{y'}(\mathbf{r}_0)|0)}{(\omega_{n0} - \omega)^2 + \gamma_n^2(\omega)}\right.$$
$$\left. + \frac{\gamma_n(-\omega)(n|G_{x'}(\mathbf{r})|0)(0|G_{y'}(\mathbf{r}_0)|n)}{(\omega_{n0} + \omega)^2 + \gamma_n^2(-\omega)}\right\}.$$

It is easy to see that

$$Q_{y'x'}(\mathbf{r}_0, \mathbf{r}; \omega) = Q^*_{x'y'}(\mathbf{r}, \mathbf{r}_0; \omega),$$
$$R_{y'x'}(\mathbf{r}_0, \mathbf{r}; \omega) = -R^*_{x'y'}(\mathbf{r}, \mathbf{r}_0; \omega),$$
$$Q_{x'y'}(\mathbf{r}, \mathbf{r}_0; \omega) = Q^*_{x'y'}(\mathbf{r}, \mathbf{r}_0; -\omega),$$
$$R_{x'y'}(\mathbf{r}, \mathbf{r}_0; \omega) = \overline{R}^*_{x'y'}(\mathbf{r}, \mathbf{r}_0; -\omega).$$

Here the first two identities show that Q and R are the Hermitian and anti-Hermitian parts of K respectively. The last two identities express the fact that (10) is real.

For a system with a continuous spectrum, the matrix elements $(0|\mathbf{G}(\mathbf{r})|n)$ differ from zero for a wide range of values of $\mathbf{r}$. Hence the portion of (12) which results from these states leads to a considerable spatial dispersion in (11).

3. DISPERSION RELATIONSHIPS FOR THE POLARIZABILITY KERNEL

Taking into account the spatial dispersion, the polarization, which depends causally on the strength of the solenoidal field, can be represented in the form

$$P_{x'}(\mathbf{r}, t) = \sum_{y'} \iint_0^\infty K_{x'y'}(\mathbf{r}, \mathbf{r}_0; \tau)\, E_{y'}^{(\perp)}(\mathbf{r}_0, t - \tau)\, d\tau\, d\mathbf{r}_0, \quad (14)$$

where $K_{x'y'}(\mathbf{r}, \mathbf{r}_0; \tau)$ is real. This is in full agreement with the results obtained above. At the same time, for the case of harmonic time-dependence we obtain, from (11),

$$P_{x'}(\mathbf{r}, t) = \sum_{y'} \int K_{x'y'}(\mathbf{r}, \mathbf{r}_0; \omega) \exp(-i\omega t)\, E_{y'}^{(\perp)}(\mathbf{r}_0)\, d\mathbf{r}_0 + \text{c.c.} \quad (15)$$

For the case of an arbitrary time-dependence of the field,

$$\mathbf{E}^{(\perp)}(\mathbf{r}, t) = \int_0^\infty \exp(-i\omega t)\, \mathbf{E}^{(\perp)}(\mathbf{r}, \omega)\, d\omega + \text{c.c.} \quad (16)$$

and (15) leads to

$$P_{x'}(\mathbf{r}, t) = \sum_{y'} \iint_0^\infty K_{x'y'}(\mathbf{r}, \mathbf{r}_0; \omega) \exp(-i\omega t)\, E_{y'}^{(\perp)}(\mathbf{r}_0, \omega)\, d\omega\, d\mathbf{r}_0 + \text{c.c.} \quad (17)$$

On the other hand, by substituting (16) into (14) we also obtain (17), since

$$K_{x'y'}(\mathbf{r}, \mathbf{r}_0; \omega) = \int_0^\infty \exp(i\omega\tau)\, K_{x'y'}(\mathbf{r}, \mathbf{r}_0; \tau)\, d\tau.$$

As a result of its finite relaxation time, the function $K_{x'y'}(\mathbf{r}, \mathbf{r}_0; \tau)$ in the case of a dielectric tends to zero as $\tau \to \infty$, being finite for all values of τ. Hence, if ω is taken as the complex variable, the function $K_{x'y'}(\mathbf{r}, \mathbf{r}_0; \omega)$ will have no singularities in the entire upper half-plane (including the real axis). As $\omega \to \infty$ along any path in the upper half-plane, $K_{x'y'}(\mathbf{r}, \mathbf{r}_0; \omega) \to 0$. From the foregoing properties of this function, we obtain in the usual way[3]

$$\int_{-\infty}^{+\infty} \frac{K_{x'y'}(\mathbf{r}, \mathbf{r}_0; x)}{x - \omega}\, dx - i\pi K_{x'y'}(\mathbf{r}, \mathbf{r}_0; \omega) = 0.$$

Inserting (13) here and separating the Hermitian and anti-Hermitian parts of the equation so obtained, we obtain the dispersion relationships that connect the Hermitian and anti-Hermitian parts of the polarizability kernel:

$$R_{x'y'}(\mathbf{r}, \mathbf{r}_0; \omega) = -\frac{i}{\pi} \int_{-\infty}^{+\infty} \frac{Q_{x'y'}(\mathbf{r}, \mathbf{r}_0; x)}{x - \omega}\, dx,$$

$$Q_{x'y'}(\mathbf{r}, \mathbf{r}_0; \omega) = -\frac{i}{\pi} \int_{-\infty}^{+\infty} \frac{R_{x'y'}(\mathbf{r}, \mathbf{r}_0; x)}{x - \omega}\, dx. \quad (18)$$

These relationships represent a generalization of the Kramers-Kronig formulas to the case when spatial dispersion is taken into account.

The formulas (18), which apply to the polarizability kernel, will in general not be valid for the complex refractive index, which has been introduced formally and measured experimentally. This fact has been observed in experiments.[4]

4. OUTLINE OF THE SOLUTION OF MAXWELL'S EQUATIONS

The total strength of the macroscopic electric field is

$$\mathbf{E}(\mathbf{r}, t) = \exp(-i\omega t)\, \mathbf{E}(\mathbf{r}) + \text{c.c.},$$

in which $\mathbf{E}(\mathbf{r})$ can be divided into solenoidal and irrotational parts:

$$\mathbf{E}(\mathbf{r}) = \mathbf{E}^{(\perp)}(\mathbf{r}) + \mathbf{E}^{(\parallel)}(\mathbf{r}), \quad \operatorname{div} \mathbf{E}^{(\perp)}(\mathbf{r}) = 0, \quad \operatorname{curl} \mathbf{E}^{(\parallel)}(\mathbf{r}) = 0.$$

Similarly, we put

$$\mathbf{P}(\mathbf{r}) = \mathbf{P}^{(\perp)}(\mathbf{r}) + \mathbf{P}^{(\parallel)}(\mathbf{r}).$$

This corresponds to the separation

$$K_{x'y'}(\mathbf{r}, \mathbf{r}_0; \omega) = K_{x'y'}^{(\perp)}(\mathbf{r}, \mathbf{r}_0; \omega) + K_{x'y'}^{(\parallel)}(\mathbf{r}, \mathbf{r}_0; \omega),$$

$$\operatorname{div}_r \mathbf{K}_{y'}^{(\perp)}(\mathbf{r}, \mathbf{r}_0; \omega) = 0, \quad \operatorname{curl}_r \mathbf{K}_{y'}^{(\parallel)}(\mathbf{r}, \mathbf{r}_0; \omega) = 0,$$

where $(\mathbf{K}_{y'})_{x'} = K_{x'y'}$. In this case

$$P_{x'}^{(\perp)}(\mathbf{r}) = \sum_{y'} \int K_{x'y'}^{(\perp)}(\mathbf{r}, \mathbf{r}_0; \omega)\, E_{y'}^{(\perp)}(\mathbf{r}_0)\, d\mathbf{r}_0, \quad (19)$$

$$P_{x'}^{(\parallel)}(\mathbf{r}) = \sum_{y'} \int K_{x'y'}^{(\parallel)}(\mathbf{r}, \mathbf{r}_0; \omega)\, E_{y'}^{(\perp)}(\mathbf{r}_0)\, d\mathbf{r}_0. \quad (20)$$

From Maxwell's equations we find

$$\mathbf{E}^{(\parallel)}(\mathbf{r}) + 4\pi \mathbf{P}^{(\parallel)}(\mathbf{r}) = 0 \quad (21)$$

and, taking (19) into account,

$$\Delta^2 E_{x'}^{(\perp)}(\mathbf{r}) + (\mu\omega^2/c^2)\, E_{x'}^{(\perp)}(\mathbf{r}) + (4\pi\mu\omega^2/c^2) \sum_{y'} \int K_{x'y'}^{(\perp)}(\mathbf{r}, \mathbf{r}_0; \omega)\, E_{y'}^{(\perp)}(\mathbf{r}_0)\, d\mathbf{r}_0 = 0, \quad (22)$$

where μ is the magnetic permeability, which for simplicity will be considered to be a scalar. (22) is a system of equations for the determination of $\mathbf{E}^{(\perp)}(\mathbf{r})$. When $\mathbf{E}^{(\perp)}(\mathbf{r})$ has been found it is then possible, according to (20) and (21), to find

$$E_{x'}^{\parallel}(\mathbf{r}) = -4\pi \sum_{y'} \int K_{x'y'}^{(\parallel)}(\mathbf{r}, \mathbf{r}_0; \omega)\, E_{y'}^{(\perp)}(\mathbf{r}_0)\, d\mathbf{r}_0.$$

Note that the expression $\exp(i\mathbf{k} \cdot \mathbf{r})$ is not, generally speaking, a solution of (22), since the spatial dispersion leads to complications in the spatial behavior of monochromatic waves.

The application of the theory developed here to the case of exciton states in a crystal will be given later.

---

[1] S. I. Pekar, JETP **33**, 1022 (1957), **34**, 1176 (1958), **36**, 451 (1959); Soviet Phys. JETP **6**, 785 (1958), **7**, 813 (1958), **9**, 314 (1959).

[2] M. Born and Kun Huang, Dynamical Theory of Crystal Lattices, Oxford, 1954.

[3] L. D. Landau and E. M. Lifshitz, Электродинамика сплошных сред (Electrodynamics of Continuous Media), Gostekhizdat, M. (1957).

[4] M. S. Brodin and M. S. Soskin, Izv. Akad. Nauk SSSR, Ser. Fiz. **22**, 1316 (1958), Columbia Tech. Transl. p. 1308; Brodin, Prikhot'ko, and Soskin, Оптика и спектроскопия (Optics and Spectroscopy) **6**, 28 (1959).

Translated by D. C. West
171

SOVIET PHYSICS JETP VOLUME 11, NUMBER 3 SEPTEMBER, 1960

GYROMAGNETIC RESONANCE ABSORPTION OF ELECTROMAGNETIC WAVES IN A PLASMA

B. N. GERSHMAN

Radiophysics Institute, Gorkiĭ State University

Submitted to JETP editor September 3, 1959

J. Exptl. Theoret. Phys. (U.S.S.R.) 38, 912-924 (March, 1960)

The absorption of characteristic waves in a uniform magnetoactive plasma at frequencies close to the gyromagnetic frequency and multiples of this frequency is investigated, taking account of the thermal motion of the electrons. Collisions and specific plasma absorption mechanisms are considered.

In an earlier work of the author[1] (referred to hereinafter as I) the absorption of electromagnetic waves in a plasma (with thermal motion of the electrons taken into account) was investigated by means of a general dispersion equation for characteristic waves of all three possible types: ordinary waves, extraordinary waves, and plasma waves (denoted 1, 2 and 3). However, we have not analyzed in I cases in which the frequency is close to the gyromagnetic frequency ω_H or its multiples $2\omega_H$, $3\omega_H$, etc. In the present work we investigate absorption at these gyromagnetic frequencies, so that this paper represents a direct extension of I.

The theory of gyromagnetic resonance absorption of waves in a plasma has already been developed.[2-4] In certain respects the present analysis is more general. Both the damping in time and the absorption in space are determined for all three types of waves. The first resonance and certain problems associated with collision effects are considered in greater detail. In addition, we make estimates of certain quantities, give numerical examples, and refine certain of the results obtained in references 2 and 3.

We determine the absorption by starting with the dispersion equation of I [(Eq. 1.8)], which will not be written out completely here. This equation was obtained by solving a linearized system of the electrodynamic equations and the kinetic equation for the electrons. The problem was formulated as follows: We assume that at an arbitrary time t the value of the non-equilibrium part of the distribution function is given in the plane $z = 0$. Then, as the perturbations propagate along the z axis $(z > 0)$, the asymptotic behavior of the fields is determined by a function of the form $e^{i\tilde{k}z} = e^{ikz-qz}$, where k is the wave number and q is the absorption factor. Another formulation of the problem, such as used in references 2 – 4, is possible. In an infinite space, at $t = 0$, we may prescribe a periodic perturbation with wave number k. Then the field varies in time in accordance with the asymptotic relation $e^{pt} = e^{-i\omega t-\gamma t}$ where γ is the damping factor.

Below, in Section I, we calculate absorption in the frequency region close to ω_H. In Section II we analyze absorption at $\omega \approx 2\omega_H$ and $\omega \approx 3\omega_H$. In the last section we discuss the results and give numerical examples.

I. ABSORPTION IN THE REGION OF THE FIRST GYROMAGNETIC RESONANCE

In this section we investigate the absorption, assuming that the frequency ω is close to the gyromagnetic frequency ω_H, so that

$$|(\omega - \omega_H)/\omega_H| \ll 1. \qquad (1.1)$$

Furthermore, in accordance with I, we assume that the following condition is satisfied:

$$\delta = (\varkappa T/m)(k^2 \sin^2\alpha/\omega_H^2) \ll 1, \qquad (1.2)$$

where α is the angle between the direction of propagation and the direction of the fixed magnetic field H_0, κ is the Boltzmann constant, T is the electron temperature, and $\omega_H = eH_0/mc$ (e and m are the charge and mass of the electron). Taking account of the conditions given in (1.1) and (1.2), we can omit a number of unimportant terms from the general dispersion equation. We thus obtain the equation used as the starting point for this section:

$$
\begin{aligned}
& i\omega\omega_0^6 \{2\pi I_2 I_0^- I_0^+ - (\widetilde{k}^2 \sin^2\alpha / 2\omega_H^2)\, I_0^- I_1^{+2}\} + \omega_0^4 \{I_0^+ I_0^- (\omega^2 - c^2\widetilde{k}^2 \sin^2\alpha) + \pi I_2 (I_0^+ + I_0^-) \langle 2\omega^2 - c^2\widetilde{k}^2 (1 + \cos^2\alpha)\rangle \\
& \quad + (\widetilde{k}^2 \sin^2\alpha I_1^{+2} / 4\omega_H^2) \langle c^2\widetilde{k}^2 (1 + \cos^2\alpha) - 2\omega^2\rangle - (c^2\widetilde{k}^3 / \omega_H) \sin^2\alpha \cos\alpha I_0^- I_1^+\} \\
& \quad - (i\omega_0^2 / 2\omega)(c^2\widetilde{k}^2 - \omega^2) \{(c^2\widetilde{k}^2 \sin^2\alpha - 2\omega^2)(I_0^+ + I_0^-) + 4\pi (c^2\widetilde{k}^2 \cos^2\alpha - \omega^2) I_2 + (2c^2\widetilde{k}^3 \sin^2\alpha \cos\alpha / \omega_H) I_1^+ \\
& \quad + \delta \langle 2\pi c^2\widetilde{k}^2 \cos^2\alpha I_2^+ - c^2\widetilde{k}^2 \sin^2\alpha (I_0^+ - I_0^{++})\rangle\} - (c^2\widetilde{k}^2 - \omega^2)^2 = 0,
\end{aligned} \tag{1.3}
$$

where $\widetilde{k} = k + iq$, and $\omega_0 = \sqrt{4\pi e^2 N/m}$ is the frequency of the plasma oscillations (N is the electron concentration). The integrals $I_0^\pm$, $I_1^\pm$, and $I_2^\pm$ are given by

$$
\begin{aligned}
I_0^\pm &= \sqrt{\frac{m}{2\pi\varkappa T}} \int\limits_C \frac{\exp(-mv_z^2 / 2\varkappa T)\, dv_z}{i(-\omega \pm \omega_H) + \nu + i\widetilde{k}v_z \cos\alpha}, \\
I_1^\pm &= \sqrt{\frac{m}{2\pi\varkappa T}} \int\limits_C \frac{v_z \exp(-mv_z^2 / 2\varkappa T)\, dv_z}{i(-\omega \pm \omega_H) + \nu + i\widetilde{k}v_z \cos\alpha}, \\
I_2^\pm &= \left(\frac{m}{2\pi\varkappa T}\right)^{3/2} \int\limits_C \frac{v_z^2 \exp(-mv_z^2 / 2\varkappa T)\, dv_z}{i(-\omega \pm \omega_H) + \nu + i\widetilde{k}v_z \cos\alpha},
\end{aligned} \tag{1.4}
$$

where ν is the effective number of collisions between electrons and other particles. The expressions for I_0, I_1 and I_2 are obtained by putting $\omega_H = 0$ in Eq. (1.4). In computing all these integrals (I), the integration is carried out over a contour C which is chosen in the same way as in reference 1.

We shall be concerned here mostly with weakly attenuated waves. The necessary conditions for weak attenuation, as can be verified by calculation, are the inequalities

$$
\omega \gg \sqrt{\varkappa T / m}\, k \cos\alpha, \quad \omega \gg \nu. \tag{1.5}
$$

Using the conditions (1.5), we can obtain the usual approximate expressions for all the I integrals except $I_{0,1,2}^+$. The denominators of the integrands in the latter contain the difference $\omega - \omega_H$. The computation of these terms will be considered in detail. In considering the resonance integrals $I_{0,1,2}^+$, we must choose a path C such that the singularity (pole) $v_z = \hat{v}_z$ is encircled from below. This applies for all the I integrals. If the pole is in the lower half plane, the integration must be carried out over the path C shown in Fig. 1a. However, if the point $v_z = \hat{v}_z$ lies in the upper half plane, it is sufficient to integrate along the real axis, as in Fig. 1b. From the fact that the denominators in the integrands of $I_{0,1,2}^+$ vanish, we have when $q \ll k$

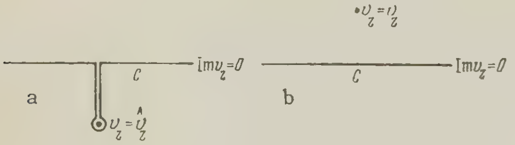

FIG. 1. Integration paths C for the integrals in Eq. (1.4) for $\operatorname{Im}\hat{v}_z < 0$ and $\operatorname{Im}\hat{v}_z > 0$.

$$
\begin{aligned}
\operatorname{Re} \hat{v}_z &= \frac{1}{\cos\alpha}\left(\frac{\omega - \omega_H}{k} + \frac{\nu q}{k^2}\right), \\
\operatorname{Im} \hat{v}_z &= \frac{1}{\cos\alpha}\left(\frac{\nu}{k} - \frac{q(\omega - \omega_H)}{k^2}\right).
\end{aligned} \tag{1.6}
$$

If $q(\omega - \omega_H)/k > \nu$, as is possible only when $\omega > \omega_H$, the integration is carried out over the contour shown in Fig. 1a. Furthermore, it can be shown that if $q \ll k$, then $\operatorname{Re} \hat{v}_z = (\omega - \omega_H)/k \cos\alpha$ so that $|\operatorname{Re} \hat{v}_z| \gg |\operatorname{Im} \hat{v}_z|$. When these considerations are taken into account, it is easy to compute the contribution in $I_{0,1,2}^+$ due to integration around the singularity. Denoting the appropriate parts of the integrals by the symbol I, we have

$$
\begin{aligned}
I_{0\mathrm{I}}^+ &= \frac{2}{k\cos\alpha}\sqrt{\frac{m\pi}{2\varkappa T}} \exp\left\langle -\frac{m(\omega - \omega_H)^2}{2\varkappa T k^2 \cos^2\alpha}\right\rangle, \\
I_{1\mathrm{I}}^+ &= \frac{\omega - \omega_H}{k\cos\alpha} I_{0\mathrm{I}}^+, \quad I_{2\mathrm{I}}^+ = \frac{m(\omega - \omega_H)^2}{2\pi\varkappa T k^2 \cos^2\alpha} I_{0\mathrm{I}}^+.
\end{aligned} \tag{1.7}
$$

If, however, $q(\omega - \omega_H)/k < \nu$ it must be assumed that $I_{0,1,2,\mathrm{I}}^+ = 0$.

We now determine the contribution due to integration along the real axis. For example, consider the integral

$$
I_{0\mathrm{II}}^+ = \sqrt{\frac{m}{2\pi\varkappa T}} \int\limits_{-\infty}^{+\infty} \frac{\exp(-mv_z^2 / 2\varkappa T)\, dv_z}{-i(\omega - \omega_H) + \nu + i\widetilde{k}v_z \cos\alpha}. \tag{1.8}
$$

Following the method of reference 5 for the analysis of such integrals, and substituting $v_z = \sqrt{2\kappa T/m}\, y$, we obtain

$$
I_{0\mathrm{II}}^+ = \frac{i}{\widetilde{k}\cos\alpha}\sqrt{\frac{m}{2\pi\varkappa T}} \int\limits_{-\infty}^{+\infty} dy\, e^{-y^2} / (z - y), \tag{1.9}
$$

where

$$
\begin{aligned}
\operatorname{Re} z &= \frac{(\omega - \omega_H)k + \nu q}{(k^2 + q^2)\sqrt{2\varkappa T / m}\cos\alpha}, \\
\operatorname{Im} z &= \frac{\nu k - q(\omega - \omega_H)}{(k^2 + q^2)\sqrt{2\pi T / m}\cos\alpha}.
\end{aligned} \tag{1.10}
$$

For weak absorption and $|z| \gg 1$, we have

$$
\int\limits_{-\infty}^{+\infty} dy\, e^{-y^2} / (z - y) \approx \frac{\sqrt{\pi}}{z}\left(1 + \frac{1}{2z^2} + \frac{3}{4z^4} + \cdots\right) - \pi i e^{-z^2} \operatorname{sgn} \operatorname{Im} z. \tag{1.11}
$$

This formula is applicable only when $|\operatorname{Re} z| \gg |\operatorname{Im} z|$. If this condition is not satisfied, the exponential term must be omitted (the remaining terms are not changed). When $|z| \ll 1$ we use the expansion

$$\int_{-\infty}^{+\infty} dye^{-y^2} / (z-y) \approx \sqrt{\pi z} - \pi i \operatorname{sgn} \operatorname{Im} z. \qquad (1.12)$$

Using Eqs. (1.11) and (1.12) we can compute $I_0^+ \text{II}$ in various cases. The integrals $I_1^+ \text{II}$ and $I_2^+ \text{II}$ can be expressed in terms of $I_0^+ \text{II}$:

$$I_{1\text{II}}^+ = \frac{1}{i\tilde{k}\cos\alpha} \langle 1 + [i(\omega-\omega_H) - \nu] I_{0\text{II}}^+ \rangle,$$

$$I_{2\text{II}}^+ = \frac{[i(\omega_H-\omega)+\nu]\, m}{2\pi\varkappa T\tilde{k}^2\cos^2\alpha} \langle 1 + [i(\omega-\omega_H) - \nu] I_{0\text{II}}^+ \rangle. \qquad (1.13)$$

We can now proceed with the absorption calculation. We assume at the outset that collisions are relatively unimportant so that

$$\nu \ll \sqrt{\varkappa T/m}\, k\cos\alpha. \qquad (1.14)$$

We consider first the frequency region close to ω_H, which lies outside the direct resonance region; we call this the outer region. In this case

$$|\omega-\omega_H| \gg \sqrt{\varkappa T/m}\, k\cos\alpha. \qquad (1.15)$$

Assuming that $q \ll k$, we find from Eq. (1.10) that $|z| \gg 1$. Using Eqs. (1.7), (1.11), and (1.13) we arrive at the customary expansion, which is applicable both for $\operatorname{Im} z > 0$ and $\operatorname{Im} z < 0$:

$$I_0^+ = \frac{1}{\nu + i(\omega_H-\omega)} - \frac{\tilde{k}^2\varkappa T\cos^2\alpha}{m[\nu + i(\omega_H-\omega)]^3}$$

$$+ \frac{1}{k\cos\alpha}\sqrt{\frac{m\pi}{2\varkappa T}} \exp\left(-\frac{m(\omega-\omega_H)^2}{2\varkappa T k^2\cos^2\alpha}\right)$$

$$I_1^+ = -\frac{\varkappa T\tilde{k}\cos\alpha}{m[\nu + i(\omega_H-\omega)]^2}$$

$$+ \frac{(\omega-\omega_H)}{k^2\cos^2\alpha}\sqrt{\frac{m\pi}{2\varkappa T}} \exp\left(-\frac{m(\omega-\omega_H)^2}{2\varkappa T k^2\cos^2\alpha}\right),$$

$$I_2^+ = \frac{1}{2\pi[\nu + i(\omega_H-\omega)]} - \frac{3\varkappa T\tilde{k}^2\cos^2\alpha}{2\pi m[\nu + i(\omega_H-\omega)]^3}$$

$$+ \frac{(\omega-\omega_H)^2}{\sqrt{\pi}\, k^3\cos^3\alpha}\left(\frac{m}{2\varkappa T}\right)^{3/2} \exp\left(-\frac{m(\omega-\omega_H)^2}{2\varkappa T k^2\cos^2\alpha}\right). \qquad (1.16)$$

Similar expansions obtain for $I_{0,1,2}$ and $I_{0,1,2}^-$. To convert to the formulas for $I_{0,1,2}$, we must put in Eq. (1.16) $\omega_H = 0$; for $I_{0,1,2}^-$ we must replace in Eq. (1.16) $\omega - \omega_H$ by $\omega + \omega_H$. Since we are interested only in gyromagnetic absorption, exponential terms can be omitted from the last six integrals. Expansions of the type given in (1.16) for $I_{0,1,2}$ and $I_{0,1,2}^-$ are used here throughout.

Substituting expressions such as Eq. (1.16) for the I integrals in Eq. (1.3), we neglect absorption completely in the first approximation (we assume that $\nu = 0$ and omit the exponential terms). We thus arrive at the equation

$$\beta^2 vRn^6 - (1-u-v+uv\cos^2\alpha)\, n^4 + [2(1-v)^2$$
$$+ uv(1+\cos^2\alpha) - 2u]\, n^2 + (1-v)[u-(1-v)^2] = 0, \qquad (1.17)$$

which determines the square of the index of refraction, $n^2 = c^2k^2/\omega^2$, for the extraordinary ($n^2 = n_1^2$), ordinary ($n^2 = n_2^2$), and plasma ($n^2 = n_3^2$) waves. In Eq. (1.17) $v = \omega_0^2/\omega^2$, $u = \omega_H^2/\omega^2$, and $\beta = \sqrt{\kappa T/mc^2}$ is the ratio of the mean thermal velocity to the velocity of light c. The general expression for R is given in references 1 and 6–8 (cf. also below). When $\beta^2 \ll 1$, the root of Eq. (1.17) corresponding to the plasma wave is

$$n_3^2 = \frac{1-u-v+uv\cos^2\alpha}{\beta^2 vR} =$$

$$= \frac{1-u-v+uv\cos^2\alpha}{\beta^2 v\langle 3\sin^4\alpha/(1-4u) + \sin^2\alpha\cos^2\alpha[1+(5-u)/(1-u)^2] + 3(1-u)\cos^4\alpha\rangle}. \qquad (1.18)$$

According to Eq. (1.1), $|1-u| \approx 2|1-\sqrt{u}| \approx 2|\omega-\omega_H|/\omega_H \ll 1$. For values of α which are not too close to $\alpha = 0$ or $\alpha = \pi/2$, we have from Eq. (1.18) $n_3^2 \approx -(1-u)^2/4\beta^2\cos^2\alpha$. Since $n_3^2 < 0$, plasma waves cannot propagate when $u \approx 1$. At small α ($\alpha \ll |1-u|/v$), this relation does not apply. We then have $n_3^2 \approx (1-v)/3\beta^2 v$, corresponding to the isotropic case. Here it is clear that gyromagnetic resonance absorption is not important. When $\alpha \approx \pi/2$, we have $n_3^2 = 1/\beta^2$. Although $n_3^2 > 0$, wave 3 (plasma wave) does not propagate because one of the initial conditions (1.2) is violated and there should be appreciable absorption ($q \sim k$). For this reason there is no need to compute the absorption of plasma waves at $\omega \approx \omega_H$ in detail. In this section we discuss therefore gyromagnetic resonance absorption of wave 1 and wave 2 only.

Because plasma waves are neglected [we also neglect the transiton region between waves 3 and 1 (or 3 and 2)$^{6-8}$] we can neglect the $\beta^2 vRn^6$ term. Then, in the second approximation, when $q \neq 0$, we obtain from (1.3), using (1.16) and similar expansions,

$$\frac{q}{k} = \frac{s}{2vn^2}\, \frac{2(v-1)n^4 + 2(v^2-4v+2)n^2 - 3v^2 + 6v - 2}{-2\sin^2\alpha n^2 + 2 + \sin^2\alpha - 2v + 4(1-\sqrt{u})(1-v)n^2/v}$$

$$+ \sqrt{\frac{\pi}{2}}\, \frac{(1-\sqrt{u})^2}{v\beta n^3\cos\alpha}$$

$$\times \frac{(v\cos 2\alpha - 1)n^4 + (-{}^1\!/_4\, v^2\sin^2\alpha - 2v\cos^2\alpha + 2)n^2 + (v-1)(1-v^2/4)}{-2\sin^2\alpha n^2 + 2 + \sin^2\alpha - 2v + 4(1-\sqrt{u})(1-v)n^2/v}$$

$$\times \exp\langle -(1-\sqrt{u})^2/2\beta^2 n^2\cos^2\alpha\rangle, \qquad (1.19)$$

where $s = \nu/\omega$. In obtaining Eq. (1.19) we have discarded small terms [terms proportional to $(1-\sqrt{u})^2$ and certain terms proportional to $(1-\sqrt{u})$]. We have used the first-approximation equation (1.17), where we put $\beta^2 vRn^6 = 0$. We may note that it would not be correct to take $u = 1$ at the outset in this equation. It is obvious that the first term in Eq. (1.19) is due to collisions while the second derives from a specific absorption mechanism. It can easily be established that actually $q \ll k$ under the restrictions given above.

When $\alpha = 0$, for wave 1 when $n_1^2 \approx 1 - v/(1-\sqrt{u})$, we have for the slow waves ($n_1^2 \gg 1$), from Eq. (1.19),

$$\frac{q_1}{k} = \frac{s}{2(\sqrt{u}-1)} + \frac{\sqrt{u}-1}{\beta n}\sqrt{\frac{\pi}{8}} \exp\left\langle -\frac{(1-\sqrt{u})^2}{2\beta^2 n^2}\right\rangle. \tag{1.20}$$

This formula has been obtained by Shafranov[9] for the case $s = 0$ and has been considered as a special case in I. From Eq. (1.15) we find that $|1 - \sqrt{u}| \gg \beta n \cos \alpha$. If, however, we use Eq. (1.20) with $s = 0$ in the region where $|1 - \sqrt{u}| \sim \beta n$, we find that $q \sim k$. Thus when $|\omega - \omega_H| \sim \sqrt{\kappa T/m}\, k$ the absorption of wave 1 must be appreciable. The same holds at small values of α, except that there is appreciable absorption of wave 1 only when $v < 1$; when $v > 1$ it is wave 2 that is strongly absorbed, rather than wave 1 (this effect is considered in greater detail in I; the statement in I that at small values of α only wave 2 is absorbed for any value of v is in error). If however $n_{1,2}^2 \sim 1$, as is the case for values of α which are not too small, then we obtain from Eq. (1.19), for $|1-\sqrt{u}| \sim \beta n \cos \alpha$, a specific absorption $q/k \sim \beta$, i.e., $q \ll k$. This estimate is in agreement with a calculation for the inner resonance region, which we now consider.

In the inner region we assume that the following condition [the inverse of (1.15)] is satisfied:

$$|\omega - \omega_H| \ll \sqrt{\kappa T/m}\, k \cos\alpha, \tag{1.21}$$

all other restrictions remaining the same as before. Now we must use the expansion (1.13). As before, we again assume that the absorption is weak. This assumption will be violated only at small values of α (if $\alpha = 0$ exactly, this is the case for wave 1), and also in the case of quasi-transverse propagation, i.e., when $\alpha \approx \pi/2$. The first case can be considered by means of our general formulas. We shall not do this because when $\sqrt{u} > 1$, and $n_1^2 > 0$ if thermal motion is neglected, our results agree with those obtained in reference 9 where it is assumed that $\alpha = 0$ exactly. The second case ($\alpha \approx \pi/2$) cannot be analyzed correctly in a nonrelativistic approximation. We may note, however, that according to Eq. (1.21) the inner regions, in which the absorption is large, become very narrow when $\cos \alpha \ll 1$.

Because of the condition (1.14), we can neglect the effect of collisions since under the restrictions of Eq. (1.21) the calculation yields $q_{\text{spec}} \sim \beta k$, while the collision contribution is $q_{\text{coll}} \sim sk$, so that $q_{\text{spec}} \gg q_{\text{coll}}$. Putting $\nu = 0$ and assuming that $q \ll k$, we obtain the following expressions for the integrals $I_{0,1,2}^{+}$:

$$I_0^{+} = \frac{1}{\tilde{k}\cos\alpha}\sqrt{\frac{\pi m}{2\kappa T}},$$

$$I_1^{+} = \frac{1}{i\tilde{k}\cos\alpha}, \qquad I_2^{+} = -\frac{im(\omega-\omega_H)}{2\pi\kappa T\tilde{k}^2\cos^2\alpha} \tag{1.22}$$

After substitution of the above values in the dispersion equation (1.3), we again obtain as a first approximation Eq. (1.17), where we may take $\beta = 0$ and $u = 1$. In the next approximation, we obtain the following expression for the absorption factor q:

$$\begin{aligned} q/k = {} & \sqrt{2/\pi}\,(\beta\cos\alpha/vn)\,(2v - 2 - \sin^2\alpha + 2\sin^2\alpha n^2)^{-1} \\ & \times \Big\{\Big[1 - \Big(1 - \tfrac{7}{4}\sin^2\alpha\Big)v\Big]n^4 - \Big[2 + v\Big(\tfrac{7}{4}\sin^2\alpha - \tfrac{5}{2}\Big) \\ & + \tfrac{1}{4}v^2(2\cos 2\alpha - \tan^2\alpha)\Big] + \Big[1 - \tfrac{3}{2}v + \tfrac{1}{2}v^2(1 - \tan^2\alpha) \\ & + \tfrac{1}{4}v^3\tan^2\alpha\Big]\Big\}. \end{aligned} \tag{1.23}$$

It follows from Eq. (1.23) that $q/k \sim \beta$ when $n_{1,2}^2 \sim 1$. Equation (1.23) is similar to that obtained earlier by Sitenko and Stepanov.[2] The difference lies in the expression inside the curly brackets and is apparently due to the fact that the I_1^{+2} terms have not been considered in reference 2 [(cf. Eq. 1.3)]. We may note that our formula, as has already been indicated, does not apply when $\alpha \approx \pi/2$ (roughly, when $\cos\alpha \lesssim \beta$). The analogous formula in reference 2 does not contain a similar singularity, which appears at $\alpha \to \pi/2$ or $\omega \approx 2\omega_H$, $3\omega_H$, etc. in the inner resonance regions.

Up to this point we have considered the propagation of waves of a given frequency ω and have determined the spatial attenuation of the field. However, as was mentioned in the introduction, another formulation of the problem is possible: in this approach the wave number k is assumed known and the time-damping term $e^{-\gamma t}$ is determined.[10] Solving the problem in this second formulation, as has been done earlier by a number of authors[2-4,6,10] and assuming that the damping γ is weak, we have in the inner resonance region

$$\begin{aligned} \frac{\gamma}{\omega} = {} & \frac{s}{2}\,\frac{2(v-1)n^4 + 2(v^2 - 4v + 2)n^2 - 3v^2 + 6v - 2}{(v-1)n^4 + [2v^2 - (6+\sin^2\alpha)v + 2]n^2 + v(v-2)^2 + (2v-1)(1-v)} + \sqrt{\frac{\pi}{2}}\,\frac{(1-\sqrt{u})^2}{\beta n\cos\alpha} \\ & \times \frac{(v\cos 2\alpha - 1)n^4 + (-{}^1\!/_4\, v^2\sin^2\alpha - 2v\cos^2\alpha + 2)n^2 + (v-1)(1-v^2/4)}{(v-1)n^4 + [2v^2 - (6+\sin^2\alpha)v + 2]n^2 + v(v-2)^2 + (2v-1)(1-v)} \exp\left(-(1-\sqrt{u})^2/2\beta^2 n^2\cos^2\alpha\right). \end{aligned} \tag{1.24}$$

It is easy to show that q in Eq. (1.19) and γ in Eq. (1.24) are related by the expression

$$\gamma = q\, d\omega/dk, \tag{1.25}$$

where $d\omega/dk$ is the projection of the group velocity in the direction of the vector **k**. The latter can be computed from Eq. (1.17) if we assume for waves 1 and 2 that $\beta^2 \rightarrow 0$. An expression similar to Eq. (1.24) has been obtained earlier by Stepanov.[3] Our expression appears in somewhat different form. However, if we compare Eq. (1.24) with $s = 0$ with the analogous relation in reference 3, and take the transformations used here into account, there is a discrepancy in the denominators of the expressions which multiply the exponentials. We may note that there is also a discrepancy of this kind for the other gyromagnetic resonances (cf. below).

When $\alpha = 0$, we have from Eq. (1.24), for the slow wave 1

$$\gamma = \nu + \sqrt{\pi/2}\,[(1-\sqrt{u})^2/\beta n]\ \exp\left\langle -(1-\sqrt{u})^2/2\beta^2 n^2\right\rangle.$$

This formulas has been given in I.

A direct calculation of γ for the inner resonance region leads to an equation which can be solved only by numerical methods. However, for not too small values of α, we may take for waves 1 and 2 tentatively $\gamma/\omega \sim \beta n$, which corresponds to the estimate made on the basis of Eq. (1.24) for $|1-\sqrt{u}| \sim \beta n$. It should be noted that Eq. (1.25) does not apply in this case. This formula is valid only for weak attenuation; however, the condition $\omega \gg \gamma$, which is satisfied for the inner region when α is not small, is insufficient. The condition $\gamma \ll \sqrt{\kappa T/m}\,k$ must also be satisfied. The latter condition is not satisfied in the inner region when $\omega \approx \omega_H$, since $\gamma \sim \beta n\omega = \sqrt{\kappa T/m}\,k$.

Up to this point we have used the assumption given in Eq. (1.14). We now consider the inverse case, when

$$\nu \gg \sqrt{\kappa T/m}\,k \cos\alpha. \tag{1.26}$$

Turning now to Eq. (1.10), we obtain for the parameter z, which appears in the integrals $I_{0,1,2}$, (assuming that $q/k \sim \gamma/\omega \ll 1$),

$$\operatorname{Re} z = [(\omega-\omega_H)k + \nu q]/k^2\sqrt{2\kappa T/m}\cos\alpha,$$

$$\operatorname{Im} z = \nu/k\sqrt{2\kappa T/m}\cos\alpha \gg 1.$$

In this case we may use an expansion such as (1.11), since $|z| \gg 1$. If we assume that $|\omega-\omega_H| \ll \nu$, then $|\operatorname{Im} z| \gg |\operatorname{Re} z|$ and, in general, the exponential terms, which take account of the specific absorption, do not appear. If $|\omega-\omega_H| \gg \nu$, however, although the $\sim e^{-z^2}$ term does not vanish, its contribution is negligibly small. Hence, the specific absorption can be neglected both for $|\omega-\omega_H| \gg \nu$ and $|\omega-\omega_H| \ll \nu$.

We thus conclude that if (1.26) is satisfied, the absorption of waves 1 and 2 in the region $\omega \approx \omega_H$ is determined exclusively by collisions. For the very simple approximation of the collision integral we have used (cf. I), there is no point at all in carrying out a kinetic analysis; we can limit ourselves to the formulas of the elementary theory, which does not take account of the thermal spread in the electron velocities.[11]

2. ABSORPTION IN FREQUENCY REGIONS CLOSE TO $2\omega_H$ AND $3\omega_H$

In this section we analyze absorption in frequency regions near $\omega \approx 2\omega_H$ and $\omega \approx 3\omega_H$ when the following conditions are satisfied, respectively:

$$|(\omega-2\omega_H)/\omega| \ll 1, \qquad |(\omega-3\omega_H)/\omega| \ll 1. \tag{2.1}$$

To consider cases simultaneously we must supplement Eq. (1.8) of I with I_0^{+++} terms. As a result we start from the following equation:

$$\begin{aligned}
&2\pi i\omega\omega_0^6 I_2 I_0^- I_0^+ + \omega_0^4\{I_0^- I_0^+(\omega^2 - c^2\tilde{k}^2\sin^2\alpha)\\
&\quad + \pi I_2(I_0^+ + I_0^-)[2\omega^2 - c^2\tilde{k}^2(1+\cos^2\alpha)]\}\\
&\quad - (i\omega_0^2/2\omega)(c^2\tilde{k}^2 - \omega^2)\ \{(c^2\tilde{k}^2\sin^2\alpha - 2\omega^2)(I_0^+ + I_0^-)\\
&\quad + 4\pi(c^2\tilde{k}^2\cos^2\alpha - \omega^2) I_2 + \delta c^2\tilde{k}^2(2\pi\cos^2\alpha\, I_2^+\\
&\quad - \sin^2\alpha\, I_0^+)\} - (c^2\tilde{k}^2 - \omega^2)^2\\
&\quad + \delta(I_0^{++} + \tfrac{3}{8}\delta I_0^{+++})\{2\pi i\omega\omega_0^6 I_0^- I_2\\
&\quad - \omega_0^4\langle(c^2\tilde{k}^2\sin^2\alpha - \omega^2) I_0^- - \pi[c^2\tilde{k}^2(1+\cos^2\alpha) - 2\omega^2] I_2\rangle\\
&\quad + (i\omega_0^2/2\omega)(c^2\tilde{k}^2 - \omega^2)(2\omega^2 - c^2\tilde{k}^2\sin^2\alpha)\} = 0.
\end{aligned} \tag{2.2}$$

The integrals I_0^{++} and I_0^{+++} in Eq. (2.2) can be computed by starting from the expression for I_0^+ in Eq. (1.4) and replacing ω_H by $2\omega_H$ or ω_H by $3\omega_H$.

Assuming that (1.5) is satisfied, we first consider the case (1.14) when the number of collisions is relatively small. In Eq. (2.2), for $I_{0,1,2}^+$ we use the approximations in (1.16); for $I_{0,1,2}$ and $I_{0,1,2}^-$ we use expansions similar to (1.16), omitting the exponential terms. The analysis of the resonance integrals I_0^{++} (when $\omega \approx 2\omega_H$) or I_0^{+++} (when $\omega \approx 3\omega_H$) is carried out the same way as in Sec. 1 (for I_0^+).

Considering the absorption of waves 1 and 2, and assuming that $q \ll k$ we use, as before, a successive-approximation method. Neglecting absorption, we arrive at Eq. (1.17), in which we must assume that $\beta^2 \nu R n^6 = 0$. In the next approximation we obtain relations for the absorption factor q. In this case, in contrast with the first gyromagnetic resonance, the absorption in the inner and outer regions for $\omega \approx 2\omega_H$ (or $\omega \approx 3\omega_H$) can be described by a single formula.

Finally, for waves 1 and 2 we have

$$\frac{q}{k} = \frac{s}{2} A\left(u = \frac{1}{4}\right) + \frac{1}{2}\sqrt{\frac{\pi}{8}}\, v \frac{\beta n \sin^2\alpha}{\cos\alpha} B\left(u = \frac{1}{4}\right) \exp\left\langle -\frac{(1-2\sqrt{u})^2}{2\beta^2 n^2 \cos^2\alpha}\right\rangle, \tag{2.3}$$

$$\frac{q}{k} = \frac{s}{2} A\left(u = \frac{1}{9}\right) + \frac{27}{16}\sqrt{\frac{\pi}{8}}\, v \frac{\beta^3 n^3 \sin^4\alpha}{\cos\alpha} B\left(u = \frac{1}{9}\right) \exp\left\langle -\frac{(1-3\sqrt{u})^2}{2\beta^2 n^2 \cos^2\alpha}\right\rangle. \tag{2.4}$$

For the functions A(u) and B(u) we have

$$A(u) = \frac{(2v+u-3)n^4 + (2v^2-8v-2u+6)n^2 - 3v^2 + 6v + u - 3}{n^2\,[2(1-u-v+uv\cos^2\alpha)n^2 - 2(1-v)^2 - (1+\cos^2\alpha)uv + 2u]},$$

$$B(u) = \frac{(u-1)}{un^2}\,\frac{{}^1/_2 n^4 \sin^2\alpha + \{v[{}^1/_2 + {}^1/_2\cos^2\alpha + \sin^2\alpha/(1+\sqrt{u})]}{2(1-u-v+uv\cos^2\alpha)\,n^2} \longrightarrow$$

$$\longrightarrow \frac{-(1+{}^1/_2\sin^3\alpha)\}n^2 + (1-v)[1-v/(1+\sqrt{u})]}{-2(1-v)^2 - (1+\cos^2\alpha)\,uv + 2u}. \tag{2.5}$$

When $\omega \approx 2\omega_H$, we take $u = 1/4$ in Eq. (2.5) and when $\omega \approx 3\omega_H$ we use $u = 1/9$.

It follows from Eqs. (2.3) and (2.4) that the change in the specific absorption with frequency, q_{spec}, is determined in the region $\omega = 2\omega_H$ or $\omega = 3\omega_H$ by an exponential resonance factor. Under the conditions considered here, the absorption due to collisions is of non-resonant nature and the value of q_{coll} depends to a considerable extent on the quantity $s = \nu/\omega$. As a very rough maximum, we can take $q_{spec} \sim \beta$ at $\omega \approx 2\omega_H$ and $q_{spec} \sim \beta^3$ at $\omega \approx 3\omega_H$ (for simplicity we assume that $\alpha \sim 1$). Because $\beta^2 = \kappa T/mc^2$ is small, the value of q_{spec} falls off rapidly as the number of the resonance increases. It can be shown that when $\omega \approx 4\omega_H$, $q_{spec} \lesssim \beta^5$ and when $\omega \approx 5\omega_H$, $q_{spec} \lesssim \beta^7$. Thus the largest specific absorption for waves 1 and 2 obtains for $\omega \approx \omega_H$ and $2\omega_H$, in which case $q_{spec} \lesssim \beta$. If one speaks of specific absorption, Eqs. (2.3) and (2.4) are not meaningful in the inner resonance regions [cf. the condition in Eq. (1.21), where we must replace ω_H by $2\omega_H$ or $3\omega_H$] when $\alpha \approx \pi/2$. This is approximately the case for the second gyromagnetic resonance when $\cos\alpha \lesssim \beta$ and for the third when $\cos\alpha \lesssim \beta^3$. When $\cos\alpha \ll 1$, the inner resonance regions are very narrow.

We now consider the absorption of the plasma wave (wave 3). For this wave $n_3^2 \gg 1$ in all cases. We shall not dwell on the properties of these waves, but shall concentrate our attention on the question of absorption. In considering absorption, one must keep in mind the fact that these waves are damped if $\beta n \sim 1$,[2,6-8] regardless of the gyromagnetic resonance mechanism. The attenuation is small when

$$|1-u-v+uv\cos^2\alpha| \ll 1. \tag{2.6}$$

At the same time, the quantity $|1-u-v+uv\cos^2\alpha|$ must not be too small if we are to avoid the transition region between waves 3 and waves 1 (or 2).[6-8] We shall not analyze absorption in the transition region.

For wave 3, analysis of the resonance is more simple at $\omega \approx 3\omega_H$ than that at $\omega \approx 2\omega_H$. This situation results from the fact that the term with I_0^{+++} in Eq. (1.2) does not change the first-approximation equations (1.17), unlike the terms with I_0^{++}. For $\omega \approx 3\omega_H$, the absorption for waves 3, as well as waves 1 and 2, can be given by a single formula. From Eq. (2.2), and Eq. (1.17) we have, when $n_3^2 \gg 1$ and $q_3 \ll k$

$$\frac{q_3}{k} = \frac{s}{2} C\left(u = \frac{1}{9}\right) + \frac{27}{16}\sqrt{\frac{\pi}{8}}\, \frac{\beta^3 n^3 v \sin^4\alpha}{\cos\alpha} D\left(u = \frac{1}{9}\right) \exp\left(-\frac{(1-3\sqrt{u})^2}{2\beta^2 n^2\cos^2\alpha}\right), \tag{2.7}$$

with

$$C(u) = \frac{3-2v-u}{1-u-v+uv\cos^2\alpha},$$

$$D(u) = \frac{(1-u)\sin^4\alpha}{2u(1-u-v+uv\cos^2\alpha)}. \tag{2.8}$$

If α is small, we must introduce certain corrections in the second relation of (2.8). When $\alpha \ll 1$, however, because of the presence of the $\sin^8\alpha$ factor, the absorption is relatively small.

When $\omega \approx 2\omega_H$, we again obtain a formula similar to Eq. (2.7); this formula applies only when $|\omega - 2\omega_H| \gg \sqrt{\kappa T/mk}\cos\alpha$ (in the outer region):

$$\frac{q_3}{k} = \frac{s}{2} C\left(u = \frac{1}{4}\right) + \sqrt{\frac{\pi}{8}}\, \frac{v\beta n \sin^2\alpha}{2\cos\alpha} D\left(u = \frac{1}{4}\right) \exp\left(-\frac{(1-2\sqrt{u})^2}{2\beta^2 n^2\cos^2\alpha}\right), \tag{2.9}$$

As the frequency $\omega = 2\omega_H$ is approached (in the outer region), the absorption becomes appreciable ($q_3 \sim k$). We shall not give formulas for this case, but simply indicate the following point of interest. From Eq. (1.18), we have when $\omega \approx 2\omega_H$

$$n_3^2 \approx \left\{\left[\frac{3}{4}(1-v) - \frac{1}{4} v \sin^2\alpha\right] \Big/ 3\beta^2 v \sin^4\alpha\right\}(1-4u).$$

Whence it is apparent that n_3^2 changes sign on going through $u = 1/4$. Thus, the region of strong specific absorption is not isolated, but is contiguous with the region in which $n_3^2 < 0$ and propagation is forbidden. Under these conditions it becomes more difficult to isolate the specific absorption effect than in the cases when there are isolated, broad absorption lines (this is the case for waves 1 and 2 for large values of α, or waves 3 at $\omega \approx 3\omega_H$).

We now consider the formulas for the damping factor γ, limiting ourselves to waves 1 and 2. Solving the problem in the second formulation (cf. Introduction and I) we have

$$\frac{\gamma}{\omega} = \frac{s}{2} F\left(u = \frac{1}{4}\right) + \sqrt{\frac{\pi}{8}} \frac{v\beta n \sin^2\alpha}{2\cos\alpha} G\left(u = \frac{1}{4}\right) \exp\left(-\frac{(1 - 2\sqrt{u})^2}{2\beta^2 n^2 \cos^2\alpha}\right), \tag{2.10}$$

$$\frac{\gamma}{\omega} = \frac{s}{2} F\left(u = \frac{1}{9}\right) + \sqrt{\frac{\pi}{8}} \frac{27 v\beta^3 n^3 \sin^4\alpha}{16\cos\alpha} G\left(u = \frac{1}{9}\right) \exp\left(-\frac{(1 - 3\sqrt{u})^2}{2\beta^2 n^2 \cos^2\alpha}\right), \tag{2.11}$$

where

$$F(u) = \frac{(2v + u - 3) n^4 + (2v^2 - 8v - 2u + 6) n^2}{(2 - v - u) n^4 - \langle 2(1 - v)^2 + uv(1 + \cos^2\alpha)} \rightarrow$$

$$\rightarrow \frac{-3v^2 + 6v + u - 3}{-4(u + v - 1)\rangle n^2 - (v - 2)[(1 - v)^2 - u] - (1 - v)(u + 2v - 2)}. \tag{2.12}$$

$$G(u) = \frac{(1 - u)\{{}^1\!/_2 n^4 \sin^2\alpha + \langle v[{}^1\!/_2 + {}^1\!/_2 \cos^2\alpha + \sin^2\alpha/(1 + \sqrt{u})]}{u\{(2 - v - u) n^4 - \langle 2(1 - v)^2 + uv(1 + \cos^2\alpha)} \rightarrow$$

$$\rightarrow \frac{-(1 + {}^1\!/_2 \sin^2\alpha)\rangle n^2 + (1 - v)[1 - v/(1 + \sqrt{u})]\}}{-4(u + v - 1)\rangle n^2 - (v - 2)[(1 - v)^2 - u] - (1 - v)(u + 2v - 2)\}}. \tag{2.13}$$

Equation (2.10), which reflects in part the contribution of a specific damping mechanism, applies only in the outer region; on the other hand, Eq. (2.11) can be applied to both the outer and inner resonance regions when $\omega \approx 3\omega_H$. In this connection, we note that Eq. (1.25) does not apply for the inner resonance region when $\omega \approx 2\omega_H$. Thus, the last relation is violated for the inner resonance region when $\omega \approx \omega_H$ and $\omega \approx 2\omega_H$. It does apply to all other cases considered here (for $\nu \ll \omega$).

A comparison of Eqs. (2.10) and (2.11) (with $s = 0$) with the analogous relations from reference 3 indicates a discrepancy, due to the differences between the denominators in Eq. (2.13) and the corresponding formula of reference 3.

In concluding this section, we note that if the inequality (1.26) is satisfied, the absorption of waves 1 and 2 is determined by collisions exclusively, as in Sec. 1. If the collision frequency ν is assumed given, the absorption calculation can be carried out in the framework of the elementary theory.[11] A similar conclusion applies to the gyromagnetic resonance absorption of waves 3. However, because the latter waves are slow ($n_3^2 \gg 1$), inequality (1.26) is satisfied only at relatively high values of the collision frequency ν. In passing we also note that in the case of wave 3 and in the transition region collisions may affect absorption and propagation even when $\omega \gg \nu$.[12]

3. EXAMPLES AND ESTIMATES

In this section we discuss the results obtained, using certain estimates and numerical examples. We use the relations derived in Secs. 1 and 2, as well as the results obtained in I, in which the non-resonance absorption of waves in a plasma is considered.

In comparing absorption due to collisions and due to specific damping mechanisms, in accordance with Eqs. (1.14) and (1.26), we must compare ν and the quantity $\sqrt{\kappa T/mk} \cos\alpha = \omega\beta n \cos\alpha$. Typical values of ν and β for different conditions are given in the table. The table is in no way complete nor highly accurate, but is given merely for purposes of illustration. A high-temperature, completely ionized plasma[13] which is the best approximation to the example in the table is the plasma in the solar corona.

	ν, sec^{-1}	β
Solar corona	$10 - 10^{-3}$	10^{-2}
Solar chromosphere	10^3	$2 - 4 \cdot 10^{-3}$
Ionosphere E layer	10^5	$2{,}5 \cdot 10^{-4}$
Ionosphere F layer	$10^3 - 10^4$	$4 - 6 \cdot 10^{-4}$
Plasma in a gas-discharge tube	$10^9 - 10^{10}$	$1 - 2 \cdot 10^{-3}$

For non-resonance absorption associated with the Cerenkov losses in the plasma,[9] damping due to the specific absorption mechanism is important only for relatively slow waves. When $\beta n \cos\alpha \ll 1$ the smallness of this absorption is determined by the factor $\exp\{-1/2\beta^2 n^2 \cos^2\alpha\}$; however, if $\beta n \gtrsim 1$, the absorption can be noticeable. When $\beta n \sim 1$ the phase velocity $v_{ph} = c/n$ is of the same order of magnitude as the thermal velocity of the electrons, $v_t = \sqrt{\kappa T/m}$. If the inequality $\beta n \ll 1$ is well satisfied, the specific non-resonance absorption is insignificant. For plasma waves which do not satisfy (2.6), specific absorption becomes significant so that $q_3 \gtrsim k$ ($\gamma_3 \gtrsim \omega$). The strong absorption found when $\beta n_3 \sim 1$ can be seen from Eqs. (2.12) and (2.14) of I, in spite of the fact that here we are somewhat outside the range of applicability of these equations. If the condition $\beta n_3 \ll 1$ is well satisfied, the non-resonance specific absorption is vanishingly small and is unimportant compared with absorption due to collisions. As is clear from the above, the inverse is true only when $\beta n_3 \gtrsim 1$ and $\omega \gg \nu$.

In contrast with plasma waves, the slow low-frequency ordinary waves (cf. I) are not strongly absorbed even when $\beta n_2 \cos\alpha \sim 1$. Thus, from Eq. (2.18) of I it follows that $q_{2,\mathrm{spec}}/k \lesssim \omega/\omega_H \times \cos\alpha$. At the same time, in accordance with Eq. (2.15) of I, $\omega_H \cos\alpha \gg \omega$, so that $q_{2,\mathrm{spec}}/k \ll 1$. It is apparent that the specific absorption obtains also when $\omega_H \cos\alpha \sim \omega$. To carry out an exact calculation of the absorption here, it would be necessary to extend the analysis of the particular case given in I. At the same time, as we have indicated, it is possible to have a case in which $q_2/k \ll 1$ over an appreciable frequency range, but in which the absorption is not a vanishingly small quantity. In the propagation of low-frequency noise in the upper atmosphere (atmospheric whistlers), which are believed to be groups of type-2 waves, as a rule $\omega_H \cos\alpha \gg \omega$. At the same time, in the passage of an atmospheric at great heights above the earth, it is also possible to have $\omega_H \cos\alpha \sim \omega$. In this case the frequencies $f = \omega/2\pi \sim 10^4$ in the spectrum of the atmospheric approach the high-frequency limit (frequencies exceeding this limit are blocked in the ionosphere). A noticeable contribution due to the specific absorption can be expected only when $\beta n_2 \gtrsim 1$. This condition can hardly be realized in the upper atmosphere under non-turbulent conditions. However, the situation may change if there are strong corpuscular perturbations. A calculation of the specific absorption under such conditions can be found in a paper by the author.[14]

We now return to the gyromagnetic resonance absorption and consider the absorption of waves 1 and 2. For these waves, (if we neglect propagation at angles close to $\alpha = 0$ and $\alpha = \pi/2$) the following rough approximations hold: $q_{\mathrm{spec}} \lesssim \beta k$ for $\omega \approx \omega_H$ and $2\omega_H$, and $q_{\mathrm{spec}} \lesssim \beta^3 k$ for $\omega \approx 3\omega_H$. The effect of collisions is roughly determined by $q_{\mathrm{coll}} \sim sk = k\nu/\omega$. To compare the contributions of the different absorption mechanisms it is necessary to estimate the ratios $r_{1,2} = \beta\omega/\nu$ and $r_3 = \beta^3\omega/\nu$. If we are interested in radio waves ($\omega \approx 10^6 - 10^{10}$), $r_3 \ll 1$ for all the cases indicated in the table, except the solar corona.

It is clear even from this estimate that the greatest specific absorption can occur when waves propagate in a hot, highly ionized plasma such as the solar corona. Thus, under the conditions which obtain in the solar corona, in contrast with the other examples, it is quite possible to have a case in which $r_3 \gg 1$ and moreover $r_4 = \beta^5\omega/\nu \gtrsim 1$. The ratio $r_{1,2}$ can be large under the conditions found in the chromosphere. In the ionosphere [excluding very high frequencies, when the ionosphere has no noticeable effect on the propagation ($\omega < 10^8$)] we find that the condition $r_{1,2} \gtrsim 1$ can be realized only at the level of the maximum of the F-layer or higher. Collisions are always predominant in absorption of radio waves in the lower ionospheric layers.

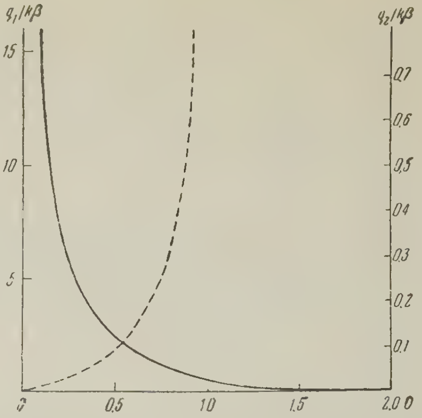

FIG. 2. Curves characterizing the specific absorption of wave 1 (solid curve) and wave 2 (dashed curve) as a function of the parameter $v = \omega_0^2/\omega^2$ for $\omega = \omega_H$ and $\alpha = 45°$.

It should be emphasized that the estimates given above are extremely coarse. It is possible that an exact calculation with the formula given in Secs. 1 and 2 would show great differences in the values of the absorption factors. This statement can be illustrated by curves such as those shown in Figs. 2 and 3. In Fig. 2 we show the curves $q_1/k\beta$ and $q_2/k\beta$ (in different scales), which characterize the specific absorption of wave 1 and wave 2, on the basis of Eq. (1.23), for the inner resonance region $\omega \approx \omega_H$ at $\alpha = 45°$. For a given value of α, the absorption given by the curves in Fig. 2 represents the maximum or at least the order of magnitude of the maximum. The shape of the specific absorption line close to $\omega = \omega_H$ has not been obtained, but the width of this line is of order $\Delta\omega \sim \omega\beta n \cos\alpha$.

In Fig. 3 we show similar curves for wave 1 and wave 2, also when $\alpha = 45°$ but with $\omega = 2\omega_H$. The shape of the absorption line close to $\omega = 2\omega_H$ is given by the factor

$$\exp\{-(\omega - 2\omega_H)^2 / 2\omega^2\beta^2 n^2 \cos^2\alpha\},$$

and it is apparent that the curves in Fig. 3 determine the maximum absorption values. It follows from Figs. 2 and 3 that the absorption of wave 1 differs greatly from that of wave 2 under the same

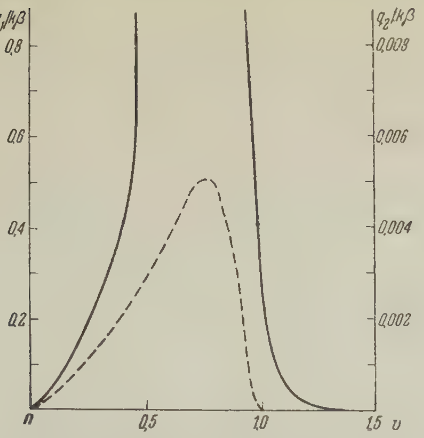

FIG. 3. Curves characterizing the specific absorption of wave 1 (solid curve) and wave 2 (dashed curve) as a function of the parameter $v = \omega_0^2/\omega^2$ for $\omega = 2\omega_H$ and $\alpha = 45°$.

conditions; this is why different scales must be used. The absorption of a given wave in a plasma at its wavelength λ $(q/k = 2\pi q\lambda = 2\pi q\lambda_0/n)$ changes considerably as the parameter v is changed.

The differences indicated above in the values of the absorption factors again emphasize the need for exact calculations.

We note in connection with Figs. 2 and 3 that the curves corresponding to different characteristic waves lack those sections where $n^2 < 0$ and propagation is forbidden (in Fig. 2 this is the case, for example, for wave 2 at $v > 1$). The relatively high values of absorption in Fig. 2 are due to the fact that $n_1 \rightarrow 0$ and $n_2 \rightarrow 0$ as $v \rightarrow 0$ and $v \rightarrow 1$, respectively (we determine the absorbtion per wavelength in the medium, $\lambda = \lambda_0/n$). If, however, we relate the absorption coefficient to the wave number in free space, $k_0 = 2\pi/\lambda_0$, the increase in the values of $q/k_0\beta$ is not so great. In Fig. 3 the increase in $q/k\beta$ close to $v = 6/7$ arises because at this value $n_1^2 \rightarrow \infty$. Actually, it is necessary to take account of the effect of thermal motion on propagation in the region $v \approx 6/7$. In this case plasma waves exist in the region $v < 6/7$. In this region the gyromagnetic absorption must be analyzed by means of Eq. (2.9) (cf. also the remarks following this formula).

The author is indebted to Professor V. L. Ginzburg for his continued interest in this work.

---

[1] B. N. Gershman, JETP **37**, 695 (1959), Soviet Phys. JETP **10**, 497 (1960).

[2] A. G. Sitenko and K. N. Stepanov, JETP **31**, 642 (1956), Soviet Phys. JETP **4**, 512 (1957).

[3] K. N. Stepanov, JETP **35**, 283 (1958), Soviet Phys. JETP **8**, 195 (1959).

[4] K. N. Stepanov and V. S. Tkalich, J. Tech. Phys. (U.S.S.R.) **28**, 1789 (1958), Soviet Phys.-Tech. Phys. **3**, 1649 (1959).

[5] A. I. Akhiezer and Ya. B. Faĭnberg, JETP **21**, 1262 (1951).

[6] B. N. Gershman, JETP **24**, 659 (1953).

[7] Gershman, Ginzburg, and Denisov, Usp. Fiz. Nauk **61**, 561 (1957).

[8] B. N. Gershman, Сб. памяти А. А. Андронова (Coll. In Memoriam A. A. Andronov) Acad. Sci. Press, p. 599; JETP **31**, 707 (1956), Soviet Phys. JETP **4**, 582 (1957).

[9] V. D. Shafranov, JETP **34**, 1475 (1958), Soviet Phys. JETP **7**, 1019 (1958).

[10] L. D. Landau, JETP **16**, 574 (1946).

[11] Al'pert, Ginzburg, and Faĭnberg, Распространение радиоволн (Propagation of Radio Waves) Gostekhizdat (1953).

[12] B. N. Gershman and M. S. Kovner, Изв. высш. шк., Радиофизика (News of the Higher Schools, Radiophysics) **2**, 28 (1959).

[13] R. F. Post, Revs. Modern Phys. **28**, 338 (1956); Usp. Fiz. Nauk **61**, 491 (1957).

[14] B. N. Gershman, loc. cit. ref. 12, **1**, 49 (1958).

Translated by H. Lashinsky
172

SOVIET PHYSICS JETP VOLUME 11, NUMBER 3 SEPTEMBER, 1960

THE INDIRECT INTERACTION OF d ELECTRONS IN TRANSITION METALS. II. ANTIFERROMAGNETISM

B. V. KARPENKO and A. A. BERDYSHEV

Ural State University

Submitted to JETP editor September 12, 1959

J. Exptl. Theoret. Phys. (U.S.S.R.) **38**, 925-928 (March, 1960)

Antiferromagnetic substances are considered within the framework of Vonsovskiĭ's s-d-exchange model. The energy of the spin waves is determined by perturbation-theory methods. The possibility of the existence of an antiferromagnetic state in the absence of direct d-d-exchange interaction is discussed.

In their previous work[1] the authors expressed opinions regarding the necessity of studying the indirect interaction of electrons in the unfilled inner shells of the atoms of transition metals (d electrons) and rare earths (f electrons). It was shown that the indirect interaction of d electrons by means of the conduction electrons can lead to ferromagnetism. In the present paper a study of the role of the indirect interaction of d electrons is carried out for the antiferromagnetic state.

The Hamiltonian of an antiferromagnet in the s-d-exchange model has the form[2]

$$
\begin{aligned}
H = {} & \sum_{k\sigma} E(k)\, a^{+}_{k\sigma} a_{k\sigma} - J \sum_{\langle nm\rangle} S_n S_m \\
& - \frac{I}{V} \sum_{k_1 k_2 n} e^{i(k_2-k_1)n} [(S - S^z_n)\, a^{+}_{k_1} a_{k_2} + (S^x_n - iS^y_n)\, a^{+}_{k_1} a_{k_2}(-) \\
& + (S^x_n + iS^y_n)\, a^{+}_{k_1}(-)\, a_{k_2} + (S + S^z_n)\, a^{+}_{k_1}(-)\, a_{k_2}(-)] \\
& - \frac{I}{V} \sum_{k_1 k_2 m} e^{i(k_2-k_1)m} [(S - S^z_m)\, a^{+}_{k_1} a_{k_2} + \\
& + (S^x_m - iS^y_m)\, a^{+}_{k_1} a_{k_2}(-) + (S^x_m + iS^y_m)\, a^{+}_{k_1}(-)\, a_{k_2} \\
& + (S + S^z_m)\, a^{+}_{k_1}(-)\, a_{k_2}(-)],
\end{aligned}
$$

where a_k and $a_k(-)$ are the Fermi operators of second quantization for electrons with a momentum k and with positive and negative spins, S_n is the spin operator of the n-th lattice point, J is the d-d-exchange integral between two nearest neighbors, I is the s-d-exchange integral (independent, in our approximation, of the electron momentum), V is the volume of the system, n and m are the numbers of lattice points of two different sublattices, the sign $< >$ denotes summation over the nearest neighbors, $E(k) = Ak^2$ is the conduction-electron energy, and A is the transport integral.

We go over from the spin operators to the Bose operators of the spin shift

$$
S^z_n = {}^1\!/_2 - b^{+}_n b_n, \quad S^x_n + iS^y_n = b_n, \quad S^x_n - iS^y_n = b^{+}_n,
$$

$$
S^z_m = -{}^1\!/_2 + c^{+}_m c_m, \quad S^x_m + iS^y_m = c^{+}_m, \quad S^x_m - iS^y_m = c_m
$$

for the two sublattices, respectively. Then, going over to the Bose operators in wave-number space according to the formulas

$$
b_n = \left(\frac{2}{V}\right)^{1/2} \sum_{\lambda} e^{-in\lambda}\, b_\lambda, \qquad c_m = \left(\frac{2}{V}\right)^{1/2} \sum_{\lambda} e^{im\lambda}\, c_\lambda,
$$

we obtain the Hamiltonian in the form

$$
\begin{aligned}
H = {} & \sum_{k\sigma} E(k)\, a^{+}_{k\sigma} a_{k\sigma} - \frac{zJ}{2} \sum_{\lambda} [b^{+}_\lambda b_\lambda + c^{+}_\lambda c_\lambda + \gamma_\lambda (b_\lambda c_\lambda + b^{+}_\lambda c^{+}_\lambda)] \\
& - \frac{I}{V} \sum_{k\lambda} (b^{+}_\lambda b_\lambda - c^{+}_\lambda c_\lambda)(a^{+}_k a_k - a^{+}_k(-)\, a_k(-)) \\
& - \frac{I}{\sqrt{2V}} \sum_{k_1 k_2 \lambda} \delta(k_2 - k_1 + \lambda) [(c_\lambda + b^{+}_\lambda)\, a^{+}_{k_1} a_{k_2}(-) \\
& + (c^{+}_\lambda + b_\lambda)\, a^{+}_{k_2}(-)\, a_{k_1}],
\end{aligned}
$$

where z is the number of nearest neighbors of a given atom, $\gamma_\lambda = 1/z \sum_{\rho} e^{i\rho\lambda}$, and ρ is the radius vector from the given atom to its nearest neighbor. The part of the Hamiltonian quadratic with respect to the Bose operators is easily diagonalized with the aid of the linear substitution

$$
b_\lambda = \alpha_{1\lambda} \xi_{1\lambda} + \alpha_{2\lambda} \xi^{+}_{2\lambda}, \qquad c_\lambda = \alpha_{2\lambda} \xi^{+}_{1\lambda} + \alpha_{1\lambda} \xi_{2\lambda}.
$$

The commutation relations between the operators, and the requirement that the coefficients in the nondiagonal parts of the energy operator equal zero, lead to equations for the transformation coefficients:

$$
\alpha^2_{1\lambda} - \alpha^2_{2\lambda} = 1,
$$

$$
2\alpha_{1\lambda} \alpha_{2\lambda} + \gamma_\lambda (\alpha^2_{1\lambda} + \alpha^2_{2\lambda}) = 0.
$$

Having determined these coefficients, we obtain the transformed Hamiltonian in the form

$$H = H_0 + H_{int},$$
$$H_0 = \sum_{k\sigma} E(k)\, a_{k\sigma}^+ a_{k\sigma} + \sum_{\lambda} \varepsilon(\lambda)\,(\xi_{1\lambda}^+ \xi_{1\lambda} + \xi_{2\lambda}^+ \xi_{2\lambda}),$$
$$H_{int} = -\frac{I}{V}\sum_{k\lambda}(a_k^+ a_k - a_k^+(-)\, a_k(-))\,(\xi_{1\lambda}^+ \xi_{1\lambda} - \xi_{2\lambda}^+ \xi_{2\lambda})$$
$$- \frac{I}{\sqrt{2V}} \sum_{k_1 k_2 \lambda} \delta(k_2 - k_1 + \lambda)\, g(\lambda)\, [(\xi_{1\lambda}^+ + \xi_{2\lambda})\, a_{k_2}^+ a_{k_1}(-)$$
$$+ (\xi_{1\lambda} + \xi_{2\lambda}^+)\, a_{k_2}^+(-)\, a_{k_1}], \tag{1}$$

where $\epsilon(\lambda) = -J(z/2)^{1/2}\lambda$ is the spin-wave energy, and

$$g(\lambda) = \alpha_{1\lambda} + \alpha_{2\lambda} = (2\lambda^2/z)^{1/4}.$$

Unlike in previous work,[1] perturbation theory will be applied here not to an arbitrary spectrum but to a given unperturbed-energy level. We are interested in the correction to the elementary excitation energy of the Bose branch $\epsilon(\lambda)$ due to the interaction terms. In accordance with perturbation theory, the spin-wave energy $\tilde{\epsilon}(\lambda)$ of interest to us is equal, up to terms of the second order, to

$$\tilde{\varepsilon}(\lambda) = \varepsilon(\lambda) + \langle C_v \xi_{1\lambda} H_{int} \xi_{1\lambda}^+ C_v\rangle$$
$$- \langle C_v \xi_{1\lambda} H_{int} (H_0 - E_0 - \varepsilon(\lambda))^{-1} H_{int} \xi_{1\lambda}^+ C_v\rangle, \tag{2}$$

where

$$C_v = \prod_{k \leqslant k_F} \delta(N_k^+, 1)\, \delta(N_k^-, 1) \prod_{\lambda} \delta(n_{1\lambda}, 0)\, \delta(n_{2\lambda}, 0)$$

represents the unperturbed wave function of the ground state. N_k^+ and N_k^- are the occupation numbers of conduction electrons with positive and negative spins, respectively, n are the occupation numbers of the spin waves, $E_0 = 2\sum_{k \le k_F} E(k)$ is the ground-state energy of the unperturbed system, and k_F is the boundary Fermi momentum. Calculating the matrix elements in (2), we obtain

$$\tilde{\varepsilon}(\lambda) = \varepsilon(\lambda) - \frac{I^2 g^2(\lambda)}{2V} \sum_{\substack{k_1 > k_F > k_2 \\ (k_1 - k_2 = \lambda)}} \Bigl(\frac{1}{E(k_1) - E(k_2) + \varepsilon(\lambda)}$$
$$+ \frac{1}{E(k_1) - E(k_2) - \varepsilon(\lambda)}\Bigr).$$

For the right-hand side we can substitute the integral

$$\frac{V}{(2\pi)^3}\int\Bigl(\frac{1}{E(k_1) - E(k_2) + \varepsilon(\lambda)}$$
$$+ \frac{1}{E(k_1) - E(k_2) - \varepsilon(\lambda)}\Bigr)\, \delta(k_1 - k_2 - \lambda)\, d^3k_1\, d^3k_2,$$

which can be easily calculated in the approximation $\lambda/k_F \ll 1$.[3] Substituting $k_2 + \lambda$ for k_1, discarding in the denominator terms with λ/k_F to a power greater than 1, and taking into account that $k_2 + \lambda > k_F$, we obtain for the integral

$$\frac{V}{(2\pi)^3}\int_0^{2\pi} d\varphi \int_0^1 d\mu \int_{k_F'}^{k_F} k_2^2\, dk_2 \Bigl(\frac{1}{2Ak_F\lambda\mu + \varepsilon(\lambda)} - \frac{1}{2Ak_F\lambda\mu - \varepsilon(\lambda)}\Bigr),$$

where μ is the cosine of the angle between k_2 and λ, and $k_F' = k_F(1 - 2\mu q/k_F)^{1/2}$.

Finally we find that

$$\tilde{\varepsilon}(\lambda) = \varepsilon(\lambda) - \frac{I^2 g^2(\lambda)\, k_F}{(4\pi)^2 A}\Bigl[2 + \frac{\varepsilon(\lambda)}{2A\lambda k_F}\ln\frac{1 - 2A\lambda k_F/\varepsilon(\lambda)}{1 + 2A\lambda k_F/\varepsilon(\lambda)}\Bigr]. \tag{3}$$

To analyze this expression formally, we can consider the two limiting cases: a) $2A\lambda k_F/\epsilon(\lambda) \ll 1$, and b) $2A\lambda k_F/\epsilon(\lambda) \gg 1$. The first case corresponds to the approximation in which the energy of the virtual electron transitions is assumed to be considerably smaller than the energy of the corresponding spin wave. Expanding the expression in square brackets in (3) into a series in $2A\lambda k_F/\epsilon(\lambda)$ and limiting ourselves to the first nonvanishing terms of the third order, we obtain

$$\tilde{\varepsilon}(\lambda) = J_{\text{eff}}\lambda, \quad J_{\text{eff}} = -J\sqrt{\frac{z}{2} + \frac{\sqrt{2}}{3\pi^2 z^{3/2}} k_F^3 A \frac{I^2}{J^2}}\,.$$

Thus, in our case the indirect interaction favors antiferromagnetic ordering, increasing the effective exchange integral.

The second case corresponds to the approximation for which the energy of virtual electron transitions is considerably larger than the spin-wave energy. In this case we obtain from (3)

$$\tilde{\varepsilon}(\lambda) = \varepsilon(\lambda) - I^2 g^2(\lambda)\, k_F / 8\pi^2 A$$

or

$$\tilde{\varepsilon}(\lambda) = J_{\text{eff}}\lambda, \qquad J_{\text{eff}} = -J\sqrt{\frac{z}{2}} - \frac{I^2 k_F}{8\pi^2 A}\sqrt{\frac{2}{z}}\,.$$

The effective integral in this case, as in case a), consists of two terms corresponding to direct and indirect exchange. However, in this case the indirect exchange decreases the effective exchange integral, and in the absence of direct d-d-exchange coupling $(J = 0)$ the effective integral becomes negative. Consequently, the energies of the elementary excitations and of the spin waves become negative, which means that the antiferromagnetic state becomes energetically unfavorable and, therefore, does not come into being.

Case a), although it offers the possibility that indirect exchange favors antiferromagnetic ordering, is nevertheless of no physical significance, since the inequality $2A\lambda k_F/\epsilon(\lambda) \ll 1$ is not fulfilled in any of the known estimates. Therefore, this case need be considered only as a purely formal possibility.

Thus, the general conclusion is that indirect interaction of d electrons through conduction electrons in transition metals decreases the antiferromagnetic exchange coupling, preventing the formation of antiferromagnetic ordering and, consequently, cannot lead, in the absence of direct d–d-exchange interaction or of some other ordering mechanism, to antiferromagnetism.

The calculations in the present paper are exact up to second-order terms of perturbation theory. The calculation of higher-order corrections, beginning with the third, require that account be taken of Hamiltonian terms which contain products of four or more Bose operators, and which were left out in the derivation of (1). Thus, the precision of the calculations increases when the system is considered at low temperatures.

The authors express their gratitude to L. Ya. Kobelev for useful advice.

---

[1] A. A. Bardyshev and B. V. Karpenko, JETP **36**, 819 (1959), Soviet Phys. JETP **9**, 577 (1959).

[2] S. V. Vonsovskiĭ and A. A. Berdyshev, Izv. Akad. Nauk SSSR, Ser. Fiz. **18**, 328 (1954), Columbia Tech. Transl. p. 23.

[3] N. M. Hugenholtz, Physica **23**, 533 (1957).

Translated by Z. Barnea
173

SOVIET PHYSICS JETP VOLUME 11, NUMBER 3 SEPTEMBER, 1960

THE SIGNIFICANCE OF STRANGE PARTICLES IN FERMI'S STATISTICAL THEORY

V. I. RUS' KIN and P. A. USIK

Institute of Nuclear Physics, Academy of Sciences, Kazakh S.S.R.

Submitted to JETP editor September 18, 1959

J. Exptl. Theoret. Phys. (U.S.S.R.) **38**, 929-933 (March, 1960)

It is shown that account of resonance interaction of two π mesons in Fermi's statistical theory permits one to explain a number of experimental facts which remained inexplicable by the statistical theory which takes into account only the nucleonic "isobar" ($^3/_2$, $^3/_2$). Such facts are the mean multiplicity of π and K mesons in $p\bar{p}$ annihilations, mean multiplicity of strange particles in meson-nucleon collisions, and angular correlations between π mesons in π^-p interactions at an energy of 1.0 Bev.

BARASHENKOV and Mal'tsev[1] have reported a confirmation that account of resonance $\pi\pi$ interaction worsens the agreement of the Fermi statistical theory with experiment. In this research we shall show that there is no foundation for such a conclusion at the present time.

It is known that resonance interaction of two particles can be considered within the framework of the statistical theory of Fermi. Account of resonant interaction of a π meson with a nucleon (nucleonic "isobar") considerably improves the agreement of statistical theory with experiment.[2] However a series of experimental facts remained unexplained even in this case: 1) the mean multiplicity of π mesons in $p\bar{p}$ annihilation was shown to be significantly smaller, while the percent of cases of annihilation with the formation of K mesons was significantly larger than observed by experiment; 2) the presence of maxima in the angular distribution among the π mesons and in the momentum representation of nucleons in π^-p collisions at energies of 1.0 Bev was not explained; 3) the multiplicity of "strange" particles in meson-nucleon collisions remained significantly larger than that experimentally observed.

There is at the present time a sufficient amount of indirect experimental and theoretical indications on the presence of resonance interaction of two π mesons. By considering this resonance interaction as the presence of a π-meson "isobar" with isospin $T = 1$ and effective mass $\mu = 0.47$* we shall attempt to improve the relation of the statistical theory with the experimental facts just enumerated.

1. Resonance $\pi\pi$ interaction in a state with isospin $T = 0$ in the process of $p\bar{p}$ annihilation was considered by Eberle,[3]* who obtained the mean multiplicity of π mesons, $\bar{n}_\pi = 3.8$, and the percent of cases of annihilation with formation of the observed K mesons, $P_K = 12$ per cent. According to experimental data given by Segré at the 1959 Ninth International Conference on High-Energy Physics in Kiev, $\bar{n}_\pi = 4.7 \pm 0.1$, $P_K = (3 \pm 1)$ per cent. In order to improve the agreement between theory and experiment, Eberle made use of the assumption of Barashenkov[5] on the creation of the K meson in its volume V_K [$V_K = (^4/_3)\pi r_K^3$, where $r_K = 1/M_K$] and obtained $\bar{n}_\pi = 4.4$. Here the percentage of cases with formation of the observed K mesons appears to be greatly reduced, $P_K = 0.35$ per cent. We note that the annihilation of a strongly slowed or arrested antinucleon is the most advantageous process for verification of the assumption on the production of K mesons in the volume V_K, since only K mesons are produced from the "strange" particles in this case. By considering the resonance interaction of two π mesons in a state with isospin $T = 1$, we obtain the following statistical weight of the finite state of $p\bar{p}$ annihilation (normalized to 100 per cent):

2π	3π	4π	5π	6π	7π	$2K$	$2K\pi$	$2K2\pi$	$2K3\pi$
1.0	9.8	21.2	13.5	38.5	0.6	1.2	4.8	7.1	2.3

For the calculations, we have assumed that the K mesons, like the π mesons, are produced in the Fermi volume $V_\pi = (^4/_3)\pi r_\pi^3$, where r_π is the π-meson Compton wavelength. From the statistical weight of possible finite states given above, it follows that the mean multiplicity of the π mesons is $\bar{n}_\pi = 4.5$, while the percentage of cases with formation of observed K mesons is $P_K = 7.7$. The distribution of charged products of $p\bar{p}$ annihilation was also computed by us according to the number of prongs:

---

*Here and below, $\hbar = c = M_{\text{nucl.}} = 1$.

*Resonance $\pi\pi$ interaction was considered by Goto.[4] However, in this research the calculation of the statistical weights of all processes was carried out according to the same very approximate formula.

0-prong cases — 2 (5); 2-prong cases — 38 (40);
4-prong cases — 56 (50); 6-prong cases — 4 (5);
8-prong cases — 0 (0).

Here the figures in parentheses correspond to the experimental data,[6] normalized to 100 per cent. The statistical weight of cases with the formation of two charged π mesons ($p + \bar{p} \rightarrow \pi^+ + \pi^-$) was shown to be less than one per cent. The results that were obtained were in reasonable agreement with the experimental data given by Segrè.[6]

Taking into account the resonance $\pi\pi$ interaction in the state with T = 1, S = 1, and effective mass $\mu = 0.60$, we obtain better agreement with experiment: $\bar{n}_\pi = 4.9$, $P_K \approx 4$ per cent.

2. In the majority of researches on the statistical theory of multiple production of particles, correlations between the directions of motion of the secondary particles have not been taken into consideration. At the same time, an investigation of this problem would permit one to decide on the necessity of taking into account resonance interaction of two particles, since this interaction ought to lead to the appearance of definite angular correlations. In the general case, this problem is very complicated and evidently cannot be solved without consideration of the law of conservation of momentum, which is neglected at the present time. However, in the case of $\pi^- p$ interaction in the energy region of 1.0 Bev, where the processes

$$\pi + N \rightarrow N + \pi + \pi, \tag{1}$$

$$\pi + N \rightarrow N' + \pi \rightarrow N + \pi + \pi, \tag{2}$$

$$\pi + N \rightarrow \Pi + N \rightarrow N + \pi + \pi \tag{3}$$

play the principal role, with relative statistical weights 41.9, 41.9, and 16.2, the distribution over angles among the π mesons can easily be found. For this purpose it suffices to assume that the characteristic features of this distribution are brought about by the resonance processes (2) and (3), and therefore one can neglect angular correlations in the process (1).

In the process (2) (here the symbol N′ denotes the nucleonic "isobar"), the meson moves in a direction which is strongly opposed to the direction of the "isobar." Therefore, the angle φ between the direction of motion of the "isobar" and the direction of motion of the π meson from decay of the "isobar" will be connected with the angle θ between the directions of motion of both π mesons by the relation $\varphi + \theta = \pi$. Making use of the angular distribution of π mesons from the decay of the "isobar," given in the review of Rozental',[7] one can easily obtain the distribution over the angle θ for the secondary π mesons.

The angular distribution over the π mesons in the process (3) (here the symbol Π denotes the π-meson "isobar") can be obtained if use is made of the dependence of the angle θ between the two π mesons from the decay of the π-meson "isobar" on the energy of the π mesons E_1.[8] Transforming from the energy distribution of one of the π mesons to the angular distribution between them, we obtain

$$\begin{aligned} N(\theta)\, d\cos\theta = d\cos\theta \Big\{ & M^2 \cos\theta \sqrt{M^4/4 - E_0^2 \mu^2 \cos^2\theta} \\ & - (\cos^2\theta + 1)\left(\tfrac{1}{4} M^4 - E_0^2 \mu^2 \sin^2\theta\right) \\ & - \cos^2\theta \sin^2\theta E_0^2 \mu^2 \Big\} (4 p_c \gamma v \sin^4\theta)^{-1} \\ & \times \left(\tfrac{1}{4} M^4 - E_0^2 \mu^2 \sin^2\theta\right)^{-1/2} \Big(\tfrac{1}{4} E_0^2 + \mu^2 - \frac{M^2}{2\sin^2\theta} \\ & + \frac{\cos\theta}{\sin^2\theta} \sqrt{M^4/4 - E_0^2 \mu^2 \sin^2\theta}\Big)^{-1/2}, \end{aligned}$$

where E_0 and v are the energy and velocity of the π-meson "isobar" in the center of mass of the meson and nucleon; $\gamma = (1 - v^2)^{-1/2}$; M is the mass of the π-meson "isobar," equal to 0.47; μ is the mass of the π meson; p_c is the momentum of the π meson from the decay of the π-meson "isobar" in its rest system; θ is the angle between the two π mesons from the decay of the π-meson "isobar." The limits of variation of the angle θ are easily obtained from the usual formulas given in a review by Rozental'.[7]

Distribution over the angles between the π mesons in the reactions

$$\pi^- + p \rightarrow p + \pi^- + \pi^0, \qquad \pi^- + p \rightarrow n + \pi^+ + \pi^- \tag{4}$$

was computed by us for an energy of 1.0 Bev. The resultant distribution is plotted in the drawing, where the experimental data of reference 9 are represented by the histogram, while our calculations are given by the solid curve. As is seen from the drawing, the results obtained here are in excellent qualitative agreement with experiment. The maximum is brought about by process (3) when $\cos\theta = 0.2$ and by process (2) when $\cos\theta = -0.8$. A certain quantitative discrepancy comes about here by the fact that we have neglected angular correlations in process (1).

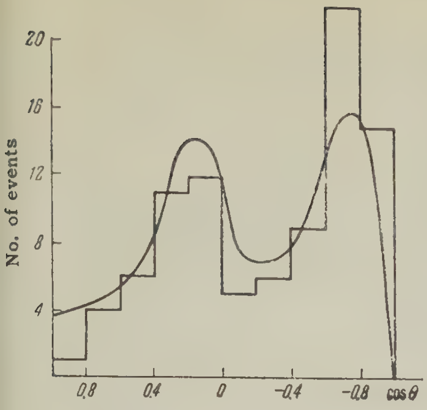

Distribution according to the angles between the π mesons in reactions (4) at an energy of 1.0 Bev. Histogram from the experiment in reference 9; smooth curve – calculated according to the statistical theory with account of resonance interactions (nuclear and π-meson "isobar").

The effect of consideration of resonance $\pi\pi$ interaction on the momentum distribution of the π mesons and nucleons, obtained theoretically for the reactions considered above, has been investigated by us in reference 10; therefore, we shall not dwell on it. We only note that consideration of resonance interaction of two π mesons allows one to explain the characteristic maximum in the momentum distribution of nucleons in $\pi^- p$ collisions at 1.0 Bev. (The momentum distribution of the secondary particles, calculated with account of the π-meson "isobar" in a state with isospin $T = 0$, differs slightly from the momentum distribution computed with account of the π-meson "isobar" in a state with isospin $T = 1$.)

3. We shall further consider the effect of resonance $\pi\pi$ interaction on the multiplicity of strange particles in meson-nucleon collisions. It is known that the statistical theory of Fermi, which takes into account only the nucleonic isobar $(3/2, 3/2)$, gives a ratio of the cross section of production of strange particles to the cross section of production of π mesons, $\sigma_{str}/\sigma_\pi = 0.3$.[2] By taking into account (along with the nucleonic isobar) the resonance $\pi\pi$ interaction in the state with isospin $T = 1$, it is possible to lower this ratio to 0.08.[11] However, both in reference 2 and in reference 11, calculation of the statistical weights of processes with four and more particles was carried out by approximate formulas. Therefore, some of the reactions with strange particles were not considered in these researches. More exact calculations increase the ratio given above by a factor of more than 2.5. Therefore, although calculation of the resonance $\pi\pi$ interaction significantly lowers the ratio σ_{str}/σ_π, this ratio still remains larger than that experimentally observed.[12]

In the first part of this paper, we showed that account of the resonance interaction of two π mesons in a state with isospin $T = 1$ in the case of $p\bar{p}$ annihilation, where only K mesons are produced from the strange particles, allows one to obtain a reasonable multiplicity of strange particles. Starting out from this situation, one can attempt to improve the agreement of the statistical theory with experiment by assuming that in the case of meson-nucleon collisions, the statistical weight of all strange particles (hyperons and K mesons) is determined by the statistical weight of processes with the production of only meson pairs $K + \bar{K}$. The scheme of elementary particles advanced by Goldhaber (see reference 13) lends some support to this assumption; in this scheme the hyperons are the product of a medium-strong interaction of secondary $\bar{K}$ mesons with secondary nucleons. The given assumption makes it possible to lower the ratio σ_{str}/σ_π to 0.14. In the calculation of this ratio, reactions previously omitted[11] have been taken into account.* The experimental value is $\sigma_{str}/\sigma_\pi = 0.04$.[12] This ratio is known to be too low, since the strange particles in reference 12 were established only by the decay. Therefore, the ratio that we have found of $\sigma_{str}/\sigma_\pi = 0.14$ can be regarded as not very far from the correct one.

We note that if the scheme of elementary particles of Goldhaber is correct, then in those cases in which the energy of the emitted π mesons in meson-nucleon collisions is below the threshold of formation of two K mesons (1.34 Bev), formation of the latter is possible only virtually in an intermediate state. Consequently, formation of strange particles up to this energy region cannot be considered within the framework of the statistical theory of Fermi. It is quite evident that all other consequences of the Goldhaber scheme remain valid under such considerations.

In conclusion, we take up the principal objection against calculation in the statistical Fermi theory of resonance $\pi\pi$ interaction, put forward in the work of Barashenkov and Mal'tsev.[1] This objection is that in the case of consideration of a π-meson "isobar" the theoretically determined distribution of charged products of $\pi^- p$ collisions according to the number of prongs differs from that experimentally observed. As seen from reference 11, the distribution computed with account of the π-meson "isobar" is in better agreement with experiment than that which takes into account only the nucleon isobar if in this case we can take into account the formation of strange particles. The departure from the experimentally observed distribution is evidently brought about by the crudeness of the statistical theory.

---

*We are grateful to V. S. Barashenkov and V. M. Mal'tsev for making it possible for us to use their calculations of the statistical weights of the reactions omitted by us in reference 11, and for discussion of the problem.

Actually, for example, the state with isospin $T = 3/2$ and $T = -1/2$ can be resolved into two π mesons and a nucleon in two ways:

$$[3/2, -1/2] = \sqrt{2/5}\,[1/2, -1/2]\,[2, 0] + \sqrt{3/5}\,[1/2, 1/2]\,[2, -1],$$
$$[3/2, -1/2] = \sqrt{2/3}\,[1/2, -1/2]\,[1, 0] + \sqrt{1/3}\,[1/2, 1/2]\,[1, -1].$$

Within the framework of the statistical theory, these two distributions are considered equally probable. Account of the interaction matrix element H_{if} should lead to a deviation from this equality of probability. Processes taking place close to threshold (see, for example, the appendix to reference 2) represent a trivial example of such a discrepancy.

---

[1] V. S. Barashenkov and V. M. Mal'tsev, JETP **37**, 884 (1959), Soviet Phys. JETP **10**, 630 (1959).

[2] Belen'kiĭ, Maksimenko, Nikishev, and Rozental', Usp. Fiz. Nauk **62**, 1 (1957).

[3] E. Eberle, Nuovo cimento **8**, 610 (1958).

[4] T. Goto, Nuovo cimento **8**, 625 (1958).

[5] V. S. Barashenkov, JETP **34**, 1016 (1958), Soviet Phys. JETP **7**, 701 (1958).

[6] E. Segré, Ninth International Conference on High-Energy Physics, Kiev, 1959.

[7] I. L. Rozental', Usp. Fiz. Nauk **54**, 405 (1954).

[8] G. I. Kopylov, preprint P-166, Dubna, 1958.

[9] Walker, Hushfar, and Shephard, Phys. Rev. **104**, 526 (1956).

[10] V. I. Rus'kin, JETP **37**, 105 (1959), Soviet Phys. JETP **10**, 74 (1960).

[11] V. I. Rus'kin, JETP **36**, 164 (1959), Soviet Phys. JETP **9**, 113 (1959).

[12] Maenchen, Fowler, Powell, and Wright, Phys. Rev. **108**, 850 (1957).

[13] M. A. Markov, Гипероны и *K*-мезоны (Hyperons and K Mesons) Fizmatgiz, 1958.

Translated by R. T. Beyer
174

SOVIET PHYSICS JETP VOLUME 11, NUMBER 3 SEPTEMBER, 1960

CERENKOV RADIATION FROM A CHARGED PARTICLE WITH INTRINSIC MAGNETIC MOMENT

LI MENG-HA

Moscow State University

Submitted to JETP editor September 25, 1959

J. Exptl. Theoret. Phys. (U.S.S.R.) **38**, 934-936 (March, 1960)

The effect of spin on the intensity and polarization of the radiation produced in a ferrite by a charged particle with intrinsic magnetic moment is considered by quantum electrodynamic methods. The radiation is analyzed near threshold.

THE Cerenkov radiation produced by electrons, and its polarization, have been studied by a number of authors;[1–5] a number of other authors have considered the radiation due to a "superluminal" magnetic moment.[6,7] In this note we consider the "mixed" case, i.e., the radiation from a charged particle with intrinsic magnetic moment.

As is well known, the operator associated with the energy of interaction between a charged particle, having intrinsic magnetic moment, and an electromagnetic field in a medium, is given by

$$W = e(\boldsymbol{\alpha}\mathbf{A}) + \mu_0\{\rho_3(\boldsymbol{\sigma}\mathbf{B}) + \rho_2(\boldsymbol{\sigma}\mathbf{E})\}, \tag{1}$$

where ρ_3, ρ_2, $\boldsymbol{\alpha}$, and $\boldsymbol{\sigma}$ are Dirac matrices. The vector potential $\mathbf{A}$ for the quantized transverse electromagnetic field in a medium characterized by $\epsilon(\omega)$ and $\mu(\omega)$ can be written in the form[8]

$$\mathbf{A} = L^{-3/2}\sum_{\varkappa}(2\pi c''\hbar/\varkappa)^{1/2}[\mathbf{a}\exp(-ic'\varkappa t + i\boldsymbol{\varkappa}\mathbf{r}) + \mathbf{a}^{+}\exp(ic'\varkappa t - i\boldsymbol{\varkappa}\mathbf{r})], \tag{2}$$

where $c'' = c'\mu$, $c' = c/n$, $n = \sqrt{\epsilon\mu}$ and $\hbar\boldsymbol{\kappa}$ is the momentum of the photon.

In order to investigate the polarization of the radiation, we separate the amplitude of the vector potential into two components:[9]

$$\mathbf{a} = \mathbf{a}_2 + \mathbf{a}_3 = \boldsymbol{\beta}_2 q_2 + \boldsymbol{\beta}_3 q_3,$$
$$\boldsymbol{\beta}_2 = [\boldsymbol{\varkappa}^0\times\mathbf{k}^0]/\sqrt{1-(\boldsymbol{\varkappa}^0\mathbf{k}^0)^2}, \quad \boldsymbol{\beta}_3 = [\boldsymbol{\varkappa}^0\times\boldsymbol{\beta}_2] \tag{3}$$

for linear polarization and

$$\mathbf{a} = \mathbf{a}_1 + \mathbf{a}_{-1} = \boldsymbol{\beta}_1 q_1 + \boldsymbol{\beta}_{-1}q_{-1},$$
$$\sqrt{2}\boldsymbol{\beta}_\lambda = \boldsymbol{\beta}_2 + i\lambda\boldsymbol{\beta}_3 \quad (\lambda = 1, -1) \tag{4}$$

for circular polarization. Here $\boldsymbol{\kappa}^0 = \boldsymbol{\kappa}/\kappa$, $\mathbf{k}^0 = \mathbf{k}/k$, and the q_j $(j = 2, 3, 1, -1)$ are the quantum-mechanical operators of the vector potential $\mathbf{A}$.

If there are no photons at the initial time, the interaction-energy operator (cf. Eq. 1) becomes

$$W_j^{+} = L^{-3/2}\sum_{\varkappa}(2\pi c''\hbar/\varkappa)^{1/2}\exp\{i(c'\varkappa t - \boldsymbol{\varkappa}\mathbf{r})\}$$
$$\times\{e(\boldsymbol{\alpha}\mathbf{a}_j^{+}) - i\mu_0[\rho_3(\boldsymbol{\sigma}[\boldsymbol{\varkappa}\times\mathbf{a}_j^{+}]) + \varkappa n^{-1}\rho_2(\boldsymbol{\sigma}\mathbf{a}_j^{+})]\}, \tag{5}$$

where multiple photon production has been neglected.

Using perturbation-theory methods, we can find the radiation probability for a charged particle with intrinsic magnetic moment:[4]

$$W_j = \frac{2\pi}{c\hbar^2}\sum_{\mathbf{k}',\boldsymbol{\varkappa}} R_j^{+}R_j\delta_{\mathbf{k},\mathbf{k}'+\boldsymbol{\varkappa}}\delta(K' + \varkappa/n - K),$$

$$R_j = L^{-3/2}(2\pi c''\hbar/\varkappa)^{1/2}b'^{+}\{e(\boldsymbol{\alpha}\mathbf{a}_j^{+})$$
$$- i\mu_0[\rho_3(\boldsymbol{\sigma}[\boldsymbol{\varkappa}\times\mathbf{a}_j^{+}]) + n^{-1}\varkappa\rho_2(\boldsymbol{\sigma}\mathbf{a}_j^{+})]\}b, \tag{6}$$

where $\hbar\mathbf{k}$, $c\hbar K$, and $\hbar\mathbf{k}'$, $c\hbar K'$ are the momentum and energy of the particle before and after it radiates, and $\hbar k_0/c$ is the particle mass. Computing the necessary matrix elements in Eq. (6),[10] we can obtain an expression for the radiation intensity per unit path for the case of linear polarization $(j = 2, 3)$:

$$W_{j\,\text{tot}}^{s,s'} = W_{j\,\text{ch}}^{s,s'} + W_{j\,\text{m}}^{s,s'} + W_{j\,\text{cr.}}^{s,s'} \tag{7}$$

Here

$$W_{j\,\text{cm}}^{s,s'} = \frac{e\mu_0}{2}\int\limits_{\cos\theta\leqslant 1}\mu(\omega)\frac{\hbar n^2\omega^3}{pc^4\beta}\sqrt{1-\beta^2}\{(1-n^{-2})$$
$$+ ss'\xi[1 + n^{-2} - (2/\beta n)\cos\theta - 2(j-2)n^{-2}\sin^2\theta]\}\,d\omega;$$

and $W_{j\,\text{ch}}^{s,s'}$ and $W_{j\,\text{m}}^{s,s'}$ are the radiation intensities for the charge and magnetic moment respectively; these have been found earlier;[7,11]

$$\xi = \left[1 + \frac{\hbar^2n^2\omega^2}{p^2c^2} - \frac{2\hbar n\omega}{pc}\cos\theta\right]^{-1/2}, \quad \cos\theta = \frac{1}{\beta n} + \frac{\hbar n\omega}{2pc}(1-n^{-2}).$$

In what follows we will consider only the cross term $W_{j\,\text{cr}}^{s,s'}$.

If the spin orientation is unknown before and after emission of the photon and the total radiation intensity is measured, then we must average over initial spin states and sum over final spin states in Eq. (7); this procedure yields

$$W_{j\,\text{cr}} = e\mu_0\int\limits_{\cos\theta\leqslant 1}\mu(\omega)\frac{\hbar n^2\omega^3}{pc^4\beta}\sqrt{1-\beta^2}(1-n^{-2})\,d\omega, \tag{8}$$

whence it is apparent that the polarization is not linear. In the relativistic or classical approximations, the cross term $W_{j\,\mathrm{cr}}$ tends toward zero, in complete agreement with the classical theory.

It follows from Eq. (7) that close to threshold ($\cos\theta \approx 1$) the intensity is given by

$$W_{j\,\mathrm{cr}}^{s,s'} = \frac{e\mu_0}{2} \int\limits_{\cos\theta\leqslant 1} \mu(\omega)\frac{\hbar n^2\omega^3}{pc^4\beta}\sqrt{1-\beta^2}\,(1-n^{-2}) \times (1-ss')\,d\omega \quad (j=2,3). \tag{9}$$

Whence, $W_{j\,\mathrm{cr}}^{s,s'} = 0$ for $ss' = +1$; for $ss' = -1$, however,

$$W_{j\,\mathrm{cr}}^{s,s'} = e\mu_0 \int\limits_{\cos\theta\leqslant 1} \mu(\omega)\frac{\hbar n^2\omega^3}{pc^4\beta}\sqrt{1-\beta^2}\,(1-n^{-2})\,d\omega, \tag{10}$$

that is to say, the radiation near threshold is associated with a spin flip, a pure quantum effect. The fact that the threshold radiation is finite is a consequence of this quantum effect.

Using similar techniques we can obtain an expression for the radiation intensity per unit path in the case of circular polarization

$$W_{j\,\mathrm{tot}}^{s,s'} = W_{j\,\mathrm{ch}}^{s,s'} + W_{j\,\mathrm{m}}^{s,s'} + W_{j\,\mathrm{cr}}^{s,s'} \qquad (j = 1, -1), \tag{11}$$

where

$$W_{j\,\mathrm{cr}}^{s,s'} = \frac{e\mu_0}{2} \int\limits_{\cos\theta\leqslant 1} \mu(\omega)\frac{\hbar n^2\omega^3}{pc^4\beta}\sqrt{1-\beta^2}\Big\{(1-n^{-2}) \times \Big[1 + js\cos\theta - js'\xi\Big(\cos\theta - \frac{\hbar n\omega}{pc}\Big)\Big] + ss'\xi\Big[1 + n^{-2} - \frac{2}{\beta n}\cos\theta - n^{-2}\sin^2\theta\Big]\Big\}\,d\omega.$$

Using Eq. (11), we can determine the threshold radiation for a particle with oriented spin:

$$W_{j\,\mathrm{cr}}^{s,s'} = \frac{e\mu_0}{2} \int\limits_{\cos\theta\leqslant 1} \mu(\omega)\frac{\hbar n^2\omega^3}{pc^4\beta}\sqrt{1-\beta^2} \times (1-n^{-2})(1+js)(1-ss')\,d\omega. \tag{12}$$

It will be apparent that near threshold the radiation is associated with a spin flip; for a flux of particles characterized by spin $s = +1$, the radiation near threshold exhibits right-circular polarization ($j = +1$) while if $s = -1$ it exhibits left-circular polarization ($j = -1$), since $W_{j\,\mathrm{cr}}^{s,s'} \neq 0$ only when $js = +1$.

It should be noted that the radiation described by Eq. (8) is not polarized, because we have averaged over initial spin states so that particles characterized by $s = +1$ and $s = -1$ make equal contributions.

In conclusion, the author wishes to express his gratitude to Professor A. A. Sokolov for guidance in this work and to Yu. M. Loskutov for discussion of the results.

---

[1] P. A. Cerenkov, Dokl. Akad. Nauk **2**, 451 (1934); **12**, 413 (1936); **14**, 103 (1937).

[2] I. E. Tamm and I. M. Frank, Dokl. Akad. Nauk **14**, 107 (1937).

[3] E. Fermi, Phys. Rev. **57**, 485 (1940).

[4] A. A. Sokolov, Dokl. Akad. Nauk **28**, 415 (1940).

[5] A. A. Sokolov and Yu. M. Loskutov, JETP **32**, 630 (1957), Soviet Phys. JETP **5**, 523 (1957).

[6] V. L. Ginzburg, JETP **10**, 589 (1940).

[7] Yu. M. Loskutov and A. B. Kukanov, JETP **34**, 477 (1958), Soviet Phys. JETP **1**, 328 (1958).

[8] A. A. Sokolov and V. N. Tsytovich, JETP **30**, 136 (1956), Soviet Phys. JETP **3**, 94 (1956).

[9] A. A. Sokolov and I. M. Ternov, JETP **31**, 473 (1956), Soviet Phys. JETP **4**, 396 (1957).

[10] A. A. Sokolov, Введение в квантовую электродинамику (Introduction to Quantum Electrodynamics) Fizmatgiz, Moscow, 1958.

[11] Yu. M. Loskutov, Научн. докл. высш. шк., серия физ.-мат. (Science Notes from the Higher Schools, Phys.-Math Series), **4**, 103 (1958).

Translated by H. Lashinsky
175

SOVIET PHYSICS JETP VOLUME 11, NUMBER 3 SEPTEMBER, 1960

ON THE STRUCTURE OF THE Be^9 *NUCLEUS*

I. Sh. VASHAKIDZE, T. I. KOPALEĬSHVILI, V. I. MAMASAKHLISOV, and G. A. CHILASHVILI

Physics Institute, Academy of Sciences, Georgian S.S.R.

Submitted to JETP editor October 1, 1959

J. Exptl. Theoret. Phys. (U.S.S.R.) **38**, 937-941 (March, 1960)

For the Be^9 nucleus viewed as consisting of two α particles and a neutron, the equilibrium distances between the α particles and between the neutron and the centers of the α particles have been determined from the condition of minimum energy. Vibrations along the axis of symmetry and about the center of mass of the α particles are considered and the energy levels of the Be^9 nucleus are derived. The results obtained are compared with data relating to the $_\Lambda Be^9$ hypernucleus.

1. The model of the Be^9 nucleus in which the odd neutron moves in the centrally symmetric field of the residual Be^8 nucleus has been effectively used by many authors[1,2] to investigate the disintegration of this nucleus by photon and electron modes. Since the lifetime of the excited state, in the reactions investigated, was significantly shorter than the lifetime of the Be^8 nucleus as regards decay of the latter into two α particles, it appears more or less valid to neglect the structure of the residual Be^8 nucleus as was done by these authors. However, for the ground state or for those excitations of the Be^9 nucleus which are not attended by emission of the odd neutron, we must evidently presume that the residual Be^8 nucleus consists of two α particles located a certain distance apart.

Blair and Henley[3] recently proposed to explain some of the Be^9 excited levels as being rotational, viewing the nucleus as a system consisting of two α particles and a neutron. Furthermore, Suh[4] has shown that the binding energy value of the Λ particle in the $_\Lambda Be^9$ hypernucleus can be made to agree with experiment only if it is assumed that this particle moves in the field of the two α particles.

The aim of the present paper is to examine the stability of such a system and to explain the observed energy spectrum of the Be^9 nucleus.

2. The Hamiltonian of a system consisting of two α particles and a neutron has the form

$$H = -(\hbar^2/2\mu_\alpha)\Delta_u - (\hbar^2/2\mu)\Delta_\rho + V_{n\alpha}(|\boldsymbol{\rho} - \mathbf{u}/2|) + V_{n\alpha}(|\boldsymbol{\rho} + \mathbf{u}/2|) + V_{\alpha\alpha}(u) + C_{\alpha\alpha}(u), \tag{1}$$

where $\mathbf{u}$ is the relative α-particle radius-vector; $\boldsymbol{\rho}$ is the neutron radius vector relative to the center of the two α particles; $V_{n\alpha}$ and $V_{\alpha\alpha}$ are the potential energies of the nuclear interaction of the neutron with the α particles and between the two α particles, respectively; $C_{\alpha\alpha}$ is the potential energy of the Coulomb interaction of the α particles; $\mu_\alpha = 2M$ and $\mu = 8M/9$, where M is the nucleon mass.

In order to determine $V_{n\alpha}$, we follow Suh and proceed from the nucleon-nucleon interaction, which we take in the form

$$V_{nn} = -V_0 e^{-\beta^2 r^2}, \tag{2}$$

where, as shown by Hochberg et al.,[5] $\beta^2 = 0.266 \times 10^{26}\ \mathrm{cm}^{-2}$; we then normalize the expression by using a distribution of the nuclear material in the α particles in the form

$$P_\alpha(r) = 4(\alpha^2/\pi)^{3/2} e^{-\alpha^2 r^2}. \tag{3}$$

For the rms radius of the α particle we use the value $\sqrt{\overline{r^2}} = \sqrt{3/2\alpha^2} = 1.44$ fermis found by Hofstadter.[6] For the n-α interaction we therefore obtain

$$V_{n\alpha}(r) = -4V_0\left(\frac{\alpha^2}{\alpha^2+\beta^2}\right)^{3/2} \exp\left(-\frac{\alpha^2}{\alpha^2+\beta^2}\beta^2 r^2\right). \tag{4}$$

Following Suh,[4] we select the potential $V_{\alpha\alpha}$ in the form

$$V_{\alpha\alpha} = Ae^{-\delta^2 u^2} - Be^{-\epsilon^2 u^2}, \tag{5}$$

where $\delta^2 = 0.406 \times 10^{26}\ \mathrm{cm}^{-2}$, $\epsilon^2 = 0.116 \times 10^{26}\ \mathrm{cm}^{-2}$, A = 96 Mev, B = 30 Mev. The potential (5), which shows short-range repulsion and long-range attraction, best describes the experimental results of low-energy α scattering.

To find the Coulomb potential $C_{\alpha\alpha}$, we assume that the α-particle charge distribution follows a law analogous to Eq. (3). Noting that the odd neutron in Be^9 is in a p state, we take a zero-approximation trial function of the form

$$\Psi(\boldsymbol{\rho}, \mathbf{u}) = \frac{16}{3\pi}\sqrt{2a^5 b^5}\, u e^{-a^2u^2} e^{-b^2\rho^2} \rho Y_{1m}(\mathbf{n}_\rho), \tag{6}$$

where a and b are variation parameters established by the mean-square distance between the α particles and between the neutron and the center of the α particles respectively; $\mathbf{n}_\rho$ is the unit vector with direction $\boldsymbol{\rho}$. We point out that the presence of the factor u guarantees a null value for the wave function describing the relative motion of the two α particles at the coordinate origin; this tallies with short-range repulsion.

On the basis of Eqs. (1), (4), (5), and (6) we finally obtain for the mean energy value of the system under investigation

$$E(x, y) = \omega x + my - \frac{V_0 M (xy)^{5/2}}{(8xy + 4x + y)^{5/2}}\left[3 + \frac{5}{2(8xy + 4x + y)}\right]$$

$$+ \frac{\rho x^{5/2}}{(2x + p)^{5/2}} - \frac{nx^{5/2}}{(2x + q)^{5/2}} + \frac{kx^{1/2}(6x + j)}{(4x + j)^{3/2}}, \qquad (7)$$

where

$\omega = 7\hbar^2 l^2/6\mu_\alpha, \qquad m = 5\hbar^2 l^2/2\mu,$

$M = (2^{10}\sqrt{2/3})(\alpha^2/(\alpha^2 + \beta))^{3/2},$

$\rho = 4\sqrt{2}A, \qquad n = 4\sqrt{2}B, \qquad k = 2^5 e^2\alpha/3\sqrt{2\pi},$

$l^2 = \alpha^2\beta^2/(\alpha^2 + \beta^2), \qquad x = a^2/l^2, \qquad y = b^2/l^2,$

$p = \delta^2/l^2, \qquad q = \varepsilon^2/l^2, \qquad j = \alpha^2/l^2.$

In expression (7), x and y are the variation changes; V_0 is a parameter requiring determination which enters into the expression for the Gaussian potential (2); e is the electron charge.

To determine the possible values of V_0, we proceed from the experimental fact that there is no bound state of $He^4 + n$, i.e., that there is no binding of a neutron to a single α particle. It is easily seen that in the solution of variational problems for the system $He^4 + n$, we find the same parameters α, β, and γ that occur in our problems. If we require that the minimum energy value of the system $He^4 + n$ be positive or zero, it is possible to determine the possible values of V_0. As a result, it turns out that $V_0 \leq 26.6$ Mev.

3. As can be seen from (7), it is impossible to find the minimum of the function E (x, y) analytically. Therefore this function was tabulated within the square $0 \leq x \leq 5$, $0 \leq y \leq 5$ in steps of 0.5 for three values of V_0 ($V_0 = 26.6$, 20, and 15 Mev). We note that the interval in question for x and y corresponds to the mean square distance from ∞ to 1×10^{-13} cm.

Calculation shows that the function E (x, y) has a minimum in the region of negative values only when 26.6 Mev $\geq V_0 \geq$ 20 Mev. For $V_0 <$ 20 Mev the curve of E (x, y) is positive in the square of interest, and with further decrease of V_0 the minimum gradually flattens out and finally vanishes.

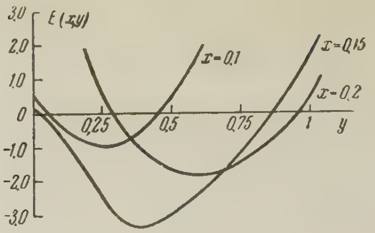

The figure shows curves expressing the dependence of E (x, y) on y for x = 0.10, 0.15, and 0.20, using $V_0 = 26.6$ Mev in every case. As can be seen from the figure, the function E (x, y) has an absolute minimum for $x = x_0 = 0.15$ and $y = y_0 = 0.40$, for which the corresponding energy value is −3 Mev.

If we require that the energy at the minimum should coincide with the observed 1.6 Mev binding energy of Be^9 when considered in the form of two α particles and a neutron, then we obtain a value of 24 Mev for V_0. It can easily be seen that for this case the minimum point coordinates x_0 and y_0 hardly move. To these values of x_0 and y_0 there correspond the distance between α particles $R_\alpha = 5.8 \times 10^{-13}$ cm and the distance between the neutron and the center of mass of the α particles $R_n = 3.6 \times 10^{-13}$ cm. The fact that on the average $R_n < R_\alpha$ gives us a basis for assuming that the Be^9 neutron moves in an axially symmetric field whose axis passes through the centers of the α particles. If it had happened that $R_n > R_\alpha$, then the existence of two centers would have been immaterial to the state of the neutron in the Be^9 nucleus. From the condition $R_n < R_\alpha$ it also ensues that the neutron in Be^9 must spend the major part of its time between the α particles, as if it were implementing the bond between them.

4. Since the Be^9 nucleus is characterized by axial symmetry, it follows that it must possess rotational and vibrational excitation levels. The rotational levels have been investigated by Blair and Henley,[3] who used them in calculating certain effects related to the excitation of these levels. Upon requiring that the energy of the second excited level, which appears under the rotational assumption, should coincide with the experimentally observed level (2.4 Mev), Blair and Henley found $R_\alpha = 4.6 \times 10^{-13}$ cm, which is satisfactorily close to our value of 5.8×10^{-13} cm.

Using this value of R_α, the above-mentioned authors likewise calculated other possible values of rotational level energies, but these values are in poor agreement with experimental data. Therefore we must conclude that only the second excited level of Be^9 with 2.4 Mev energy appears to be a rotational level. As regards the remaining Be^9 levels, we can assume that all of them are vibrational, as will be shown below. For this purpose

n_2	n_1	E_{exp}	E_{theor}	n_2	n_1	E_{exp}	E_{theor}
1	0	1.7	1,7	0	4	—	12.4
0	1	3.1	3.1	1	4	—	14.1
1	1	4.8	4.8	0	5	—	15.5
0	2	6.8	6.2	1	5	17,3(17.5)	17,2
1	2	7.9	7.9	0	6	18,2	18.6
0	3	—	9,3	1	6	19,9	20,3
1	3	11.3	11.0	0	7	21.7	21.7

we shall consider the Be^9 nucleus as a combination of two independent oscillators with frequencies ω_1 and ω_2, one of which corresponds to vibration along the axis of symmetry, and the other corresponds to vibration of the neutron about the center of gravity of the system. The first of these can be described as a vibration of the α particles along the axis connecting their centers, while the second can be described as a vibration of the odd neutron about the center of mass of the two α particles.

We shall designate by n_1 and n_2 the quantum numbers characterizing these vibrational modes. Then for the total excitation energy, reckoned from a given level, we can write

$$E_{n_1n_2} = n_1\hbar\omega_1 + n_2\hbar\omega_2. \tag{8}$$

If we require that the first 1.7-Mev Be^9 level correspond to excitation of only the first neutron vibration ($n_1 = 0$, $n_2 = 1$), while the 3.1-Mev level correspond to excitation of only the first α-particle vibration ($n_1 = 1$, $n_2 = 0$), it is possible to determine the frequencies ω_1 and ω_2. Assigning the values $n_1 = 0, 1, 2, 3, 4, 5, 6, \ldots$ for $n_2 = 0$ and for $n_2 = 1$, it is possible to obtain the entire excitation energy spectrum for the Be^9 nucleus with the exception, as is to be expected, of the 2.4 Mev energy level, which appears to be purely rotational according to Blair and Henley.

The table shows theoretical values of the Be^9 excitation energies calculated by Eq. (8), and also shows the experimental data contained in references 7 and 3.

As can be seen from the table, the agreement of the theoretical results with experimental data appears to be quite satisfactory. It should be noted however, that (8) predicts levels of energies 9.3, 12.4, 14.1, and 15.5 Mev, which have not yet been found experimentally. If we consider that the interval between the two neighboring observed levels at 11.3 and 17.2 Mev (like the one between 7.9 and 11.3 Mev) appears to be so large that it does not correspond to the observed level density found for other energy values, then this appears to make plausible the existence of the levels predicted by theory.

In addition, experiment shows two very close levels at 17.27 and 17.47 Mev, while the theoretical value corresponding to a vibrational level is 17.2 Mev. This could lead to the assumption that one of these levels is rotational. However, calculation shows that it is impossible to obtain a rotational level of 17.2 or 17.5 Mev for any value whatsoever of the moment J for the Be^9 nucleus if we proceed from the Blair and Henley value $R_\alpha = 4.6 \times 10^{-13}$ cm. This leads to one of two choices: either these levels coincide, in which case we really have only one level to deal with, or else a level uncoupling occurs which is not covered by our Eq. (8).

It is possible to conclude from the basic data given in the table that all the Be^9 levels fall into two series, characterized by $n_2 = 0$ and $n_2 = 1$, for each of which $n_1 = 0, 1, 2, 3, 4, 5, 6, \ldots$ The first spectral series corresponds to the excitation of vibrational modes along the axis of symmetry, when the odd neutron is found in the first excited state of vibrational motion.

Our assignment of the quantum number n_1 to vibration along the axis of symmetry and n_2 to vibration of the neutron about the center of mass is related to the fact, known from experiment, that the reaction for electron and photon disintegration of Be^9 with emission of a neutron is observed beginning with 1.7 Mev energy, which corresponds to the neutron binding energy. Since our investigation shows that the single-particle model as applied to the neutron is valid in several cases, it is reasonable to assume that when a Be^9 state has an excitation energy greater than 1.7 Mev, the neutron cannot receive more than 1.7 Mev of this energy. It follows that there cannot be a series with $n_2 > 1$. In fact, all the experimentally observed lines fall into series with $n_2 = 0$ or $n_2 = 1$.

5. Let us compare our deductions with results dealing with the $_\Lambda Be^9$ hypernucleus. For $_\Lambda Be^9$ there have been obtained[4] the values $R'_\alpha \approx 2.5 \times 10^{-13}$ cm and $R_\Lambda \approx 2 \times 10^{-13}$ cm. We observe here that $R_\Lambda < R'_\alpha$, just as in our case before. The smaller values of R_Λ and R'_α for the $_\Lambda Be^9$ hypernucleus than for the Be^9 nucleus can be explained by the fact that the Λ particle in the $_\Lambda Be^9$

hypernucleus is in an s state, while the neutron in the Be^9 nucleus is in a p state; it is therefore obvious why $R_n > R_\Lambda$. Furthermore, if we consider that the interaction radius of the Λ particle with a nucleon is smaller than the nucleon-nucleon interaction radius, and that consequently the Λ-α interaction radius is smaller than the n-α interaction radius, then we can assume that $R'_\alpha < R_\alpha$, since the Λ particle does the binding in the ${}_\Lambda Be^9$ hypernucleus while the neutron does the binding in the Be^9 nucleus. This conclusion seems all the more plausible, because the binding energy of the Λ particle in the ${}_\Lambda Be^9$ hypernucleus is greater than the binding energy of the neutron in the Be^9 nucleus.

In conclusion we wish to express our thanks to our associates at the Computer Center of the Academy of Sciences of the Armenian S.S.R., and especially to F. M. Ter-Mikaelyan and R. A. Aleksandryan for preparing the table of functions on the "Erevan" computer.

Added in proof (February 12, 1960): A recent paper [H. H. Thies and B. M. Spicer, J. Astr. Phys. **12**, 293 (1959)] shows the nuclear spectrum of Be^9 with the following new levels: 6.2, 9.2, and 13.3 Mev. As can be seen from our table, the first two are in good agreement with our values of 6.2 and 9.3 Mev, while the 13.3-Mev level falls between our theoretical values 12.4 and 14.1 Mev. The 6.8-Mev level, also observed experimentally, does not fit into our scheme and evidently has some other origin.

---

[1] V. I. Mamasakhlisov, J. of Phys. **7**, 239 (1943).

[2] E. Guth and C. J. Mullin, Phys. Rev. **76**, 234 (1949).

[3] J. S. Blair and E. M. Henley, Phys. Rev. **112**, 2029 (1958).

[4] K. S. Suh, Phys. Rev. **111**, 941 (1958).

[5] Hochberg, Massey, and Underhill, Proc. Phys. Soc. **A67**, 957 (1954).

[6] R. Hofstadter, Revs. Modern Phys. **28**, 214 (1956).

[7] F. Ajzenberg and T. Lauritsen, Revs. Modern Phys. **27**, 77 (1955).

Translated by D. A. Kellogg
176

SOVIET PHYSICS JETP VOLUME 11, NUMBER 3 SEPTEMBER, 1960

ON THE NUCLEAR ORIENTATION ASSOCIATED WITH A SATURATED FORBIDDEN RESONANCE AND WITH DOUBLE RESONANCE

G. R. KHUTSISHVILI

Institute of Physics, Academy of Sciences, Georgian S.S.R.

Submitted to JETP editor October 3, 1959

J. Exptl. Theoret. Phys. (U.S.S.R.) **38**, 942-947 (March, 1960)

Parameters f_k, characterizing the degree of nuclear orientation, are calculated for orientation produced by saturating a forbidden resonance and for a double resonance. Modifications of the double resonance method are examined.

1. During 1956 and 1957, Feher and Jeffries proposed two new methods for obtaining polarized nuclei. Jeffries' method[1] is based on the saturation of a forbidden paramagnetic resonance, while Feher's uses double resonance.[2] Experimentally both methods have led to observable polarizations.[3-8] In this paper we calculate the quantities f_k which characterize the degree of orientation,[9] and discuss the two methods.

2. Let the sample be a paramagnetic salt or silicon (or germanium) doped with nuclei having valence five or three. We assume that the nuclei of the paramagnetic ions, or of the impurity atoms, have spin, and if the sample is a paramagnetic salt, assume that the electron cloud in the paramagnetic ion has effective spin $\frac{1}{2}$. For silicon or germanium, we assume that the temperature is so low that the impurity atoms are not ionized.

Such a system can be thought of as a set of electron clouds with spin S, and a set of nuclei with spin I, the electron clouds being those of the paramagnetic ions (with an extra electron or hole). In a strong magnetic field, the energy levels of such a system are given by the equation

$$E_{Mm} = Mg\beta H + KMm + O(B^2/g\beta H,\ g_I\beta H,\ P). \qquad (1)$$

The notation is standard (in particular, M and m are the projections of the electron and nuclear spins respectively on the axis of quantization).

Figure 1 shows the energy levels when all terms can be neglected, except the Zeeman energy of spin S (as is the case when computing Boltzmann factors). For conciseness, the state $M = \frac{1}{2}$, m will be denoted by m′, while the state $M = -\frac{1}{2}$, m will be denoted by m.

The ordinary paramagnetic resonance lines induced by the alternating field are due to transitions with selection rules $\Delta M = \pm 1$, $\Delta m = 0$, and energy differences given approximately by $g\beta H + Km$. Those transition which have selection rules $\Delta M = 0$, $\Delta m = \pm 1$ and energy differences $\approx K/2$ correspond to nuclear magnetic resonance (more precisely, there will be correction terms of order $B^2/g\beta H$, $g_I\beta H$, and P).

The forbidden paramagnetic resonance lines correspond to transitions with $\Delta M = \pm 1$, $\Delta m = \pm 1$ and energy differences of about $g\beta H + K(m + \frac{1}{2})$.[10,11] In particular, if the spin Hamiltonian is axially symmetric about the direction of the magnetic field, then transitions will occur with $\Delta M = -\Delta m = \pm 1$ (provided that the alternating field has a non-zero component along the main field). In other cases, other transitions will be possible, with selection rules $\Delta M = \Delta m = \pm 1$.

There are also relaxation transitions, as follows:

1. Vertical transitions: $\Delta M = \pm 1$, $\Delta m = 0$ (purely electronic relaxation).
2. Horizontal transitions: $\Delta M = 0$, $\Delta m = \pm 1$ (purely nuclear relaxation).
3. Flip-flop transitions: $\Delta M = -\Delta m = \pm 1$.
4. Flip-flip transitions: $\Delta M = \Delta m = \pm 1$.
5. Quadratic transitions: $\Delta M = 0$, $\Delta m = \pm 2$.

We note that the contact interaction between electronic and nuclear spins can give only flip-flop transitions. The dipole-dipole interaction between these spins can give transitions of type 1, 2, 3, and

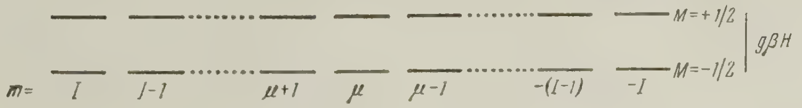

FIG. 1

4. The quadrupole interaction between the nucleus and the electric field of the electron cloud gives rise to transitions of types 5 and 2.

3. Jeffries' method is based on saturating the forbidden paramagnetic resonance and can be used when the vertical relaxation is predominant over other modes. These conditions are always fulfilled for paramagnetic salts, and also for silicon, doped for example, with As^{76} or Sb^{122}. In general, it need not be more difficult to saturate a forbidden resonance than an allowed one. Forbidden transitions are less likely than allowed ones, but on the other hand the relaxation rate of the forbidden transition is usually smaller than that of an allowed one.

Returning to Fig. 1, suppose that one of the transitions $\Delta M = -\Delta m = \pm 1$ is saturated (in particular, the transition $\mu \longleftrightarrow \mu - 1'$ where μ can take on values $I, I-1, \ldots -I+1$). Figure 2 shows three pairs of levels from Fig. 1, the levels corresponding to nuclear spin projections $\mu + 1$, μ and $\mu - 1$. Let $W(\mu)$ be the probability (per unit time) that the alternating field induces the transitions $\mu \longleftrightarrow \mu - 1'$. In this case there are three characteristic times: the time $T_r = 1/W(\mu)$ required for the alternating field to cause one transition (on the average), the vertical relaxation time T_e, and the nuclear relaxation time T_n (i.e., the relaxation time associated with changing m).

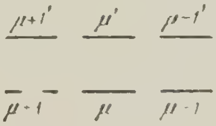

FIG. 2

Suppose these times satisfy the inequalities

$$T_r \ll T_e \ll T_n.$$

In this case, in a relaxation time of order T_r, the alternating field will make the populations of the states μ and $\mu - 1'$ equal. In a time of order T_e equilibrium will be established between the states μ and μ', and also between $\mu - 1$ and $\mu - 1'$. In a time T_n, full equilibrium will be established. We will use indices r, e, and n to distinguish between the orientation parameters corresponding to these three stages.

It is easy to obtain the results*

$$f_1^r = -\frac{\tanh\delta}{2I(2I+1)}, \qquad f_2^r = -\frac{3(2\mu-1)}{2I(2I+1)(2I-1)}\tanh\delta; \quad (2)$$

$$f_1^e = -\frac{\tanh\delta}{I(2I+1)}, \qquad f_2^e = -\frac{3(2\mu-1)}{I(2I+1)(2I-1)}\tanh\delta, \quad (3)$$

where $\delta = g\beta H/2kT$.

It is also easy to find an expression for the mean value of m^k (where k is an arbitrary, positive integer):

$$\langle m^k\rangle - \langle m^k\rangle_0 = -\alpha\tanh\delta\cdot[\mu^k - (\mu-1)^k]/(2I+1), \quad (4)$$

In Eq. (4), the index zero denotes no saturation, α is $\frac{1}{2}$ in the first stage (r), and 1 in the second (e). From this last formula, it is easy to find the values of f_3, f_4, etc in the first two stages. It turns out that

$$f_k^e = 2f_k^r \quad (5)$$

for all k.

Buishvili[12] has obtained the following expressions for f_1^n and f_2^n, on the assumption that the nuclear relaxation is due to the contact interaction only:

$$f_1^n = -\frac{[I(I+1) - \mu(\mu-1)]\sinh\delta}{I[(I+1-\mu)e^{-\delta} + (I+\mu)e^{\delta}]};$$
$$f_2^n = -\frac{[I(I+1) - \mu(\mu-1)](2\mu-1)\sinh\delta}{I[(I+1-\mu)e^{-\delta} + (I+\mu)e^{\delta}](2I-1)}. \quad (6)$$

What is the physical meaning of these results? f_1 is negative because the alternating field causes more transitions from μ to $\mu - 1'$ than the other way around (the population of the state μ being larger before saturation), with the result that the mean value of the projection of the nuclear spin decreases. Similarly, it is easy to see why f_2 is proportional to $1 - 2\mu$. Indeed, it can be shown that if $\mu > \frac{1}{2}$, then $\langle m^2\rangle$ decreases when the resonance $\mu \longleftrightarrow \mu - 1'$ is saturated, while if $\mu < \frac{1}{2}$, then $\langle m^2\rangle$ increases.

From the formulas for f_1 it follows that

$$|f_1^r| < |f_1^e| < |f_1^n|,$$

which is also not difficult to understand. After the populations of the states μ and $\mu - 1'$ have become equal, vertical relaxation occurs between the states μ' and μ, as well as $\mu - 1'$ and $\mu - 1$, followed by transitions $\mu \rightarrow \mu - 1'$ induced by the alternating field. When nuclear relaxation enters the picture, there will be transitions between the levels on the left in Fig. 1 to those on the right. All this increases the population of states with small m.

If the inequality $T_r \ll T_e$ does not hold, equilibrium under the alternating field and under vertical relaxation will be established simultaneously, and formulas (2) will not be applicable. If the inequality $T_e \ll T_n$ is violated, vertical and nuclear relaxations will establish equilibrium at the same time, and formula (3) will no longer hold.

The equations (6) remain valid in all cases, except that if the transitions $\mu \longleftrightarrow \mu - 1'$ are not completely saturated (which will be the case if T_r

---

*The f_k are normalized so that their maximum value is 1.[9]

$\sim T_n$), then the right hand sides must be multiplied by a factor $s(\mu)$ which tells how saturated is the transition.[12]

At first sight it would appear that to get maximum polarization, T_n should be as small as possible. However, this is not the case because when the nuclei relax quickly it is hard to saturate the forbidden transition.

Finally, it is easy to show that if the forbidden transition $\mu \longleftrightarrow \mu+1'$ is saturated, the minus sign in formulas (2) and (3) has to be replaced* by a plus sign, and $2\mu-1$ replaced by $2\mu+1$. The formulas for f_1^n and f_2^n become much more complicated because in this case the alternating field and the nuclear relaxation cause different transitions.

4. We now consider the double resonance method of orienting nuclei. Bloch has shown[13] that an adiabatic fast passage through a resonance results in an inversion of the two populations, provided the resonance is swept through quickly enough. In the following, the inverted pair of levels i and k will be denoted by the symbol $[i, k]$.

In Fig. 1 (or 2), let the pair of levels $[\mu, \mu']$ be inverted. The nuclei will not be polarized as a consequence of this, and so the amount of polarization will remain small. Now let us invert one of the pairs $[\mu, \mu-1]$, $[\mu, \mu+1]$, $[\mu', \mu-1']$, or $[\mu', \mu+1']$. This will result in a significant nuclear polarization.

For example, the two inversions $[\mu, \mu']$ and $[\mu', \mu-1']$ are equivalent to exchanging the populations of the levels μ and $\mu-1'$. As a result, the number of nuclei with spin projection $\mu-1$ will increase, while the number with spin μ will decrease. This leads to a negative nuclear polarization ($f_1 < 0$).

The final expressions for f_1 and f_2 in the four possible cases are given below:

$$f_1 = \pm \frac{\tanh \delta}{I(2I+1)}, \qquad f_2 = \pm \frac{3(2\mu-1)}{I(2I+1)(2I-1)} \tanh \delta, \tag{7}$$

the upper sign corresponding to inverting first the pair $[\mu, \mu']$ and then $[\mu, \mu-1]$, while the lower sign corresponds to inverting first $[\mu, \mu']$ and then $[\mu', \mu-1']$. Furthermore,

$$f_1 = \mp \frac{\tanh \delta}{I(2I+1)}, \qquad f_2 = \mp \frac{3(2\mu+1)}{I(2I+1)(2I-1)} \tanh \delta, \tag{8}$$

where the upper sign corresponds to the inversion $[\mu, \mu+1]$ after $[\mu, \mu']$ while the lower one corresponds to $[\mu', \mu+1']$ after $[\mu, \mu']$.

Formulas (7) and (8) are applicable only in the case where the time between the two inversions is significantly smaller than the vertical relaxation time T_e. If this inequality does not hold, less orientation will result because partial equilibrium between the levels μ and μ' will have been established by the time the second inversion occurs.

The orientation obtained by Feher's method will decay away with the nuclear relaxation time T_n. Although vertical relaxation transitions occur between the two inversions, they do not change the projection of the nuclear spin.

From the results given above, it follows that the values of the f_k obtained by Feher's method are the same as those in the second stage of Jeffries' method. For example, inverting the two pairs $[\mu, \mu']$ and $[\mu', \mu-1']$ gives the same result as saturating the forbidden transition $\mu \longleftrightarrow \mu-1'$. Clearly, the two inversions can be replaced by one — the one being an inversion of the two levels in the forbidden transition. For example, instead of inverting the pairs $[\mu, \mu']$ and $[\mu', \mu-1']$, it is sufficient to invert the pair $[\mu, \mu-1']$.

5. Different variations have been proposed on the method discussed above.[14,15] For example, we could saturate the transition $\mu \longleftrightarrow \mu'$, and then either saturate or invert one of the horizontal pairs (see Fig. 2). It is easy to see that if we were to saturate the transition $\mu \longleftrightarrow \mu'$ and then invert one of the pairs $[\mu, \mu+1]$, $[\mu, \mu-1]$, $[\mu', \mu+1']$, or $[\mu', \mu-1']$, the resulting orientations f_k would be half as big as those given by formulas (7) and (8). In other words, the values of f_k so obtained would be those corresponding to the first stage in Jeffries' method. The orientation would decay to its equilibrium value with a relaxation time of order T_n.

The values of the f_k would not change if the saturating field were to be removed after the horizontal pair of levels was inverted. When the saturating field goes off, vertical transitions between the levels μ and μ' take place, but these do not change the projection of the nuclear spin.

6. Another possibility is to saturate one of the vertical and also one of the horizontal pairs of levels. It is not difficult to show that

$$\langle m^k\rangle - \langle m^k\rangle_0 = -\frac{1}{2I+1}\Big\{[\mu^k + (\mu-1)^k] - \frac{2}{3+e^{\mp 2\delta}}[2\mu^k + (\mu-1)^k(1+e^{\pm 2\delta})]\Big\}, \tag{9}$$

where k is any positive integer and the upper sign in the exponents corresponds to saturating the transitions $\mu \longleftrightarrow \mu'$ and $\mu' \longleftrightarrow \mu-1'$, while the lower one corresponds to $\mu \longleftrightarrow \mu'$ and $\mu \longleftrightarrow \mu-1$. The index zero denotes no saturation. Furthermore,

---

*On the right hand side of formula (4), $\mu-1$ must be replaced by $\mu+1$.

$$\langle m^k\rangle - \langle m^k\rangle_0 = -\frac{1}{2I+1}\Big\{[\mu^k + (\mu + 1)^k] - \frac{2}{3+e^{\pm 2\delta}}\,[2\mu^k + (\mu+1)^k(1+e^{\pm 2\delta})]\Big\}, \qquad (10)$$

where the upper sign in the exponents corresponds to saturating the transitions $\mu \longleftrightarrow \mu'$ and $\mu' \longleftrightarrow \mu + 1'$ while the lower one refers to $\mu \longleftrightarrow \mu'$ and $\mu \longleftrightarrow \mu + 1$. As in the preceding cases, the polarization decays away with the relaxation time T_n.

If both saturating fields are turned off, the degree of nuclear orientation will not change for times less than T_n. When the field saturating the transition $\mu \longleftrightarrow \mu'$ is turned off, vertical transitions will occur, but these do not change the projection of the nuclear spin. When the field saturating the horizontal transitions is turned off, transitions will occur with relaxation time T_n.

---

[1] C. D. Jeffries, Phys. Rev. **106**, 164 (1957).

[2] G. Feher, Phys. Rev. **103**, 500 (1956).

[3] Abraham, Kedzie, and Jeffries, Phys. Rev. **106**, 165 (1957).

[4] G. Feher and E. A. Gere, Phys. Rev. **103**, 501 (1956).

[5] F. M. Pipkin and J. W. Culvahouse, Phys. Rev. **106**, 1102 (1957).

[6] J. W. Culvahouse and F. M. Pipkin, Phys. Rev. **109**, 319 (1958).

[7] F. M. Pipkin and J. W. Culvahouse, Phys. Rev. **109**, 1423 (1958).

[8] F. M. Pipkin, Phys. Rev. **112**, 935 (1958).

[9] G. R. Khutsishvili, JETP **28**, 496 (1955), Soviet Phys. JETP **1**, 390 (1955).

[10] Bleaney, Scovil, and Trenam, Proc. Roy. Soc. (London) **A223**, 15 (1954).

[11] L. L. Buishvili and G. R. Khutsishvili, Оптика и спектроскопия (Optics and Spectroscopy) in press.

[12] L. L. Buishvili, JETP **36**, 1926 (1959), Soviet Phys. JETP **9**, 1369 (1959).

[13] F. Bloch, Phys. Rev. **70**, 460 (1946).

[14] A. Kastler, Compt. rend. **233**, 1444 (1951).

[15] G. Feher, Phys. Rev. **103**, 835 (1956).

Translated by R. Krotkov
177

SOVIET PHYSICS JETP VOLUME 11, NUMBER 3 SEPTEMBER, 1960

INTERNAL BREMSSTRAHLUNG IN THE β DECAY OF POLARIZED NUCLEI

CH'ING CH'EN-JUI* and F. YANOUKH†

Nuclear Physics Institute, Moscow State University

Submitted to JETP editor October 8, 1959

J. Exptl. Theoret. Phys. (U.S.S.R.) **38**, 948-951 (March, 1960)

Internal bremsstrahlung in the β decay of polarized nuclei is studied. The general form of angular distributions is given. It is shown that a measurement of the correlation between the direction of emission of the internal bremsstrahlung photon and the nuclear polarization provides information on the form of the β interaction.

1 It is well known that as a consequence of parity nonconservation in β decay the emitted β electrons are longitudinally polarized. Therefore the internal bremsstrahlung of these electrons will be circularly polarized. The theory of internal bremsstrahlung was studied by a number of authors;[1-3] effects due to parity nonconservation were also discussed.[4-6] In particular the degree of circular polarization of the internal bremsstrahlung has been calculated for allowed and once forbidden β transitions.[5,6]

We wish to discuss the internal bremsstrahlung in the β decay of polarized nuclei. As a result of parity nonconservation there exist in this case correlations between the direction of emission of the photon and the polarization direction of the nucleus (of the type $\boldsymbol{\eta}\cdot\mathbf{k}$ where η is the polarization direction of the nucleus and $\mathbf{k}$ the momentum of the photon), and also between the direction of emission of the β electron after the internal bremsstrahlung and the nucleus polarization direction (of the type $\boldsymbol{\eta}\cdot\mathbf{p}$ where $\mathbf{p}$ is the β-electron momentum after the internal bremsstrahlung), if the direction of emission of the neutrino is not observed.

A measurement of the correlation between the direction of emission of the internal bremsstrahlung photon and the nucleus polarization provides information on the form of the β interaction. Consequently the study of internal bremsstrahlung of polarized nuclei is of well defined interest, particularly since it may turn out in a number cases that, due to considerations forced by experimental methods, an observation of this effect will be more convenient than the study of the angular distribution of β electrons in the β decay of polarized nuclei (this is due to the difficulties encountered in measurements of the β electron energy as a consequence of their scattering in the source, etc).

2. The calculation of the internal bremsstrahlung in the β decay of polarized nuclei is carried out for allowed transitions on the assumption of the V-A interaction form. The matrix element for the internal bremsstrahlung is written in the same form as in references 3 and 5.

The angular distribution of particles emitted in the β decay of polarized nuclei, accompanied by internal bremsstrahlung, may be written for the general case as follows:

$$w(\theta_{kp}, \theta_{\eta k}, \theta_{\eta p}) = A(\theta_{kp}) + B_k(\theta_{kp})\cos\theta_{\eta k} + B_p(\theta_{kp})\cos\theta_{\eta p} + \mu[C(\theta_{kp}) + D_k(\theta_{kp})\cos\theta_{\eta k} + D_p(\theta_{kp})\cos\theta_{\eta p}], \tag{1}$$

where

$$A(\theta_{kp}) = \frac{2}{\varepsilon_p p'^2 k^3}\Big[\Big\{|\langle 1\rangle|^2\delta_{j_2 j_1} + \frac{2j_2+1}{2j_1+1}|\langle\sigma\rangle|^2\Lambda^2\Big\}\{p^2(\varepsilon_p + k)\sin^2\theta_{kp} - k^2p'\}\Big], \tag{2}$$

$$B_k(\theta_{kp}) = \frac{2P_n}{\varepsilon_p p'^2 k^3}\Big[\Big\{-2\delta_{j_2 j_1}\sqrt{\frac{j_1}{j_1+1}}\Lambda\langle\sigma\rangle\langle 1\rangle + \frac{2j_2+1}{2j_1+1}g|\langle\sigma\rangle|^2\Lambda^2\Big\}\{k^2p' - kp^2 + kp\varepsilon_p\cos\theta_{kp}\}\Big], \tag{3}$$

$$B_p(\theta_{kp}) = \frac{2P_n}{\varepsilon_p p'^2 k^3}\Big[\Big\{-2\delta_{j_2 j_1}\sqrt{\frac{j_1}{j_1+1}}\langle\sigma\rangle\langle 1\rangle\Lambda + \frac{2j_2+1}{2j_1+1}g|\langle\sigma\rangle|^2\Lambda^2\Big\}\{pkp' - p^3\sin^2\theta_{kp}\}\Big], \tag{4}$$

$$C(\theta_{kp}) = \frac{2}{\varepsilon_p p'^2 k^3}\Big[\Big\{\delta_{j_2 j_1}|\langle 1\rangle|^2 + \frac{2j_2+1}{2j_1+1}|\langle\sigma\rangle|^2\Lambda^2\Big\}(kp^2\sin^2\theta_{kp} - k^2p')\Big], \tag{5}$$

$$D_k(\theta_{kp}) = \frac{2P_n}{\varepsilon_p p'^2 k^3}\Big[-2\delta_{j_2 j_1}\sqrt{\frac{j_1}{j_1+1}}\langle\sigma\rangle\langle 1\rangle\Lambda\,\{-\varepsilon_p k(k - p\cos\theta_{pk}) - 2p^2k + 2k^2p'\} + \frac{2j_2+1}{2j_1+2}g|\langle\sigma\rangle|^2\Lambda^2\{\varepsilon_p kp\cos\theta_{kp} - p^2k + k^2p'\}\Big], \tag{6}$$

$$D_p(\theta_{kp}) = \frac{2P_n}{\varepsilon_p p'^2 k^3}\Big[\Big\{-2\delta_{j_2 j_1}\sqrt{\frac{j_1}{j_1+1}}\langle\sigma\rangle\langle 1\rangle\Lambda + \frac{2j_2+1}{2j_1+1}g|\langle\sigma\rangle|^2\Lambda^2\Big\}kpp'\Big]. \tag{7}$$

---

*Nuclear Physics Institute, Peking University.

†Institute for Nuclear Research, Czechoslovak Academy of Sciences, Prague.

The notation used in Eqs. (1) — (7) is as follows: $\mathbf{k}$, k — momentum and energy of bremsstrahlung photons; $\mathbf{p}$, ϵ_p — momentum and energy of β electrons after bremsstrahlung; μ — sign of circular polarization of the internal bremsstrahlung photons ($\mu = \pm 1$); θ_{kp} — angle between directions of emission of the photon and β electron; $\theta_{\eta k}$ — angle between direction of photon and nucleus polarization; $\theta_{\eta p}$ — angle between direction of emission of β electron (after bremsstrahlung) and nucleus polarization; $\langle 1 \rangle$ and $\langle \sigma \rangle$ — matrix elements of the Fermi and Gamow-Teller type; $p' = -\epsilon_p + p \cos\theta_{kp}$; j_1, j_2 — nucleus spin in initial and final state; P_n — degree of nuclear polarization; $\Lambda = C_A/C_V = 1.19 \pm 0.04$.[7]

The coefficient g depends on the change in the nucleus angular momentum in the given β transition and is equal to

$$g = \begin{cases} -1 & \text{for transitions } j_2 = j_1 + 1, \\ +1/(j_1+1) & \text{for transitions } j_2 = j_1, \\ +1 & \text{for transitions } j_2 = j_1 - 1. \end{cases}$$

3. Next we analyze expression (1). We note that for internal bremsstrahlung in the β decay of unpolarized nuclei the terms proportional to B_k, B_p and D_k, D_p vanish. Therefore the expression

$$w_0(\theta_{kp}) = A(\theta_{kp}) \tag{8}$$

represents the probability for unpolarized internal bremsstrahlung in the β decay of unpolarized nuclei and it differs from previously given expressions[1-3] only in the inclusion of parity nonconservation. On the other hand the expression

$$w_1(\theta_{kp}) = A(\theta_{kp}) + \mu C(\theta_{kp}) \tag{9}$$

represents the probability for circularly polarized internal bremsstrahlung in the β decay of unpolarized nuclei. We note that the degree of circular polarization of the internal bremsstrahlung (for the V and A interaction variants) is equal to

$$P = \mu\frac{C}{A} = \mu\,\frac{p^2 k \sin^2\theta_{kp} - k^2 p'}{p^2(\varepsilon_p + k)\sin^2\theta_{kp} - k^2 p'}, \tag{10}$$

which agrees in magnitude with but differs in sign from the expression previously derived.[5,6] The disagreement in sign is a result of different assumptions regarding the ratio of the constants C and C′. Namely, we assume, in agreement with recent data,[8] that for the V and A interaction variants the relation $C = +C'$ holds; whereas Sawicki and Szymanski[5,6] assumed $C = -C'$.

Let us further note that the terms in expression (1) proportional to D_k and D_p are not due to parity nonconservation and represent scalars of the type $(\boldsymbol{\sigma}_\gamma \cdot \mathbf{k})(\mathbf{k}\cdot\boldsymbol{\eta})$ and $(\boldsymbol{\sigma}_\gamma\cdot\mathbf{k})(\mathbf{p}\cdot\boldsymbol{\eta})$ where $\boldsymbol{\sigma}_\gamma$ is the circular polarization vector of the photon.

Lastly, the expression

$$w_2(\theta_{kp}, \theta_{\eta p}, \theta_{\eta k}) = A(\theta_{kp}) + B_k(\theta_{kp})\cos\theta_{\eta k} + B_p(\theta_{kp})\cos\theta_{\eta p} \tag{11}$$

represents the desired angular distribution of unpolarized photons from the β decay of polarized nuclei, accompanied by internal bremsstrahlung.

4. Let us look in more detail at expression (11). After integrating it over the angle $\theta_{\eta p}$ we obtain the expression for the angular distribution of unpolarized internal bremsstrahlung photons from the β decay of polarized nuclei in the form

$$w_k \sim 1 + \alpha_k \cos\theta_{\eta k}, \tag{12}$$

where the asymmetry coefficient α_k is given by

$$\alpha_k = P_n\,\frac{[-2\delta_{j_2 j_1}\sqrt{j_1/(j_1+1)}\langle\sigma\rangle\langle 1\rangle\Lambda + [(2j_2+1)/(2j_1+1)]g|\langle\sigma\rangle|^2\Lambda^2]}{[\delta_{j_2 j_1}|\langle 1\rangle|^2 + [(2j_2+1)/(2j_1+1)]|\langle\sigma\rangle|^2\Lambda^2]} \times \Phi(\Delta, k), \tag{13}$$

and $\Phi(\Delta, k)$ is a function of the β-transition energy and the photon energy k given by

$$\Phi(\Delta, k) = \frac{6\varepsilon_p + 4k - p^{-1}[\varepsilon_p^2 + m^2 + (\varepsilon_p + k)^2]\ln[(\varepsilon_p + p)/(\varepsilon_p - p)]}{-4(\varepsilon_p + k) + p^{-1}[\varepsilon_p^2 + (\varepsilon_p + k)^2]\ln[(\varepsilon_p + p)/(\varepsilon_p - p]} \tag{14}$$

The table shows numerical values of the function Φ integrated over the β-electron energy (all energies expressed in units of mc^2). It is seen from the table that the asymmetry coefficient is quite large and does not depend strongly on either the energy of the β transition or on the photon energy.

Values of the function $\Phi(\Delta, k)$

Δ	k		
	0.1	0.5	1.0
4.0	−0.58	−0.64	−0.78
3.5	−0.55	−0.58	−0.71
2.2	−0.53	−0.55	—

By integrating expression (11) over the angle $\theta_{\eta k}$ we get the angular distribution of β electrons, which have emitted a bremsstrahlung photon, from the β decay of polarized nuclei; this represents one of the radiative corrections to the asymmetry coefficient in the Wu effect.

In conclusion the authors express their deep gratitude to Prof. Shapiro for suggesting this problem and for useful discussions.

---

[1] C. S. Chang and D. Falkoff, Phys. Rev. **76**, 365 (1949).

[2] Madansky, Lipps, Bolgiano, and Berlin, Phys. Rev. **84**, 596 (1951).

[3] R. Cutkovsky, Phys. Rev. **95**, 1222 (1954).

[4] R. Cutkovsky, Phys. Rev. **107**, 330 (1957).

[5] J. Sawicki and J. Szymanski, Nuovo cimento **10**, 982 (1957).

[6] J. Sawicki and J. Szymanski, Bull. Acad. Polon. Cl. III, **5**, 897 (1957).

[7] Sosnovskiĭ, Spivak, Prokof'ev, Kutikov, and Dobrynin, Report at the International Conference on Peaceful Uses of Atomic Energy, Geneva, 1958.

[8] A. I. Alikhanov, Report at the Kiev Conference on High Energy Physics, 1959.

Translated by A. M. Bincer
178

SOVIET PHYSICS JETP VOLUME 11, NUMBER 3 SEPTEMBER, 1960

SUPERFLUIDITY OF LIGHT NUCLEI

V. B. BELYAEV, B. N. ZAKHAR'EV, and V. G. SOLOV'EV

Joint Institute of Nuclear Research

Submitted to JETP editor October 12, 1959

J. Exptl. Theoret. Phys. (U.S.S.R.) **38**, 952-954 (March, 1960)

The physical ideas and the mathematical methods developed in superconductivity theory are applied to a study of the properties of light nuclei. On the basis of the shell model of the nucleus, it is shown that account of the residual interactions of protons and neutrons located near the Fermi surface leads to the appearance of superfluid states. Data on the binding energy of the last neutron in the $22 \le A \le 32$ region indicate the presence of paired (pp), (nn), and (np) correlations with the same quantum numbers s and m connected with the superfluidity of light nuclei.

APPLICATION of physical ideas and mathematical methods developed in superconductivity theory[1] to the theory of heavy nuclei has proved to be very fruitful. The residual interactions of protons and neutrons found in the outer shell of light nuclei can also lead to a large role for pair correlations and to the appearance of a superfluid state, i.e., to an energetically more favorable state than that of complete degeneracy of the Fermi gas. In this connection, it is of interest to consider the possibility of the appearance of a superfluid state of a light nucleus and to investigate its basic properties. The present paper is devoted to the study of these questions.

Taking the shell model of the nucleus as a base, we shall investigate certain properties of light nuclei with atomic weight A lying in the range $16 < A < 40$, where one can still use the hypothesis of isotopic invariance. We shall assume that the protons and neutrons forming the closed shell $Z = 8$, $N = 8$ create a radially symmetric field, which is distorted somewhat by nucleons lying outside this shell. Therefore our consideration applies directly to even weakly deformed nuclei (this restriction evidently has a purely methodological character), i.e., to nuclei lying in the $22 \le A \le 32$ interval.[2] We consider the residual interactions of protons and neutrons lying in the outer shell. The most significant difference of these interactions in light nuclei in comparison with heavy nuclei is the presence of neutron-proton interactions in addition to pp and nn interactions. We shall characterize the state of the nucleon by a choice of quantum numbers s, the quantum number m (the absolute value of the projection of the momentum along the axis of symmetry of the nucleus), and the number $\rho = \pm 1$ (the sign of this projection), while in the case of LS coupling ρ also characterizes the direction of the spin.

The Hamiltonian of the residual interactions of the nucleons close to the Fermi surface, i.e., in the region $E_F - \delta \le E(s, m) \le E_F + \Delta$, will be written in the isotopically symmetric form; that is,

$$\begin{aligned}H = \Sigma \{E(s, m) - \lambda\} \{a_{\rho m}(s)^+ a_{\rho m}(s) + b_{\rho m}(s)^+ b_{\rho m}(s)\} \\ + {}^1/_4 \Sigma J(s_1, s_2, s_2', s_1' \mid \rho_1 m_1, \rho_2 m_2;\ \rho_2' m_2', \rho_1' m_1') \\ \times \{a_{\rho_1 m_1}(s_1)^+ a_{\rho_2 m_2}(s_2)^+ a_{\rho_2' m_2'}(s_2')\, a_{\rho_1' m_1'}(s_1') \\ + b_{\rho_1 m_1}(s_1)^+ b_{\rho_2 m_2}(s_2)^+ b_{\rho_2' m_2'}(s_2')\, b_{\rho_2' m_2'}(s_2') \\ + 2a_{\rho_1 m_1}(s_1)^+ b_{\rho_2 m_2}(s_2)^+ b_{\rho_2' m_2'}(s_2')\, a_{\rho_1' m_1'}(s_1')\}. \quad (1)\end{aligned}$$

Here summation is carried out over s, s_1, s_2, s_1', s_2' for all positive values of m, m_1, m_2, m_1', m_2', and for $\rho = \pm 1$, while

$$\rho_1 m_1 + \rho_2 m_2 = \rho_1' m_1' + \rho_2' m_2', \quad \rho_1 m_1 \neq \rho_1' m_1',$$

$a_{m\rho}(s)$, $b_{m\rho}(s)$ are the operators of absorption of a proton and a neutron, λ is a parameter playing the role of a chemical potential, which is defined by the condition

$$n = \sum_{s, m, \rho} \{\overline{a_{\rho m}(s)^+ a_{\rho m}(s)} + \overline{b_{\rho m}(s)^+ b_{\rho m}(s)}\}. \quad (2)$$

We carry out a linear canonical transformation

$$\begin{aligned}a_{\rho m}(s) = u_m(s)\,\alpha_{m,-\rho} + \rho v_m(s)\,\alpha_{m\rho}^+ + i n_m(s)\,\beta_{m,-\rho} \\ + i\rho w_m(s)\beta_{m\rho}^+, \\ b_{\rho m}(s) = u_m(s)\,\beta_{m,-\rho} + \rho v_m(s)\,\beta_{m\rho}^+ + i n_m(s)\,\alpha_{m,-\rho} \\ + i\rho w_m(s)\,\alpha_{m\rho}^+, \quad (3)\end{aligned}$$

where the real functions u_m, v_m, n_m, w_m are related by the following relation

$$u_m(s)^2 + v_m(s)^2 + n_m(s)^2 + w_m(s)^2 = 1. \tag{4}$$

We determine the new vacuum state by the relation

$$\alpha_{\rho m}(s)\,\Psi = \beta_{\rho m}(s)\,\Psi = 0. \tag{5}$$

Solving (5), we obtain a wave function of the new vacuum state in the following form

$$\Psi = \prod_{s,\ m} \{(u_m^2 + n_m^2) + (v_m^2 + w_m^2)\, a_{m+}^{+} a_{m-}^{+} b_{m+}^{+} b_{m-}^{+} + (u_m v_m - w_m n_m)(a_{m+}^{+} a_{m-}^{+} - b_{m+}^{+} b_{m-}^{+}) + i\,(u_m w_m + n_m v_m)(a_{m+}^{+} b_{m-}^{+} - a_{m-}^{+} b_{m+}^{+})\}\,\Psi_0, \tag{6}$$

where $a_{\rho m}(s)\,\Psi_0 = 0$. The canonical transformation (3) is so chosen that the np interaction is taken into account, i.e., so that

$$(\Psi^{*} a_{\rho m} b_{\rho m} \Psi) \equiv \langle a_{\rho m} b_{\rho m} \rangle \neq 0.$$

Further, proceeding as in reference 3, we find the mean value of the energy operator $\overline{H}$ over the new vacuum state, and we determine the $u_m(s)$, $v_m(s)$, $n_m(s)$, and $w_m(s)$ from the condition of the minimum $\overline{H}$; as a result, we get

$$C_m(s) + {}^1/_2 \sum_{s'm'} J(s,\ s' \mid m, -m; -m',\ m') \frac{C_{m'}(s')^2}{\sqrt{\xi(s',\ m')^2 + 2C_{m'}(s')^2}} = 0, \tag{7}$$

$$u_m v_m - w_m n_m = u_m w_m + n_m v_m = -C_m(s)/2\varepsilon(s,\ m); \tag{8}$$

where

$$C_m(s) = \sum_{s'm'} J(s,\ s' \mid m, -m; -m',\ m')\,(u_{m'}(s')\,v_{m'}(s') - n_{m'}(s)\,w_{m'}(s')),$$

$$\varepsilon(s,\ m) = \sqrt{\xi(s,\ m)^2 + 2C_m(s)^2}, \quad \xi(s,\ m) = E(s,\ m) - \lambda,$$

$$u_m^2 + n_m^2 = {}^1/_2(1 + \xi(s,\ m)/\varepsilon(s,\ m)),$$

$$\times\, v_m^2 + w_m^2 = {}^1/_2(1 - \xi(s, m)/\varepsilon(s, m)).$$

Let us consider the approximation

$$J = \text{const}, \qquad \rho = \text{const}, \tag{9}$$

i.e., J and the level density ρ are constant in the energy range $E_F - \delta \leq E \leq E_F + \Delta$. We solve Eqs. (7) and (2) in the same way as in reference 4 and obtain

$$C = \frac{\sqrt{(4\Omega - n)\,n}}{e^{2/G} - 1}\,\frac{e^{1/G}}{2\sqrt{2\rho}}; \tag{10}$$

$$E_F - \lambda = \frac{2\Omega - n}{2\rho}\,\frac{1}{e^{2/G} - 1}, \tag{11}$$

where $G = -\rho J$, n = number of neutrons, while Ω is the number of levels in the outer shell of the nucleus. We note that $C = C_0/\sqrt{2}$, $\epsilon = \epsilon_0$, where C_0 and ϵ_0 correspond to the case of the absence of np interaction.[4]

Thus, if the model considered for a light nucleus is valid, then the residual (after separation of the self-consistent field) np, pp, and nn interactions lead to the formation of a superfluid state of the nucleus. It should be noted that the energy of the ground state of an even nucleus does not depend on how the nucleons are coupled together: protons with protons or neutrons with neutrons or also coupling of protons with neutrons takes place.

The first excited state in light even-even nuclei (and also in odd-odd nuclei, in which $N = Z$, when the last neutron and proton are described by the same quantum numbers) is separated from the ground state by an energy gap of order 2ϵ, and the behavior of single particle excitation levels in these nuclei ought to be similar to the same degree to which isotopic invariance is valid. However, for the explanation of energy levels and the energy of coupling of nuclei in the region $22 \leq A \leq 32$, one must take into consideration the quadruple correlation of α-particle-like nucleons in addition to pair correlations; these new correlations evidently play a very important role and somewhat mask the effect of pair correlations.

We now consider the data of Brink and Kerman[2] pertaining to the coupling energy of the last neutron in light nuclei. The binding energy of the last nucleon in ${}_{12}\text{Mg}_{14}^{26}$, ${}_{13}\text{Al}_{14}^{27}$, and ${}_{15}\text{P}_{16}^{31}$, where all the neutrons are coupled, is of the order of 11 Mev, while in the nuclei ${}_{12}\text{Mg}_{13}^{25}$, ${}_{12}\text{Mg}_{15}^{27}$, and ${}_{14}\text{Si}_{15}^{29}$, where the last neutron is not coupled, it is of the order of 7 Mev. Further neutron-proton couplings in ${}_{11}\text{Na}_{11}^{22}$, ${}_{13}\text{Al}_{13}^{26}$, and ${}_{15}\text{P}_{15}^{30}$ reduce to a last-neutron binding energy of the order of 11 Mev, and in odd-odd nuclei, where the last proton and neutron are described by different quantum numbers and therefore the pair correlation between them does not exist, the binding energy of the last neutron is also of the order of 7 Mev.

Thus the data on the binding energies of the last neutron in light nuclei confirm our assumption of the presence of np, pp, and nn pair correlations with identical quantum numbers s and m, leading to a superfluid state of light nuclei.

In conclusion we express our gratitude to N. N. Bogolyubov for his very interesting discussions.

---

[1] Bogolyubov, Tolmachev, and Shirkov, Новый метод в теории сверхпроводимости (A New Method in the Theory of Superconductivity) Acad. Sci. Press, 1958; English Translation, Consultants Bureau, N. Y., 1959.

[2] D. M. Brink and A. K. Kerman, Nucl. Phys. **12**, 314 (1959).

[3] V. G. Solov'ev, Dokl. Akad. Nauk SSSR **123**, 652 (1958), Soviet Phys.-Doklady **3**, 1197 (1959); Nucl. Phys. **9**, 655 (1959).

[4] V. G. Solov'ev, JETP **36**, 1869 (1959), Soviet Phys. JETP **9**, 1331 (1959).

Translated by R. T. Beyer
179

SOVIET PHYSICS JETP VOLUME 11, NUMBER 3 SEPTEMBER, 1960

EXCITATION OF FISSION FRAGMENTS AND THEIR MASS DISTRIBUTION

B. T. GEĬLIKMAN

Submitted to JETP editor October 15, 1959

J. Exptl. Theoret. Phys. (U.S.S.R.) **38**, 955-958 (March, 1960)

The influence of shell effects on elastic constants and mass coefficients of vibrational degrees of freedom of a nucleus, on the mass distribution of fission fragments, and on the magnitude of their excitation energy is considered.

1. The fission asymmetry and the excitation of the fragments have previously been considered.[1,2] It was shown that the degree of asymmetry and the magnitude of the excitation energy of the fragments depend on the values of the elastic constants for vibrational degrees of freedom of the fragments, and the excitation energy also depends on the mass coefficients of these degrees of freedom.

In references 1 and 2 it was noted that experiments on the Coulomb excitation of nuclei give evidence of a considerable deviation of the true values of the elastic constants and mass coefficients from their theoretical values calculated on the basis of the liquid-drop model. However, in references 1 and 2 elastic constants and mass coefficients calculated on the basis of the liquid-drop model were used in estimating the degree of asymmetry and the excitation energies of the fragments. Recently, Belyaev[3] showed a method for calculating the elastic constants and mass coefficients for vibrational quadrupole degrees of freedom of the nucleus, taking account of shell effects and of nucleon-nucleon interaction. According to Belyaev,[3] the potential energy of the nucleus, which depends on the deformation, has the form (a simpler case, when only one type of nucleon is present, was considered in reference 3)

$$U_d = \tfrac{1}{2}(k-\varkappa)Q_c^2 + \tfrac{1}{2}\varkappa\gamma_p Q_p^2 + \tfrac{1}{2}\varkappa\gamma_n Q_n^2 - \varkappa(Q_cQ_p + Q_cQ_n + Q_pQ_n), \qquad (1)$$

where Q_c, Q_p, Q_n are the (volume) quadrupole moments of the filled shell, and of the protons and nucleons outside the filled shell, respectively.

For small Q_p and Q_n

$$\gamma_p = \frac{\Theta_{p0}}{\Theta_p(1-\varkappa/k)} - 1, \qquad \gamma_n = \frac{\Theta_{n0}}{\Theta_n(1-\varkappa/k)} - 1;$$

Θ_{p0} and Θ_{n0} are numerical parameters characteristic of the given shell, and Θ_p and Θ_n are the occupation factors:

$$\Theta_p = \frac{4N_p}{N_{p\,max}}\left(1 - \frac{N_p}{N_{p\,max}}\right), \qquad (2)$$

where N_p is the number of protons in the unfilled shell, and $N_{p\,max}$ is the maximum number of protons possible in this shell. Θ_n has an analogous form. The notation is the same as in reference 3. The values of the elastic constants k and $\varkappa$ must be found from experiment ($\varkappa \approx k/2$, cf. reference 3).

The kinetic energy T is of the form

$$T = \tfrac{1}{2}B_c\dot{Q}_c^2 + \tfrac{1}{2}B_p\dot{Q}_p^2 + \tfrac{1}{2}B_n\dot{Q}_n^2;$$

B_c has the same meaning as in the liquid drop model: $B_c = 5m/24AR^2$; B_p and B_n are considerably larger:

$$B_p = \frac{\hbar^2}{(GN_{p\,max}/2)^2}\,\frac{\Theta_{p0}}{\Theta_p}\,\frac{\varkappa k}{k-\varkappa};$$

for B_n we have an analogous expression. Here m is the nucleon mass, A — the atomic weight, R — the nuclear radius, and G — the mean matrix element of the interaction energy; G is connected with the magnitude of the energy gap. The normal coordinates Q_1, Q_2, Q_3, and the frequencies of the normal vibrations for the Hamiltonian $H = T + U_d$ are easily found. The main role is played by the lowest frequency ω_1

$$\omega_1^2 \approx \frac{\varkappa k}{2(k-\varkappa)}\left\{\frac{1}{B_p}\left(\frac{\Theta_{p0}}{\Theta_p}-1\right) + \frac{1}{B_n}\left(\frac{\Theta_{n0}}{\Theta_n}-1\right) - \left[\left(\frac{1}{B_p}\left(\frac{\Theta_{p0}}{\Theta_p}-1\right) - \frac{1}{B_n}\left(\frac{\Theta_{n0}}{\Theta_n}-1\right)\right)^2 + \frac{4}{B_nB_p}\right]^{1/2}\right\}; \qquad (3)$$

if ω_1 is real, the nucleus is spherical.[3]

The probability of Coulomb excitation is determined by the matrix element of the operator $Z_cQ_c/A_c + Q_p$ of the oscillator ψ functions for Q_1. Comparing the theoretical values of the frequencies ω_1 thus found and the probabilities of Coulomb excitation with the experimental data on the values of the vibrational levels and on the probability of Coulomb excitation (cf. reference 4), it is possible to find Θ_{n0}, Θ_{p0}, $\varkappa$, and k (S. T. Belyaev, private communication).

The potential energy of the fissioning nucleus before scission is determined by the deformation energy of the future fragments; this deformation energy depends on the total deformation of the fragments, i.e., on the total quadrupole moment $Q = Q_c + Q_p + Q_n$ (cf. reference 1). Since the deformation process of the fissioning nucleus is quasistatic, it can be assumed that Q_p and Q_n take on values which correspond to a minimum of the energy U_d. Thus, to find the deformation energy of a fragment before scission, the potential energy U_d in (1) must be expressed in terms of Q, Q_p, and Q_n, and minimized with respect to Q_p and Q_n for a given Q. Here $U_d = C_Q Q^2/2$, where

$$C_Q = \varkappa \frac{1-\Theta_p/\Theta_{p0}-\Theta_n/\Theta_{n0}}{\Theta_p/\Theta_{p0}+\Theta_n/\Theta_{n0}+\varkappa/(k-\varkappa)}. \qquad (4)$$

It is easily seen that C_Q has maxima for filled shells. However, these maxima are not as sharp as the maxima of the frequency ω_1, of the elastic constant, and the mass coefficient for the normal coordinate Q_1 with a frequency ω_1. These sharp maxima are observed on the experimental curves of the elastic constants and mass coefficients in references 4 and 5. In C_Q values of k, $\varkappa$, Θ_{n0}, Θ_{p0}, found from a comparison with experimental data should be substituted (see above).

Since C_Q has a maximum for filled shells, the sum of the deformation energy of both fragments will, for the same parameters of the fragment deformation Q, be larger for magic than for nonmagic fragments. This effect will counteract the shell effects as far as the binding energy of spherical nuclei is concerned[1] and, consequently, will not favor asymmetric fission. However, an estimate of C_Q according to (4) shows that with the new values of C_Q the energy minimum of the fissioning nucleus is increased only by 1 – 2 Mev compared with calculations based on the liquid drop model,[1] and corresponds, as before, to asymmetric fission. Numerical calculations of the energy of the fissioning nucleus with new values of C_Q will be published in another paper.

2. Taking account of shell effects on the elastic constants and mass coefficients of the nucleus also changes the excitation energies of the fragments. The fragment excitation energy E_∞ consists of the energy of the inner degrees of freedom of the fragments at the instant of scission E_0, and of the additional excitation energy after scission $E_\infty - E_0$ (reference 2). In reference 2 the author showed that $E_\infty - E_0 \ll E_0$; however, there the calculations were made on the basis of the liquid-drop model. In accordance with the new model, instead of a single parameter of quadrupole fragment deformation $\alpha_2^{(i)}$, i.e., $Q^{(i)}$ $(i = 1, 2)$, three normal coordinates $Q_1^{(i)}$, $Q_2^{(i)}$, $Q_3^{(i)}$, have to be introduced, and the deformation energy U_d and the Coulomb interaction energy U_{int}, depending on $\alpha_2^{(i)}(Q^{(i)})$ (cf. reference 2), have to be expressed in terms of these normal coordinates. However, at the same time, only those terms depending on the coordinate $Q_1^{(i)}$, which corresponds to the lowest frequency $\omega_1^{(i)}$, can be retained in U_d and U_{int}, since higher excited frequencies will be considerably weaker. An estimate shows that here too, as before, $E_\infty - E_0 \ll E_0$. Therefore, for an approximate estimate of the excitation energy E_∞ it is sufficient to calculate E_0 corresponding to the most probable fragment mass ratio $A_1/A_2 \equiv A_{light}/A_{heavy}$. The value of E_0 depends only on $\alpha_2^{(i)}$ (i.e., on $Q^{(i)}$) and on $\alpha_3^{(i)}$ (cf. reference 2). Numerical calculations of E_0 and E_∞ as functions of Z and A of the fissioning nucleus will be published elsewhere.

Of great interest is also the calculation of the excitation energy of each fragment separately for different mass ratios A_1/A_2. The figure gives the values of the total energy $E_0^{(i)} = U_d^{(i)} + T^{(i)}$ (in units of e^2/r_0; for $r_0 = 1.22 \times 10^{-13}$ cm, $e^2/r_0 \approx 1.18$ Mev) at the instant of scission, calculated for three nuclei on the basis of the liquid drop model. In calculating $T^{(i)}$ in the expression for $(\alpha_2)_{eff}$ the term $\Delta U(A_1/A_2)$ [cf. formula (7) in reference 2] was, for simplicity, not taken into account. The fragment deformation energy $U_d^{(i)}$,

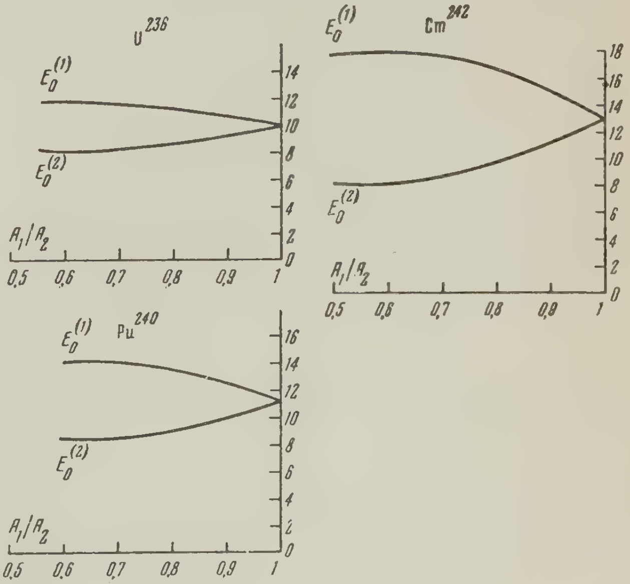

unlike the energy of the vibrational degrees of freedom $T^{(i)}$, changes little with A_1/A_2; only when $A_1/A_2 \ll 1$ is the energy $U_d^{(1)}$ noticeably smaller than $U_d^{(2)}$. The ratio $T^{(1)}/T^{(2)}$, however, as was to be expected,[2] increases sharply when A_1/A_2 decreases. On account of this E_0 becomes larger for a lighter fragment. In the new model, which takes into account shell effects on the elastic constants $C_Q^{(i)}$, $U_d^{(1)}$ and $U_d^{(2)}$ will, obviously, no longer remain practically constant while A_1/A_2 changes, but will increase from A_1/A_2 equal to unity up to A_1/A_2 corresponding to magic or nearly-magic fragments (that is near the most probable value of A_1/A_2); then, upon further change of A_1/A_2 they will decrease. $E_0^{(1)}$ and $E_0^{(2)}$ should prove to be more sensitive functions of A_1/A_2. Taking account of $\Delta U\,(A_1/A_2)$ leads to the same results, since $|\Delta U|$ (and, consequently, also $T^{(1)} + T^{(2)}$) has a maximum for the most probable value of A_1/A_2.

For such calculations of $E_0^{(1)}$ and $E_0^{(2)}$ we assume that scission takes place at the neck thickness d_n which is close to zero, for instance for $d_n \approx (0.1 \text{ to } 0.15)\,R$ (R is the radius of the fissioning nucleus) (cf. reference 2), and at that, in the most narrow place of the neck. However, as O. Bohr noted (private communication), if the fluctuations of the scission location are taken into account, an even stronger dependence of $E_0^{(1)}/E_0^{(2)}$ on A_1/A_2 may be obtained in the region where A_1/A_2 is close to unity. Indeed, if for a given position of the narrowest part of the neck the scission point is moved towards the heavier fragment, the energy of the lighter fragment is increased, since its deformation becomes larger. Inasmuch as a very strong dependence of the excitation energy ratio $E_0^{(1)}/E_0^{(2)}$ is observed[6] in the region of $A_1/A_2 = 1$, the effect of the fluctuation of the fracture location evidently plays an important role.

In conclusion, I wish to express my gratitude to S. T. Belyaev for an interesting discussion, and to I. G. Krutikova for carrying out the numerical calculations.

---

[1] B. T. Geĭlikman, Атомная энергия (Atomic Energy) **6**, 290 (1959).

[2] B. T. Geĭlikman, Атомная энергия (Atomic Energy) **6**, 297 (1959).

[3] S. T. Beliaev, Kgl. Danske Videnskab. Selskab, Mat.-fys. Medd **31**, No. 11 (1958).

[4] Alder, Bohr, Huus, Mottelson, and Winther, Деформация атомных ядер (Coll. Deformation of Atomic Nuclei) IIL, 1958, p. 210.

[5] G. M. Temmer and N. P. Heydenburg, Phys. Rev. **104**, 967 (1956).

[6] R. B. Leachman, Nuclear Fission, Paper at the International Conference on the Peaceful Uses of Atomic Energy, Geneva, 1955.

Translated by Z. Barnea
180

SOVIET PHYSICS JETP VOLUME 11, NUMBER 3 SEPTEMBER, 1960

ON THE ENERGY LEVELS OF μ MESIC ATOMS

N. I. ZHIRNOV

Moscow State Pedagogical Institute

Submitted to JETP editor October 16, 1959

J. Exptl. Theoret. Phys. (U.S.S.R.) **38**, 959-962 (March, 1960)

An approximate method is proposed for the calculation of the energy levels of μ mesic atoms from radial Dirac equations with a potential which simultaneously accounts for both nuclear volume and screening effects.

1. For the calculation of the energy levels and the wave functions of the meson in mesic atoms it is necessary to solve the quantum mechanical problem of the motion of a meson in the electrostatic field of the nucleus with the most reasonable (from the point of view of nuclear physics) distribution of protons. In the case of μ mesons one usually solves the relativistic Dirac equation with the potential

$$V(r) = Ze(3R^2 - r^2)/2R^3 \qquad (r < R),$$
$$V(r) = Ze/r \qquad (r > R), \qquad (1)$$

which corresponds to a proton distribution whose density is constant inside, and zero outside the nucleus. The screening effect is neglected by assuming that the electrons, which move at relatively large distances from the nucleus, do not have any appreciable effect on the μ meson which moves close to, or inside, the nucleus.

These considerations, however, are not the only reason for neglecting the screening effect in the calculation of the energy levels. Another reason which made the inclusion of the screening effect impossible was the absence of reliable approximate methods for integrating the Dirac equation with a combined potential of more complicated form than the potential (1). We note that even the integration of the radial Dirac equations with a potential of such a simple structure as potential (1) cannot be done exactly. The most exact solution of this problem is obtained by joining the wave functions at the boundary of the nucleus.[1]

In the present paper we propose the use of the quasi-classical method of solving the radial Dirac problem (see reference 2) for the calculation of the energy levels of μ mesic atoms including nuclear volume and screening effects.

2. We propose to take account simultaneously of both the nuclear volume and screening effects in the calculation of the energy levels of μ mesic atoms with the help of a combined potential which inside the nucleus is a Thompson oscillator potential and outside, a nonrelativistic statistical Thomas-Fermi potential, corrected at small distances from the nucleus:

$$U(r) = Ze(3R^2 - r^2)/2R^3 \qquad (r < R),$$
$$U(r) = Ze[1 - B(r - R)]/r \qquad (R < r < a_0/Z),$$
$$U(r) = e/r + (Z-1)e\varphi_0(r/\mu)/r \qquad (r > a_0/Z), \qquad (2)$$

where R is the radius of the nucleus, $\varphi_0(r/\mu)$ is the universal function of the statistical model of the atom, $\mu = 0.8853\,a_0/(Z-1)^{1/3}$, and a_0 is the Bohr radius of the hydrogen atom. The constant B, as determined from the continuity condition on the potential (2) at $r = a_0/Z$, is equal to

$$B = (Z-1)[1 - \varphi_0(a_0/\mu Z)]/(a_0 - RZ). \qquad (3)$$

The qualitative agreement of potential (2) with potential (1) allows us to solve the radial Dirac problem with the potential (2) for the μ mesic atom with the help of the quasi-classical method developed by the author,[2] by constructing an approximate quasi-classical solution of the radial Dirac problem with the potential (2) from the more exact solution of the analogous problem with the potential (1), obtained by the method of joining the wave functions at the nuclear boundary.[1]

As was shown earlier,[2] the approximate eigenvalues of the radial Dirac problem are, in the above-mentioned quasi-classical method, determined by the equations (14a) and (14b), which in our case have the form

$$\int_{r_1}^{r_2} K(\rho)\,d\rho = \int_{s_1}^{s_2} L(\sigma)\,d\sigma \quad (\text{for states with } \varkappa \neq -1), \qquad (4)$$

$$\int_{0}^{r_1} K(\rho)\,d\rho = \int_{0}^{s_1} L(\sigma)\,d\sigma \qquad (\text{for S states; } \varkappa = -1), \qquad (5)$$

where κ is the quantum number of the radial Dirac problem, and r_1 and r_2 are the zeroes of the function under the integral sign, $K(\rho)$; s_1 and s_2 are the zeroes of $L(\sigma)$. The functions $K(\rho)$ and $L(\sigma)$ have the form

$$K^2(\rho) = \alpha^2\left[E + \frac{Z}{2R^3}(3R^2 - \rho^2)\right]^2 + 2\left[E + \frac{Z}{2R^3}(3R^2 - \rho^2)\right]$$

$$- \frac{\varkappa(\varkappa + 1)}{\rho^2}$$

$$+ \frac{Z\varkappa}{(E + 2/\alpha^2 + 3Z/2R)R^3 - Z\rho^2/2} \quad (\text{for } \rho \leqslant R);$$

$$K^2(\rho) = \alpha^2(E - ZB + Z^*/\rho)^2$$

$$+ 2(E - ZB + Z^*/\rho) - \frac{\varkappa(\varkappa + 1)}{\rho^2}$$

$$+ \frac{Z^*\varkappa}{\rho^2[Z^* + (E - ZB + 2/\alpha^2)/\rho]} \qquad (\text{for } \rho \geqslant R), \tag{6}$$

where $Z^* = Z(1 + BR)$ and α is the fine-structure constant;

$$L^2(\sigma) = \alpha^2\left[\varepsilon + \frac{Z}{2R^3}(3R^2 - \sigma^2)\right]^2$$

$$+ 2\left[\varepsilon + \frac{Z}{2R^3}(3R^2 - \sigma^2)\right] - \frac{\varkappa(\varkappa + 1)}{\sigma^2}$$

$$+ \frac{Z\varkappa}{(\varepsilon + 2/\alpha^2 + 3Z/2R)R^3 - Z\sigma^2/2} \qquad (\text{for } \sigma \leqslant R);$$

$$L^2(\sigma) = \alpha^2(\varepsilon + Z/\sigma)^2 + 2(\varepsilon + Z/\sigma) - \frac{\varkappa(\varkappa + 1)}{\sigma^2}$$

$$+ \frac{Z\varkappa}{\sigma^2[Z + (\varepsilon + 2/\alpha^2)\sigma]} \qquad (\text{for } \sigma \geqslant R). \tag{7}$$

In formulas (6) and (7) ϵ is the level energy calculated from the Dirac equations with account of the nuclear volume effect, but neglecting the screening effect, by the method of joining the wave functions at the nuclear boundary;[3] E is the required level energy which includes both the nuclear volume and screening effects. The energies ϵ and E are measured in units of $e^2/r_0 = 5.6366$ kev, where

$$r_0 = \hbar^2/m_\mu e^2 = 2.555 \cdot 10^{-11} \text{ cm};$$

ρ, σ, and R are measured in units of r_0 and the constant B in units of r_0^{-1}. In the functions $K(\rho)$ and $L(\sigma)$ in formulas (6) and (7) we did not include the terms corresponding to the third line of the potential (2), since we do not have to know these terms in the solution of (4) and (5) (the zeros of these functions which are farthest away from the center of the nucleus, r_2 and s_2, lie considerably closer to the nucleus than the point $r = a_0/Z$).

3. The method outlined above was used for the calculation of a number of energy levels of μ mesic lead. The results of the computation are shown in the figure. The comparison of these results with the values of the level energies of μ mesic lead calculated earlier by Pustovalov[3] without account of the screening effect shows that the screening of the nuclear field by the electrons moving at the periphery of the mesic atom leads to an additional level shift which amounts to about 0.03% of the 1S level energy, to 0.15 to 0.25% of the 2P and 2S level energies, and to 0.46 to 0.63% of the energies of the levels 3D, 3P, and 3S. However, this should not lead one to think that these results are unimportant.

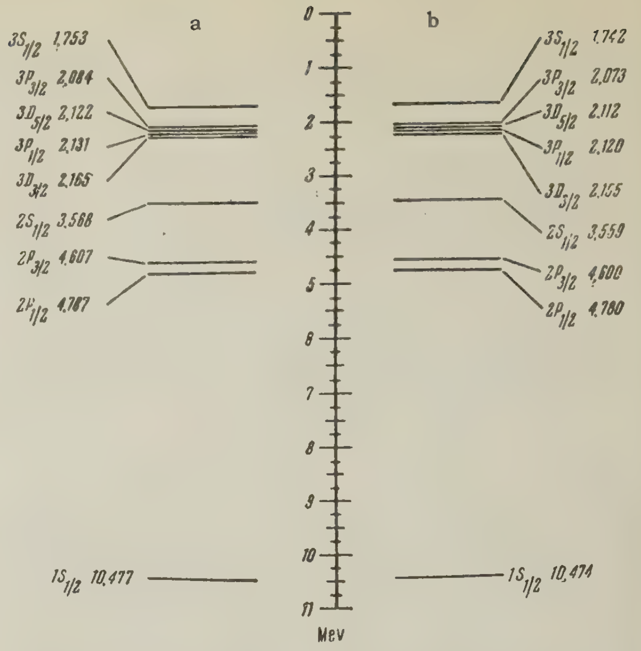

Energy levels of μ mesic lead, calculated with account of the nuclear volume effect (for constant density distribution of the protons): a – not including the screening effect, solving the Dirac equations by the method of joining the wave functions at the nuclear boundary;[3] b – including the screening effect, solving the Dirac equations by the quasi-classical method. The numbers near the levels give the values of their energies in Mev. The mass of the meson is 207 m_e, the radius of the nucleus is $1.2 \times 10^{-13} A^{1/3}$ cm, where A = 208.

The results obtained become of definite interest if we compare them with the Lamb shift of the levels in μ mesic lead which is mainly due to the polarization of the electron-positron vacuum. Pustovalov showed[3] that in μ mesic lead the polarization shift of the 1S level is 53 kev, that of the 2P levels is 28 kev, and that of the 2S level 17 kev, if nuclear volume effects are included. The additional level shift due to the screening effect is therefore about 5.7% of the Lamb shift of the 1S level, 25% of the Lamb shift of the 2P levels, and about 53% of the Lamb shift for the 2S level.

A serious shortcoming of the quasi-classical method used in the calculations is the absence of a rigorous criterion for its applicability, as was already pointed out in reference 2. To estimate the accuracy of our calculations we therefore resort to the criterion for the applicability of the usual WKB method in the case of the Coulomb field: the extent of the region which is important in our calculations is mainly given by the potential $Ze[1-B(r-R)]/r$, which is essentially a potential of the Coulomb type. The above-mentioned criterion (the absolute value of the energy of the μ meson must be small compared with its energy in the first Bohr orbit[4]) is satisfied (poorly at first, but then better and better), starting with the 2P states. The additional shift of 3 kev of the 1S level can be crudely estimated as the energy of the electrostatic interaction (repulsion) between the μ meson inside the nucleus and the $(Z-1)$ electrons which are separated from it by a mean distance of the Bohr radius. This crude estimate gives about 2.2 kev.

In conclusion we note that our method of including simultaneously the nuclear volume and screening effects in the calculation of the energy levels of μ mesic atoms can also be applied in the case of an arbitrary distribution of positive charge over the volume of the nucleus.

The author expresses his gratitude to B. T. Geĭlikman for his interest in the present work.

---

[1] A. Sommerfeld, Z. Physik **118**, 295 (1941). D. Ivanenko and N. Kolesnikov, Dokl. Akad. Nauk SSSR **91**, 47 (1953).

[2] N. I. Zhirnov, JETP **37**, 1619 (1959), Soviet Phys. JETP **10**, 1148 (1960).

[3] G. E. Pustovalov, JETP **32**, 1519 (1957), Soviet Phys. JETP **5**, 123 (1957).

[4] L. D. Landau and E. M. Lifshitz, Квантовая механика (Quantum Mechanics), pt. I, Gostekhizdat (1948); Engl. Transl., L. D. Landau and E. M. Lifshitz, Quantum Mechanics, Non-Relativistic Theory, Pergamon Press, London (1958).

Translated by R. Lipperheide
181

SOVIET PHYSICS JETP VOLUME 11, NUMBER 3 SEPTEMBER, 1960

A VARIATIONAL PRINCIPLE FOR THE CALCULATION OF A CORRECTION, QUADRATIC WITH RESPECT TO THE MAGNETIC FIELD INTENSITY, TO THE ELECTRON ENERGY IN A MOLECULE

T. K. REBANE

L. Ya. Karpov Physico-Chemical Institute

Submitted to JETP editor October 17, 1959

J. Exptl. Theoret. Phys. (U.S.S.R.) **38**, 963-965 (March, 1960)

A variational principle is formulated for the calculation of the diamagnetic correction to the ground-state energy of an electron in a molecule. The method is based on the variation of the gauge-transformation functions of the vector potential.

IN a constant magnetic field

$$\mathbf{H} = \operatorname{curl} \mathbf{A} \tag{1}$$

the correction to the i-th nondegenerate electron energy level in a molecule, quadratic with respect to H, is represented in the form

$$E_i^{(2)} = \frac{e^2}{2mc^2}\langle i\,|\,\mathbf{A}^2\,|\,i\rangle + \frac{e^2h^2}{m^2c^2}\sum_{k\neq i}\frac{|\langle k\,|\,\mathbf{A}\nabla + {}^1/_2\operatorname{div}\mathbf{A}\,|\,i\rangle|^2}{E_i - E_k}. \tag{2}$$

Here E_i and ψ_i are the energy and wave function of the i-th stationary state in the absence of a magnetic field,

$$\langle k\,|\,L\,|\,i\rangle = \int \psi_k L \psi_i d\tau. \tag{3}$$

The functions ψ_k are assumed real. This corresponds to an absence of orbital magnetic moments in unperturbed states. The summation over the index k denotes here and below summation over the discrete and integration over the continuous spectrum of the unperturbed problem.

Unlike the first (so-called "diamagnetic") term of formula (2), the computation of the second ("paramagnetic"*) term causes serious difficulties, since it requires the knowledge of all eigenvalues and eigenfunctions of the unperturbed problem. We shall show that these difficulties can be avoided if we use the gauge invariance of H.

We shall represent the vector potential in the form

$$\mathbf{A} = \mathbf{A}_0 + \nabla f, \tag{4}$$

where $\mathbf{A}_0$ is some fixed vector potential, satisfying the conditions

$$\operatorname{curl} \mathbf{A}_0 = \mathbf{H}, \qquad \operatorname{div} \mathbf{A}_0 = 0. \tag{5}$$

The value of $E_i^{(2)}$ is invariant with respect to the choice of the function f. However at the same time the individual terms in (2) depend substantially on the form of the function f. In particular, the "paramagnetic" term in (2) becomes zero if we assume in (4) that $f = f_i$ where the function f_i satisfies the equation

$$\tfrac{1}{2}\psi_i \nabla^2 f_i + \nabla\psi_i \nabla f_i + \mathbf{A}_0 \nabla \psi_i = 0. \tag{6}$$

The solution of this equation can be found by various approximation methods as well as by expansion in the functions ψ_k. In the latter case we have, for example

$$f_i = \frac{1}{\psi_i}\sum_{k\neq i}\frac{\langle k\,|\,\mathbf{A}_0\nabla\,|\,i\rangle}{E_k - E_i}\psi_k. \tag{7}$$

The important point now is the existence of a solution of Eq. (6). $E_i^{(2)}$ is now represented in the form

$$E_i^{(2)} = \frac{e^2}{2mc^2}\int \psi_i^2 (\mathbf{A}_0 + \nabla f_i)^2 d\tau. \tag{8}$$

Multiplying (4) by $\psi_i f_i$ and integrating, we obtain

$$\int \psi_i^2 (\mathbf{A}_0 \nabla f_i + \nabla f_i \nabla f_i)\, d\tau = \int [\psi_i^2 (f_i \mathbf{A}_0 + f_i \nabla f_i)]\, dS = 0. \tag{9}$$

Taking (9) into account, expression (8) is transformed into the form

$$E_i^{(2)} = (e^2/2mc^2)\int \psi_i^2 (\mathbf{A}_0^2 + \mathbf{A}_0 \nabla f_i)\, d\tau. \tag{10}$$

Since the integral (8) is not negative, the magnetic susceptibility of the electron in a state with zero orbital momentum is of diamagnetic character.* One must, however, take it into account that the proof of the inequality $E_i^{(2)} \geq 0$ is based on the existence of the volume integrals entering Eqs. (8) and (9). From (7) it can be seen that the integral $\int \psi_i^2 \nabla f_i \nabla f_i d\tau$ may not exist if the functions ψ_i have a nodal surface (or surfaces). Therefore, the statement about the diamagnetic character of the magnetic susceptibility is proved only for the ground state $(i = 1)$. For excited states of the electron $(i > 1)$, $E_i^{(2)}$ may be smaller than zero. This is in agreement with the results of direct calculations of the diamagnetic susceptibility of π electrons in aromatic molecules and (in contradiction to reference 1) indicates that in principle the existence of the so-called van Fleck temperature-independent paramagnetism is possible.

---

*We note that this term is unconditionally paramagnetic only for the lowest energy level (for i = 1).

*The inequality $E_1^{(2)} > 0$ for real wave functions was first proved by a different method.[1]

The above considerations allow a formulation of the following variational principle. The correction, quadratic with respect to the constant magnetic field intensity, to the electron energy for the ground state with a real wave function ψ_0, is equal to the minimum of the integral

$$I_0 = (e^2 / 2mc^2) \int \psi_0^2 (\mathbf{A}_0 + \nabla f)^2 d\tau, \qquad (11)$$

which is a functional of the function f [here, as in (4), A_0 is some fixed vector potential satisfying conditions (5)]. Indeed, Euler's equation for the function f is identical with Eq. (6) and, consequently, the minimum of I_0 is equal to $E_1^{(2)}$ [see Eqs. (11) and (8)]. The significance of minimizing I_0 lies in the search of a vector-potential gauge for which the paramagnetic term in (2) vanishes. The variational principle (11) is very convenient for practical calculations. In addition, the form of functional (11) emphasizes the diamagnetic character of the correction $E_i^{(2)}$ and shows that it is fully determined by the density distribution of the electron charge in the ground state.

---

[1] Guy, Tillieu, and Baudet, Compt. rend. **246**, 574 (1958).

Translated by Z. Barnea
182

SOVIET PHYSICS JETP VOLUME 11, NUMBER 3 SEPTEMBER, 1960

INTERACTIONS BETWEEN ELECTRONS AND LATTICE VIBRATIONS IN A SUPERCONDUCTOR

G. M. ÉLIASHBERG

Leningrad Physico-Technical Institute, Academy of Sciences, U.S.S.R.

Submitted to JETP editor October 18, 1959

J. Exptl. Theoret. Phys. (U.S.S.R.) **38**, 966-976 (March, 1960)

A perturbation theory is developed for the Green's function in which the Green's function calculated for the superconducting ground state is used as the zero approximation. Dyson equations are written down from which the electron Green's function can be determined. Interaction between electrons and phonons is not assumed to be small. The spectrum and the damping of the excitations are calculated.

1. INTRODUCTION

As Migdal[1] has shown in his work, a perturbation series for the vertex function of electron-phonon interaction converges rapidly, independent of whether the interaction is weak or strong. The expression $\lambda_0 h\omega_0/E_F$ served as the expansion parameter, where $\lambda_0 \lesssim 1$, ω_0 — maximum frequency of the phonons, E_F – Fermi energy. For this reason, it was possible to solve the Dyson equation and find the Green's function of the electrons and the phonons with accuracy up to $\lambda_0 h\omega_0/E_F$.

Application of this method to the study of the superconducting state is not possible if one starts out from the states of non-interacting electrons. Contemporary superconductivity theory makes use of a new system of approximate wave functions.[2,3] The corresponding energy spectrum has a gap

$$\varepsilon(k) = \sqrt{\xi^2(k) + C^2(k)},$$

where $\xi(k)$ is the spectrum of the normal state reckoned from the Fermi surface and $C(k)$ is a quantity defining the gap. The wave functions of the new collection of states depend both on the $C(k)$ and on the parameter. It is possible to determine them, for example, by a variational method[2] or by the method of Bogolyubov.[3] Starting out from the new states, Bogolyubov determined the single particle spectrum of the superconductor with accuracy up to $\lambda_0 h\omega_0/E_F$.[4]

It is of interest to apply the Migdal method, using superconductivity theory, to the determination of the Green's functions of the electrons in the superconductor. In addition to the results of Bogolyubov et al.,[4] this also allows us to compute the damping of the excitation.

The Green's functions of the electrons in a superconductor were computed by Gor'kov[5] for a model with a simplified four-fermion interaction. Use of a simplified Hamiltonian assumes the averaging of all quantities over the region with linear dimensions of order $v_0/\omega_0 \sim 10^{-5}$ cm (v_0 — velocity of electrons on the Fermi surface). Since the depth of penetration of the magnetic field in a superconductor far removed from the transition point has the same order of magnitude, then the obtaining of equations of the type of the Gor'kov equations for the Fröhlich Hamiltonian is of particular interest. Such equations are derived in the present work with the aid of superconductivity theory, in which the Green's functions computed for the "superconducting" BCS-Bogolyubov ground state are used as the zero approximation.

2. ZERO HAMILTONIAN IN THE INTERACTION REPRESENTATION

Following the work of Migdal, we shall consider a system with the Fröhlich Hamiltonian (the system of units is used in which $h = m = 1$):

$$H = \int d\mathbf{x} \{\psi_\sigma^+(\mathbf{x}) [H(\mathbf{x}) - \mu] \psi_\sigma(\mathbf{x}) + \psi_\sigma^+(\mathbf{x}) \psi_\sigma(\mathbf{x}) \varphi(\mathbf{x})\} + H_{ph}, \tag{1}$$

$$\psi_\sigma(\mathbf{x}) = V^{-1/2} \sum_{\mathbf{k}} a_{\mathbf{k}\sigma} e^{i\mathbf{k}\mathbf{x}},$$

$$\varphi(\mathbf{x}) = V^{-1/2} \sum_{q<q_M} \alpha_q (b_{\mathbf{q}} + b_{-\mathbf{q}}^+) e^{i\mathbf{q}\mathbf{x}}. \tag{2}$$

Here $H(x)$ is the one-electron Hamiltonian, q_M is the maximum momentum of the phonons; for $q \ll q_M$,

$$\alpha_q^2 = \lambda_0 \pi^2 s q / k_0, \tag{3}$$

$\lambda_0 \lesssim 1$ is the dimensionless parameter of Fröhlich, k_0 is the Fermi momentum, s is the sound velocity. The chemical potential μ is included in the Hamiltonian, since states will be used with a variable number of electrons. The explicit form of the phonon Hamiltonian is not needed.

We now introduce an abbreviated notation which is suitable for further exposition. We number the operators $\psi_{1/2}$, $\psi_{-1/2}$, $\psi^{+}_{-1/2}$, $\psi^{+}_{1/2}$ and will then deal with the "vector" ψ_α ($\alpha = 1, 2, 3, 4$). The operators ψ_α satisfy the commutation relations

$$\{\psi_\alpha(\mathrm{x}),\ \psi_\beta(\mathrm{x}')\} = I_{\alpha,\beta}\delta(\mathrm{x}-\mathrm{x}'), \tag{4}$$

$$\hat{I} = \begin{pmatrix} 0 & 0 & 0 & 1 \\ 0 & 0 & 1 & 0 \\ 0 & 1 & 0 & 0 \\ 1 & 0 & 0 & 0 \end{pmatrix}, \tag{5}$$

$\hat{I}^2 = \hat{E}$ ($\hat{E}$ is the unit matrix).

Along with ψ_α, we shall consider

$$\psi^\alpha = I_{\alpha\beta}\psi_\beta, \tag{6}$$

such that

$$\{\psi^\alpha(\mathrm{x}),\ \psi_\beta(\mathrm{x}')\} = \delta_{\alpha\beta}\delta(\mathrm{x}-\mathrm{x}'). \tag{7}$$

In this notation, the Hamiltonian has the following form:

$$H = H_{el} + H_{ph} + H_{int},$$
$$H_{el} = \int d\mathrm{x}\psi^\alpha(\mathrm{x})\,[H(\mathrm{x}) - \mu]\,\psi_\beta(\mathrm{x})\,N_{\beta\alpha},$$
$$H_{int} = \int d\mathrm{x}\psi^\alpha(\mathrm{x})\,\psi_\beta(\mathrm{x})\,\varphi(\mathrm{x})\,N_{\beta\alpha}. \tag{8}$$

The matrix $\hat{N}$ guarantees the normal order of the operators:

$$\hat{N} = \begin{pmatrix} 1 & 0 & 0 & 0 \\ 0 & 1 & 0 & 0 \\ 0 & 0 & 0 & 0 \\ 0 & 0 & 0 & 0 \end{pmatrix}, \tag{9}$$

As has already been noted, application of perturbation theory to the Hamiltonian of non-interacting electrons H_{el} does not lead to superconductivity in any finite order, independently of whether we expand the Green's function or the vertex function in a series. Our aim is to construct a perturbation theory for the Green's function on the basis of the collection of states employed in contemporary superconductivity theory. Bogolyubov[3,6] determined these states as the eigenstates of the operator of the number of particles

$$\int dx\,[\chi_0^+(\mathrm{x})\,\chi_0\,\mathrm{x} + \chi_1^+(\mathrm{x})\,\chi_1(\mathrm{x})],$$

where χ^+, χ are the creation and annihilation operators of the excitations, introduced by means of the canonical transformation

$$\chi_0(\mathrm{x}) = \int dy\,[U(\mathrm{x},\ \mathrm{y})\,\psi_{+1/2}(\mathrm{y}) - V(\mathrm{x},\ \mathrm{y})\,\psi^{+}_{-1/2}(\mathrm{y})],$$
$$\chi_1(\mathrm{x}) = \int dy\,[U(\mathrm{x},\ \mathrm{y})\,\psi_{-1/2}(\mathrm{y}) + V(\mathrm{x},\ \mathrm{y})\,\psi^{+}_{+1/2}(\mathrm{y})]. \tag{10}$$

U and V are, generally speaking, complex functions. Such conditions should be imposed on them that the operators χ satisfy the commutation relations for Fermi operators. The ground state is determined as a vacuum excitation.

In connection with what has been pointed out, we redetermine the zero Hamiltonian and write down the total Hamiltonian in the following form:

$$H = H_0 + H', \qquad H_0 = \widetilde{H}_{el} + H_{ph},$$
$$H' = H_{int} - (\widetilde{H}_{el} - H_{el});$$
$$\widetilde{H}_{el} = \int \widetilde{H}_{\alpha\beta}(\mathrm{x},\ \mathrm{y})\,\psi^\beta(\mathrm{x})\,\psi_\alpha(\mathrm{y})\,dx\,dy,$$
$$\widetilde{H}_{\alpha\beta}(\mathrm{x},\ \mathrm{y}) = \widetilde{H}^*_{\beta\alpha}(\mathrm{y},\ \mathrm{x}). \tag{11}$$

In order that the matrix $\widetilde{H}_{\alpha\beta}$ be diagonal in the χ-representation, it must have the following form in the representation of the ψ-operators:

$$\tilde{\widetilde{H}}(\mathrm{x},\ \mathrm{y}) = \begin{pmatrix} \widetilde{H}(\mathrm{x},\ \mathrm{y}) & 0 & \frac{1}{2}C(\mathrm{x},\ \mathrm{y}) & 0 \\ 0 & \widetilde{H}(\mathrm{x},\ \mathrm{y}) & 0 & -\frac{1}{2}C(\mathrm{x},\ \mathrm{y}) \\ \frac{1}{2}C^*(\mathrm{y},\ \mathrm{x}) & 0 & 0 & 0 \\ 0 & -\frac{1}{2}C^*(\mathrm{y},\ \mathrm{x}) & 0 & 0 \end{pmatrix}. \tag{12}$$

In the absence of external fields, $\widetilde{H}(\mathrm{x},\mathrm{y})$ and $C(\mathrm{x},\mathrm{y})$ are real functions of the difference in the arguments. We denote their Fourier components by $\tilde{\xi}(k)$ and $C(k)$, respectively. As we shall see, $\tilde{\xi}(k)$ will represent the renormalized energy of the electron excitations in the normal state, while $C(k)$ will determine the energy gap. The transformation functions (10) are also real if there are no external fields; their Fourier components are connected with $\tilde{\xi}(k)$ and $C(k)$ in the following fashion:

$$u_k^2 = \tfrac{1}{2}\left(1 + \tilde{\xi}(k)/\sqrt{\tilde{\xi}^2(k) + C^2(k)}\right),$$
$$v_k^2 = \tfrac{1}{2}\left(1 - \tilde{\xi}(k)/\sqrt{\tilde{\xi}^2(k) + C^2(k)}\right). \tag{13}$$

We now determine the Green's functions

$$G_\alpha^\beta(\mathrm{x},\ t;\mathrm{x}',\ t') = -i\langle T\psi_\alpha(\mathrm{x},t)\,\psi^\beta(\mathrm{x}',\ t')\rangle, \tag{14}$$
$$D(\mathrm{x},t;\ \mathrm{x}',\ t') = -i\langle T\varphi(\mathrm{x},t)\,\varphi(\mathrm{x}',t')\rangle. \tag{15}$$

For brevity, we shall call the matrix $\hat{G}$ with the matrix elements (14) the electron Green's function. Sometimes we shall find it convenient to deal with quantities

$$G_{\alpha\beta}(\mathbf{x},t;\ \mathbf{x}',t') = -i\langle T\psi_\alpha(\mathbf{x},t)\psi_\beta(\mathbf{x}',t')\rangle.$$

The electron Green's function of zero approximation satisfies the matrix equation

$$i\frac{\partial}{\partial t}\hat{G}^{(0)}(\mathbf{x},t;\mathbf{x}',t') - \int d\mathbf{y}\,\hat{H}(\mathbf{x},\mathbf{y})\hat{G}^{(0)}(\mathbf{y},t;\ \mathbf{x}',t')$$

$$= \hat{E}\delta(\mathbf{x}-\mathbf{x}')\delta(t-t'),$$

$$\hat{H}(\mathbf{x},\mathbf{y}) = \hat{\tilde{H}}(\mathbf{x},\mathbf{y}) - \hat{I}\hat{\tilde{H}}^*(\mathbf{x},\mathbf{y})\hat{I}$$

$$= \begin{pmatrix} \tilde{H}(\mathbf{x},\mathbf{y}) & 0 & C(\mathbf{x},\mathbf{y}) & 0 \\ 0 & \tilde{H}(\mathbf{x},\mathbf{y}) & 0 & -C(\mathbf{x},\mathbf{y}) \\ C^*(\mathbf{y},\mathbf{x}) & 0 & -\tilde{H}^*(\mathbf{x},\mathbf{y}) & 0 \\ 0 & -C^*(\mathbf{y},\mathbf{x}) & 0 & -\tilde{H}^*(\mathbf{x},\mathbf{y}) \end{pmatrix}. \tag{16}$$

Transforming to Fourier components in x and t, we obtain

$$[\omega\hat{E} - \hat{H}(k)]\hat{G}^{(0)}(k,\omega) = \hat{E}. \tag{17}$$

The solution of Eq. (17) can be written as follows:

$$\hat{G}^{(0)}(k,\omega)$$

$$= \begin{pmatrix} G^{(0)}(k,\omega) & 0 & F^{(0)}(k,\omega) & 0 \\ 0 & G^{(0)}(k,\omega) & 0 & -F^{(0)}(k,\omega) \\ F^{(0)}(k,\omega) & 0 & -G^{(0)}(k,-\omega) & 0 \\ 0 & -F^{(0)}(k,\omega) & 0 & -G^{(0)}(k,-\omega) \end{pmatrix}$$

$$G^{(0)}(k,\omega) = \frac{u_k^2}{\omega - \varepsilon(k) + i\delta} + \frac{u_k^2}{\omega + \varepsilon(k) - i\delta}$$

$$F^{(0)}(k,\omega) = \frac{C(k)}{(\omega - \varepsilon(k) + i\delta)(\omega + \varepsilon(k) - i\delta)}$$

$$\left(\varepsilon(k) = \sqrt{\xi^2(k) + C^2(k)}\right). \tag{18}$$

The imaginary part was determined by a theorem of Landau.[7] The functions $G^{(0)}$ and $F^{(0)}$ have the same structure as the corresponding Gor'kov functions.[5]

To construct a perturbation theory, it is necessary to establish the rule of calculation of the averages, over the ground state of the Hamiltonian H_0, of the T-product of the ψ-operators in the interaction representation. Direct application of the Wick theorem is not possible, since the concept of a normal product does not exist for the ψ-operators. We transform to χ-operators by means of the transformation (10), which we shall write for brevity in the form $\psi_\alpha = U_{\alpha\beta}\chi_\beta$. With reference to the χ-operators, the ground state is a vacuum one. Therefore, the usual rules of calculation of the mean are applicable. Considering the T-product of four operators for simplicity, we obtain

$$\langle T\psi_\alpha\psi_\beta\psi_\gamma\psi_\delta\rangle = U_{\alpha\alpha_1}U_{\beta\beta_1}U_{\gamma\gamma_1}U_{\delta\delta_1}\langle T\chi_{\alpha_1}\chi_{\beta_1}\chi_{\gamma_1}\chi_{\delta_1}\rangle$$

$$= U_{\alpha\alpha_1}U_{\beta\beta_1}U_{\gamma\gamma_1}U_{\delta\delta_1}\{\langle T\chi_{\alpha_1}\chi_{\beta_1}\rangle\langle T\chi_{\gamma_1}\chi_{\delta_1}\rangle$$

$$- \langle T\chi_{\alpha_1}\chi_{\gamma_1}\rangle\langle T\chi_{\beta_1}\chi_{\delta_1}\rangle + \langle T\chi_{\alpha_1}\chi_{\delta_1}\rangle\langle T\chi_{\beta_1}\chi_{\gamma_1}\rangle\}$$

$$= \langle T\psi_\alpha\psi_\beta\rangle\langle T\psi_\gamma\psi_\delta\rangle$$

$$- \langle T\psi_\alpha\psi_\gamma\rangle\langle T\psi_\beta\psi_\delta\rangle + \langle T\psi_\alpha\psi_\delta\rangle\langle T\psi_\beta\psi_\gamma\rangle.$$

Here it is evident that, in the notation used, the average vacuum states are computed according to the usual rules. In this case the matrix $\hat{G}^{(0)}$ serves as the Green's function.

3. DERIVATION OF THE EQUATIONS AND CALCULATIONS OF THE ELECTRON GREEN'S FUNCTION

We begin with the equation for the Green's function

$$\left[i\frac{\partial}{\partial t}\delta_{\alpha\gamma} - H^{(0)}_{\alpha\gamma}(\mathbf{x}) + \mu\Gamma^{(0)}_{\alpha\gamma}\right]G^{\beta}_{\gamma}(\mathbf{x},t;\ \mathbf{x}',t')$$

$$= \delta_{\alpha\beta}\delta(\mathbf{x}-\mathbf{x}')\delta(t-t')$$

$$- i\Gamma^{(0)}_{\alpha\gamma}\langle T\varphi(\mathbf{x},t)\psi_\gamma(\mathbf{x},t)\psi^\beta(\mathbf{x}',t')\rangle, \tag{19}$$

$$\hat{H}^{(0)}(\mathbf{x}) = \begin{pmatrix} H(\mathbf{x}) & 0 & 0 & 0 \\ 0 & H(\mathbf{x}) & 0 & 0 \\ 0 & 0 & -H^*(\mathbf{x}) & 0 \\ 0 & 0 & 0 & -H^*(\mathbf{x}) \end{pmatrix},$$

$$\hat{\Gamma}^{(0)} = \hat{N} - \hat{I}\hat{N}\hat{I} = \begin{pmatrix} 1 & 0 & 0 & 0 \\ 0 & 1 & 0 & 0 \\ 0 & 0 & -1 & 0 \\ 0 & 0 & 0 & -1 \end{pmatrix}. \tag{20}$$

Introducing the matrix $\hat{\Sigma}(\mathbf{x},t;\ \mathbf{x}',t)$, we write (19) as follows:

$$\left[i\frac{\partial}{\partial t}\hat{E} - \hat{H}^{(0)}(\mathbf{x}) + \mu\hat{\Gamma}^{(0)}\right]\hat{G}(\mathbf{x},t;\ \mathbf{x}',t')$$

$$= \hat{E}\delta(\mathbf{x}-\mathbf{x}')\delta(t-t')$$

$$+ \int d\mathbf{y}\,d\tau\,\hat{\Sigma}(\mathbf{x},t;\ \mathbf{y},\tau)\hat{G}(\mathbf{y},\tau;\ \mathbf{x}',t'). \tag{21}$$

In the absence of an external field in (21), we can transform to the Fourier components in x and t:

$$[\omega\hat{E} - \xi(k)\hat{\Gamma}^{(0)} - \hat{\Sigma}(k,\omega)]\hat{G}(k,\omega) = \hat{E}. \tag{22}$$

For the study of the structure of the self energy, we shall expand $\langle T\varphi(\mathbf{x},t)\psi_\gamma(\mathbf{x},t)\psi^\beta(\mathbf{x}',t')\rangle$ in a perturbation-theory series. Since the vacuum averages in the interaction representation are expressed in terms of the matrix $\hat{G}^{(0)}$ by the usual rules, we can make use of the usual graphical techniques. To each solid or dashed line, there corresponds an electron or phonon Green's function, multiplied by i, and to the simple vertex there corresponds the matrix $\hat{\Gamma}^{(0)}$ [see (20)]. We recall that by the electron Green's function we mean the matrix $\hat{G}^{(0)}$, defined by (17).

It is now clear that we can write down the Dyson equation which defines the connection of the self energy $\hat{\Sigma}$ with the exact Green's functions and the total vertex function $\hat{\Gamma}$:

$$\hat{\Sigma}(\mathbf{k}, \omega) = \frac{i}{(2\pi)^4} \hat{\Gamma}^{(0)} \int d\mathbf{k}_1 \, d\omega_1 \, \hat{G}(\mathbf{k}_1, \omega_1)$$

$$\times D(\mathbf{k} - \mathbf{k}_1; \omega - \omega_1) \, \hat{\Gamma}(\mathbf{k}, \omega; \mathbf{k}_1, \omega_1).$$

To expand $\hat{\Gamma}$ in a perturbation theory series, we need to know the zeroth Green's functions which contain the (still undetermined) quantities $\tilde{\xi}(k)$ and $C(k)$. We shall assume that we are limited to a simple vertex $\hat{\Gamma}^{(0)}$. There is no necessity in the exact expressions for $\tilde{\xi}$ and C for an estimate of the contribution of higher approximations.

For a normal metal, as has already been pointed out, we can replace the vertex function by a simple vertex. Calculations, completely analogous to those performed by Migdal, lead to the conclusion that in our case we can, with the same accuracy, neglect all corrections and limit ourselves to a simple vertex. Without presenting the calculations here, we shall make only a few remarks. For computation of $\hat{\Sigma}$, the larger values of the transferred momentum $q \sim k_0$ are important. Therefore, for example, in a simple tripole, both electron Green's functions enter with a large difference in the argument, and are therefore shown to be almost orthogonal. The difference of the "superconducting" Green's function from the "normal" does not appear to be essential here. It would have been necessary to take into account the counter term of H' only in the calculation of subsequent corrections to the vertex function.

Thus, replacing $\hat{\Gamma}$ by $\hat{\Gamma}^{(0)}$, we obtain the following expression for $\hat{\Sigma}$:

$$\hat{\Sigma}(\mathbf{k}, \omega) = \frac{i}{(2\pi)^4} \hat{\Gamma}^{(0)} \int d\mathbf{k}_1 \, d\omega_1 \hat{G}(\mathbf{k}_1, \omega_1)$$

$$\times D(\mathbf{k} - \mathbf{k}_1; \omega - \omega_1) \, \hat{\Gamma}^{(0)}. \tag{23}$$

The phonon Green's functions of the superconductor and the normal metal are practically identical, since the region of momenta which is important for the determination of D is large in comparison with the region of momenta close to the Fermi surface which is responsible for superconductivity. Therefore, we can use for D the expression of Migdal:[1]

$$D(q, \omega) = \alpha_q^2 \frac{\omega_q^{(0)}}{\omega_q} \left(\frac{1}{\omega - \omega_q + i\delta_1(q)} - \frac{1}{\omega + \omega_q - i\delta_1(q)} \right),$$

$$\omega_q^2 = (\omega_q^{(0)})^2 (1 - \lambda_0 + \lambda_0 q^2/8k_0^2),$$

$$\delta_1(q) = \pi\lambda_0 (\omega_q^{(0)})^2/4k_0 q. \tag{24}$$

Equations (22) and (23) now form a closed system. We eliminate Σ from the equations and write down the resultant matrix equation in the coordinate representation:

$$\left[i \frac{\partial}{\partial t} \hat{E} - \hat{H}^{(0)}(\mathbf{x}) + \mu\hat{\Gamma}^{(0)} \right] \hat{G}(\mathbf{x}, t, \mathbf{x}', t') = \hat{E}\delta(\mathbf{x} - \mathbf{x}') \, \delta(t - t')$$

$$+ i \int d\mathbf{y} d\tau \, \hat{\Gamma}^{(0)} \hat{G}(\mathbf{x}, t; \mathbf{y}, \tau)$$

$$\times D(\mathbf{x}, t; \quad \mathbf{y}, \tau) \, \hat{\Gamma}^{(0)} \hat{G}(\mathbf{y}, \tau; \mathbf{x}', t'). \tag{25}$$

If we were to write out this equation in detail, then it would be seen that the system obtained here has the structure of the Gor'kiĭ equations. Equation (25) was derived for the case in which external fields are absent. However, it can be expected that it remains valid even when $H(x)$ contains an external field, for example, a magnetic field. We note that it has a gauge invariant form.

We now turn our attention to Eqs. (22) and (23). The matrices $\hat{G}$ and $\hat{\Sigma}$ in them also have the same matrix structure as the matrix $\hat{G}^{(0)}$ [see (18)]. The formula for $\hat{G}$ is obtained from (18) if the index zero in the latter is omitted; $\hat{\tilde{\Sigma}}$ is obtained from (18) if we replace $\hat{G}^{(0)}$ and $F^{(0)}$ by Σ_1 and Σ_2, respectively, where

$$\Sigma_1(\mathbf{k}, \omega) = \frac{i}{(2\pi)^4} \int d\mathbf{k}_1 d\omega_1 G(\mathbf{k}_1, \omega_1) \, D(\mathbf{k} - \mathbf{k}_1, \omega - \omega_1), \tag{26a}$$

$$\Sigma_2(\mathbf{k}, \omega) = \frac{i}{(2\pi)^4} \int d\mathbf{k}_1 d\omega_1 F(\mathbf{k}_1, \omega_1) \, D(\mathbf{k} - \mathbf{k}_1, \omega - \omega_1). \tag{26b}$$

It will be convenient for us to solve the equation for $\hat{\Sigma}$; therefore, we express $\hat{G}$ in terms of $\hat{\Sigma}$ by means of (22):

$$G = [\omega + \xi(k) + \Sigma_1(k, -\omega)] / \Omega(k, \omega),$$

$$F(k, \omega) = \Sigma_2(k, \omega) / \Omega(k, \omega),$$

$$\Omega(k, \omega) = [\omega - \xi(k) - \Sigma_1(k, \omega)]$$

$$\times [\omega + \xi(k) + \Sigma_1(k_1 - \omega)] - [\Sigma_2(k, \omega)]^2. \tag{27}$$

We divide $\Sigma_1(k, \omega)$ into an odd $f(k, \omega)$ and an even $\mu_1(k, \omega)$ part relative to ω. Then, by substituting in (26a) the expression for G from (27), we get the equations

$$f(\mathbf{k}, \omega) = \frac{i}{(2\pi)^4} \int d\,\mathbf{k}_1 d\omega_1 \, \frac{\omega_1 - f(\mathbf{k}_1, \omega_1)}{\Omega(\mathbf{k}_1 \omega_1)} D(\mathbf{k} - \mathbf{k}_1, \omega - \omega_1), \quad (28)$$

$$\mu_1(\mathbf{k}, \omega) = \frac{i}{(2\pi)^4} \int d\,\mathbf{k}_1 \, d\omega_1 \, \frac{\xi(\mathbf{k}_1) + \mu_1(\mathbf{k}_1, \omega_1)}{\Omega(\mathbf{k}_1, \omega_1)} \times D(\mathbf{k} - \mathbf{k}_1, \omega - \omega_1). \quad (29)$$

In Eq. (29), we divide the region of integration over $\mathbf{k}_1$ into two parts, with $|\xi(\mathbf{k}_1)| < \xi_1$ and $|\xi(\mathbf{k}_1)| > \xi_1$, respectively, where $\omega_0 \ll \xi_1 \ll E_F$. The integration over the first part vanishes because of the odd nature of the integrand relative to ξ (we can include the μ_1 in ξ under the integral). In the integral over the second part, we neglect Σ in comparison with ξ. We can then complete the integration over ω_1. Then, transforming from integration over the angles to integration over $q = |\mathbf{k} - \mathbf{k}_1|$, and taking it into account that in the important region, $\omega_q \ll |\xi|$, we obtain for μ_1 the expression

$$\mu_1(k, \omega) = -\frac{1}{8\pi^2 k} \int_0^{q_M} q\alpha_q^2 \frac{\omega_q^{(0)}}{\omega_q} \, dq \cdot \mathrm{P} \int \frac{\xi(k_1) k_1}{\xi^2(k_1) - \omega^2} dk_1. \quad (30)$$

For $\omega \ll E_F$ and $k \sim k_0$, the function μ_1 does not depend on k and ω, and represents a correction to the chemical potential

$$\mu = E(k_0) + \mu_1.$$

Before proceeding to solve the equation for f and Σ_2, let us investigate certain analytical properties of the electron Green's function in a superconductor. We shall not undertake a rigorous derivation of these properties, and therefore shall consider for simplicity the Green's function of zero approximation (18). The function $G^{(0)}(k, \omega)$ can be written as

$$G^{(0)}(k, \omega) = (\omega + \xi(k)) / (\omega - \varepsilon(k) + i\delta)(\omega + \varepsilon(k) - i\delta).$$

Simultaneously, we consider the function of complex argument

$$\widetilde{G}^{(0)}(k, z) = (z + \xi(k)) / [z - \varepsilon(k)][z + \varepsilon(k)],$$

which is analytic at all points in the z plane except the parts of the real axis $(-\infty, -\Delta)$ and $(\Delta, +\infty)$, where $\Delta = \epsilon(k_0)$ (Fig. 1). In the interval $(-\Delta, +\Delta)$, we have $\widetilde{G}^{(0)} = G^{(0)}$. For $\omega \leq -\Delta$, the value of $G^{(0)}$ coincides with $\widetilde{G}^{(0)}$ on the lower side of the cut, while for $\omega \geq \Delta$, on the upper side of the cut. The values of $\widetilde{G}^{(0)}$ on the opposite sides of the cuts are complex conjugates. Analytic continuation of $G^{(0)}$ in the upper half plane for $\omega < -\Delta$, and in the lower half plane for $\omega > \Delta$, has poles which determine the single particle spectrum of the system. Here, the path along which the analytic continuation follows must intersect the real axis outside the cut $(-\Delta, \Delta)$. Everything that has been said also applies to the function $F^{(0)}$. The exact function G and F must also possess the general properties that have been enumerated. For $\Delta = 0$, these properties coincide with the analytical properties of the Green's function obtained in reference 8. Thus we can assume that the functions $\widetilde{\Sigma}_1(k, z)$ and $\widetilde{\Sigma}_2(k, z)$ exist and are analytic everywhere except for the parts of the real axis $(-\infty, -\Delta)$ and $(\Delta, +\infty)$ and coincide respectively with $\Sigma_1(k, \omega)$ and $\Sigma_2(k, \omega)$ on the lower side of the cut $(-\infty, -\Delta)$, at the cut of the real axis $(-\Delta, \Delta)$, and on the upper side of the cut $(\Delta, +\infty)$. The values of $\widetilde{\Sigma}_1$ and $\widetilde{\Sigma}_2$ on the upper side of the cut $(-\infty, -\Delta)$ and on the lower side of the cut $(\Delta, +\infty)$ are equal to Σ_1^* and Σ_2^*, respectively.

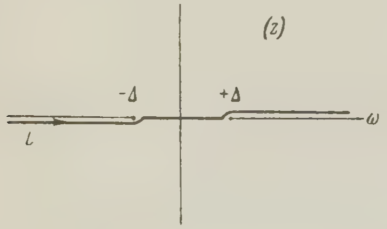

FIG. 1

We shall now employ these properties in the solution of the equations. We transform in (28) from integration over the real axis to integration over the contour L (Fig. 1), replacing the functions of real argument ω by the corresponding analytical functions. Moreover, we transform from integration over k_1 to integration over ξ, $q = |\mathbf{k} - \mathbf{k}_1|$ and φ. Since $k \sim k_0$, and the integral over k_1 converges in the interval $\mathbf{k}_1 \sim \mathbf{k}_0$, then $d\mathbf{k}_1 \approx q\,dq\,k_0^{-1} d\xi\, d\varphi$. As a result, f is shown not to be dependent on k. In what follows, we shall see that Σ_2 also does not depend on k. Therefore, we can write Eq. (28) in the form

$$f(\omega) = -\frac{i}{(2\pi)^3 k_0} \int_0^{q_1} q\alpha_q^2 \frac{\omega_q^{(0)}}{\omega_q} \, dq \int_{-\infty}^{\infty} d\xi \int_L dz \, \frac{z - \widetilde{f}(z)}{\xi^2 - \widetilde{\Omega}_1^2(z)} \times \left(\frac{1}{z - \omega - \omega_q + i\delta_1(q)} - \frac{1}{z - \omega + \omega_q - i\delta_1(q)} \right),$$

where $q_1 = \min(2k_0, q_M)$ and the notation

$$\Omega_1^2(\omega) = [\omega - f(\omega)]^2 - [\Sigma_2(\omega)]^2$$

has been introduced.

The function $[z - \omega - \omega_q + i\delta_1(q)]^{-1}$ is analytic in the upper half plane. Therefore, in the corresponding part of the integral, the contour L can be deformed into the contour L_1. By analogy, in this part of the integral, which contains $[z - \omega + \omega_q - i\delta_1(q)]^{-1}$, the contour L can be deformed into L_2 (Fig. 2). Further, since $[z - f(z)][\xi^2 - \widetilde{\Omega}_1^2(z)]^{-1}$ is an odd function, one can proceed from integration over L_1 to integration over L_2. Finally,

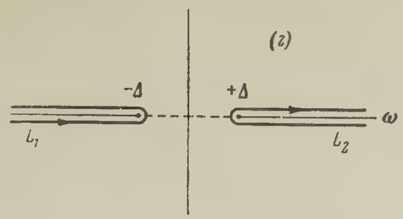

FIG. 2

by carrying out integration over ξ, we arrive at the equation

$$f(\omega) = -\frac{1}{8\pi^2 k_0}\int_0^{q_1} q\alpha_q^2 \frac{\omega_q^{(0)}}{\omega_q}\,dq \int_{L_2} dz\,\frac{z-\widetilde{f}(z)}{\widetilde{\Omega}_1(z)}\,\mathrm{sign}\,\mathrm{Im}\,\{\widetilde{\Omega}_1(z)\}$$
$$\times [1/(z-\omega+\omega_q-i\delta_1(q)) - 1/(z+\omega+\omega_q-i\delta_1(q)].$$

On the upper side of the cut, $\mathrm{Im}\{\Omega_1\} > 0$, and it appears that on the lower side, $\mathrm{Im}\{\Omega_1\} < 0$. Taking this into account, we obtain

$$f(\omega) = -\frac{1}{4\pi^2 k_0}\int_0^{q_1} q\alpha_q^2 \frac{\omega_q^{(0)}}{\omega_q}\,dq \int_\Delta^\infty d\omega_1\,\mathrm{Re}\left\{\frac{\omega_1 - f(\omega_1)}{\Omega_1(\omega_1)}\right\}$$
$$\times\left(\frac{1}{\omega_1-\omega+\omega_q-i\delta_1(q)} - \frac{1}{\omega_1+\omega+\omega_q-i\delta_1(q)}\right).$$

We introduce the function

$$Q(\omega) = \Sigma_2(\omega)/(1 - f(\omega)/\omega).$$

As we shall see, for $\omega = \Delta$, the imaginary part of Q vanishes, while the real part is equal to Δ. For $\omega > \Delta$, we have $\mathrm{Re}\,Q < \Delta$, $\mathrm{Im}\,Q \ll \Delta$. Therefore,

$$\mathrm{Re}\,\{(\omega_1 - f(\omega_1)/\Omega_1(\omega_1)\} \approx \omega_1/\sqrt{\omega_1^2-\Delta^2}.$$

Since $\delta_1(q)/\omega_q \sim \lambda_0\omega_0/E_F$, then

$$\mathrm{Re}\,f(\omega) \equiv f_0(\omega)$$
$$= -\frac{\omega}{2\pi^2 k_0}\int_0^{q_1} q\alpha_q^2\frac{\omega_q^{(0)}}{\omega_q}\,dq\int_0^\infty \frac{d\omega_1}{(\omega_1+\omega_q)^2-\omega^2}. \qquad (31)$$

Here we take it into account that in the integral $\omega_1 \sim \omega_0 \gg \Delta$. For $\omega \ll \omega_0$,

$$f_0(\omega) = -\lambda\omega, \quad \lambda = 2\ln\frac{1-\lambda_0+\lambda_0 q_1^2/8k_0^2}{1-\lambda_0}. \qquad (32)$$

We see that $f_0(\omega)$ coincides with the corresponding part of the characteristic energy of the electrons in the ground state.[1]

In the calculation of the imaginary part of $f(\omega)$, we should, in the limits of the desired accuracy, assume that $\delta_1(q)$ is an infinitely small quantity, since $\delta_1(q) \ll \Delta$. Therefore, for $\omega > 0$ $[f(\omega) = -f(-\omega)]$,

$$\mathrm{Im}\,f(\omega) \equiv f_1(\omega)$$
$$= -\frac{1}{4\pi k_0}\int_0^{q_1} q\alpha_q^2\frac{\omega_q^{(0)}}{\omega_q}\,\frac{\omega-\omega_q}{\sqrt{(\omega-\omega_q)^2-\Delta^2}}\,\theta(\omega-\omega_q-\Delta)\,dq,$$
$$\theta(\omega) = \begin{cases}1 \text{ for } \omega > 0,\\ 0 \text{ for } \omega < 0.\end{cases} \qquad (33)$$

It is therefore evident that $f_1(\omega) = 0$ for $\omega \le \Delta$. For $\alpha \equiv (\omega-\Delta)/\Delta \ll 1$, it is not difficult to obtain the result that

$$f_1(\omega) = -\frac{\pi\lambda_0(2-\lambda_0)}{(1-\lambda_0)^2}\left(\frac{2\Delta}{\omega_0}\right)^2\left(\frac{8}{15}\,\alpha^{5/2} + O[\alpha^{7/2}]\right)\Delta. \qquad (34)$$

For $\omega \gg \Delta$, the quantity f_1 transforms into the imaginary part of the self energy of the normal state:

$$f_1(\omega) = -\frac{\pi\lambda_0(2-\lambda_0)}{6(1-\lambda_0)^2}\left(\frac{\omega}{\omega_0}\right)^3\omega_0, \quad \omega_0 = 2sk_0\sqrt{1-\lambda_0/2}. \qquad (35)$$

Applying the same considerations as in the derivation of the equation for $f(\omega)$, we can get from (26b) and (27) the following equation for $\Sigma_2(\omega)$:

$$\Sigma_2(\omega) = \frac{1}{4\pi^2 k_0}\int_0^{q_1} q\alpha_q^2\frac{\omega_q^{(0)}}{\omega_q}\,dq$$
$$\times\int_\Delta^\infty \mathrm{Re}\left\{\frac{\Sigma_2(\omega_1)}{\Omega_1(\omega_1)}\right\}\left(\frac{1}{\omega_1-\omega+\omega_q-i\delta} + \frac{1}{\omega_1+\omega+\omega_q-i\delta}\right)d\omega_1.$$

Introducing the function $Q(\omega)$ in place of $\Sigma_2(\omega)$, we get

$$Q(\omega) = \frac{1}{4\pi^2 k_0}\left[1 - f(\omega)\frac{1}{\omega}\right]^{-1}\int_0^{q_1} q\alpha_q^2\frac{\omega_q^{(0)}}{\omega_q}\,dq\int_\Delta \mathrm{Re}\left\{\frac{Q(\omega_1)}{\sqrt{\omega_1^2-\Delta^2}}\right\}$$
$$\times\left(\frac{1}{\omega_1-\omega+\omega_q-i\delta} + \frac{1}{\omega_1+\omega+\omega_q-i\delta}\right)d\omega_1. \qquad (36)$$

For $\omega \ll \omega_0$, the quantity $\mathrm{Im}\,f/\omega \ll 1$, and consequently,

$$\mathrm{Re}\,Q(\omega) \equiv C(\omega) = \frac{1}{4\pi^2 k_0}\,\frac{1}{1+\lambda}\int_0^{q_1} q\alpha_q^2\frac{\omega_q^{(0)}}{\omega_q}\,dq\int_0^\infty\frac{C(\omega_1(\xi))}{\sqrt{\xi^2+\Delta^2}}$$
$$\times\left(\frac{1}{\omega_1(\xi)-\omega+\omega_q} + \frac{1}{\omega_1(\xi)+\omega+\omega_q}\right)d\xi. \qquad (37a)$$

The integral is calculated in the sense of the principal value; λ is determined by Eq. (32). We have carried out the substitution $\omega_1 \to \sqrt{\xi^2+\Delta^2}$ under the integral sign.

For $\omega \sim \omega_0$, the imaginary part of $f(\omega)$ is comparable with ω if $\lambda_0 \sim 1$. Therefore, for $\lambda_0 \sim 1$, determination of the spectrum in this region of values of ω no longer makes much sense. For $\omega \gg \omega_0$, we have $f(\omega)/\omega \ll 1$, and therefore

$$C(\omega)=\frac{1}{4\pi^2k_0}\int\limits_0^{q_1} q\alpha_q^2\frac{\omega_q^{(0)}}{\omega_q}\,dq\int\limits_0^{\infty}\frac{C(\omega_1(\xi))}{\sqrt{\xi^2+\Delta^2}}\,\frac{\omega_1(\xi)}{\omega_1^2(\xi)-\omega^2}\,d\xi. \tag{37b}$$

The result for C, obtained by Bogolyubov,[4] can be written in the following fashion:

$$C(\omega)=\frac{1}{2\pi^2k_0}\left[1-\frac{f_0(\omega)}{\omega}\right]^{-1}$$

$$\times\int\limits_0^{q_1} q\alpha_q^2\frac{\omega_q^{(0)}}{\omega_q}\,dq\int\limits_0^{\infty}\frac{C(\omega_1(\xi))}{\sqrt{\xi^2+\Delta^2}}\,\frac{d\xi}{\omega_1(\xi)+\omega+\omega_q}. \tag{38}$$

For $\omega \ll \omega_0$, our result does not differ from (38) and, in particular, the results for the gap Δ coincide. However, the behavior of $C(\omega)$ for $\omega \gtrsim \omega_0$ is different in the two cases. This difference, which does not exist for many problems, is connected with the following. The equation (38) is obtained from the principle of compensation of dangerous diagrams, which are actually dangerous only for $\omega \ll \omega_0$. Our formulas are derived from the Dyson equation, i.e., actually, are the summation of a definite class of diagrams, which exclude all "dangerous" diagrams. Therefore, (36) and (37) describe the behavior of $C(\omega)$ more exactly for large ω than does (38).

The imaginary part of $Q(\omega)$ is equal, for $\omega \ll \omega_0$, to

$$\operatorname{Im} Q(\omega)\equiv C_1(\omega)=\frac{1}{4\pi k_0}\,\frac{1}{1+\lambda}\int\limits_0^{q_1} q\alpha_q^2\frac{\omega_q^{(0)}}{\omega_q}\,\frac{C(\omega-\omega_q)}{\sqrt{(\omega-\omega_q)^2-\Delta^2}}$$

$$\times\,\theta(\omega-\omega_q-\Delta)\,dq+\frac{1}{1+\lambda}\,\frac{f_1(\omega)}{\omega}\,C(\omega).$$

The principal terms of both components for $\alpha = (\omega-\Delta)/\Delta \ll 1$ are proportional to $\alpha^{5/2}$. They differ only in sign and cancel out. For thisis reason $C_1(\omega) \sim \alpha^{7/2}$, for $\alpha \ll 1$, and makes no contribution in practice to the imaginary part of the Green's function. For $\omega \gg \Delta$, the quantity C_1 does not play a role.

The spectrum and the damping of the excitations are determined by the roots of the equation

$$[\omega-f(\omega)]^2-[\xi(k)+\mu_1]-[\Sigma_2(\omega)]^2=0,$$

whence, for $\omega \ll \omega_0$,

$$\omega(k)=\varepsilon(k)-i\gamma(k),\quad \varepsilon(k)=\sqrt{\tilde{\xi}^2(k)+C^2(k)},$$

$$\gamma(k)=-f_1(\varepsilon(k))/(1+\lambda), \tag{39}$$

where $\tilde{\xi} = (\xi + \mu_1)/(1 + \lambda)$ is the renormalized energy of the electron of the normal metal, reckoned from μ.

For $(\epsilon(k) - \Delta)/\Delta \ll 1$,

$$\gamma(k)=\frac{8}{15}\,\frac{\pi\lambda_0(2-\lambda_0)}{(1-\lambda_0)^2}\left(\frac{2\Delta}{\omega_0}\right)^2\left(\frac{\xi(k)}{2\Delta}\right)^5\Delta. \tag{40}$$

In the normal metal, the damping of the excitations in the vicinity of the Fermi surface falls off as ξ^3 for $\xi \gg \omega_0^2/E_F$ and as ξ^2 for $\xi \ll \omega_0^2/E_F$. The much faster decrease of $\gamma(k)$ for $k \to k_0$ is connected with the fact that the important part of the interaction of the electrons with phonons close to the Fermi surface is contained in the zero Hamiltonian.

The author thanks L. É. Gurevich for his numerous valuable suggestions and discussions.

---

[1] A. B. Migdal, JETP **34**, 1438 (1958), Soviet Phys. JETP **7**, 996 (1958).

[2] Bardeen, Cooper, and Schrieffer, Phys. Rev. **108**, 1175 (1957).

[3] N. N. Bogolyubov, JETP **34**, 58 (1958), Soviet Phys. JETP **7**, 51 (1958).

[4] Bogolyubov, Tolmachev, and Shirkov, Новый метод в теории сверхпроводимости (New Method in the Theory of Superconductivity) Acad. Sci. Press Moscow, 1958.

[5] L. P. Gor'kov, JETP **34**, 735 (1958), Soviet Phys. JETP **7**, 505 (1938).

[6] N. N. Bogolyubov, Usp. Fiz. Nauk **67**, 549 (1959), Soviet Phys.-Uspekhi **2**, 236 (1959).

[7] L. D. Landau, JETP **34**, 262 (1958), Soviet Phys. JETP **7**, 182 (1958).

[8] V. M. Galitskiĭ and A. B. Migdal, JETP **34**, 139 (1958), Soviet Phys. JETP **7**, 96 (1958).

Translated by R. T. Beyer
183

SOVIET PHYSICS JETP VOLUME 11, NUMBER 3 SEPTEMBER, 1960

CONTRIBUTION TO THE THEORY OF ABSORPTION OF ULTRASOUND IN METALS

V. P. SILIN

P. N. Lebedev Physics Institute, Academy of Sciences, U.S.S.R.

Submitted to JETP editor October 24, 1959

J. Exptl. Theoret. Phys. (U.S.S.R.) **38**, 977-983 (March, 1960)

The absorption of sound is considered in the low-temperature region, where absorption is due to electrons, and for frequencies sufficiently high so that the acoustic wavelength is small in comparison with the mean free path. The anisotropy of the Fermi surface is taken into account, as are interactions due to the electromagnetic field and to the variation in electron energy as a result of lattice deformations. The acoustic absorption is determined. In the region of wavelengths close to the thickness of the anomalous skin layer at the acoustic frequency, it is shown that a decrease in the ratio of the absorption coefficient to the frequency should be observed with increasing frequency.

1. It is well known that in the low-temperature region the absorption of sound in metals is due to the electrons. Moreover, although it is reasonable to discuss the usual picture of absorption as due to an electronic viscosity in the region where the wavelength $\bar{\lambda}$ is considerably greater than the electron mean free path l, this is not at all true of the opposite case of short waves.

In what follows we consider precisely the latter case. In the limit of sufficiently short waves, the mean free path can be considered infinite. Therefore the processes that occur under such conditions are similar to those in a rarefied electron gas. The damping of sound waves in this case is analogous in nature to the well known damping of plasma waves, first discovered by Landau,[1] and is due to the possibility of the absorption and emission of acoustic waves by electrons moving in phase with the waves. It is plain, therefore, that the consideration of the absorption of sound in the short wavelength region ($\bar{\lambda} \ll l$) should lead to corresponding analogous considerations in an electron gas. This is exactly how the decay of longitudinal sound waves was treated in a paper by the author,[2] in which a linear dependence of the absorption upon frequency was obtained. Pippard[3] developed a method which is also applicable to the case $\bar{\lambda} \ll l$ and gives a description of the absorption of both longitudinal and transverse sound waves.

The limitations of references 2 and 3 are, first, that they refer to electronic models with spherical Fermi surfaces and, secondly, that they do not take into account the variation of the electron energy under the influence of the sound wave.[4] The next step was therefore to consider a theory of sound absorption using a more realistic model. In spite of the fact that such attempts have been made, it must be admitted that at the present time there is not a single theory of sound absorption which is consistent and free from the deficiencies of references 2 and 3.

In our view, the reason for this state of affairs is that up to now the peculiarities of sound absorption in the region of indefinitely long free paths have not been sufficiently realized. Only in this way, for example, is it possible to explain the attempts to calculate sound absorption in this region with the aid of the heat release formula $Q = T\,dS/dt$, where S is the entropy of the electrons. When the mean free paths of the electrons are infinitely long, it is clear that their entropy is conserved, and therefore if the above formula is used correctly in the calculations, nothing can result.

In what follows we shall put forward a theory of sound absorption which, in the first place, does not make use of the rate of change of electron entropy or of collision integrals (which are equal to zero in our case of infinitely long free paths) in determining the absorption; which, in the second place, is valid for any arbitrary Fermi surface having a center of symmetry; and which, thirdly, takes into account not only the electromagnetic field arising from the passage of the sound wave, but also the variation in electron energy as a result of the lattice deformation. Finally, the idea of a complex modulus of elasticity tensor will be introduced, and in Appendix A the rotation of the plane of polarization of sound will be considered from this point of view.

2. Because of the deformation that occurs in a lattice upon the passage of a sound wave, the energy of the electrons is altered:[4]

$$\varepsilon(\mathbf{p}, \mathbf{r}) = \varepsilon(\mathbf{p}) + \Lambda_{ik}(\mathbf{p})\, \partial u_i / \partial x_k. \tag{1}$$

Here $\epsilon(\mathbf{p})$ is the energy of an electron in the absence of the deformation, $\mathbf{u}$ is the deformation vector, and $\Lambda_{ik}(\mathbf{p})$ is a tensor depending on the quasi-momentum of the electron. Using (1), one can write the following kinetic equation for the electrons:

$$\frac{\partial f}{\partial t} + \mathbf{v}\frac{\partial f}{\partial \mathbf{r}} + \left\{ e\left(\mathbf{E} + \frac{1}{c}\, [\mathbf{v}\times\mathbf{H}] \right) - \Lambda_{ik}\, \frac{\partial^2 u_i}{\partial \mathbf{r}\, \partial x_k} \right\} \frac{\partial f}{\partial \mathbf{p}} = 0. \tag{2}$$

Here collisions have been neglected and it has also been assumed that, in addition to the Lorentz forces, there is a force acting on the electrons due to the dependence of the electron energy on the lattice deformation. Furthermore, formula (1) yields for the velocity $\mathbf{v}$

$$\mathbf{v} \equiv \frac{\partial \varepsilon(\mathbf{p}, \mathbf{r})}{\partial \mathbf{p}} = \frac{\partial \varepsilon}{\partial \mathbf{p}} + \frac{\partial \Lambda_{ik}}{\partial \mathbf{p}} \frac{\partial u_i}{\partial x_k}. \tag{3}$$

In order to determine the electromagnetic field we need to know the charge density and current density of the electrons. These are found in the usual form, with the aid of the solutions of (2) and the velocity formula (3):

$$\rho_{\mathrm{e}} = e \int d\mathbf{p} f, \qquad \mathbf{j}_{\mathrm{e}} = e \int d\mathbf{p}\, f \mathbf{v}.$$

We describe the lattice vibrations by the equation

$$\rho_m \ddot{u}_i = \lambda^{(0)}_{ikjl} \frac{\partial^2 u_j}{\partial x_k \partial x_l} + \rho_{\mathrm{p}} E_i + \frac{1}{c} [\mathbf{j}_l \times \mathbf{H}]_i + \frac{\partial}{\partial x_k} \int \Lambda_{ik} f\, d\mathbf{p}. \tag{4}$$

Here ρ_{m} is the density of the material in the lattice, $\lambda^{(0)}_{\mathrm{ijk}l}$ is the modulus of elasticity tensor, and ρ_l and $\mathbf{j}_l = \rho_l \dot{\mathbf{u}}$ are the charge density and current density of the lattice. The final term on the right-hand side of (4) represents the vibration-electron interaction, which appears in (2).

It should be mentioned that the consideration of the electric field, which in itself leads to an interaction between the electrons and the lattice, and also the consideration of the interaction due to the variation of electron energy in the sound-wave field (2), lead to the appearance of an additional elasticity. In other words, the interactions under consideration lead to a renormalization of the elastic-modulus tensor, and consequently to a renormalization of the speed of sound. Thus, in fact, in Eq. (4), $\lambda^{(0)}_{\mathrm{ijk}l}$ must be interpreted as the renormalized elasticity tensor. Note that the appearance of similar renormalizations in the modulus, even when electric interactions alone are considered, is evident from references 2 and 5, in which no elasticity is taken into account except what results from the electrical forces acting between the electrons and the ions. In a model that takes into account an interaction of the type (1), such as Fröhlich's model,[6-8] the occurrence of renormalization in the speed of sound is also well known.

The electromagnetic field is described by Maxwell's equations. For wavelengths large in comparison with the radius of the longitudinal screening field, the equation

$$\rho_{\mathrm{e}} + \rho_l = 0 \tag{5}$$

can be used in place of the equation $\operatorname{div} \mathbf{E} = 4\pi(\rho_{\mathrm{e}} + \rho_l)$. Accordingly, if we neglect the displacement current, we obtain from Maxwell's system of equations

$$\operatorname{curl}\operatorname{curl} \mathbf{E} = -\frac{4\pi}{c^2}\frac{\partial}{\partial t}(\mathbf{j}_{\mathrm{e}} + \mathbf{j}_l). \tag{6}$$

Equations (2), (4), (5), and (6) constitute a system which permits us to describe the sound absorption in which we are interested.

3. The subsequent treatment must be devoted to the elimination of all quantities except the lattice-vibration variables from the above system of equations. For this purpose Eq. (4) can be written as

$$\ddot{u}_i \rho_m = \partial \sigma_{ij} / \partial x_j, \tag{4'}$$

where

$$\sigma_{ij}(\mathbf{r}, t) = \int_{-\infty}^{t} dt' \int d\mathbf{r}\, \hat{\lambda}_{ij\,lm}(t - t', \mathbf{r} - \mathbf{r}')\, \frac{\partial u_l(\mathbf{r}', t)}{\partial x'_m}. \tag{7}$$

The relationship (7) can be considered as a generalization of the usual connection between the stress tensor and the strain to the case of dispersion of the elastic modulus. In treating the propagation and absorption of sound it is convenient to use the quantity

$$\lambda_{ij\,lm}(\omega, \mathbf{k}) = \int d\mathbf{r}\, e^{-i\mathbf{k}\mathbf{r}} \int_0^{\infty} dt\, e^{i\omega t} \hat{\lambda}_{ij\,lm}(t, \mathbf{r}) = \lambda'_{ijlm} + i\lambda''_{ijlm}, \tag{8}$$

which we shall call the complex modulus of elasticity tensor. In the problem of sound absorption in metals, which is treated in this paper, the dispersion of the real part λ' proves to be extremely small, and will not be considered. On the other hand, the dispersion of the imaginary part λ'', both in time and in space, is of considerable importance [see Eq. (16)].

With the aid of (4′) it is easy to show that the energy lost by the sound wave per unit time is given by

$$Q = {}^1\!/_4 i\omega\,(\lambda_{ijlm} - \lambda^*_{lmij})\,k_jk_mu_i^*u_l. \qquad (9)$$

According to Onsager's symmetry relations, we have also

$$k_jk_m\lambda_{ijlm}(\mathbf{H}_0, \omega, \mathbf{k}) = k_jk_m\lambda_{lmij}(-\mathbf{H}_0, \omega, -\mathbf{k}) \qquad (10)$$

(H_0 — constant magnetic field).

In what follows we shall determine the complex modulus of elasticity tensor within the framework of the model outlined in Sec. 2.

4. We take the decrement of the acoustic damping to be small compared with the frequency. In particular, this will enable us to assume a time dependence of the form $\exp(-i\omega t)$ in all equations except (4). If we then assume that there is no constant field, and take the coordinate dependence to be of the form $\exp(-i\mathbf{k}\cdot\mathbf{r})$, we obtain with the aid of (2) the following expression for the nonequilibrium addition to the electron distribution function:

$$\delta f = \frac{\partial f_0}{\partial \varepsilon}\Big(e\frac{\partial \varepsilon}{\partial \mathbf{p}}\,\mathbf{E} + \Lambda_{jl}k_lu_j\mathbf{k}\frac{\partial \varepsilon}{\partial \mathbf{p}}\Big)\Big(\mathrm{P}\,\frac{i}{\mathbf{k}\,\partial\varepsilon/\partial\mathbf{p} - \omega}$$
$$- \pi\delta\,\Big[\mathbf{k}\frac{\partial \varepsilon}{\partial\,\mathbf{p}} - \omega\Big]\Big). \qquad (11)$$

The occurrence of the delta function $\delta_+(\omega - \mathbf{k}\partial\epsilon/\partial\mathbf{p})$ corresponds to adiabatically turning on the interaction an infinite time ago.*

We have at our disposal a parameter of smallness given by the ratio of the speed of sound to the electron velocity at the Fermi surface. If we limit the expansion in terms of this parameter to the most important terms, after substituting (11) into (5) and (6), we obtain equations for the transverse field $\mathbf{E}^\perp$ and the longitudinal field $\mathbf{E}\cdot\mathbf{k}/k$:

$$E^\perp_\alpha = ie\omega B^{-1}_{\alpha\beta}\Big\{u_jk_l\Big\langle\frac{v^\perp_{0\beta}}{\mathbf{k}\mathbf{v}_0}\Big(\Lambda_{jl} - \frac{\langle\Lambda_{il}\rangle}{\langle 1\rangle} - \frac{N\delta_{jl}}{\langle 1\rangle}\Big)\Big\rangle + Nu^\perp_\beta\Big\}, \qquad (12)$$

$$\frac{e\mathbf{k}\mathbf{E}}{k^2} = -\frac{u_jk_l}{\langle 1\rangle}\langle\Lambda_{jl} + N\delta_{jl}\rangle - \frac{e\,\mathbf{E}^\perp}{\langle 1\rangle}\Big\langle\frac{\mathbf{v}^\perp_0}{\mathbf{k}\mathbf{v}_0}\Big\rangle$$
$$- \frac{i\,\pi\omega}{\langle 1\rangle}\Big\langle\,\delta(\mathbf{k}\mathbf{v}_0)\,\Big(\Lambda_{jl} - \frac{\langle\Lambda_{jl}\rangle}{\langle 1\rangle} - \frac{N\delta_{jl}}{\langle 1\rangle}\Big)\Big\rangle u_jk_l. \qquad (13)$$

Here $\mathbf{v}_0$ is the electron velocity, N is the number of electrons per unit of volume, $<\ >$ denotes the mean value calculated according to the formula† $\langle A\rangle = \int d\mathbf{p}\,A\,\partial f_0/\partial\epsilon$, and, finally, the tensor $B_{\alpha\beta}$ is of the form

$$B_{\alpha\beta} = -\pi e^2\langle v^\perp_{0\alpha}v^\perp_{0\beta}\delta(\mathbf{k}\mathbf{v}_0)\rangle - i\,(c^2k^2/4\pi\omega)\,\delta_{\alpha\beta}. \qquad (14)$$

The relationships (11), (12), and (13) enable us to represent Eq. (4) in the form (4′). When this is done,

$$k_mk_l\lambda'_{imjl} = k_mk_l\Big\{\lambda^{(0)}_{imjl} + \langle\Lambda_{im}\Lambda_{jl}\rangle - \frac{1}{\langle 1\rangle}(\langle\Lambda_{im}\rangle$$
$$+ N\delta_{im})\,(\langle\Lambda_{jl}\rangle + N\delta_{jl})\Big\}, \qquad (15)$$

$$k_mk_l\lambda''_{imjl} = \pi\omega\,\langle\delta(\mathbf{k}\mathbf{v}_0)\,L_iL_j\rangle - \omega e^2\Big(\Big\langle\frac{v^\perp_{0\alpha}}{\mathbf{k}\mathbf{v}_0}\,L_i\Big\rangle$$
$$+ \delta_{i\alpha}N\Big)\,\mathrm{Im}\,(iB^{-1}_{\alpha\beta})\Big(\Big\langle\frac{v^\perp_{0\beta}}{\mathbf{k}\mathbf{v}_0}\,L_j\Big\rangle + \delta_{j\beta}N\Big). \qquad (16)$$

The summation with respect to α and β on the right-hand side of (16) is carried out over the components that are perpendicular to the direction of the wave vector $\mathbf{k}$. In addition we introduce the notation

$$L_i = k_m\Big(\Lambda_{im} - \frac{\langle\Lambda_{im}\rangle}{\langle 1\rangle} - \frac{N\delta_{im}}{\langle 1\rangle}\Big).$$

It follows from (15) that the introduction of the interaction between the sound wave and the electrons has led to a renormalization of the elastic modulus. Furthermore, owing to the symmetry of equations (15) and (16) with respect to the indices i and j, the absorption is determined by the expression (16), according to formula (9).

5. We first compare the results achieved so far with some already known.

In the simplest case, where $\Lambda_{ij} = 0$ and $\lambda^{(0)}_{ijkl} = 0$, taking only the electrical forces into account, we have for an isotropic Fermi surface (this corresponds to the results of reference 2)

$$\lambda'_{imjl} = \delta_{im}\delta_{jl}p_0v_0N/3, \qquad \omega^2 = p_0v_0k^2N/3\rho_m,$$

$$q^t = (\pi/2)\,(\omega^2/v_0k).$$

Here p_0 and v_0 are the momentum and velocity of an electron at the Fermi surface, and q^t is the ratio of the energy lost by the wave per unit time to the energy of the wave; the frequency ω is given by $|\,\delta_{il}\rho_m\omega^2 - k_jk_r\lambda'_{ijlr}\,| = 0$, as usual. We also note that in the isotropic case, when $\lambda^{(0)} \neq 0$ and $\Lambda_{ij} = 0$, the renormalization occurs only for the hydrostatic-compression modulus. Hence the velocity of transverse sound is not renormalized.

The case is quite different if the electric field is completely neglected, but the changes in energy due to lattice deformations are considered. In this case we have

$$k_jk_m\,(\lambda' - \lambda^{(0)})_{ijlm} = k_jk_m\,\langle\Lambda_{im}\Lambda_{jl}\rangle,$$

$$k_mk_l\lambda''_{imjl} = \pi\omega\,\langle\delta(\mathbf{k}\mathbf{v}_0)\,\Lambda_{im}\Lambda_{jl}\rangle\,k_mk_l.$$

For the case of the Fröhlich model, considered above, $\Lambda_{ij} = C\delta_{ij}$, and we obtain

---

*In all that follows, $1/\mathbf{k}\cdot\mathbf{v}$ will be understood to mean its principal value.

†Here the process of integration is understood to include also summation over the zones.

$$\delta\lambda'_{imjl}k_m k_l = -3k^2\delta_{lj}(C^2/p_0 v_0)N,$$

$$\delta\omega^2 = -3(C^2/p_0 v_0)(N/\rho_m)k^2,$$

$$q^t = (3\pi/2)(C^2/p_0 v_0)(N/\rho_m)(k/v_0),$$

which corresponds to the results of references 6 – 8.

Let us now consider the frequency dependence of the absorbed energy. To this end, we must first consider the behavior of the tensor $B_{\alpha\beta}$. The real part of the tensor $B_{\alpha\beta}$ has appeared before, in the theory of the anomalous skin effect.[9]* Its order of magnitude is $\mathrm{Re}\, B \sim e^2N/p_0 k$. Hence, for acoustic wavelengths satisfying the condition

$$\lambda \gg \delta \approx [p_0 c/e^2 N\omega]^{1/3}, \qquad (17)$$

the imaginary part of $B_{\alpha\beta}$ can be completely neglected. It should be mentioned that in the inequality (17) δ represents the depth of the skin layer corresponding to the frequency ω in the case of the anomalous skin-effect. What is important is that if condition (17) is fulfilled, both the first term on the right hand side of (16) and the second term, which depends on the transverse field, are of the same order of magnitude, generally speaking. On the other hand, in the region of acoustic wavelengths small compared with the skin depth, for ordinary metals when $\omega/2\pi > 10^9\ \mathrm{sec}^{-1}$, the imaginary part of the tensor $B_{\alpha\beta}$ turns out to be considerably larger than the real part. In this connection, the contribution due to the transverse field turns out to be relatively small, and the second term in (16) can be neglected.

It can thus be stated that in both the regions $\lambda \gg \delta$ and $\lambda \ll \delta$ the sound-absorption coefficient is proportional to the first power of the frequency. However, the ratio q^t/ω, which is a constant for each of these regions, must in general decrease noticeably upon changing from a wavelength greater than the corresponding skin depth to one which is smaller. We note that this picture is nearly the same as the one obtained by Pippard in the isotropic model for the absorption of transverse sound. The essential difference is that in our case the absorption coefficient, generally speaking, does not remain constant when $\lambda \ll \delta$, as it does in Pippard's model. The reason for this is chiefly our allowance for the anisotropy of the Fermi surface.

APPENDIX A

ROTATION OF THE PLANE OF POLARIZATION OF SOUND

Consider a non-absorbing medium. Then, from (9),

$$k_j k_m \lambda_{ijlm} = k_j k_m \overset{*}{\lambda}_{lmij},$$
$$k_j k_m \lambda'_{ijlm} = k_j k_m \lambda'_{lmij},\quad k_j k_m \lambda''_{ijlm} = -\lambda''_{lmij} k_j k_m.$$

For an antisymmetric imaginary part, the expressions can be rewritten in terms of the dual vector $\rho_m k^2 \mathbf{G}$

$$k_j k_r \lambda''_{ijlr} = e_{irl} G_r \rho_m k^2.$$

We choose the coordinate axes along the principal axes of the tensor

$$k_j k_r \lambda'_{ijlr} = \delta_{il}\rho_m \omega_i^2.$$

(On the right hand side of this equation, as well as in the following one, (4″), there is no summation over repeated indices!) Then (4′) takes on the form

$$(\omega^2 - \omega_i^2)u_i + ik^2[\mathbf{u}\times\mathbf{G}]_i = 0. \qquad (4'')$$

It is easy to verify that if all three values of ω_i are quite different from each other, then the changes in the natural frequencies and, consequently, the rotation of the plane of polarization, will be quadratic in **G**. A different picture emerges if two values of ω_i coincide. An isotropic medium is a trivial case. For oscillations in the plane corresponding to the coinciding ω, we have $\omega^2 = \omega_1^2 \pm G_\perp k^2$, where $G_\perp$ is the projection of **G** on the axis perpendicular to the plane of the coinciding principal values. The corresponding angle of rotation per unit length is equal to $\frac{1}{2}(k^3/\omega_1^2)G_\perp$. The most obvious reason for the occurrence of the gyration is the presence of a magnetic field.[10]

Another possible cause of rotation of the plane of polarization of the sound is natural optical activity.* In particular, in optically-active media one would expect a considerable rotation of the plane of polarization of sound (comparable in order of magnitude with the optical rotation), under conditions in which the acoustic wavelength is equal to (or smaller than) the wavelength of a light beam

---

*In the region of wavelength which we are considering, the inequalities $kl \gg 1$ and $kv_0 \gg \omega$, characteristic for the anomalous skin effect in the radio frequency region, are satisfied. In this case the complex dielectric constant of the metal has a spatial dispersion; in other words, it depends not only on the frequency but also on the wave vector. Under these circumstances the longitudinal component of the dielectric-constant tensor is negligibly small in comparison with the transverse components, for which the following expression is valid:

$$\varepsilon_{\alpha\beta} = -(4\pi i/\omega)\,\pi e^2 < v_{0\alpha}^{\perp} v_{0\beta}^{\perp}\delta(\mathbf{k}\mathbf{v}_0) >.$$

From this it is plain that the real part of the tensor $B_{\alpha\beta}$ is none other than the conductivity tensor of the metal, corresponding to the region of anomalous skin effect.

*Attention has already been called to this possibility by V. L. Ginzburg, who has kindly informed me that a study of this question has also been undertaken by A. A. Andronov.

which undergoes a noticeable rotation of the plane of polarization. Such conditions can be realized at frequencies $\omega/2\pi \sim 10^9$ to 10^{10} $\sec^{-1}$.

APPENDIX B

INFLUENCE OF LIQUID EFFECTS

Let us consider what changes would be introduced, by comparison with the results of Sec. 4, by taking into account the fact that the electrons in a metal form a liquid rather than a gas. For this purpose we use Landau's theory of a Fermi liquid.[11] Then instead of Eq. (2) we must use a kinetic equation of the form

$$\frac{\partial \delta f}{\partial t} + \mathbf{v}\frac{\partial}{\partial \mathbf{r}}\left(\delta f - \frac{\partial f_0}{\partial \varepsilon}\,\delta\varepsilon\right) + e\mathbf{E}\frac{\partial f_0}{\partial \mathbf{p}} - \Lambda_{jl}\frac{\partial^2 u_j}{\partial \mathbf{r}\,\partial x_l}\,\frac{\partial f_0}{\partial \mathbf{p}} = 0. \tag{2'}$$

Here $\delta\epsilon(\mathbf{p}, \mathbf{r}) = \int d\mathbf{p}'\,\Phi(\mathbf{p}, \mathbf{p}')\,\delta f(\mathbf{p}', \mathbf{r})$. We also denote by $R(\mathbf{p}, \mathbf{p}')$ the operator which enables the solution of the equation $\delta f - \delta\epsilon\,\partial f_0/\partial\epsilon = A(\mathbf{p})\,\partial f_0/\partial\epsilon$ to be expressed in the form

$$\delta f = (\partial f_0/\partial\varepsilon)\int R(\mathbf{p}, \mathbf{p}')\,A(\mathbf{p}')\,d\mathbf{p}'\partial f_0/\partial\varepsilon'.$$

Because of the fact that $\Phi(\mathbf{p}, \mathbf{p}') = \Phi(\mathbf{p}', \mathbf{p})$, there is also an analogous identity for the operator just introduced: $R(\mathbf{p}, \mathbf{p}') = R(\mathbf{p}', \mathbf{p})$.

Continuing the treatment in a manner analogous to that in Sec. 4, we obtain, instead of (15) and (16)

$$\begin{aligned} k_m k_l(\lambda'_{imjl} - \lambda^{(0)}_{imjl}) = {} & k_m k_l\{\langle\Lambda_{im}(\mathbf{p})\,R(\mathbf{p},\mathbf{p}')\,\Lambda_{jl}(\mathbf{p}')\rangle_2 \\ & - \langle R(\mathbf{p},\mathbf{p}')\rangle_2^{-1}\,(\langle\Lambda_{im}R\rangle_2 + N\delta_{im})\,(\langle\Lambda_{il}R\rangle_2 + N\delta_{jl})\}, \end{aligned} \tag{15'}$$

$$\begin{aligned} k_m k_l\lambda''_{imjl} = {} & \pi\omega\,\langle L_i^R(\mathbf{p})\,R(\mathbf{p},\mathbf{p}')\,\delta(\mathbf{k}\mathbf{v}')\,R(\mathbf{p}',\mathbf{p}'')\,L_j^R(\mathbf{p}'')\rangle_3 \\ & - \omega e^2\left\{\left\langle\frac{v_\alpha^\perp}{\mathbf{k}\mathbf{v}}R(\mathbf{p},\mathbf{p}')\,L_i^R(\mathbf{p}')\right\rangle_2 + \delta_{i\alpha}N\right\}\operatorname{Im}(iB^{-1}_{\alpha\beta}) \\ & \times\left\{\left\langle\frac{v_\beta^\perp}{\mathbf{k}\mathbf{v}}R(\mathbf{p},\mathbf{p}')\,L_j^R(\mathbf{p}')\right\rangle_2 + \delta_{j\beta}N\right\}. \end{aligned} \tag{16'}$$

Here we have used the notation

$$\langle F(\mathbf{p}_1,\ldots,\mathbf{p}_n)\rangle_n = \int d\mathbf{p}_1\ldots d\mathbf{p}_n\frac{\partial f_0}{\partial\varepsilon_1}\cdots\frac{\partial f_0}{\partial\varepsilon_n}F(\mathbf{p}_1,\ldots,\mathbf{p}_n),$$

$$L_j^R = k_l\left\{\Lambda_{jl} - \frac{\langle R\Lambda_{jl}\rangle_2}{\langle R\rangle_2} - \frac{N\delta_{jl}}{\langle R\rangle_2}\right\}.$$

It follows from formulas (15′) and (16′) that in cases where the electron pair correlation characterized by the function $\Phi(\mathbf{p}, \mathbf{p}')$ is not small, the influence of the liquid effects cannot be small either.

In conclusion, I should like to express my gratitude to V. L. Ginzburg for discussing the results of the present work.

---

[1] L. D. Landau, JETP **16**, 574 (1946).

[2] V. P. Silin, JETP **23**, 649 (1952).

[3] A. B. Pippard, Phil. Mag. **46**, 1104 (1955).

[4] A. I. Akhiezer, JETP **8**, 1318 (1938).

[5] D. Bohm and T. Staver, Phys. Rev. **84**, 836 (1951).

[6] H. Fröhlich, Phys. Rev. **79**, 845 (1950).

[7] A. B. Migdal, JETP **34**, 1438 (1958), Soviet Phys. JETP **7**, 996 (1958).

[8] Yu. L. Klimontovich and S. V. Temko, JETP **35**, 1141 (1958), Soviet Phys. JETP **8**, 799 (1959).

[9] M. I. Kaganov and M. Ya. Azbel', Dokl. Akad. Nauk SSSR **102**, 49 (1955).

[10] K. B. Vlasov, Физика металлов и металловедение (Phys. of Metals and Met. Res.) **7**, 447 (1959).

[11] L. D. Landau, JETP **30**, 1058 (1956), Soviet Phys. JETP **3**, 920 (1956). V. P. Silin, JETP **33**, 495 (1957) and **34**, 707 (1958), Soviet Phys. JETP **6**, 387 (1958) and **7**, 486 (1959).

Translated by D. C. West
184

Letters to the Editor

THE MAGNETOELECTRIC EFFECT IN ANTIFERROMAGNETICS

D. N. ASTROV

Institute for Physico-Technical and Radio-Technical Measurements

Submitted to JETP editor December 28, 1959

J. Exptl. Theoret. Phys. (U.S.S.R.) **38**, 984-985 (March, 1960)

LANDAU and Lifshitz[1] showed the possibility of the existence of a linear relationship between the electric and magnetic field in a substance for certain types of magnetic crystal symmetry.

When a crystal of this type is placed in a magnetic (electric) field, an electric (magnetic) moment proportional to the field should appear. Dzyaloshinskiĭ[2] showed that the magnetic symmetry group of Cr_2O_3, whose magnetic structure is well known from neutron-diffraction measurements[3] and from magnetic susceptibility data,[4] admits of the existence of terms proportional to EH in the thermodynamic potential and, consequently, the magnetoelectric effect should occur in Cr_2O_3.

Figure 1 is a schematic drawing of the device used to observe the magnetic moment appearing in a sample 1 of Cr_2O_3 when placed in an alternating electric field established by the electrodes 2. The signal from the astatic pair of measuring coils 3, which arises with the appearance of a magnetic moment, was fed to the input of a measuring amplifier through a balancing transformer. The noise level at the input of the amplifier did not exceed 10^{-7} v. The temperature was measured with a copper-constantan thermocouple 6 and could be controlled with the help of heater 4. Careful electrostatic shielding 5 was used. The measurements took place at a frequency of 10^4 cps. The effective value of the ac field was about 500 v/cm.

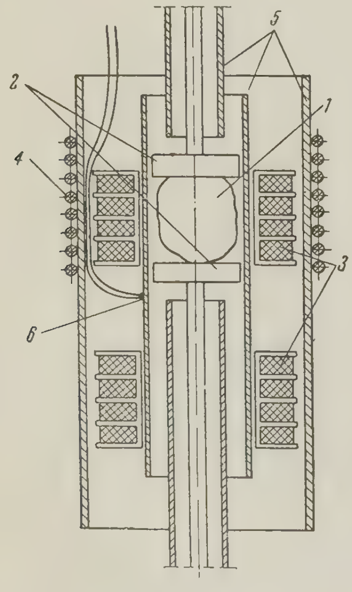

FIG. 1

Figure 2 shows the temperature dependence of the signal at the output of the measurement amplifier for a field intensity of 430 v/cm (curve 1) and 230 v/cm (curve 2). The data was obtained with a single-crystal sample of Cr_2O_3. The sample was kindly provided by the Institute of Physical Problems.* The sample was kept for about 10 minutes at the temperature corresponding to each point. The temperature of the antiferromagnetic transition was found to be 312°K.

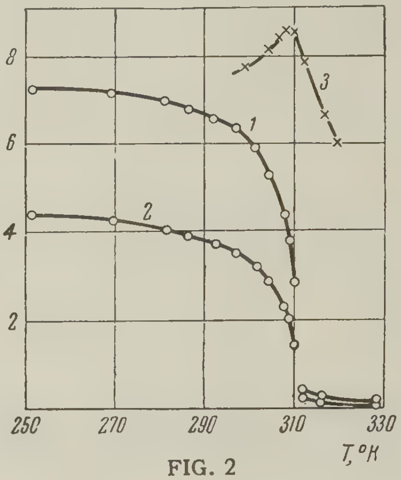

FIG. 2

The absence in the sample of ferromagnetic impurities, which could in the antiferromagnetic ordering lead to a temperature dependence of the measured signal similar to that described by curves 1 and 2, was checked by measuring the magnetic susceptibility of the sample at various temperatures near the transition point. The temperature dependence of the magnetic susceptibility (in relative units) is described by curve 3 and is of a form characteristic for an antiferromagnetic transition. The susceptibility was measured in the same device in an alternating magnetic field with an intensity of 6 oe and at a frequency of 10^4 cps, which was established by a solenoid mounted on the device.

Apparently, curves 1 and 2 should be considered as referring to the temperature dependence of the magnetic moment arising as a result of the magnetoelectric effect. The coefficient of proportionality α between the resultant magnetic moment and the applied electric field which characterizes the extent of the effect (cf. reference 2) was estimated to be 1.2×10^{-5} at a temperature of 0° C.

The sample used had an irregular form and in estimating the coefficient α no correction for the demagnetizing factor was introduced. The large nonuniformity of the applied electric field was also not taken account of.

The author expresses his deep gratitude to Acad. P. L. Kapitza and I. E. Dzyaloshinskiĭ for their interest in the work and for valuable advice, and also to A. S. Borovik-Romanov for a useful discussion of the results.

---

[*] The author expresses his gratitude to A. A. Popova of the Institute of Crystallography of the U.S.S.R. Academy of Sciences for growing the Cr_2O_3 single crystals.

---

[1] L. D. Landau and E. M. Lifshitz, электродинамика сплошных сред (Electrodynamics of Continuous Media) Gostekhizdat, 1957.

[2] I. E. Dzyaloshinskiĭ, JETP **37**, 881 (1959), Soviet Phys. JETP **10**, 628 (1960).

[3] B. N. Brockhouse, J. Chem. Phys. **21**, 961 (1953).

[4] McGuire, Scott, and Grannis, Phys. Rev. **98**, 1562 (1955).

Translated by Z. Barnea
185

ON THE MOMENTUM SPECTRUM OF π^+ MESONS FROM THE REACTION $\pi^+ + p \rightarrow 2\pi^+ + n$

V. A. ASTAF'EV

Institute of Nuclear Physics, Moscow State University

Submitted to JETP editor November 9, 1959

J. Exptl. Theoret. Phys. (U.S.S.R.) **38**, 985-987 (March, 1960)

In the observation of the reaction $\pi^- + \pi^+ + \pi^- + n$ for an incident-meson energy $E_\pi = 1.37$ Bev[1] in the laboratory system, the histogram representing the momentum spectrum of the π^+ and π^- meson was found to have two maxima: broad and low at small values of momentum and narrower and higher at large values of momentum. This was explained by Sternheimer and Lindenbaum[2] by means of the real isobaric nucleon model ($T = J = 3/2$). It should be mentioned that, according to this model, a similar momentum spectrum should also be observed in the reactions $\pi^- + p \rightarrow \pi^- + \pi^0 + p$ and $\pi^+ + p \rightarrow 2\pi^+ + n$. The first of these reactions was studied in reference 1. The shape of the total momentum spectrum in this case is in better agreement with the statistical theory of Fermi, which gives one maximum at medium energies. Disparities with the conclusions of the isobaric theory are also mentioned in reference 3. In this connection, we should draw attention to the formal possibility, existing in theory, of not employing the notion of a real isobaric nucleon.

For simplicity, we consider the reaction $\pi^+ + p \rightarrow 2\pi^+ + n$, which occurs in the isotopic state with total angular momentum $T = 3/2$ and total meson angular momentum $\Lambda = 2$. We denote the momentum of the incident meson in the center-of-mass system by $\mathbf{k}_0$ and the momenta of the emitted mesons by $\mathbf{k}_1$ and $\mathbf{k}_2$. As is known, this reaction is described by the matrix $\langle \mathbf{k}_1, \mathbf{k}_2 | T^{3/2;2} | \mathbf{k}_0 \rangle$, whose elements in the total angular momentum representation are $T^{3/2;2}_{J,lL(l_1,l_2)}(k_1, k_2, k_0)$, where J is the total angular momentum, l is the orbital angular momentum of the incident meson, L is the total and l_1, l_2 the partial orbital angular momenta of the radiated mesons (see references 4 and 5); $L = l \pm 1$, $|l_1 - l_2| \leq L \leq l_1 + l_2$. The probability of observing a π^+ meson in a final state with a momentum of absolute magnitude k is given by the expression

$$w(k) = \frac{v}{2}\int_0^\pi \sin\theta d\theta \left\{ \left(\frac{d\sigma(k_1, k_2, \theta)}{dk_1} \right)_{k_1=k} + \left(\frac{d\sigma(k_1, k_2, \theta)}{dk_2} \right)_{k_2=k} \right\}, \tag{1}$$

where v is the velocity of the incident π meson, and θ the angle between the vectors $\mathbf{k}_1$ and $\mathbf{k}_2$; k_1 is determined from k_2 (and conversely) by the relativistic energy-momentum conservation law.

We shall be interested in the qualitative comparison of the spectra resulting from the individual partial states, i.e., $w_{L(l_1 l_2)}(k)$. We consider part of the matrix of the process under study $T' = \{A + B(\mathbf{k}_1\mathbf{k}_0)^2\}(\sigma\mathbf{k}_0)$. Representing $(\mathbf{k}_1\mathbf{k}_0)^2$ in an expansion in Legendre polynomials, we obtain

$$T' = \left\{ \left(A + \tfrac{1}{3} k_1^2 k_0^2 B \right) P_0(\cos\vartheta_{10}) + \tfrac{2}{3} k_1^2 k_0^2 B P_2(\cos\vartheta_{10}) \right\} (\sigma\mathbf{k}_0).$$

If the coefficient of P_2 is very much less than the coefficient of P_0, then $T' \approx A(\sigma\mathbf{k}_0)$. Applying a similar argument to the matrix as a whole, we find that if

$$|T^{3/2;2}_{J',l'L'(l_1'l_2')}| \ll |T^{3/2;2}_{J,lL(l_1 l_2)}|$$

for $l_1' + l_2' \geq l_1 + l_2 + 2$, and if the matrix does not have singularities, then

$$T^{3/2;2}_{J,lL(l_1l_2)}(k_1, k_2; k_0) \approx N k_1^{l_1} k_2^{l_2} \tau^{3/2;2}_{J,lL(l_1l_2)}(k_0), \qquad (2)$$

where N is a normalizing factor and $\tau(k_0)$ is a function very weakly dependent on k_1, k_2. For energies ~ 1.3 Bev, π mesons with $l \leq 5$ take part in π-N scattering (see the survey article of Gell-Mann and Watson,[6] Fig. 1). This gives 4 and 6 for the maximum $L = l \pm 1$. Taking into account the expenditure of energy on the production of the additional π meson, we thus assume (underestimating somewhat) that the states with $l_1' + l_2' \geq 4$ do not essentially contribute to the matrix element. Then, for energies ~ 1.3 Bev, approximation (2) can be used for the cases in which $l_1 + l_2 \geq 2$.

In the figure are shown the momentum spectra for some partial states and for $E_\pi = 1.37$ Bev, calculated from approximation (2). The normalization makes the area of each curve equal to unity. The spectra corresponding to states with $l_1 = l_2$ have single maxima, and the greater the angular momentum, the sharper the peak. For $l_1 \neq l_2$ the shape of the spectrum changes with increasing $\Delta l = |l_1 - l_2|$, and acquires the character of a double-humped curve.* The total momentum spectrum is formed by the superposition of the partial spectra (with the interference of the partial states taken into account) with weights determined by the specific character of the interaction; the spectrum can take on all intermediate shapes, from a curve with one sharp maximum to a curve with two characteristic maxima. If it is assumed that the weight of the orbital angular momentum is due to one of the mesons, then the total momentum spectrum of the π^+ mesons, for sufficiently large energies, will be represented by a double-humped curve. A similar result can be expected for the total momentum spectra of the π mesons in other reactions mentioned above.

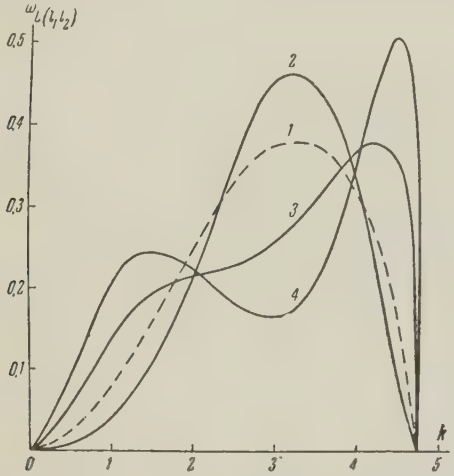

Curve 1 – Statistical theory; Curve 2 – $L(l_1l_2) = 2(11)$; Curve 3 – $L(l_1l_2) = 2(20), 2(02)$; Curve 4 – $L(l_1l_2) = 3(30), 3(03)$.

The author thanks M. A. Markov for helpful advice and A. M. Baldin, A. I. Lebedev, and V. A. Petrun'kin for discussion of the results.

---

*This result may be explained by an extreme simplification of the problem. If the mesons are assumed to be ultra-relativistic and the nucleon is assumed to be at rest, then the law of conservation of energy gives $k_1 + k_2 = \epsilon$, where ϵ is the total energy minus the mass of the nucleon. In this case $w_{L(ll)}(k) \sim k^{2l}(\varepsilon - k)^{2l}\rho(k)$, $w_{L(l0)+L(0l)}(k) \sim [k^{2l} + (\varepsilon - k)^{2l}]\rho(k)$, where $\rho(k)$ is the state density function; $\rho(0) = \rho(\epsilon) = 0$, and $\rho(\epsilon/2) = \rho_{\max}$. For sufficiently large l, the second probability has two maxima.

---

[1] Eisberg, Fowler, Lea, Shephard, Shutt, Thorndike, and Whittemore, Phys. Rev. **97**, 797 (1955).

[2] R. M. Sternheimer and S. J. Lindenbaum, Phys. Rev. **109**, 1723 (1958).

[3] R. C. Whitten and M. M. Block, Phys. Rev. **111**, 1676 (1958).

[4] B. d'Espagnat, Kgl. Danske Videnskab Selskab., Mat-fys Medd. **28**, 11 (1954).

[5] V. A. Astaf'ev, JETP **36**, 98 (1959), Soviet Phys. JETP **9**, 70 (1959).

[6] M. Gell-Mann and K. M. Watson, Annual Review of Nuclear Science **4**, 219 (1954) [Russ. Transl., Usp. Fiz. Nauk **59**, 399 (1956)].

Translated by E. Marquit
186

THEORETICAL INTERPRETATION OF ELASTIC π^--p SCATTERING EXPERIMENTS ON THE PROTON SYNCHROTON OF THE JOINT INSTITUTE FOR NUCLEAR RESEARCH

I. PATERA and Ch. D. PALEV

Moscow State University

Submitted to JETP editor November 16, 1959

J. Exptl. Theoret. Phys. (U.S.S.R.) 38, 987-989 (March, 1960)

EXPERIMENTS on π^--p scattering at high energies are of great interest for the study of nucleon structure. In particular, it is possible from the analysis of such experiments to obtain data on the distribution of nuclear matter in the proton and also the value of the mean square of its radius.[1]

Using the experimental data obtained in Dubna[3] at an energy of 7 Bev, we computed the phase shifts of the elastic scattering by a method described in reference 1. From these we then obtained the absorption coefficient of pions in a proton as a function of the distance from its center, and also the mean square of the "pion" radius of the nucleon. In references 1 and 2 such computations were carried out for energies of 1.3 and 5 Bev.

In the region of small angles we approximated the differential elastic scattering cross section in accordance with the optical law $4\pi\lambda\!\!\!^{-}\,\mathrm{Im}\,F(0) = \sigma_t$ (assuming that $\mathrm{Re}\,F = 0$). The value of the total interaction cross section σ_t was assumed to be (30 ± 5) mb (reference 3). As a result of our computations we obtained

$$\sigma_{in} = \sum_{l=0}^{12} \sigma_{in}(l) = (24.3 \pm 4.2)\ \text{mb},$$

$$\sigma_d = \sum_{l=0}^{12} \sigma_d(l) = (6.6 \pm 1.1)\ \text{mb},$$

which is in good agreement with the experimental data. We have neglected the partial cross sections with $l > 12$. As can be seen in Fig. 1, their relative contributions are sufficiently small.

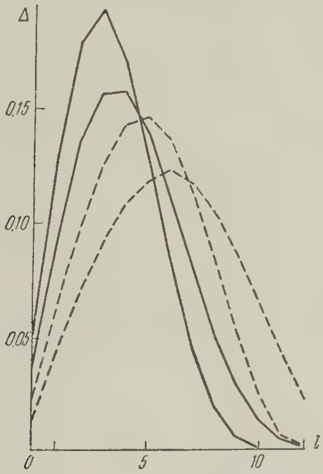

FIG. 1. Relative value of the partial elastic (solid curves) and inelastic (dashed curves) cross sections:

$$\Delta_{in} = \sigma_{in}(l)/\sigma_{in}, \qquad \Delta_d = \sigma_d(l)/\sigma_d.$$

The two curves correspond to the angular distributions with largest and smallest curvature.

Figure 2 shows the dependence of the computed absorption coefficient on the distance from the center of the proton. The curve $K(r)$ is most reliable for intermediate values of r, since for small values it is determined by an approximation of the angular distribution for large angles, and for large values by the optical law and the assumption $\mathrm{Re}\,F = 0$. To make the curve more precise in the extremal regions, measurements of the elastic scattering at small and large angles are needed.

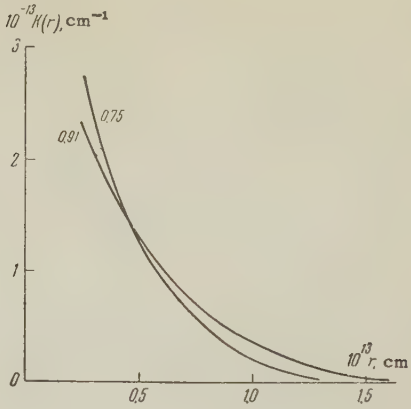

FIG. 2. Absorption coefficient as a function of the distance from the center of the proton. The two curves correspond to the angular distributions with largest and smallest curvatures.

A value of $\sqrt{\langle r^2 \rangle} = (0.83 \pm 0.08) \times 10^{-13}$ cm was obtained for the mean square of the "pion" radius of the proton. This is in good agreement with the value obtained in reference 1 and with the value of the "electromagnetic radius" in reference 4.

A comparison with the curves of references 1 and 2 showed that, within the limits of experimental error, the proton absorption coefficient does not depend on the energy.

It is also important to emphasize that, unlike for high-energy p-p scattering, the experimental data for π^--p scattering can be explained on the assumption of a purely absorbing proton model ($\mathrm{Re}\ F = 0$). For a more precise check of this conclusion measurements of the elastic scattering in the region of small angles, on the order of several degrees, are necessary.

In conclusion, we express our gratitude to V. S. Barashenkov, under whose guidance this work was carried out.

---

[1] Blochincev, Barashenkov, and Grishin, Nuovo cimento **9**, 249 (1958); Blokhintsev, Barashenkov, and Barbashov, Usp. Fiz. Nauk **68**, 417 (1959), Soviet Phys.-Uspekhi **2**, 505 (1960).

[2] Blokhintsev, Barashenkov, and Grishin, JETP **35**, 311 (1958), Soviet Phys. JETP **8**, 215 (1959).

[3] Wang Kang-Ch'ang, M. I. Solov'ev, et al., Материалы Киевской конференции по физике высоких энергий (Proceedings of the Kiev Conference on High-Energy Physics), 1959.

[4] R. Hofstadter, Revs. Modern Phys. **28**, 214 (1956); D. R. Yennie et al., Revs. Modern Phys. **29**, 144 (1957).

[5] Tsyganov, Shafranova, Markov, et al., loc. cit. reference 3.

Translated by Z. Barnea
187

MEASUREMENTS OF THE ENERGY DEPENDENCE OF RADIATIVE NEUTRON CAPTURE IN IRON, SILVER, AND GOLD AT ENERGIES UP TO 30 kev

A. I. ISAKOV, Yu. P. POPOV, and F. L. SHAPIRO

P. N. Lebedev Physics Institute, Academy of Sciences, U.S.S.R.

Submitted to JETP editor November 20, 1959

J. Exptl. Theoret. Phys. (U.S.S.R.) **38**, 989-992 (March, 1960)

A spectrometer employing the neutron slowing-down time in lead[1] was used to measure the energy dependence of the cross section for radiative capture of neutrons in chlorine,[2,3] iron, silver, and gold. The measurement procedure and the reduction of the experimental data were described in detail in reference 2.

1. Iron. The measurements were made on samples of varying thicknesses of Armco iron (type "A", approximately 99.7% iron) and iron oxide (chda). The cross section of the (n, γ) reaction was obtained up to neutron energies of approximately 50 kev (Fig. 1). In the region up to 600 ev, the cross section obeys the 1/v law within 3 to 5%. For the iron level at $E_0 = 1180 \pm 80$ ev, a value $\sigma_0\Gamma_\gamma = 74 \pm 7$ ev-bn was obtained (only the statistical error is indicated). This value is half the preliminary result reported earlier.[3]

Measurements of the area of the resonance peak as a function of $\overline{l}^{-1/2}$, where $\overline{l}$ is the effective thickness of the sample, are presented in Fig. 2. The crosses denote the points used to calculate the preliminary value of $\sigma_0\Gamma_\gamma$. The reason for the deviation of the points is not clear, but numerous subsequent measurements, performed with considerably better statistics, lead us to assume the value indicated above for the strength of the level.

If the peak at $E_0 = 1180$ ev is due to one level, then $\Gamma_\gamma \gtrsim 0.8$ ev regardless of the isotope to which this level is assigned. At the same time, the neutron width Γ_n depends substantially on the spin and the isotope to which this resonance is ascribed (in particular, for s neutrons and Fe^{56}, $\Gamma_n \sim 5 \times 10^{-2}$ ev). This level cannot explain the thermal cross section of the iron.

From the results shown in Fig. 1, it follows that for iron the resonant capture integral $R_\gamma = \int \sigma_\gamma(E)\, dE/E$ should differ little, within the range from 0.49 to 2×10^6 ev, from the value $R_\gamma(1/v) = 1.1 \pm 0.03$ bn, calculated by extrapolating the capture cross section from the thermal region in accordance with the 1/v law, namely $R'_\gamma = R_\gamma - R_\gamma(1/v) = 0.12 \pm 0.02$ bn. The principal contribution, 0.1 ± 0.01 bn, is made to this quantity by the 1180 ev level. The contribution of the levels $E_0 = 7$ to 8 kev amounts to approximately 0.01 bn; all the higher levels make contributions that add up to approximately the same value.* The given value of R'_γ is one order of magnitude less than the value obtained by subtracting $R_\gamma(1/v)$ from the experimental data of references 4 — 6. The reason for the discrepancy remains unclear.

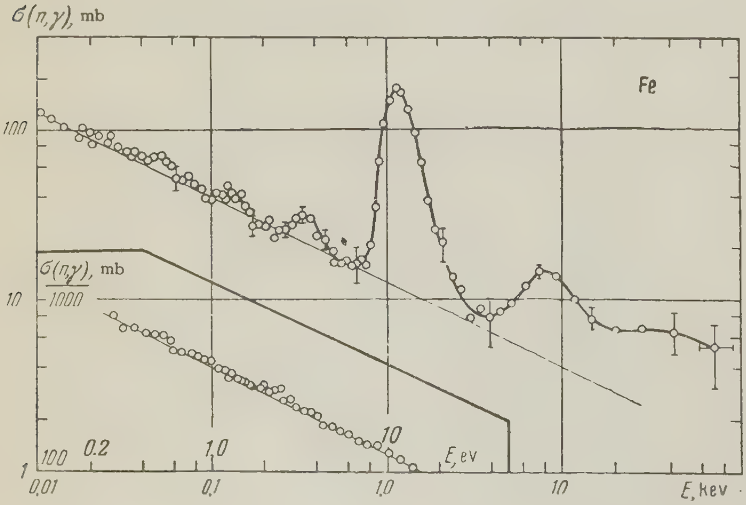

FIG. 1. Energy dependence of the neutron capture cross section in iron. The curve was normalized to the capture cross section $\sigma = 2.53 \pm 0.06$ bn at $E = 0.025$ ev.[8]

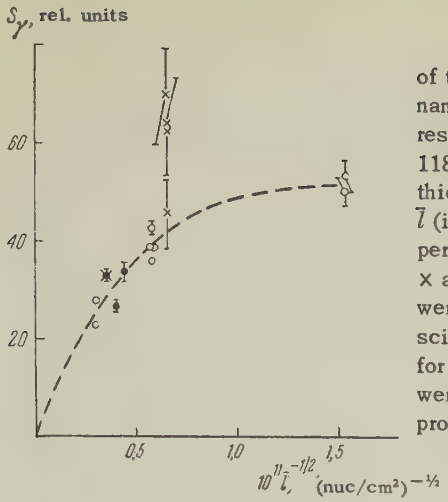

FIG. 2. Dependence of the effective resonance integral for the resonance of iron at 1180 ev on the effective thickness of the specimen $\bar{l}$ (in number of nuclei per cm²). For the points × and ●, the γ rays were registered with a scintillation counter; for the points ○ they were registered with a proportional counter.

On the other hand, the contribution to R'_γ, which we measured in the energy region E > 6 kev, agrees with the value calculated by Goldstein and Kolos[7] on the basis of the parameters of known resonances of iron.

2. Silver and Gold. Measurements of the average cross sections were made with samples of metallic silver (effective thicknesses 0.6 and 0.2 mm) and gold (effective thicknesses 0.6 and 0.2 mm) with the aid of scintillation counters.

Figures 3 and 4 show the energy dependence of the cross sections of the (n, γ) reactions for silver and gold (dark and light circles — measurement data with samples of 0.2 and 0.6 mm effective thickness, respectively). For R < 1 kev, at an effective specimen thickness $\bar{l} \gtrsim 0.2$ mm, the result is influenced by the thickness of the specimen (the well known effect of the blocking of strong resonances).

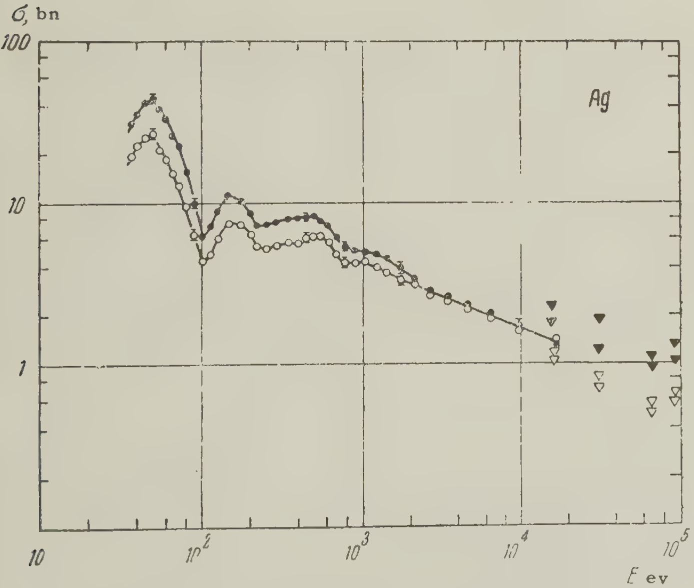

FIG. 3. Energy dependence of the neutron-capture cross section in silver. ∇ – points taken from the first edition of the handbook[8] (1955). ▼ – points taken from the second edition of the handbook[8] (1958).

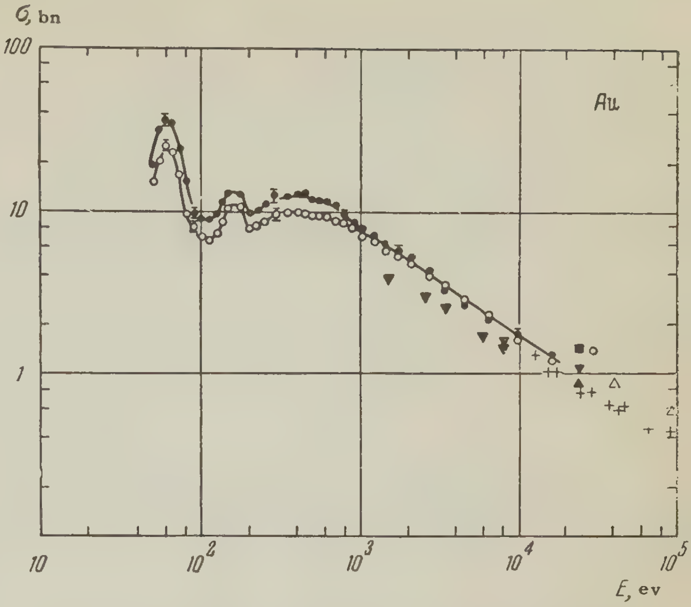

FIG. 4. Energy dependence of the neutron-capture cross section in gold. The points outside the smooth curve were taken from the handbook.[8] The notation of reference 8 was retained.

In the case of silver, the measurements of the average cross sections of the reaction (n, γ) were carried out earlier only for E > 10 kev, but the data given in the first and second editions of the cross-section handbook[8] differ from each other by a factor of 2.

The energy variation of the cross section in the region E ~ 10 kev agrees in the case of gold with other data,[8] but for E ~ 1 kev our results are 30 to 40% higher.

---

*To explain the irregularities in the regions of 50, 130, and 360 ev it is enough to propose the presence of molybdenum (0.03%, based on the number of nuclei), cobalt (0.008%), and manganese (0.05%) impurities. No chemical analysis of the specimens was made. The total contribution of these impurities to R'_γ amounts to approximately 1×10^{-2} bn and is not included in the value of $R'_\gamma = 0.12$ bn.

---

[1] Bergman, Isakov, Murin, Shapiro, Shtranikh, and Kazarnovskiĭ, Paper P-642, Transactions of the Geneva Conference **4**, 166 (1955).

[2] Kashukeev, Popov, and Shapiro, Атомная энергия (Atomic Energy), in press.

[3] Bergman, Isakov, Popov, and Shapiro, JETP **33**, 9 (1957), Soviet Physics JETP **6**, 6 (1958); Ядерные реакции при малых и средних энергиях (Nuclear Reactions at Small and Medium Energies), Academy of Sciences Press, 1958, p. 140.

[4] Spivak, Erozolimskiĭ, Dorofeev, and Lavrenchik, Transactions of the Geneva Conference **5**, 113 (1955).

[5] R. McClean and H. Pomeranz, ibid. **5**, 119 (1955).

[6] V. B. Klimentov and V. M. Gryazev, Атомная энергия (Atomic Energy) 3, 507 (1957).

[7] H. Goldstein and M. Kolos, Transactions of the International Conference on the Interaction Between Neutrons and Nuclei, New York, 1957, p. 30.

[8] D. J. Hughes and R. B. Schwartz, Neutron Cross Sections, 2nd edition BNL, 1958, p. 325.

Translated by J. G. Adashko
188

STRUCTURE OF THE GIANT RESONANCE IN PHOTONUCLEAR REACTIONS

E. V. INOPIN

Physico-Technical Institute, Academy of Sciences, U.S.S.R.

Submitted to JETP editor November 24, 1959

J. Exptl. Theoret. Phys. (U.S.S.R.) 38, 992-994 (March, 1960)

IT was shown in the work of Danos[1] and Okamoto[2] that, in the case of nuclei having the shape of an ellipsoid of revolution, the cross section for photonuclear reactions should have two maxima, rather than one as in the case of spherical nuclei. These authors began from a two-fluid model of the nucleus, which leads to the equation and boundary condition

$$\nabla^2 \Psi + k^2 \Psi = 0, \qquad (\mathbf{n}\,\mathrm{grad}\,\Psi)_S = 0, \qquad (1)$$

where Ψ is the deviation of the proton density from its equilibrium value, k is the wave vector connected with the frequency of vibration ω by the relation $k = \omega/u$ (u is the velocity of "sound" in the nucleus), n is the normal to the surface of the nucleus and S is the surface of the nucleus.

Solution of Eq. (1) in spheroidal functions, and subsequent calculation of eigenvalues k for dipole oscillations, showed that the eigenvalues could be approximately represented by the formula $k_i = 2.08/R_i$, where R_i is the corresponding axis of the ellipsoid. The question arises as to whether this result is still valid in the general case of an ellipsoid with three axes. This is of particular interest in connection with the theory of nonaxially symmetric nuclei, developed by Davydov and his collaborators.[3] In fact, the presence of three maxima in the region of the giant resonance would be the most direct demonstration of the existence of nonaxially symmetric nuclei.

In calculating the eigenvalues we use a variational principle,[4] according to which the eigenvalues of (1) are obtained from the minima of the corresponding functional

$$k^2 = \min \int (\nabla \Psi)^2 \, dV \Big/ \int \Psi^2 \, dV, \qquad (2)$$

where the integration is carried out over the nuclear volume. In so far as (2) possesses a stationary property, we can choose as trial functions the functions Ψ_i^0 which are solutions to (1) for a spherical nucleus of equal volume:

$$\Psi_1^0 = j_1(k_0 r) \cos \vartheta, \qquad \Psi_2^0 = j_1(k_0 r) \sin \vartheta \cos \varphi,$$
$$\Psi_3^0 = j_1(k_0 r) \sin \vartheta \sin \varphi, \qquad (3)$$

where $k_0 = 2.08/R_0$ (R_0 is the radius of the nucleus). Since the values k_0 are three-fold degenerate, then, in general, one should take linear combinations of the functions (3) as trial functions and then vary the coefficients in these linear combinations. However, there is no need for this in our case; the functions (3) are already the correct functions. This is connected with the fact that they transform according to different representations of the symmetry group of the ellipsoid (group D_{2h}).

Substitution of (3) into (2) and calculation of the integrals to within quantities of first order in the deformation of the nucleus leads to the result

$$k_i = \frac{2.08}{R_i}\left(1 + 0.08\,\frac{\Delta R_i}{R_0}\right), \qquad \Delta R_i = R_i - R_0. \qquad (4)$$

Comparison of this formula in the axially symmetrical case with exact calculations of Danos[1] shows that the values of k_i are given, in the worst case, to an accuracy of 1%.

Splitting of the giant resonance into three maxima, as given by (4), appears to be shown in the experiments of Fuller and Weiss[5] in the nucleus Tb^{159} (see the figure), although this has not been noted by them. Approximating the experimental data by the sum of three resonance curves gives

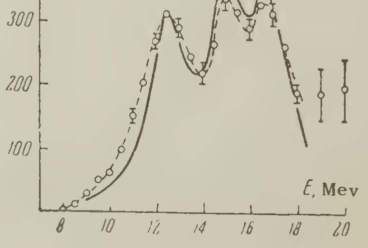

Giant resonance in the (γ, n) reaction in Tb^{159}. The circles show the experimental points, and the dashed curve is drawn through these points. The solid curve represents the sum of three resonance curves within the parameters indicated in the text.

for the resonance energies $E_1 = 16.8$ Mev, $E_2 = 15.0$ Mev, $E_3 = 12.5$ Mev, and for the widths $\Gamma_1 = \Gamma_2 = \Gamma_3 = 1.9$ Mev (it is clear that even better agreement would be obtained if the widths were chosen to be somewhat different). Using these E_i ($E_i = \mathrm{const} \cdot k_i$) in Eq. (4), calculation of the deformation gives $\beta = 0.30$ and $\gamma = 19°$. Calculation of β from $Q_0 = 6.9$ b (Coulomb excitation[6]) gives $\beta = 0.35$ (for $R_0 = r_0 A^{1/3}$ and $r_0 = 1.2 \times 10^{-13}$ cm).[7] The value of γ for Tb^{159} is not given from other sources; however, from the nearby nuclei[8] Gd^{154} and Dy^{160}, $\gamma = 14°$ and 12°, respectively.[8] Thus, the proposed interpretation of the (γ, n) data for Tb^{159} agrees satisfactorily with data obtained from other sources.

In conclusion, I would like to express my deep gratitude to A. K. Val'ter, who brought this problem to my notice, and also to S. P. Kamerdzhiev for help in carrying out the calculations.

---

[1] M. Danos, Nuclear Phys. **5**, 23 (1958).

[2] K. Okamoto, Phys. Rev. **110**, 143 (1958).

[3] A. S. Davydov and G. F. Filippov, JETP **35**, 440 (1958), Soviet Phys. JETP **8**, 303 (1959); Nuclear Phys. **8**, 237 (1958).

[4] P. M. Morse and H. Feshbach, *Methods of Theoretical Physics*, Part II, New York-Toronto-London, 1953.

[5] E. G. Fuller and M. S. Weiss, Phys. Rev. **112**, 560 (1958).

[6] Alder, Bohr, Huus, Mottelson, and Winther, Revs. Modern Phys. **28**, 432 (1956).

[7] R. Hofstadter, Amer. Rev. Nuclear Sci. **7**, 231 (1957).

[8] A. S. Davydov, Izv. Akad. Nauk SSSR, Ser. Fiz. **23**, 792 (1959), Columbia Tech. Transl., in press.

Translated by G. E. Brown
189

ANGULAR DISTRIBUTION OF Na^{24} *NUCLEI AND FISSION FRAGMENTS PRODUCED BY INTERACTIONS BETWEEN HIGH-ENERGY PROTONS AND* Au *AND* U *NUCLEI*

A. K. LAVRUKHINA, L. P. MOSKALEVA,
V. A. MALYSHEV, L. M. SATAROVA, and
SU HUNG-KUEI

Institute of Geochemistry and Analytical Chemistry, Academy of Sciences, U.S.S.R.

Submitted to JETP editor December, 1959

J. Exptl. Theoret. Phys. (U.S.S.R.) **38**, 994-995 (March, 1960)

IN this communication we present the preliminary results on the angular distribution of Na^{24} nuclei and the fission fragments Sr^{91}, Br^{76}, I^{131}, $I^{130+133}$ from gold and uranium irradiated by 660-Mev protons. The experiment was carried out with the synchrocyclotron of the Joint Institute of Nuclear Studies. Sheets of metallic beryllium 50 μ thick were used as absorbing foils. The proton beam was monitored by the reaction $Al^{27}(p, 3pn)Na^{24}$. After irradiation, the beryllium sheets were dissolved in acid containing isotopic carriers of the produced elements, after which the elements were separated chemically and purified. The apparatus for measuring the activity and identifying the isotopes consisted of twin end-window counters of type T-25-BFL working in anti-coincidence with a ring of MS-9 counters to reduce the background. The geometric efficiency was about 70%.

Two series of experiments were made to determine the "forward-backward" ratio and to study the angular distribution from 0 to 180° in angular intervals of 30°.

1. An investigation of the "forward-backward" ratio was carried out for the isotopes Na, Sr, Br, and I emitted from plates of metallic uranium of size 20 × 15 × 1 mm. A second beryllium foil was placed as a shield between the aluminum foil-monitor and the absorbing sheet of beryllium. It was found that, in the laboratory system, the "forward-backward" ratio for the fission fragments Sr^{91} was 1.1; for Br^{76}, 1.0; for I^{131}, 0.6; for $I^{130+133}$, 1.0. The error in determining the ratio did not exceed 20%.

The calculation of the "forward-backward" ratio for Na^{24} was made more complicated by the presence of an impurity due to silicon in the beryllium sheets (1%). In order to introduce a correction for the production of Na^{24} from the silicon, a control experiment was made, in which the beryllium sheets were irradiated with 660-Mev protons, and the sodium was subsequently separated. Such an experiment made it possible to introduce a correction for Na^{24} produced from silicon in the "forward-backward" experiments. In making the comparison with the control experiments, all the variable factors were taken into account: a) proton stream, b) chemical yields, c) weight of the beryllium sheets, d) time of irradiation and time between the end of the irradiation and the beginning of the counting, e) isotopic composition. After the introducing of these corrections, it was found that in the rear beryllium sheet (with respect to the direction of the proton beam) the entire activity was due to the admixture of silicon, and in the front sheet the activity produced by the reaction on silicon $Si^{28}(p, 4pn)N^{24}$ constituted only 20% of the total Na^{24} activity. Hence the major part of all Na^{24} nuclei produced from uranium is emitted in the forward direction.

2. An investigation of the angular distribution from 0 to 180° in angular intervals of 30° was carried out for Na^{24} and Sr^{91} nuclei emitted from a gold thread $300\,\mu$ in diameter (see reference 1 for the experimental arrangement). The angular distribution obtained for S^{91} was isotropic within the limits of error. The small anisotropy in the angular distribution of fission fragments observed by other authors[2,3] was not observed in the present work.

In view of the difficulty in making a correction for the admixture of silicon in the experiments on the angular distribution, the results for Na^{24} cannot be considered conclusive; nevertheless, there was an appreciable sharp asymmetry in the forward direction. After introducing the correction for the admixture of silicon, we observed that the activity of Na^{24} due to nuclei emitted from the gold thread are distributed in the angular intervals $0-30°$, $30-60°$ as follows: If the activity of Na^{24} in the interval $0-30°$ is taken as unity, then the Na^{24} activity in the interval $30-60°$ is 0.4. The major part of the Na^{24} activity in the angular intervals $60-90°$, $90-120°$, $120-150°$, $150-180°$ is apparently due only to the admixture of silicon.

Comparison of the data obtained for the angular distribution of Na^{24} nuclei and the fission fragments Sr^{91}, Br^{76}, I^{131}, and $I^{130+133}$ indicates that the greater part of the Na^{24} nuclei are apparently not produced in the fission process, which is contrary to the previous assumptions.[4] The Na^{24} nuclei apparently cannot be produced in an evaporation process, since in this case their angular distribution should be close to isotropic.

At present, the investigation of the angular distribution is being continued. Materials not containing admixtures of heavy elements are being used as absorbing foils, which will make it possible to obtain more accurate data.

---

[1] Borisova, Kuznetsova, Kurchatova, Mekhedov, and Chistyakov, JETP **37**, 366 (1959), Soviet Phys. JETP **10**, 261 (1960).

[2] Lozhkin, Perfilov, and Shamov, JETP **29**, 292 (1955), Soviet Phys. JETP **2**, 116 (1956).

[3] J. W. Meadows, Phys. Rev. **110**, 1109 (1958).

[4] Lavrukhina, Moskaleva, Krasavina, and Grechishcheva, Атомная энергия (Atomic Energy) **3**, 285 (1957).

Translated by E. Marquit
190

SCATTERING AND RADIATIVE CAPTURE OF Λ PARTICLES

A. M. KOL'CHUZHKIN and N. N. KOLESNIKOV

Moscow State University

Submitted to JETP editor December 18, 1959

J. Exptl. Theoret. Phys. (U.S.S.R.) **38**, 996-997 (March, 1960)

In the interaction of low energy Λ particles with even-even nuclei, the spin, noncentral, and spin-orbit forces do not come into play. This permits us to estimate the magnitude of the scattering cross section for slow Λ particles in a simple fashion, provided that we know the parameters of the central spin-independent part of the Λ-N interaction, which is weaker and has smaller range than the N-N forces.[1,2] Regarding the range of the Λ-N forces as small in comparison with the radius of the nucleus and neglecting the deformation of the core,[2] we can write the potential of the interaction of the Λ particle with the nucleus in the form

$$V(r) = \int \rho(r_1) V_{\Lambda N}(r_{12})\, dv_1 \approx \rho(r) C_{\Lambda N} (1 + R_2^2 / R^2(r)),$$

$$R_2^2 = C_{\Lambda N}^{-1} \int V_{\Lambda N}(r_{12})\, r_{12}^2 dv_{12},$$

$$R^2 = \rho^{-1}(r) \left\{ \frac{1}{2} \frac{d^2\rho(r)}{dr^2} + \frac{2}{3r^2} \frac{d\rho(r)}{dr} \right\},$$

$$\mathbf{r}_1 = \mathbf{r} + \mathbf{r}_{12}, \qquad C_{\Lambda N} = \int V_{\Lambda N}(r_{12})\, dv_{12}, \tag{1}$$

where $\rho(\mathrm{r})$ is the nucleon density in the nucleus, $V_{\Lambda N}$ is the potential of the Λ-N interaction, $\mathbf{r}$ is the distance of the Λ particle from the center of the nucleus, while $C_{\Lambda N}$ characterizes the strength and R_2 the range of the Λ-N interaction.

The de Broglie wavelength of Λ particles with energies of the order of a few Mev is considerably greater than the range of the potential well (1). Therefore, only S wave scattering is important, and we can use the approximation which is independent of the form of the potential between the Λ particle and the nucleus. In this approximation the phase shift δ is related to the scattering length a and the range of interaction r_0 by the well known equation[3,4]

$$k \cot \delta = -1/a + r_0 k^2/2, \tag{2}$$

where $k = \sqrt{2ME}/\hbar$, and M is the reduced mass; the cross section is

$$\sigma(k^2) = 4\pi / [k^2 + (r_0 k^2/2 - 1/a)^2]. \tag{3}$$

Since the numerical values of the parameter R_2 are not yet known exactly, we restrict ourselves in the numerical calculations to the case where the range of the Λ-N forces is zero. In this case we have for the nucleus He_2^4

$$B_\Lambda \approx 2.9\,\text{Mev}, \qquad C_{\Lambda N} \approx 180\,\text{Mev.}\,f^3$$

Furthermore, according to the electron scattering experiments,[6]

$$\rho(r) = \rho_0 \exp(-r^2/b^2),$$

where the parameter b, which also incorporates the proton radius, is equal to 1.14 f. The numerical solution gives in this case a = 2.57 f, r_0 = 1.04 f. The scattering cross section at zero energy is $\sigma(0) = 0.8$ b.

We should like to emphasize that it is possible, in principle, to determine the parameters $C_{\Lambda N}$ and R_2 more exactly from the experimental cross sections for the scattering of Λ particles by nuclei. Up to the present time, however, only very preliminary results on the scattering of Λ particles with energies of 75 to 150 Mev in hydrogen[7] have been published (see also reference 8).

Besides the elastic scattering, the radiative capture of Λ particles may play an important role in the region of small energies. If we restrict ourselves to Λ particles of extremely low energy, we may assume that the capture leads only from an S state of the continuous spectrum to an S state of the hypernucleus. The parities of the initial and final states are identical, so that this capture process may be accompanied by the emission of a magnetic dipole γ quantum. The cross section for capture with emission of magnetic dipole radiation with frequency ω is given by the formula[3]

$$\sigma_{\Lambda\gamma} = \frac{16\pi}{9}\left(\frac{\omega}{c}\right)^3 \frac{M}{\hbar^2 k} \sum_m |\mathfrak{M}'_{1m}|^2, \tag{4}$$

where

$$\mathfrak{M}'_{1m} = \frac{e\hbar}{2M_p c}\,\frac{M_p}{M_\Lambda}\sqrt{\frac{3}{4\pi}}\,\mu_\Lambda \sum \int (\overset{*}{\varphi}_b \sigma \varphi_a) \nabla\, r_{(m)},\, d\tau$$

$$r_{(0)} = z, \qquad r_{(\pm 1)} = (x \pm iy)/\sqrt{2}, \tag{5}$$

μ_Λ is the magnetic moment of the Λ particle in nuclear magnetons, and M_p and M_Λ are the mass of the proton and of the Λ particle, respectively; φ_b and φ_a are the wave functions of the final (b) and initial (a) states; $\hbar\omega = E_a - E_b$; the summation goes over the spins of the final state. Assuming zero range of the interaction between the Λ particle and the nucleus, we can write φ_a and φ_b in the form

$$\varphi_a = \chi_a \sin(kr + \delta)/kr, \qquad \varphi_b = \sqrt{2\beta/4\pi}\, e^{-\beta r} \chi_b, \tag{6}$$

where $\beta = \sqrt{2MB_\Lambda}/\hbar$, and χ_a and χ_b are the spinor functions of the initial and final states. From (4) – (6) follows

$$\sigma_{\Lambda\gamma} = \pi\alpha \left(\frac{\hbar}{M_p c}\right)^4 \left(\frac{M_p}{M}\right)^2 \mu_\Lambda^2\, \frac{k^2+\beta^2}{k}\, \frac{(\beta a - 1)^2 \beta}{a^2 k^2 + 1}, \tag{7}$$

where $\alpha = e^2/\hbar c$. In the region of extremely small energies the ratio of $\sigma_{\Lambda\gamma}$ and the corresponding cross section for the radiative capture of neutrons by protons is

$$\frac{\sigma_{\Lambda\gamma}}{\sigma_{n\gamma}} \sim \left(\frac{M_\Lambda}{M_n - M_p}\right)^2 \cdot 10^{-2}$$

and $\sigma_{\Lambda\gamma}$ is of the order of 10^{-7} b at energies of ~ 20 Mev. Despite the fact that the capture cross section of Λ particles can reach large values in the region of very low energies, there will be practically no capture of Λ particles because of their short lifetime. (The ratio of the capture and decay probabilities for Λ particles is ~ 10^{-7} to 10^{-9}.) However, it could well be that radiative capture is to be observed for heavier nuclei.

---

[1] D. D. Ivanenko and N. N. Kolesnikov, JETP **30**, 800 (1956), Soviet Phys. JETP **3**, 955 (1959).

[2] R. H. Dalitz and B. W. Downs, Phys. Rev. **111**, 967 (1958).

[3] A. S. Davydov, Теория атомного ядра (Theory of the Atomic Nucleus) Fizmatgiz, M. (1958). J. Blatt and V. Weisskopf, Theoretical Nuclear Physics, J. Wiley and Sons, N. Y. (1952).

[4] J. M. Blatt and J. D. Jackson, Phys. Rev. **76**, 18 (1949).

[5] L. M. Brown and M. Peshkin, Phys. Rev. **107**, 272 (1957).

[6] R. Hofstadter, Revs. Modern Phys. **28**, 214 (1956).

[7] Crawford et al., Phys. Rev. Lett. **2**, 174 (1959).

[8] J. S. Kovacs and D. B. Lichtenberg, Nuovo cimento **13**, 371 (1959); C. G. Gardner and T. A. Welton, Phys. Rev. Lett. **3**, 281 (1959).

Translated by R. Lipperheide
191

COMPARISON OF THE PROBABILITIES OF THE TRIPLE FISSION OF U^{233}, U^{235}, *AND* Pu^{239}

V. N. DMITRIEV, L. V. DRAPCHINSKIĬ, K. A. PETRZHAK, and Yu. F. ROMANOV

Radium Institute, Academy of Sciences, U.S.S.R.

Submitted to JETP editor October 26, 1950

J. Exptl. Theoret. Phys. (U.S.S.R.) **38**, 998-999 (March, 1960)

RECENTLY there has been a considerable increase in the interest in nuclear fission accompanied by the emission of long-range α particles. A study of this phenomenon yields more information on the fission mechanism, since the emission of the α particle is connected with the initial stage of the process and characterizes the state of the nucleus during the instant of fission.

One of the most important characteristics of nuclear fission with emission of long-range particles is the probability of the given process relative to the fission into two fragments. The determination of the probability of triple fission of U^{235} induced by slow neutrons has been the subject of many investigations,[1-9] but U^{233} and Pu^{239} have not been sufficiently investigated in this respect. Thus, data on the relative probabilities of triple fission of Pu^{239} and U^{235}, determined by Farewell et al.[4] and Allen and Dewan,[6] do not agree with each other — whereas it follows from reference 4 that the probability of triple fission of Pu^{235} is half that of U^{235}, reference 6 yields a probability that is 1.14 times greater. It is therefore interesting to obtain more exact values for the relative probabilities of triple fission of U^{233}, U^{235}, and Pu^{239}, induced by slow neutrons.

We used for this purpose a setup intended for the investigation of the energy distribution of triple-fission fragments.[10] The triple fissions were identified by the coincidences of the pulses from the fragment chamber and from the α-particle chamber. The fraction of registered triple fissions depended on the solid angle of the α chamber relative to the target of the fissioning substances, on the argon pressure in the chamber, and on the degree of pulse discrimination in the α channel. Under the condition of the present experiment, a calculation of this fraction is subject to great errors, and therefore the determination of the absolute probabilities of triple fission does not seem advisable. The apparatus used can measure, with great accuracy, the ratios of probabilities of triple fission of different nuclei. The geometry of the chamber and the chosen argon pressure resulted in maximum pulses from the α particles with the most probable energies. It is known that the energy spectra of long-range α particles, emitted upon fission of the investigated nuclei, are nearly equal.[6] The measurement conditions in experiments with different nuclei remained unchanged. Consequently, the sought ratio of probabilities of triple fission of nuclei 1 and 2 is

$$\eta_1 / \eta_2 = (N_{\mathrm{tr}} / N_{\mathrm{d}})_1 / (N_{\mathrm{tr}} / N_{\mathrm{d}})_2,$$

where N_{tr} is the number of triple fissions and N_d is the number of double fissions registered per unit time.

The targets were irradiated with slow neutrons in the experimental reactor of the U.S.S.R. Academy of Sciences. The measurement results are listed in the table, and the background of random coincidences, which amounted to 3% of N_{tr}, was taken into account. The statistical errors are indicated.

Nucleus	N_{tr}, pulse/min	N_d, pulse/min
U^{233}	7.45 ± 0.15	28600 ± 140
U^{235}	8.86 ± 0.18	41600 ± 200
Pu^{239}	18.53 ± 0.37	74000 ± 400

The resultant data were used to determine the ratios of triple-fission probabilities:

$$\eta(U^{233}) / \eta(U^{235}) = 1.22 \pm 0.06,$$

$$\eta(Pu^{239}) / \eta(U^{235}) = 1.18 \pm 0.06.$$

According to the results of Allen and Dewan,[6] these values are 1.25 ± 0.22 and 1.14 ± 0.23 respectively.

Thus, the probability ratios obtained in the present work agree with those calculated from the data of Allen and Dewan. The use of the method of relative measurements ensured a higher accuracy of the results.

---

[1] Tsien, Ho, Chastel, and Vigneron, J. phys. radium 8, 165, 200 (1947).

[2] L. L. Green and D. L. Livesey, Nature, No. 4036, 332 (1947).

[3] L. L. Green and D. L. Livesey, Phil. Trans. **241**, 323 (1948).

[4] Farewell, Segré, and Wiegand, Phys. Rev. **71**, 327 (1947).

[5] L. Marshall, Phys. Rev. **75**, 1339 (1949).

[6] K. W. Allen and J. T. Dewan, Phys. Rev. **80**, 181 (1950).

[7] E. W. Titterton, Nature **168**, 590 (1951).

[8] D. Hill, Phys. Rev. **87**, 1049 (1952).

[9] C. B. Fulmer and B. L. Cohen, Phys. Rev. **108**, 370 (1957).

[10] Dmitriev, Drapchinskiĭ, Petrzhak, and Romanov, Dokl. Akad. Nauk SSSR **127**, 531 (1959), Soviet Phys.-Doklady **4**, 823 (1960).

Translated by J. G. Adashko
192

LONGITUDINAL RELAXATION OF NUCLEAR SPINS IN A PARAMAGNETIC CRYSTAL AT VERY LOW TEMPERATURES

B. I. KOCHELAEV

Kazan' State University

Submitted to JETP editor December 11, 1959

J. Exptl. Theoret. Phys. (U.S.S.R.) **38**, 999-1000 (March, 1960)

IT is well known that at sufficiently low temperatures, the specific heat associated with the lattice of a paramagnetic crystal becomes negligible compared with the specific heat of spin systems. In this case, the spin system of paramagnetic atoms will be the thermostat determining the equilibrium population distribution among nuclear spin levels, and the longitudinal nuclear relaxation time T_1 will be the time required to establish thermodynamic equilibrium between the electronic and nuclear spin systems. It is the purpose of this note to describe some calculations of this time.

At low temperatures, the energy levels of most paramagnetic atoms in an external magnetic field can be described by an effective spin $S = \frac{1}{2}$ with an anisotropic g factor, i.e., with the magnetic moment of an atom being given by $\mu = \beta \mathbf{g} \mathbf{S}$, where $\mathbf{g}$ is a tensor of the second rank and β is the Bohr magneton. We assume that the electric field inside the crystal has axial symmetry and that the Zeeman energy is much greater than either kT or the mean interaction energy of magnetic dipoles. In this case Bogolyubov's approximate method for second quantization can be used to find the energy spectrum of the interacting electron spins. This spectrum turns out to be equivalent to the spectrum of a system of non-interacting Bose particles with Hamiltonian

$$\mathcal{H} = E_0 + \sum_{\mathbf{k}} E_{\mathbf{k}} N_{\mathbf{k}}, \quad N_{\mathbf{k}} = b_{\mathbf{k}}^{+} b_{\mathbf{k}},$$

$$E_0 = g_{\parallel} \beta H N, \quad E_{\mathbf{k}} \approx \frac{10\pi}{a} g_{\perp}^2 \beta^2 (k^2 - 3k_z^2), \tag{1}$$

where $b_{\mathbf{k}}^{+}$, $b_{\mathbf{k}}$ are creation and destruction operators for Bose particles with wave vector $\mathbf{k}$, N is the number of paramagnetic atoms, a is the shortest distance between them and $g_{\parallel}$, $g_{\perp}$ are the principal values of the tensor $\mathbf{g}$. In our calculations we used the fact that to find the spectrum of a spin system in a strong magnetic field it is only necessary to consider the diagonal and semi-diagonal parts of the operator for the dipole-dipole interaction.[2] It was also assumed that the paramagnetic atoms were arranged in a simple cubic lattice, that the magnetic field $\mathbf{H}$ is directed along the symmetry axis of the crystal field, and the lattice sums can be approximated by integrals.

Suppose the nuclear spins are coupled to the paramagnetic atoms only through the dipole-dipole interaction. We shall find the probability of a transition in which one boson is created, another destroyed, the energy difference between them being equal to the energy required to re-orient a nuclear spin in the external field, $E_{\mathbf{k}_1} - E_{\mathbf{k}_2} = 2 g_N \beta_N H$ (where g_N is the nuclear magnetic moment in nuclear magnetons β_N). Assuming that $2 g_N \beta_N H \ll \beta^2 g_{\perp}^2 / a^3$ and using the standard formulas of perturbation theory, we find that the probability of a transition is

$$P(m+1, m) = \frac{9}{20\pi^2 \hbar} \left(\frac{g_{\parallel}}{g_{\perp}}\right)^2 g_N^2 \beta_N^2 \frac{a^3}{r^6} \sin^2 2\theta$$

$$\times \exp\left(\frac{2 g_{\parallel} \beta H}{kT}\right) (I + m + 1)(I - m), \tag{2}$$

where $\mathbf{r}$ is the radius vector from a paramagnetic atom to a nuclear spin $\mathbf{I}$; θ is the angle between the direction of the magnetic field and $\mathbf{r}$, and m is the magnetic quantum number of the nucleus.

Experimentally, the method of a saturated nuclear magnetic resonance has been used to measure a nuclear spin relaxation time in a paramagnetic crystal. The measurement was made on the protons in the water of crystallization of $Ce_2Mg_3(NO_3)_{12} \cdot 24H_2O$ at 0.086°K.[3] It was impossible to achieve saturation, and only an upper bound on the relaxation time was obtained: $T_1 < 32$ sec. A rough estimate using formula (2) yields $T_1 \approx 10^{-1}$ sec. The estimate is rough because $g_{||} = 0.25$ for the Ce^{3+} ion[4] and the condition $2g_{||}\beta H \gg kT$ is poorly fulfilled. This result does not contradict the experimental one.

The author would like to thank S. A. Al'tshuler for discussion of his results.

---

[1] N. N. Bogolyubov, Лекции по квантовой статистике (Lectures on Quantum Statistics) Kiev, 1949.

[2] J. H. Van Vleck, Phys. Rev. **74**, 1168 (1948).

[3] Estle, Hart, and Wheatley, Phys. Rev. **112**, 1576 (1958).

[4] K. D. Bowers and J. Owen, Reports on Progress in Physics **18**, 304 (1955).

Translated by R. Krotkov
193

SEMICONDUCTOR AMPLIFIERS AND GENERATORS WITH CARRIERS HAVING NEGATIVE EFFECTIVE MASS

N. G. BASOV, O. N. KROKHIN, and Yu. M. POPOV

P. N. Lebedev Physics Institute, Academy of Sciences, U.S.S.R.

Submitted to JETP editor December 17, 1959

J. Exptl. Theoret. Phys. (U.S.S.R.) **38**, 1001-1002 (March, 1960)

KRÖMER[1] proposed the use of the negative effective mass of carriers in a semiconductor for the amplification and generation of electromagnetic waves, for when such carriers move in a field they give up their energy to the field interacting with them, i.e., they possess negative losses. To obtain such states, the use of a constant electric field is proposed.

In the present communication we shall show that it is impossible to obtain a state with negative losses by using a constant electric field in a semiconductor.

In fact, negative losses mean that, at least for some ϵ_1 and ϵ_2 $(\epsilon_2 > \epsilon_1)$, the following condition is fulfilled:

$$wf(\varepsilon_2)[1 - f(\varepsilon_1)]\,n(\hbar\omega) - wf(\varepsilon_1)[1 - f(\varepsilon_2)]\,n(\hbar\omega) = wn(\hbar\omega)\{f(\varepsilon_2) - f(\varepsilon_1)\} > 0, \quad (1)$$

where $f(\epsilon)$ is the distribution function for electrons, $n(\hbar\omega)$ is the number of photons of energy $\hbar\omega = \epsilon_2 - \epsilon_1$, and w is the probability of spontaneous emission. We do not consider spontaneous transitions, since they are not relevant to the process of amplification. From (1) it follows that at least at some points in the interval $\epsilon_2 - \epsilon_1$, $\partial f(\epsilon)/\partial\epsilon > 0$ should hold. At thermodynamic equilibrium, $\partial f/\partial\epsilon < 0$ always holds for any ϵ, independently of the type of distribution of the particles, and consequently amplification is impossible.

The creation of a semiconductor amplifier or generator using the effect of negative losses should be considered from the viewpoint of the possible destruction of thermodynamic equilibrium and the attainment of states with $\partial f/\partial\epsilon > 0$ in some interval of energy. However, in the steady state in a constant electric field E, as assumed by Krömer,[1] it is impossible to obtain such states for a semiconductor, as direct calculation shows.[2-5] The distribution functions found up to the highest values of fields, have $\partial f(\epsilon, E)/\partial\epsilon < 0$ for all values of ϵ $[\partial f(\epsilon, E)/\partial\epsilon \to 0$ as $E \to \infty]$. In very strong fields when the processes of electron scattering at lattice phonons are unimportant, it is also impossible to obtain an amplifying state, even if impact ionization and the Zener effect are ignored. In this case the electron will oscillate periodically between the upper and lower edges of the permitted band, so that electron states with positive and negative masses are equally probable.

Everything that has been said above can be generalized directly to the case of an anisotropic band in which, for some values of the quasi-momentum $\mathbf{p}$, some components of the tensor-effective mass are negative; here, too, it is impossible to have $\partial f/\partial\epsilon > 0$ in a constant electric field, since in semiconductors the constants of interaction with acoustical and optical phonons are of the same order of magnitude.

Thus, to create semiconducting systems with negative losses, it is necessary to obtain a state with negative temperature, where $\partial f/\partial\epsilon > 0$. Such states can in principle be attained by excitation of the electrons with sufficiently powerful monochromatic radiation, causing transitions between the levels of one band or different bands using a pulsed system or a steady state system, as in molecular generators and amplifiers, or using pulsed excitation by an electric field.[6]

We note that to obtain a negative temperature using a pulsed electric field, it is expedient to use interband transitions of electrons, and not transitions inside a single band, since the time for which negative temperatures exist is much shorter in the latter case.

---

[1] H. Krömer, Proc. I.R.E. **47**, 397 (1959); Phys. Rev. **109**, 1856 (1958).

[2] B. I. Davydov, JETP **7**, 1068 (1937).

[3] I. Yamashita and M. Watanabe, Progr. Theor. Phys. 12, 443 (1954).

[4] R. Stratton, Proc. Roy. Soc. **A242**, 355 (1957).

[5] L. V. Keldysh, JETP **37**, 713 (1959).

[6] Basov, Vul, and Popov, JETP **37**, 587 (1959), Soviet Phys. JETP **10**, 416 (1960).

Translated by K. F. Hulme
194

ON POSSIBLE PROPERTIES OF D^0 MESONS

I. V. CHUVILO

Joint Institute for Nuclear Research

Submitted to JETP editor December 28, 1959

J. Exptl. Theoret. Phys. (U.S.S.R.) **38**, 1002-1003 (March, 1960)

IN connection with the communication on the D^+ meson,[1] various "peculiar" decays of unstable particles,[2] which were observed in the past, are being reanalyzed.[2] An opinion becoming prevalent is that the D^+ meson, and in accordance with presently popular systematics of elementary particles (e.g., the Gell-Mann-Nishijima scheme[3]) also the D^- meson, exist, have a mass of 742 ± 20 Mev, decay according to the scheme

$$D^{\pm} \to K + \pi + Q, \tag{1}$$

and are particles of strangeness ±2. Thus from among all the bosons of the Gell-Mann-Nishijima scheme only the ρ_0 meson has not been detected experimentally.

In the notation of the Salam-Polkinghorne scheme[4]

$$Q/e = \tau_3 + \mu_3 \tag{2}$$

(Q — magnitude of electric charge, τ_3 corresponds to the isospin and μ_3 to the strangeness) the $D^{\pm}$ mesons are described by $\tau_3 = 0$ and $\mu_3 = \pm 1$. If we also include $\tau_3 = 0$ and $\mu_3 = 0$ here, we obtain a triplet D^+, D^0, D^- which may be viewed as a vector in μ-isospace. Consequently the suggestion occurs that this group of isotopic singlets may have similar properties. If such a view were to be accepted then the D^0 meson would also have a mass of the order of the mass of the charged D mesons, and decay according to the scheme

$$D^0 \to K^{\pm 0} + \pi^{\mp 0}. \tag{3}$$

We wish to call attention to the communications existing in the literature on the decay of neutral particles according to the scheme

$$V_3^0 \to K^{\pm} + \pi^{\mp} \tag{4}$$

with $m(V_3^0) \approx 650 - 700$ Mev.[5] Thus there are indications that a neutral unstable particle exists with a mass and a mode of decay analogous to the characteristics of the $D^{\pm}$ mesons. If we identify the V_3^0 particle with the above indicated D^0 meson, we come to the conclusion that an isotopic singlet D^0 meson exists with strangeness $S = 0$ which, although it could formally undergo a fast decay into π mesons satisfying the condition $\Delta S = 0$,[6] decays slowly into decay products with strangeness ±1. However this conclusion contradicts the premises on which the indicated systematics are based unless fast decays of the type $\Sigma^0 \to \Lambda^0 + \gamma$ and $D^0 \to n\pi$ are somehow forbidden.

The most convenient method for production of such D^0 mesons would be from reactions of the type

$$\pi^- + p \to n + D^0, \tag{5}$$

and also from photoproduction of the type studied by Bernardini et al.[7]

We have analyzed over 50 "anomalous" V^0 events detected at various times in cosmic ray experiments.[8] We obtained the following results: 1) no neutral meson exists with a mass of the order of 750 Mev and a decay mode (3); 2) the published anomalous V^0 events are more likely evidence for the existence of two neutral cascade mesons D_1^0 and D_2^0 with the above indicated decay mode (3) with $Q_1 = 38$ Mev and $Q_2 = 63$ Mev; 3) the flux of these mesons amounts to 1 — 2% of the flux of Λ^0 and θ^0 particles (there were approximately 30 of them among the 50 "anomalous" V^0 events); 4) the decays of both D_1^0 and D_2^0 through the two channels $K^+ + \pi^-$ and $K^- + \pi^+$ are in the ratio of 1 : 1.

In connection with the questions discussed here it would be of interest to check the data obtained with bubble chambers irradiated with π-meson beams with momenta in excess of 1 Bev/c. The purpose of this check would be a systematic search for and study of unstable neutral particles with properties different from the Λ^0 and θ^0 particles, since the information on the number of D^0 mesons and their properties is of great importance for the systematics of elementary particles.

The author is grateful fo Prof. D. I. Blokhintsev and M. A. Markov for useful discussions on the problems raised here.

---

[1] Wang Kang-Ch'ang, Report at the Kiev Conference on High Energy Physics, July 1959 (in press).

[2] T. Yamanouchi, Phys. Rev. Lett. **3**, 480 (1959).

[3] M. Gell-Mann, Probl. sovr. fiz. 11 (1956).

[4] A. Salam and J. C. Polkinghorne, Nuovo cimento **2**, 685 (1955).

[5] Leighton, Wanlass, and Anderson, Phys. Rev. **89**, 148 (1953).

[6] M. A. Markov, Гипероны и *K*-мезоны (Hyperons and K Mesons), Fizmatgiz. 1958, p. 156.

[7] Bernardini, Querzoli, Salvini, Silverman, and Stoppini, Nuovo cimento **14**, 268 (1959).

[8] R. Thompson, Cosmic Ray Physics, ed. by J. G. Wilson (Russ. Transl.) 3, IIL, 1958. K. H. Barker, Proc. Roy. Soc. **A221**, 328 (1954). Kadyk, Trilling, Leighton, and Anderson, Phys. Rev. **105**, 1862 (1957). D'Andlau, Armenteros, Astier, DeStaebler, Gregory, Leprince-Riguet, Muller, Peyroe, and Tinlot, Nuovo cimento **6**, 1135 (1957).

Translated by A. M. Bincer
195

ANGULAR DISTRIBUTION OF DECAY PRODUCTS OF $\Sigma^\pm$ -HYPERONS PRODUCED BY PROTONS IN PHOTOEMULSION

L. P. DZHANELIDZE, K. V. MANDRITSKAYA,
O. A. SHAKHULASHVILI, D. K. KOPYLOVA,
Yu. B. KORELEVICH, N. I. PETUKHOVA,*
D. TUVDENDORZH, CHENG P'U-YING, and
N. I. KOSTANASHVILI

Joint Institute of Nuclear Research

Submitted to JETP editor December 31, 1959

J. Exptl. Theoret. Phys. (U.S.S.R.) **38**, 1004-1005 (March, 1960)

SOLOV'EV[1] stressed the importance of studying the longitudinal asymmetry in the angular distribution of π mesons produced in hyperon decays. During a study of the strange-particle production by 9-Bev protons, Kostanashvili and Shakhulashvili[2] obtained an indication as to the possible existence of such an asymmetry in the decay of $\Sigma^\pm$ hyperons. In view of this, we undertook an experiment to improve the data on the angular distribution of $\pi^\pm$ mesons from the decay of $\Sigma^\pm$ hyperons produced in interactions between 9-Bev protons and photoemulsion nuclei. Our main concern was to choose a method of searching for hyperons free from any experimental bias and to identify carefully the cases of decay that were found.

The search for Σ hyperons was carried out by following the tracks from stars produced by the interaction of the primary protons with emulsion nuclei (NIKFI BR-400 emulsion). Each layer of the emulsion stack was area-scanned for stars with $N_h \geq 10$ in which there was at least one track satisfying the following conditions: a) the particle producing the track is emitted in the direction of the forward hemisphere relative to the motion of the proton beam; b) the line of horizontal projection of the track in one layer of emulsion was ≥ 3 mm; c) the value of the ionization I was within the limits of $1.5 I_{\min} \leq I \leq 7 I_{\min}$. Tracks satisfying these conditions were followed a distance of at least 2 cm or to the end if their length was less than 2 cm. The Σ -hyperon decays in flight via the scheme $\Sigma^\pm \rightarrow \pi^\pm + n$ were selected primarily by inspection. To do this, all points of disappearance of the tracks of particles which clearly did not stop within the layer of emulsion were carefully examined under high magnification (60 × 10 × 1.5) to seek a secondary relativistic or almost relativistic track. Such cases could represent the decay in flight of $\Sigma^\pm$ hyperons or $K^\pm$ mesons, where it may be expected beforehand that, owing to the great difference in the lifetimes of these two particles, the contamination of K mesons should be extremely slight.

The final identification was made on the basis of multiple scattering and ionization measurements. The values of the velocity (β) of the hyperon and K meson corresponding to the measured value of $p\beta$ and calculated with the tables in reference 3 were compared with the results of the ionization measurement by the method given in reference 4. The statistical error of the measurement of the quantity $p\beta$, as a rule, did not exceed 10 — 15%, and the relative error in the ionization measurement did not exceed 6 — 8%. Measurements to such an accuracy proved to be sufficient for a reliable identification of hyperons. Analogous measurements were made for control purposes on tracks of known K mesons (the K mesons were found incidentally, when extending the tracks from the selected stars) in the interval of ionization $(2.5-7)\ I_{\min}$; in all cases, the identification of the particles proved to be correct. Moreover, for two hyperons found by the above-described method the tracks of the π mesons produced in the decay could be followed. The ranges of the π mesons were in good agreement with the kinematics of the decay via the scheme $\Sigma^{\pm} \rightarrow \pi^{\pm} + n$.

In the method chosen for searching for the decays, the only cause for the missing of $\pi^{\pm}$ mesons could have been a low efficiency in detecting relativistic particles. To estimate this efficiency, we investigated 226 cases of $\pi \rightarrow \mu$ decay in which the μ meson stopped inside the emulsion stack. The electrons from the μ meson were not observed in eight cases. On this basis, one can evidently assume that there was no preferential selection of $\pi^{\pm}$ mesons in any direction in the $\Sigma^{\pm}$-hyperon decays found.

In all, 72 cases of $\Sigma^{\pm}$-hyperon decays in flight were found in this way. If it is assumed that the angular distribution has the form $(1 + a \cos\theta)$, where θ is the angle between the direction of flight of the Σ hyperon and the π meson in the hyperon rest system, then the value of a turns out to be 0.09 ± 0.2. After adding seven cases found by the same method, but under somewhat different conditions, we obtained $a = 0.03 \pm 0.2$.

In the process of searching for and identifying the hyperons, two cases were observed in which the secondary particle turned out to be an electron. The kinetic energies of the electrons were equal to ~ 1.5 Mev and (11 ± 2) Mev. Both cases could be explained by the proton undergoing charge exchange in a carbon nucleus of the emulsion and the subsequent β decay of the resulting nitrogen isotope N^{12}:

$$p + C^{12} \rightarrow N^{12} + n, \qquad N^{12} \rightarrow C^{12} + \beta^{+}.$$

The authors express their deep appreciation to É. L. Andronikashvili for his constant interest in this work, to M. Danysz and M. I. Podgoretskiĭ for their valuable advice and discussions during the course of the work, and also to V. V. Glagolev, R. M. Lebedev, and O. G. Khakhanashvili for assistance in the work.

---

*Deceased.

[1] V. G. Solov'ev, Joint Institute of Nuclear Studies, preprint P-147, Dubna, 1958.

[2] N. I. Kostanashvili and O. A. Shakhulashvili, JETP **36**, 1006 (1959), Soviet Phys. JETP **9**, 713 (1960).

[3] Fay, Gottstein, and Hain, Nuovo cimento Suppl. **2**, 234 (1954).

[4] P. H. Fowler and D. H. Perkins, Phil. Mag. **46**, 587 (1955).

Translated by E. Marquit
196

ON THE POSSIBILITY OF MEASURING IN THE LABORATORY THE SPEED OF PROPAGATION OF GRAVITATIONAL WAVES

V. B. BRAGINSKIĬ, D. D. IVANENKO, and G. I. RUKMAN

Moscow State University

Submitted to JETP editor January 3, 1960

J. Exptl. Theoret. Phys. (U.S.S.R.) **38**, 1005-1007 (March, 1960)

In recent years there has been some discussion[1-5] of possible new experiments to investigate the gravitational field, in particular, experiments to detect gravitational waves, terrestrial tests of general relativistic effects, a repetition of the classical Eötvös experiment, and so on. In view of the recent developments in electronics, it is natural to use the most modern, sensitive measuring techniques. The question of whether we can measure the speed of gravitational waves has been discussed in reference 5. To do this it is necessary to have a gravitational oscillator, radiating an intense, high-frequency gravitational wave, and, at some distance, a gravitational receiver. To use language borrowed from electrodynamics, we can say that a gravitational experiment with macroscopic objects must necessarily be done in the "induction zone," i.e., the distance between the oscillator and receiver must be less than a wavelength.

In the linear approximation to Einstein's equations, a weak gravitational field is described by D'Alembert's equation, with a suitable right-hand side. We therefore write a tentative expression for a typical component of the field strength, at distances small compared with a wavelength, with a dipole frequency ω (reference 6)

$$E_R = 2p_0 e^{i\omega t} R^{-3} \cos\theta \,(1 + k^2R^2/2 - ik^3R^3/2 + \ldots), \quad (1)$$

where $k = \omega/c_g$, c_g is the speed of propagation of the gravitational field in the wave zone, p_0 is the dipole moment, and R is the distance. This expression holds for $kR \ll 1$. There are two "nonstatic" terms in the brackets: $k^2R^2/2$ and $ik^3R^3/2$

(the other terms are of higher order). The first term takes into account the effect of c_g on the amplitude of the field, while the second essentially expresses the "phase shift" associated with the finiteness of c_g. Thus, in principle, c_g can be obtained from a measurement of E_R. In reference 5 it is proposed to measure the phase shift to obtain c_g; however, it should be noted that while reference 5 claims this phase shift to be a first-order effect (kR), it is really of third order, $ik^3R^3/2 \approx iv^3/c_g^3$, as is evident from (1) (v is the amplitude associated with the linear velocity of the oscillator). For the experiment proposed in reference 5, it would be necessary to measure an angle $\approx 10^{-17}$ radian, taking $c_g = 3 \times 10^{10}$ cm/sec. At the present time, phase shifts of $10^{-5} - 10^{-6}$ radian are known to have been measured.[7]

From (1) we see that the decrease in amplitude is frequency dependent and at a frequency $\omega/2\pi \sim 200$ cps, and at a distance $R = 1$ m, we have $k^2R^2/2 \approx 10^{-11}$. Such a small decrease in amplitude can be measured if the oscillator frequency is modulated at some low frequency, ≈ 0.5 cps, and the signal detected synchronously. With such an arrangement, the band-width could be decreased to $\approx 10^{-3}$ cps.

As a detector of the gravitational field, Weber[1] has proposed a piezoelectric transducer, together with associated amplifiers. Such a transducer would consist of a piezoelectric crystal between two sufficiently large masses; the inhomogeneous gravitational field due to the oscillator would lead to a stress in the crystal. We note a number of technical difficulties which would have to be solved before such a scheme would work.

The frequency response of transducer plus amplifiers would have to be horizontal to at least one part in 10^{11}. This implies that the transducer and the reactive elements in the amplifier would have to be temperature controlled within 0.1° C. After demodulation, the signal, proportional to k^2R^2, has an amplitude of only 10^{-10} volts.

Such small signals can be measured with the photo-electric amplifier built by Kozyrev.[8] The oscillator can be a mechanical rotator with diameter $D_0 = 2$ m, operating at a frequency 25 — 50 cps, and with four additional masses distributed along its circumference. The stress appearing upon rotation is $\approx 10^3$ kg/cm² which is not too large for the usual grades of steel.

In conclusion the authors would like to thank V. V. Migulin and M. S. Akulin for their discussions of versions of the experiments.

---

[1] J. Weber, Revs. Modern Phys. **31**, 681 (1959); Science News Letter 5, 17 (1959).

[2] R. H. Dicke, Science **129**, 621 (1959).

[3] V. L. Ginzburg, Usp. Fiz. Nauk **59**, 1 (1956).

[4] C. Møller, Dan. Mat. Fys. Medd. **30**, No. 10 (1955).

[5] I. L. Bershteĭn and M. E. Gertsenshteĭn, JETP **37**, 1832 (1959), Soviet Phys. JETP **10**, 1293 (1960).

[6] L. D. Landau and E. M. Lifshitz, Теория поля (Field Theory) Gostekhizdat; Engl. transl., Addison Wesley, 1951.

[7] M. E. Zhabotinskiĭ and E. I. Sverchikov, Приборы и техника эксперимента (Instrum. and Meas. Engg.) No. 3, 74 (1956).

[8] V. P. Kozyrev, Электричество (Electricity) No. 2, 47 (1956).

Translated by R. Krotkov
197

ON THE RADIATIVE CORRECTION IN WEAK-INTERACTION PROCESSES

Ya. A. SMORODINSKIĬ and HO TSO-HSIU

Joint Institute for Nuclear Research

Submitted to JETP editor January 15, 1960

J. Exptl. Theoret. Phys. (U.S.S.R.) **38**, 1007-1008 (March, 1960)

It has been shown in a number of papers[1-4] that, in first order in α, the radiative corrections to μ-meson decay lead to a finite renormalization of the interaction constants (with different renormalization for the vector and axial-vector parts). At the same time the analogous correction for β decay, for example that of the neutron, diverges, and moreover this divergence cannot be removed by ordinary mass renormalization.

The cause of the different behavior is that the diagram for μ decay is of a type analogous to the diagram for the emission of a photon. In fact, the interaction Hamiltonian for the decay of a μ meson can be written either in the ordinary V-A form

$$H = \frac{G}{\sqrt{2}} \langle \nu | \gamma_\alpha (1 + \gamma_5) | \mu \rangle \langle e | \gamma_\alpha (1 + \gamma_5) | \nu \rangle, \qquad (1)$$

or in the equivalent form

$$H = \frac{\bar{G}}{\sqrt{2}} \langle e | \gamma_\alpha (1 + \gamma_5) | \mu \rangle \langle \nu | \gamma_\alpha (1 + \gamma_5) | \nu \rangle; \qquad (2)$$

the change from form (1) to form (2) consists only in interchange of two particles of the same helicity, ν and e. In the latter expression the radiation corrections affect only the first factor (there are no charged particles in the second), which differs from the electrodynamic current $\langle e | \gamma_\mu | e \rangle$ by the fact that the mass of the particle changes in the transition, and also by the presence of the factor γ_5 (the current axial vector is $\gamma_5\gamma_\alpha$).

Since, as is well known, the divergent integrals in electrodynamics do not depend on the mass of the particle, the fact that it changes cannot invalidate the conclusion from Ward's theorem[5] that the vertex-part and self-mass divergences cancel. The factor γ_5 can also change nothing in this connection, since the replacement of the wave function ψ by $\gamma_5\psi$ leads only to a change of the mass.

It follows that a finite result will be obtained when one calculates the radiative corrections to μ-meson decay (and to any other process of interaction of μ mesons with electrons: $\mu \rightarrow e + \nu + \bar{\nu} + \gamma$, $e + \nu \rightarrow e + \nu$, $\mu + \nu \rightarrow \mu + \nu$, and so on) in any order (in e^2) of perturbation theory.

In the case of the β decay of the neutron or the capture of a μ meson by a proton the Hamiltonian does not reduce to the electrodynamic form. In fact,

$$H = \frac{G}{\sqrt{2}} \langle p | \gamma_\alpha (1 + \gamma_5) | n \rangle \langle e | \gamma_\alpha (1 + \gamma_5) | \nu \rangle \tag{3}$$

and it is not possible by interchanging particles of the same helicity to group the charged particles in one factor — to do so one must interchange n and e. This latter interchange does not leave the Hamiltonian in the same form, but changes it to[6]

$$H = \sqrt{2}\, G \langle e | (1 - \gamma_5) | \bar{p} \rangle \langle \bar{n} | (1 + \gamma_5) | \nu \rangle, \tag{4}$$

which, as is well known, is not renormalizable (even if one does not take into account the magnetic moment of the neutron). It can be seen from this that only for processes in which no particles appear except electrons, μ mesons, neutrinos, and photons is it possible to calculate the radiative corrections.

In this connection one cannot at the present time predict theoretically the relative size of the constants calculated, on one hand, from the lifetime of the neutron, and on the other hand from β transitions between nuclei of spin zero ($0^+ \rightarrow 0^+$ transitions); the experimental determination of this ratio is an important problem.

---

[1] Behrends, Finkelstein, and Sirlin, Phys. Rev. **101**, 866 (1956).

[2] S. M. Berman, Phys. Rev. **112**, 267 (1958).

[3] T. Kinoshita and A. Sirlin, Phys. Rev. **113**, 1652 (1959).

[4] V. P. Kuznetsov, JETP **37**, 1102 (1959), Soviet Phys. JETP **10**, 784 (1960).

[5] J. Ward, Phys. Rev. **78**, 182 (1950).

[6] Ho Tso-Hsiu and Chu Hung-Yüan (preprint).

Translated by W. H. Furry
198

ON AN ESTIMATE OF THE MINIMUM RADIUS OF TWO-PARTICLE INTERACTIONS AT HIGH ENERGIES

V. G. GRISHIN and V. I. OGIEVETSKIĬ

Joint Institute for Nuclear Research

Submitted to JETP editor January 6, 1960

J. Exptl. Theoret. Phys. (U.S.S.R.) **38**, 1008-1009 (March, 1960)

It is impossible in practice to carry out a phase-shift analysis at high energies, owing to the large number of partial waves participating in the interaction. It is therefore important to establish what information may be extracted from the experimental data.

In this note we show how to determine the minimum number of partial waves $L_{\min}$ necessary to describe the experimentally known total elastic scattering cross section σ_{el} and the differential cross section at a given angle $\sigma(\vartheta_1)$. The following inequalities may be proved:

a) Spinless particles:

$$\Sigma_0 \geqslant 4\pi\sigma(\vartheta_1) / \sigma_{el}. \tag{1}$$

b) Interaction between particles of spin 0 and $\frac{1}{2}$:

$$\max\{\Sigma_0, \ \Sigma_1\} \geqslant 4\pi\sigma(\vartheta_1) / \sigma_{el}. \tag{2}$$

c) Not identical Dirac particles:

$$\max\{\Sigma_0, \ \Sigma_1, \ \Sigma_2\} \geqslant 4\pi\sigma(\vartheta_1) / \sigma_{el}. \tag{3}$$

d) Identical Dirac particles:

$$\max\{\Sigma_0', \ \Sigma_0'', \ \Sigma_1', \ \Sigma_1'', \ \Sigma_2', \ \Sigma_2''\} \geqslant 4\pi\sigma(\vartheta_1) / \sigma_{el}. \tag{4}$$

In these inequalities

$$\Sigma_m = \sum_{l=m}^{L} (2l+1) \frac{(l-m)!}{(l+m)!} [P_l^{(m)}(\cos\vartheta_1)]^2,$$

$$\Sigma_m' = \sum_{l=m}^{L} [1-(-1)^l](2l+1) \frac{(l-m)!}{(l+m)!} [P_l^{(m)}(\cos\vartheta_1)]^2,$$

$$\Sigma_m'' = \sum_{l=m}^{L} [1+(-1)^l](2l+1) \frac{(l-m)!}{(l+m)!} [P_l^{(m)}(\cos\vartheta_1)]^2. \tag{5}$$

The largest of the entries in the curly brackets is to be used on the left hand sides of Eqs. (2) — (4).

At large energies, when L is sufficiently large, $\Sigma'_m \approx \Sigma''_m \approx \Sigma_m$. If the angle ϑ_1 is small, then Σ_0 will be larger than Σ_1 and Σ_2 since the latter contain the associated Legendre polynomials. Therefore in practice one can always use the inequality (1). Let us write it out in more detail:

$$\sum_0^L (2l+1)\,[P_l(\cos\vartheta_1)]^2 \geqslant 4\pi\sigma(\vartheta_1)/\sigma_{el}. \qquad (1')$$

It is obvious that (1′) will begin to be valid only for $L \geq L_{\min}$. In a quasiclassical approach one may associate with $L_{\min}$ a minimum interaction radius $R_{\min} \approx L_{\min}\bar{\lambda}$.

As an example we discuss pp scattering at 8.5 Bev. According to Tsyganov et al.[1] we have in this case

$$\sigma_{el} = (8.6 \pm 0.8)\ \text{mb},$$
$$\sigma(2.5° - 5.5°) = 123 \pm 18\ \text{mb/sr}.$$

From the inequality (1′) we find $L_{\min} = 16 \pm 3$. The optical model, when used to describe the same data, gives an effective L equal to 16. The corresponding interaction radius is $R \approx 1.6 \times 10^{-13}$ cm. It follows from our results that any other model will lead to the same or larger interaction radius.

The inequality (1′) may be viewed as a stronger version of the Rarita-Schwed[2] inequality:

$$(L+1)^2 \geqslant k^2\sigma_t^2/4\pi\sigma_{el}, \qquad (6)$$

which, as is easy to see, follows from (1′) for $\vartheta = 0$ in the case of a vanishing real part of the scattering amplitude. Thus, in the example considered above, the inequality (6) yields the weaker estimate $L_{\min} = 8 \pm 1$ if $\sigma_t = (30 \pm 3)$ mb.

In conclusion we note that all our results hold as well for inelastic two-particle reactions of the type $\pi^- + p \rightarrow \Sigma^- + K^+$. In this case one should replace σ_{el} by the total cross section for the reaction under study.

The authors are indebted to L. G. Zastavenko for discussions.

---

[1] V. I. Veksler, Report at the International Conference on High Energy Physics, Kiev, 1959.

[2] W. Rarita and P. Schwed, Phys. Rev. **112**, 271 (1958).

Translated by A. M. Bincer

CREATION OF ANTIPROTONS IN INTERACTION OF NEGATIVE PIONS WITH NUCLEONS

WANG KANG-CH'ANG, WANG TS'U-TSENG, TING TA TS'AO, V. G. IVANOV, E. N. KLADNITSKAYA, A. A. KUZNETSOV, NGUYEN DIN-TY, A. V. NIKITIN, S. Z. OTVINOVSKIĬ, and M. I. SOLOV'EV

Submitted to JETP editor January 6, 1959

J. Exptl. Theoret. Phys. (U.S.S.R.) **38**, 1010-1011 (March, 1960)

UP to now there apparently has been no observed case of direct production of antiprotons in πN interactions. We have found several cases of production of antiprotons by negative pions on nucleons, two of which are reported in this letter.

The work was carried out on the proton synchrotron of the Joint Institute for Nuclear Research with a propane bubble chamber[1] in a permanent magnetic field of 13,700 gauss.

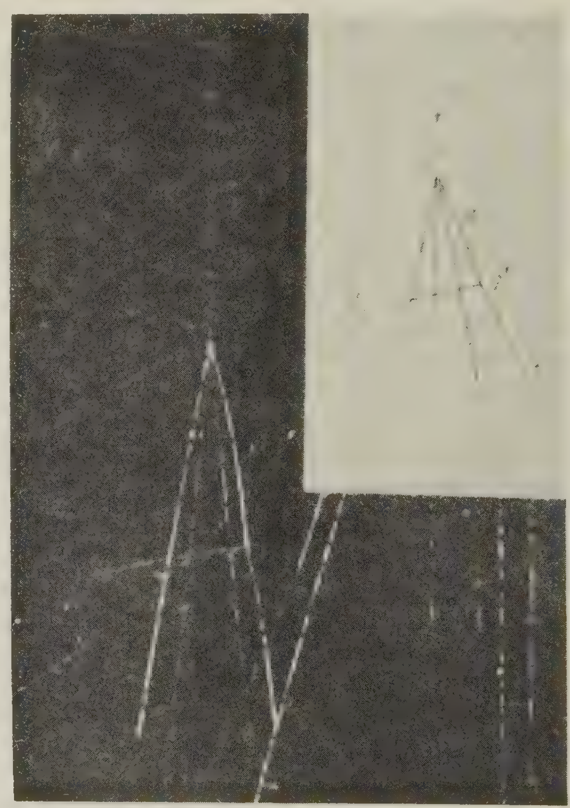

FIG. 1

Figure 1 shows a case where a primary negative pion with approximate energy 7 Bev crosses at the point O a star with four prongs. Prong a is determined unambiguously as an antiproton. The prong a experiences scattering by approximately 5°, 2.3 cm away from the point O, and travels another 3.3 cm before it is stopped at the point O′, where it is apparently annihilated, with the proton forming, in addition to neutral particles, two charged particles f^- and g^+. The momentum of the f particle is 138 ± 6 Mev/c, while that of the g particle is 170 ± 12 Mev/c. The angle between f and g is 126 ± 1°. It must be emphasized that the star O′ cannot be caused by any other process except annihilation.

Let us consider the possible reactions:

1. $K^- + p \rightarrow \Lambda^0 + \pi^+ + \pi^-$

(for the free and bound proton);

2. $K^- \rightarrow \pi^- + \pi^0 + \pi_0$;

3. $K^- \rightarrow \pi^- + \pi^0$;

4. $\overline{p} + p \rightarrow \pi^+ + \pi^- + (n\pi^0)$.

1. The $\pi^\pm$ mesons (f and g) cannot be produced by reaction 1, from energy considerations. This conclusion is not changed if it is assumed that the K^- mesons interact in flight, because the angle between a and f at O is greater than 90°, and the angle between a and g is close to 90°.

2. Reaction 2 is also impossible from energy considerations, even if it is assumed that one of the γ quanta from the π^0-meson decay produces immediately a positron, and the electron receives no energy at all.

3. If it is assumed, on the other hand, that reaction (3) takes place, then the negative pion should have a momentum of 205 Mev/c; measurements yield 130 ± 6 Mev/c. Furthermore, the positive g particle should be a positron and carry away the total momentum of the γ quantum, on the order of 100 Mev/c. Actually the measurements show the particle to have a momentum of 170 ± 12 Mev/c.

4. Only the last possibility remains: g and f are positive and negative pions respectively, created simultaneously with the other neutral particles during the act of annihilation.

Figure 2 shows the second case of creation of a slow antiproton by a negative pion of energy 8 Bev. The negative pion interacts with the carbon nucleus and produces at the point O a three-pronged star. Particle a, which has a negative charge, covers 12.9 cm in the chamber and is stopped at the point O′, where it is annihilated with the nucleon in the carbon nucleus, forming a star of seven prongs, three of which have minimum ionization.

Track b, one of the three prongs with minimum ionization, formed by the positive particle, has a momentum of 566 ± 34 Mev/c, i.e., it is a positive pion. This fact confirms that the a particle is an antiproton (or, less probably, $\overline{\Sigma}^+$), since no other known particle can produce a pion with so large a momentum when stopped. The momenta of the other prongs of this star cannot be measured with reliable accuracy, since they have a very small length in the chamber and all go outside the working volume.

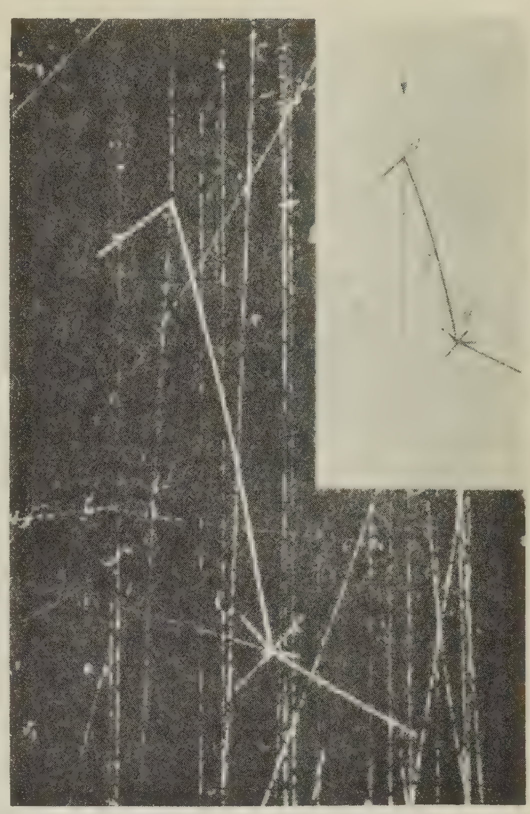

FIG. 2

The mechanism of production of these two antiprotons, and also several cases of production of antiprotons with momenta greater than 1.5 Bev/c, will be described in detail in another article.

An estimate of the cross section for the production of antiprotons by negative pions with energies 7 — 8 Bev in propane gives a lower value of 10^{-30} cm^2 per nucleon.

---

[1] Wang, Solov'ev, and Shkobin, Приборы и техника эксперимента (Intruments and Measurement Engineering) No. 1, 41 (1959).

Translated by J. G. Adashko
200

NEW ISOMER Sn^{113m}

I. P. SELINOV and V. L. CHIKHLADZE

Submitted to JETP editor January 19, 1960

J. Exptl. Theoret. Phys. (U.S.S.R.) **38**, 1012 (March, 1960)

ACCORDING to the systematics of the half-lives of the isomers, one would expect the long-lived (T = 119 days) tin isotope Sn^{113} to have an isomer with a half-life somewhat shorter than that of Cd^{111m} (T = 48.7 min). Actually, an investigation of the isotope Sb^{113} (T = 7 min) with a double-lens β spectrometer has disclosed that, as a result of positron decay, this isotope is partially transmuted into a new isomer, Sn^{113m}, with a half-life of 27 ± 3 min.

There have been observed in the conversion spectrum of Sb^{113} electrons with energies 49.6, 75.3, and 77.4 kev, corresponding to conversion of γ radiation of energy 79.3 ± 0.5 kev on the K, L, and M shells. The ratio of the conversion on the K shell to that on the L shell is 1.75.

Theoretical values of this ratio, for transitions of various multipolarities, are: E1 — 9.45, E2 — 3.8, E3 — 0.95, M1 — 7.55, M2 — 3.8, and M3 — 3.56. The extrapolated value for M4 is about 1.7. Consequently, the isomer transition from the metastable state of Sn^{113m} has a multipolarity M4.

Translated by J. G. Adashko
201

REMARK ON THE DECAY OF THE CASCADE HYPERON

I. Yu. KOBZAREV, L. B. OKUN', and A. P. RUDIK

Submitted to JETP editor January 23, 1960

J. Exptl. Theoret. Phys. (U.S.S.R.) **38**, 1012-1013 (March, 1960)

IF the spin of the cascade hyperon is ½, the amplitude of its decay

$$\Xi^0 \to \Lambda^0 + \pi^0, \quad \Xi^- \to \Lambda^0 + \pi^- \tag{1}$$

can be written in the form

$$A = 2\bar{u}_\Lambda (a + be^{i\varphi}\sigma\mathbf{n})\, u_\Xi. \tag{2}$$

Here a and b denote the amplitude for the formation of Λ^0 and π in the S and P states, respectively, and φ is the difference of the phase shifts for the scattering of the π meson by the Λ hyperon in these states. The unit vector **n** is directed along the momentum of the Λ^0 hyperon in the rest system of the Ξ hyperon, the σ's are the Pauli matrices, and u_Λ and u_Ξ are two-component spinors.

If the polarization vector of the Ξ hyperon (in the rest system of Ξ) is denoted by η and the polarization vector of the Λ hyperon (in the rest system of Λ) by ζ, the probability of the decay of a polarized Ξ hyperon with formation of a polarized Λ hyperon, as calculated with the help of the amplitude (2), has the form

$$W(\mathbf{n}, \eta, \zeta) = a^2 + b^2 + 2ab\cos\varphi\,(\zeta\mathbf{n} + \eta\mathbf{n}) + (a^2 - b^2)\,\zeta\eta + 2b^2(\zeta\mathbf{n})(\eta\mathbf{n}) + 2ab\sin\varphi\,[\eta\zeta]\,\mathbf{n}. \tag{3}$$

Formula (3) contains, of course, all possible correlations which were recently considered by Teutsch, Okubo, and Sudarshan.[1] With regard to this formula we should like to make the following observation. As is seen from formula (3), the polarization of the Λ hyperons in the direction perpendicular to the plane defined by the vectors η and **n** will be zero unless $\varphi \neq 0$. The study of the polarization of the Λ hyperons in this direction (together with the measurement of the longitudinal polarization of the Λ hyperons, for example) permits, therefore, the determination of the difference of the S and P phase shifts in the scattering of π mesons by Λ hyperons.

We note that, by isotopic invariance, the value of φ_-, obtained from the decay of the Ξ^- hyperon, and of φ_0, obtained from the decay of the Ξ^0 hyperon, should be identical.

For comparison we mention that the S phase shifts for the scattering of a π meson by a nucleon at corresponding energies (the momentum in the center-of-mass system is equal to $m_\pi c$) are approximately equal to $\alpha_1 \approx -7°$ for the channel $T = 1/2$ and to $\alpha_3 \approx +10°$ for $T = 3/2$ (reference 2). The resonance P phase is equal to $\alpha_{33} \approx 12°$, while the other P phases are close to zero.

---

[1] Teutsch, Okubo, and Sudarshan, Phys. Rev. **114**, 1148 (1959).

[2] J. Orear, Phys. Rev. **100**, 288 (1955).

Translated by R. Lipperheide
202

CONCERNING THE ARTICLE BY S. M. BILEN'KIĬ, R. M. RYNDIN, Ya. A. SMORODINSKIĬ, AND HO TSO-HSIU, "ON THE THEORY OF NEUTRON BETA DECAY"

Submitted to JETP editor January 27, 1960

J. Exptl. Theoret. Phys. (U.S.S.R.) **38**, 1013 (March, 1960)

WEINBERG[1] proved a theorem from which it follows that the full probability for a process of the type $\alpha \rightarrow \beta + l + \bar{\nu}$ (α and β are arbitrary strongly interacting particles and l is a lepton) does not contain V-A interferences. It is easy to see that the expression (12) for the total probability of neutron decay given in our paper[2] satisfies this condition, since the dependence on the first power of λ is only apparent. Indeed, in the approximation $E_0/M = \Delta/M$, which we used, expression (12) may be rewritten as follows:

$$W = \frac{G^2}{(2\pi)^3}(1+3\lambda^2)\Big\{m^4\Big(E_0 - \frac{m^2+2E_0^2}{2M}\Big)\ln\frac{E_0+\sqrt{E_0^2-m^2}}{m} + \frac{2}{15}\sqrt{E_0^2-m^2}\Big[E_0^4 - \frac{9}{2}E_0^2m^2 - 4m^4 + \frac{E_0}{M}\Big(E_0^4 - 2E_0^2m^2 + \frac{49}{4}m^4\Big)\Big]\Big\}.$$

We are grateful to Prof. J. Bernstein for bringing the work of Weinberg to our attention.

---

[1] S. Weinberg, Phys. Rev. **115**, 481 (1959).

[2] Bilenkiĭ, Ryndin, Smorodinskiĭ, and Ho Tso-Hsiu, JETP **37**, 1758 (1959), Soviet Phys. JETP **10**, 1241 (1960).

Translated by A. M. Bincer
203

PRODUCTION OF "SUPERCOLD" POLARIZED NEUTRONS

G. M. DRABKIN and R. A. ZHITNIKOV

Leningrad Physico-Technical Institute, Academy of Sciences, U.S.S.R.

Submitted to JETP editor January 27, 1960

J. Exptl. Theoret. Phys. (U.S.S.R.) **38**, 1013-1014 (March, 1960)

THE rapidly developing research on "cold" neutrons could be greatly widened if "supercold" neutrons with energies of the order of 10^{-4} to 10^{-6} °K could be successfully obtained. However, at moderator temperatures of 1°K, the yield of neutrons with energies of the order of 10^{-5} degrees K amounts to only 10^{-11} of the total flux. To increase the yield of "supercold" neutrons, a new moderation method is proposed below, based on the interaction of the neutron's magnetic moment with a non-uniform magnetic field.

When a neutron crosses a magnetic field H, the change in the kinetic energy ϵ of the neutron will be equal to

$$\Delta\varepsilon = \int_0^s \mu_{\mathrm{eff}} \frac{\partial H}{\partial s} ds,$$

where μ_{eff} is the component of the neutron's magnetic moment in the direction of the field H, and s is the path traversed by the neutron in the field. Since the region affected by a magnetic field can be separated into two parts, in which the gradients are directed in opposite directions, then for $\mu_{\mathrm{eff}} = \mathrm{const}$ we have $\Delta\epsilon = 0$.

The neutron energy can be changed by a corresponding change in the sign of μ_{eff}, i.e., by a reorientation of the neutron spin at the instant when it passes through the maximum of the magnetic field. For this purpose a uniform magnetic field, falling off to zero at the ends, is applied along the neutron path. When a neutron with its moment opposed to the field enters the field, it is acted on by a retarding force $F = \mu_{\mathrm{eff}}\,\partial H/\partial s$ (neutrons with spins oriented in the opposite direction will be accelerated). At the instant when it reaches the maximum field H_0, where $\Delta\epsilon = \mu_{\mathrm{eff}} H_0$, the change in speed will equal

$$\Delta v_1 \approx \mu_{\mathrm{eff}} H_0 / m v_0,$$

where m is the mass and v_0 the initial velocity of the neutron.

If a field H_1 of radio frequency $\omega = \gamma H_0$ is applied in a direction perpendicular to H_0, and if it satisfies the condition $H_1 \Delta t = \hbar/g\mu_N$ (Δt being the time of flight of the neutron through the field H_1, g the gyromagnetic ratio, and μ_N the nuclear magneton), then the result will be a reversal of the spin of the traveling neutron, and consequently a change in the sign of μ_{eff}. This will cause retardation of the neutron during its exit from the constant-field region as well as during its entrance, and the total loss in velocity will be $2\Delta v_1$. The reorientation of neutron spins can be accomplished in a field H_0 of length 2 to 5 cm, with $H_1 \sim 1$ gauss. The velocity lost by a neutron during a single passage through the field is very small. Thus, if $H_0 = 20{,}000$ gauss and the initial velocity is 2×10^3 cm/sec we have $2\Delta v_1 = 100$ cm/sec.

By passing the neutrons successively through a series of regions of uniform retarding fields H_0, it is possible to attain a considerable reduction in the velocity of the neutrons. For instance, to retard neutrons having an initial velocity $v_0 = 2 \times 10^3$ cm/sec to a velocity $v = 40$ cm/sec with $H_0 \approx 2 \times 10^4$ gauss requires sending the neutrons successively through 15 to 20 retarding fields, and the flight path will be of the order of 200 cm. Under these circumstances the relative flux of neutrons with energies of 10^{-5} degrees K, emerging from a moderator at $T = 1°K$, will be increased more than a thousandfold, and will amount to 10^{-7} of the total current.

These neutrons can be separated from the rest of the flux by reflection from a magnetic mirror, after which the reflected neutrons will be completely polarized. In the case of a pulsed neutron source, the moderation can be effected by a traveling magnetic field.

Translated by D. C. West
204

POSSIBLE SYMMETRY PROPERTIES FOR THE π-K SYSTEM

CHOU KUANG CHAO

Joint Institute for Nuclear Research

Submitted to JETP editor January 27, 1960

J. Exptl. Theoret. Phys. (U.S.S.R.) **38**, 1015-1016 (March, 1960)

THE Hamiltonian describing the π-K system has the form

$$H = H_\pi + H_K + g\pi_\alpha\pi_\alpha K^{+}_{\lambda}K_\lambda, \tag{1}$$

where H_π is the pion Hamiltonian including the $\pi\pi$ interaction, H_K is the K-meson Hamiltonian, and g is the coupling constant of the $\pi\pi$KK interaction.[1] It is assumed in (1) that the π-meson and K-meson interactions with baryons can be neglected.

The Hamiltonian (1) is invariant under rotations of the pion field operator in isospin space with the K-meson field operator held fixed. In other words, it is possible to consider the pion as an isovector in one space and the K meson as an isospinor in another space. The Hamiltonian (1) is invariant under rotations in either space.

Let us denote pion—K-meson scattering amplitudes by $f(\pi + K \rightarrow \pi + K)$. Then from the above symmetry properties we obtain the following selection rules:

1) The following scattering amplitudes are equal to each other:

$$f(\pi^\pm + K^\pm \rightarrow \pi^\pm + K^\pm) = f(\pi^0 + K^\pm \rightarrow \pi^0 + K^\pm)$$
$$= f(\pi^\pm + K^0 \rightarrow \pi^\pm + K^0) = f(\pi^\pm + \overline{K}^0 \rightarrow \pi^\pm + \overline{K}^0)$$
$$= f(\pi^0 + K^0 \rightarrow \pi^0 + K^0) = f(\pi^0 + \overline{K}^0 \rightarrow \pi^0 + \overline{K}^0). \tag{2}$$

2) The charge-exchange amplitudes vanish:

$$f(\pi^+ + K^- \rightarrow \pi^0 + \overline{K}^0) = f(\pi^- + K^+ \rightarrow \pi^0 + K^0)$$
$$= f(\pi^+ + K^0 \rightarrow \pi^0 + K^+) = f(\pi^- + \overline{K}^0 \rightarrow \pi^0 + K^-) = 0.$$

3) The $K + \overline{K} \rightarrow n\pi$ annihilation process proceeds only through the isoscalar state.

To obtain experimental verification of these selection rules, one can study the angular distribution of the products in the reaction $K + N \rightarrow K + N + \pi$, for which the one-meson term in the cross section is proportional to

$$\Delta^2(\Delta^2 + \mu^2)^{-2}|f(\pi + K \rightarrow \pi + K)|^2, \tag{3}$$

where Δ^2 is the square of the nucleon momentum transfer. Expression (3) has a maximum for $\Delta^2 = \mu^2$ in the physical region.[2] A measurement of the form of this maximum would provide information on the amplitudes $f(\pi + K \rightarrow \pi + K)$.

According to the theory of Okun' and Pomeranchuk[3] and Chew and Mandelstam[4] the scattering phase shifts in high angular momentum states are determined by diagrams with the smallest number of exchanged π mesons. If the K^+ and K^0 have the same parity then the $K + N \rightarrow K + N$ scattering phase shifts in high angular momentum states are determined by diagrams with two mesons exchanged. Consequently a phase shift analysis of the process $K + N \rightarrow K + N$ would give certain information about the amplitudes $f(\pi + K \rightarrow \pi + K)$.

A violation of these selection rules would imply that the Hamiltonian contains terms with derivatives of the form

$$g'\boldsymbol{\pi} \times \frac{\partial}{\partial x_\mu}\boldsymbol{\pi} \cdot K^*\boldsymbol{\tau}\frac{\partial}{\partial x_\mu}K$$

or that baryon pairs play an important role in πK interactions. Since g′ is not dimensionless, a new fundamental length would appear in the Hamiltonian (in the first version).

The author is grateful to Prof. M. A. Markov and V. I. Ogievetskiĭ for their interest in this work and valuable discussions.

---

[1] S. Barshay, Phys. Rev. **109**, 2160; **110**, 743 (1958).

[2] C. Goebel, Phys. Rev. Lett. **1**, 337 (1958).

[3] L. B. Okun' and I. Ya. Pomeranchuk, JETP **36**, 300 (1959), Soviet Phys. JETP **9**, 207 (1959).

[4] G. F. Chew, Report at the 1959 Kiev Conference (in press).

Translated by A. M. Bincer
205

SOVIET PHYSICS JOURNALS

Published in English by the American Institute of Physics

Soviet Physics—JETP

A translation, beginning with 1955 issues of "Zhurnal Eksperimental'noi i Teoreticheskoi Fiziki" of the USSR Academy of Sciences. Leading physics journal of Soviet Union. Similar to "The Physical Review" in quality and range of topics. Outstanding new work is most likely to appear in this journal.

Twelve issues, approximately 4000 pages. $75 domestic, $79 foreign. Libraries $35 domestic, $39 foreign. Single copies, $8.*

Soviet Physics—SOLID STATE

A translation, beginning with 1959 issues of "Fizika Tverdogo Tela" of the USSR Academy of Sciences. Offering results of theoretical and experimental investigations in the physics of semiconductors, dielectrics, and on applied physics associated with these problems. Also publishes papers on electronic processes taking place in the interior and on the surface of solids.

Twelve issues, approximately 2000 pages. $55 domestic, $59 foreign. Libraries $25 domestic, $29 foreign. Single copies, $8.*

Soviet Physics—TECHNICAL PHYSICS

A translation, beginning with 1956 issues of "Zhurnal Tekhnicheskoi Fiziki" of the USSR Academy of Sciences. Contains work on plasma physics and magnetohydrodynamics, aerodynamics, ion and electron optics, and radio physics. Also publishes articles in mathematical physics, the physics of accelerators, and molecular physics.

Twelve issues, approximately 2000 pages, $55 domestic, $59 foreign. Libraries $25 domestic, $29 foreign. Single copies, $8.*

Soviet Physics—ACOUSTICS

A translation, beginning with 1955 issues of "Akusticheskii Zhurnal" of the USSR Academy of Sciences. Devoted principally to physical acoustics but includes electro-, bio-, and psychoacoustics. Mathematical and experimental work with emphasis on pure research.

Four issues, approximately 500 pages. $12 domestic, $14 foreign. (No library discounts.) Single copies, $4.

Soviet Physics—DOKLADY

A translation, beginning with 1956 issues of the physics sections of "Doklady Akademii Nauk SSSR," the proceedings of the USSR Academy of Sciences. All-science journal offering four-page reports of recent research in physics and borderline subjects.

Six issues, approximately 1500 pages. $35 domestic, $38 foreign. Libraries $15 domestic, $18 foreign. Single copies Vols. 1 and 2, $5; Vol. 3 and later issues, $7.*

Soviet Physics—CRYSTALLOGRAPHY

A translation, beginning with 1957 issues of the journal "Kristallografiya" of the USSR Academy of Sciences Experimental and theoretical papers on crystal structure, lattice theory, diffraction studies, and other topics of interest to crystallographers, mineralogists, and metallurgists.

Six issues, approximately 1000 pages. $25 domestic, $27 foreign. Libraries $10 domestic, $12 foreign. Single copies, $5.*

SOVIET ASTRONOMY—AJ

A translation, beginning with 1957 issues of "Astronomicheskii Zhurnal" of the USSR Academy of Sciences. Covers various problems of interest to astronomers and astrophysicists including solar activity, stellar studies, spectroscopic investigations of radio astronomy.

Six issues, approximately 1100 pages. $25 domestic, $27 foreign. Libraries $10 domestic, $12 foreign. Single copies, $5.*

Soviet Physics—USPEKHI

A translation, beginning with September, 1958, issue of "Uspekhi Fizicheskikh Nauk" of the USSR Academy of Sciences. Offers reviews of recent developments comparable in scope and treatment to those carried in "Reviews of Modern Physics." Also contains reports on scientific meetings within the Soviet Union, book reviews, and personalia.

Six issues, approximately 1700 pages. (Contents limited to material from Soviet sources.) $45 domestic, $48 foreign. Libraries $20 domestic, $23 foreign. Single copies $9.*

*For libraries of nonprofit academic institutions.
Subscription prices subject to annual variation, depending on size of Russian originals.

Please send orders and inquiries to

American Institute of Physics
335 East 45 Street, New York 17, N.Y.